

NASA SP 33 PART 3

SPACE FLIGHT HANDBOOKS

Volume 1

Orbital Flight Handbook

NATIONAL AERONAUTICS AND SPACE ADMINISTRATION



SPACE FLIGHT HANDBOOKS
Volume 1

Orbital Flight Handbook

PART 3 - REQUIREMENTS

Prepared for the
**GEORGE C.
MARSHALL SPACE FLIGHT CENTER**
Huntsville, Alabama
Under Contract NAS 8-5031



Office of Scientific and Technical Information

NATIONAL AERONAUTICS AND SPACE ADMINISTRATION

Washington, D. C.

1963

FOREWORD

This handbook has been produced by the Space Systems Division of the Martin Company under Contract NAS8-5031 with the George C. Marshall Space Flight Center of the National Aeronautics and Space Administration. The handbook expands and updates work previously done by the Martin Company and also incorporates, as indicated in the text, some of the work done by Space Technology Laboratories, Inc. and Norair Division of Northrop Corporation under previous contracts with the George C. Marshall Space Flight Center. The Orbital Flight Handbook is considered the first in a series of volumes by various contractors, sponsored by MSFC, treating the dynamics of space flight in a variety of aspects of interest to the mission designer and evaluator. The primary purpose of these books is to serve as a basic tool in preliminary mission planning. In condensed form, they provide background data and material collected through several years of intensive studies in each space mission area, such as earth orbital flight, lunar flight, and interplanetary flight.

Volume I, the present volume, is concerned with earth orbital missions. The volume consists of three parts presented in three separate books. The parts are:

- Part 1 - Basic Techniques and Data
- Part 2 - Mission Sequencing Problems
- Part 3 - Requirements

The Martin Company Program Manager for this project has been Jorgen Jensen; George Townsend has been Technical Director. George Townsend has also had the direct responsibility for the coordination and preparation of this volume. Donald Kraft is one of the principal contributors to this volume; information has also been supplied by Jyri Kork and Sidney Russak. Barclay E. Tucker and John Magnus have assisted in preparing the handbook for publication.

The assistance given by the Future Projects Office at MSFC and by the MSFC Contract Management Panel, directed by Conrad D. Swanson, is gratefully acknowledged.

CONTENTS

Volume I, Part 3 - Requirements

| | | |
|------|---|--------|
| X | Waiting Orbit Criteria | X-1 |
| XI | Orbit Computations | XI-1 |
| XII | Guidance and Control Requirements | XII-1 |
| XIII | Mission Requirements | XIII-1 |
| | Appendix A | A-1 |
| | Appendix B | B-1 |
| | Index | i |

The preceding contents are Part 3 of Volume I. The remaining two parts of Volume I contain the following:

Volume I, Part 1 - Basic Techniques and Data

| | | |
|-----|-------------------------------|-------|
| I | Introduction | I-1 |
| II | Physical Data | II-1 |
| III | Orbital Mechanics | III-1 |
| IV | Perturbations | IV-1 |
| V | Satellite Lifetimes | V-1 |

Volume I, Part 2 - Mission Sequencing Problems

| | | |
|------|------------------------------|--------|
| VI | Maneuvers | VI-1 |
| VII | Rendezvous | VII-1 |
| VIII | Orbital Departure | VIII-1 |
| IX | Satellite Re-Entry | IX-1 |

CHAPTER X

WAITING ORBIT CRITERIA

| | Page |
|---|------|
| Symbols | X-1 |
| A. Introduction | X-2 |
| B. Payload and Geometrical Restrictions | X-2 |
| C. Vehicle Temperature Control | X-4 |
| D. Cryogenic Propellant Storage | X-10 |
| E. References | X-15 |
| Illustrations | X-21 |

LIST OF ILLUSTRATIONS

| Figure | | Page |
|--------|--|------|
| 1 | Equilibrium Temperature of Inert Sphere | X-23 |
| 2 | Equilibrium Temperature of a Thin Plate Normal to the Sun | X-23 |
| 3 | Effect of Attitude on Equilibrium Temperature of a Thin Plate Located at One Astronomical Unit from the Sun | X-24 |
| 4 | Effect of Added Heat Input on Equilibrium Tempera- ture | X-24 |
| 5 | Vapor Pressure of Cryogenic Fluids | X-25 |
| 6 | Heat Transfer Rates of Cryogenic Insulations, Thermal Conductivity Versus Vacuum Pressure | X-25 |
| 7 | Thermal Conductivity at Various Wall Temperatures . | X-26 |
| 8 | Heat Flux from Sun. | X-26 |
| 9 | Solar Heating--Temperature of Outer Wall | X-27 |
| 10 | Heat Transfer to Hydrogen and Oxygen. | X-27 |
| 11 | No-Loss (Pre-Boiloff) Time--LH ₂ Tank. | X-28 |
| 12 | System Factors (S) Versus Time $S = I_w + \frac{tQ_l T}{v}$. . | X-28 |
| 13 | Propellant Boiloff Plus Insulation Weight at Optimum Insulation Thickness for Spherical Tanks on the Lunar Surface | X-29 |
| 14 | Boiloff Losses for Liquids Contained in Spherical Tanks, General Case | X-30 |

X. WAITING ORBIT CRITERIA

| <u>SYMBOLS</u> | | | |
|----------------|---|------------|--|
| A | Right ascension | \vec{S} | Unit vector specified by launch time and time of flight to injection point |
| A_e, A_i | Reference areas for emitted and incident energy | T | Absolute temperature |
| c_p | Specific heat at constant pressure | W | Weight |
| G | Solar flux | α | Absorptivity |
| k | Thermal conductivity | γ | Ratio of specific heats |
| l | Thickness | ϵ | Emissivity |
| L | Latitude | θ | True anomaly |
| p | Pressure | Λ | Longitude |
| \vec{P} | Unit vector to perigee | ν | Heat of vaporization |
| Q | Transmitted heat flux | ρ | Density |
| \hat{R} | Unit vector to the injection point | σ | Stefan-Boltzmann constant |
| | | τ | Orbital period |

A. INTRODUCTION

In the previous chapters of this manual, the concept of waiting orbits or parking orbits was introduced. In some of these discussions the parking orbit was defined completely (i.e., all six elements were obtained) by the mission to be accomplished. The rendezvous discussion utilizing the intermediate orbit is an example of such cases. In other discussions, however, one or more of the orbital elements could be selected based on considerations other than those of the mechanics of the mission. When these degrees of freedom exist, the following factors are among those which become of interest:

| | Chapter |
|--|---------|
| (1) the radiation environment | II |
| (2) the meteoroid environment | II |
| (3) atmospheric factors, heating, etc. | II, V |
| (4) orbital perturbations | IV, V |
| (5) satellite lifetimes | V |
| (6) maneuver requirements | VI |
| (7) recovery considerations | VIII |
| (8) trajectory error sensitivities | XII |
| (9) guidance and navigation philosophies | XII |
| (10) solar elevation and eclipses | XIII |
| (11) tracking station, area, and point coverage optimization | XIII |
| (12) ground tracks and or synchronous behavior | XIII |
| (13) optical resolution, etc. | XIII |
| (14) staging considerations, reignition and economics | XIII |
| (15) radiation heat loads and cryogenic storage | |

Because of the number of constraints which can be imposed, no single set of rules can be constructed which will yield the best orbit in the sense that each constraint is satisfied. Indeed, it is necessary to assign weights to each factor and to select the elements of the intermediate trajectory for each particular mission by a study of the tradeoffs involved. This phase of study will not be attempted here because of the scope of the task and the fact that the 15 previous constraints can be permuted into

different combinations (taken n at a time) and $\frac{15!}{(15-n)!}$ different permutations.

All of these factors except the last two are discussed within the manual. The next to last item is a practical limitation imposed by the nature of the vehicle used to boost the satellite to orbit and as such was not covered within the present scope of study. Later paragraphs will, however, provide a short qualitative treatment. The final item on the list, though far from completing the possible list of constraints (e.g., human tolerances to radiation), falls into the same general classification of material. However, because of the fact that propellant is required for maneuvers and because radiation heat loads cause problems of storability and boiloff, some of the problems are presented. The level of these discussions, however, will be superficial since the theory of heat transfer is a study in itself

and since in any case the specific vehicle must be considered to obtain design data. The presentation of this material, though brief, will begin to tie the purely mechanical analyses of the remainder of the manual to system or operational requirements.

B. PAYLOAD AND GEOMETRICAL RESTRICTIONS

The parking orbit concept was introduced in several chapters (e.g., VII and IX) to assure that some given parameter (usually time) could be factored into the 3-dimensional analysis without requiring drastic maneuvers at launch. Thus, the primary advantage was in the area of timing the mission. However, there are three other distinct advantages:

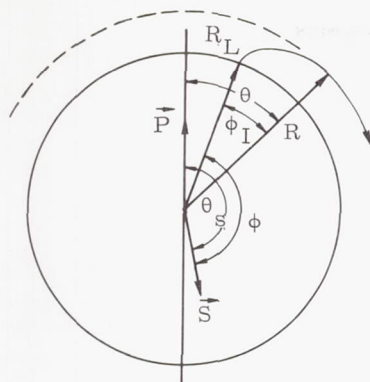
- (1) Flexibility
- (2) Energy reductions
- (3) Error correction.

Flexibility in planning and executing the mission is afforded because the intermediate orbit, if selected properly, increases the number of times at which transfer to a given position or orbit is possible. Also, since the orbit is to be utilized in any event, the launch can occur at any of the crossings of the orbital plane by the launch site. Thus, the effects of countdown holds can be reduced.

The energy requirement utilizing this technique is generally reduced because of two factors. First, the out-of-plane maneuver can be eliminated (or nearly so if there are small launch time errors) and secondly, the type of transfer trajectories can be energy optimized since the timing problem is handled separately. It is noted, however, that there may be times in which parking orbits will require an increase in energy. These cases are those for which the problem timing was correct for direct launch and ascent via a near optimum trajectory since under such conditions the work expended in transporting propellant to an intermediate orbit for future burning is not recoverable. (If this situation is in fact true, it can, however, be assessed so that in no case should an unnecessarily high energy requirement exist.) This energy loss points up the case for a low altitude parking orbit. The practical limit for this orbit will be mentioned later.

The third advantage is that of affording a convenient interval for either correcting for launch errors or computing changes in the transfer trajectory to compensate for them. Because of this feature, the intermediate orbit approach will result in smaller errors in the position and velocity in space at the time of arrival at the designated transfer point.

The discussions which follow combine the flexibility and energy considerations in a brief summary of some of the material presented elsewhere in the manual (the emphasis here being in the selection of the intermediate orbit). Consider the following sketch and angular definitions:

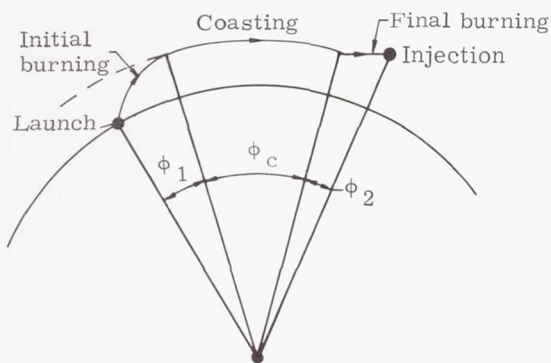


$$\theta = \theta_s - \phi + \phi_I$$

where

- θ_s = perigee-outward radial angle
- ϕ = launch-outward radial angle
- ϕ_I = total burning arc (launch-to-injection)
- \vec{P} = unit vector directed toward perigee
- \vec{S} = unit vector in outward radial direction (specified by launch date and flight time).

Since θ_s and ϕ_I are relatively invariant (with zero coast capability), it is necessary to vary ϕ by launch azimuth or outward radial declination. (Launch azimuth is restricted by range safety; to change the outward radial declination the mission must be altered). By employing a variable coasting, arc ϕ_I may be replaced by $\phi_1 + \phi_c + \phi_2$ where ϕ_1 is the burning arc necessary to get into the parking orbit and ϕ_2 is the burning arc from parking orbit to final injection. Given a launch azimuth (or time) and mission (outward radial declination), the powered flight is matched to the post-injection trajectory by varying launch time (or azimuth) and parking orbit coast time. This is illustrated in the following sketch.



$$\theta = \theta_s - \phi + (\phi_1 + \phi_c + \phi_2)$$

The lowest possible altitude should be selected for the parking orbit from energy considerations. Since the energy requirement is lower, this selection also provides the greatest payload capability. The minimum altitude which can be utilized, however, depends on vehicle engineering constraints such as aerodynamic heating and structural loading, on guidance constraints, such as minimum elevation angle, and on mission constraints requiring specified orbital characteristics (all enumerated in the introduction). However, if the payload capability outweighs the other factors, a parking orbit altitude in the vicinity of 100 to 110 naut mi (i.e., 185 to 204 km) appears to be the best choice.

Thus everything is defined in terms of the parameters of the problem save the vector \hat{R} . This unit vector is obtained utilizing the spherical trigonometric relationships in Chapter III for right ascension and declination or latitude and the identity

$$\hat{R} = \cos A \cos L \hat{x} + \sin A \cos L \hat{y} + \sin L \hat{z}$$

where

- \hat{R} = unit vector directed from earth's center to injection
- A_I = right ascension of injection
- L_I = injection latitude
- $\hat{x}, \hat{y}, \hat{z}$ = unit vectors, earth centered inertial cartesian system (aligned as x, y, z) with x toward vernal equinox

This location will of course vary considerably with launch time delays since the interval in the intermediate orbit must be adjusted accordingly.

Corresponding to this value of A and L, there is a unique value of longitude for injection. This value may be obtained from the following equation.

$$\Lambda_I = A_I - A_L - \Omega_e t_I + \Lambda_L$$

where

- A_L = launcher right ascension
- Λ_L = launcher longitude

$$t_I = t_1 + t_2 + \phi_c / \dot{\phi}_c$$

$$\begin{aligned} \dot{\phi}_c &= \text{constant parking orbital rate,} \\ &= \frac{2\pi}{\tau} = \sqrt{\frac{\mu}{a^3}} \end{aligned}$$

This brief review points up some of the factors affecting the selection of a parking orbit and indicates the desirability of restricting the altitude of such an orbit. The discussion has, however, been purely qualitative since more complete discussions are available in Chapters VI and VIII as well as in the literature.

C. VEHICLE TEMPERATURE CONTROL (REF. 1)

The general temperature control problem can be conveniently subdivided into two requirements.

- (1) Maintaining the mean temperature of the spacecraft components within limits dictated by tolerances of the components.
- (2) Preventing fluctuations about the mean temperature which might impair the general reliability.

Depending on the mission requirements, there are several possible solutions for these problems:

- (1) Independent local control of sensitive components.
- (2) General control of the mean temperature of the total spacecraft.
- (3) General control of the mean temperature of the total spacecraft plus control of the fluctuations about the mean temperature.
- (4) Various combinations of the above.

The major factors involved in the temperature control problem will be examined leading to a discussion of various control methods.

1. Heat Balance

The mean temperature of an object in space is determined by the energy balance on that object. Except for the dwell time in a planetary atmosphere, a spacecraft is generally in a vacuum far below that which will support conductive or convective transfer, and since mass transfer is generally negligible, the only significant exchange is by radiation. Consider for simplicity a satellite made of a material of infinite thermal conductivity so that it is at a uniform temperature throughout. If it is not in the vicinity of a planet and has no internal power its energy balance, at equilibrium, is found by equating the absorbed solar energy with the infrared energy emitted from the spacecraft:

$$\alpha G A_i = \epsilon \sigma T^4 A_e$$

$$T^4 = \frac{\alpha}{\epsilon} \frac{G}{\sigma} \frac{A_i}{A_e} \quad (1)$$

where T is the absolute temperature, α is the absorptance of the surface coating for the zero air mass solar spectrum, ϵ is the emittance of the surface for the black body infrared spectrum corresponding to the temperature of the spacecraft, G is the solar flux at the local radial distance of the spacecraft from the sun, σ is the Stefan-Boltzmann constant, A_i is the cross-sectional area intercepting solar energy, and A_e is the emitting surface area. Kirchhoff's law for opaque materials states that absorptance equals emittance (for bodies at the same temperature) at a given wavelength or integrated over the same spectral curve. But since the two bodies of this problem are not at the same temperature and since α is here reserved for the solar wavelengths and ϵ for the infrared wavelengths, α in general does not equal

ϵ . The fourth power of the temperature is seen in Eq (1) to be proportional to the ratio of α to ϵ so that the ratio itself becomes a convenient material property of interest (see Fig. 1).

If internal power w is uniformly dissipated throughout the imaginary spacecraft, the energy balance then becomes

$$\alpha G A_i + w = \epsilon \sigma T^4 A_e$$

$$T^4 = \frac{\alpha}{\epsilon} \frac{G}{\sigma} \frac{A_i}{A_e} + \frac{w}{\epsilon \sigma A_e} \quad (2)$$

The effect of the internal power on the mean temperature depends on the ease with which that energy can reach the surface and be radiated away, which in the case of our infinite conductivity spacecraft is a function of the emittance ϵ only. Thus, the emittance must be considered separately as well as in the ratio of α/ϵ . It has often been the case that the second term on the right of Eq (2), the internal power term, is small relative to the first term, so that the internal power produces a minor effect on the spacecraft mean temperature.

It has been assumed that the spacecraft exterior is a continuous surface of a single material. This is generally not the case. However, under the assumption of infinite conductivity the case of multiple surface materials with no internal power, is expressed by

$$T^4 = \frac{G}{\sigma} \left[\frac{\alpha_1 A_{i1} + \alpha_2 A_{i2} + \dots}{\epsilon_1 A_{e1} + \epsilon_2 A_{e2} + \dots} \right] \quad (3)$$

where the numerical subscripts represent the n surface materials. If the idealized isothermal spacecraft has moved to the vicinity of a planet, the energy balance including the transient effect becomes:

[the absorbed solar energy + the absorbed solar energy reflected from the planet + the absorbed planet emitted energy + the internally dissipated power + the stored energy] equated to the infrared energy emitted by the spacecraft.

Symbolically,

$$\sum \alpha_j G A_{iSj} + \sum \alpha'_j E_R A_{iRj} + \sum \epsilon'_j E_E A_{iEj}$$

$$+ w + Wc_p \frac{dT}{dt} = \sum \epsilon_j \sigma T_j^4 A_{ej} \quad (4)$$

where G is the solar flux at local distances of spacecraft from sun, E_R is the flux of solar energy reflected from the planet, E_E is the flux of planet emitted energy at the altitude of the spacecraft, A_{iS} is the area absorbing direct solar energy, A_{iR} is the area absorbing reflected solar energy, A_{iE} is the area absorbing the planet's emitted energy, α' is the absorptance of the solar reflected energy, ϵ' is the absorptance for the planet's emitted energy, w represents the internally dissipated power, Wc_p the thermal capacity of the shell, t is time, and the summation signs indicate that the appropriate terms are summed over the j isothermal surface areas.

Depending on the spacecraft thermal design, and its particular orbit and altitude, the magnitude of the energy exchanges shown in Eq (4) varies, in turn causing changes in the mean temperature of the spacecraft. These factors are discussed qualitatively in the following sections. More detailed analytic discussions are to be found in the bibliography.

a. Solar flux input

The mean value and variations about the mean are most strongly affected by direct solar radiation. Solar flux input is dependent on orientation of the surface, time of exposure, look angles with respect to sun, wavelength of received and emitted radiation. In addition there is the problem of solar eclipses due to the planets (see Chapter XIII).

One effect of the eclipse of an earth satellite is the transient cooling during the eclipse. The extent of this, in a simplified model, depends on the thermal capacity of the satellite and the external radiation resistance as determined by the surface infrared emittance. In an actual satellite the various components each have different thermal capacities and different thermal couplings to the exterior, and will therefore experience different transient thermal behavior during the eclipse. The other important thermal effect is due to the reduction in the total solar radiation input integrated around the orbit. For example, a satellite in a polar orbit will at one time during the year experience full sun, and at another time of the year, if in a low altitude orbit, the total solar flux averaged around the orbit will be only slightly greater than one-half of the nominal value. The present best estimate of the nominal value of the solar flux at the earth's mean orbital distance from the sun is 442 Btu/hr-ft^2 (1199 kcal/hr-m^2) with an uncertainty of $\pm 2\%$. The ellipticity of the earth's orbit results in a $\pm 3.7\%$ fluctuation in the solar input throughout the year, so that other factors remaining constant, a satellite will be about 9° R (5° K) hotter in December than in June. The limit cases for the effect of earth orbits in solar radiation input may be divided as:

Ecliptic. A satellite whose orbit lies in the ecliptic plane at same time will be eclipsed by the planet once each orbit throughout the time required for the planet to rotate the orbital plane out of the ecliptic by an amount dependent on the orbital elements.

Equatorial. If the orbit lies in the equatorial plane, and is at a relatively low altitude, the satellite will be eclipsed each orbit. At a sufficiently great altitude, because of the 23-degree tilt of the earth's equatorial plane, the satellite will experience an eclipse once each orbit during two periods of the year and will experience no eclipses for the other two periods. This is the case for a satellite in a circular, equatorial 24-hour orbit about the earth.

Polar. The polar orbit is similar to the high altitude equatorial case in that the satellite is eclipsed once each revolution for two periods during the year and is in full sunlight for the other two periods. Each of the two eclipsing intervals

start out with an eclipse of momentary duration, gradually increasing to an eclipse of maximum duration (the time depending on the satellite velocity) and gradually decreasing the shorter eclipse durations.

Special. One special class of orbits [approximately 81° retrograde, depending on the semilatus rectum] has the property that the nodes regress such that the 1° per day shift in the direction to the sun is canceled. In this orbit the satellite will be in full sun continuously throughout the year or, depending on the launch time during the day, eclipsed once each orbit throughout the year. The duration of the eclipse depends on the altitude of the satellite and the ellipticity of the orbit. For example, in a highly elliptical orbit it is possible to have very long eclipses, if they occur at the apogee of the orbit; however, it is possible to delay the occurrence of such an apogee eclipse (resulting from orbital precession) for several years, depending upon the orbit characteristics, by suitable choice of launch time.

b. Planetary emitted flux

For the earth and presumably for any planet with an appreciable atmosphere the infrared energy emitted by the planet is relatively independent of latitude and longitude and varies in a predictable manner with altitude. In the case of the earth at low altitudes the flux is about 68 Btu/hr-ft^2 (184 kcal/hr-m^2). In cases where there is no atmosphere, as for the moon, the emitted flux must be considered to vary with angular position measured from the subsolar point because of the large temperature variations on the surface.

The earth-emitted flux injects two sources of error which must be accounted for in the thermal design of the spacecraft. One is the magnitude of the flux, which is known with much less precision than that of the solar flux. (This lack of knowledge is even more applicable of the moon, and for the other planets there is relatively poor knowledge of the planetary thermal balance conditions and the emitted flux). The second is the lack of adequate knowledge of the emission spectral characteristics. In the case of the earth, for example, it is known that the emitted flux comes primarily from the surrounding gaseous atmosphere which has spectral characteristics differing significantly from the black body spectrum corresponding to the earth's equilibrium temperature. Lack of knowledge of this spectral characteristic results in an uncertainty in the effective absorptance of the spacecraft surface material for the earth emitted energy.

c. Planetary reflected solar energy

The same altitude dependence applies for the solar energy reflected from the earth or nearby planet as for the infrared energy emitted by the planet. In addition the reflected solar energy varies with the orbit plane attitude with respect to the sun and the instantaneous position in the orbit. For example, in a twilight polar orbit the reflected solar flux is approximately constant, whereas in a noon orbit in which the sun

lies in the orbit plane the reflected flux varies from zero to a maximum of about 160 Btu/hr-ft² (434 kcal/hr-m²) at the sub-polar point.

The magnitude of this flux is approximately as uncertain as that of the earth emitted flux and is known to vary with such factors as cloud coverage. The absorptance of the surface materials for the planetary reflected solar energy is not precisely the same as for the direct solar flux because of changes in the spectral characteristics after reflection from the planet and its atmosphere. The magnitude of these changes and the corresponding change in the effective absorptance for this flux is not well known.

d. Spacecraft characteristics affecting heat balance

The internal and surface characteristics of the vehicle itself are important in temperature control since they define the radiation losses to space and to internal heat boundaries (equipment heat dissipation and thermal inertias). A thorough review of thermal balance and uncertainties is given by Comack and Edwards (Ref. 2) and a qualitative discussion is presented below.

Thermal radiation properties. Knowledge of the thermal radiation properties of the spacecraft surfaces can be deficient in two respects. The first has to do with uncertainties in measurement of the properties in the laboratory, and the second is concerned with the changes in those properties due to handling and exposure to the air before launch, to heating during ascent to orbit, and to exposure to the space environment.

Shape and attitude considerations. A spin stabilized spacecraft has the spin axis nominally fixed in inertial space, though various disturbing torques and tip-off errors can decrease the spin rate and gradually shift the spin axis attitude in space. An attitude controlled spacecraft is not affected as much by these uncertainties. Cornog (Ref. 3) shows that if the attitude of the vehicle can be controlled, the same aspect of the vehicle can be presented to the sun at all times. If low vehicle temperatures are desired, the portions of the surface exposed to the sun can be made highly reflective, the unexposed portions can be covered with some material having good radiative properties, and by changing the shape or treating each vehicle quadrant with the desired α/ϵ materials, the effective absorptive area exposed to sunlight can be made quite small.

Internal temperature gradients. The preceding factors all result in either variations or uncertainties in the spacecraft mean temperature. (Mean temperature can be defined as that temperature which the spacecraft would attain assuming zero thermal resistances.) In an actual vehicle, temperature variation can be quite large. For example, temperature differences exceeding 100° F (38° C) were encountered in Explorer VI. Thus a given component in this spacecraft located near one end of the thermal gradient would experience large changes in temperature as the sun orientation changes and during the spacecraft lifetime.

Internal power fluctuations. As various components are turned on and off, or changed in power level, the locally dissipated energy causes local temperature changes, the amount depending on the power dissipated and the particular thermal circuitry of the spacecraft interior. This internal power dissipation may range from a few watts to kilowatts depending on the equipments required for the mission.

2. The Effects of Thermal and Optical Properties on Temperature Control

a. Thermal radiation properties and materials

Coating the surface of the spacecrafts external structure with thin lightweight material may provide the needed thermal radiation properties. These coatings may in some instances be more effective if applied in patterns of several materials (for example the combination of vacuum deposited aluminum and anodized aluminum in adjacent areas). Values of solar absorptance α and infrared emittance ϵ covering the entire range from 0 to 1 are useful for these coatings. In particular, both high and low values of the ratio of α/ϵ are especially useful for certain forms of active temperature control systems. A good material should absorb over the entire thermal spectrum, that is, have high α and high ϵ . (Materials which reflect well over the entire spectrum, that is, have low values of α and ϵ , are also useful, although this combination can sometimes be achieved by insulation.)

A great body of thermal radiation data exists in the literature. While these data are useful as a guide to the kinds of properties obtainable with various types of materials, most of it is useless for space applications. There are a variety of reasons for this fact:

(1) The data is not applicable because of the following reasons: much of it is reported for radiation properties not directly applicable to the spacecraft thermal control problem; in general, the diffuse properties are required, but most data reported is for specular properties; for emittance, hemispherical values are generally required, but most data reported is for normal or near-normal angles; absorptance data is not available as a function of incident angle but most data reported is for a single near-normal angle; much emittance data reported is for a total measurement, which is often made at a relatively high temperature (such data is applicable to a somewhat incorrect spectral curve and to the wrong material temperature); finally the total solar absorptances are often measured directly with the solar energy as it exists at the laboratory (this spectrum is generally markedly different from the solar spectrum in space).

(2) Measurement errors. Only in the past few years have the subtleties of the various types of radiation measurements and techniques been fully appreciated (Refs. 4 and 5). Equipment and techniques to measure directly the appropriate properties are in many cases still lacking. From the standpoint of the designer using the data, such errors represent serious shortcomings and must

be fully recognized. A few of the common sources of errors are: lenses and mirrors which do not have spectrally flat optical characteristics are often present in the instrument optical path; water vapor may be present in detrimental amounts; the reflecting surface in integrating spheres, often MgO, is sensitive to water vapor and may have to be renewed frequently; MgO is partially transparent in the wavelengths for which it is used and must be applied in a relatively heavy coat to avoid erroneous data, a fact not always appreciated by the experimenter; nonuniform wall temperatures with variances in the infrared reflectance yield erroneous data; spectral measurements are difficult to obtain at wavelengths longer than about $50\ \mu$, and much of the available equipment is limited to about $25\ \mu$. This last point is significant in its effect on the property obtained for a low temperature spectrum (for example, 18% of the energy of a 50°F (10°C) black-body spectrum and 36% of a -100°F (-73°C) spectrum are both beyond $25\ \mu$).

(3) Materials not well defined. Much of the reported data represents materials which are poorly defined. For example, the surface optical properties are usually sensitive to the details of a materials processing technique. Because of incomplete or inadequate description of the material, the materials cannot generally be duplicated, rendering useless a large part of the reported data. In most cases the only solution to this situation is to measure the required properties for each material.

Once the spacecraft has been prepared with materials of the desired properties, there remains a practical problem of making certain that the properties remain unchanged before the spacecraft reaches altitudes above the atmosphere. A certain amount of handling of the exterior surfaces may be unavoidable. Some of the more delicate coatings can be protected by plastic peel-coats until a few days before the scheduled launch, but if any last minute cleaning is necessary to remove fingerprints, grease, dirt, etc., there is always a danger that the cleaning process itself may affect delicate surface properties. During the launch interval the satellite and its materials are presumably protected from aerodynamic heating by a protective fairing, which is jettisoned after leaving the sensible atmosphere. Because of the weight penalty in carrying the fairing along longer than necessary, there is often a tendency to jettison it too soon, thereby heating the satellite surfaces to a level which may affect the optical properties of the surfaces.

b. Optical properties in the space environment

Most of the factors of the space environment represent new and untried conditions for spacecraft materials. Whether these materials and in particular their sensitive surface optical properties remain stable in this environment is a question of importance for all spacecraft with long intended lifetimes. Among the factors of importance are:

- (1) The vacuum of space, in which the pressure is such that sublimation and decomposition occur virtually unimpeded.

- (2) Ultraviolet radiation, X-rays, and the harder radiation of the radiation belts.
- (3) Single particle radiation.
- (4) Micrometeorites.

Certain of these factors may present no problems. For example, micrometeorites are generally believed to be of sufficiently low flux that they will have no significant effect in spacecraft thermal control (Ref. 6). Many of the other factors of the space environment are difficult or impossible to reproduce in the laboratory, even singly, let alone in combination. In addition, the designer does not always have the freedom to choose materials which are rugged since certain optical properties are available only in delicate, vacuum deposited forms. Since these surfaces can be delicate, sufficient flexibility must be allowed to provide for some change in materials' optical properties due to exposure in the space environment. (Some of the important optical properties of various materials are summarized in Table 1.)

3. Vehicle Temperature Control Systems

a. Passive

A passive thermal control system is defined here to be one employing fixed external coatings in which there is no active element either mechanical or electrical. Since the mission requirements in orbit, the lifetime, the internal component complexity, etc., have generally been sufficiently simple from the thermal environment standpoint to allow a passive system to be used successfully, the great majority of spacecraft flown to date have had passive thermal control systems. Experience demonstrates that a passive design can achieve a spacecraft mean temperature in orbit within about 5 to 10°F (2.8 to 5.6°C) of the designed mean temperature (for example, in the case of Explorer VI).

An interesting application of a passive design was that of Pioneer V, a spacecraft designed to reach the vicinity of the Venus orbit. In the course of its journey, it would experience approximately a doubling of the solar flux from that occurring at the earth's distance from the sun. This spacecraft was spin stabilized, that is, with its spin axis fixed in inertial space. In an approximate manner, the trajectory flown may be considered to be such that the sun moved half-way around the spin axis during the half orbit to Venus. That is, the sun look-angle would increase from zero, looking straight down the spin axis at one end of the spacecraft, to 180° , looking at the opposite end of the spin axis and spacecraft. If the external coating was chosen to be appropriate for the solar flux at the earth's distance from the sun at the start of the flight (sun look-angle equal to zero) and also chosen appropriately on the other half of the spacecraft for the Venus distance from the sun, then in a rough sense the coating would be appropriate at both the earth and at Venus. In actual fact, partly because of three-dimensional effects and partly because of other considerations, the orbit that was flown resulted in a sun look-angle of 35° at the start,

TABLE 1
Optical Properties of Various Materials (Ref. 3)

| Material | Degrees Fahrenheit | Degrees Centigrade | Absorption Number α | Emissivity ϵ | Ratio α/ϵ |
|---|--------------------|--------------------|----------------------------|-----------------------|-------------------------|
| Silver | 100 | 37.7 | 0.04 | 0.02 | 2.0 |
| Aluminum, polished | 100 1000 | 37.7 538 | 0.10 - | 0.05 0.06 | 2.0 |
| Aluminum, 2024, buffed and polished | 100 | 37.7 | 0.34 to 0.37 | 0.03 | 12.0 |
| Stainless steel, black | 100 1000 | 37.7 538 | - - | 0.90 0.90 | - - |
| Stainless steel, polished | 100 | 37.7 | 0.40 | 0.05 | 8.0 |
| Fused quartz, bricks, hard rubber, asbestos | 100 1000 | 37.7 538 | 0.1 to 0.4 - | 0.90 0.90 | 0.2 - |
| Lamp black | 100 1000 | 37.7 538 | 0.95 - | 0.95 0.95 | 1.0 - |
| SiO on polished metal | 100 | 37.7 | 0.1 | 0.90 | 0.1 |
| MgO | 100 | 37.7 | 0.15 | 0.97 | 0.15 |
| Titanium, 6A1-4V | 100 | 37.7 | 0.8 | 0.18 | 4.4 |

decreasing to about 15° at 20 days, back to 35° in about 40 days, and increasing to 135° upon reaching the Venus orbit at approximately 105 days after launch. A pattern was chosen using two materials, one with an α of 0.92 and ϵ of 0.87 and the other with an α of 0.25 and an ϵ of 0.85. A pattern was achieved which maintained a mean temperature within the desired range over the entire trajectory, as well as at the end points of Earth and Venus. During the 3-1/2 months of transmitted data, the measured temperatures followed the predicted curve within about 5° to 10° F. The flight path that was finally selected was not the optimum one from trajectory considerations but rather was chosen to satisfy a thermal control requirement that the sun look-angle increase from approximately 0 to approximately 180°. It would be entirely possible, from trajectory considerations alone, for the sun look-angle to start at 90° at the earth, decrease to zero and increase back to 90° at the Venus orbit. Clearly the coating pattern and therefore the effective α/ϵ of the spinning spacecraft at both the earth and Venus would be the same and would therefore not compensate for the increase in solar flux. The actual sun look-angle history noted above was about the limit of allowable deviation from the ideal 0 to 180° change.

b. Active

A variety of mechanizations of active control may be envisioned:

- (1) The spacecraft can be kept relatively cool by means of passive coatings, but still warm enough to satisfy the majority of the components. (Local thermostatically controlled electrical dissipation can be provided to warm those few components

requiring a higher temperature.) While this scheme is quite feasible, the types of components which require the heating, (such as liquid fuel tanks and secondary storage batteries) may be so large that the "local" heating may involve a large fraction of the spacecraft power. Unless excess power is available such a design may not be practical from the point of view of the overall system.

- (2) With a nonspherical shape, such as a relatively flat disc, the mean temperature can be increased or decreased by orienting the spacecraft so as to increase or decrease the surface area intercepting solar energy (see Figs. 2, 3 and 4). However, normally, this design would not be practical in view of other conflicting requirements for the spacecraft attitude control system.
- (3) A number of materials change optical properties as a function of temperature. For example, silicon monoxide and other materials like it have the self-controlling tendency to increase in emittance as temperature increases, thus tending to limit the temperature rise, and vice versa. Various experimenters are currently examining such materials, but the materials unfortunately have a general characteristic that their emissivity is too weak a function of temperature to be advantageously employed.
- (4) Some number of materials undergo reversible optical property changes as a result of phase changes, Curie point

transitions, etc. For example, the so-called thermochromic materials reversibly change color, and therefore solar absorptance, as a sharp function of temperature. Unfortunately these materials may be in the form of gels, liquids, etc., generally with low vapor pressures and therefore unsuitable for the exterior surface. They could be encapsulated in materials transparent in solar wave lengths but at the present at least they would not seem to offer enough advantages to overcome their obvious shortcomings for use in a temperature control system.

- (5) Mechanical changes of radiation properties and areas are the systems presently given most consideration.

These mechanizations are embodied in two general types of active vehicle temperature control designs, the radiation balance design and the insulated design. Any thermal design is at least partially a combination of the two and there are many designs in which both the external radiation balance and the insulated features are combined in a single application.

Radiation balance type. In a radiation balance design the internally dissipated power is generally a small factor in the overall heat balance and therefore contributes only in a minor way to the mean temperature level, although the dissipated power may have important local effects. The energy relationship is then a balance, in the equilibrium state, between the absorbed incident radiant energy and the emitted radiant energy. Active control of the temperature may be effected by varying the exposed areas of two materials, one with a relatively high α/ϵ ratio and one with a relatively low α/ϵ ratio. This can be accomplished by a venetian blind arrangement, moving vanes, or in a variety of other ways.

The first spacecrafts with such a temperature control system were the Atlas/Able 4 and Able 5 satellites. These were intended to be orbiting satellites of the moon, to be put into lunar orbit by means of monopropellant hydrazine engine aboard the spacecraft to reduce the approach velocity sufficiently to allow lunar capture. Partly because of the hydrazine fuel and fairly severe environmental conditions, such as lunar eclipse durations exceeding two hours, it was necessary to employ an active thermal control system. The spacecraft was spin stabilized, thus an arbitrary sun orientation with respect to the spin axis was possible during the spacecraft lifetime.

Briefly, the thermal design was as follows. Thermal energy exchange took place primarily at 50 circular areas well distributed over the external skin. Each circle consisted of an alternating arrangement of two materials in the eight 45° sectors of the circle, one material with a high α/ϵ ratio and the other a low α/ϵ ratio. The circular areas were covered by a four bladed mask which could completely cover one or the other of the two materials, or some fraction of each at any intermediate position. The mask was driven by a bimetallic spring device at the inner end of the body, arranged so that the bimetallic device sensed a

portion of the spacecraft interior. The plastic body of the unit was made of a poor thermal conductor so that the bimetallic spring was better coupled thermally to the spacecraft interior than it was to the skin of the spacecraft. The mask was rotated the 45° of its travel by a 25° F change in temperature of the spring. With the spring at 50° F the mask fully exposed the high α/ϵ material, and at 75° F the low α/ϵ material was fully exposed. The activation thus provided self-powered, closed-loop control of the interior temperature. The remainder of the spacecraft's skin, outside the control circles, was covered with a material of low α and low ϵ so that the contribution to the overall energy balance from the uncontrolled area would be as small as possible. That area was vacuum-deposited aluminum, over a smooth plastic substrate, with an absorptance of 0.10 and an emittance of 0.05. The high α/ϵ material in the control areas was a form of titanium dioxide with an α of 0.65 and an ϵ of 0.13, and the low α/ϵ material was a particular form of anodized aluminum with an α of 0.20 and an ϵ of 0.80. A more complete description of this system is given in Ref. 7.

The system has the capability of compensating for fairly large changes in the external environment, such as an interplanetary mission to Venus, and furthermore it minimizes the decrease in temperature during long eclipses because the masks automatically decrease the effective emittance of the spacecraft during this time.

Insulated type. If a spacecraft is always oriented so that the sun irradiates only certain of its sides but not others, as may be the case in a fully attitude controlled or a spin stabilized spacecraft, it is possible to insulate the solar irradiated sides so that the solar input plays little or no part in the spacecraft energy balance. (A very high order of insulation may be achieved for the spacecraft sides with multiple layer reflective insulation.) If for simplicity the spacecraft is considered to be far removed from a planet, then the energy balance is achieved between the internally dissipated power, the transmitted solar heat load and the spacecraft emitted energy. The unirradiated, uninsulated faces are covered with a surface of high emittance, and the emitted radiation is controlled by a set of louvers (external coverings to the radiation plate). The emitting area is then a function of the louver position, which may be controlled by sensors measuring the radiation plate temperature to which the spacecraft components are mounted. If the louver is irradiated, the system may still be employed if the radiation plate is covered with a material of sufficiently low α and high ϵ , to minimize the solar input. It is required that the internally dissipated power be at least as great as the heat losses from the entire spacecraft when the louvers are fully closed.

The advantages of this design are that the spacecraft is insensitive to eclipses and other changes in the solar flux, such as would occur on an interplanetary journey. The temperatures within the spacecraft are much more uniform than in the radiation balance design since there is no large external input over any part of the surface, and the problem of sensitivity of optical properties

of the space environment is greatly diminished. The primary property of interest is the high emittance on the radiating plate, but this is a property which tends to be stable in space environment (Ref. 8).

D. CRYOGENIC PROPELLANT STORAGE (Ref. 9)

Cryogenics is concerned with the phenomena of low temperatures, normally those below $T \approx -250^\circ \text{F}$ (-157°C). To be more specific, cryogenic storability involves the prevention of excessive boiloff of cryogenic fluids (e.g., liquid oxygen, liquid fluorine, liquid nitrogen, liquid hydrogen, and liquid helium) over varying periods of time. These stored fluids can be used for any of the following purposes:

- (1) Supplying other vehicles or stations (logistic use).
- (2) Maintaining state-of-readiness in ballistic missiles or for satellite propulsion (operational use).
- (3) Thermal shielding during times of increased flux.

1. Properties of Cryogenic Fluids

Insofar as space vehicles are concerned, there are six important cryogenic fluids: liquid hydrogen, liquid helium, liquid nitrogen, liquid fluorine, liquid oxygen, and liquid ozone. Table 2 gives the basic properties, except vapor pressure, of these fluids and of liquid neon and liquid argon. Figure 5 presents the vapor pressure of these fluids as a function of temperature and pressure. Definition of properties is as follows:

- (1) Heat of vaporization (ν). The number of heat units required to vaporize one unit weight of liquid at its normal boiling point.
- (2) Boiling point. Absolute temperature, at which liquid boils under one atmosphere of pressure.
- (3) Freezing point. Absolute temperature, at which the liquid freezes, under one atmosphere of pressure (except liquid helium).
- (4) Critical point. The combination of pressure and temperature of a liquid and its vapor under equilibrium conditions that causes the two phases to be indistinguishable.
- (5) Density (ρ). Density of the gas phase in units of force per unit volume.
- (6) Specific heat ratio (γ). Ratio of specific heat at constant pressure (c_p) to specific heat at constant volume (c_v).
- (7) Vapor pressure (p). The vapor pressure of a liquid is defined as the pressure of saturated vapor over the liquid. It varies with temperature. In the design of cryo-

genic tankage, the relationship of vapor pressure to other pressures (see below) is of importance in calculating boil-off and "no-loss" times. Figure 5 gives the variation of vapor pressure with temperatures for liquid nitrogen, liquid oxygen, liquid hydrogen, and liquid helium.

2. Properties of Insulations

In the past few years a number of new insulations of extreme value in cryogenic service have been developed. With these much more efficient insulations, the mission analyst is able to plan space flights involving much greater weight of payload and vehicle.

There are six types of insulation now in use for various types of cryogenic service. Some are useless with regard to space vehicles, because of too high a conductivity or density. Others (Fiberglas, SI-4, NRC-2) have great potential in space applications, since the environmental vacuum (either moderate or high) prevents heat leaks into the fluids due to gas conduction and convection. The substance added, whether powder, Fiberglas, aluminum foil, etc., is intended to reduce the radiation heat leak across the vacuum into the fluid.

a. Types of insulation

- (1) Cellular. Actually consists of a silica gel with very high absorbing or absorbing surface.
- (2) Powder. An organic powder, usually perlite, is introduced into a space held at a moderate vacuum ($< 100\mu \text{Hg}$).
- (3) Opacified powder. Aluminum or bright copper flakes are added to the powder to increase the radiation shielding. The vacuum must be high ($< 10\mu \text{Hg}$).
- (4) Fiberglas. A very low density inorganic substance placed in a high vacuum ($< 1\mu \text{Hg}$).
- (5) Organic foams. Usually polystyrene, foamed either with air or freon. These foams have a cell structure which isolates one cell from another. When placed next to a fluid at cryogenic temperatures, the gas condenses within each cell, creating a partial vacuum, which is the insulating agent. Use of such foams with liquid oxygen or liquid fluorine is highly dangerous, due to their organic nature.
- (6) Multiple radiation shield. This type has the highest insulating qualities (but also requires high order vacuum for most efficient usage ($< 1\mu \text{Hg}$)). One type (Linde SI series) consists of alternate layers of aluminum foil and glass fiber paper. Usually 50 to 80 layers are used. NRC-2 uses approximately 100 layers of crinkled mylar which has been aluminized on both sides.

b. Table of properties

Table 3 lists all types of insulations, with some of them reported under different conditions. The properties of Santogel A, given for an ambient operating pressure and under moderate vacuum, show the effect of vacuum on these insulations. The thermal conductivity (k) of Linde SI-4 and the Fiberglas insulations, is measured both in the compressed and uncompressed states. The increase in k value under compression indicates that such insulations must be maintained in an uncompressed state for greatest efficiency, but will also have a reasonable insulating effect when compressed. This fact may be of considerable importance for the insulation of space vehicle stages during flight through the atmosphere. Outer insulation blankets must be compressed to prevent their being lost due to air friction. Once in orbit, or in space flight, the compressing device may be removed, and the high vacuum of space will raise the insulation to its full efficiency.

c. Relationship of thermal conductivity to operating pressure

To obtain the very low thermal conductivity values shown in Table 3, the insulations must be in vacuum. Hence, a double wall is required for most tankage applications--except in space, where the environment is already a vacuum. The thermal conductivity is a function of the degree of vacuum in the interspace. Figure 6 indicates that, in general, the powder and cellular types of insulation are less affected by vacuum changes than the radiation shield and fiber glass types. With the latter, there is a sharp lowering in efficiency when the operating pressure rises above about 10μ of mercury; while with the former, the change in k is more gradual, and pressures of 100 to 1000 μ Hg can be tolerated with not too great a degradation of insulating qualities. It may also be seen from Fig. 6 that the multiple radiation shield insulations (at high vacuum) are more efficient than other types by an order of magnitude.

One other criterion for efficient insulation is given in the last column of Table 3 where the thermal conductivity (k) is multiplied by the density of the insulation (ρ). It may be seen that the product $k\rho$ for the multiple radiation shields is one to three orders of magnitude lower than other types. Hence, for orbital operations, it is concluded that the multiple radiation shield insulations must be used. In the remainder of this section, the insulation used in all calculations will be the Linde SI-4.

d. Relationship of thermal conductivity to wall temperatures

The temperatures of the inner (cold) wall and the outer (warm) wall of the insulation have decided effect on the value of the thermal conductivity factor (Fig. 7). The thermal conductivity varies by about a factor of 30 as the outer wall temperature (T_1) varies by a factor of 10 [100° to 1000° R (56 to 560° K)] for any constant inner wall temperature (T_2). The value of k varies much less with inner wall temperature for constant T_1 , and is essentially independent of the value of T_1 .

3. Design of Cryogenic Tanks

In order to design cryogenic tankage for space applications, one must determine the heat input into the cryogenic fluid. In order to do this, the temperature of the outer wall must be determined. If the insulation has been selected and the cryogenic fluid specified, all else is known. The ultimate factor to be calculated is the evaporation, or boil-off rate, of the cryogenic fluid.

Space vehicles, or orbiting tankage, receive heat from the sun according to the distance from the sun. Figure 8 shows the relationship of heat flux from the sun (G_s) and the distance from the sun. If the surface of the tankage were either a perfect absorber or a perfect reflector, the problem would be simple. However, since this is not the case, the absorptivity (α) and the emissivity (ϵ) of the surface must be taken into account. Normally, the parameter used is the ratio of these terms, α/ϵ . The higher this ratio, the more heat absorbed, and the higher the temperature T_1 .

Figure 9 shows the variation of T_1 with $\alpha A_s/\epsilon A_w$ (where A_s = surface area exposed to the sun and A_w = area of the total outer surface of the tank). The greater the proportion of the outer surface exposed to the sun, the greater the heat absorbed.

It is possible to determine the outer wall temperature (T_1) from Fig. 9, once the shape and size of the tankage are known. One first assumes a value of α/ϵ , the practical lower limit of which is approximately 0.25. From the general shape and orientation of the space vehicle or tank, A_s/A_w may be estimated. After obtaining $\alpha A_s/\epsilon A_w$, it is possible to interpolate in Fig. 9 at the expected distance from the sun, reading the temperature. Note that orbits about the earth may be assumed at the same distance as the earth from the sun, with negligible error. Even on the moon at its nearest point to the sun, the temperature of the outer wall will maximize at essentially the same value as if the vehicle were on earth.

Knowing the temperature of the outer wall, it is then possible to determine the heat flux (Q_ℓ) into the cryogenic fluid.

$$Q_\ell = \frac{k}{\ell} (T_1 - T_2)$$

where k/ℓ is the ratio of the thermal conductivity to the thickness of the insulation, and Q_ℓ is the heat flux to the exposed surface. Figure 10 shows the results of calculations for several values of T_1 (thus, for several values of α/ϵ), and for various thicknesses and thermal conductivities.

a. Total heat input

The total heat input per hour into the cryogenic liquid will be $Q_{\ell T} = Q_\ell A_w (A_s/A_w)$ where A_s/A_w = estimated percentage of surface exposed to the sun. From a knowledge of $Q_{\ell T}$, the weight of the cryogenic liquid at the start,

TABLE 2
Properties of Cryogenic Fluids

| Element | Mol Weight | Heat of Vaporization | | Boiling Point (° R at 1 atm) | Freezing Point (° R at 1 atm) | Critical Point | | Density | | Gas Volume of Liquid | | Gas Constant (R) | Specific Heat $\gamma = c_p/c_v$ | Weight of Liquid | |
|----------|------------|----------------------|---------------|---------------------------------|----------------------------------|----------------------|---|-----------------------|--------------------------|----------------------|-------------------------|---------------------|-------------------------------------|------------------|----------------|
| | | (Btu/lb) | (kcal/newton) | | | Temperature (° R) | Pressure (10^6 newtons/m ²) | (lb/ft ³) | (newton/m ³) | (cu ft/gal) | (m ³ /liter) | | | (lb/gal) | (newton/liter) |
| Hydrogen | 2.02 | 194.2 | 11.00 | 36.54 | 25 | 59.87 | 1.297 | 0.0052 | 0.817 | 114.3 | 0.735 | 772 | 1.4 | 0.54 | 0.55 |
| Helium | 4.00 | 10.3 | 0.583 | 7.596 | 0 (25 atm) | 9.49 | 0.230 | 0.0103 | 1.62 | 101.0 | 0.640 | 386.3 | 1.66 | 1.043 | 1.053 |
| Neon | 20.20 | 37.5 | 2.124 | 48.96 | 43.0 | 89.02 | 2.716 | 0.0522 | 8.20 | 192.0 | 1.234 | | 1.64 | 10.0 | 10.10 |
| Nitrogen | 28.02 | 85.7 | 4.855 | 139.32 | 113.0 | 227.91 | 3.395 | 0.0725 | 11.39 | 93.0 | 0.598 | 55.1 | 1.4 | 6.73 | 6.80 |
| Oxygen | 32.00 | 91.7 | 5.20 | 162.36 | 99.0 | 277.85 | 5.078 | 0.0828 | 13.01 | 115.3 | 0.741 | 48.3 | 1.4 | 9.53 | 9.62 |
| Fluorine | 38.00 | 74.1 | 4.20 | 153.00 | 97.0 | 259.50 | 557.4 | 0.0983 | 15.44 | 128.5 | 0.826 | | 1.4 | 12.6 | 12.7 |
| Argon | 39.91 | 72.0 | 4.08 | 157.14 | 151.0 | 271.40 | 4.865 | 0.1034 | 16.24 | 112.0 | 0.720 | 38.7 | 1.67 | 11.56 | 11.67 |
| Ozone | 48.00 | 136.1 | 7.710 | 290.34 | 144.0 | 469.91 | 5.533 | 0.1230 | 19.32 | 91.6 | 0.589 | | 1.4 | 11.28 | 11.39 |

1 Btu/lb = 0.5665 kcal/newton

1 ft³/gal = 0.006428 m³/liter1 lb/ft² = 157.084 newtons/m²1 lb/in.² = 144 lb/ft² = 6894.4 newtons/m²

1 lb/gal = 1.00976 newtons/liter

TABLE 3
Properties of Insulations

| Insulation | Type | Density (ρ) | | Vacuum Space Pressure (microns Hg, μ) | Thermal Conductivity (k) A* | | Thermal Conductivity (k) B* | | k ρ (Btu-lb/hr-ft ⁴ -° R) A*/B* | |
|------------------|--|-----------------------|---------------------------|---|--------------------------------|--|--------------------------------|--|---|-----------------------|
| | | (lb/ft ³) | (newtons/m ³) | | (Btu/hr-ft ² -° R) | ($\frac{\text{kcal}}{\text{sec-m}^2\text{-}^\circ\text{K}}$) | (Btu/hr-ft ² -° R) | ($\frac{\text{kcal}}{\text{sec-m}^2\text{-}^\circ\text{K}}$) | | |
| Santocel A | Cellular | 6.0 | 940 | Ambient | 1400×10^{-5} | 1780×10^{-9} | 1400×10^{-5} | 1780×10^{-9} | 8400×10^{-5} | 8400×10^{-5} |
| Santocel A | Cellular | 6.0 | 940 | < 100 μ | 120×10^{-5} | 153×10^{-9} | 96×10^{-5} | 123×10^{-9} | 720×10^{-5} | 576×10^{-5} |
| Polystyrene foam | Freon filled cellular | 3.0 | 470 | < 100 μ | 900×10^{-5} | 1150×10^{-9} | 700×10^{-5} | 890×10^{-9} | 2700×10^{-5} | 2100×10^{-5} |
| Polystyrene foam | Air filled cellular | 2.4 | 377 | Ambient | -- | -- | 1900×10^{-5} | 2400×10^{-9} | -- | 4500×10^{-5} |
| Perlite | Powder | 8.0 | 1260 | < 100 μ | 90×10^{-5} | 115×10^{-9} | 72×10^{-5} | 92×10^{-9} | 720×10^{-5} | 576×10^{-5} |
| Linde CS-5 | Powder w/Cu flakes | 11.0 | 1730 | < 10 μ | 22×10^{-5} | 28×10^{-9} | 17.6×10^{-5} | 22.5×10^{-9} | 242×10^{-5} | 194×10^{-5} |
| Linde SI-12 | Multiple radiation shields (Al foil + fiber glass) | 2.5 | 390 | < 1 μ | 17×10^{-5} | 22×10^{-9} | 10×10^{-5} | 13×10^{-9} | 42.5×10^{-5} | 25×10^{-5} |
| Linde SI-4 | Multiple rad shield | 4.0 | 630 | < 1 μ | 2.5×10^{-5} | 3.2×10^{-9} | 2×10^{-5} | 2.6×10^{-9} | 12.0×10^{-5} | 9.4×10^{-5} |
| Linde SI-4 | Compressed mult rad shield | 20.0 | 3140 | < 1 μ | 80.0×10^{-5} | 102×10^{-9} | 64.0×10^{-5} | 81.6×10^{-9} | 1600×10^{-5} | 1280×10^{-5} |
| NRC-2 | Multiple rad (aluminated mylar) | 3.0 | 470 | < 1 μ | 3×10^{-5} | 3.8×10^{-9} | 2.6×10^{-5} | 3.3×10^{-9} | 9×10^{-5} | 7.8×10^{-5} |
| Fiber glass | Fiber | 2.5 | 390 | < 1 μ | 40.0×10^{-5} | 51.0×10^{-9} | 32.0×10^{-5} | 40.8×10^{-9} | 100×10^{-5} | 80×10^{-5} |
| Fiber glass | Compressed fiber | 10.0 | 1570 | < 1 μ | 80×10^{-5} | 102×10^{-9} | 64×10^{-5} | 82×10^{-9} | 800×10^{-5} | 640×10^{-5} |

*A--between 560° R - 162° R (LN₂BP)*B--between 560° R - 36° R (LH₂BP) $\frac{1 \text{ Btu-lb}}{\text{hr-ft}^4\text{-}^\circ\text{R}} = 2.0042 \times 10^{-2} \frac{\text{kcal-newton}}{\text{sec-m}^2\text{-}^\circ\text{K}}$ $\frac{1 \text{ Btu}}{\text{hr-ft}^2\text{-}^\circ\text{R}} = 1.27588 \times 10^{-4} \frac{\text{kcal}}{\text{sec-m}^2\text{-}^\circ\text{K}}$

and the heat of vaporization of the cryogenic liquid, some knowledge of the evaporation rate can be gained.

- b. Relationship of tank pressure, vapor pressure and designed vent pressure

The phenomena occurring in a tank of cryogenic liquid are complex. If the vapor pressure = tank pressure = vent pressure, then the evaporation rate is easily determined. There appear, however, to be three thermodynamic phenomena that occur in distinct phases. When the heat inflow begins, normally the vapor pressure will be below the tank pressure. As heat continues to flow in, the temperature of the liquid increases according to

$$\Delta T = \frac{Q_{LT} t}{W c_p}$$

where

t = time in hours

W = weight of cryogenic fluid, and

c_p = specific heat of liquid at constant pressure.

Thus, the pressure is raised, as shown in Fig. 5. During Phase 1, no evaporation can occur because all of the heat used in raising the temperature of the liquid, merely increases its vapor pressure.

Phase 1 ends when the vapor pressure equals the tank pressure. In Phase 2, these two pressures will always be equal, since, if the vapor pressure were greater, evaporation from the liquid into the ullage space would increase the tank pressure. Thus, in Phase 2, the liquid temperature, the vapor pressure and tank pressure all increase, until finally the vent pressure is reached. Although the liquid has evaporated, it has not yet been lost from the tank. It is, however, unusable as a propellant, although it could be used to aid in a pressure transfer of the fluid, if required.

Based on perfect gas laws, the total heat input during Phase 2 can be conveniently divided in the following way

$$t Q_{LT} = \Delta T W c_p + M_1 v \left[\frac{p_2 T_1}{p_1 T_2} - 1 \right]$$

where

M_1 = mass of gas initially in ullage space

p_1, p_2 = initial and final Phase 2 tank pressures

v = heat of vaporization of cryogenic liquid, and

ΔT = total temperature change of liquid.

The first term in this equation is the heat input which raises the temperature of the liquid, and

the second term is the heat input which vaporizes the liquid. The duration of Phase 2 is given by

$$t = \frac{1}{Q_{LT}} \left[\Delta T W c_p + M_1 v \left(\frac{p_2 T_1}{p_1 T_2} - 1 \right) \right]$$

if aerodynamic heating is neglected. A term Q_{aero}/Q_{LT} must be subtracted from the time to account for this phenomenon.

If the ullage space is small, t can be considered the preboil-off time, because in this case the boil-off time is much less than the liquid heating time. If the ullage is less than 10 to 15% of the total volume,

$$t \approx \frac{\Delta T W c_p}{Q_{LT}} \text{ hours,}$$

this is the time during which no boil-off occurs.

Phase 3 is that period during which tank pressure is equivalent to vent pressure. It is during this time that the liquid actually boils off.

$$W_{BO} = \frac{t Q_{LT}}{v}$$

This equation shows that the boil-off for reasonably well designed systems is moderate even for long times for good quality insulation in moderate thicknesses.

If the tank is filled at the vent pressure then the process will be in Phase 1 until the vapor pressure reaches the vent pressure, at which time the process becomes Phase 3. Thus, preboil-off time and the actual boil-off can be regulated by varying the design vent pressure. Phase 2 is completely eliminated from consideration. Such a system will have the disadvantages of requiring external pressure sources (helium bottles) and a pressure relief system. Thus, by setting a high vent pressure and maintaining a small ullage space, the pre-boil-off (no loss) time can be extended considerably (see Fig. 11).

c. Insulation performance factor

The weight of the insulation, I_w , represents a performance penalty and since insulation is not perfect, a certain amount of boil-off will be associated with the weight of insulation determined by the $t Q_{LT}/v$. The penalty exists when

$$I_w + t Q_{LT}/v > (\text{uninsulated tank boil-off}).$$

Let

$$S = I_w + \frac{t Q_{LT}}{v}$$

be called the insulation performance factor. Thus, it is desired to minimize S . Since

$$\ell = \frac{I_w}{\rho A}$$

and

$$Q_{LT} = \frac{k \rho A^2 (T_1 - T_2)}{I_w}$$

then

$$S = I_w + \frac{t}{\nu} \left[\frac{k\rho A^2 (T_1 - T_2)}{I_w} \right]$$

and S is a minimum when

$$I_w^2 = \frac{K\rho A^2 (T_2 - T_1) t}{\nu}$$

Thus, the total weight is minimized when the insulation weight is just equal to the weight of the boiled-off liquid. Finally,

$$S_m = 2\sqrt{\frac{K\rho (T_1 - T_2) t_A^2}{\nu}}$$

Figure 12 is a plot of the insulation performance factor versus time-in-storage for a 6000-lb (26,700 newton) liquid hydrogen tank under a specific set of conditions and with a surface area of 10^3 ft^2 (93 m^2).

If it is assumed that it is required to have a given amount of LH_2 left (from a 6000-lb [26,700 newton] initial capacity) after a given time and the amount of insulation is to be found, enter Fig. 12 at the time and read S. Subtract the permissible weight of the boiled-off liquid hydrogen, the remainder is left for the weight of the insulation. From Table 3, the density of SI-4 is read. Thus, the volume of SI-4 required to meet the prescribed boil-off can be computed.

Now, since the area of the outer surface of such a tank is known, the thickness of SI-4 wrapped about the tank necessary to provide the proper insulation can be estimated. Before proceeding, it is noted that the insulation for such a tank may actually weigh slightly more than the uninsulated tank.

Once the thickness of insulation is determined, all that remains is to determine the no-loss time (Fig. 11), the boil-off during Phase 3, and the weight of tankage required.

d. Application to other cryogenic fluids

In order to apply the previous discussions to the design of tankage for cryogenic fluids other than liquid hydrogen, the following factors must be taken into account.

- (1) The ratio of the weight of the new cryogenic fluid to liquid hydrogen.
- (2) Boiling point of the new cryogenic fluid related to LH_2 .
- (3) The volume occupied by one pound of the new liquid.

It is then possible by means of ratios to use the figures given here to obtain tank designs for all other cryogenic fluids. What must be kept in mind is the high weight of propellants other than hydrogen and helium.

4. Example

The problem is to find the optimum insulation thickness for insulating spherical tanks placed on the illuminated lunar surface (Refs. 10 and 11), that is, to find the minimum combined weight of vaporized propellant and insulation for tanks containing liquid hydrogen, oxygen or fluorine.

For tanks on the lunar surface, an external insulation surface temperature of 607° R (337° K) was assumed (based on an average of the lunar surface temperature and the radiation equilibrium temperature of a surface exposed at normal incidence to solar radiation).

The only need for insulation during the lunar night would be to prevent freezing of the fluorine or oxygen (at 97° to 99° R [54° and 55° K], respectively) and to limit the hydrogen boil-off. However, the average external insulation temperature is estimated to be about 108° R (60° K), so that freezing of fluorine and oxygen will not occur, and the hydrogen vaporization rate will be only about 15% of the day condition. Therefore, the day condition is controlling for insulation thickness if the conservative approach of designing is chosen for propellant tanks to be exposed on either the illuminated or shadowed surface of the moon.

Propellant losses on the lunar surface. The weight shown in Fig. 13 is the sum of insulation weight and boil-off, the two being equal at the optimum. The results are based on conduction through the insulation only. In actual practice the heat leaks through tank support structure are about equal to the heat flow through the insulation. An approximation to the real case would be to increase the value read from the curve by about 70%. The propellant weight loss would then be the total value of the ordinate and the insulation weight would be 70% of that value.

Propellant losses during transfer. To determine losses from the tanks during the earth-moon transfer phase:

- (1) Determine optimum insulation thickness based on the lunar day condition and increase by 40%

$$\ell_i = (1.40) \sqrt{\frac{k\Delta T t}{\rho_i \nu}}$$

- (2) Calculate $\Delta T/\nu$ from Table 4.
- (3) Enter Fig. 14 to find " β ." Vaporized propellant then equals

$$W = \frac{tD^2}{\ell_i} \beta$$

- (4) Double the weight found in step (3) to account for heat leaks, and add the insulation weight

$$W_i = A_i \ell_i \rho_i$$

Propellant losses in lunar orbit. Propellant loss from tanks that do not land on the moon but which are a part of the boost, transfer and de-boost system are more difficult to define due to their inherently integral fabrication with the flight structure. However, for hydrogen the loss will probably lie between 0.01 to 0.10% per hour of the initial hydrogen weight. The lower value would be a design goal for a thermally well designed flight vehicle with separate tankage. The oxidizer boil-off can be assumed zero for the "well designed" case since the major heat exchange, even with separate tanks, is from the oxidizer to the hydrogen with other modes relatively small so that the oxidizer may actually experience some cooling.

TABLE 4
Propellant Parameters

| Propellant | ΔT_a ($^{\circ}$ R) | | ν | |
|----------------|------------------------------|----------|--------|-------------|
| | Lunar Day | Transfer | Btu/lb | kcal/newton |
| H ₂ | 567 | 460 | 190 | 10.7 |
| O ₂ | 445 | 338 | 92 | 5.2 |
| F ₂ | 454 | 347 | 72 | 4.1 |

1 Btu/lb = 0.05667 kcal/newton

E. REFERENCES

1. Lipkis, R. P., "Temperature Control of Spacecraft," Space Technology Laboratories, Inc., Memorandum, August 1961.
2. Camack, Walter G., and Edwards, Donald K., "Effect of Surface Thermal Radiation Characteristics on the Temperature Problem in Satellites," Surface Effects on Spacecraft Materials, John Wiley and Sons, 1960.
3. Cornog, R. A., "Temperature Equilibria in Space Vehicles," part of Space Technology Laboratories Engineering Design Manual, 1961.
4. Bevans, J. T., "A Review of Thermal Radiation Properties and Measuring Techniques," Space Technology Laboratories, Inc., TN-60-0000-09096, 24 June 1960.
5. Dunkle, R. V., "Thermal Radiation Characteristics of Surfaces," Invited Paper at the American Society of Mechanical Engineers Annual Meeting, 1960, to be published in the Journal of Heat Transfer, Trans ASME.
6. Beard, David B., "Interplanetary Dust Distribution and Erosion Effects," Surface Effects on Spacecraft Materials, John Wiley and Sons, 1960.
7. Acker, R. M., Lipkis, R. P., and Vehrencamp, J. E., "Temperature Control System for the Atlas Able-4 Lunar Satellite," presented at the Aviation Conference, Dallas, Texas, 5 to 9 June 1960.

8. Fried, E., and Costello, F. A., "The Interface Thermal Contact Resistance Problem in Space Vehicles," Presented at ARS Lifting Re-entry Vehicles Conference, Palm Springs, California, 4 to 6 April 1961.
9. Wolverton, R. W., ed., "Flight Performance Manual for Orbital Operations," Space Technology Laboratories (LA), September 1961 (U).
10. Perkins, D. S., "Cryogenic Propellant Considerations, Lunar Return Vehicle," STL Memo 9862-2-47, 13 July 1961.
11. Fuil, A., "First Approximation to Optimizing Insulation Weight on Propellant Tanks for Long Term Space Storability of Cryogenics," STL Memo 9862-36, 19 July 1961.

F. BIBLIOGRAPHY

1. Bibliography for Staging of Vehicles

(See other chapters for geometrical restrictions and bibliography of pertinent references.)

- Amass, W., Bullard, S. A., and Teegarden, W. T., "Collection of Parametric Performance Studies," The Martin Company, Baltimore, Maryland, TM 491/2-02-60, January 1960.
- Arens, M., "Staging of Cruising Vehicles," ARS Journal, Vol. 31, No. 6, June 1961, pp 824 to 825.
- Ashley, H., and Asher, G. W., "The Virtual Mass of Clustered Boosters," ARS Journal, Vol. 31, No. 6, June 1961, pp 757 to 763.
- Builder, C. H., "A General Solution for Optimization of Staging of Multistaged Boost Vehicles," ARS Journal, Vol. 29, No. 7, July 1959, pp 497 to 499.
- Byrum, B. L., and Grady, E. R., "General Airframe Dynamics of a Guided Missile," Journal of the Aeronautical Sciences, Vol. 22, No. 8, August 1955.
- "Kinematics and Kinetics of Aerospace Vehicles," The Martin Company, Baltimore, Maryland, Engineering Report No. ER 10920, June 1960.
- Chase, R. L., "Multistage Rocket Staging Optimization," American Astronautical Society, Preprint No. 60-41, January 1960.
- Chin, S. S., "Missile Design Criteria," The Martin Company, Orlando, Florida, Report No. OR-1272, 10 October 1960.
- Cobb, E. R., "Optimum Staging Technique to Maximize Payload Total Energy," ARS Journal, Vol. 31, No. 3, March 1961, pp 342 to 344.
- Cohen, A. D., and Rhodes, H. H., "Evaluation of Coasting Flight of an Ascending Satellite Vehicle for Circular Orbits," ARS Journal, Vol. 30, No. 8, August 1960, pp 768 to 769.

- Cole, D. M., and Epstein, L. I., "Interpretation of Malina-Summerfield Criterion for Optimization of Multistage Rockets," *Jet Propulsion*, Vol. 26, No. 3, March 1956, p 188.
- Cole, D. M., and Marrese, M. A., "Optimization of Rockets for Maximum Payload Energy," *American Rocket Society Journal*, Vol. 29, No. 1, January 1959, p 71.
- Coleman, J. J., "Optimum Stage-Weight Distribution of Multistage Rockets," *ARS Journal*, Vol. 31, No. 2, February 1961, pp 259 to 260.
- Dergarabedian, P., and Ten Dyke, R. P., "Estimating Performance Capabilities of Boost Rockets," Los Angeles, California, Space Technology Laboratories, September 1959, Report No. TR-59-0000-00792.
- Dini, D., "Distribution of the Stages of a Missile to Obtain Minimum Takeoff Weight, Minimum Cost, and Maximum Payload Kinetic Energy," *L'Aerotecnica*, Vol. 41, No. 1, February 1961, pp 3 to 13 (in Italian).
- Ehricke, K. A., "Powered Flight," *Handbook of Astronautical Engineering*, New York, McGraw-Hill Book Company, 1961 (Koelle, ed.)
"Ascent of Orbital Vehicles," *American Rocket Society*, Preprint No. 146-54, 1954.
- Fiul, A., and Braham, H., "Optimization of Vehicles and Trajectories for the Twenty-Four Hour Equatorial Satellite Mission," *American Rocket Society*, Paper No. 1120-60, 1960.
- Fried, B. D., "On the Powered Flight Trajectory of an Earth Satellite," *Jet Propulsion*, Vol. 27, No. 6, June 1957.
- Froehlich, J. E., "Capabilities of Multistaged Chemical Rocket Systems," *Astronautica Acta*, Vol. 6, No. 6, 1960, pp 311 to 321.
- Geckler, D., "Ideal Performance of Multistage Rockets," *ARS Journal*, Vol. 30, No. 6, June 1960, pp 531 to 536.
- Goldsmith, M., "On the Optimization of Two Stage Rockets," *Jet Propulsion*, Vol. 27, April 1957, p 415.
- Hall, H. H., and Zambelli, E. D., "On the Optimization of Multistage Rockets," *Jet Propulsion*, Vol. 28, No. 7, July 1958, pp 463 to 465.
- Hughes, J. V., et al., "Trajectories for Continuously Applied Propulsion Thrust," *Proceedings of the 4th Symposium on Ballistic Missile and Space Technology* (Los Angeles, 1959). New York, Pergamon Press, 1960. (Also, *Planetary and Space Science*, July 1961, Vol. 7.)
- Koelle, H. H., "Optimization Considerations for Orbital Payload Capabilities," *American Rocket Society*, Preprint No. 491-57, October 1957.
- Krause, H. G. L., Koelle, H. H., and Kuebler M. E., "Analytical Method for the Determination of Powered Rocket Trajectory Elements, with a Specific Turning Program and Consideration of Air Drag and Thrust Variation," Stuttgart, Astronautical Research Institute, Report No. 3, Chapter 2, August 1953, pp 18 to 25. (ASTIA Document No. AD-115961.)
- MacDonald, J. A., "Probability Approach to Outage Prediction (U)," *The Martin Company*, Baltimore, Maryland, Engineering Report No. 11712, 1961.
- Mackay, J. S., and Weber, R. J., "Performance Charts for Multistage Rocket Boosters," NASA TN D-582, January 1961.
- Pollak, R. J., "Rapid Determination of the Interaction Between the Rocket Vehicle and Its Trajectory," Lockheed Aircraft Corporation, Missiles and Space Division, Sunnyvale, California, *American Rocket Society*, Preprint No. 1476-60, 1960.
- Ragsac, R. V., and Patterson, P. L., "Multistage Rocket Optimization," *ARS Journal*, Vol. 31, No. 3, March 1961, pp 450 to 451.
- Schmidt, R., "Preliminary Calculation and Layout Method for Single and Multistage Ballistic and Space Rockets, Huntsville, Alabama, Army Ballistic Missile Agency, Redstone Arsenal, Report No. RA-TR-1-61, 10 February 1961.
- Schurmann, E. E. H., "Optimum Staging Technique for Multistaged Rocket Vehicles," *Jet Propulsion*, Vol. 27, August 1957, p 863.
- Subotowicz, M., "The Optimization of the N-Step Rocket with Different Construction Parameters and Propellant Specific Impulses in Each Stage," *Jet Propulsion*, Vol. 28, No. 7, July 1958, pp 460 to 463.
- Ten Dyke, R. P., "Computation of Rocket Step Weights to Minimize Initial Gross Weight," *Jet Propulsion*, Vol. 28, May 1958, p 338.
- Townsend, G., "Ascent to Orbit," *Design Guide to Orbital Flight*, McGraw-Hill Book Company, New York, Chapter 6, 1962.
- Van Pelt, J. M., "Optimum Propellant Distribution for Two-Stage Ballistic Missiles," *The Martin Company*, Baltimore, Maryland, TM 491/2-66, January 1959.
- Vargo, L. G., and Bruce, R. W., "Preliminary Optimization of Clustered Rocket Vehicles," *Aeronutronic*, Newport Beach, California, November 1959.
- Vertregt, M.
"Calculation of Step-Rockets," *Journal of the British Interplanetary Society*, Vol. 14, January 1955, p 20.
"A Method for Calculating the Mass Ratios of Step-Rockets," *Journal of the British Interplanetary Society*, Vol. 15, March 1956, p 94.

- Wang, C. J., et al., "Thrust Optimization of a Nuclear Rocket of Variable Specific Impulse," ARS Journal, Vol. 29, No. 5, 1959, pp 341 to 344.
- Weisbord, L.,
 "A Generalized Optimization Procedure for N-Staged Missiles," Jet Propulsion, Vol. 28, July 1958, p 164.
 "Optimum Staging Techniques," ARS Journal Vol. 29, June 1959, p 445.
- Wilson, M. L., "The Calculation of Fuel Distribution in Step-Rocket," Journal of the British Interplanetary Society, Vol. 16, No. 77, October to December 1957, pp 211 to 215.
2. Bibliography for Thermal Control and Cryogenic Storage
- Adelberg, M., "Storage of Cryogenics in Space," STL Report TN-59-0000-00324, 28 September 1959.
- Altshuler, T. L., "A Method for Calculating the Thermal Irradiance Upon a Space Vehicle and Determining Its Temperature," General Electric Company, R60SD386, August 1960.
- Ballinger, J., et al., "Thermal Environment of Space," Convair Astronautics Division, General Dynamics Corporation, ERR-AN-016, November 1960.
- Berenson, P., "Transition Boiling Heat Transfer from a Horizontal Surface," AIChE Paper No. 18, ASME-AIChE Heat Transfer Conference, Buffalo, August 1960.
- Bevans, J. T., Grier, J. T., and Dunkle, R. V., "Comparison of Total Emittances with Values Computed from Spectral Measurements," Trans. ASME, Vol. 80, No. 7, October 1958, p 1405.
- Birkebak, R. C., and Hartnett, J. P., "Measurements of the Total Absorptivity for Solar Radiation of Several Engineering Materials," ASME Paper 57-SA-27.
- Blanchero, J. T., Barker, G. E., and Boll, R. H., "Heat Transfer Characteristics of Boiling Oxygen, Fluorine, and Hydrazine," Eng. Res. Inst., University of Michigan (1951). See also Chem Eng Progr Symposium, Serial No. 17, Vol. 51, 1955, p 21.
- Boelter, L. M. K., et al., "A Mechanical Integrator for Determination of Illumination from Diffuse Surface Sources," Transactions of the Illuminating Engineering Society, Vol. 34, No. 9, November 1939, p 1085 to 1092.
- Brandt, J. A., Irvine, T. F., and Eckert, E. R. G., "A Method of Measuring Total Hemispherical Emissivities at Low Temperatures--Results for Pure Iron from 300 to 500° R," Proceedings, Heat Transfer and Fluid Mechanics Institute, Stanford University, 1960.
- Brock, O. K., "Thermal Radiation Interchange Between Black and Grey Surfaces," Convair, Fort Worth, General Dynamics Corporation, PT-23, 3 June 1960.
- Bromley, L. A., "Heat Transfer in Stable Film Boiling," Chem Eng Prog, Vol. 46, 1950, pp 221 to 227.
- Brown, A. I., and Marco, S. M., "Introduction to Heat Transfer," McGraw-Hill Book Company, New York, 1942.
- Carlsaw, H. S., and Jaeger, J. C., "Heat Conduction in Solids," 2nd Edition, Oxford Press, 1959.
- Chang, Y. P., and Snyder, N. W., "Heat Transfer in Saturated Boiling," AIChE Preprint No. 104, Third National Heat Transfer Conference, August 1959.
- Chelton, D. B., and Mann, D. B., "Cryogenic Data Book," WADC TR 59-8, March 1959.
- Class, C. R., DeHaan, J. R., Piccone, M., and Cost, R. B.,
 "Pool Boiling Heat Transfer to a Cryogenic Liquid," WADC Tech Rep 58-528, 1958.
 "Boiling Heat Transfer to Liquid Hydrogen from Flat Surfaces," Advances in Cryogenic Engineering, Vol. 5, 1960, K. D. Timmerhaus, Editor.
- Dean, L. E., and Thompson, L. M., "Heat Transfer Characteristic of Liquid Nitrogen," Bell Aircraft Corporation, Rep No. 56-982-035, 1955. See also ASME Paper 56-SA-4.
- Deissler, R. G.,
 "Heat Transfer and Fluid Friction for Fully Developed Turbulent Flow of Air and Supercritical Water with Variable Fluid Properties," Trans Am Soc Mech Engrs, 76, pp 73 to 85, 1954.
 "Analysis of Turbulent Heat Transfer, Mass Transfer, and Friction in Smooth Tubes at High Prandtl and Schmidt Numbers," NACA Report 1210, 1955.
- Drayer, D. E., and Timmerhaus, K. D., "An Experimental Investigation of the Individual Boiling and Condensing Heat Transfer Coefficients for Hydrogen," Paper J-6, Advances in Cryogenic Eng., Vol. 7, 1962, p 401.
- Driscoll, D. G., "Cryogenic Tankage for Space Flight Applications," Linde Company, Cryogenics Engineering Conference, 1959.
- Dunkle, R. V.,
 "Thermal Radiation Characteristics of Surfaces," Lecture presented at Symposium on Theory and Fundamental Research in Heat Transfer, ASME, November 1960; also in Theory and Fundamental Research in Heat Transfer, J. A. Clark, Editor, Pergamon Press, 1962.
 "Thermal Radiation Tables and Applications," Trans ASME, Vol. 76, 1954, pp 549 to 552.

- Durham, T. F., McClintock, R. M., and Reed, R. P., "Cryogenics Materials Data Handbook," Cryogenics Engineering Laboratory, National Bureau of Standards, U. S. Department of Commerce, Contract AF04(647)-59-3, 8th Quarterly Report, Boulder, Colorado.
- Dusinberre, G. M., "Heat Transfer Calculations by Finite Differences," International Textbook Company, 1961.
- Eckert, E. R. G., "Introduction to the Transfer of Heat and Mass," McGraw-Hill Book Company, New York, 1950.
- Eckert, E. R. G., and Drake, R. M., Jr., "Heat and Mass Transfer," McGraw-Hill Book Company, New York, 1959.
- Elrod, H. G., "New Finite-Difference Method for the Solution of the Heat Conduction Equation, Especially near Surfaces with Convective Heat Transfer," Trans. ASME, Vol. 79, No. 7, October 1957, p 1519.
- Farkas, A., "Orthohydrogen, Parahydrogen, and Heavy Hydrogen, Cambridge University Press, London, 1935, p 20.
- Fenechi, H., "Thermal Conductance of Metallic Surfaces in Contact," SM Thesis, MIT, 1957.
- Fenster, S. K., VanWylen, G. J., and Clark, J. A., "Transient Phenomena Associated with the Pressurization of Liquid Nitrogen Boiling at Constant Heat Flux," Advances in Cryogenic Engineering, K. D. Timmerhaus, Editor, Vol. 5, 1960, p 226.
- Forster, H. E., and Zuber, N., "Dynamics of Vapor Bubbles and Boiling Heat Transfer," AIChE Journal, Vol. 1, 1955, p 531.
- Frainier, R. J., "Experimental Performance and Selection of Rocket Insulation Systems," Linde Company, Cryogenic Engineering Conference (Reprint), 1960.
- Frederking, T. H. K., "Film Boiling of Helium I and Other Liquefied Gases on Single Wires," AIChE, J. Vol. 5, No. 3, 1959, p 403.
- "Remarks on the Heat Transport in Helium II at High Heat Flux Values," University of California, Los Angeles, Report No. 62-5, February 1962.
- Frederking, T. H. K., and Clark, J. A., "Natural Convection Film Boiling on a Sphere," Paper submitted to 1962 Cryogenic Engineering Conference Committee, K. D. Timmerhaus, Secretary, May 1962.
- Fritz, S., "The Albedo of the Planet Earth and of Clouds," Journal of Meteorology, 1949.
- Fulk, M. M., Reynolds, M. M., and Park, O. E., "Thermal Radiation Absorption by Metals," Proceedings, 1954 Cryogenic Engineering Conference, p 151.
- Gebhart, B., "Unified Treatment for Thermal Radiation Transfer Processes--Gray Diffuse Radiators and Absorbers," ASME Paper No. 57-A-34. See also, "Heat Transfer," B. Gebhart, McGraw-Hill, 1961.
- Giedt, W. H., "Principles of Engineering, Heat Transfer," D. Van Nostrand Company, Princeton, New Jersey, 1958.
- Graham, R. W., Hendricks, R. C., Hsu, Y. V., and Friedman, R., "Experimental Heat Transfer and Pressure Drop of Film Boiling Liquid Hydrogen Flowing Through A Heated Tube," Advances in Cryogenic Engineering, K. D. Timmerhaus, Editor, Vol. 6, 1961, p 517.
- Hamilton, D. C., and Morgan, W. R., "Radiant-Interchange Configuration Factors," National Advisory Committee for Aeronautics, NACA TN 2836, 1952.
- Haselden, G. G., and Prosad, S., "Heat Transfer from Condensing Oxygen and Nitrogen Vapours," Trans Inst Chem Eng (London), Vol. 27, 1949, pp 195 to 200.
- Haselden, G. G., and Peters, J. I., "Heat Transfer to Boiling Liquid Oxygen and Liquid Nitrogen," Trans Am Inst Chem Eng (London), Vol. 27, 1949, pp 201 to 208.
- Holten, D. C., "A Study of Heat and Mass Transfer to Uninsulated Liquid Oxygen Containers," Advances in Cryogenic Engineering, Vol. 6, K. D. Timmerhaus, Editor, 1961, p 499.
- Holter, F. J., "Simplified Matrix Technique for Determining the Average Surface Temperatures of an N-Surface Enclosure Radiation to Space," Personal Communication to J. A. Clark, November 1961.
- Hottel, H. C., "Some Problems in Radiative Transport," Lecture presented at 1961 International Heat Transfer Conference, Boulder, Colorado, London, England.
- "Radiant Heat Transmission," Mechanical Engineering, Vol. 52, No. 7, July 1930, pp 699 to 704.
- Hsu, Y. Y., and Smith, J. M., "The Effect of Density Variation on Heat Transfer in the Critical Region," Am Soc Mech Engr, Paper 60-HT-8, 1960.
- Irvine, T. F., Hartnett, J. P., and Eckert, E. P. G., "Solar Collector Surfaces with Wave Length Selective Radiation Characteristics," Solar Energy, Vol. II, No. 2-3, July to October 1958. See also addendum: Solar Energy, Vol. III, No. 2, April 1959, p 38.
- Ivey, H. J., "Preliminary Results on the Effect of Acceleration on the Critical Heat Flux in Pool Boiling," Reactor Development Division Report AEEW-R99, AEE, Dorchester, Dorset, England, September 1961.
- Jakob, M., "Heat Transfer," Vol. I and II, John Wiley and Sons, 1949, 1960.

- Kamius, M., and Zabel, E., "Manufacture and Delivery of Liquid Oxygen and Liquid Nitrogen to ICBM Sites," Rand Report, STL 59-3357.
- Karagounis, A., "Heat Transfer Coefficient for Liquid Helium," (in French), Bull Inst Intern Froid, Annexe 2. 195-9, 1956.
- Keenan, J. H., "Thermodynamics, John Wiley and Sons, Inc., New York, 1941.
- King, C. R., "Compilation of Thermodynamic Properties, Transport Properties and Theoretical Rocket Performance of Gaseous Hydrogen," NASA TN D-275, 1960.
- Knudsen, J. G., and Katz, D. L., "Fluid Dynamics and Heat Transfer," McGraw-Hill Book Company, Inc., 1958.
- Kreith, F.,
"Principles of Heat Transfer," International Textbook Company, 1960.
"Radiation Heat Transfer for Spacecraft and Solar Power Plant Design," International Textbook Company, 1962.
- Kreith, F., and Summerfield, M., "Investigation of Heat Transfer at High Heat Flux Densities; Experimental Study with Water of Friction Drop and Forced Convection with and Without Surface Boiling in Tubes," Jet Propulsion Lab Progress Report 4-68, 1948.
- Kropschot, R. H., "Insulation Principles," Lecture No. 3, UCLA Symposium, Cryogenic Technology, 1962.
- Leonhard, K. E., and McMordie, R. K., "The Nonadiabatic Flow of Evaporating Cryogenic Fluid Through a Horizontal Tube," Advances in Cryogenic Engineering, Vol. 6, K. D. Timmerhaus, Editor, 1961, p 481.
- Leuenberger, H., and Person, R. A., "Radiation Shape Factors for Cylindrical Assemblies," American Society of Mechanical Engineers, Paper 56-A-144.
- Loper, J. L., and Heatherly, E. R., "Vapor Losses in Cylindrical Containers of Aluminum and Fiberglass Laminate Filled with Liquid Nitrogen and Exposed to Climatic Heating," Tech Note No. G-002, Structures and Mechanics Laboratory, ABMA, Huntsville, Alabama, 4 August 1955.
- McAdams, W. H., "Heat Transmission," 3rd Edition, McGraw-Hill, 1954.
- McCue, G. A.,
"Program for Determining Temperatures of Orbiting Space Vehicles," Space and Information Systems Division, North American Aviation, Inc., SID 61-105, 20 April 1961.
"Eclipse Characteristics of Close Earth Satellite Orbits," Space and Information Systems Division, North American Aviation, Inc., SID 61-50, February 1961.
- McMordie, R. K., "Steady-State Conduction with Variable Thermal Conductivity," Trans ASME, Heat Transfer Journal, Vol. 84, No. 1, February 1962, p 92.
- Merte, H., and Clark, J. A., "Boiling Heat Transfer Data for Liquid Nitrogen at Standard and Near-Zero Gravity," Advances in Cryogenic Engineering, Vol. 7, 1962, K. D. Timmerhaus, Editor.
- Moon, P., "The Scientific Basis of Illuminating Engineering," McGraw-Hill Book Company, New York, 1936.
- Monroe, A. G., Bristow, A. S., and Newell, J. E., "Heat Transfer to Boiling Liquids at Low Temperatures and Elevated Pressures," J. Appl Chem, Vol. 2, 1952, pp 613 to 624.
- Mulford, R. N., Nigon, J. P., Dash, J. G., and Keller, W. E., "Heat Exchange Between a Copper Surface and Liquid Hydrogen and Nitrogen," Ext from Secret Doc, LAMS-1443.
- Nordwall, H. L., "Geometrical Configuration Factor Program," Space and Information Systems Division, North American Aviation, Inc., SID 61-90, 30 April 1960.
- Obert, E. F., "Elements of Thermodynamics and Heat Transfer," McGraw-Hill Book Company, New York, 1949.
- Oppenheim, A. K., "Radiation Analysis by the Network Method," Transaction ASME, Vol. 78, No. 1, May 1956, pp 725 to 735.
- Perkins, W. E., and Frainier, R. J., "Practical Storage of Liquid Hydrogen and Helium," Linde Company, 1959 Cryogenic Engineering Conference.
- Perry, J. H., "Chemical Engineer's Handbook," McGraw-Hill Book Company, New York, 3rd Edition, 1950, p 205.
- Peterson, M., "Radiation Effects," Los Angeles Division, North American Aviation, Inc., NA-56-399, 1956.
- Pope, D. H., Killian, W. R., and Corbett, R. J., "Single-Phase Flow Tests with Liquid Hydrogen," Advances in Cryogenic Engineering, Vol. 5, K. D. Timmerhaus, Editor, Plenum Press, 1960, p 449.
- Richards, R. J., Robbins, R. F., Jacobs, R. B., and Holten, D. C., "Heat Transfer to Boiling Liquid Nitrogen and Hydrogen Flowing Axially Through Narrow Annular Passages," Adv in Cryogenic Eng., K. D. Timmerhaus, Ed., Plenum Press, Inc., New York, Vol. 3, 1960, p. 375.
- Richards, R. J., Steward, W. G., and Jacobs, R. B., "A Survey of the Literature on Heat Transfer from Solid Surfaces to Cryogenic Fluids," NBS TN 122, Boulder Laboratories, October 1961.

- Richtmyer, R. D., "Difference Methods for Initial-Value Problems," Interscience Publishers, Inc., New York, 1957.
- Riede, P. M., and Wang, D., "Characteristics and Applications of Some Super Insulations," Linde Company, 1959 Cryogenic Engineering Conference (Reprint).
- Rohsenow, W. M., and Clark, J. A., "Mechanism of Boiling Heat Transfer," Trans ASME, Vol. 73, July 1951.
- "Heat Transfer and Pressure Drop Data for High Heat Flux Densities to Water at High Subcritical Pressures," Heat Transfer and Fluid Mechanics Institute, Stanford University, 1951.
- Rohsenow, W. M., "Correlating Heat Transfer Data for Surface Boiling Liquids," Trans ASME, Vol. 74, 1952.
- Rohsenow, W. M., and Choi, H., "Heat, Mass and Momentum Transfer," Prentice-Hall, 1961.
- Ruzicka, J., "Heat Transfer to Boiling Nitrogen," Problems of Low Temperature Physics and Thermodynamics, Pergamon Press, 1959, p 323.
- Schneider, P. J., "Conduction Heat Transfer," Addison-Wesley, 1955.
- Scott, R. B., "Cryogenic Engineering," D. Van Nostrand Company, 1959.
- Smolak, G. R., and Knoll, R. H., "Cryogenics Propellant Storage for Round Trips to Mars and Venus," IAS Paper No. 60-23, presented at the 28th Annual IAS Meeting, New York, 25 to 27 January 1960.
- Stevenson, J. A., and Grafton, J. C., "Radiation Heat Transfer Analysis for Space Vehicles," Space and Information Division, North American Aviation, Inc., Downey, California, ASD Technical Report 61-119, Part I, December 1961.
- Stock, B. J., "Observations on Transition Boiling Heat Transfer Phenomena," Argonne National Lab, ANL-6175, June 1960.
- Sydoriak, S. G., and Roberts, T. R., "A Study of Boiling in Short Narrow Channels and Its Application to Design of Magnets Cooled by Liquid H_2 and N_2 ," J Appl Phys, Vol. 28, No. 2, 1957, pp 143 to 148.
- Thompson, W. R., and Geery, E. L., "Heat Transfer to Cryogenic Hydrogen at Super-Critical Pressure," Advances in Cryogenic Engineering, Vol. 7, K. D. Timmerhaus, Editor, 1962, p 391.
- Timmerhaus, K. D., Editor, "Advances in Cryogenic Engineering," Vol. 1 to 7, Plenum Press.
- Usiskin, C. M., and Siegel, R., "An Experimental Study of Boiling in Reduced and Zero Gravity Fields," Trans ASME, Journal of Heat Transfer, Vol. 83, No. 3, August 1961.
- Van Gundy, D. A., and J. R. Uglum, "Heat Transfer to an Uninsulated Surface at 20° K," Advances in Cryogenic Engineering, Vol. 7, K. D. Timmerhaus, Editor, Paper No. J-3, 1962.
- Van Vliet, K. M., "Selective Coatings for Extraterrestrial Solar Energy Conversion, A Fundamental Analysis," Wright Air Development Division, WADD TR 60-773, 1960.
- Von Glahn, U. H., and Lewis, J. P., "Nucleate and Film Boiling Studies with Liquid Hydrogen," Advances in Cryogenic Engineering, Vol. 5, K. D. Timmerhaus, Editor, 1960.
- Walters, H. H., "Single Tube Heat Transfer Tests with Liquid Hydrogen," Advances in Cryogenic Engineering, K. D. Timmerhaus, Editor, Vol. 6, 1961, p 509.
- Wooley, H. W., Scott, R. B., and Brickwedde, F. G., "Compilation of Thermal Properties of Hydrogen in Its Various Isotopic and Orthopara Modifications," J. Research National Bureau Standards 41, November 1948, pp 379 to 476.
- Wright, C. C., "Design, Construction and Testing of a Helium-To-Hydrogen Heat Exchanger," Advances in Cryogenic Engineering, Vol. 5, K. D. Timmerhaus, Editor, Plenum Press, 1960, p 248.
- Zuber, N., and Fried, E., "Two Phase Flow and Boiling Heat Transfer to Cryogenic Liquids," American Rocket Society, Propellants, Combustion and Liquid Rockets Conference, April 1961.

ILLUSTRATIONS

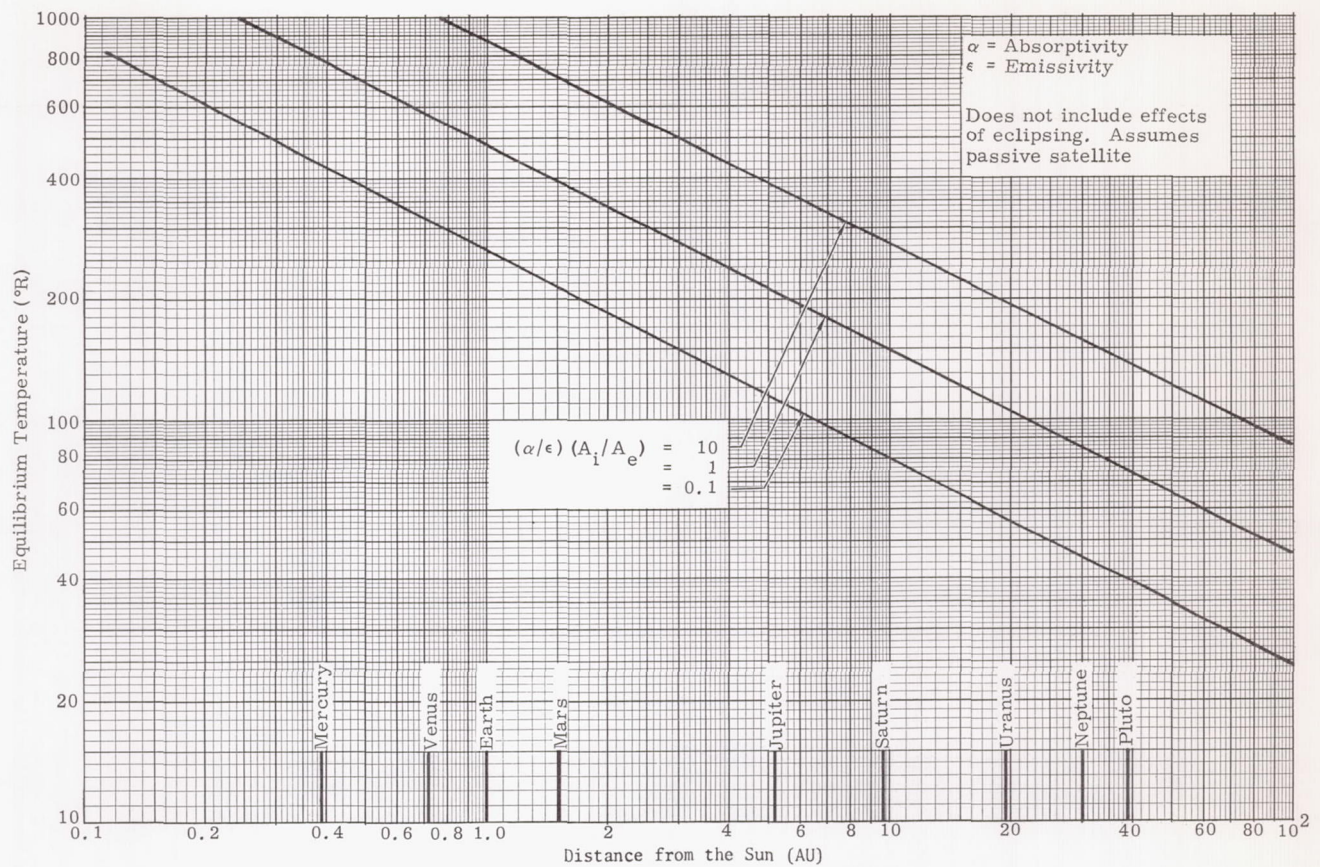


Fig. 1. Equilibrium Temperature of Inert Sphere

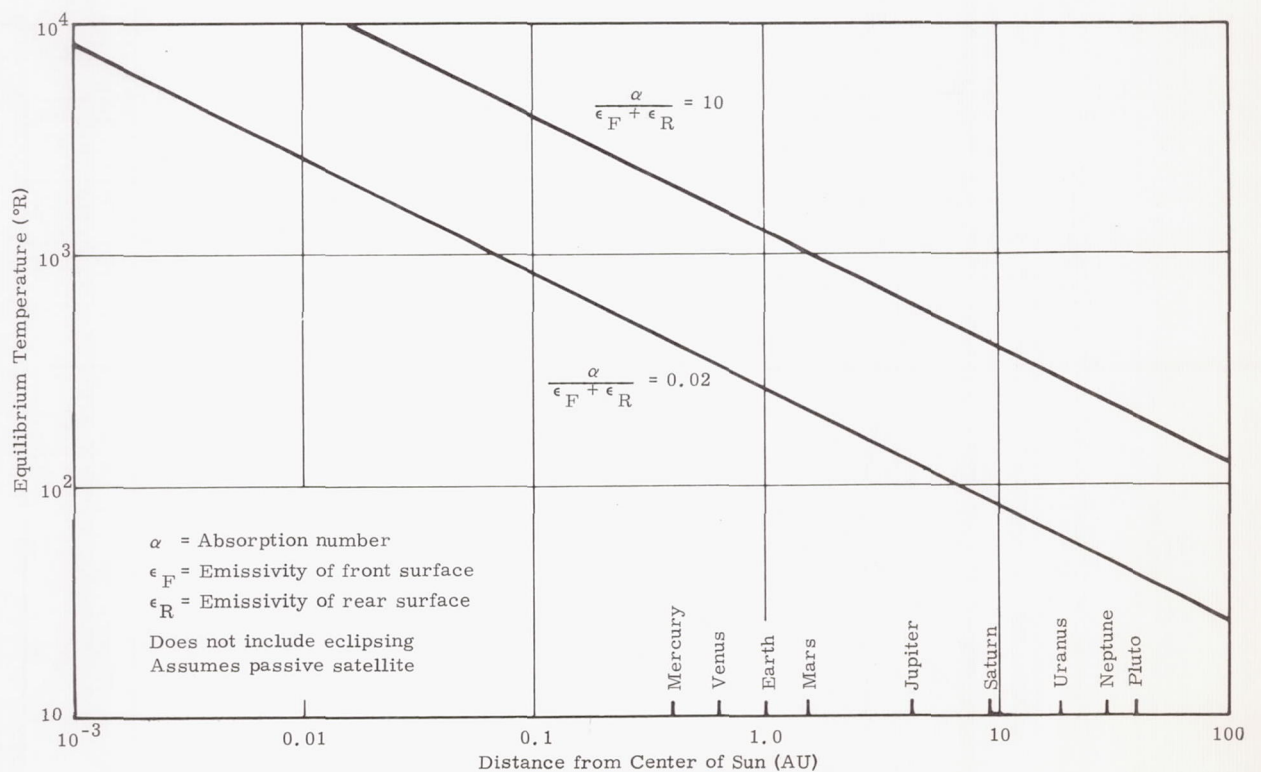


Fig. 2. Equilibrium Temperature of a Thin Plate Normal to the Sun (Ref. 3)

Preceding Page Blank

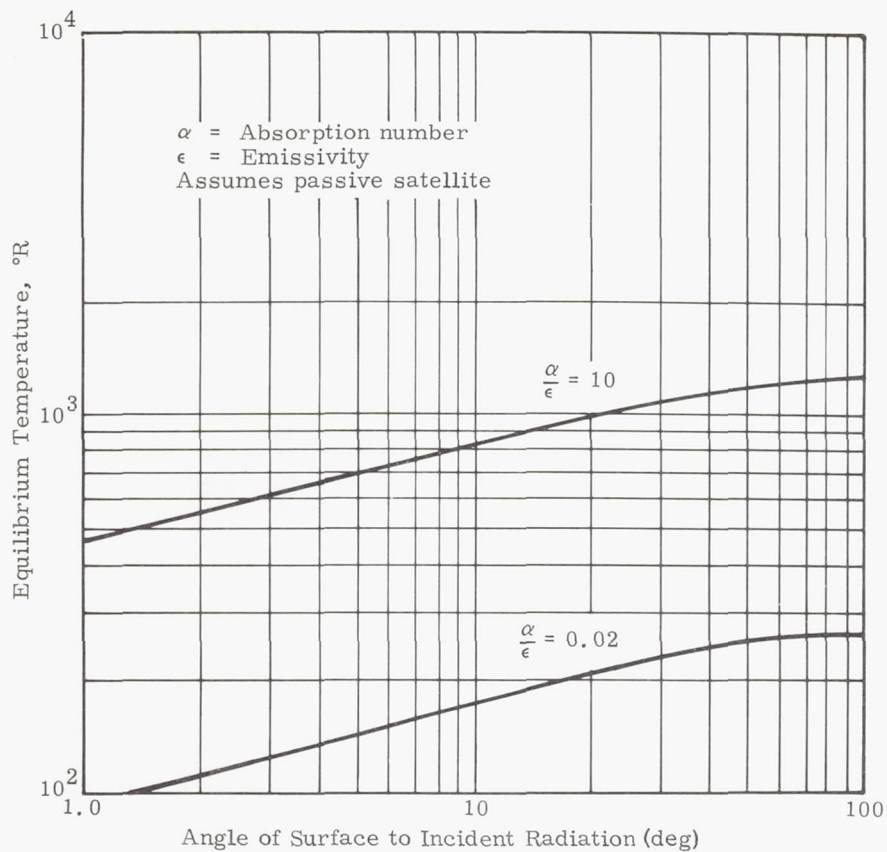


Fig. 3. Effect of Attitude on Equilibrium Temperature of a Thin Plate Located at One Astronomical Unit from the Sun (Ref. 3)

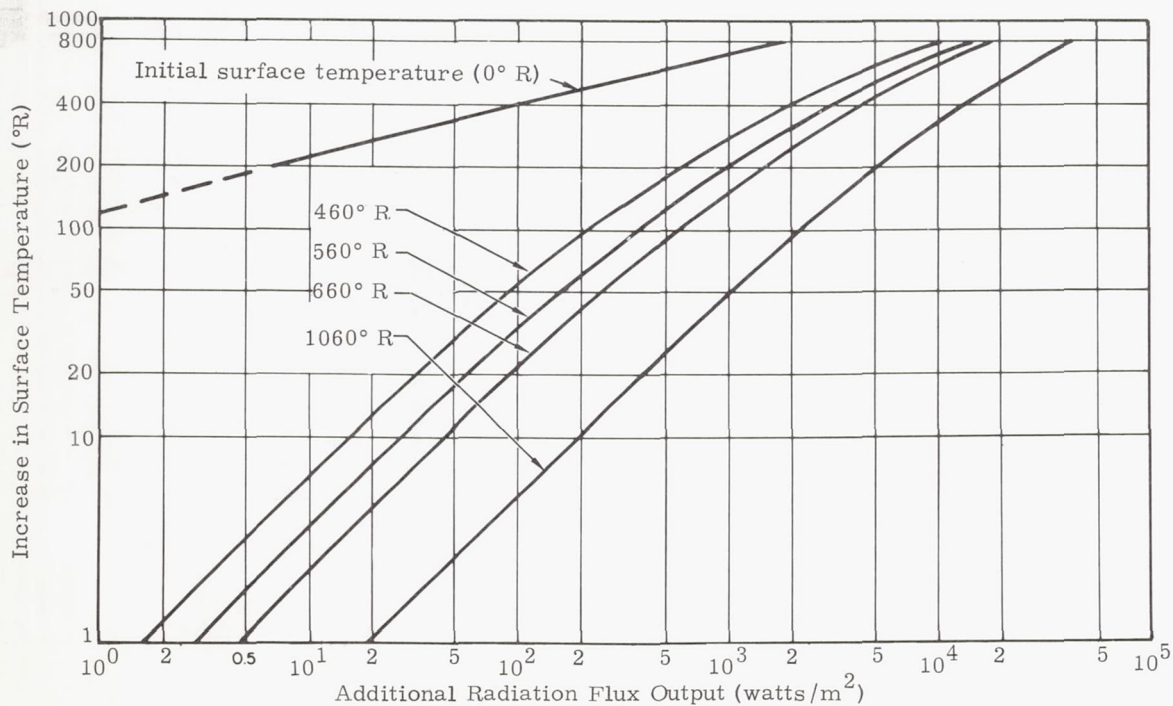


Fig. 4. Effect of Added Heat Input on Equilibrium Temperature
 (1 w/ft² = 10.76 w/m²) (Ref. 3)

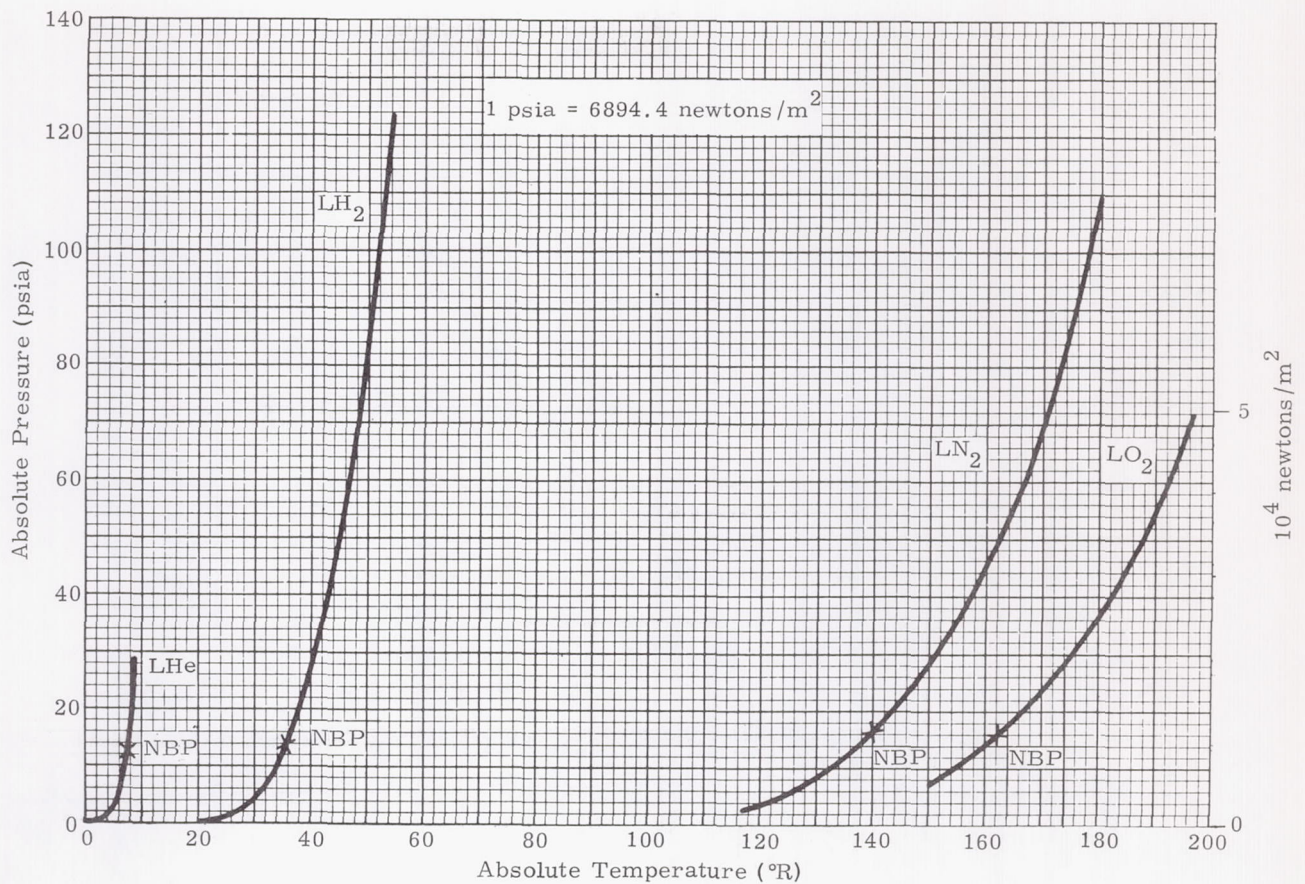


Fig. 5. Vapor Pressure of Cryogenic Fluids

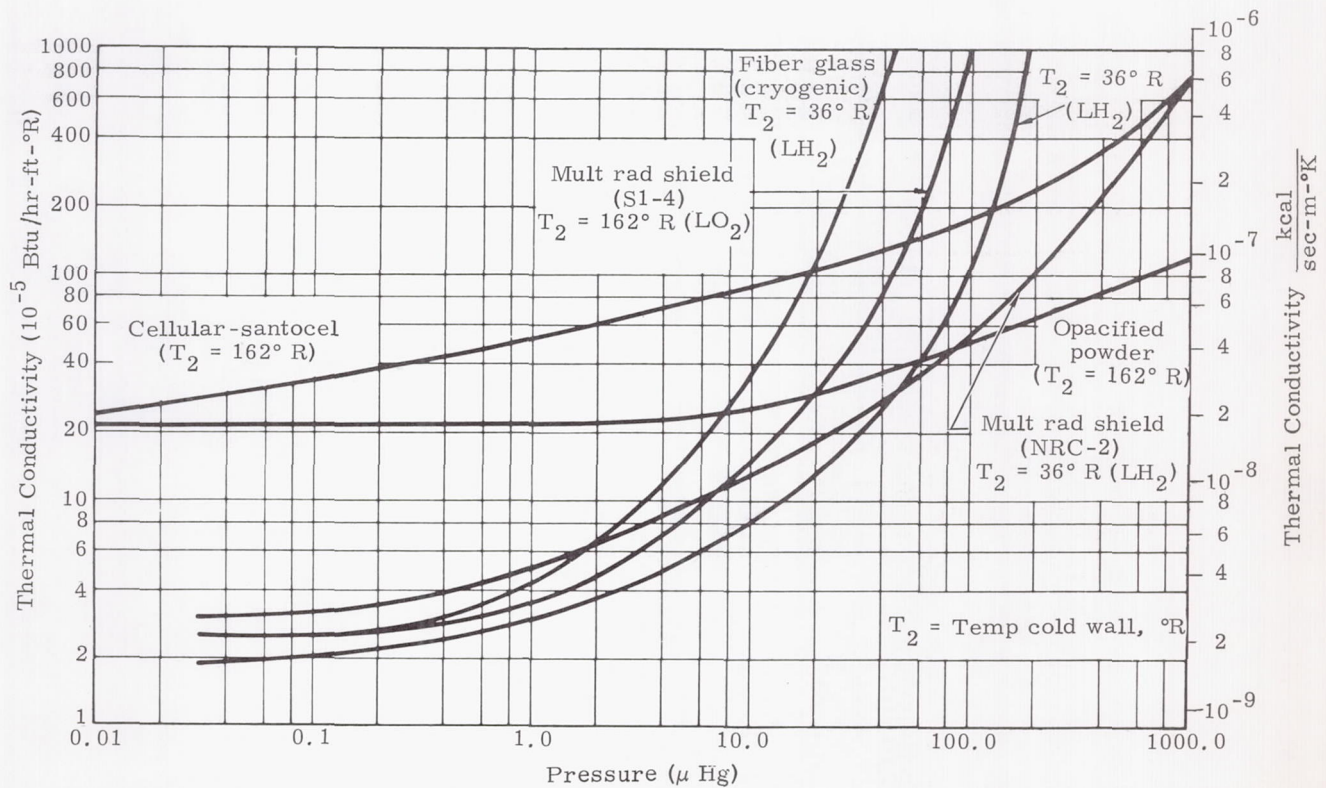


Fig. 6. Heat Transfer Rates of Cryogenic Insulations, Thermal Conductivity Versus Vacuum Pressure (1 Btu/hr-ft-°R = 1.27588 x 10⁻⁴ kcal/sec-m-°K)

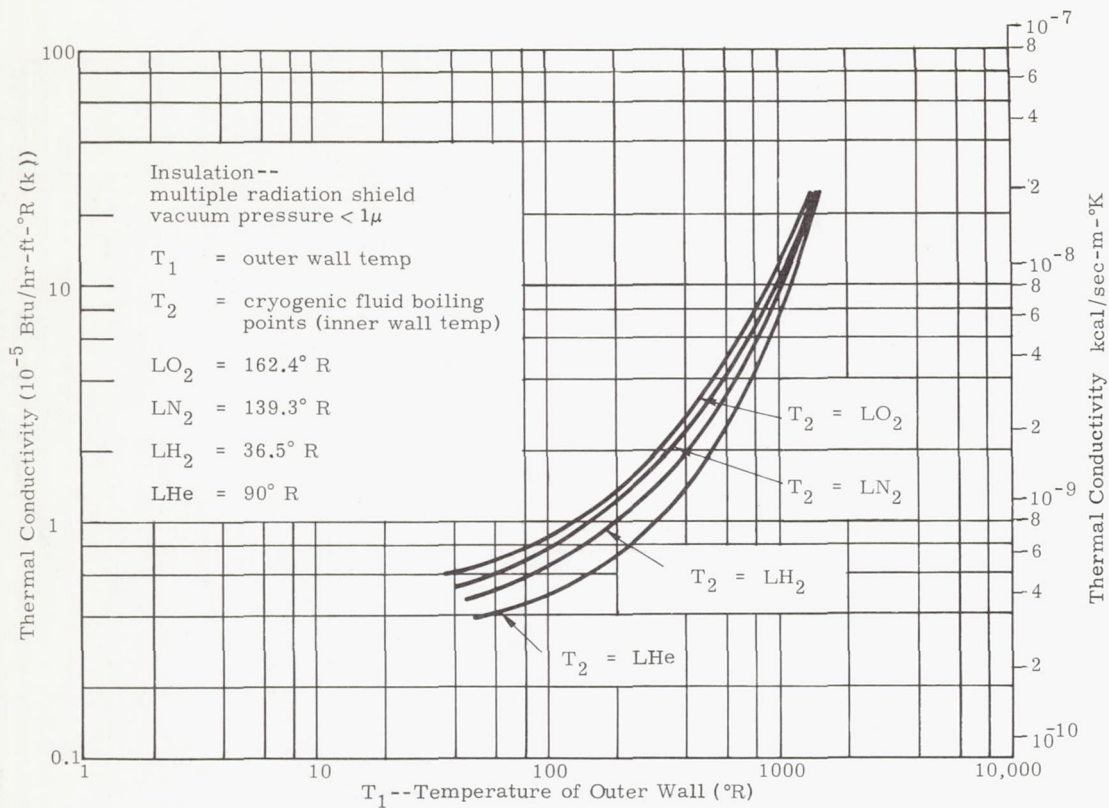


Fig. 7. Thermal Conductivity at Various Wall Temperatures
 (1 Btu/hr-ft- $^\circ R = 1.27588 \times 10^{-4}$ kcal/sec-m- $^\circ K$)

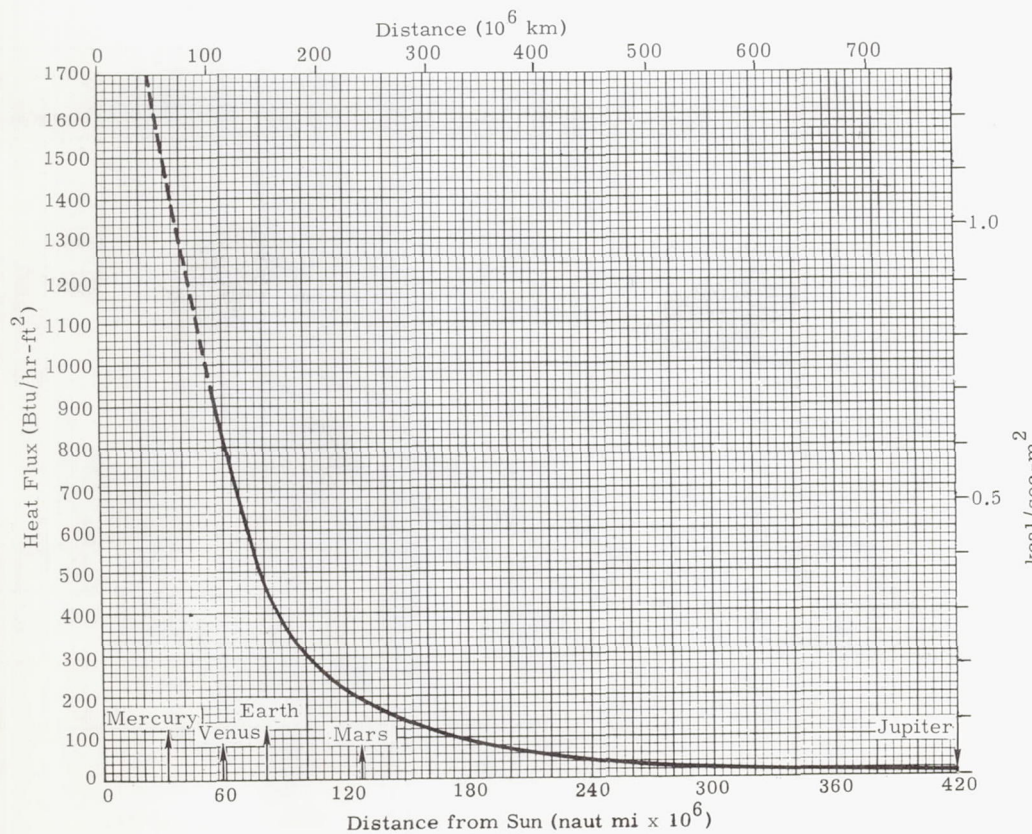


Fig. 8. Heat Flux from Sun (1 Btu/hr-ft $^2 = 0.75347 \times 10^{-3}$ kcal/sec-m 2)

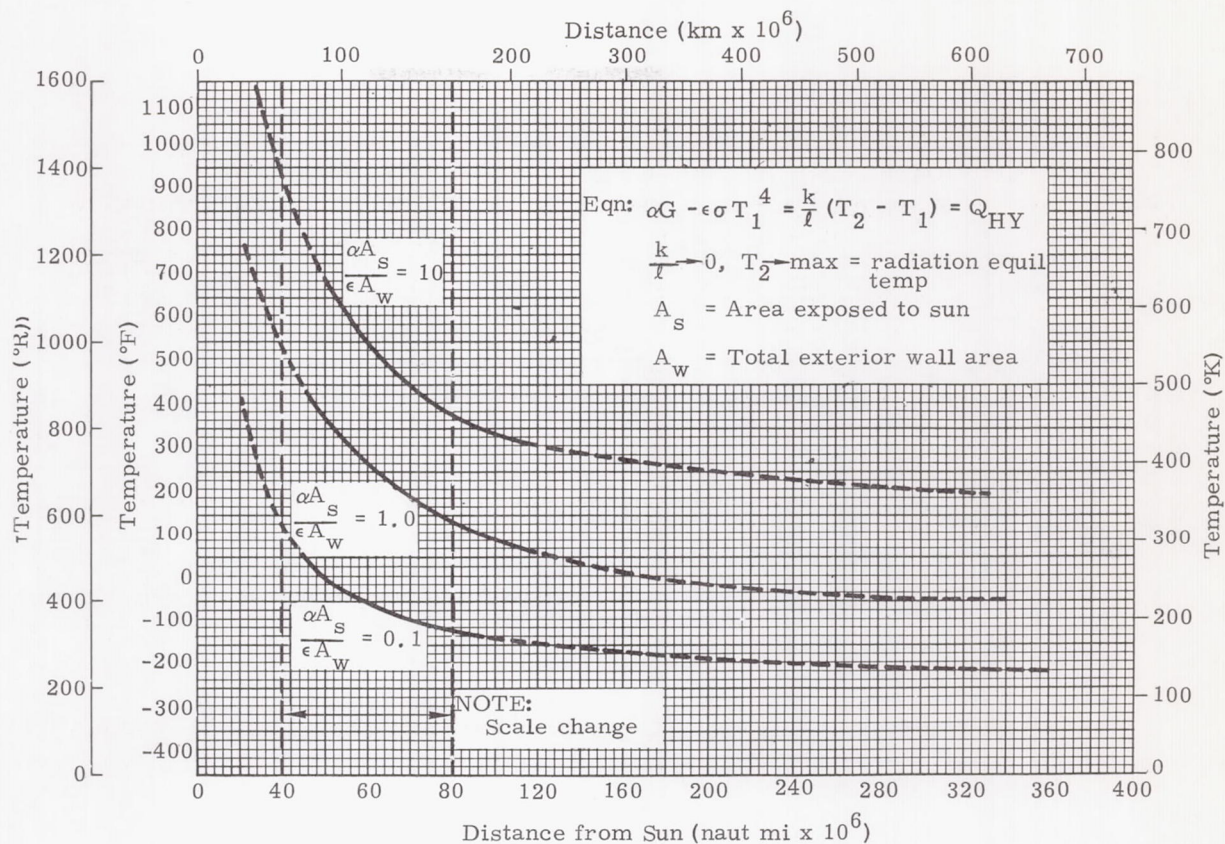


Fig. 9. Solar Heating--Temperature of Outer Wall

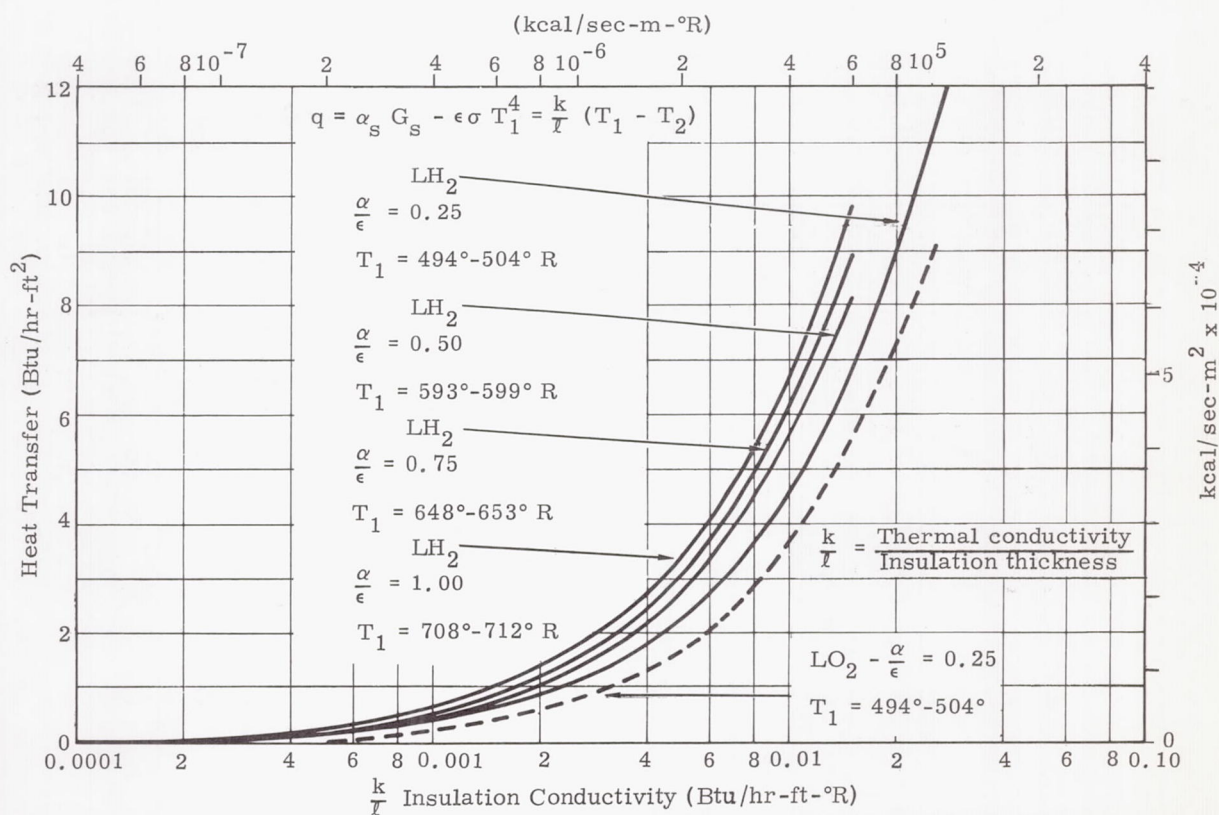


Fig. 10. Heat Transfer to Hydrogen and Oxygen (1 Btu/hr-ft² = 0.75347 x 10⁻³ kcal/sec-m²)

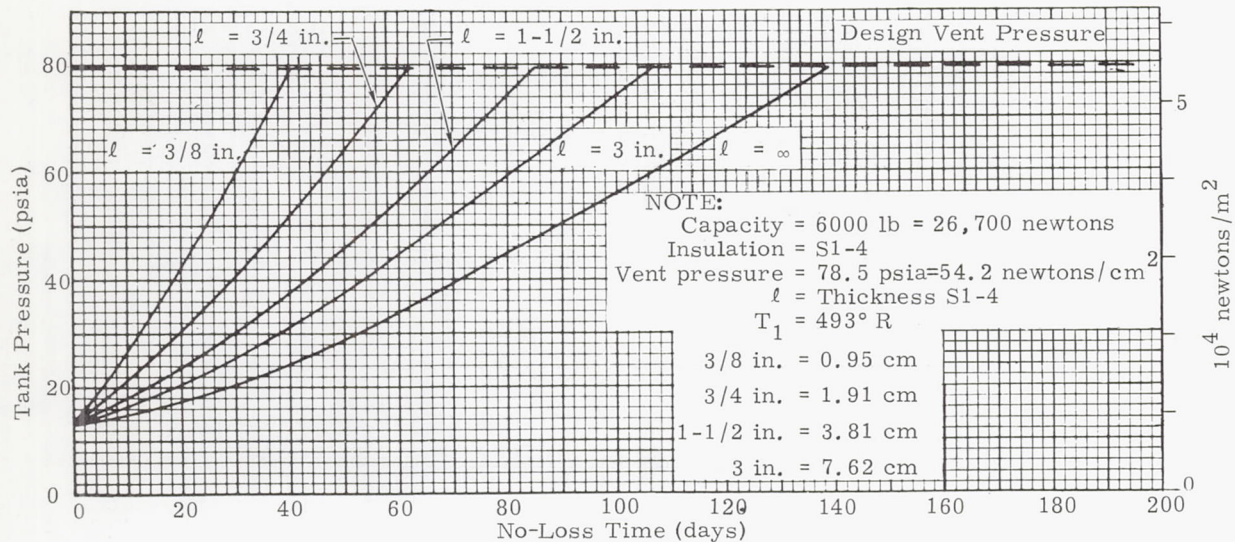


Fig. 11. No-Loss (Pre-Boiloff) Time--LH₂ Tank (1 psia = 6894.4 newtons/m²)

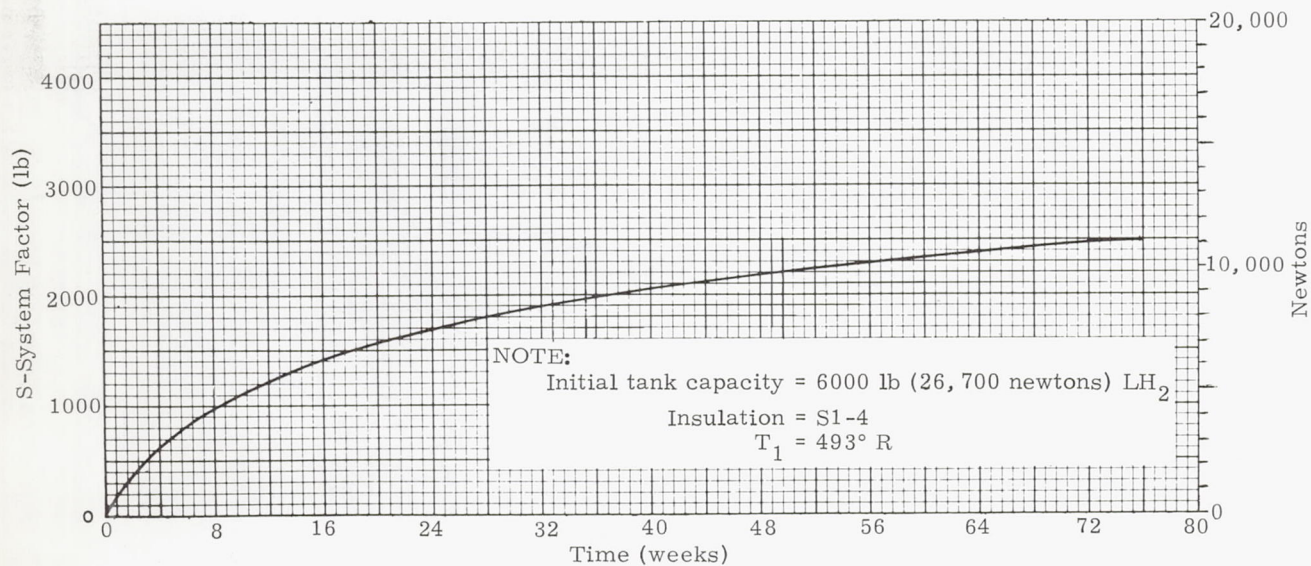


Fig. 12. System Factor (S) Versus Time $S = I_w + \left(\frac{tQ T}{v} \right)$ (1 lb = 4.448 newtons)

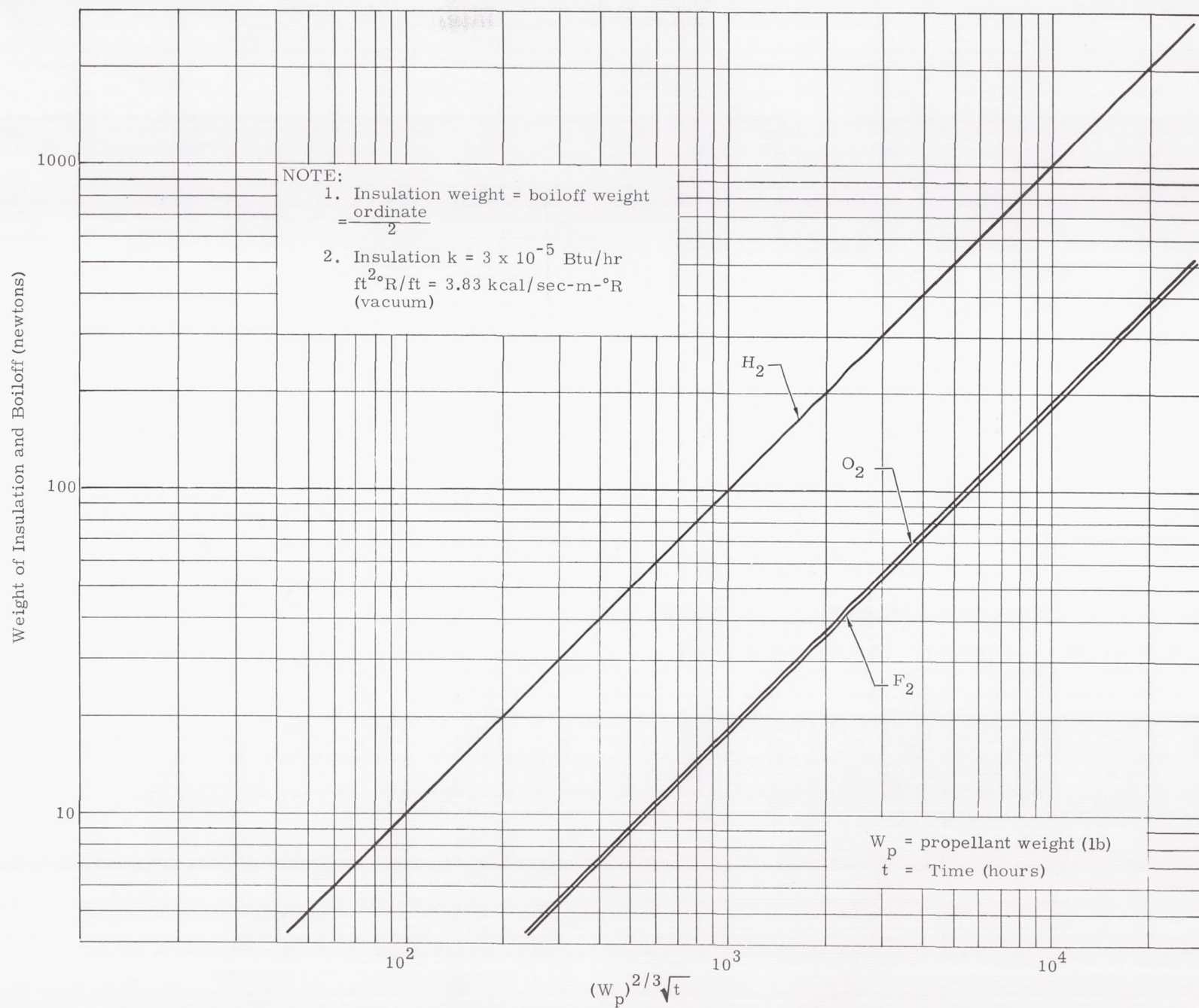


Fig. 13. Propellant Boiloff Plus Insulation Weight at Optimum Insulation Thickness for Spherical Tanks on the Lunar Surface (1 lb = 4.448 newtons)

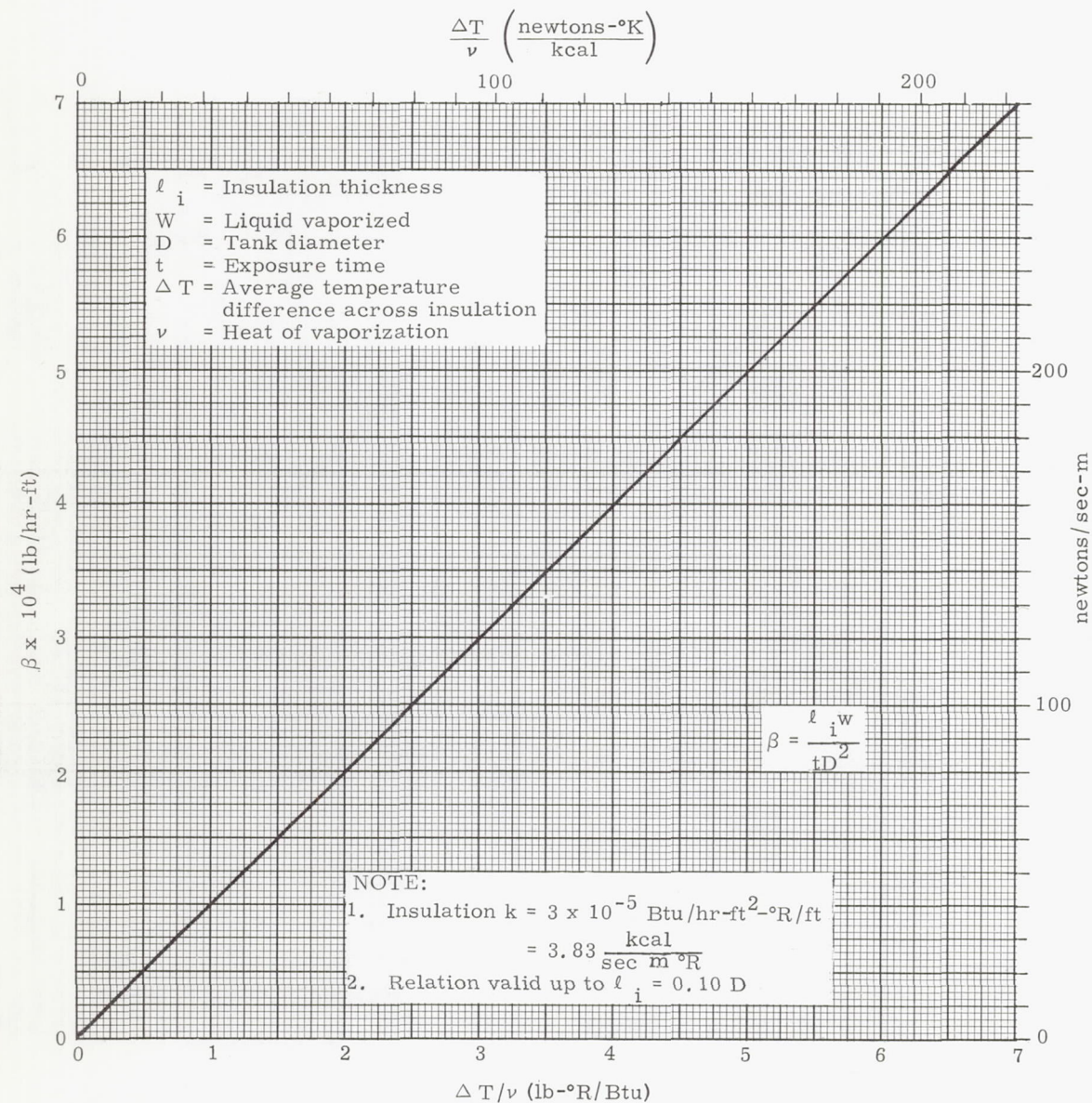


Fig. 14. Boiloff Losses for Liquids Contained in Spherical Tanks, General Case

CHAPTER XI

ORBIT COMPUTATIONS

Prepared by:

J. D. Kraft
Martin Company (Baltimore)
Aerospace Mechanics Department
March 1963

| | Page |
|--|-------|
| Symbols | XI-1 |
| A. Introduction. | XI-2 |
| B. Coordinate Systems and Transformations | XI-2 |
| C. Acquisition of Data | XI-14 |
| D. Determination of Preliminary Orbit Elements | XI-22 |
| E. Theory of Observation Error | XI-28 |
| F. Orbit Improvement | XI-37 |
| G. Accuracy Determinations | XI-43 |
| H. References | XI-47 |
| I. Bibliography | XI-47 |
| Illustrations | XI-51 |

LIST OF ILLUSTRATIONS

| Figure | | Page |
|--------|--|-------|
| 1 | Interferometer System | XI-53 |
| 2 | Minitrack Modified Interferometer System | XI-53 |
| 3 | Effect of Spread and Number of Data on Accuracy of Eccentricity Determination | XI-54 |
| 4 | Effect of Spread and Number of Data on Accuracy of Semilatus Rectum Determination | XI-54 |
| 5 | Effect of Spread of Data on Accuracy of In- clination and Nodal Longitude Determination | XI-55 |
| 6 | Effect of a Limited Number of Data on Ac- curacy of Orbit Determination | XI-56 |
| 7 | Effect of a Limited Number of Data on Ac- curacy of Orbit Determination | XI-56 |
| 8 | Angular Observation Errors, σ_A Versus σ_ϵ ($\sigma_\rho^* = 0.3$ mps) | XI-57 |
| 9 | Angular Observation Errors, σ_D Versus σ_ϵ ($\sigma_\rho^* = 0.3$ mps) | XI-57 |
| 10 | Angular Observation Errors, σ_v Versus σ_ϵ ($\sigma_\rho^* = 0.3$ mps) | XI-58 |
| 11 | Angular Observation Errors, σ_η Versus σ_ϵ ($\sigma_\rho^* = 0.3$ mps) | XI-58 |
| 12 | Angular Observation Errors, σ_r Versus σ_ϵ ($\sigma_\rho^* = 0.3$ mps) | XI-59 |
| 13 | Angular Observation Errors, σ_v Versus σ_ϵ ($\sigma_\rho^* = 0.3$ mps) | XI-59 |

LIST OF ILLUSTRATIONS (continued)

| Figure | | Page |
|--------|---|-------|
| 14 | Angular Observation Errors, σ_a Versus σ_ϵ ($\sigma_\rho^* = 0.3$ mps)..... | XI-60 |
| 15 | Angular Observation Errors, σ_e Versus σ_ϵ ($\sigma_\rho^* = 0.3$ mps)..... | XI-60 |
| 16 | Angular Observation Errors, σ_i Versus σ_ϵ ($\sigma_\rho^* = 0.3$ mps)..... | XI-61 |
| 17 | Angular Observation Errors, σ_Ω Versus σ_ϵ ($\sigma_\rho^* = 0.3$ mps)..... | XI-61 |
| 18 | Angular Observation Errors, σ_ω Versus σ_ϵ ($\sigma_\rho^* = 0.3$ mps)..... | XI-62 |
| 19 | Angular Observation Errors, σ_M Versus σ_ϵ ($\sigma_\rho^* = 0.3$ mps)..... | XI-62 |
| 20 | Angular Observation Errors, σ_A Versus σ_ϵ ($\sigma_\rho = 183$ m)..... | XI-63 |
| 21 | Angular Observation Errors, σ_D Versus σ_ϵ ($\sigma_\rho = 183$ m)..... | XI-63 |
| 22 | Angular Observation Errors, σ_v Versus σ_ϵ ($\sigma_\rho = 183$ m)..... | XI-64 |
| 23 | Angular Observation Errors, σ_η Versus σ_ϵ ($\sigma_\rho = 183$ m)..... | XI-64 |
| 24 | Angular Observation Errors, σ_v Versus σ_ϵ ($\sigma_\rho = 183$ m)..... | XI-65 |

LIST OF ILLUSTRATIONS (continued)

| Figure | | Page |
|--------|--|-------|
| 25 | Angular Observation Errors, σ_r Versus σ_ϵ ($\sigma_\rho = 183$ m) | XI-65 |
| 26 | Angular Observation Errors, σ_a Versus σ_ϵ ($\sigma_\rho = 183$ m) | XI-66 |
| 27 | Angular Observation Errors, σ_e Versus σ_ϵ ($\sigma_\rho = 183$ m) | XI-66 |
| 28 | Angular Observation Errors, σ_i Versus σ_ϵ ($\sigma_\rho = 183$ m) | XI-67 |
| 29 | Angular Observation Errors, σ_Ω Versus σ_ϵ ($\sigma_\rho = 183$ m) | XI-67 |
| 30 | Angular Observation Errors, σ_ω Versus σ_ϵ ($\sigma_\rho = 183$ m) | XI-68 |
| 31 | Angular Observation Errors, σ_M Versus σ_ϵ ($\sigma_\rho = 183$ m) | XI-68 |
| 32 | Range Observation Errors, σ_A Versus σ_ρ ($\sigma_\epsilon = 0.05$ deg) | XI-69 |
| 33 | Range Observation Errors, σ_D Versus σ_ρ ($\sigma_\epsilon = 0.05$ deg) | XI-69 |
| 34 | Range Observation Errors, σ_v Versus σ_ρ ($\sigma_\epsilon = 0.05$ deg) | XI-70 |
| 35 | Range Observation Errors, σ_η Versus σ_ρ ($\sigma_\epsilon = 0.05$ deg) | XI-70 |

LIST OF ILLUSTRATIONS (continued)

| Figure | | Page |
|--------|---|-------|
| 36 | Range Observation Errors, σ_v Versus σ_ρ ($\sigma_\epsilon = 0.05$ deg) | XI-71 |
| 37 | Range Observation Errors, σ_r Versus σ_ρ ($\sigma_\epsilon = 0.05$ deg) | XI-71 |
| 38 | Range Observation Errors, σ_e Versus σ_ρ ($\sigma_\epsilon = 0.05$ deg) | XI-72 |
| 39 | Range Observation Errors, σ_a Versus σ_ρ ($\sigma_\epsilon = 0.05$ deg) | XI-72 |
| 40 | Range Observation Errors, σ_i Versus σ_ρ ($\sigma_\epsilon = 0.05$ deg) | XI-73 |
| 41 | Range Observation Errors, σ_Ω Versus σ_ρ ($\sigma_\epsilon = 0.05$ deg) | XI-73 |
| 42 | Range Observation Errors, σ_ω Versus σ_ρ ($\sigma_\epsilon = 0.05$ deg) | XI-74 |
| 43 | Range Observation Errors, σ_M Versus σ_ρ ($\sigma_\epsilon = 0.05$ deg) | XI-74 |

XI. ORBIT COMPUTATION

SYMBOLS

| | | | |
|------------------|--|----------------------|--|
| a | Orbit semimajor axis | x | } Cartesian coordinates. See section A.1 for definitions of the various coordinate systems |
| A | Right ascension | y | |
| c | Speed of light; also, variance-covariance matrix | z | |
| D | Declination | α | Azimuth angle |
| e | Orbit eccentricity | δ | Residual |
| E | Eccentric anomaly | ϵ | Elevation angle |
| f | Flattening; also, two-way phase coherent Doppler frequency shift | η | Angle of the velocity vector with north on the local horizontal plane; also, sector-triangle ratio |
| f_{non} | Noncoherent Doppler frequency | θ | True anomaly |
| h | Altitude above the surface of the earth | ι | Obliquity of the ecliptic |
| H | Hour angle | λ | Celestial longitude |
| i | Inclination of the orbit to the equatorial plane | Λ | Geocentric longitude |
| l | Celestial latitude | μ | Gravitational constant; also, mean value |
| L | Geocentric latitude | $\hat{\mu}$ | Maximum likelihood estimator for the mean |
| L' | Geodetic latitude | ν | Angle of the velocity vector to the local geocentric vertical; also, refractive index |
| m | Mass | ρ | Range, the distance from the observer to a body |
| M | Mean anomaly | $\dot{\rho}$ | Range rate |
| N | Electron density | σ | Standard deviation |
| p | Semilatus rectum (semiparameter) | $\hat{\sigma}^2$ | Maximum likelihood estimate of the variance |
| r | Radius vector | τ | Orbit period |
| R | Radius of the earth | ω | Argument of perigee |
| R_c | Radius of the earth at the observation site | Ω | Right ascension or longitude of the ascending node |
| t | Time | Ω_e | Rotation rate of the earth, 0.7292115×10^{-4} rad/sec |
| t_p | Time when the vehicle encounters perigee | Υ | Vernal equinox (Aries) |
| t_s | Local sidereal time | $\underline{\Omega}$ | Autumnal equinox (Libra) |
| T | Transformation matrix | | |
| v | Velocity; also, diagonal matrix of the inverse variances | | |

A. INTRODUCTION

The basic problem of orbit computation is the determination, from a set of observations, of six parameters which define an orbit. These parameters may be the Cartesian position and velocity components at some epoch, the classical orbit elements (semimajor axis, eccentricity, inclination, argument of perigee, longitude of ascending node, and mean anomaly at epoch), or any other set of independent quantities which uniquely determine the orbit. The orbit computation problem may involve determination of quantities other than the six orbit parameters, however. For example, improved values of physical constants, drag coefficients, tracking station locations or thrust corrections may also be determined in the orbit computation process.

Whether the goal of a satellite vehicle mission is gathering of accurate geophysical data or safe recovery of a manned capsule, accurate orbit computation is a prime requirement since gravity field or atmospheric density information is only as accurate as the satellite position time-histories from which it is derived. In addition, there is a requirement for continual precise knowledge of the position of manned satellites for the safety of the pilot. The increasing requirement for fast, highly accurate determination of orbits has led to many new developments of theories, techniques and systems as well as modifications of existing astronomical methods. This chapter comprises a general exposition of some methods and system capabilities for locating an earth satellite and predicting its future positions and velocities. Specifically, the areas considered are tracking networks and their capabilities, tracking techniques, data reduction, initial determination of the orbit elements and improvement of the computed orbit.

B. COORDINATE SYSTEMS AND TRANSFORMATIONS

1. Coordinate System Definition

In the determination of orbits a multitude of coordinate systems are frequently used. It is convenient to define these various systems before considering the principal problem of orbit determination, so that the definitions will be available for reference.

Complete specification of a coordinate system involves three geometric quantities, an origin, a principal direction and a fundamental plane. For example, the origin might be an observer on the earth's surface (a topocentric system), the center of the earth (a geocentric system), the center of the moon (selenocentric), the center of the sun (heliocentric), or any other convenient point. The principal direction might be the south point on the horizon, vernal equinox, or any of a number of such directions; and the fundamental plane might be one of the customary planes of reference, i. e., the local horizontal, equatorial or ecliptic planes, or any other convenient plane. In addition, coordinate systems may be time dependent (rotating systems) or fixed in spatial orientation (inertial systems). Table 1

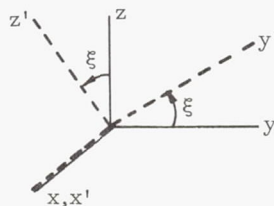
defines the most frequently used systems of coordinates. A list of definitions of the various terms involved in this table and subsequent discussions is presented in Appendix B.

2. Transformation of Coordinates

A rotation ξ about a certain axis is considered positive if counterclockwise as viewed from the positive end of that axis. The general forms for rotations of $+\xi$ about the x, y, and z axes are as follows:

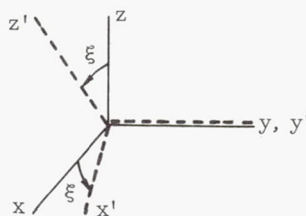
$$\begin{bmatrix} x' \\ y' \\ z' \end{bmatrix} = \begin{bmatrix} 1 & 0 & 0 \\ 0 & \cos \xi & \sin \xi \\ 0 & -\sin \xi & \cos \xi \end{bmatrix} \begin{bmatrix} x \\ y \\ z \end{bmatrix} \quad (1)$$

$$\equiv T_{x, \xi} \{x, y, z\}$$



$$\begin{bmatrix} x' \\ y' \\ z' \end{bmatrix} = \begin{bmatrix} \cos \xi & 0 & -\sin \xi \\ 0 & 1 & 0 \\ \sin \xi & 0 & \cos \xi \end{bmatrix} \begin{bmatrix} x \\ y \\ z \end{bmatrix} \quad (2)$$

$$\equiv T_{y, \xi} \{x, y, z\}$$



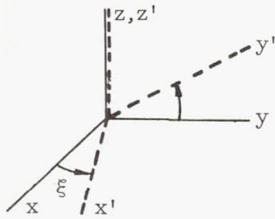
$$\begin{bmatrix} x' \\ y' \\ z' \end{bmatrix} = \begin{bmatrix} \cos \xi & \sin \xi & 0 \\ -\sin \xi & \cos \xi & 0 \\ 0 & 0 & 1 \end{bmatrix} \begin{bmatrix} x \\ y \\ z \end{bmatrix} \quad (3)$$

$$\equiv T_{z, \xi} \{x, y, z\}$$

These general rules may be used to derive transformations between the various coordinate systems defined in the preceding subsection.

TABLE 1
Coordinate Systems

| Coordinate System | Basis | Origin | Principal Direction | Principal Plane | Poles | Secondary Great Circles | Parallels | Angular Coordinates | Cartesian Coordinates | Transformation References (sections) |
|-------------------------------------|---------------------------------------|--|---|-----------------|--|-----------------------------|--------------------------|--|--|---|
| Geocentric (geographic) (rotating) | Rotation of earth | Center of earth | Intersection of greenwich meridian with equatorial plane | Equatorial | North and south terrestrial poles (or north and south celestial poles) | Meridians | Parallels of latitude | Geocentric latitude L Geocentric longitude Λ | | B. 2. a (geodetic) B. 2. d (topocentric) |
| Geodetic (rotating) | Reference spheroid, rotation of earth | Intersection of normal to geoid with major axis of earth | Intersection of greenwich meridian with equatorial plane | Equatorial | North and south celestial poles | Meridians | Parallels of latitude | Geodetic latitude L Geodetic longitude Λ | | B. 2. a (geocentric) B. 2. f (general) |
| Topocentric (horizontal) (rotating) | Direction of gravity | Observer | South point of horizon | True horizon | Zenith and nadir | Vertical circles | Almucantars | Azimuth α Elevation ϵ | x_{oh} y_{oh} z_{oh} | B. 2. b B. 2. c |
| Equatorial (rotating) | Rotation of earth | Observer or center of earth | Intersection of observer's meridian with equatorial plane | Equator of date | North and south terrestrial poles | Meridians | Parallels of latitude | Declination D or geocentric latitude L Hour angle H or relative longitude $\Delta\Lambda$ | x_r y_r z_r | |
| Earth centered inertial (ECI) | Diurnal motion of celestial sphere | Center of earth | Vernal equinox of date | Equator of date | North and south celestial poles | Hour circles | Parallels of declination | Declination $D = L$ Right ascension A | x_e y_e z_e | B. 2. e (general) B. 2. h (orbit) |
| General equatorial (inertial) | Diurnal motion of celestial sphere | Any convenient point | Intersection of any convenient secondary circle with the equatorial plane | Equator of date | North and south celestial poles | Meridians | Parallels of declination | Declination D Relative right ascension ΔA | x_i y_i z_i | B. 2. e (ECI) B. 2. f (geodetic) B. 2. g (ecliptic) |
| Orbit (inertial) | Orbital motion of satellite vehicle | Focus | Orbit major axis in direction of perifocus | Orbit plane | Normal to orbit plane | | | True anomaly θ | x_ω y_ω z_ω | B. 2. h (ECI) |
| Ecliptic (inertial) | Orbital motion of earth | Any convenient point | Vernal equinox of date | Ecliptic | Ecliptic poles | Secondaries to the ecliptic | Parallels of latitude | Celestial latitude ℓ Celestial longitude λ | x_ϵ y_ϵ z_ϵ | B. 2. g. (general) |
| Galactic (inertial) | Geometry of visible universe | Any convenient point | Intersection of galactic circle with celestial equator | Galactic circle | Galactic poles | Secondaries to the galactic | Parallels of latitude | Galactic latitude Galactic longitude | | |



Transformation of geodetic latitude L' to geocentric latitude L

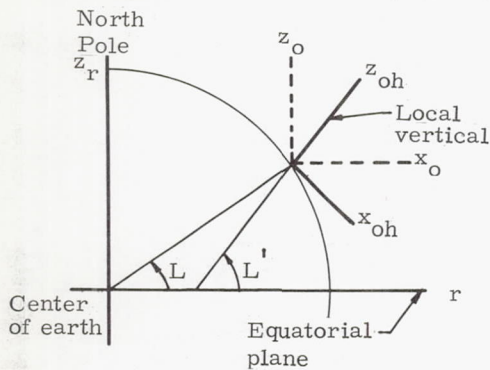
$$L = L' - 695''.6635 \sin 2L' + 1''.1731 \sin 4L'$$

$$-0''.0026 \sin 6L' \quad (4)$$

or $\tan L = (1-f)^2 \tan L'$ where

$$f = \frac{1}{298.24} = \text{flattening}$$

Transformation from topocentric horizontal (x_{oh}, y_{oh}, z_{oh}) axes to topocentric equatorial (x_o, y_o, z_o) rotating axes

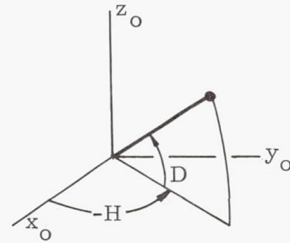
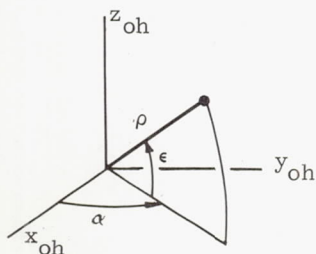


$$\begin{bmatrix} x_o \\ y_o \\ z_o \end{bmatrix} = \begin{bmatrix} \sin L' & 0 & \cos L' \\ 0 & 1 & 0 \\ -\cos L' & 0 & \sin L' \end{bmatrix} \begin{bmatrix} x_{oh} \\ y_{oh} \\ z_{oh} \end{bmatrix} \quad (5)$$

polar coordinates:

$$\left. \begin{aligned} x_{oh} &= \rho \cos \epsilon \cos \alpha \\ y_{oh} &= \rho \cos \epsilon \sin \alpha \\ z_{oh} &= \rho \sin \epsilon \end{aligned} \right\} \quad (6)$$

where ϵ = elevation, α = azimuth



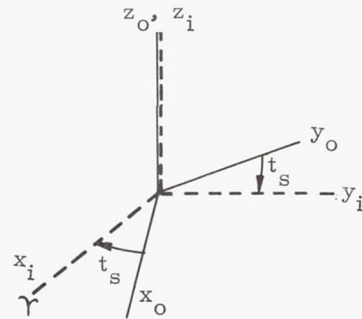
$$\begin{aligned} \sin D &= \sin L' \sin \epsilon - \cos L' \cos \epsilon \cos \alpha \\ \sin H &= -\frac{\sin \alpha \cos \epsilon}{\cos D} \end{aligned} \quad (7)$$

Transformation from topocentric equatorial (x_o, y_o, z_o) rotating axes to topocentric equatorial inertial axes (x_i, y_i, z_i)

$$\begin{bmatrix} x_i \\ y_i \\ z_i \end{bmatrix} = \begin{bmatrix} \cos t_s & -\sin t_s & 0 \\ \sin t_s & \cos t_s & 0 \\ 0 & 0 & 1 \end{bmatrix} \begin{bmatrix} x_o \\ y_o \\ z_o \end{bmatrix} \quad (8)$$

where

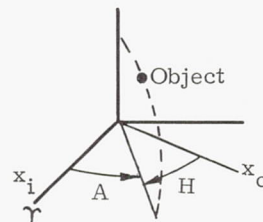
- t_s = local sidereal time
- = hour angle of vernal equinox
- = right ascension of local meridian.



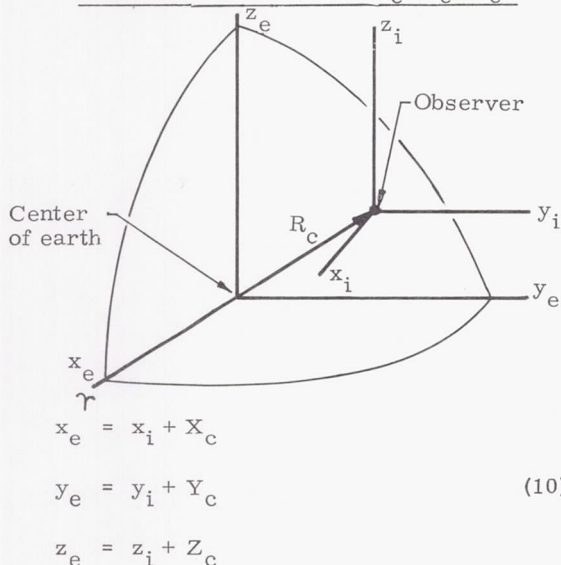
The polar coordinates are related as follows:

$$A = t_s - H \quad (9)$$

D is the same as in subsection b.



Transformation from topocentric equatorial inertial axes (x_i, y_i, z_i) to geocentric equatorial inertial axes (x_e, y_e, z_e)



where

$$\begin{aligned} X_c &= (C + h_o) \cos L' \cos t_s \\ Y_c &= (C + h_o) \cos L' \sin t_s \\ Z_c &= (S + h_o) \sin L' \end{aligned} \quad (11)$$

are the coordinates of the observer in the equatorial inertial system and

t_s = local sidereal time

L' = geodetic latitude

h_o = observer's height above sea level in units of the equatorial radius of the earth

$$C = \frac{1}{\sqrt{1 - (2f - f^2) \sin^2 L'}}$$

$$S = C(1 - f)^2$$

$$f = \frac{1}{298.24} = \text{flattening of the earth}$$

(C and S , as defined by $\frac{R_c}{R_e} \sin L = S \sin L'$ and

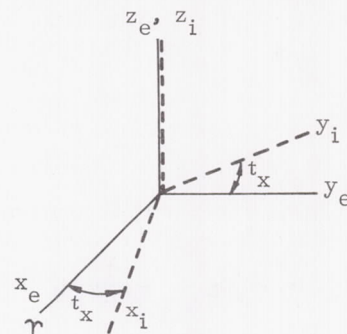
$\frac{R_c}{R_e} \cos L = C \cos L'$, are tabulated in the American Ephemeris and Nautical Almanac).

$$\begin{aligned} R_c &= R_e C \sqrt{\cos^2 L' + (1 - f)^4 \sin^2 L'} \\ &= \frac{R_e (1 - f)}{\sqrt{1 + f(f - 2) \cos^2 L}} \end{aligned} \quad (12) \quad (13)$$

where

R_e = equatorial radius.

Transformation from general equatorial inertial coordinates (x_i, y_i, z_i) to earth-centered inertial axes (x_e, y_e, z_e)



$$\begin{bmatrix} x_e \\ y_e \\ z_e \end{bmatrix} = \begin{bmatrix} \cos t_x & -\sin t_x & 0 \\ \sin t_x & \cos t_x & 0 \\ 0 & 0 & 1 \end{bmatrix} \begin{bmatrix} x_i \\ y_i \\ z_i \end{bmatrix} \quad (14)$$

where

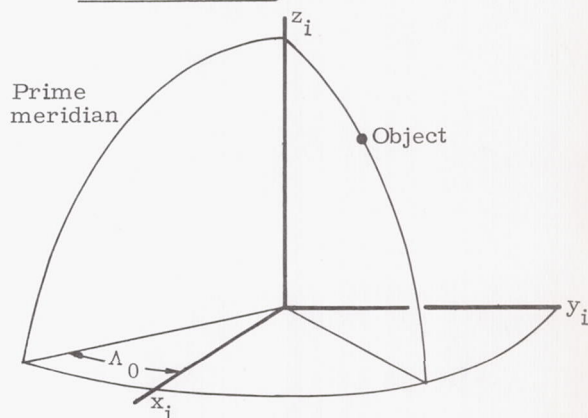
t_x = right ascension of the x_i -axis meridian

$$A = t_x + \Delta \Lambda \quad (15)$$

D is the same as in subsection b

$\Delta \Lambda$ = difference in geocentric longitude between the x_i -axis and the object being located.

Transformation from general equatorial inertial coordinates (x_i, y_i, z_i) to geodetic coordinates



Geodetic or geocentric longitude:

$$\Lambda = \Lambda_0 + \tan^{-1} \frac{y_i}{x_i} - \frac{\Omega_e}{\Delta t} \quad (16)$$

Geodetic latitude:

$$L' = \tan^{-1} \left[\frac{1}{(1-f)^2} \frac{z_i}{\sqrt{x_i^2 + y_i^2}} \right] \quad (17)$$

where

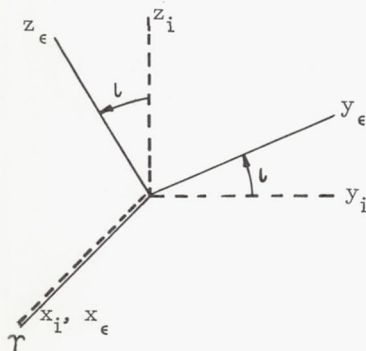
Λ_0 = geodetic longitude of the prime direction x_i at the time of transformation

Ω_e = rotation rate of the earth,
 0.7292115×10^{-4} rad/sec

Δt = time elapsed since the time of transformation

f = flattening = $\frac{1}{298.24}$

Transformation from equatorial inertial coordinates (x_i, y_i, z_i) to ecliptic inertial coordinates (x_e, y_e, z_e)



$$\begin{bmatrix} x_e \\ y_e \\ z_e \end{bmatrix} = \begin{bmatrix} 1 & 0 & 0 \\ 0 & \cos l & \sin l \\ 0 & -\sin l & \cos l \end{bmatrix} \begin{bmatrix} x_i \\ y_i \\ z_i \end{bmatrix} \quad (18)$$

or, since

$$\begin{aligned} x_i &= r_i \cos D \cos A \\ y_i &= r_i \cos D \sin A \\ z_i &= r_i \sin D \end{aligned} \quad (19)$$

and

$$\begin{aligned} x_e &= r_e \cos l \cos \lambda \\ y_e &= r_e \cos l \sin \lambda \\ z_e &= r_e \sin l \end{aligned} \quad (20)$$

$$\cos l \cos \lambda = \cos D \cos A$$

$$\cos l \sin \lambda = \cos l \cos D \sin A + \sin l \sin D \quad (21)$$

$$\sin l = -\sin l \cos D \sin A + \cos l \sin D$$

where

l = obliquity of the ecliptic

$$= 23^\circ 27' 08''.26 - 0''.4684 (t_{\text{years}} - 1900)$$

$r_i = r_e$ = radius vector

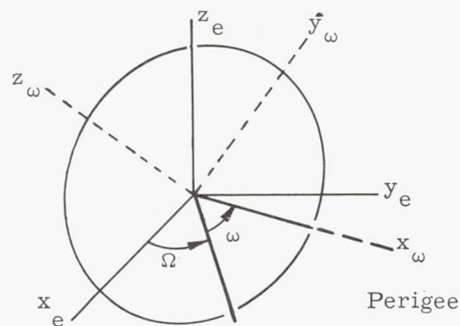
A = right ascension

D = declination

l = celestial latitude

λ = celestial longitude.

Transformation from orbit system coordinates (x_w, y_w, z_w) to earth-centered inertial coordinates (x_e, y_e, z_e)



Rotation routine:

- (1) Rotation in the orbit plane about the z_w axis through $-\omega$, $T_{-\omega}$
- (2) Rotation about the line of nodes through $-i$, T_{-i}
- (3) Rotation in the equatorial plane through $-\Omega$, $T_{-\Omega}$

then

$$\{x_e, y_e, z_e\} = T_{-\Omega} T_{-i} T_{-\omega} \{x_w, y_w, z_w\} \quad (22)$$

where

$$T_{-\Omega} T_{-i} T_{-\omega} = \begin{bmatrix} \cos \Omega \cos \omega & -\cos \Omega \sin \omega & \sin \Omega \sin i \\ -\sin \Omega \cos i \sin \omega & -\sin \Omega \cos i \cos \omega & -\cos \Omega \sin i \\ \sin \Omega \cos \omega & -\sin \Omega \sin \omega & \cos i \\ +\cos \Omega \cos i \sin \omega & +\cos \Omega \cos i \cos \omega & \sin i \\ \sin i \sin \omega & \sin i \cos \omega & \cos i \end{bmatrix}$$

The elements of this transformation matrix are frequently assigned the following symbols for convenience:

$$T_{-\Omega} T_{-i} T_{-\omega} = \begin{bmatrix} P_x & Q_x & R_x \\ P_y & Q_y & R_y \\ P_z & Q_z & R_z \end{bmatrix} \quad (23)$$

3. Data Correction

Various data corrections are usually required to convert apparent coordinates to true coordinates. Depending on the nature of the measurement, corrections may be required to account for aberration, refraction, precession, proper motion, nutation and parallax.

a. Aberration

Since light travels at a finite velocity, the apparent coordinates of any body in space depend upon the motion of the body and the motion of the observer on earth during the time interval required for light from the body to arrive at the observer. This apparent displacement of a body from its actual position due to the finite speed of light and the motions of the observer and the body is called aberration. To elaborate, the observer perceives a ray of light which originated at the body sometime before the instant of observation and which traveled toward a position that the earth would occupy sometime after the ray originated. Therefore, at the time of observation, the moving body is no longer located in the direction from which the light ray is observed. Also, since the earth is moving, the apparent direction of the ray differs from the true direction. Thus the observed direction relative to the stars is neither the actual direction at the time of observation nor the direction to the position of the body at the time the ray was emitted.

Various types of aberration are distinguished. Planetary aberration is the displacement of the observed apparent position from the actual position at the instant of observation. Stellar aberration, a part of the planetary aberration, is the displacement of the observed position from the actual position of the body at the instant when the light ray was emitted. The stellar aberration consists of two parts, diurnal aberration and annual aberration. Diurnal aberration is that part due to the rotation of the earth on its axis. Annual aberration is due to the orbital motion of the earth about the sun.

Obviously, most corrections for aberration are significant only for astronomical determinations on relatively remote bodies. Even for observations of the sun, only stellar aberration need be considered. In the case of a satellite, observed as to its distance and angular position relative to the earth, the stellar aberration may be neglected as being essentially the same for the satellite and the earth. Also, a satellite experiences very nearly the same heliocentric motion as the earth. Therefore, aberration corrections for satellites in practice need include only the effect of motion of the satellite relative to the earth during the

time required for light from the satellite to arrive at the observer. (For example, during the time for light to pass from the moon to the earth, the moon moves about 0."7 in geocentric longitude.) Planetary aberration is larger for artificial satellites. In a circular satellite orbit, central angle traversed is proportional to time, i.e.,

$$\frac{\Delta\theta}{2\pi} = \frac{t}{\tau} \quad (\Delta\theta \text{ in radians}).$$

Since the period is

$$\tau = 2\pi r \sqrt{\frac{r}{\mu}},$$

$$\Delta\theta = \frac{t}{r} \sqrt{\frac{\mu}{r}}$$

where r is the satellite orbit radius. The time required for light to travel from an overhead satellite to the earth is

$$t = \frac{r - R}{c}$$

where R is the radius of the earth and c is the speed of light. Therefore, the planetary aberration is

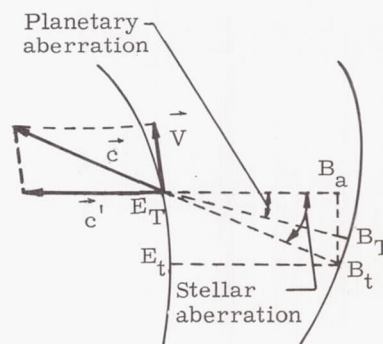
$$\Delta\theta = \frac{r - R}{cr} \sqrt{\frac{\mu}{r}}.$$

This quantity has a maximum for $r = 3R$,

$$\Delta\theta_{\max} \approx 2".1$$

The following sections briefly consider methods used for computing the effect of aberration. A more detailed description is contained in Ref. 1.

(1) Stellar aberration



In stellar aberration determinations the following notation is used:

\vec{v} = earth's orbital velocity in inertial, fixed-origin coordinates (x, y, z)

\vec{c} = velocity vector of the actual light ray

\vec{c}' = relative velocity vector of the light ray

T = instant when an observation is made

t = earlier time when the ray observed left the body

E_T, E_t = actual positions of the earth at the times T and t, respectively

B_T, B_t = actual positions of a body at the times T and t, respectively

B_a = apparent position of the body at time T

$\tau = T - t$ = time for light to travel from the body to earth

$\rho = \tau c$ = geometric distance $E_T B_t$

Λ_a, Λ_T = longitudes of the apparent direction $E_T B_a$ and the true light path $E_T B_T$, respectively

L_a, L_T = latitudes corresponding to Λ_a, Λ_T .

Then the direction cosines of $E_T B_a$ are

$$\begin{aligned}\cos L_a \cos \Lambda_a &= \cos L_T \cos \Lambda_T + \frac{v_x}{c} \\ \cos L_a \sin \Lambda_a &= \cos L_T \sin \Lambda_T + \frac{v_y}{c} \\ \sin L_a &= \sin L_T + \frac{v_z}{c}\end{aligned}\quad (24)$$

where V_x, V_y, V_z are the components of v

These direction cosines give

$$\begin{aligned}\tan (\Lambda_a - \Lambda_T) &= \frac{-\sec L_T (v_x \sin \Lambda_T - v_y \cos \Lambda_T)}{c + \sec L_T (v_x \cos \Lambda_T + v_y \sin \Lambda_T)} \\ \tan (L_a - L_T) &= \frac{v_z \cos L_T - (v_x \cos \Lambda_T + v_y \sin \Lambda_T) \sin L_T}{v_z \sin L_T + (v_x \cos \Lambda_T + v_y \sin \Lambda_T) \cos L_T + c} \\ &+ O\left(\sin^2 \frac{\Lambda_a - \Lambda_T}{2}\right)\end{aligned}\quad (25)$$

where:

$O\left(\sin^2 \frac{\Lambda_a - \Lambda_T}{2}\right)$ denotes terms of the order of the quantity in the brackets.

In rectangular coordinates,

$$\begin{aligned}X_a - X_t &= \frac{v_x \rho_t}{c} = v_x \tau \\ Y_a - Y_t &= \frac{v_y \rho_t}{c} = v_y \tau\end{aligned}$$

$$Z_a - Z_t = \frac{v_z \rho_t}{c} = v_z \tau \quad (26)$$

where

(X_a, Y_a, Z_a) are the apparent coordinates of the body at the instant of observation T

(X_t, Y_t, Z_t) are the true coordinates of the body at the time the light left the body.

(2) Planetary aberration

The planetary aberration is the stellar aberration corrected for the motion of the body from B_t to B_T during the time for light from the body to reach earth (see previous sketch). This correction may be computed from a Taylor series, e.g.,

$$X_T - X_t = \dot{X}_t \tau + \frac{1}{2} \ddot{X}_t \tau^2 + \frac{1}{6} \dddot{X}_t \tau^3 + \dots$$

Then the rectangular components of the planetary aberration are

$$\begin{aligned}X_a - X_T &= (V_x - \dot{X}_t) \tau - \frac{1}{2} \ddot{X}_t \tau^2 - \frac{1}{6} \dddot{X}_t \tau^3 \dots \\ Y_a - Y_T &= (V_y - \dot{Y}_t) \tau - \frac{1}{2} \ddot{Y}_t \tau^2 - \frac{1}{6} \dddot{Y}_t \tau^3 \dots \\ Z_a - Z_T &= (V_z - \dot{Z}_t) \tau - \frac{1}{2} \ddot{Z}_t \tau^2 - \frac{1}{6} \dddot{Z}_t \tau^3 \dots\end{aligned}\quad (27)$$

where (X_t, Y_t, Z_t) are given in the preceding subsection. The terms of order τ^2 and higher can usually be neglected. In terms of right ascension and declination the planetary aberration can then be expressed as

$$\begin{aligned}\Delta A &= -A \frac{R_T}{c} \\ \Delta D &= -D \frac{R_T}{c}\end{aligned}\quad (28)$$

$$\text{where } R_T = \sqrt{X_T^2 + Y_T^2 + Z_T^2}$$

(3) Diurnal aberration

Because of the earth's rotation, the observer moves toward the east at a rate

$$\zeta = 464 \frac{R_c}{R_e} \cos L \quad \text{meters/sec} \quad (29)$$

where

R_c = radius of the earth at the observer's location

R_e = equatorial radius of the earth

L = geocentric latitude of the observer.

This motion causes a shift in apparent position of remote bodies toward the east given by

$$\frac{\zeta}{\alpha} \sin \xi$$

where ξ is the angular distance from the east point to the body. Then, in terms of right ascension and declination, the diurnal aberration is

$$\left. \begin{aligned} \Delta A &= 0''.319 \frac{R_c}{R_e} \cos L \cos H \sec D \\ \Delta D &= 0''.319 \frac{R_c}{R_e} \cos L \sin H \sin D \end{aligned} \right\} \quad (30)$$

where H = hour angle of the body.

The effect of diurnal aberration may be neglected except where relative positions of widely separated bodies are being measured.

(4) Annual aberration

The annual aberration, due to the earth's orbital motion, in terms of right ascension and declination is

$$\begin{aligned} \Delta A &= C_1 c_1 + C_2 c_2 \\ \Delta D &= C_1 c_1' + C_2 c_2' \end{aligned} \quad (31)$$

where

$$\begin{aligned} c_1 &= \cos A \sec D \\ c_2 &= \sin A \sec D \\ c_1' &= \tan \iota \cos D - \sin A \sin D \quad [\iota = \text{obliquity}] \\ c_2' &= \cos A \sin D \end{aligned}$$

and

$$C_1 = -20''.47 \cos \lambda_{\odot} \cos \iota$$

$[\lambda_{\odot} = \text{true longitude of sun}]$

$$C_2 = -20''.47 \sin \lambda_{\odot}$$

are tabulated in the American Ephemeris.

b. Precession

Precession is the combination of the slow change of direction of the earth's axis of rotation and the slower change of direction of the axis perpendicular to the ecliptic. The first effect is due to the action of the sun and the moon (luni-solar precession), the second is due to the action of the planets (planetary precession).

As a result of precession the vernal equinox is slowly regressing at a rate of about 50 sec of arc per year; therefore, any coordinate system which has as the principal direction the vernal equinox must specify a date to which it is referred.

To change from one equatorial system, say

referred to the mean equinox of date, to another, say to the mean equinox of some other standard date (like 1950.0), the following operations should be performed:

$$\begin{aligned} x_d &= X_x x_{1950} + Y_x y_{1950} + Z_x z_{1950} \\ y_d &= X_y x_{1950} + Y_y y_{1950} + Z_y z_{1950} \\ z_d &= X_z x_{1950} + Y_z y_{1950} + Z_z z_{1950} \end{aligned} \quad (32)$$

or

$$\begin{aligned} x_{1950} &= X_x x_d - Y_x y_d - Z_x z_d \\ y_{1950} &= -X_y x_d + Y_y y_d + Z_y z_d \\ z_{1950} &= -X_z x_d + Y_z y_d + Z_z z_d \end{aligned}$$

where the subindex

d = mean equinox of date

1950 = mean equinox of 1950.0

and

$$X_x = 1.000\,000\,00 - 0.000\,296\,97\,T^2 - 0.000\,000\,13\,T^3$$

$$Y_x = -X_y = -0.022\,349\,88\,T - 0.000\,006\,76\,T^2 + 0.000\,002\,21\,T^3$$

$$Z_x = -X_z = -0.009\,717\,11\,T + 0.000\,002\,07\,T^2 + 0.000\,000\,96\,T^3$$

$$Y_y = 1.000\,000\,00 - 0.000\,249\,76\,T^2 - 0.000\,000\,15\,T^3$$

$$Z_y = Y_z = -0.000\,108\,59\,T^2 - 0.000\,000\,03\,T^3$$

$$Z_z = 1.000\,000\,00 - 0.000\,047\,21\,T^2 + 0.000\,000\,02\,T^3$$

where T is measured in Julian centuries from 1950.0.

The Julian Calendar is discussed and a table presenting Julian Day Numbers presented in Chapter II.

$T = [\text{Julian date number for epoch} -$

Julian date number for 1950.0] / 36525

c. Nutation

Due to the solar and lunar attractions on the equatorial protuberance of the earth, the celestial pole travels in a small ellipse around its mean position on the circular precessional path. The correction for nutation is very small and may generally be neglected except in precise astronomical determinations.

Tables for nutation in longitude and in obliquity are tabulated in the American Ephemeris and Nautical Almanac each year. An explanation of how those tables are obtained is given in Astronomical Papers of the American Ephemeris, vol. XV, Part I, p. 153, 1953, and in the joint supplement to the American Ephemeris and Nautical Almanac entitled "Improved Lunar Ephemeris 1952 - 1959," pp. ix-x, 1954.

To obtain rectangular coordinates referred to the mean equinox of date when those referred to the true equinox are available, perform the following computations:

$$\begin{aligned}x &= x_d x_y - y_d y_z - z_d z_z \\y &= -x_d x_y + y_d y_z + z_d z_z \\z &= -x_d x_z + y_d y_z + z_d z_z\end{aligned}\quad (33)$$

where

$$\begin{aligned}z_z &= y_y = x_x = 1 \\-y_x &= x_y = \Delta\psi \cos l \sin 1'' \\-z_x &= x_z = \Delta\psi \sin l \sin 1'' \\-z_y &= y_z = \Delta l \sin 1'' \\l &= \text{obliquity of ecliptic}\end{aligned}$$

and

Δl and $\Delta\psi$ are, respectively, the rates of nutation in obliquity and in longitude (obtained from the tables mentioned above) in units of seconds of arc.

d. Refraction

Refraction is another source of deviation between the apparent and true directions of optical or radio measurements. The curvature of electromagnetic rays due to refraction is greatest for measurements of small elevation above the horizontal plane. From Snell's law, the correction to be added to the observed elevation is

$$\Delta\epsilon = \int_b^o \frac{ds}{\rho_c} = - \int_b^o \frac{\hat{n} \cdot \nabla \nu}{\nu} ds \quad (34)$$

where the integral along the ray path is taken from the body observed, b, to the observer, o, and

$$\begin{aligned}\rho_c &= \text{radius of curvature of the ray path} \\ \nu &= \text{refractive index} \\ \hat{n} &= \text{unit vector normal to the ray path} \\ s &= \text{arc length along the ray path}\end{aligned}$$

Specification of the variation in ν along the path may be very difficult. One approach is numerical

integration of the integral expressed as

$$\sum_i a_i \tan^{(2i+1)} z_a$$

where the a_i 's are empirical coefficients and z_a is the apparent zenith distance. In several studies of radio wave refraction, two components of the refractive index are distinguished:

tropospheric refraction:

$$\begin{aligned}(\nu - 1) 10^6 &= \frac{103.49}{K} (p_a - p_w) + \left[\frac{86.26}{K} \right. \\ &\quad \left. \cdot \left(1 + \frac{5748}{K} \right) p_w \right]\end{aligned}\quad (35)$$

where

$$\begin{aligned}p_a &= \text{air pressure, mm of mercury} \\ p_w &= \text{water pressure, mm of mercury} \\ K &= \text{temperature in degrees Kelvin}\end{aligned}$$

or

$$\begin{aligned}\nu - 1 &= 105 \times 10^{-6} e^{-0.142(h-a)} \\ &(\pm 15\%, h \geq 9 \text{ km})\end{aligned}$$

ionospheric refraction:

$$\nu = \sqrt{1 - \frac{4\pi N \epsilon^2}{\epsilon_0 m \omega^2}} = \sqrt{1 - \frac{3.18 \times 10^9 N}{\omega^2}} \quad (36)$$

where

$$\begin{aligned}N &= \text{electron density, electrons/cm}^3 \\ \epsilon &= \text{charge of the electron} \\ m &= \text{mass of an electron} \\ \epsilon_0 &= \text{dielectric constant} \\ \omega &= \text{frequency in radians per second}\end{aligned}$$

Electron density is tabulated in Chapter II. Ref (2) enumerates the phase changes which occur in propagation for the various radio tracking techniques:

Range measurement:

$$\Delta\phi_t = \frac{\omega}{c} \left(\int_{\text{up}} \nu ds + \int_{\text{down}} \nu ds \right) \quad (37)$$

Doppler measurement:

$$\begin{aligned}\Delta\phi &= \frac{\omega}{c} \frac{d}{dt} \left(\int \nu ds \right) = \frac{\omega}{c} \left(\nu_b \hat{t}_b \cdot \dot{\hat{\rho}} + \int \frac{\partial \nu}{\partial t} ds \right) \\ &(\text{assuming isotropic } \nu)\end{aligned}\quad (38)$$

Interferometer measurement :

$$\Delta \phi_s = \frac{\omega}{c} \left(\int_1 v ds - \int_2 v ds \right) \quad (39)$$

$$\delta \Delta \phi = \frac{\omega}{c} \Delta x \sin \epsilon \Delta \epsilon \quad (40)$$

where the integrals are taken over the ray path and

ρ = range

$\Delta \phi_t$ = temporal phase difference

$\Delta \phi_s$ = spatial phase difference

$\Delta \dot{\phi}$ = difference in rate of change of phase

ω = frequency (rad/sec)

c = speed of light

ν = refractive index

b = subscript indicating a value of the body

\hat{t} = unit vector tangent to the ray

Δx = interferometer baseline length

and $\Delta \epsilon$ = is defined in Eq (34)

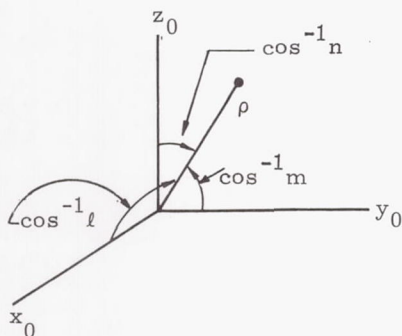
4. Data conversions

Transformation between topocentric coordinates and direction cosine data

$$l = \cos \epsilon \cos \alpha = \frac{x_{oh}}{\rho}$$

$$m = \cos \epsilon \sin \alpha = \frac{y_{oh}}{\rho}$$

$$n = \sqrt{1 - l^2 - m^2} = \sin \epsilon = \frac{z_{oh}}{\rho} \quad (41)$$



From the differentials of these relations

$$dl = \frac{dx_{oh}}{\rho} - \frac{x_{oh}}{\rho^3} (x_{oh} dx_{oh} + y_{oh} dy_{oh} +$$

(continued)

$$\begin{aligned} & + z_{oh} dz_{oh}) \\ dm &= \frac{dy_{oh}}{\rho} - \frac{y_{oh}}{\rho^3} (x_{oh} dx_{oh} + y_{oh} dy_{oh} \\ & + z_{oh} dz_{oh}) \\ dn &= \frac{dz_{oh}}{\rho} - \frac{z_{oh}}{\rho^3} (x_{oh} dx_{oh} + y_{oh} dy_{oh} \\ & + z_{oh} dz_{oh}) \end{aligned}$$

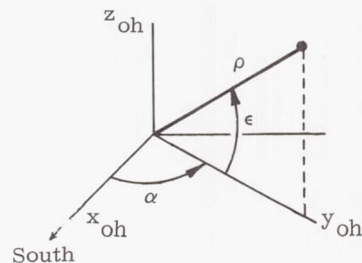
the correction relationship is

$$\begin{bmatrix} d\ell \\ dm \\ dn \end{bmatrix} = \begin{bmatrix} 1 - l^2 & -lm & -ln \\ -lm & 1 - m^2 & -mn \\ -ln & -mn & 1 - n^2 \end{bmatrix} \begin{bmatrix} \frac{dx_{oh}}{\rho} \\ \frac{dy_{oh}}{\rho} \\ \frac{dz_{oh}}{\rho} \end{bmatrix} \quad (42)$$

$$\equiv T_I \left\{ \frac{d\vec{r}_{oh}}{\rho} \right\}$$

Transformation between topocentric coordinates and radar data

$$\begin{aligned} x_{oh} &= \rho \cos \epsilon \cos \alpha \\ y_{oh} &= \rho \cos \epsilon \sin \alpha \\ z_{oh} &= \rho \sin \epsilon \end{aligned} \quad (43)$$



where

ρ = range

α = azimuth

ϵ = elevation

The inverse relationships are

$$\begin{aligned} \rho &= \sqrt{x_{oh}^2 + y_{oh}^2 + z_{oh}^2} \\ \sin \epsilon &= \frac{z_{oh}}{\rho} \\ \tan \alpha &= \frac{y_{oh}}{x_{oh}} \end{aligned} \quad (44)$$

The sensitivities of topocentric coordinates to radar data corrections are obtained from the differentials of the above expressions.

$$\begin{aligned}
 d\rho &= \frac{1}{\rho} (x_{oh} dx_{oh} + y_{oh} dy_{oh} + z_{oh} dz_{oh}) \\
 \cos \epsilon d\epsilon &= \frac{dz_{oh}}{\rho} - \frac{z_{oh}}{\rho^2} (x_{oh} dx_{oh} + y_{oh} dy_{oh} + z_{oh} dz_{oh}) \\
 \sec^2 \alpha d\alpha &= \frac{dy_{oh}}{x_{oh}} - \frac{y_{oh}}{x_{oh}^2} dx_{oh} \\
 \begin{bmatrix} d\rho \\ \cos \epsilon d\epsilon \\ d\epsilon \end{bmatrix} &= \begin{bmatrix} \cos \epsilon \cos \alpha & \cos \epsilon \sin \alpha & \sin \epsilon \\ -\frac{1}{\rho} \sin \alpha & \frac{1}{\rho} \cos \alpha & 0 \\ -\frac{1}{\rho} \sin \epsilon \cos \alpha & -\frac{1}{\rho} \sin \epsilon \sin \alpha & \frac{1}{\rho} \cos \epsilon \end{bmatrix} \begin{bmatrix} dx_{oh} \\ dy_{oh} \\ dz_{oh} \end{bmatrix} \quad (45)
 \end{aligned}$$

The transformations of the time rates of these variables are as follows:

$$\begin{aligned}
 \dot{\rho} &= \frac{1}{\rho} (x_{oh} \dot{x}_{oh} + y_{oh} \dot{y}_{oh} + z_{oh} \dot{z}_{oh}) \\
 \dot{\alpha} &= \frac{x_{oh} \dot{y}_{oh} - y_{oh} \dot{x}_{oh}}{x_{oh}^2 + y_{oh}^2} \quad (46) \\
 \dot{\epsilon} &= \frac{z_{oh} (x_{oh} \dot{x}_{oh} + y_{oh} \dot{y}_{oh}) - \dot{z}_{oh} (x_{oh}^2 + y_{oh}^2)}{-\rho^2 \sqrt{x_{oh}^2 + y_{oh}^2}}
 \end{aligned}$$

C. ACQUISITION OF DATA

1. Tracking Techniques

Orbit data are chiefly acquired by either optical or radio techniques. Optical trackers have the advantage of extremely accurate topocentric angular measurements, and the disadvantage of not being able to measure range directly (range is found by triangulation). Radar trackers, using much longer wave lengths (1 in. to 50 ft), have the advantage of accurate line-of-sight measurements but the disadvantage of relatively poor accuracy in angular measurements. The radar trackers are able to attain their high accuracy in line-of-sight measurements because radio waves can be generated with very narrow bandwidths; hence, the measurements of single frequencies are practical. Since the velocity of electromagnetic wave propagation is known rather accurately, the range (the velocity of light times the transit time) can be measured with good accuracy. The other line-of-sight measurement based on the doppler effect involves a comparison of the transmitter frequency to the received frequency in order to deduce range rate. Since the frequencies of a light

transmitter spread out over a wide band and are uncorrelated, great difficulty is encountered in attempting to follow any one frequency and measure its Doppler effect. Only recently has pure light, with a very narrow bandwidth, been generated with high intensity.

Thus optical cameras such as the Baker-Nunn camera are used to measure the topocentric angles of satellites and radars are used for both line-of-sight measurements and angles (even though angles degrade the accuracy).

a. Optical systems

Optical systems which may be used are: Baker-Nunn camera, recording optical tracking instrument (ROTI). Cine theodolite, and ballistic cameras. A complete description of one, the Baker-Nunn camera, follows:

| | |
|----------------|---|
| Features: | field of view = $5^\circ \times 30^\circ$ focal length = 20 in. = 50.8 cm accuracies = 2" (claimed) limiting magnitude: 17.2 (when tracking object on celestial equator). |
| Description: | Modification basic Schmidt design which has wider field of view than most telescopes or cameras; uses three-element correcting system for aberrations. |
| Advantages: | Wide field of view, without excessive aberration. |
| Disadvantages: | Slow processing; no direct range or range rate measurements, sometimes takes a week to process a single photograph, sometimes the star background is too sparse. |

b. Radio trackers

Various techniques have been developed to obtain the highest accuracy from radar measurements. Three broad classes of techniques are discussed:

- (1) Radar measurements
- (2) Interferometer techniques
- (3) Special techniques to reduce measurement errors.

Radar measurements can be classified into line-of-sight measurements and angular measurements. Line-of-sight measurements are range and range rate; angular measurements are usually azimuth and elevation. Since the wave lengths of the radio waves used by radars are relatively large compared with the dimensions of the typical radar antenna, the angular measurements are usually less accurate than the line-of-sight measurements. Many systems such as Minitrack and General Electric Mod II use triangulation schemes with only range measurements. By using

at least three stations in a coherent manner, the topocentric angles of the satellite can be computed. Generally, range measurements use monopulse systems.

(1) Range measurements

There are two types of range radars.

Skin track radars depend on the reflection properties of the satellite's skin to reflect the transmitted pulse back to the receiver. Of course, the reflected pulse is greatly reduced in amplitude. Since the reflected pulse is weak, and since it is desirable to send out as many pulses as possible during a pass, complex gates must be built into the receiver and usually high redundancy must be in each pulse to help separate the signal from the noise.

Beacon track radars can either be monopulse or continuous wave-single frequency carrier types. Beacon track radars depend on a transmitter on board the satellite which can be interrogated by a ground transmitter. Since the return pulse is much stronger than that of the skin track radar, beacon track radars are more accurate in range measurements. However, the added weight of the onboard transmitter sometimes precludes using beacon track radars.

(2) Doppler systems

Another radar technique is to measure the change in carrier frequency as the satellite either recedes or approaches the radar station. One of the differences between this technique and the above pulsed systems is that the transmitter and receiver of the tracking station must be phase locked onto the satellite in order to obtain accuracy, which means that phase information of the carrier is retained. The frequency transmitted can be measured by counting its energy maxima or minima; the received frequency is measured the same way. The result is a frequency difference which is proportional to the range rate of the satellite. Range can sometimes be measured by integrating the range rate (provided the constant of integration is known).

(3) Angular measurements

Direct angular measurements (that is, not using triangulation techniques with line-of-sight measurements) can be made as follows: Suppose a radar antenna is highly directional so that when it does not point directly at the satellite (assuming a satellite beacon and neglecting refraction effects), the signal strength falls off. The signal strength is at a maximum when the antenna points directly at the satellite. When the maximum signal strength is indicated the orientation of the antenna can be measured in azimuth and elevation.

(4) Interferometer systems

Interferometer systems measure the difference in times that a radio wave front from a satellite strikes differently located tracking stations (see Fig. 1). By the time that the wave front reaches the tracking stations it is almost planar; and the approximation that

$$b \cos \epsilon = \lambda = c (t_2 - t_1)$$

is fairly accurate. The elevation ϵ can be found

from the above formula.

Minitrack is an example of a tracking system which uses the above interferometer technique in modified form. The tracking portion (distinguished from the acquisition portion) of each Minitrack "station" consists of five antennas. The central antenna transmits and receives; each of the others only receives. Two of the receivers form a north-south line with central included; the other two receivers form an east-west line with central. The resulting beam width from the length of the baselines is 100° (north-south) by 11° (east-west). See Fig. 2.

Notice that, since the antennas are fixed in direction, the Minitrack station cannot track unless a satellite passes through its fan-shaped radio beam.

(5) Special techniques

Noise reduction techniques may be listed as

- (1) Low noise receivers
- (2) Choice of frequency
- (3) Modulation scheme and redundancy (coding, correlation)
- (4) Frequency diversity to avoid multipath errors
- (5) Time standards and synchronization
- (6) Search or acquisition techniques
- (7) Antenna design
- (8) Coherent and noncoherent systems

Low noise receivers. These receivers are the masers and reactance amplifiers. Masers (microwave amplification by stimulated emission of radiation) utilize the high Q properties of the natural resonance frequencies of certain materials such as ammonia, cesium vapor and rubidium.

A reactance amplifier increases the signal-to-noise ratio of the receiver by pumping energy into the signal in a manner related to the phase of the incoming signal. In this manner the phase information redundancy of a carrier is not thrown away.

Choice of frequency. The atmosphere is opaque to most radio frequencies; however, there is a "window" to radiation in the region from 300 to 10,000 Mc. Water vapor absorption limits the upper frequencies and thermal excitation limits the lower end of the spectrum.

Modulation schemes and redundancy. One scheme for using the redundancy of the signal has already been mentioned. The common modulation schemes are amplitude modulation, frequency modulation and pulse time.

Frequency diversity. Frequency diversity systems use two or more carrier frequencies to minimize frequency effects in propagation. One of the major sources of error in propagation

is the ionosphere, which acts as a time varying dielectric, thus changing the frequency of a carrier in an unpredictable manner. The ionosphere also refracts radio beams, thus changing the direction of the beam. The following formula shows how the index of refraction is a function of frequency and ion density:

$$\nu = \sqrt{1 - \frac{81N}{f^2}}$$

where

ν = index of refraction

N = ion density in particles/cm³

f = carrier frequency in kc

Using two frequencies allows the index of refraction to be estimated, thus minimizing the error due to bending of the radio wave.

The change in frequency due to the variable index of refraction has been calculated by Guier and Weiffenbach to be:

$$f - f_0 = \nu_0 \frac{r_c f_0}{c} \left(\cos h \frac{d\psi}{dt} + \frac{1}{r} \frac{dr}{dt} \sqrt{r^2 \frac{\nu}{\nu_0} - \cos^2 h} \right)$$

where

ν_0 = equivalent refractive index at earth's surface

r_c = the geocentric distance of the station

$\psi(t)$ = angle between the station vector and the geocentric distance vector of the satellite

r = geocentric distance

h = height

c = velocity of light $\approx 3.00 \times 10^{10}$ cm/sec

Time standards and synchronization. Some classes of orbits and some types of orbit computations (determinations) require very tight synchronization, whereas others need considerably less. If three stations are to take simultaneous range measurements, then the simultaneity requirement will generally limit the three stations to smaller baselines, and complicated synchronization techniques are needed. On the other hand, overdetermined orbits do not need such tight synchronization and baselines as wide as the earth are feasible (satellites could also be used for tracking stations resulting in very wide baselines).

One technique for synchronization of precision radars is to use gas filled wave guides in which the temperature and pressure can be controlled to the extent that the velocity of propagation is very precise. Generally, a central station is connected via wave guides to outlying stations; the signals and time are sent to central

from the other stations via the wave guides. If line-of-sight radio beams were to be used instead of wave guides, then significant errors, such as multipath errors and variable time delays due to temperature sensitive dielectric constants of the propagation medium, would occur.

Another technique used for synchronization when the time requirements are not quite so stringent, is to use WWV receivers. WWV transmits very accurate radio pulses on frequencies of 2.5, 5, 10, 15, 20, 25 Mc. Through the use of new techniques such as parametric amplifiers, the frequencies are accurate to several parts in 10^{11} . Received frequencies, if by line of sight, can be nearly as accurate as the frequency transmitted by WWV; if the received frequency is received via the ionosphere reflection, then the accuracy varies, sometimes degrading to a few parts in 10^6 during solar storms.

2. Station Properties

Table 2 lists some of the existing satellite tracking stations and their properties. Where the information is incomplete or changes are anticipated, blanks are left so that insertions or modifications can be made. The information presented should allow a good first estimate of whether or not a station might usefully support a given mission.

Additional information on these and other stations is available from Goddard Space Flight Center, Greenbelt, Maryland, attention Code 531.3.

Explanation of Table 2

Station number--An arbitrarily assigned serial number for cross referencing within this handbook.

System--The net of tracking facilities, if any, to which the particular station is assigned.

Cognizant agency--This is the activity responsible for the scheduling and operation of the station; if should be contacted to obtain support from this station. Abbreviations are:

| | |
|------|---|
| AMR | Atlantic Missile Range Cape Canaveral, Florida |
| APL | Applied Physics Laboratory Johns Hopkins University Silver Spring, Md. |
| BRL | Ballistics Research Laboratory Aberdeen Proving Ground Aberdeen, Md. |
| GE | General Electric Corporation General Engineering Laboratory Schenectady, New York |
| GSFC | Goddard Space Flight Center Anacostia Naval Station Anacostia, Maryland |

| | |
|--------|--|
| JPL | Jet Propulsion Laboratory California Institute of Technology Pasadena, California |
| MIT | Lincoln Laboratories Massachusetts Institute of Technology Boston, Mass. |
| NAA | Space and Information Systems Division North American Aviation, Inc. Downey, California |
| NERA | Radio Receiving Station NERA Nederhorstenden, Netherlands |
| NSSC | National Space Surveillance Center (Spacetrack) Code CRRKI, AFCRC L. G. Hanscom Field Bedford, Mass. |
| PMR | Pacific Missile Range Pt. Mugu, California |
| RADC | Rome Air Development Command Griffiss AFB Rome, New York |
| SRI | Stanford Research Institute Menlo Park, California |
| STL | Space Technology Laboratories One Space Park Redondo Beach, California |
| UILL | Electrical Engineering Re- search Laboratory University of Illinois Champaign, Illinois |
| USASRD | US Army Astro Scientific Research and Development Laboratory Deal, New Jersey |
| VAFB | Vandenberg AFB Lompoc, California |
| WRE | Weapons Research Establish- ment Woomera, Australia |
| WSMR | White Sands Missile Range White Sands, New Mexico |

Station name--A designation descriptive of location and/or equipment.

Installation type--Equipment classification (e.g., FPS-16). Several widely distributed radio systems are described in Table 3. Where the installation type is unique or at least not widely used at present, the table gives the particular antenna configuration. In this case, generally only the primary antenna is described, and there may be others for different frequencies or purposes.

Local designation--A code used by the cognizant agency to identify the station within the agency.

N Lat (deg)--The geodetic north latitude of the station, measured in degrees.

E Long. (deg)--The geodetic east longitude of the station, measured in degrees.

Altitude (meters)--The height of the antenna feed at zero degree elevation above mean sea level, measured in meters.

Survey reference--The basic survey to which the station's location is referenced.

Data reported--Advertised and/or known observations from a given station. More may be available.

α azimuth measurement

ϵ elevation or astronomical altitude measurement

H hour angle

D declination

ρ range measurement

$\dot{\rho}$ range rate

f_{non} noncoherent Doppler frequency, the received frequency from the satellite being tracked, including Doppler frequency shifts

f two-way phase coherent Doppler frequency shift. Range rate can be accurately and directly extracted from f in most cases

Tel telemetry, analog or digital coded information communicated from the satellite

Units--Basic measurement system in which the data is reported. Data reported and units are on the same respective lines in Table 2.

Coordinate system--Indicates how the station's antenna is mounted and calibrated. Antenna steering data (ephemerides) should be supplied in the system and units specified. The asterisk means that the units desired differ from those reported and are artillery mils for angular measurements.

Accuracy (3σ)--This is statistical 3σ to which a given measurement is accurate.

Data formats--Indicates the data output equipment available. Most manual outputs work into a teletype system. Almost all automatic outputs work into a teletype system. Almost all automatic output systems may be read manually, so only the higher order available output is shown.

Data delay--The estimated nominal time for handling data at the station before it is transmitted to the user. Abbreviations are as follows:

RT Real time, which signifies that the data is transmitted via an on-line process and will be received by the user essentially the same time that the station observes it.

NRT Near real time--less than 1-min delay--essentially the same as real time except for slight delays such as those caused by data going through teletype tape loops, etc.

Maximum range--The range limit on the particular installation when tracking a passive 1-m^2 target.

Antenna gain/frequency--The advertised approximate antenna gain in a particular frequency band.

Table 3 contains descriptions of some of the more widely used radio tracking systems.

3. Data Acquisition

Mission constraints generally dictate the data sources and tracking time available to each source for a given pass. Low altitude earth satellites are usefully visible from a given station for about 5 to 20 min, and, if the satellite's period is on the order of 120 min, three to four stations more or less evenly spaced along the ground track of the satellite can track and produce data so that data processing facilities will not be overloaded. Pre-launch planning must always include the possibility of a nonnominal orbit, and data handling and orbit computation operations must be capable of producing results under this "worst condition." Orbit determination tasks seldom have the problem of an overload of data, and, when it arises, it is easily controlled.

The threat of insufficient data is best met by considered overdesign of the tracking network. Some redundancy in the tracking systems is desirable, so that failure of a single system will not require reliance on optical or skin track radar methods for further data. Optical methods are slow and dependent on such uncontrollable items as weather, and large skin track radars generally have other commitments. One tracking station with high acquisition reliability should be able to track immediately after injection of the satellite into its free flight orbit, since in many cases the data is better at shorter ranges and time-propagating position errors are reduced. Accurate determination of the time of injection (orbit epoch) is possible from telemetry or Doppler data.

The problem of locating tracking stations to provide maximum certainty in orbit determination involves three considerations:

- (1) Maximizing basic orbital information.
- (2) Maximizing the visibility period, consistent with other requirements.
- (3) Measuring with maximum certainty.

Maximizing the basic orbital information depends strongly on what part of the orbit is being observed. For any given coordinate system, there exist orbits and locations on the orbit path which give ambiguous coordinates. For example: (1) it is very difficult to resolve the line of nodes (intersection of orbit plane and equatorial plane) if the orbit is equatorial or near equatorial; (2) it is also extremely difficult to locate perigee when the orbit is nearly circular; (3) if a station is located such that it observes perigee passage, the orbit determination might be very poor because so few observations would be obtained and the noise on the observations would obscure such vital information as time of perigee; (4) in the least-squares fitting of observations in orbit determination (described in Section E. 2) the partial derivatives (of the observation quantities with respect to the orbital elements) can be manipulated to indicate the information content of a pass, orbit, orbits, etc.

Maximizing the visibility period means more observations for a given situation, but careful notice must be taken of the information gained from each observation. This requirement can be approached by attempting to either adjust the network to maximize visibility or to adjust orbits to existing networks. Most system designs are compromises of the above two approaches.

Measuring with maximum certainty means measuring in such a manner that most errors are minimized.

Data rate. To minimize random errors, the highest data rate possible is desirable in order to obtain the maximum number of data per pass. However, the assumptions of independent data become poorer as the data rate is increased.

If the correlation between measurements falls off exponentially with time, then there is a predictable data rate above which greater errors are given in the orbit determination rather than less.

Measurement ambiguities. A simple example of a measurement ambiguity to be avoided follows.

Suppose the tracking station measures range ρ , azimuth α and elevation ϵ , of the satellite with respect to the radar location.

It can be seen that when ϵ equals exactly 90° , the azimuth measurement is ambiguous; and when ϵ only approaches 90° , the azimuth measurements become more uncertain.

Transformation ambiguities. Transformation ambiguities may result in the trigonometric transformations of the topocentric coordinates into orbital elements. An example of this is the transformation of the inertial, geocentric spherical coordinates r , A and D , into the radar quantities ρ , α and ϵ .

One possible transformation equation is

$$\sin(D_S - D) = \frac{\rho}{r} (\cos \epsilon \cos \alpha)$$

TABLE 2
Tracking Systems

| No. | System | Cognizant Agency | Station Name | Installation Type | Local Designation | N Lat | E Long. | Altitude (m) | Survey Ref | Data | Units | Coord System | Accuracy 3σ | Data Formats | Data Delay | Max Range (passive 1-sq m target) | Ant Gain/Oper Freq Band | Comments | | | |
|-----|------------------------|------------------|--------------------------------|-----------------------|-------------------|-----------|--------------|--------------|------------|--------------------------|--------------------|---------------------|---|--------------|-------------------|--|-------------------------|--|-----------------------------|----------------------|-----------|
| 1 | Minitrack | GSFC | Coolidge Field, Antigua Island | Radio inter-ferometer | B point [UHF VHF] | 17.15 | 298.217 | | | f _{non} | Cycles | | | | | | | Minitrack R&D sta. cape has vertical baseline for UHF, provides greater coverage than most Minitrack stations | | | |
| 2 | | | Antofagasta, Chile | | | -23.6389 | 289.7278 | | | | | | | | | | | | | | |
| 3 | | | Blossom Point, Md. | | | 38.43045 | 282.9134 | 4.9 | | | | | | | | | | | | | |
| 4 | | | Cape Canaveral | | | 28.45866 | 279.43095 | 6.1 | | | | | α, ε | Degrees | | | | | 1 min | | 21 db/UHF |
| 5 | | | East Grand Forks, Minn. | | | 47.93 | 262.98 | | | | | | | | | | | | | | 30 db/L |
| 6 | | | Fairbanks, Alaska | | | 64.73 | 212.35 | | | | | | | | | | | | | | 12 db/UHF |
| 7 | | | Fort Meyers, Fla. | | | 26.62 | 278.15 | | | | | | | | | | | | | | VHF |
| 8 | | | Fort Stewart, Ga. | | | 31.9806 | 278.5083 | | | | | | f _{non} | Cycles | Azimuth elevation | 3 cps; [theoretical, 20" of arc (0.006°), 1 millisecond of time; experimental 200" of arc (0.06°)] | Manual variable | | | 500 n mi S (14 db N) | |
| 9 | | | Grand Turk Is. | | | 21.52 | 288.90 | | | | | | | | | | | | | | |
| 10 | | | Johannesburg, S. Africa | | | -26.1825 | 28.7356 | | | | | | | | | | | | | | |
| 11 | | | Lima, Peru (Ancon) | | | -11.7778 | 282.8444 | | | | | | | | | | | | | | |
| 12 | | | Mayaguana Is. | | | 22.3750 | 286.9917 | | | | | | | | | | | | | | |
| 13 | | | Quito, Ecuador (Mt. Cotopaxi) | | | -0.6278 | 281.4389 | | | | | | | | | | | | | | |
| 14 | | | St Johns, Newfoundland | | | 50.00 | 304.50 | | | | | | | | | | | | | | |
| 15 | | | San Diego, Navy Elect. Lab | | | 32.5806 | 243.0278 | | | | | | | | | | | | | | |
| 16 | | | Santiago, Chile (Peldehue) | | | -33.1528 | 289.3277 | | | | | | | | | | | | | | |
| 17 | | | South Dakota | | | | | | | | | | | | | | | | | | |
| 18 | | | Spain | | | | | | | | | | | | | | | | | | |
| 19 | | | Woomera, Australia | | | -31.1026 | 136.7882 | 160.0 | | | | | | | | | | | | | VHF |
| 20 | Atlantic Missile Range | AMR | Cape Canaveral | Azusa | | 28.49137 | 279.44104 | | | ρ, α, ε | | Azimuth elevation | | | | | 33 db/C-band | Experimental model XN-1 Model XN-2 prototype (5000-mi range capability proposed for all FPS-16's except XN-2) Proposed | | | |
| 21 | | | Cape Canaveral | Azusa MK II | | 28.41295 | 279.40752 | | | ρ, α, ε dir cos rates | | Azimuth elevation | Range 3 ft; 6 pts/million nonambiguous dir cos; 0.75 pts/million ambiguous cos rate | | | | 35 db/C-band | | | | |
| 22 | | | Cape Canaveral | Extradop receiver | | 28.45 | 279.43 | | | | | | | | | | | | 36,864 mc | | |
| 23 | | | Bassett Cove, GBI | | | 26.60 | 280.68 | | | | | | | | | | | | or | | |
| 24 | | | West End, GBI | | | 26.65 | 281.08 | | | | | | | | | | | | 73,728 mc | | |
| 25 | | | Jupiter, Fla. | | | 26.95 | 279.93 | | | | | | | | | | | | | | |
| 26 | | | Cape Canaveral | Mod II | Radar 1.3 | 28.49245 | 279.42419 | 15.7 | | ρ, α, ε | Ft deg | Azimuth elevation | 12 m 1.5 mils | | | | | | 33 db/2650 to 33 db/2950 mc | | |
| 27 | | | Grand Bahama Is. | | Radar 3.1 | 26.61645 | 281.64006 | 16.3 | | | | | | | | | | | | | |
| 28 | | | Eleuthera Is | | Radar 4.1 | 25.26760 | 283.68677 | 37.5 | | | | | | | | | | | | | |
| 29 | | | San Salvador Is. | | Radar 5.1 | 24.06664 | 285.46366 | 14.6 | | | | | | | | | | | | | |
| 30 | | | Grand Turk Is. | | Radar 7.1 | 21.43328 | 288.85452 | 25.3 | | | | | | | | | | | | | |
| 31 | Antigua | | Radar 9.1 | 17.17540 | 292.91181 | 408.2 | | | | | | | | | | | | | | | |
| 32 | Ascension Is. | | Radar 12.1 | -7.93148 | 345.59709 | 275.2 | | | | | | | | | | | | | | | |
| 33 | Cape Canaveral | FPS-8 | | 28.4 | 279.4 | | | | | | | | | | | 220 n mi | 35 db/L-band | | | | |
| 34 | Grand Bahama Is. | | | | 26.61 | 281.64 | | | | | | | | | | | | | | | |
| 35 | Cape Canaveral | FPS-16 | 116 | 28.48133 | 279.52327 | 13.7 | AMS spheroid | ρ, α, ε | Ft deg | Azimuth elevation | 50 ft 0.012 deg | Auto-matic variable | NRT | 500 stat mi | | 44.5 db/C-band | | | | | |
| 36 | Patrick AFB | | 216 | 28.22647 | 279.40054 | 8.3 | | | | | | | | | | | | | | | |
| 37 | Grand Bahama Is. | | 316 | 26.61527 | 281.65189 | 14.1 | | | | | | | | | | | | | | | |
| 38 | San Salvador | | 516 | 24.11837 | 285.49560 | 13.1 | | | | | | | | | | | | | | | |
| 39 | Ascension Is. | | 1216 | -7.95175 | 345.58739 | 94.6 | | | | | | | | | | | | | | | |
| 40 | Antigua | | | 916 | 17.14250 | 298.20667 | 45.7 | | | | | | | | | | | | | | |

TABLE 2 (continued)

| No. | System | Cognizant Agency | Station Name | Installation Type | Local Designation | N Lat | E Long. | Altitude (m) | Survey Ref | Data | Units | Coord System | Accuracy 3 σ | Data Formats | Data Delay | Max Range (passive 1-sq m target) | Ant. Freq Gain Band | Oper | Comments |
|-----|------------------------|------------------|-------------------------|----------------------|-------------------|----------|-----------|--------------|----------------|-------------------------------------|--------------------------------|------------------------|------------------------|--------------------|------------|-----------------------------------|---------------------|------|--|
| 41 | Atlantic Missile Range | AMR | Tele-2 | 60-ft parabolic dish | BTM | 28.51351 | 279.22347 | 20.9 | | Tel α, ϵ | Deg | Azimuth elevation | 0.75 deg | Manual variable | 5 min | | 28 db/VHF | | Primary telemetry station at Cape Canaveral |
| 42 | | | Tele-3 | | | 28.46289 | 279.41667 | 20.7 | | | | | | | | | 32 db/UHF | | |
| 43 | | | AMR mobile | 28-ft parabolic dish | | | | | | Tel $\Delta f, \alpha, \epsilon$ | Cycles, deg | Azimuth* elevation* | 3 cps 1.5 deg | Automatic fixed | NRT | | UHF UHF VHF | | Has autotrack capability once signal is acquired |
| 44 | Pacific Missile Range | PMR | South Arguello | FPS-16 | 023001 | 34.58276 | 239.43944 | 661.6 | | ρ, α, ϵ | Ft, deg | Azimuth elevation | 150 ft, 0.03 deg | Automatic variable | RT | 200 mi | 44.5 db/C-band | | Planned 5000-mi range part of Mercury net |
| 45 | | | North Arguello | | 023002 | 34.58305 | 239.43989 | 661.6 | | | | | | | | 500 mi | | | Planned 500-mi range |
| 46 | | | South Mugu | | 003001 | 34.12144 | 240.84933 | 12.8 | | | | | | | | 200 mi | | | Planned 500-mi range (Mugu has a total of 4 FPS-16's) |
| 47 | | | North Mugu | | 003002 | 34.12122 | 240.84812 | 12.8 | | | | | | | | 200 mi | | | 500-mi and 5000-mi range capability is planned for one of four FPS-16's on San Nicolas |
| 48 | | | San Nicolas Island | SCR-584/615 | No. 15 No. 30 | | | | | | | | | | | 200 mi | | | Kokee has planned 5000-mi range capability |
| 49 | | | Kokee, Kauai, Hawaii | | | | | | | | | | | | | 500 mi | | | There are 6 SCR-584/615's at Point Mugu and 4 at San Nicolas |
| 50 | | | Point Mugu | | | 34.121 | 240.848 | 12.8 | | | Yd, mil | | 100 yd, 10 mil | | | 440 km | S-band | | Two verlorts being acquired |
| 51 | | | San Nicolas | | | | | | | | | | | | | | | | |
| 52 | | | Point Arguello | Verlort | | 34.58 | 239.439 | 661.6 | | | | | 20 yd, 1 mil at 3°/sec | | | 1800 km | | | |
| 53 | | | Kauai, Hawaii | | | | | | | | | | | | | | | | |
| 54 | | | Point Mugu | Microlock | | 34.121 | 239.439 | 661.6 | | f | | | | | | | 108 mc | | |
| 55 | | | South Point, Hawaii | | | 18.94 | 204.33 | | | | | | | | | | 70 mc | | |
| 56 | Transit Program Net | APL | Howard County | 20-ft dish | 0.01 | 39.1635 | 283.1010 | 145.0 | No. Amer Datum | Tel f_{non} | Cycles | Azimuth elevation | 0.75 cps | Automatic fixed | NRT | | VHF 23db/UHF | | Receiver has parametric amplifier uses atomichron time standard |
| 57 | | | Austin | | 0.02 | 30.28861 | 262.26861 | 179.8 | | | | | 1.5 cps | | | 60 min | VHF | | |
| 58 | | | Las Cruces | | 0.03 | 32.28157 | 253.28222 | 1218.4 | | | | | | | | | VHF | | |
| 59 | | | Seattle | | 0.04 | 47.56107 | 237.64471 | 83.5 | | | | | | | | | VHF | | |
| 60 | | | Argentina | | 0.05 | 47.31529 | 306.01029 | 13.8 | | | | | | Manual variable | | | VHF | | |
| 61 | | | Sao Paulo | | 0.08 | | | | | | | | | | | | VHF | | |
| 62 | Deep Space | JPL | Goldstone, Calif. | 85-ft parabolic dish | GS | 35.3895 | 243.1518 | 1054.6 | | H, D f_{non} Tel | Deg, Cycles | Hour angle declination | 0.15 deg 39 cps | Automatic fixed | NRT | | UHF | | 200- to 250-ft dia parabolic antennas are planned for each DSN site, the first for Goldstone in 1965 |
| 63 | | | Woomera, Australia | | W | -31.382 | 136.886 | | | H, D | Deg | | 0.15 deg | | | | | | Goldstone also has Az-B1 antennas |
| 64 | | | Johannesburg, S. Africa | | J | -25.891 | 27.675 | | | | | | | | | | | | |
| 65 | Space-track Net | MIT | Millstone Hill | 84-ft parabolic dish | | 42.617 | 288.509 | 156.1 | | ρ, α, ϵ β | Km, deg | Azimuth elevation | 18.3 km 1.2 deg | Automatic variable | NRT | | 36 db/UHF | | High power skin tracking |
| 66 | | BRL | BRL Lab | Unihelix | | 39.4744 | 283.9278 | 18.3 | | $\Delta f, \alpha, \epsilon$ | Cycles, deg | | 9 cps 12 deg | Manual variable | 1 min | | 1.4 db/UHF | | |
| 67 | | RADC | Rome ADC | 28-ft parabolic dish | | 43.2234 | 284.5792 | 164.0 | | f_{non} α, ϵ | Cycles | | 60 cps 15 deg | | 10 min | | 28 db/UHF | | |
| 68 | | NSSC | Sagamore Hill Telescope | 84-ft parabolic dish | | 42.6311 | 289.1846 | 74.7 | | H, D f_{non} | Hr, min, sec, deg, min, cycles | Hour angle declination | 3 deg 9 cps | | 15 min | | 37 db/UHF | | |

TABLE 2 (continued)

| No. | System | Cognizant Agency | Station Name | Installation Type | Local Designation | N Lat | E Long. | Altitude (m) | Survey Ref | Data | Units | Coord System | Accuracy 3 σ | Data Formats | Data Delay | Max Range (passive 1 sq m target) | Ant. Gain | Oper Freq Band | Comments |
|-----|---------------------------|------------------|------------------------|----------------------|-------------------|-----------|-----------|--------------|-----------------|--|-------------|-------------------|-------------------------|-------------------------|------------|-----------------------------------|---------------------------|----------------|--|
| 69 | Space-track Net | SRI | Stanford Research | 61-ft parabolic dish | | 37.4031 | 237.8247 | 150.0 | | f_{non} α, ϵ | Cycles, deg | Azimuth elevation | 3000 cps 5.25 deg | Manual variable | | | 33 db/UHF | | |
| 70 | White Sands Missile Range | WSMR | White Sands, N. Mex. | FPS-16 | R-113 | 32.35795 | 253.60737 | 1234.2 | | ρ, α, ϵ | Yd deg | Azimuth elevation | 15 yd 0.015 deg | Automatic variable | 30 min | | 44.5 db/C-band | | Part of Mercury program net |
| 71 | | | Holloman AFB | | R-123 | 32.91589 | 253.90139 | 1264.8 | | | | | | | | | | | |
| 72 | | | Mid White Sands | | R-112 | 32.35795 | 253.62977 | 1234.0 | | | | | | | | | | | |
| 73 | | | East White Sands | | R-114 | 32.35795 | 253.63171 | 1233.6 | | | | | | | | | | | |
| 74 | | | South Holloman | | R-122 | 32.90222 | 253.90139 | 1264.5 | | | | | | | | | | | |
| 75 | | WRE/GSFC | Red Lake | | | -30.81931 | 136.85847 | 128.1 | | | Yd art mils | | 150 ft 0.015 deg | Automatic fixed | 60 min | 500 mi | | | Part of Mercury Program net. Data in octal artillery mils |
| 76 | | WRE | Mirikata | | | -29.87147 | 135.241 | 219.1 | | | | | | | | | | | |
| 77 | | STL | GGS | Quad helix | | 28.44853 | 279.41929 | 3.5 | AMS spheroid | Δf | Cycles | | 0.18 cps | Manual auto-matic fixed | 15 min | | 15 db/UHF | | |
| 78 | Courier Program | USASRD | Fort Monmouth | 50-ft parabolic dish | Decour | 40.1833 | 285.9431 | 31.7 | | f_{non} α, ϵ | Cycles, deg | Azimuth Elevation | 2 cps 0.5 deg | Manual variable | NRT | | 33 db/UHF | | Receiver has parametric amplifier |
| 79 | | GE | GE | 28-ft parabolic dish | | 42.84806 | 285.92917 | 403.9 | | f_{non} α, ϵ | Cycles | | 15 cps 12 deg | | 5 min | | 26 db/UHF | | |
| 80 | | GSFC | Huntsville | 15-ft parabolic dish | | 34.6670 | 273.3564 | 181.4 | | f_{non} α, ϵ | Cycles, deg | | 30 cps 6 deg | | 60 min | | 19.5 db/UHF | | |
| 81 | | U. Ill. | University of Illinois | | | 40.1050 | 271.7731 | 240.2 | | | | | 300 cps 6 deg | | 2 min | | 28 db/UHF | | |
| 82 | | NERA | NERA Tracking | 10-m parabolic dish | | 52.233 | 5.083 | 0.0 | | Tel f | Cycles | | 0.3 pts/ million cps | | 8 hr | | | | |
| 83 | | RADC | GE-Trinidad | 84-ft parabolic dish | | 10.73923 | 298.3910 | 273.3 | Clarke spheroid | ρ, α, ϵ | Km, deg | | 18 km 1.2 deg | | 5 min | | 36 db/UHF VHF | | High power skin tracking |
| 84 | | NAA | NAA Tracking | Quad helix | | 33.92472 | 241.87268 | 39.6 | | f_{non} α, ϵ | Cycles, deg | | 7.5 cps 15 deg | | 15 min | | 22 db/UHF | | |
| 85 | | RCA | Moorestown | FPS-49 | | | | | | $\rho, \beta, \alpha, \epsilon$ | | | | | | | 39 db/UHF | | Data smoothing interval is 10 sec High power skin tracking |
| 86 | | GSFC | Cape Canaveral | 6-ft parabolic dish | Hangar S | 28.48794 | 279.41378 | 7.6 | | f_{non} | Cycles | | 30 cps | | 15 min | | 15 db/UHF | | |
| 87 | | NASA | Cape Canaveral | Microlock | | 28.41483 | 279.40583 | 6.1 | | α | Deg | | 1.5 deg | | | | | | |
| 88 | | | | | | 28.41436 | 279.40584 | 6.1 | | | | | | | | | | | |
| 89 | | | | | | 28.41405 | 279.40625 | 6.1 | | | | | | | | | | | |
| 90 | | NASA | Cape Canaveral | Microlock | | 28.41464 | 279.40516 | 10.4 | | α, ϵ Tel | Deg | Azimuth Elevation | 15 deg 3 deg | Manual variable | | | 13 db/VHF 33 db/L-band | | Uses atom-ichron time standard |
| 91 | Dis-coverser Net | VAFB | Cook Tracking | 60-ft parabolic dish | | 34.82565 | 239.49507 | 306.3 | | α | | | 0.06 deg | | 5 min | | 28 db/VHF UHF | | |
| 92 | SPANDAR | NASA | Wallops Island | 60-ft parabolic dish | | 37.8546 | 284.4866 | 29.0 | | α, ϵ | | | 0.03 deg | | | | S-band | | |
| 93 | Relay | NASA | Andover, Maine | Cassegrain antenna | | 44.6319 | 289.3017 | | | | | | 0.06 deg | | | | | | |
| 94 | | | Goonhilly, England | | | 50.0494 | 354.8253 | | | | | | 6 min of arc | | | | | | |
| 95 | | | Nutley, N. J. | | | 40.816 | 285.833 | | | | | | | | | | | | |
| 96 | | | Pleumeur-Bodou, France | | | 48.7869 | 356.4758 | | | | | | | | | | | | |
| 97 | | | Rio de Janeiro, Brazil | | | -22.9525 | 316.6314 | 9.8 | | | | | | | | | | | |
| 98 | | | Fucino, Italy | | | 41.9781 | 13.6014 | 640.1 | | | | | | | | | | | |

TABLE 3
Tracking Facility Characteristics

| Name | Manufacturer | Antenna Type | System Type | Scan Rate | Coverage | Beam Width | Frequency |
|-----------------------------------|-------------------|--|--|--|--|--|---|
| Minitrack | Navy | Fixed array | CW-bistatic | Stationary | Vertical fan | 0.3° x 140° | 108 and 135 mc |
| AN/FPS-16 | RCA | 12-ft parabolic 44.5-db gain | Monopulse; skin or beacon automatic tracking | Range: 10,000 yd/sec Azimuth: 40°/sec Elevation: 30°/sec | 360° az; -10° + 85° el (raster, circu- lar and sector scan) | 1.2° | 5400 to 5900 mc |
| Verlort | Reeves | 10-ft parabolic | Monopulse; skin or beacon automatic tracking | Range: 10,000 yd/sec Az and El: 900 mils/sec | 360° az; -11.25 to 90° el | 2.5° | S-band |
| FPS-49 (BMEWS) | RCA | 84-ft parabolic 39-db gain | Pulse-doppler, steerable automatic tracking | 3° to 15°/sec | 330° az 0 to 90° el | 2° x 2° pencil | 425 mc |
| FPS-50 Surveillance (BMEWS) | RCA | 165- x 400-ft torus 45-db gain | 88 feed horns and 2 dual organ pipe scan- ners | 5°, 6-2/3° and 10°/sec in azimuth | 2 fans--3.5° and 7° el angles | 1° elev width | 425 mc |
| Millstone FPS-44 | Lincoln Labs, MIT | 84-ft parabolic 37.3-db gain | | 2°/sec | 360° az 0 to 90° el (conical scan) | 2.1° | 440 mc |
| Trinidad FPS-44 | GE | 84-ft parabolic 37.5-db gain | | 4.5°/sec (slew) | 360° az 0 to 90° el | 2.25° | 425 and 438 mc |
| Goldstone | NASA | 85-ft HA-DEC parabolic | Deep space | 1.0° and 0.03°/sec | 360° az 5° to 90° el | 1° at 960 mc 0.4° at 2295 mc | 890/960 mc 2115/2295 mc (1963) |
| Stanford Research | SRI | 60-ft parabolic | Monostatic pulse | 4°/sec (slew) | 360° az 0° to 90° el | 12° | 106.1 mc Calif. 200 to 400 mc Alaska |
| Doploc | Army BRL-ARPA | Tunable 16-db gain | CW doppler | Stationary | 3 fans | 8° x 76° | 108 mc |
| Spasur (detection) | NRL-ARPA | 50-dipole receiver 400 ft long (1600 ft being installed) | Detection only CW-tristatic fence interferometer | Stationary | Vertical fan | 0.4° x 160° (0.3° x 160° proposed) | 108 mc (108 and 428 mc proposed) |
| ESAR | Bendix | 90-element linear array | | | ±45° az ±45° el | Transmit 1.5° pencil Receive 1.5° cluster | 425 mc 850 mc 1275 mc |

where

- D = declination of the satellite in inertial coordinates
- D_s = declination of the station in inertial coordinates
- r = geocentric distance of the satellite.

Examination of this equation shows that D information is lost when the azimuth α measurements approach 90° , that is, when the satellite heads due east from the station. In a like manner, all coordinate transformations have ambiguous answers where the inertial orbital element cannot be determined at that time. One of the ways of resolving ambiguities is to have an overdetermined orbit; another way is to adjust the orbit or the station location such that the ambiguities do not occur.

Errors may be minimized by suitable station calibration techniques and methods.

It is undesirable to attempt an orbit determination from a single station's data on one pass. The station's random errors generally preclude computation or an orbit sufficiently accurate to furnish position predictions which will enable a narrow beam radar to acquire one orbit revolution later. Experience dictates that data from at least one tracking pass from each of two well spaced stations (preferably through apogee, and 90° to 180° from apogee) is required to determine the initial orbit achieved.

Satellites in highly elliptical orbits (perigee high enough to be free from drag effects) and space probes present less stringent requirements on the tracking system, unless midcourse guidance is involved, because more stations have visibility for longer periods of time and data is plentiful. Midcourse guidance requires rapid and accurate orbit determination if satellite fuel requirements are to be kept within reason. As little as an hour may be available to track the satellite, process data, determine the orbit, and calculate the time and duration of the rocket firing for correction of the satellite trajectory.

Under these conditions, prelaunch planning must include limitations on the tracking time and the number of data points, to ensure that adequate computation time is available. Several data handling modes should be available so that last minute equipment failures do not jeopardize the mission.

4. Data Handling

Communications should be established at least one hour prior to the earliest scheduled liftoff to ascertain that complete circuit communication is available. Once liftoff occurs, data should begin to arrive from the tracking stations.

Teleprinter circuits are a favored method for transmitting data because they:

- (1) Are readily available as a leased service.
- (2) Are the most reliable rapid communication.
- (3) Produce punched paper tape and printed, multicopy output.
- (4) May be gauged together on a single circuit at little extra cost.

The received information may be:

- (1) Supplied as electrical impulses in teletype code to electronic conversion equipment which writes it on a magnetic tape in computer code, or enters it directly into the computer.
- (2) Punched onto cards by passing the paper tape through a tape-to-card machine. (These cards are checked for bad points and are then read into the computer.)
- (3) Manually transcribed to load sheets, keypunched to cards, and then read into the computer. (This method is used if the data is irregular in some respect and cannot be handled as described in the first two methods.)

The availability of at least two of the above methods is recommended. Experience has shown that flexibility is a prime data handling requirement. Extremely useful observations may be received in an irregular format when previously coordinated sources have failed to acquire the satellite, and the orbit determination agency should be prepared to use them.

Generally, the transmission of information from tracking stations to a central data gathering center is over a narrow bandwidth channel such as a telephone circuit. This means that the information cannot be fed over the lines very rapidly. Error checking slows down the rate even more; to check for all errors would require an extremely long time. The result is that high probability error classes are checked automatically or semi-automatically; low probability errors are not excluded.

5. Data Filtering

Two extreme cases of how the data could be processed are: (1) the raw data could be fed into a central data gathering center and processed there and (2) the data could be processed at each station. If each tracking station completely processes its own data, there is not only a duplication of computing equipment (one for each station) but each station is not taking full advantage of other stations' data. If all data is fed raw from each tracking station to one central computer, then far too much bad data gets into the orbit determination routine. The usual compromise is to have one central computer do the final editing, smoothing and orbit determination, but have each tracking station perform its own local calibrations

and some data smoothing and editing for grossly erroneous data.

When a sufficient number of points have accumulated, the preliminary precision orbit is determined. The differential correction technique using least squared errors is the method usually used; it is described later.

An optimum filtering scheme has two conflicting requirements imposed on it: (1) to use all the information contained in the observation and (2) to reject all misinformation contained in the observations.

Since there are no perfect data, all observations have varying degrees of noise or unknown errors associated with them. Using all the information contained implies accepting all data points. Rejecting all misinformation implies rejecting all data points. Filtering schemes attempt to improve the accuracy of an orbit determination by various compromises with the two above contradictory requirements. One such compromise is to reject all "obviously" bad data. Such data only degrade the curve fits, since they contain so little information. Another compromise is to maximize the probability of the accuracy of the estimates of the orbit parameters. This compromise is effected by determining the maximum likelihood estimates of the orbital parameter. There are two different ways of determining a bad point: (1) by taking more observations, thus increasing the probability of obtaining a more accurate fit, or (2) by a priori knowledge of the true trajectory or a priori knowledge that a given point is bad.

The best filtering of the data, if random errors (only) are present, uses a least square fit (described in Sections E.2 and F) to curves constrained by the known (i.e., well determined) laws of physics. Unfortunately, to use all the points in the curve fitting procedure would degrade the orbit determination so much that the computation would almost always result in an ambiguous answer. (In other words, so many orbits would fit the set of observations that the estimates would not be consistent.) Additionally, if much of the bad data had been rejected previously by quicker methods, fewer computations would be needed to reject the bad data.

An efficient filtering scheme must divide the filtering between the tracking stations and the central computer, such that most of the above problems are minimized. It is instructive to contrast the extremes of too much local filtering at the tracking stations and no local filtering.

Excessive local filtering. If data is rejected on the basis of simple curve fitting, the curve being fit would be in error and there would be a tendency to reject "good" data.

If data is fit to curves representing the known laws of orbital mechanics, then a complex computer is required at each station. However, each station would have the disadvantage of not using data from other stations.

If each station fits all data to curves representing orbital mechanics, then each is really a central station and there is inefficiency in that the same computations are being duplicated in each station.

No filtering at local station. If no filtering occurs at each station, the computation center is swamped with bad data, unknown biases (e.g., biases known to local stations but not to central), increased transmission errors, and less information per unit time being fed to central.

D. DETERMINATION OF PRELIMINARY ORBIT ELEMENTS

Two areas of the problem of orbit determination are generally distinguished:

- (1) Preliminary orbit determination--more or less approximate calculation of an orbit which was previously completely unknown.
- (2) Orbit improvement--refinement in accuracy of elements already known approximately.

This section considers the problem of preliminary orbit determination; Section F considers orbit improvement. Many methods of determining preliminary orbits are available. The best computation technique to use in a given problem depends on the types of data available. Table 4 shows the appropriate computation schemes to be used for the various combinations of observational data.

Several methods are described briefly below. Reference 4 considers some techniques in greater detail.

1. Method of Laplace

The method of Laplace depends on the solution of the differential equation of motion by Taylor series. That is, a solution of the equation

$$\frac{d^2 \vec{r}}{dt^2} = -\mu \frac{\vec{r}}{r^3} \quad (47)$$

will be written in the form

$$\vec{r} = \vec{r}_0 + \frac{d\vec{r}}{dt} \bigg|_0 (t - t_0) + \frac{1}{2} \frac{d^2 \vec{r}}{dt^2} \bigg|_0 (t - t_0)^2 + \dots \quad (48)$$

Evaluation of the derivatives (the series coefficients) of Eq (48) from Eq (47) and collection of terms gives

$$\vec{r}(t) = \left[1 - \mu \frac{(t - t_0)^2}{2 r_0^3} + \dots \right] \vec{r}_0 + \quad (49)$$

(continued)

TABLE 4*
Observation Requirements for Preliminary Orbit Determination

| Observational Data | Assumption | Method |
|--|---|--|
| Three 3-dimensional fixes | None | Herrick-Gibbs or Gibbs (with or without differential correction to reduce residuals and/or discard bad data) |
| Overdetermined system with more than three fixes | Random error distribution | Least-square differential correction of initial orbit |
| Fifteen range measurements | Low eccentricity circular orbit rectilinear parabola | Gibbs |
| Eight range measurements | | Gibbs |
| Four range measurements | | Gibbs |
| One 1-dimensional fix (can be achieved in several ways: one vector measurement of range and range rate; three range and three range-rate measurements) | None | Laplace, Lagrange |
| Two 3-dimensional fixes | None | Gauss (and variants) |
| Azimuth, elevation (α, ϵ) | None | Laplacian |
| Azimuth, elevation rate ($\dot{\alpha}, \dot{\epsilon}$) | | |
| Azimuth, elevation change of rate ($\ddot{\alpha}, \ddot{\epsilon}$) all at one time | | |
| Three elevation } Three azimuth } for three times | None | Convert to $\alpha, \epsilon, \dot{\alpha}, \dot{\epsilon}, \ddot{\alpha}, \ddot{\epsilon}$ of middle data (Laplacian) |
| (That is, each $\epsilon_i - \alpha_i$ pair is taken at three separate times) | | Retain α, ϵ |
| | | Lagrange with Herrick-Gibbs velocity |
| | | Gauss |
| | | Gibbs expansion method |
| Three range measurements | None | Differential correction of pseudo-Laplacian |
| Three range-rate measurements | | |
| Six range measurements | None | Differential correction of pseudo-Laplacian |
| Six range-rate measurements | None | Probably only differential correction |
| Other combinations of six observed quantities for three or more times | None | Needs to be developed |
| Five observed quantities for one or two times | Parabolic or one-condition orbits | Modified Olbers Laplacian or similar method |
| Four observed quantities: for example, $\alpha, \epsilon, \dot{\alpha}, \dot{\epsilon}$ for one time; $2\alpha, 2\epsilon$ for two times | Circular or two-condition orbits: for example, two ranges or two r 's are assumed | Standard circular orbit methods |
| Four ranges for four times | | |
| Two ranges, two range rates for two times | | |
| α, ϵ , range, range rate for one time | | |
| Three observed quantities | Three-condition orbit | Needs to be developed |
| Two observed quantities | Four-condition orbit | Needs to be developed |

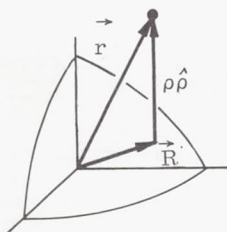
*Adapted from Ref. 3

$$+ (t - t_0) \left[1 - \mu \frac{(t - t_0)^2}{6 r_0^3} + \dots \right] \frac{d\vec{r}}{dt} \bigg|_0$$

$$\equiv s \vec{r}_0 + \sigma \dot{\vec{r}}_0 \quad (49)$$

From Eq (49), if the position vector \vec{r}_0 and the velocity vector $\dot{\vec{r}}_0$ are known for some time t_0 , and if the series s and σ converge, the radius vector at any time, $\vec{r}(t)$, is determined. But the radius vector \vec{r} is related to the observations by

$$\vec{r} = \rho \hat{\rho} + \vec{R} \quad (50)$$



where

\vec{R} = vector position of the observer

ρ = magnitude of the observation vector

$\hat{\rho}$ = unit vector in the direction of observation

Successive differentiation of Eq (50) gives

$$\ddot{\vec{r}} = \ddot{\rho} \hat{\rho} + 2 \dot{\rho} \dot{\hat{\rho}} + \rho \ddot{\hat{\rho}} + \ddot{\vec{R}} \quad (51)$$

The acceleration as given by dynamics (Eq (47)) can then be equated to that given by the geometry (Eq (51))

$$\ddot{\rho} \hat{\rho} + 2 \dot{\rho} \dot{\hat{\rho}} + \rho \ddot{\hat{\rho}} + \ddot{\vec{R}} = - \frac{\rho \hat{\rho} + \vec{R}}{r^3} \quad (52)$$

The dot product of this equation with $(\hat{\rho} \times \dot{\hat{\rho}})$ gives

$$\rho (\hat{\rho} \times \dot{\hat{\rho}} \cdot \ddot{\hat{\rho}}) = - (\hat{\rho} \times \dot{\hat{\rho}} \cdot \ddot{\vec{R}}) - \frac{\hat{\rho} \times \dot{\hat{\rho}} \cdot \vec{R}}{r^3}$$

$$= (\hat{\rho} \times \dot{\hat{\rho}} \cdot \vec{R}) \left(\frac{1}{R^3} - \frac{1}{r^3} \right) \quad (53)$$

Dotting Eq (50) into itself provides the additional relation

$$r^2 = \rho^2 + R^2 + 2 (\hat{\rho} \cdot \vec{R}) \rho \quad (54)$$

If only direction data comprise the observations, ρ and r are the only unknowns in Eqs (53) and (54). Each of the vector products can be evaluated from the observations and the known position of the observer. Three observations, each con-

sisting of two angular coordinates and the corresponding time, are sufficient to determine $\hat{\rho}_0$ and $\dot{\hat{\rho}}_0$ at some time t_0 (generally the middle of the three observations), except when $\hat{\rho} \times \dot{\hat{\rho}} \cdot \ddot{\hat{\rho}} = 0$ at $t = t_0$, or if $\dot{\hat{\rho}} = 0$ at $t = t_0$.

A convenient computation method for determination of the preliminary orbit of an earth satellite from three observations of right ascension and declination,

$$t_a: A_a \quad D_a$$

$$t_0: A_0 \quad D_0$$

$$t_b: A_b \quad D_b,$$

proceeds as follows. Four equations in the four unknowns s_a, s_b, σ_a and σ_b are obtained

$$\vec{r}_a = s_a \vec{r}_0 + \sigma_a \dot{\vec{r}}_0 = s_a (\rho_0 \hat{\rho}_0 + \vec{R}_0) + \sigma_a \dot{\vec{r}}_0$$

$$= \rho_a \hat{\rho}_a + \vec{R}_a$$

$$\vec{r}_b = s_b \vec{r}_0 + \sigma_b \dot{\vec{r}}_0 = s_b (\rho_0 \hat{\rho}_0 + \vec{R}_0) + \sigma_b \dot{\vec{r}}_0$$

$$= \rho_b \hat{\rho}_b + \vec{R}_b$$

where

$$\hat{\rho}_i = \cos A_i \cos D_i \hat{i} + \sin A_i \cos D_i \hat{j} + \sin D_i \hat{k}$$

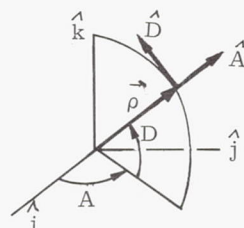
The dot products of these equations with unit vectors \hat{A} and \hat{D} ,

$$\hat{A} = -\sin A_i \hat{i} + \cos A_j \hat{j}$$

(in the direction of increasing right ascension)

$$\hat{D} = -\sin D \cos A_i \hat{i} - \sin D \sin A_j \hat{j} + \cos D \hat{k}$$

(in the direction of increasing declination)



give the following equations to be solved:

$$s_i (\hat{\rho}_0 \cdot \hat{A}_i) \rho_0 + \sigma_i \hat{A}_i \cdot \dot{\vec{r}}_0 = -s_i (\vec{R}_0 \cdot \hat{A}_i) + \vec{R}_i \cdot \hat{A}_i$$

$$s_i (\hat{\rho}_0 \cdot \hat{D}_i) \rho_0 + \sigma_i \hat{D}_i \cdot \dot{\vec{r}}_0 = -s_i (\vec{R}_0 \cdot \hat{D}_i) + \vec{R}_i \cdot \hat{D}_i \quad (55)$$

where

$$i = a, b$$

2. Method of Gauss

If three position vectors, \vec{r}_1 , \vec{r}_2 and \vec{r}_3 at times t_1 , t_2 and t_3 , are coplanar, and if \vec{r}_1 is not parallel or anti-parallel to \vec{r}_3 ,

$$\vec{r}_2 = c_1 \vec{r}_1 + c_3 \vec{r}_3. \quad (56)$$

With the notation of the previous subsection

$$\vec{r}_i = \rho_i \hat{\rho}_i + \vec{R}_i, \quad i = 1, 2, 3.$$

These two equations give,

$$c_1 \vec{\rho}_1 - \vec{\rho}_2 + c_3 \vec{\rho}_3 = -c_1 \vec{R}_1 + \vec{R}_2 - c_3 \vec{R}_3. \quad (57)$$

Also, from Eq (56),

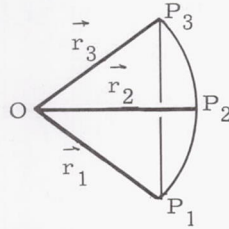
$$\vec{r}_1 \times \vec{r}_2 = c_3 \vec{r}_1 \times \vec{r}_3$$

$$\vec{r}_2 \times \vec{r}_3 = c_1 \vec{r}_1 \times \vec{r}_3,$$

so that

$$c_1 = \frac{\vec{r}_2 \times \vec{r}_3 \cdot \vec{k}}{\vec{r}_1 \times \vec{r}_3 \cdot \vec{k}} = \frac{\text{Area } \triangle OP_2P_3}{\text{Area } \triangle OP_1P_3}$$

$$c_3 = \frac{\vec{r}_1 \times \vec{r}_2 \cdot \vec{k}}{\vec{r}_1 \times \vec{r}_3 \cdot \vec{k}} = \frac{\text{Area } \triangle OP_1P_2}{\text{Area } \triangle OP_1P_3}$$



The c 's are known as "triangle ratios" "Sector-triangle ratios" can then be defined as

$$\eta_1 = \frac{\text{area of sector } OP_2P_3}{\text{area of triangle } OP_2P_3}$$

$$\eta_2 = \frac{\text{area of sector } OP_1P_3}{\text{area of triangle } OP_1P_3}$$

$$\eta_3 = \frac{\text{area of sector } OP_1P_2}{\text{area of triangle } OP_1P_2}$$

By Kepler's law of areas, the areas of the sectors are proportional to the time. Therefore,

$$c_1 = \frac{t_3 - t_2}{t_3 - t_1} \frac{\eta_2}{\eta_1} \quad (58)$$

$$c_3 = \frac{t_2 - t_1}{t_3 - t_1} \frac{\eta_2}{\eta_3} \quad (59)$$

Additional conditions are imposed by Kepler's equation,

$$\frac{1}{a} \sqrt{\frac{\mu}{a}} (t_j - t_i) = E_j - E_i - e (\sin E_j - \sin E_i) \quad (60)$$

(a dynamic condition)

where

E = eccentric anomaly

e = eccentricity of orbit

a = semimajor axis of orbit

μ = gravitational constant

and

$$r_i + r_j = 2a - ae (\cos E_i + \cos E_j) \quad (61)$$

(a geometric condition).

Defining $2E_{ij} = E_j - E_i$ as the change in eccentric anomaly and $2\theta_{ij} = \theta_j - \theta_i$ as the change in true anomaly, the last equation gives

$$r_i + r_j = 2a \sin^2 E_{ij} + 2\sqrt{r_i r_j} \cos \theta_{ij} \cos E_{ij} \quad (62)$$

and Kepler's equation becomes

$$\frac{1}{a} \sqrt{\frac{\mu}{a}} (t_j - t_i) = 2E_{ij} - \sin 2E_{ij} + \frac{2}{a} \sqrt{r_i r_j} \cos \theta_{ij} \sin E_{ij}. \quad (63)$$

The following definitions will prove convenient.

$$k^2 \equiv 4r_i r_j \cos^2 \theta_{ij}$$

$$1 + 2\ell \equiv \frac{r_i + r_j}{k}$$

$$m^2 \equiv \frac{\mu}{k^3} (t_j - t_i)^2 \quad (64)$$

$$x \equiv \sin^2 \frac{E_{ij}}{2}.$$

Solution of Eq (62) for a gives

$$2a \sin^2 E_{ij} = \frac{k (r_i + r_j)}{k} - k \cos E_{ij}$$

or

$$a = \frac{k (\ell + x)}{\sin^2 E_{ij}} \quad (65)$$

Substitution of this a , obtained from geometrical constraints, into Kepler's equation, Eq (63), gives

$$\sqrt{\mu} (t_j - t_i) = (2E_{ij} - \sin 2E_{ij}) a^{3/2} + 2 \sqrt{r_1 r_3} \cos \theta_{ij} \sin E_{ij} \sqrt{a}$$

or

$$\sqrt{\mu} (t_j - t_i) = \frac{2 E_{ij} - \sin 2 E_{ij}}{\sin^3 E_{ij}} [k (\ell + x)]^{3/2} + k^{3/2} (\ell + x)^{1/2} = mk^{3/2}$$

With the definitions

$$\ell + x \equiv \frac{m^2}{\eta}$$

$$X(x) \equiv \frac{2 E_{ij} - \sin 2 E_{ij}}{\sin^3 E_{ij}} \quad (66)$$

this equation reduces to

$$\frac{m^3}{y^3} X(x) + \frac{m}{\eta} = m \quad (67)$$

or

$$\eta = 1 + \frac{m^2}{\eta} X(x)$$

Differentiation of the above definition of $X(x)$ with respect to E_{ij} gives

$$\sin^3 E_{ij} \frac{\partial X}{\partial E_{ij}} = -3 \sin^2 E_{ij} \cos E_{ij} X + 4 \sin^2 E_{ij}$$

Then

$$\frac{dX}{dx} = \frac{dX}{dE_{ij}} \frac{dE_{ij}}{dx}$$

$$= \frac{4 - 3 \cos E_{ij} X}{\sin E_{ij}} \cdot \frac{1}{\frac{1}{2} \sin E_{ij}}$$

Then expanding $X(x)$ in series gives

$$X(x) = \sum_{i=0}^{\infty} A_i x^i$$

where

$$A_i = \frac{2i+4}{2i+3} A_{(i-1)} \text{ from } \frac{dX}{dx} = \sum_i A_i x^{i-1}$$

From Eq (66), $A_0 = \frac{4}{3}$. Therefore,

$$X(x) = \frac{4}{3} + \frac{4}{3} \cdot \frac{6}{5} x + \frac{4}{3} \cdot \frac{6}{5} \cdot \frac{8}{7} x^2 + \dots \quad (68)$$

The solution for a preliminary orbit by Gauss' method then proceeds as follows:

- (1) Select approximate values for ρ_1 , ρ_3 , $X \approx \frac{4}{3}$, $\eta_2 \approx \eta_3 \approx 1$, these values

to be improved by iteration. Take

$$c_1 \approx \frac{t_3 - t_2}{t_3 - t_1} \text{ and } c_3 \approx \frac{t_2 - t_1}{t_3 - t_1}$$

- (2) Determine r_1 and r_3 from $\vec{r}_i = \rho_i \hat{\rho}_i + \vec{R}_i$ and determine θ_1 , θ_3 and k from Eq (64).

$$\vec{r}_2 = c_1 \vec{r}_1 - c_3 \vec{r}_3$$

$$\vec{\rho}_2 = \vec{r}_2 - \vec{R}_2$$

- (3) Determine m from t_1 , t_2 and k by Eq

$$(64). \text{ Revise } \eta_2 = 1 + \frac{m^2 X_2}{\eta_2^2} \text{ (iteration loop).}$$

- (4) Derive ℓ from r_1 , r_2 and k by Eq (64).

Derive x from $x = \left(\frac{m}{\eta_2}\right)^2 - \ell$. Revise X from Eq (68) (iteration loop). From x obtain θ_j , $-\theta_i$ and a from Eqs (64) and (65). From E_{ij} and θ_i , θ_j determine ℓ .

- (5) Repeat (1) to (4) with ρ_1 , ρ_2 to get η_3 , X_3 .

- (6) Repeat (1) to (4) with ρ_2 , ρ_3 to get η_1 , X_1 .

- (7) Obtain improved values for c_1 and c_3 from Eqs (58) and (59).

- (8) Obtain improved values of ρ_1 and ρ_2 from Eq (57). Note that this is accomplished by dotting in turn by $\hat{\rho}_2 \times \hat{\rho}_3$ and $\hat{\rho}_1 \times \hat{\rho}_2$. The values of $\rho_1 + \rho_2$ are then obtained from the following equations.

$$c_1 (\hat{\rho}_1 \cdot \hat{\rho}_2 \times \hat{\rho}_3) \rho_1 = -c_1 (\vec{R}_1 \cdot \hat{\rho}_2 \times \hat{\rho}_3) + (\vec{R}_2 \cdot \hat{\rho}_2 \times \hat{\rho}_3) - c_3 (\vec{R}_3 \cdot \hat{\rho}_2 \times \hat{\rho}_3)$$

$$c_3 (\hat{\rho}_1 \cdot \hat{\rho}_2 \times \hat{\rho}_3) \rho_3 = -c_1 (\vec{R}_1 \cdot \hat{\rho}_1 \times \hat{\rho}_2) + (\vec{R}_2 \cdot \hat{\rho}_1 \times \hat{\rho}_2) - c_3 (\vec{R}_3 \cdot \hat{\rho}_1 \times \hat{\rho}_2)$$

- (9) Repeat (1) through (8) with improved values of ρ_1 , ρ_3 , until iteration converges.

3. Gibbs' Modification of Gauss' Method

There is an alternative method of solution for c_1 and c_3 in Gauss' Method due to Gibbs. If

$$T_1 = \sqrt{\mu} (t_3 - t_2)$$

$$T_2 = \sqrt{\mu} (t_3 - t_1)$$

$$T_3 = \sqrt{\mu} (t_2 - t_1),$$

$$\vec{r}_1 = \vec{a}_0 - \vec{a}_1 T_3 + \vec{a}_2 T_3^2 - \vec{a}_3 T_3^3 + \vec{a}_4 T_3^4 - \dots$$

$$\vec{r}_2 = \vec{a}_0$$

$$\vec{r}_3 = \vec{a}_0 + \vec{a}_1 T_1 + \vec{a}_2 T_1^2 + \vec{a}_3 T_1^3 + \vec{a}_4 T_1^4 + \dots$$

Determination of $\frac{d^2 \vec{r}_i}{dt^2}$ from these series, setting

$$\frac{d^2 \vec{r}_i}{dt^2} = -\mu \frac{\vec{r}_i}{r_i^3},$$

elimination of the \vec{a} 's and substitution in

$$\vec{r}_2 = c_1 \vec{r}_1 + c_3 \vec{r}_3$$

gives

$$\left. \begin{aligned} c_1 &= m \frac{1 + B_1/r_1^3}{1 - B_2/r_2^3} \\ c_3 &= n \frac{1 + B_3/r_3^2}{1 - B_2/r_2^3} \end{aligned} \right\} \quad (69)$$

Here

$$B_1 = (mn + n - m) \frac{T_2^2}{12}$$

$$B_2 = (mn + 1) \frac{T_2^2}{12}$$

$$B_3 = (mn - n + m) \frac{T_2^2}{12}$$

where

$$m + n = 1 \text{ and } n = T_3/T_2, m = T_1/T_2$$

4. Method of Olbers

The method of Olbers is a technique for determining preliminary parabolic orbits. As in Eq (57),

$$\begin{aligned} c_1 \vec{\rho}_1 - \vec{\rho}_2 + c_3 \vec{\rho}_3 &= -c_1 \vec{R}_1 + \vec{R}_2 \\ -c_3 \vec{R}_3 &\equiv \vec{V} \end{aligned} \quad (70)$$

The dot product of this equation and $(\hat{\rho}_2 \times \vec{U})$ where \vec{U} is coplanar with \vec{V} and $\vec{\rho}_2$,

$$\begin{aligned} \vec{U} &= \hat{\rho}_2 \times \vec{V} \times \frac{\hat{\rho}_2}{V} \\ \text{is} \\ c_1 \rho_1 (\hat{\rho}_2 \cdot \hat{\rho}_2 \times \vec{U}) + c_3 \rho_3 (\hat{\rho}_3 \cdot \hat{\rho}_2 \times \vec{U}) &= 0 \end{aligned} \quad (71)$$

Then

$$\rho_3 = M \rho_1 \quad (72)$$

where

$$M = - \frac{c_1 (\hat{\rho}_1 \cdot \hat{\rho}_2 \times \vec{U})}{c_3 (\hat{\rho}_3 \cdot \hat{\rho}_2 \times \vec{U})} \quad (73)$$

The computation then proceeds as follows:

- (1) Select initial approximate values for ρ_1 and for c_1 and c_3 such that

$$\frac{c_3}{c_1} = \frac{t_3}{t_1}.$$

Obtain ρ_3 from Eq (72).

- (2) Obtain \vec{r}_1 , c_2 and ρ_2 from ρ_1 , ρ_3 and c_3 by Eq (70).
- (3) Obtain \vec{r}_3 and $S = |\vec{r}_2 - \vec{r}_1|$ from the law of cosines

$$S^2 = r_1^2 + r_2^2 - 2r_1 r_2 \cos(\theta_2 - \theta_1).$$

- (4) Obtain

$$X = \frac{2\sqrt{\mu} (t_2 - t_1)}{(r_1 + r_2)^{3/2}}$$

- (5) Correct ρ_1 in step (1) by iteration until

$$(r_1 + r_3) X Y = S \quad (74)$$

where $X Y$ is the term in Euler's equation,

$$\frac{6\sqrt{\mu} (t_j - t_i)}{(r_i + r_j)^{3/2}} = (1 + X Y)^{3/2}$$

$$\pm (1 - X Y)^{3/2} = 3 X \quad (75)$$

- (6) Obtain η_1 , η_2 , η_3 from $\vec{r}_2 = c_1 \vec{r}_1 \mp c_2 \vec{r}_2$ and the sector to triangle area ratios defining the η 's.
- (7) Determine c_1 and c_3 from Eqs (58) and (59) and iterate until they agree with step (1).

- (8) From the corrected values of c_1 and c_2 calculate $\hat{\rho}_2$ and compare with the observed $\hat{\rho}_2$. This checks the assumption of Olbers' method that $e \approx 1$.

E. THEORY OF OBSERVATION ERROR

After a preliminary orbit has been determined as described in Section D, the elements thus determined, together with a theory of motion, may be used to calculate theoretical positions of the orbiting body at any time. If further observations of the body are then made, the observed positions will be found to deviate from the theoretical positions for the corresponding times. The differences in observed and computed positions, or residuals, may be attributed to three causes:

- (1) Approximations involved in the theory.
- (2) Inaccuracies in the preliminary orbit elements.
- (3) Errors in the observations.

In the problem of orbit improvement, to be considered in Section F, these residuals between observed and computed positions are used to improve the accuracy of the preliminary orbit elements. Since the methods of orbit improvement are rather complex in themselves, some benefit may be derived from a review, preparatory to considering these methods in Section F, of those areas of statistics and numerical analysis which are basic to the orbit improvement theories.

1. Data Errors

Data errors are of three types: systematic errors, which affect all measurements alike; mistakes, generally large errors due to careless reading of indicators or incorrect recording, which do not follow any law, and accidental errors, causes of which are unknown and indeterminate, and which are usually relatively small and follow the laws of probability. Systematic errors can be corrected to some extent by calibration of instruments, and large mistakes can be eliminated from data by use of an appropriate data rejection philosophy. The mathematical theory of errors to be discussed applies only to accidental errors, and only these errors will be considered in the analyses.

All kinds of accidental errors may be described by frequency distributions, or probability density functions, curves which give the relative frequency of occurrence of the various values in a set of observations. By far the most useful frequency distribution is the normal or Gaussian distribution,

$$f(x) = \frac{1}{\sqrt{2\pi}\sigma} \exp \left[-\frac{1}{2\sigma^2} (x - \mu)^2 \right] \quad (76)$$

which is found to describe most random or accidental data errors. A special usefulness of the normal distribution is also indicated by the mathematical theory as expressed in the central-limit theorem of statistics:

"If a population has a finite variance σ^2 and mean μ , then the distribution of the sample mean approaches the normal distribution with variance $\frac{\sigma^2}{n}$ and mean μ as the sample size n increases."

It is interesting that, regardless of the form of the population distribution function, the sample mean will be approximately normally distributed for large samples.

The parameters of the distribution, as previously indicated, are the variance σ^2 and the mean μ . Sometimes, however, other parameters are employed:

$$\text{modulus of precision} = h = \frac{\sigma}{\sqrt{2}}$$

$$\text{probable error} = 0.6745\sigma \text{ (normal distribution only)}$$

In practice, since the actual parameters σ and μ of the theoretical population distribution are not known, they must be estimated from the available data. Statistical analysis shows that the maximum-likelihood estimates of these parameters for the normal distribution, are

$$\hat{\mu} = \frac{1}{n} \sum_{i=1}^n x_i = \bar{x} \quad (77)$$

$$\hat{\sigma}^2 = \frac{1}{n} \sum_{i=1}^n (x_i - \bar{x})^2 \quad (78)$$

where n is the total number of data, x_i , in a sample.

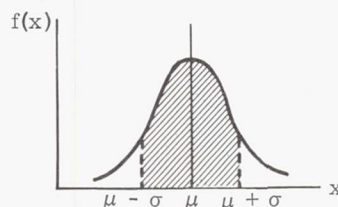
The significance of the distribution function is further indicated by noting that the area under the function contained between two arbitrary limits, x_1 and x_2 , is the probability that a given observation will lie between x_1 and x_2 , i.e.,

$$\begin{aligned} \text{Probability} \left[x_1 \leq x \leq x_2 \right] &= \int_{x_1}^{x_2} f(x) dx \\ &= \frac{1}{\sqrt{2\pi}\sigma} \int_{x_1}^{x_2} e^{-\frac{1}{2\sigma^2} (x - \mu)^2} dx \quad (79) \end{aligned}$$

Viewed from this aspect, the parameters of the normal distribution can be interpreted as follows:

μ = data value corresponding to the maximum value of the frequency distribution

σ = a span of x such that 68.26% of the area under the distribution curve is contained between the limits $\mu - \sigma$ and $\mu + \sigma$.



Probability distributions for several variables (multivariate distributions) may be defined in a similar manner, i.e.,

$$\begin{aligned} & \text{Probability } [x_1 < x < x_2, y_1 < y < y_2] \\ &= \int_{x_1}^{x_2} \int_{y_1}^{y_2} f(x, y) dy dx \end{aligned} \quad (80)$$

where $f(x, y)$ is called the joint density function for x and y . In particular, the bivariate normal distribution is

$$\begin{aligned} f(x, y) = & \frac{1}{2\pi\sigma_x\sigma_y\sqrt{1-\rho^2}} \exp \\ & \left\{ -\frac{1}{2(1-\rho^2)} \left[\left(\frac{x-\mu_x}{\sigma_x} \right)^2 \right. \right. \\ & \left. \left. - 2\rho \frac{x-\mu_x}{\sigma_x} \frac{y-\mu_y}{\sigma_y} + \left(\frac{y-\mu_y}{\sigma_y} \right)^2 \right] \right\} \end{aligned} \quad (81)$$

which represents a bell-shaped surface over the x - y plane. The parameter ρ is called the correlation between x and y . When the correlation is zero, $f(x, y)$ becomes the product of two univariate distributions

$$f(x, y) = g_1(x) g_2(y)$$

and the variates are said to be independently distributed. It is sometimes convenient to write Eq (81) in matrix notation:

$$\begin{aligned} f(x_1, x_2) = & \frac{1}{2\pi\sqrt{|\sigma_{ij}|}} \exp \\ & \left[-\frac{1}{2} \sum_{i=1}^2 \sum_{j=1}^2 \sigma^{ij} (x_i - \mu_i) (x_j - \mu_j) \right] \end{aligned} \quad (82)$$

where

$$|\sigma_{ij}| = \text{determinate of the matrix } [\sigma_{ij}]$$

$$[\sigma_{ij}] = \begin{bmatrix} \sigma_{11} & \sigma_{12} \\ \sigma_{21} & \sigma_{22} \end{bmatrix} = \text{the variance-covariance matrix}$$

$$\sigma_{11} = \sigma_x^2 \text{ and } \sigma_{22} = \sigma_y^2$$

$$\sigma_{12} = \sigma_{21} = \text{covariances}$$

$$[\sigma^{ij}] = \begin{bmatrix} \sigma_{22} & -\sigma_{12} \\ -\sigma_{21} & \sigma_{11} \end{bmatrix} = \text{inverse of } [\sigma_{ij}]$$

The extension to the general multivariate distribution is obvious:

$$\begin{aligned} f(x_1, x_2, \dots, x_k) = & \left(\frac{1}{2\pi} \right)^{\frac{k}{2}} \frac{1}{\sqrt{|\sigma_{ij}|}} \exp \\ & \left[-\frac{1}{2} \sum_{i=1}^k \sum_{j=1}^k \sigma^{ij} (x_i - \mu_i) (x_j - \mu_j) \right] \end{aligned} \quad (83)$$

Error analysis frequently requires consideration not only of random errors in measurements, but of errors in functions of the measurements. That is, the quantity sought is some known function of several measured quantities. Of particular interest is the function consisting of a linear combination of random variables. If x_1, x_2, \dots, x_k are independently and normally distributed random variables with means μ and variances σ_i^2 , and if

$$u = \sum_{i=1}^k a_i x_i, \quad (84)$$

where the a_i are arbitrary constants, then u is normally distributed with mean

$$\mu_u = \sum_{i=1}^k a_i \mu_i \quad (85)$$

and variance

$$\sigma_u^2 = \sum_{i=1}^k a_i^2 \sigma_i^2 \quad (86)$$

This case is of special interest because, even if the function of interest, u , is nonlinear, the errors in u , Δu , can usually be accurately approximated by first-order differentials, i.e.,

$$\Delta u = \frac{\partial u}{\partial x_1} \Delta x_1 + \frac{\partial u}{\partial x_2} \Delta x_2 + \dots$$

$$+ \frac{\partial u}{\partial x_k} \Delta x_k$$

which can then be treated as Eq (84).

2. The Method of Least Squares

The method of least squares is a method of finding the best possible values for a set of m unknowns, x_1, x_2, \dots, x_m , satisfying n linear equations, where $n > m$.

$$a_{11}x_1 + a_{12}x_2 + \dots + a_{1m}x_m = y_1$$

$$a_{21}x_1 + a_{22}x_2 + \dots + a_{2m}x_m = y_2$$

...

$$a_{n1}x_1 + a_{n2}x_2 + \dots + a_{nm}x_m = y_n$$

Since the number of equations exceeds the number of unknowns, and since the y_i may contain observation errors, the system of equations is not solvable exactly, i.e., there is no set x_1, x_2, \dots, x_m for which each of the n equations is exactly satisfied. Each equation then has a residual of the form

$$\delta_i = y_i - a_{i1}x_1 - a_{i2}x_2 - \dots - a_{im}x_m \quad (i = 1, 2, n) \quad (87)$$

The least squares technique attempts to find values for x_1, x_2, \dots, x_m which will make

$\sum_{i=1}^n \delta_i^2$ as small as possible. This is the criterion for "best" solutions in the least squares method. If such a set of x_i exists, it then satisfies the condition

$$\frac{\partial}{\partial x_1} \sum_{i=1}^n \delta_i^2 = 0,$$

$$\frac{\partial}{\partial x_2} \sum_{i=1}^n \delta_i^2 = 0,$$

....

$$\frac{\partial}{\partial x_n} \sum_{i=1}^n \delta_i^2 = 0$$

This differentiation results in the following m equations

$$x_1 \sum_{i=1}^n a_{i1} a_{i1} + x_2 \sum_{i=1}^n a_{i1} a_{i2} +$$

(continued)

$$\dots + x_m \sum_{i=1}^n a_{i1} a_{im} \\ = \sum_{i=1}^n a_{i1} y_i$$

$$x_1 \sum_{i=1}^n a_{i2} a_{i1} + x_2 \sum_{i=1}^n a_{i2} a_{i2} + \dots$$

$$+ x_m \sum_{i=1}^n a_{i2} a_{im} = \sum_{i=1}^n a_{i2} y_i \dots \quad (88)$$

$$x_1 \sum_{i=1}^n a_{im} a_{i1} + x_2 \sum_{i=1}^n a_{im} a_{i2} + \dots$$

$$+ x_m \sum_{i=1}^n a_{im} a_{im} = \sum_{i=1}^n a_{im} y_i$$

These equations comprise a system of m linear equations in the m unknowns x_1, x_2, \dots, x_m , which may be solved in a routine manner, e.g., by Cramer's rule. These equations are called the normal equations and are sometimes written in the following shorthand form:

$$\begin{aligned} [a_1 a_1] x_1 + [a_1 a_2] x_2 + \dots \\ + [a_1 a_m] x_m &= [a_1 y] \\ [a_1 a_2] x_1 + [a_2 a_2] x_2 + \dots \\ + [a_2 a_m] x_m &= [a_2 y] \\ \dots &\dots \\ [a_1 a_m] x_1 + [a_2 a_m] x_2 + \dots \\ + [a_m a_m] x_m &= [a_m y] \end{aligned} \quad (89)$$

These equations apply in the case in which the equations of condition, Eq (87), are of equal weight, i.e., all observations are assumed to be made with the same precision. If this is not true, then each of the residuals δ_i must be

assigned an estimated weight p_i , and each equation of condition multiplied by the square root of its weight. Then the normal equations become

$$\begin{aligned} \sum_{i=1}^n [p_i a_{i1} (x_1 a_{i1} + x_2 a_{i2} + \dots \\ + x_m a_{im} - y_i)] &= 0 \\ \sum_{i=1}^n [p_i a_{i2} (x_1 a_{i1} + x_2 a_{i2} + \dots \\ + x_m a_{im} - y_i)] &= 0 \\ \dots \\ \sum_{i=1}^n [p_i a_{im} (x_1 a_{i1} + x_2 a_{i2} + \dots \\ + x_m a_{im} - y_i)] &= 0 \end{aligned} \quad (90)$$

The weights normally utilized in these equations are inversely proportional to the variances, i. e.,

$$p_i = \frac{\sigma_i^2}{\sigma_i^2}, \quad (91)$$

where σ_i^2 is the variance corresponding to weight p_i and σ^2 is the variance corresponding to unity weight.

Use of the least squares method is not strictly limited to sets of linear equations. The method can be applied directly in the case of certain functions of an exponential type, but the usual procedure adopted in dealing with sets of nonlinear equations is to replace the functions by linear Taylor series approximations. Let the n observations α_i be related to n nonlinear functions of the unknowns to be determined, i. e.,

$$f_i(x_1, x_2, \dots, x_m) = \alpha_i - \delta_i$$

$$i = 1, 2, \dots, n, n > m$$

where the x_j are the unknowns to be determined and the δ_i are the residuals, or errors in the observations. The desired solutions may be represented by sums of approximate solutions, $(x_1)_0, (x_2)_0, \dots, (x_m)_0$, and corrections to these approximate solutions,

$$x_j = (x_j)_0 + \Delta x_j.$$

Then expansion of the f_i in Taylor series gives

$$\begin{aligned} f_i [(x_1)_0, (x_2)_0, \dots, (x_m)_0] + \left. \frac{\partial f_i}{\partial x_1} \right|_0 \Delta x_1 \\ + \left. \frac{\partial f_i}{\partial x_2} \right|_0 \Delta x_2 + \dots + \left. \frac{\partial f_i}{\partial x_m} \right|_0 \Delta x_m \\ \approx \alpha_i - \delta_i, \quad \overline{\Delta x_j}^2 \approx 0 \end{aligned} \quad (92)$$

On setting

$$\begin{aligned} \alpha_i - f_i [(x_j)_0] &\equiv y_i \\ \left. \frac{\partial f_i}{\partial x_j} \right|_0 &\equiv a_{ij}, \end{aligned}$$

Eq (92) corresponds to Eq (87), the linear equations of condition, and may therefore be solved for the "best" values of the x_j in the manner outlined previously.

For the present purposes, it is convenient to formulate the weighted least squares estimate in matrix notation. Consider the equations of condition, Eq (87)

$$\delta_i = y_i - \sum_{j=1}^m a_{ij} x_j,$$

the weighted least squares condition is that

$$\sum_{i=1}^n \frac{1}{\sigma_i^2} \left[y_i - \sum_{j=1}^m a_{ij} x_j \right]^2$$

be minimum. If the σ_i^2 do not vary significantly with x_j , setting the m derivatives

$$\frac{\partial}{\partial x_j} \sum \left(\frac{\delta_i}{\sigma_i} \right)^2 = 0$$

gives the following normal equations,

$$\sum_{i=1}^n \frac{1}{\sigma_i^2} \left[y_i - \sum_{j=1}^m a_{ij} x_j \right] a_{ik} = 0$$

$k = 1, 2, \dots, m$

or

$$\sum_{i=1}^n \frac{1}{\sigma_i^2} a_{ik} y_i - \sum_{j=1}^m \left[\sum_{i=1}^n \frac{1}{\sigma_i^2} a_{ij} a_{ik} \right] x_j = 0$$

In matrix notation, with

$$[v] \equiv \begin{bmatrix} \sigma_1^{-2} & 0 & 0 & \dots & 0 \\ 0 & \sigma_2^{-2} & 0 & \dots & 0 \\ \vdots & \vdots & \vdots & \ddots & \vdots \\ 0 & 0 & 0 & \dots & \sigma_n^{-2} \end{bmatrix}$$

the normal equations become

$$\sum_{i=1}^n [v a]_{ik} y_i - \sum_{j=1}^m \left(\sum_{i=1}^n [v a]_{ik} a_{ij} \right) x_j = 0$$

since

$$[v a]_{ik} = \sum_{\ell=1}^n v_{i\ell} a_{\ell k} = \sum_{\ell=1}^n \sigma_i^{-2} \delta_{i\ell} a_{\ell k}$$

where $\delta_{i\ell}$ is the Kronecker delta and is equal to 1 ($i = \ell$) or 0 ($i \neq \ell$). Thus, $[v a]_{ik} = \sigma_i^{-2} a_{ik}$.

But

$$\sum_{i=1}^n [v a]_{ik} y_i = \sum_{i=1}^n [v a]^t_{ki} y_i = \left([v a]^t_y \right)_k$$

and

$$\sum_{j=1}^m \left(\sum_{i=1}^n [v a]_{ik} a_{ij} \right) x_j =$$

$$= \sum_{j=1}^m \left(\sum_{i=1}^n [v a]^t_{ki} a_{ij} \right) x_j$$

(continued)

$$= \sum_{j=1}^m \left([v a]^t a \right)_{kj} x_j$$

$$= \left\{ [v a]^t a x \right\}_k$$

Therefore, the normal equations may be written

$$\left([v a]^t_y \right)_k - \left\{ \left([v a]^t a \right) x \right\}_k = 0$$

$k = 1, 2, \dots, m$

or

$$[v a]^t_y - \left([v a]^t a \right) x = 0$$

Finally, the explicit solution for the m -vector of unknowns is

$$\{x\} = \left[[v a]^t a \right]^{-1} [v a]^t \{y\}$$

or

$$\{x\} = \left[a^t v a \right]^{-1} [a]^t [v] \{y\} \quad (93)$$

where

$a = n \times m$ matrix of the a_{ij}

$v = n \times n$ diagonal matrix of the inverse variances

$y = n$ -vector of known data

Several examples of the application of the method of least squares are given in the following sections for the cases of equiweighted data.

a. Least squares fit of a straight line

The sum of the squared residuals to be minimized in fitting a straight line by the least squares technique is

$$\sum_{i=1}^n \delta_i^2 = \sum_{i=1}^n \left[y_i - (m x_i + k) \right]^2$$

$$= \sum_{i=1}^n (y_i^2 - 2 m x_i y_i - 2 k y_i + 2 k m x_i + m^2 x_i^2 + k^2)$$

which is quadratic in k , i. e.,

$$\sum_{i=1}^n \delta_i^2 = n k^2 + 2 k \left(m \sum_{i=1}^n x_i - \sum_{i=1}^n y_i \right) + C$$

where C contains all terms not involving k.

The minimum occurs for

$$\frac{\partial}{\partial k} \sum_{i=1}^n \delta_i^2 = 2nk + 2 \left(m \sum_{i=1}^n x_i - \sum_{i=1}^n y_i \right) = 0$$

or

$$\sum_{i=1}^n y_i = m \sum_{i=1}^n x_i + nk \quad (94)$$

Similarly, the quadratic in m gives

$$\sum_{i=1}^n x_i y_i = m \sum_{i=1}^n x_i^2 + k \sum_{i=1}^n x_i \quad (95)$$

Example: Consider a plot of the inverse of the nondimensional acceleration versus time. Then

$$I_{sp} = -\frac{1}{m}, x_i = \text{time points}, y_i = \frac{g}{a_t}$$

From the raw data or specific impulse of an engine in the table, compute x, y, xy and x^2 .

Raw Data for Specific Impulse of an Engine

| | \underline{x} | \underline{y} | \underline{xy} | $\underline{x^2}$ |
|-----------|---|-----------------|------------------|-------------------|
| (120 sec) | 0 | 0.1765 | 0 | 0 |
| | 0.5 | 0.1748 | 0.0874 | 0.25 |
| | 1.0 | 0.1731 | 0.1731 | 1.00 |
| | 1.5 | 0.1715 | 0.25725 | 2.25 |
| | 2.0 | 0.1697 | 0.3394 | 4.00 |
| | 2.5 | 0.1680 | 0.4200 | 6.25 |
| | 3.0 | 0.1663 | 0.4989 | 9.00 |
| | 3.5 | 0.1645 | 0.57575 | 12.25 |
| | 4.0 | 0.1627 | 0.6508 | 16.00 |
| | 4.5 | 0.1608 | 0.7236 | 20.25 |
| | 5.0 | 0.1590 | 0.7950 | 25.00 |
| | 5.5 | 0.1571 | 0.86405 | 30.25 |
| | 6.0 | 0.1553 | 0.9318 | 36.00 |
| | 6.5 | 0.1537 | 0.99905 | 42.25 |
| | 7.0 | 0.1521 | 1.0647 | 49.00 |
| | 7.5 | 0.1504 | 1.1280 | 56.25 |
| | 8.0 | 0.1484 | 1.1872 | 64.00 |
| | 8.5 | 0.1463 | 1.24355 | 72.25 |
| | 9.0 | 0.1444 | 1.2996 | 81.00 |
| | 9.5 | 0.1426 | 1.3547 | 90.25 |
| (130 sec) | 10.0 | 0.1409 | 1.4090 | 100.00 |
| | $\Sigma x = 105.0 \quad \Sigma y = 3.3381 \quad \Sigma xy = 16.00285 \quad \Sigma x^2 = 717.50 \quad (120 \text{ to } 130 \text{ sec})$ | | | |

Then, from

$$\Sigma y = m \Sigma x + n k$$

$$\Sigma xy = m \Sigma x^2 + k \Sigma x,$$

$$\begin{cases} 3.3381 = 105 m + 21 k \\ 16.00285 = 717.5 m + 105 k \end{cases}$$

Simultaneous solution of these equations gives

$$m = -0.003572207$$

$$I_{sp} = 279.938 \text{ sec from } 120 \text{ to } 130 \text{ sec.}$$

b. Least squares fit of an ellipse

A determination of the "best" elements of an ellipse from application of the least squares criterion to q sets of data (r, A, L, t),

r = radius vector

A = right ascension

L = declination (geocentric latitude)

t = time

may be based upon q sets of equations of the form

$$\begin{cases} t_k = t_p + a \sqrt{\frac{a}{\mu}} \left[\cos^{-1} \left(\frac{a - r_k}{ea} \right) \right. \\ \left. \pm \sqrt{e^2 - \left(1 - \frac{r_k}{a} \right)^2} \right] \end{cases} \quad (96)$$

$$\begin{cases} \cos A_k \cos L_k \tan i \sin \Omega \\ - \cos L_k \sin A_k \tan i \cos \Omega \\ + \sin L_k = 0 \end{cases} \quad (97)$$

where

$$k = 1, 2, \dots, q, \quad q > 3.$$

Approximate values of the elements are assumed known. These rough values will be designated a_0, e_0, t_{p0} . Then corrections $\delta a_0, \delta e_0, \delta t_{p0}$ must be computed such that

$$a = a_0 + \delta a_0$$

$$e = e_0 + \delta e_0 \quad (98)$$

$$t_p = t_{p0} + \delta t_{p0}$$

(t_p = time of perigee encounter)

are the elements that best satisfy Eq (96). Equation (96) can be written in residual form as follows:

$$\delta_k = t_{p0} + \delta t_{p0} - t_k + (a_0 + \delta a_0) \left[\frac{1}{\mu} (a_0 + \delta a_0) \right]^{1/2} \left[\cos^{-1} (a_0 + \delta a_0 - r_k) (a_0 e_0 + e_0 \delta a_0 + a_0 \delta e_0 + \delta a_0 \delta e_0)^{-1} \pm \sqrt{(e_0 + \delta e_0)^2 - \left(1 - \frac{r_k}{a_0 + \delta a_0}\right)^2} \right]$$

This equation may be linearized in terms of the corrections by means of Taylor's expansion,

$$\delta_k = \delta a_0 \frac{\partial t_k}{\partial a} + \delta e \frac{\partial t_k}{\partial e} + \delta t_p \frac{\partial t_k}{\partial t_p} + t_p - t_k + a_0 \sqrt{\frac{a_0}{\mu}} \left[\cos^{-1} \left(\frac{a_0 - r_k}{e_0 a_0} \right) \pm \sqrt{e_0^2 - \left(1 - \frac{r_k}{a_0}\right)^2} \right], \quad (99)$$

where terms of order $\{\delta(\)\}^2$ and higher have been neglected. This approximation of the Taylor series terms involving higher powers of the corrections will not affect the accuracy of the final solutions for which the corrections are very small, provided that further corrections of the form Eq (98) are applied, i. e., that the solution is obtained by a convergent iteration of the form

$$\begin{aligned} a_{n+1} &= a_n + \delta a_n \\ e_{n+1} &= e_n + \delta e_n \\ t_{p_{n+1}} &= t_{p_n} + \delta t_{p_n} \end{aligned} \quad (100)$$

Then the orbit elements which represent a least squares fit of the (r_k, t_k) data can be determined

by stipulating that $\sum_{k=1}^q \delta_k^2$ be a minimum. Evaluation of the partial derivatives of Eq (99) and substitution in Eq (100) yields the following final solutions for the planar elements:

$$a_{n+1} = a_n + \frac{1}{d} \begin{vmatrix} -\sum_k \Xi_k \Phi_k \sum_k \Xi_k \Psi_k \sum_k \Xi_k \\ -\sum_k \Psi_k \Phi_k \sum_k \Psi_k^2 \sum_k \Psi_k \\ -\sum_k \Phi_k \sum_k \Psi_k \quad q \end{vmatrix} \quad (101)$$

$$e_{n+1} = e_n + \frac{1}{d} \begin{vmatrix} \sum_k \Xi_k^2 & -\sum_k \Xi_k \Phi_k \sum_k \Xi_k \\ \sum_k \Xi_k \Psi_k & -\sum_k \Psi_k \Phi_k \sum_k \Psi_k \\ \sum_k \Xi_k & -\sum_k \Phi_k \quad q \end{vmatrix} \quad (102)$$

$$t_{p_{n+1}} = t_{p_n} + \frac{1}{d} \begin{vmatrix} \sum_k \Xi_k^2 & \sum_k \Xi_k \Psi_k & -\sum_k \Xi_k \Phi_k \\ \sum_k \Xi_k \Psi_k & \sum_k \Psi_k^2 & -\sum_k \Psi_k \Phi_k \\ \sum_k \Xi_k & \sum_k \Psi_k & -\sum_k \Phi_k \end{vmatrix} \quad (103)$$

$$\text{where } d = \begin{vmatrix} \sum_k \Xi_k^2 & \sum_k \Xi_k \Psi_k & \sum_k \Xi_k \\ \sum_k \Xi_k \Psi_k & \sum_k \Psi_k^2 & \sum_k \Psi_k \\ \sum_k \Xi_k & \sum_k \Psi_k & q \end{vmatrix}$$

$$\Xi_k = \frac{3}{2} \sqrt{\frac{a_n}{\mu}} (R_{1k} - R_{2k}) - \frac{1}{R_{2k}} \sqrt{\frac{a_n}{\mu}} \left(\frac{r_k}{a_n} \right)^2$$

$$\Psi_k = \frac{a_n}{R_{2k}} \sqrt{\frac{a_n}{\mu}} \left(\frac{a_n - r_k}{e_n a_n} - e_n \right)$$

$$\Phi_k = t_{pn} - t_k + a_n \sqrt{\frac{a_n}{\mu}} (R_{1k} - R_{2k})$$

$$R_{1k} = \cos^{-1} \left(\frac{a_n - r_k}{e_n a_n} \right)$$

$$R_{2k} = e_n \sin R_{1k}$$

In terms of true anomaly instead of time, the solution is much simpler:

$$P_n = P_{n-1} + \frac{1}{D} \left| \begin{array}{cc} \sum_{k=1}^q \Theta_k r_k - P_{n-1} & \sum_{k=1}^q \Theta_k^2 \\ P_{n-1} \sum_{k=1}^q \Theta_k^3 \cos \Theta_k & \sum_{k=1}^q \Theta_k^2 r_k \cos \Theta_k \end{array} \right| - P_{n-1} \sum_{k=1}^q \Theta_k^3 \cos \Theta_k \quad (104)$$

$$e_n = e_{n-1} + \frac{1}{D} \left| \begin{array}{cc} \sum_{k=1}^q \Theta_k^2 & \sum_{k=1}^q \Theta_k r_k - P_{n-1} \\ \sum_{k=1}^q \Theta_k^3 \cos \Theta_k & \sum_{k=1}^q \Theta_k^2 r_k \cos \Theta_k \end{array} \right| - P_{n-1} \sum_{k=1}^q \Theta_k^3 \cos \Theta_k \quad (105)$$

where

p = semilatus rectum of ellipse

$$D = \left| \begin{array}{cc} \sum_{k=1}^q \Theta_k^2 & -P_{n-1} \sum_{k=1}^q \Theta_k^3 \cos \Theta_k \\ \sum_{k=1}^q \Theta_k^3 \cos \Theta_k & P_{n-1} \sum_{k=1}^q \Theta_k^4 \cos^2 \Theta_k \end{array} \right|$$

$$\Theta_k = \frac{1}{1 + e_{n-1} \cos \Theta_k}$$

This routine is suitable for computing ellipses, parabolas or hyperbolas. There are no discontinuities since the denominator of Θ_k becomes zero only for $\cos \Theta_k = \frac{-1}{e}$, i. e., only for infinite orbital radius.

The previous routines are concerned with the computation of the elements which describe satellite position in a plane. There remains the problem of solving for the elements which define the orientation of the orbital plane in space. The equation for the orbital plane in spherical coordinates in Eq (97). Then the q data points can be used to write q residual equations.

$$P_1 \cos L_k \cos A_k - P_2 \cos L_k \sin A_k + \sin L_k = \delta_k$$

The best values of the elements Ω and i are then determined as follows

$$\Omega = \tan^{-1} \left(\frac{P_1}{P_2} \right) \quad (106)$$

$$i = \tan^{-1} \left(\frac{P_1}{\sin \Omega} \right) \quad (107)$$

where

$$P_1 = \left| \begin{array}{cc} - \sum_k \cos L_k \sin L_k \cos A_k & \sum_k \cos^2 L_k \cos A_k \sin A_k \\ \sum_k \cos L_k \sin L_k \sin A_k & \sum_k \cos^2 L_k \sin^2 A_k \end{array} \right|$$

$$P_2 = \left| \begin{array}{cc} \sum_k \cos^2 L_k \cos^2 A_k & - \sum_k \cos^2 L_k \cos A_k \sin A_k \\ - \sum_k \cos^2 L_k \sin A_k \cos A_k & \sum_k \cos^2 L_k \sin^2 A_k \end{array} \right|$$

Equations (101) through (107) may be used to investigate the effects of number, accuracy and spread of data points on the accuracy of computation.

These equations may be used to show the effects of spread of data over limited arcs of the orbit by letting sets of identical data be associated with various arc lengths. Errors due to limited sample size are to be precluded as far as possible; therefore, each set of data was selected to fit a normal distribution of zero mean and 1000-ft standard deviation in range and 0.005° in azimuth and elevation. The orbit selected for the first series of computations was the circular 6-hr orbit ($r = 5.488164 \times 10^7$ ft). The results of the computations are shown in Figs. 3, 4 and 5. Errors in computed eccentricity, semiparameter, inclination and nodal longitude are plotted against the spread of equally spaced data points for sets of four, nine and twenty-five data. For data spread over arcs of $40^\circ < \text{arc} < 90^\circ$, the iteration converged very slowly and for arcs less than 40° the solutions drifted. These figures provide a qualitative indication of the improvement of results with spread of data over wide arcs.

As indicated in the statement of the central-limit theorem in Section 0.1, the failure of a small sample of data to yield the mean of the true population gives rise to another type of error. The qualitative effect of this error may also be investigated with the previously derived solutions for least squares fit of an ellipse. Limited data samples of 6, 10, 20, 30 and 40 points were selected randomly from a normal population of $\sigma = 1000$ ft. For the case of Fig. 6, the data were taken at equal intervals over two 15° arcs at opposite sides of a 6-hr circular orbit. In Fig. 7

the results with a limited number of data are shown for data taken at equal intervals around two sample orbits, a circular 200-stat mi or 322-km orbit and an ellipse of $e = 0.4$ and $p = 3.07425 \times 10^7$ ft or 0.937031×10^4 km. The errors in computed eccentricity and semilatus rectum are shown as functions of the number of randomly selected data.

3. Other Methods of Parameter Estimation

Although the least squares method is most widely used, it is not the only technique available. Some other approaches are the minimum variance technique, the maximum likelihood estimate and the method of moments.

a. Minimum variance

The minimum variance estimate is that estimate which has a minimum variance-covariance matrix. When the errors are uncorrelated, i.e., when the covariances are zero, the minimum variance and weighted least squares methods are identical. However, when the errors are correlated, the minimum variance approach may be superior because it includes the effects of the correlations. That is, if one data type is highly correlated, the least squares technique may overly weight that data type. However, the least squares technique is generally used because the minimum variance computations are more complicated and require more detailed information about the covariances which is frequently not available. The improvement to be gained by use of the minimum variance technique is not of great significance.

The basic equations of the minimum variance approach may be developed as follows. If x_t is the true value of the unknown parameter x , and x_e is its estimated value,

$$y_i = a_i x_t + \delta_i(x_t)$$

where y_i are the observed data and $\delta_i(x_t)$ are the errors in the true unknowns, and

$$x_e = \sum_{i=1}^n b_i y_i$$

Therefore,

$$x_e = \sum_{i=1}^n b_i (a_i x_t + \delta_i)$$

is a random variable since x_e is a function of δ_i . The variance of x_e , from Eq (86), is

$$\sigma_{x_e}^2 = \sum_{i=1}^n b_i^2 \sigma_i^2$$

where

$$\sigma_i^2 = \text{variance of } \delta_i$$

if the δ_i 's are uncorrelated. If correlation exists,

$$\sigma_{x_e}^2 = \sum_{i=1}^n b_i^2 \sigma_i^2 + \sum_{\substack{i,j=1 \\ i \neq j}}^n b_i b_j \rho_{ij} \quad (108)$$

where

$$\rho_{ij} = \text{covariance of } \delta_i \text{ and } \delta_j.$$

The first summation of Eq (108) comprises the diagonal terms of the variance-covariance matrix, and the second summation represents the off diagonal terms. The minimum variance technique, as the name implies, is based on a minimization of $\sigma_{x_e}^2$, subject to the condition that the expected value of x_e is x_t . This minimization results in the following minimum variance estimates.

$$\{x_e\} = [a^t c^{-1} a]^{-1} a^t c^{-1} \{y\} \quad (109)$$

where

c = the $n \times n$ variance-covariance matrix

This equation is completely analogous to that for the least squares estimate, Eq (93), and the two estimates are obviously identical for the case of zero correlation, $c^{-1} = v$. The variance of the estimates in matrix notation is

$$\sigma_{x_e}^2 = [a^t c^{-1} a]^{-1} \quad (110)$$

b. Maximum likelihood

The maximum likelihood estimate is the estimate which maximizes the probability distribution of the data sample. If the errors are normally distributed, the maximum likelihood estimate reduces to that obtained by the minimum variance technique.

c. Method of moments

As an example of the method of moments, the problem of fitting a straight line, solved in Section D.2. a by least squares, is presented.

For a set of n values of (x_i, y_i) the r th moment of y is

$$\frac{1}{n} \sum_{i=1}^n x_i^r y_i$$

where

r is zero or a positive integer.

Now obtain two equations in m and k by equating the zeroth and first moments of the observed y 's

to the zeroth and first moments, respectively, of the y 's computed from an assumed $y = mx + k$ line fit. All moments are taken about the origin of x . These two equations may then be solved for m and k . Let o_y be observed y 's and c_y computed y 's. Then for observed y 's the first moment is

$$\frac{1}{n} \sum_{i=1}^n x_i o_{y_i}$$

and zeroth moment is

$$\frac{1}{n} \sum_{i=1}^n o_{y_i}$$

Obtain computed y 's from $c_y = mx_i + k$ and get moments

$$\frac{1}{n} \sum_{i=1}^n x_i (mx_i + k)$$

and

$$\frac{1}{n} \sum_{i=1}^n mx_i + k.$$

Equating as previously indicated,

$$\frac{1}{n} \sum_{i=1}^n y_i = \frac{1}{n} \sum_{i=1}^n (mx_i + k)$$

$$\frac{1}{n} \sum_{i=1}^n x_i y_i = \frac{1}{n} \sum_{i=1}^n [x_i (mx_i + k)]$$

Simplification of these equations gives

$$\sum_{i=1}^n y_i = m \sum_{i=1}^n x_i + nk \quad (111)$$

$$\sum_{i=1}^n x_i y_i = m \sum_{i=1}^n x_i^2 + k \sum_{i=1}^n x_i \quad (112)$$

These equations are the same as Eqs (94) and (95) in the least squares example.

Solve these for m to get

$$m = \frac{\sum_{i=1}^n y_i \sum_{i=1}^n x_i - n \sum_{i=1}^n x_i y_i}{\left(\sum_{i=1}^n x_i\right)^2 - n \sum_{i=1}^n x_i^2}$$

Example.

$$I_{sp} = -\frac{1}{m} \quad \text{when} \quad \begin{cases} x_i = \text{time points} \\ y_i = g/a_T \text{ (corresponding to } x \text{ points).} \end{cases}$$

Thus

$$I_{sp} = \frac{n \sum_{i=1}^n x_i^2 - \left(\sum_{i=1}^n x_i\right)^2}{\sum_{i=1}^n y_i \sum_{i=1}^n x_i - n \sum_{i=1}^n x_i y_i}$$

When n goes from 1, 2, ..., n

$$\sum_{i=1}^n x_i = \frac{n(n+1)}{2}$$

$$\sum_{i=1}^n x_i^2 = \frac{n(n+1)(2n+1)}{6}$$

F. ORBIT IMPROVEMENT

It has been noted that the basic problem of orbit determination is solution for the six defining parameters of an orbit from a set of observations. Orbit improvement, as distinguished from preliminary orbit determination, assumes that approximate parameters are already known and that these are to be improved in accuracy. The six parameters may be the classical orbit elements ($a, e, i, \omega, \Omega, t_p$), or the Cartesian position and velocity components at a specified time, or any set of quantities which uniquely determine the orbit. Other quantities, in addition to the six orbit parameters, could be refined in the orbit improvement process. For example, the accuracy of any geophysical constants which appear in the equations of motion (of which the six orbit parameters are constants of integration) may be improved. Examples of these constants are drag coefficients, the various coefficients of the gravitational potential function harmonics, inaccurately known locations of tracking stations, thrust corrections, etc. The basic method of computing corrections to these constants and orbit parameters is known as the differential correction technique.

1. Differential Correction Technique

The equation of motion can be written, as indicated in Chapter IV, as

$$\frac{d^2 \vec{r}}{dt^2} = -\mu \frac{\vec{r}}{r^3} + \sum_i \frac{\vec{F}_i}{m} \quad (113)$$

where the \vec{F}_i are perturbative forces due, for example, to drag, oblateness, thrust, etc. If there were no errors in the observations or inaccuracies

in the physical constants of Eq (113), all data would be exact solutions to this equation. The six constants of integration (the orbit parameters) involved in the solution of this equation could then be evaluated exactly. That is, if there existed an explicit solution for Eq (113),

$$f_i(x_1, x_2, \dots, x_m) = y_i \quad i = 1, 2, \dots, n$$

where

y_i = the observed data

x_j = the unknown orbit parameters and physical constants

f_i = some nonlinear function,

the m values of x_j would be determined if at least m values of data y_i were available. However, no observation will be exactly correct, and so this equation becomes

$$f_i(x_1, x_2, \dots, x_m) = y_i - \delta_i$$

$$i = 1, \dots, n, n > m$$

where δ_i is the error in the i th item of observed information y_i . Although the functional relationship expressed in this equation is very complicated, simple linear approximate functions of the corrections to the unknowns, Δx_i , can be written from Taylor series

$$\begin{aligned} f_i(x_{01}, x_{02}, \dots, x_{0m}) + \left. \frac{\partial f_i}{\partial x_1} \right|_0 \Delta x_1 \\ + \left. \frac{\partial f_i}{\partial x_2} \right|_0 \Delta x_2 + \dots + \left. \frac{\partial f_i}{\partial x_m} \right|_0 \Delta x_m \\ = y_i - \delta_i \end{aligned}$$

or

$$\sum_{j=1}^m \left. \frac{\partial f_i}{\partial x_j} \right|_0 \Delta x_j = \Delta y_i - \delta_i$$

where $x_{01}, x_{02}, \dots, x_{0m}$ are known approximate values of x_j , Δy_i are the differences in observed and computed or anticipated data and the corrected values of the parameters to be determined are

$$x_j = x_{0j} + \Delta x_j$$

This procedure is useful in the problem of orbit improvement, where approximate values of the parameters are assumed known from preliminary determinations. Then, if an excess of data is taken, $n > m$, the "best" values for the corrections can then be determined by the method of least squares as outlined in Section E. 2 for

$$a_{ij} = \left. \frac{\partial f_i}{\partial x_j} \right|_0$$

The normal equations corresponding to Eq (90) are

$$\sum_{i=1}^n \frac{1}{\sigma_i^2} \left[\Delta y_i - \sum_{j=1}^m \left. \frac{\partial f_i}{\partial x_j} \right|_0 \Delta x_j \right] \left. \frac{\partial f_i}{\partial x_k} \right|_0 = 0$$

$$j, k = 1, 2, \dots, m$$

(114)

This process of correcting parameters which are known approximately, is referred to as differential correction, and is not strictly limited to orbit improvement. In the case of launch of an artificial satellite, for example, the nominal trajectory parameters can be used as the initial approximate values to be refined. The only restriction is that the approximate values be sufficiently accurate to validate neglecting higher terms in the Taylor series (i.e., assure convergence of the iteration). The results of Section E are applicable to this method of estimation of orbit parameters. In particular, the matrix formulation for the estimated values, from Eq (93), is

$$\{\Delta x\} = [a^t v a]^{-1} [a]^t [v] \{\Delta y\} \quad (115)$$

where

$[a]$ = $n \times m$ matrix of the partial derivative coefficients

$[v]$ = $n \times n$ diagonal matrix of the inverse variances

and the variances of the estimated values are, from Eq (108) or Eq (110)

$$\sigma_{x_e}^2 = \sum_{i=1}^n b_i^2 \sigma_i^2 \quad (\text{no correlation})$$

or

$$\sigma_{x_e}^2 = [a^t v a]^{-1}$$

(116)

2. Determination of Partial Derivatives

In the matrix $[a^t a]$ there are elements of the form

$$\sum_{i=1}^n \left(\frac{\partial y_i}{\partial x_j} \frac{\partial y_i}{\partial x_k} \right)$$

where x_j and x_k are parameters at initial epoch. It is convenient, in the calculation of partials of the form $\frac{\partial y_i}{\partial x_j}$, to separate the partial into components which may be determined individually with greater ease.

$$\frac{\partial y_i}{\partial x_j} = \frac{\partial y_i}{\partial X} \frac{\partial X}{\partial x_j} + \frac{\partial y_i}{\partial Y} \frac{\partial Y}{\partial x_j} + \frac{\partial y_i}{\partial Z} \frac{\partial Z}{\partial x_j} + \frac{\partial y_i}{\partial \dot{X}} \frac{\partial \dot{X}}{\partial x_j} + \frac{\partial y_i}{\partial \dot{Y}} \frac{\partial \dot{Y}}{\partial x_j} + \frac{\partial y_i}{\partial \dot{Z}} \frac{\partial \dot{Z}}{\partial x_j}$$

where (X, Y, Z) and (\dot{X} , \dot{Y} , \dot{Z}) are the current position and velocity components. The partials of the observed quantities,

$$\frac{\partial y_i}{\partial X}, \frac{\partial y_i}{\partial \dot{X}},$$

etc., are derivable in analytic form from the definitions of the y_i . The derivatives

$$\frac{\partial \dot{X}}{\partial x_j}, \frac{\partial \dot{X}}{\partial \dot{x}_j}$$

etc., are obtained by numerical integration. From the equation of motion,

$$\ddot{X} = F,$$

$$\frac{d^2}{dt^2} \left(\frac{\partial X}{\partial x_j} \right) = \frac{\partial F}{\partial X} \frac{\partial X}{\partial x_j} + \frac{\partial F}{\partial Y} \frac{\partial Y}{\partial x_j} + \frac{\partial F}{\partial Z} \frac{\partial Z}{\partial x_j} + \frac{\partial F}{\partial \dot{X}} \frac{\partial \dot{X}}{\partial x_j} + \frac{\partial F}{\partial \dot{Y}} \frac{\partial \dot{Y}}{\partial x_j} + \frac{\partial F}{\partial \dot{Z}} \frac{\partial \dot{Z}}{\partial x_j}$$

Equations of this type are doubly integrated numerically to give

$$\frac{\partial X}{\partial x_j}, \frac{\partial Y}{\partial x_j}, \frac{\partial Z}{\partial x_j}$$

and differentiation of these partials yields

$$\frac{\partial \dot{X}}{\partial x_j}, \frac{\partial \dot{Y}}{\partial x_j}, \frac{\partial \dot{Z}}{\partial x_j}.$$

3. Analytic Solutions for Partial Derivatives

Corrections in a set of orbit elements may be related analytically to corrections in the Cartesian coordinates. One convenient set of orbit element corrections is $d\psi_x$, $d\psi_y$, $d\psi_z$, dM_0 , da , de , where the $d\psi$'s are rotations about the Cartesian axes,

$$dx = zd\psi_y - yd\psi_z$$

$$dy = x d\psi_z - zd\psi_x$$

$$dz = y d\psi_x - xd\psi_y \quad (117)$$

and

$$\begin{aligned} dM_0 &= \text{correction in mean anomaly} \\ da &= \text{correction in semimajor axis} \\ de &= \text{correction in eccentricity} \end{aligned}$$

The differentials dM_0 , da , de are obtained from the equations of Keplerian motion. If \hat{p} and \hat{q} are unit vectors along the x_ω and y_ω axes (the orbit plane coordinates defined in Section B.)

$$\vec{r} = a (\cos E - e) \hat{p} + a \sqrt{1 - e^2} \sin E \hat{q} \quad (118)$$

$$\begin{aligned} d\vec{r} &= \left[(\cos E - e) da + a (-\sin E dE - de) \right] \hat{p} \\ &+ \left[\sqrt{1 - e^2} (\sin E da + a \cos E dE) - a \sin E \frac{e de}{\sqrt{1 - e^2}} \right] \hat{q} \quad (119) \end{aligned}$$

The nomenclature is that of Chapter III.

But, from Kepler's equation,

$$E - e \sin E = M_0 + \frac{\sqrt{\mu}}{a^{3/2}} (t - t_0), \quad (120)$$

$$\begin{aligned} dE &= \frac{a}{r} \left[\sin E de + dM_0 \right. \\ &\quad \left. - \frac{3}{2} \frac{\sqrt{\mu}}{a^{3/2}} (t - t_0) \frac{da}{a} \right] \end{aligned}$$

Substitution of this equation in Eq (119) and noting that

$$\begin{aligned} \sin E &= - \frac{\dot{x}_\omega r}{\sqrt{\mu a}} \\ \vec{v} &= \frac{1}{r} \sqrt{\frac{\mu}{a}} \left[-a \sin E \hat{p} + a \sqrt{1 - e^2} \cos E \hat{q} \right] \quad (121) \end{aligned}$$

gives

$$\begin{aligned} dx_\omega &= \left[x_\omega + m \frac{\dot{x}_\omega}{n} \right] \frac{da}{a} - \left[a - \frac{\dot{x}_\omega}{n} \sin E \right] de + \frac{\dot{x}_\omega}{n} dM_0 \\ dy_\omega &= \left[y_\omega + m \frac{\dot{y}_\omega}{n} \right] \frac{da}{a} - \left[\frac{ey_\omega}{1 - e^2} - \frac{\dot{y}_\omega}{n} \sin E \right] de \\ &\quad + \frac{\dot{y}_\omega}{n} dM_0 \quad (122) \end{aligned}$$

where

$$n = \frac{\sqrt{\mu}}{a^{3/2}} \quad (123)$$

$$m = - \frac{3}{2} \frac{\sqrt{\mu}}{a^{3/2}} (t - t_0). \quad (124)$$

It is desirable to write the eccentricity sensitivities in the form

$$\frac{\partial x}{\partial e} = Hx + K\dot{x}, \quad x \rightarrow y, z.$$

Solving the simultaneous equations

$$\begin{cases} \frac{\partial x}{\partial e} = Hx_{\omega} + K\dot{x}_{\omega} \\ \frac{\partial y}{\partial e} = Hy_{\omega} + K\dot{y}_{\omega} \end{cases}$$

gives

$$H = \frac{\dot{y}_{\omega} \frac{\partial x}{\partial e} - \dot{x}_{\omega} \frac{\partial y}{\partial e}}{x_{\omega} \dot{y}_{\omega} - y_{\omega} \dot{x}_{\omega}}$$

$$K = \frac{x_{\omega} \frac{\partial y}{\partial e} - y_{\omega} \frac{\partial x}{\partial e}}{x_{\omega} \dot{y}_{\omega} - y_{\omega} \dot{x}_{\omega}}.$$

Substituting for $\frac{\partial x}{\partial e}$ and $\frac{\partial y}{\partial e}$ from Eq (122) and for $x_{\omega}, y_{\omega}, \dot{x}_{\omega}, \dot{y}_{\omega}$ from Eqs (118) and (121) gives

$$H = -\frac{1}{1-e^2} (\cos E + e) \quad (125)$$

$$K = \frac{1}{n} \frac{\sin E}{1-e} (2 - e^2 - e \cos E). \quad (126)$$

Then the final form of the differential correction equation is

$$\begin{bmatrix} dx \\ dy \\ dz \end{bmatrix} = \begin{bmatrix} 0 & z & -y & \frac{\dot{x}}{n} & Hx + K\frac{\dot{x}}{n}x + m & \frac{\dot{x}}{n} \\ -z & 0 & x & \frac{\dot{y}}{n} & Hy + K\frac{\dot{y}}{n}y + m & \frac{\dot{y}}{n} \\ y & -x & 0 & \frac{\dot{z}}{n} & Hz + K\frac{\dot{z}}{n}z + m & \frac{\dot{z}}{n} \end{bmatrix} \begin{bmatrix} d\psi_x \\ d\psi_y \\ d\psi_z \\ dM_0 \\ de \\ \frac{da}{a} \end{bmatrix} \quad (127)$$

where m, n, H and K are given by Eqs (123) through (126). This equation is due to Eckert and Brouwer, Ref (5). In vector notation,

$$d\vec{r} = (d\vec{\psi} \times \vec{r}) + \frac{\vec{v}}{n} dM_0 + (H\vec{r} + K\frac{\vec{v}}{n}) de + (\vec{r} + m\frac{\vec{v}}{n}) \frac{da}{a}. \quad (128)$$

Eq (127) can be transformed to the satellite oriented system (X_s, Y_s, Z_s) by

$$\begin{aligned} dx_s &= d\vec{r} \cdot \hat{r} \\ dy_s &= d\vec{r} \cdot \hat{n} \\ dz_s &= d\vec{r} \cdot \hat{m}. \end{aligned}$$

Evaluation for each term of Eq (128) proceeds as follows.

$$\begin{aligned} (d\vec{\psi} \times \vec{r}) \cdot \hat{r} &= d\vec{\psi} \cdot (\vec{r} \times \hat{r}) = 0 \\ (d\vec{\psi} \times \vec{r}) \cdot \hat{n} &= d\vec{\psi} \cdot (\vec{r} \times \hat{n}) = d\vec{\psi} \cdot r\hat{m} = rd\psi_m \\ (d\vec{\psi} \times \vec{r}) \cdot \hat{m} &= d\vec{\psi} \cdot (\vec{r} \times \hat{m}) = d\vec{\psi} \cdot (-r\hat{n}) \end{aligned}$$

$$\text{If } d\vec{\psi} = d\psi_p \hat{p} + d\psi_q \hat{q} + d\psi_s \hat{s},$$

$$\begin{aligned} (d\vec{\psi} \times \vec{r}) \cdot \hat{n} &= rd\psi_s \\ (d\vec{\psi} \times \vec{r}) \cdot \hat{m} &= -rd\psi_p p \cdot n - d\psi_q r \hat{q} \cdot \hat{n} \\ &= d\psi_p b \sin E - d\psi_q a (\cos E - e) \end{aligned}$$

Also

$$\begin{aligned} \frac{\vec{v}}{n} \cdot \hat{r} &= \frac{V}{n} = \frac{a^2}{r} e \sin E \\ \frac{\vec{v}}{n} \cdot \hat{n} &= \frac{1}{n} \frac{\sqrt{\mu p}}{r} = \frac{a^2}{r} \sqrt{1-e^2} \\ \frac{\vec{v}}{n} \cdot \hat{m} &= 0 \end{aligned}$$

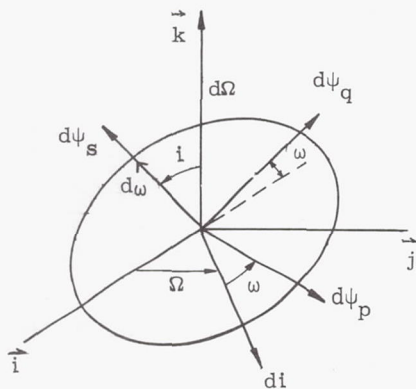
$$\begin{aligned} (H\vec{r} + K\frac{\vec{v}}{n}) \cdot \hat{r} &= rH + K\frac{a^2}{r} e \sin E \\ (H\vec{r} + K\frac{\vec{v}}{n}) \cdot \hat{n} &= K\frac{a^2}{r} \sqrt{1-e^2} \\ (H\vec{r} + K\frac{\vec{v}}{n}) \cdot \hat{m} &= 0 \\ (\vec{r} + m\frac{\vec{v}}{n}) \cdot \hat{r} &= r + m\frac{a^2}{r} e \sin E \\ (\vec{r} + m\frac{\vec{v}}{n}) \cdot \hat{n} &= m\frac{a^2}{r} \sqrt{1-e^2} \\ (\vec{r} + m\frac{\vec{v}}{n}) \cdot \hat{m} &= 0. \end{aligned}$$

Then Eq (127) can be written

$$\begin{bmatrix} dx_s \\ dy_s \\ dz_s \end{bmatrix} = \begin{bmatrix} 0 & 0 & 0 & B & rH + KB & r + mB \\ 0 & 0 & r & C & KC & mC \\ b \sin E & -a(\cos E - e) & 0 & 0 & 0 & 0 \end{bmatrix} \begin{bmatrix} d\psi_p \\ d\psi_q \\ d\psi_s \\ dM_0 \\ de \\ \frac{da}{a} \end{bmatrix} \quad (129)$$

where

$$\begin{aligned} B &= \frac{a^2}{r} e \sin E \\ C &= \frac{a^2}{r} \sqrt{1-e^2} \end{aligned}$$

$$di = d\psi_p \cos \omega - d\psi_q \sin \omega. \quad (130)$$

$$d\Omega \sin i = d\psi_a \cos \omega + d\psi_p \sin \omega. \quad (131)$$
$$d\omega + d\Omega \cos i = d\psi_g. \quad (132)$$
$$\left\{ \vec{\text{dr}}_0 \right\} = T_{-0} T_{-\Omega} T_{-i} T_{-(w+\theta)} \left\{ \vec{\text{dr}}_s \right\} \quad (133)$$

The final step in formulating the differential correction equations is the transformation to the differentials in the data. For example, from Eqs (42 or (45),

$$\begin{bmatrix} d' \\ dm \\ dn \end{bmatrix} = T_I \left\{ \vec{dr}_0 \right\} \quad (134)$$

$$\begin{bmatrix} d\rho \\ \cos \epsilon \, d\alpha \\ d\epsilon \end{bmatrix} = T_r \left\{ \vec{dr}_0 \right\} \quad (135)$$
$$\vec{v} = \frac{1}{1 - e \cos E} \sqrt{\frac{\mu}{a}} (-\sin E \hat{p} + \sqrt{1 - e^2} \cos E \hat{q}).$$
$$dE = \frac{a}{r} \left[\sin E \, de + dM_0 - \frac{3}{2} \frac{\sqrt{\mu}}{a^{3/2}} (t - t_0) \frac{da}{a} \right],$$

$$\begin{aligned} \bar{dv} = & \hat{p} \left[\left(-\frac{\dot{x}_w}{2a} - \frac{\sqrt{\mu a}}{r^3} m x_w \right) da \right. \\ & - \frac{\sqrt{\mu}}{r^3} a^{3/2} x_w dM_0 \\ & - \frac{\sqrt{\mu}}{r^2} a^{3/2} \sin E \left\{ \cos E \right. \\ & \left. + \frac{a}{r} (\cos E - e) \right\} de \left. \right] \\ & + \hat{q} \left[\left(-\frac{\dot{y}_w}{2a} - \frac{\sqrt{\mu a}}{r^3} m y_w \right) da \right. \\ & - \frac{\sqrt{\mu}}{r^3} a^{3/2} y_w dM_0 \\ & - \frac{\sqrt{\mu a}}{r} \left(\frac{a^2}{2} \sqrt{1 - e^2} \sin^2 E \right. \\ & \left. - \frac{a}{r} \sqrt{1 - e^2} \cos^2 E + \frac{e \cos E}{\sqrt{1 - e^2}} \right) de \left. \right] \end{aligned}$$

$$-\frac{\sqrt{\mu}}{r^3} a^{3/2} \vec{r} \cdot \vec{r} = -\sqrt{\frac{\mu}{a}} \left(\frac{a}{r} \right)^2$$

$$-\frac{\sqrt{\mu}}{r^3} a^{3/2} \vec{r} \cdot \hat{n} = 0$$

$$-\frac{\sqrt{\mu}}{r^3} a^{3/2} \hat{r} \cdot \hat{m} = 0$$

$$\begin{aligned} \left(-\frac{\vec{v}}{2a} - \frac{\sqrt{\mu a}}{r^3} m \vec{r} \right) \cdot \hat{r} &= -\frac{v_r}{2a} - \frac{\sqrt{\mu a}}{r^2} m \\ &= -\sqrt{\frac{\mu}{a}} - \frac{a}{r} \left(\frac{e}{2} \sin E + m \frac{a}{r} \right) \end{aligned}$$

$$\left(-\frac{\vec{v}}{2a} - \frac{\sqrt{\mu a}}{r^3} m \vec{r} \right) \cdot \hat{n} = -1/2 \frac{a}{r} \sqrt{\frac{\mu(1-e^2)}{a}}$$

$$\left(-\frac{\vec{v}}{2a} - \frac{\sqrt{\mu a}}{r^3} m \vec{r} \right) \cdot \hat{m} = 0$$

Finally,

$$\left\{ \frac{d\vec{v}}{dt} \right\} = \begin{bmatrix} 0 & 0 & \alpha_3 & \alpha_4 & \alpha_5 & \alpha_6 \\ 0 & 0 & \beta_3 & 0 & \beta_5 & \beta_6 \\ \gamma_1 & \gamma_2 & 0 & 0 & 0 & 0 \end{bmatrix} \begin{bmatrix} d\psi_p \\ d\psi_q \\ ed\psi_s \\ dM_0 + d\psi_s \\ de \\ \frac{da}{a} \end{bmatrix} \quad (136)$$

where

$$\alpha_3 = \sqrt{\frac{\mu}{a}} \frac{a}{r} \left(\frac{a}{r} \cos E + \frac{e}{1 + \sqrt{1-e^2}} \right)$$

$$\alpha_4 = \sqrt{\frac{\mu}{a}} \left(\frac{a}{r} \right)^2$$

$$\alpha_5 = \alpha_4 \sin E$$

$$\alpha_6 = \sqrt{\frac{\mu}{a}} \frac{a}{r} \left(\frac{e}{2} \sin E + m \frac{a}{r} \right)$$

$$\beta_3 = \sqrt{\frac{\mu}{a}} \frac{a}{r} \sin E$$

$$\beta_5 = \frac{a}{r} \cos E \sqrt{\frac{\mu}{p}}$$

$$\beta_6 = -1/2 \frac{a}{r} \sqrt{\frac{\mu(1-e^2)}{a}}$$

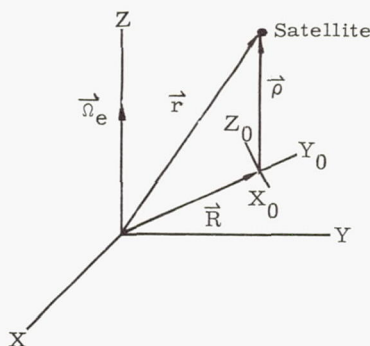
$$\gamma_1 = \sqrt{\frac{\mu a}{r}} \sqrt{1-e^2} \cos E$$

$$\gamma_2 = \sqrt{\frac{\mu a}{r}} \sin E$$

The velocity of interest is not the total velocity but the component of relative velocity along the

line of sight. If \vec{R} is the position vector of the observer in geocentric equatorial inertial coordinates (x, y, z) and $\vec{\rho}$ is the position vector of the satellite in topocentric coordinates,

$$\vec{r} = \vec{R} + \vec{\rho}$$



Differentiating,

$$\vec{v} = \frac{d\vec{R}}{dt} + \frac{d\vec{\rho}}{dt} + \vec{\Omega}_e \times \vec{\rho}$$

where $\frac{d\vec{\rho}}{dt}$ is the velocity of the satellite relative to the observer and $\vec{\Omega}_e$ is the angular velocity of the earth's rotation, or

$$\frac{d\vec{\rho}}{dt} = \vec{v} - \vec{\Omega}_e \times \vec{r}$$

The Doppler shift being measured is

$$\frac{d\rho}{dt} = \hat{\rho} \cdot \frac{d\vec{\rho}}{dt} = \hat{\rho} \cdot (\vec{v} - \vec{\Omega}_e \times \vec{r})$$

where $\hat{\rho}$ is the unit vector along the line of sight. Then, considering variations due to changes in the orbit elements only,

$$\delta \left(\frac{d\rho}{dt} \right) = \hat{\rho} \cdot (\delta \vec{v} - \vec{\Omega}_e \times \delta \vec{r}) + (\vec{v} - \vec{\Omega}_e \times \vec{r}) \cdot \delta \left[\frac{\vec{r} - \vec{R}}{\rho} \right]$$

Since $\delta \vec{R} = 0$ (i.e., the observer's position is not a function of the orbit elements) and $\delta \rho = \delta \vec{r} \cdot \hat{\rho}$,

$$\delta \left(\frac{d\rho}{dt} \right) = \hat{\rho} \cdot \{ \delta \vec{v} \} - \{ \delta \vec{r} \} \cdot \left[\vec{\rho} \times \vec{\Omega}_e - \frac{d\vec{\rho}}{dt} \frac{1}{\rho} + \left(\frac{d\vec{\rho}}{dt} \cdot \hat{\rho} \right) \frac{\hat{\rho}}{\rho} \right]$$

$$= \hat{\rho} \cdot \{ \delta \vec{v} \} - \{ \delta \vec{r} \} \cdot \left(\hat{\rho} \times \vec{\Omega}_e - \frac{d\hat{\rho}}{dt} \right)$$

where $\delta \vec{v}$ and $\delta \vec{r}$, as previously given, are the differential correction expressions involving the corrections in the elements.

G. ACCURACY OF DETERMINATIONS

1. Sources of Error

The accuracy of an orbit determination depends on not only the precision of the measurements but on knowledge of the errors and how the errors can be eliminated. Errors are broadly divided into two classes: systematic and random. Random errors can be minimized if the statistical properties of the noise spectrum are known; systematic errors, if known, can be removed by various techniques such as calibrations against known standards.

Systematic errors. Systematic errors are errors which occur in the measurements (sensors), the station location (geodetic), and the description of the orbit (simulation). Equipment sensor biases may be due to refraction effects in the measurement of angles, mechanical misalignment of the electrical axis with the geometrical axis of a parabolic reflector antenna (boresighting), drift of d-c reference voltages, surveying errors of true north or of the local horizon plane in the measurement of azimuth and elevation, error in the adopted value for the velocity of light, backlash in the servo gears which move the antenna, and sag in the antenna at different attitudes.

Range measurements, assuming a monopulse radar, can have systematic delays in propagation, false signals due to reflections, timing errors and gating errors. Some of these errors are removed by using a beacon on board the satellite which changes the frequency of the return with a known delay.

Range rate errors, using a doppler technique, can acquire systematic errors due to variable ion densities which change the frequency of the carrier to give spurious doppler effects. If a transponder is used on board, there could be small systematic retransmission errors. If the station location is not well known, there will be systematic errors for example due to errors in the calculated velocity of the station about the earth's axis.

Other geodetic uncertainties, such as in the figure of the earth, gravity anomalies, and representation of the potential function may contribute to significant errors in orbit determination. The degree of completeness of the simulation model, for example the inclusion of nongravitational losses (radiation pressure, atmospheric drag fluctuations, etc.) and perturbations due to, say, other planets or other bodies, will contribute to errors.

Noise. Some of the sources of noise which degrade observational data are atmospheric, cosmic, man-made, and thermal. Atmospheric noise is due mostly to electrical storms and varies widely throughout the year. Cosmic noise comes from the center of the galactic plane, the sun, and from a certain number of "radio" stars such as Cassiopeia.

Man-made noise comes primarily from extraneous electromagnetic radiation generated by electrical devices.

Much of the above noise can be minimized by modulation techniques which translate the information band to carrier frequencies that lie outside the noise bandwidths.

On the other hand, thermal noise covers a very wide bandwidth of frequencies and can be minimized by using specialized techniques such as phase-locked loops and cold-temperature receivers.

One obvious method of minimizing all noise is to increase the signal power. This can be accomplished by putting a transmitter on board the satellite thus eliminating the need for skin tracking.

The best set of carrier frequencies to use to minimize cosmic noise lies in the band between 1000 mc and 10,000 mc. Man-made and atmospheric noise are also extremely low in this band.

Thermal noise power at the receiver of a tracking antenna is caused by thermal agitation of electrons in the resistances in the input network. Thermal noise received power can be expressed by

$$P_N = k \cdot T \cdot \Delta f \cdot NF$$

where

P_N = Available noise power at the receiver (watts)

k = Boltzmann's constant = 1.38×10^{-32} w-sec/°K

T = Effective input temperature (not necessarily the physical ambient temperature) (°K)

Δf = Effective input noise bandwidth (cps)

NF = Noise figure of input circuit (up to the demodulator).

Reducing T , Δf , or NF will reduce the noise power. Temperature T can be reduced by bathing the receiver in a cold environment, using receivers whose effective temperature is low (such as reactive amplifiers and masers), and by "looking" only at cold space. Noise bandwidth can be reduced by using narrowband filtering but this also limits the signal bandwidth.

As long as the signal is above a certain threshold, modulation techniques such as frequency modulation and pulse code modulation can be utilized which very effectively suppress the noise. The improvement of signal to noise ratio is $\sqrt{3}$ by using an f-m system instead of an a-m system with identical input bandwidth (for random noise).

Another method of suppressing noise is to use a phase-locked loop in which a ground transmitter transmits to the satellite transponder which transmits back down to a ground receiver. The ground receiver is kept locked in phase to a multiple of the transmitter frequency by a voltage-controlled-oscillator which beats against the received frequency and whose frequency is controlled by an

error voltage from a phase detector. The voltage controlled oscillator "follows" the received frequency but with just enough lag to allow a very narrow band of frequencies to filter through the loop. This narrow band is used as the information band; and the information can be picked off by filtering. Since the bandwidth is so narrow the noise content is very small.

2. Examples of Probable Errors

Examples of the probable errors of orbit determinations based on measured standard deviations of radar stations versus various parameters follow (see Ref. 7).

Description: The sets of curves are plots of the 1 σ errors of the classical elements versus radar errors. Notice that the correlations between orbital parameters have not been plotted.

| Altitude | Observations |
|----------|--|
| 370 km | Angles and range rate (range rate held fixed) Angles and range (range held fixed) Angles and range (angles held fixed) |
| 650 km | Same |
| 930 km | Same |
| 3700 km | Same |

Briefly, the studies produced outputs which were the standard deviations (1 sigma) of the geocentric spherical coordinates (r, A, D, v, η), orbit elements ($a, e, i, \Omega, \omega, M$), and periods (τ) of various orbits of earth satellites.

Key to Symbols:

| | |
|-----------------|--|
| $L_v \Lambda_v$ | = latitude, longitude respectively of vehicle being tracked |
| $L_s \Lambda_s$ | = latitude, longitude respectively of station(s) tracking vehicle |
| A | = right ascension of vehicle |
| D | = declination of vehicle |
| v | = velocity angle with the local geocentric vertical |
| η | = velocity angle with north on the local horizontal plane |
| r | = geocentric distance |
| v | = inertial velocity |
| a | = semimajor axis of ellipse of vehicle orbit |
| e | = eccentricity axis of ellipse of vehicle orbit |
| i | = inclination of orbit plane with the equatorial plane |
| Ω | = location of node of ellipse with respect to vernal equinox τ |
| ω | = argument of perigee of ellipse |
| M | = mean anomaly |
| τ | = period of orbit |
| σ_j | = standard deviation of any quantity j ($\sigma_\alpha = \sigma_\epsilon$) |

N = number of observations

T_\oplus = distance (in degrees) of earth track of vehicle at closest approach to tracking station

h = altitude from surface of \oplus

The spherical coordinates, orbital elements and periods were calculated by the computer program and were based on least square fits of observations. The observations were generated from trajectory tapes with noise added.

The inputs to the curve fitting program were observations (range, range rate, azimuth and elevation) of a "satellite" by a tracking station(s) versus time, the station location(s), assumed standard deviations of the observational data, the nominal orbit of the satellite, and the data rate of the station(s).

To obtain the tables and graphs included in this section, many of the input variables were varied to obtain various outputs.

Quantities varied were: observational sigmas, station locations, orbit parameters, number of iterations, earth tracks of satellites and data rates. The earth track (designated \oplus track) of a satellite is the projection of the orbit upon the surface of the earth; the earth track was specified by the number of great circle degrees away from the tracking station at closest approach.

Thus graphs were obtained which were plots of $\sigma_L, \sigma_\rho, \sigma_\rho^*$

$\sigma_A, \sigma_D, \sigma_r, \sigma_v, \sigma_\eta, \sigma_v$ versus

$\sigma_\epsilon, \sigma_\rho, \sigma_\rho^*, \oplus \text{ track}, h, \tau, \Lambda, L$

$\sigma_a, \sigma_e, \sigma_i, \sigma_\Omega, \sigma_\omega, \sigma_M$ versus

$\sigma_\epsilon, \sigma_\rho, \sigma_\rho^*, \oplus \text{ track}, h, \tau, \Lambda, L$

σ_τ versus $\sigma_\epsilon, \sigma_\rho, \sigma_\rho^*, \oplus \text{ track}, h, \tau, \Lambda, L$

Only graphs showing the spherical and orbital errors versus σ_ϵ and σ_ρ are given in this section; these result in 36 graphs.

Other pertinent points:

- (1) All observations were some combination of range, range rate, azimuth and elevation.
- (2) All output sigmas are normalized to 16 observations by multiplying by $\sqrt{N/4}$ where N is the number of observations in a given pass of data.
- (3) Azimuth and elevation sigmas are always assumed equal and are usually plotted as σ_ϵ . ($\sigma_\alpha = \sigma_\epsilon$)
- (4) For comparison, most runs used only one iteration.

- (5) Asymptotes are drawn on the graphs as straight lines.

Most of the graphs tend to show diminishing returns in accuracy of orbit determination in attempting to improve the angular accuracy better than 0.5° (if the sigma of range rate is held fixed at 1 fps (0.3 mps) and no range observations are taken).

Using only range and range rate observations, the same accuracies in orbit determination as above i.e., ($\sigma_\epsilon = 0.5^\circ$, $\sigma_\rho = 1$ fps 0.3 mps) can be obtained if the deviations are 600 ft (183 m) in range and 1 fps in range rate.

Hence a "balanced" tracking system could be defined as one whose measurement standard deviations are as follows:

$$\begin{aligned}\sigma_\rho &= 1 \text{ fps } 0.3 \text{ mps (range rate observation error)} \\ \sigma_\rho &= 600 \text{ ft } 183 \text{ m (range observation error)} \\ \sigma_\epsilon &= 0.5^\circ \text{ (azimuth and elevation angular observation errors)}\end{aligned}$$

The word "balanced" used here is not to be used in the sense of optimum but rather in the sense that improving the accuracy of one (only) type of measurement does not produce a proportionate increase in the orbit determination (assuming a balanced system).

3. Graphical Display of Observation Errors

Three basic sets of information are presented for the mission analyst: (1) angular observation errors for an assumed standard deviation of 1 fps (0.3 mps) in range rate measurement σ_ρ , (2) angular observation errors for an assumed standard deviation of 600 ft (183 m) in range measurement σ_ρ , and

(3) range observation errors for an assumed standard deviation of 0.05° in azimuth and elevation angle measurement σ_ϵ . For each set are shown the six spherical coordinates (σ : A, D, r, ν , η , ν) and the six orbital elements (σ : a, e, i, Ω , ω , M) for orbits of four different altitudes (approximately 370, 650, 930 and 3700 km).

- (1) Figures 8 through 19 (Set 1). These figures show the standard deviations of the six geocentric spherical coordinates and the standard deviations of the six orbital elements as a function of the angular observation error for four altitudes, where $\sigma_\rho = 1$ fps (0.3 mps).
- (2) Figures 20 through 31 (Set 2). These figures show the same variables where $\sigma_\rho = 600$ ft (180 m).
- (3) Figures 32 through 43 (Set 3). These figures show the standard deviations of the six spherical coordinates and the six orbital elements as a function of the range observation error for four altitudes, where $\sigma_\epsilon = 0.05^\circ$.

The initial conditions for both the angular and range observation error computations are given in Table 5 as a function only of orbital altitude.

The asymptotic values of the standard deviations of the six spherical coordinates and six orbital elements for Sets 1, 2 and 3 are given in Table 6. These are the limiting values in each dependent variable as the independent variable becomes very large. Because the data rate is the same for each orbital altitude, 18 observations are contained in the results for the 365-km orbit, 27 for the 645-km orbit, 33 for the 922-km orbit and 91 for the 3710-km orbit.

TABLE 5
Initial Conditions for Angular and Range Observations
(see Figures 8 to 43)

| | Altitude (km) | | | |
|-------------|-----------------------|----------------------|-----------------------|---------------|
| | 365 | 645 | 922 | 3710 |
| t | 0 | 0 | 0 | 0 |
| L_V | 0° | 0° | 0° | 0° |
| L_S | 60° N | 60° N | 60° N | 60° N |
| Λ_V | 0° | 0° | 0° | 0° |
| Λ_S | 353° E | 353° E | 353° E | 356° E |
| A | 202.7° | 202.7° | 202.7° | 202.7° |
| D | 0° | 0° | 0° | 0° |
| ν | 90° | 90° | 90° | 90° |
| η | 0° | 0° | 0° | 0° |
| r | 6.745×10^6 m | 7.01×10^6 m | 7.300×10^6 m | 10^7 m |
| v | 7688 m/sec | 7534 m/sec | 7389 m/sec | 6286 m/sec |
| a | 6.742×10^6 m | 7.01×10^6 m | 7.300×10^6 m | 10^7 m |
| e | 0.00069 | 0.00009 | 0.0009 | 0.00012 |
| i | 90° | 90° | 90° | 90° |
| Ω | 202.7° | 202.7° | 202.7° | 202.7° |
| ω | -213.2° | -180° | -180° | -180° |
| M | 4.13 | 3.14 | 3.14 | 3.14 |
| τ | 91.86 min | 97.6 min | 103.4 min | 168.07 min |
| N | 18 | 27 | 33 | 91 |
| T_\oplus | 3.4° E | 3° E | 3° E | 10° W |

TABLE 6
Asymptotes of Dependent Variable, Figures 8 to 43

| Set of 1 as $\sigma_\epsilon \rightarrow \infty$ ($\sigma_\rho = 1 \text{ fps}$) (0.3 mps) | | | | |
|--|------------------------|------------------------|------------------------|------------------------|
| | 365 (height in km) | 645 (height in km) | 922 (height in km) | 3710 (height in km) |
| σ_A (deg) | 0.033 | 0.040 | 0.015 | 0.040 |
| σ_D (deg) | 0.041 | 0.038 | 0.017 | 0.0036 |
| σ_ν (deg) | 0.018 | 0.018 | 0.008 | 0.0012 |
| σ_η (deg) | 0.018 | 0.022 | 0.009 | 0.023 |
| σ_r (km) | 3.688 | 3.658 | 1.768 | 3.048 |
| σ_v (m/sec) | 0.43 | 4.27 | 2.0 | 0.30 |
| σ_a (m) | 96.0 | 122 | 65.8 | 131 |
| σ_e | 0.625×10^{-7} | 0.063×10^{-7} | 0.030×10^{-7} | 0.870×10^{-7} |
| σ_i (deg) | 0.018 | 0.021 | 0.009 | 0.023 |
| σ_Ω (deg) | 0.032 | 0.04 | 0.015 | 0.041 |
| σ_ω (deg) | 2.6 | 26.0 | 12.4 | 2.1 |
| σ_M (deg) | 2.6 | 26.0 | 12.4 | 2.1 |
| Set 2 as $\sigma_\epsilon \rightarrow \infty$ ($\sigma_\rho = 180 \text{ m}$) | | | | |
| σ_A (deg) | 0.040 | 0.031 | 0.026 | 0.019 |
| σ_D (deg) | 0.038 | 0.021 | 0.016 | 0.005 |
| σ_ν (deg) | 0.018 | 0.010 | 0.007 | 0.0015 |
| σ_η (deg) | 0.022 | 0.016 | 0.014 | 0.002 |
| σ_r (km) | 3.658 | 2.377 | 1.615 | 4.88 |
| σ_v (m/sec) | 4.27 | 2.0 | 1.6 | 0.30 |
| σ_a (m) | 122 | 99.1 | 94.5 | 110 |
| σ_e | 6.7×10^{-7} | 6.3×10^{-7} | 7.6×10^{-7} | 0.55×10^{-7} |
| σ_i (deg) | 0.021 | 0.017 | 0.014 | 0.019 |
| σ_Ω (deg) | 0.037 | 0.031 | 0.026 | 0.019 |
| σ_ω (deg) | 25.5 | 14.0 | 21.0 | 2.2 |
| σ_M (deg) | 25.6 | 14.0 | 21.0 | 2.2 |
| Set 3 as $\sigma_\epsilon \rightarrow \infty$ ($\sigma_\epsilon = 0.05 \text{ deg}$) | | | | |
| σ_A (deg) | 0.015 | 0.014 | 0.014 | 0.013 |
| σ_D (deg) | 0.017 | 0.017 | 0.018 | 0.022 |
| σ_ν (deg) | 0.0085 | 0.0083 | 0.0090 | 0.0085 |
| σ_η (deg) | 0.0087 | 0.0082 | 0.0082 | 0.0077 |
| σ_r (km) | 1.768 | 1.798 | 1.890 | 2.012 |
| σ_v (m/sec) | 2.01 | 1.92 | 1.89 | 1.83 |
| σ_a (m) | 70.4 | 79.2 | 88.4 | 131 |
| σ_e | 3.0×10^{-7} | 5.3×10^{-7} | 9.0×10^{-7} | 2.9×10^{-7} |
| σ_i (deg) | 0.009 | 0.008 | 0.006 | 0.008 |
| σ_Ω (deg) | 0.015 | 0.014 | 0.018 | 0.013 |
| σ_ω (deg) | 12.2 | 13.0 | 25.7 | 12.0 |
| σ_M (deg) | 12.2 | 13.0 | 25.7 | 12.0 |

H. REFERENCES

1. Brouwer, D., and Clemence, G., "Methods of Celestial Mechanics," Academic Press, New York, 1961, pp 187 to 209.
2. Kaula, W., "Celestial Geodesy," NASA TN D-1155, March 1962.
3. Baker, R., Jr., and Makemson, M., "Astrodynamics," Academic Press, 1960, pp 240, 241.
4. Herget, P., "The Computation of Orbits," published privately, 1948.
5. Eckert, W., and Brouwer, D., "The Use of Rectangular Coordinates in the Differential Correction of Orbits," *Astronomical Journal*, No. 1069, 16 August 1937.
6. Bowden, G., and Flis, J. (editors), "Notes of the Summer Institute in Dynamical Astronomy at Yale University," July 1959.
7. Ireland, R., "Tracking Studies," STL Report 7340.2-172, 30 October 1960.

I. BIBLIOGRAPHY

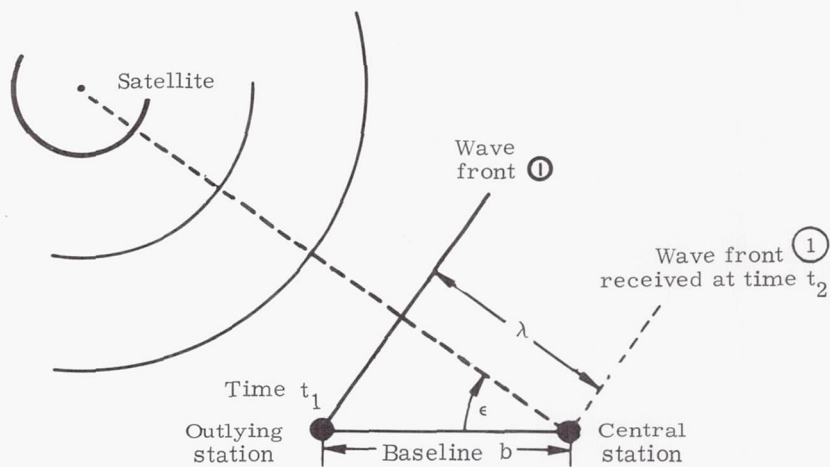
- Baker, R. M. L., Jr.,
 "High Precision Orbit Determination," ASI Monthly Progress Report, November 1958.
 (Also, ASI Monthly Progress Report, December 1958, Appendix B.)
 "Orbit Determination from Range and Range-Rate Data," American Rocket Society, 1960, Paper No. 1220-60.
- Baker, R. M. L., Jr., et al., "Efficient Precision Orbit Computation Techniques," *ARS Journal*, Vol. 30, No. 8, August 1960, pp 740 to 747. (Also, Los Angeles, California, University of California, 11 June 1959, *Astrodynamical Report No. 3.*)
- Barr, T. A., and Lundquist, C. A., "Tracking Experiments with Pioneer IV," *IRE Transactions on Military Electronics*, Vol. MIL-4, Nos. 2-3, April to July 1960, pp 355 to 359.
- Batrakov, Yu. V., "Determination of the Preliminary Orbits of Artificial Satellites from Observations with Time Approximately Known," *ARS Journal, Russian Supplement*, Vol. 30, No. 9, September 1960, pp 859 to 864.
- Berger, W. J., and Ricupita, J. R., "Prediction Theory of Missile and Satellite Orbits," *ARS Journal*, Vol. 29, No. 6, June 1959.
- Besag, P. L., and Anderson, J. T., "Determination of the Orbit of an Artificial Satellite," *IRE Proceedings*, Vol. 48, No. 5, 1960, p 950.
- Bode, H. W., and Shannon, C. E., "A Simplified Derivation of Linear Least Squares Smoothing and Prediction Theory," *IRE Proceedings*, Vol. 38, 1950, pp 417 to 425.
- Brown, D. C., "A General Solution to the Problem of the Adjustment of Trajectory Observations," RCA Data Processing, Florida, AFMTC, TM-54, 6 March 1959.
- Bryant, R.,
 "Interim Definitive Orbits Determined at the NASA Computing Center," California Institute of Technology, Jet Propulsion Laboratory, Pasadena, California, JPL Proceedings of Seminar on Orbit Prediction, February 1960.
 "NASA Computing Center Predictions," California Institute of Technology, Jet Propulsion Laboratory, Pasadena, California, JPL Proceedings of Seminar on Orbit Prediction, February 1960.
- Cahill, W. F., and Harris, I., "Determination of Satellite Orbits from Radar Data," NASA TN D-489, 1960. (Also, American Rocket Society, Preprint No. 940-59.)
- Carr, R., et al., "Tracking and Orbit Determination Program of JPL," California Institute of Technology, Jet Propulsion Laboratory, Pasadena, California, JPL Report No. TR-32-7, February 1960.
- Cormier, L. N., Goodwin, N., and Squires, R. K., "Simplified Satellite Prediction from Modified Orbital Elements," *Annals of the International Geophysical Year*, Vol. XII, Pergamon Press, New York, 1960, pp 83 to 84.
- Crawford, R. T., "Determination of Orbits of Comets and Asteroids," New York, McGraw-Hill Book Company, 1930.
- Darlington, S., "Linear Least-Squares Smoothing and Prediction with Applications," *Bell Systems Technical Journal*, Vol. 37, 1958.
- Debey, L. G., "Tracking in Space by DOPLOC," *IRE Transactions on Military Electronics*, Vol. MIL-4, Nos. 2-3, April to July 1960, pp 332 to 335.
- Deutch, A., "Orbits for Planetary Satellites from Doppler Data," *ARS Journal*, Vol. 30, No. 6, June 1960.
- Dubyago, A., "The Determination of Orbits," New York, The Macmillan Company, 1961.
- Duke, D., "Orbit Determination from Optical Tracking," *Journal of the Society of Motion Picture and Television Engineers*, Vol. 69, No. 1, 1960, pp 9 to 14.
- Eimer, M., et al., "Evaluation of Pioneer 4 Orbit Determination Program," California Institute of Technology, Jet Propulsion Laboratory, Pasadena, California, JPL Technical Release No. 34-26, February 1960.
- Friedland, B., "Least Squares Filtering and Prediction of Nonstationary Sampled Data," *Information and Control*, Vol. 1, 1958, pp 297 to 313.

- Glazier, E. V. D. (ed.), et al., "Avionics Research: Satellites and Problems of Long Range Detection and Tracking," London, Pergamon Press, 1960.
- Glover, C. C., "Optimum Prediction with a Mean Weighted Square-Error Criterion," Inst. Radio Engrs., Trans. Automatic Control, Vol. AC-6, No. 1, February 1961, pp 43 to 48.
- Guier, W. H.,
 "Doppler Tracking of Project Transit Satellites," IRE Transactions of the Space Electronics and Telemetry Symposium, September 1960.
 "A Satellite Doppler Navigation System," IRE Proceedings, Vol. 48, No. 4, 1960, pp 507 to 516.
- Harris, I., and Cahill, W. F., "Determination of Satellite Orbits from Radar Data," IRE Proceedings, Vol. 48, No. 9, September 1960, pp 1657 to 1658.
- Herrick, S.,
 "Observation Requirements for Precision Orbit Determination," Aeronautics and Astronautics, New York, Pergamon Press, 1960, pp 417 to 434.
 "Orbits from Position and Velocity," University of California, Los Angeles, California, Astrodynamical Report No. 8 (AFOSR TN 60-816), July 1960.
 "A Comparison of Astronomical and Ballistic Traditions in Orbit Computation," Astrodynamical Report No. 14, University of California Dept. of Astronomy, May 1962.
- Kaula, W. M., "Celestial Geodesy," NASA TN D-1155, March 1962.
- King-Hele, D. G., and Walker, D. M. C.,
 "Methods for Predicting the Orbits of Near Earth-Satellites," Journal of the British Interplanetary Society, Vol. 17, No. 1, 1959, pp 2 to 14.
- Kraft, J. D., "Satellite Orbit Computation," Design Guide to Orbital Flight, McGraw-Hill Book Company, New York, 1962, Chapter 11.
- Kulikov, D. K., and Batrakov, Yu. V., "Method for Improving Orbits of Artificial Satellites of the Earth Using Observations with Approximate Values of Time," ARS Journal, Russian Supplement, Vol. 30, No. 9, 1960, pp 865 to 874.
- Lane, R. E., "Mathematical Processes, Smoothing and Differentiating Experimental Data," University of Texas, Austin, Texas, MPRL-419, 18 June 1958.
- Lawden, D. F., "The Calculation of Orbits," Journal of the British Interplanetary Society, Vol. 14, No. 4, July to August 1955.
- Magness, T. A., and McGuire, J. B., "Statistics of Orbit Determination-Correlated Observations," STL Report No. 8976-6001-RU-ODO.
- Mechau, D. V., "List of Coordinates of Stations Engaged in the Observation of Artificial Earth Satellites," Cambridge, Massachusetts, Smithsonian Astrophysical Observatory, Special Report No. 45, 1960.
- Mowlem, A., "The Programming System for Orbit Determination at IBM Space Computing Center," California Institute of Technology, Jet Propulsion Laboratory, Pasadena, California, JPL Technical Release No. 34-26, February 1960.
- Muhleman, D., "Satellite Orbit Determination and Prediction Utilizing JPL Goldstone 85-Ft Antenna and JPL Tracking Program," California Institute of Technology, Jet Propulsion Laboratory, Pasadena, California, JPL Technical Release No. 34-27, February 1960.
- Munick, H., "Determination of Elements of an Elliptic Orbit from the Orbital Velocity Vector," ARS Journal, Vol. 29, No. 2, February 1959, p 150.
- Rechtin, E., "Satellite Tracking," California Institute of Technology, Jet Propulsion Laboratory, Pasadena, California, American Rocket Society Preprint No. 649-58, 1958.
- Richards, P. B., "Orbit Determination of a Nontransmitting Satellite Using Doppler Tracking Data," General Electric Company, Missile and Space Vehicle Department, Philadelphia, Pennsylvania, Institute of Aeronautical Sciences, Preprint No. 61-141-1835, June 1961.
- Rossoni, J. P., "Technical Aspects of Satellite Tracking on IBM Computers at Smithsonian Astrophysical Observatory in Cambridge," California Institute of Technology, Jet Propulsion Laboratory, Pasadena, California, JPL Technical Release No. 34-26, February 1960.
- Shapiro, L., "The Prediction of Ballistic Missile Trajectories from Radar Observations," McGraw-Hill Book Company, New York, 1957.
- Silva, R. R., "Millstone Operations Related to the Pioneer V Space Probe," Massachusetts Institute of Technology, Lincoln Laboratories, Cambridge, Massachusetts, Report No. 30-G-0007, 1960.
- Siry, J. W., "The Vanguard Orbit Determination Program," Annals of the International Geophysical Year, Vol. XII, Pergamon Press, New York, pp 91 to 104.
- Sperling, H. J.,
 "On the Computation of Keplerian Ellipses," Huntsville, Alabama, Army Ballistic Missile Agency, ABMA Report No. DA-TM-48-60, 1960.
 "Survey of Space Flight Decks Used at ABMA," California Institute of Technology, Jet Propulsion Laboratory, Pasadena, California, JPL Technical Release No. 34-26, February 1960.
- Swerling, P., "Computer Program for First Order Error Propagation in Satellite Orbit Prediction," California Institute of Technology, Jet Propulsion Laboratory, Pasadena, California, JPL Proceedings of Orbit Prediction Symposium,

- February 1960 (Martin Library No. MR 5982-Z-65).
- Szebehely, V. G., "Lunar and Interplanetary Trajectory Determination Activities at General Electric," California Institute of Technology, Jet Propulsion Laboratory, Pasadena, California, JPL Technical Release No. 34-26, February 1960.
- Tross, C., "Lunar Vehicle Orbit Determination," California Institute of Technology, Jet Propulsion Laboratory, Pasadena, California, JPL Technical Release No. 34-26, February 1960.
- Veis, G., and Moore, C., "Smithsonian Astrophysical Observatory Differential Orbit Improvement Program," California Institute of Technology, Jet Propulsion Laboratory, Pasadena, California, JPL Proceedings of Orbit Prediction Symposium, February 1960 (Martin Library No. MR 5982-Z-65).
- Walters, L. G., et al.,
 "Differential Correction Experimentation with Low Eccentricity Orbits," American Rocket Society, Preprint No. 960-59, November 1959.
 "Differential Orbit Correction Experimentation with Satellites 1958 Alpha 1 and 58 ϵ ," California Institute of Technology, Jet Propulsion Laboratory, Pasadena, California, JPL Proceedings of Seminar on Orbit Prediction, February 1960 (Martin Library No. MR 5982-Z-65).
- Wasel, A. D., "Orbital Elements, Trajectory Simulation, and Prediction for Earth Satellites," Journal of the British Interplanetary Society, Vol. 17, September to October 1959, pp 130 to 133.
- Weirauch, R. F., "On the Accuracy of an Elliptical Orbit Determination," Stockholm, XIth International Astronautical Congress, 1960.
- Welborn, E., "Mathematical Processes, Sets of Coefficients for Data Processing Formulas," University of Texas, Austin, Texas, MPRL-475, 5 May 1959.
- Westrom, G., and Van Sant, C. T., "Differential Correction of Earth Satellite Orbits Including the Drag Perturbation," Aeronutronic, Division of Ford Motor Company, Newport Beach, California, Institute of Aeronautical Sciences Preprint No. 61-140-1834, 1961.
- Williams, K. P., "The Calculation of the Orbits of Asteroids and Comets," Bloomington, Indiana, Principia Press, 1934.
- "Contribution to Astrodynamics: Astrodynamical Analysis for the National Space Surveillance Control Center," Volume I and Volume II, Aeronutronic, Newport Beach, California, Publication No. U-880, 1960.
- "Curve Fitting and Filtering Theory, Down-Range Antiballistic Measurement Program (DAMP)," RCA, MSRD, Moorestown, New Jersey.
- "Seminar Proceedings: Tracking Programs and Orbit Determination," California Institute of Technology, Jet Propulsion Laboratory, Pasadena, California, JPL Technical Release No. 34-26, February 1960 (Martin Library No. MR 5982-Z-65).

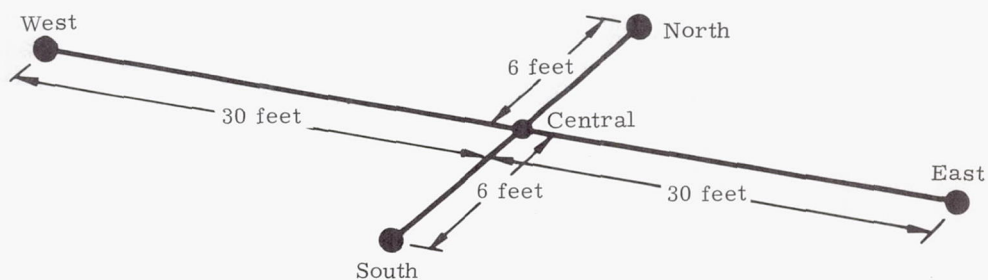
ILLUSTRATIONS

Preceding Page Blank



λ is the wavelength of the carrier from the satellite
 c is the velocity of propagation
 b is the distance between stations

Fig. 1. Interferometer System

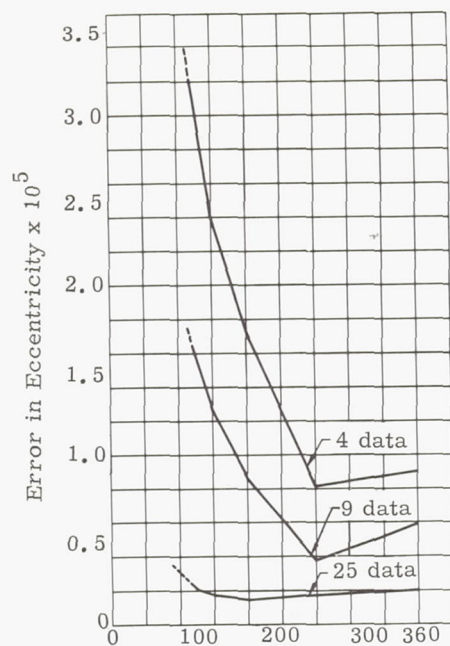


The claimed accuracy in angles: 20" to 40" (0.1 - 0.2 mrad)
 in optimum atmosphere conditions
 400" in bad weather

Frequency: 108 mc ($\lambda = 9$ ft)

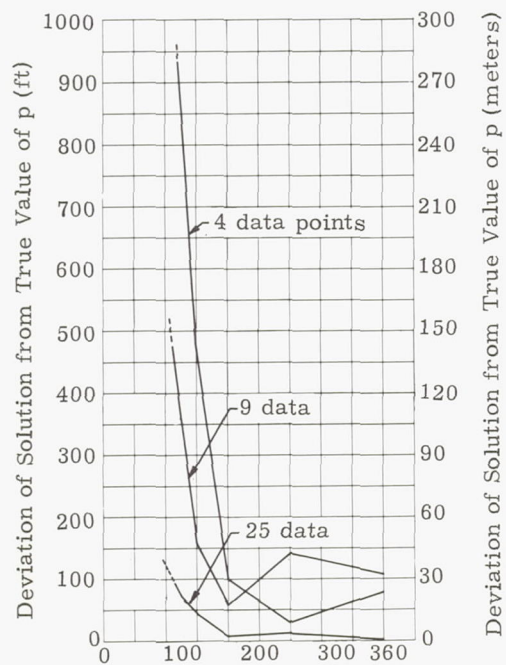
Fig. 2. Minitrack Modified Interferometer System

Preceding Page Blank



Arc over Which Equally Spaced Data Are Spread (deg)

Fig. 3. Effect of Spread and Number of Data on Accuracy of Eccentricity Determination

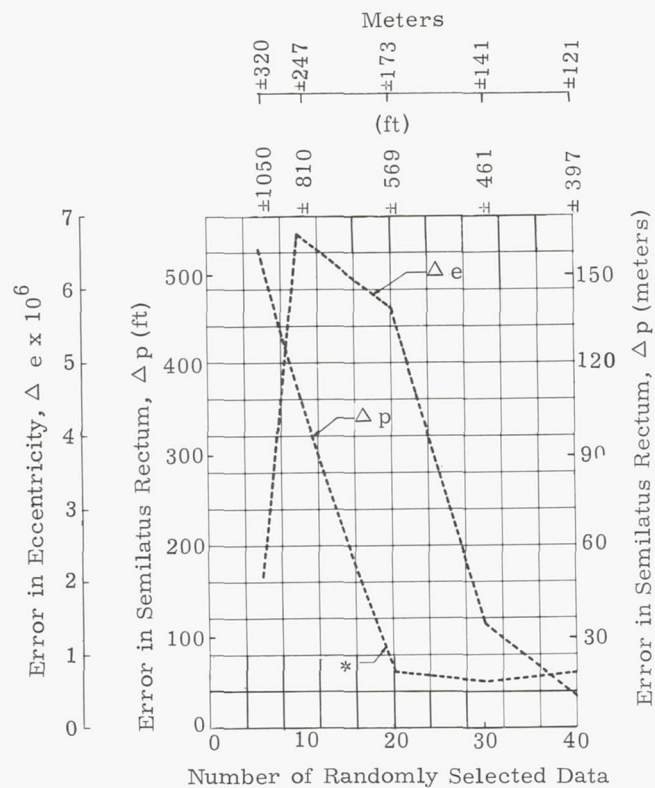


Arc over Which Equally Spaced Data Are Spread (deg)

Fig. 4. Effect of Spread and Number of Data on Accuracy of Semilatus Rectum Determination



Fig. 5. Effect of Spread of Data on Accuracy of Inclination and Nodal Longitude Determination



Confidence Interval
Associated with 0.99
Confidence Coefficient

* Data selected randomly from a normally distributed population, $\sigma = 300$ m

Data spread equally over two 15° arcs at opposite sides of a 6-hr circular orbit

Fig. 6. Effect of a Limited Number of Data on Accuracy of Orbit Determination

Data selected randomly for a normally distributed population, $\sigma = 300$ m. Data taken at equal intervals around the entire orbit

Orbits: — $p = 0.937031 \times 10^7$ m $p = 0.669307 \times 10^7$ m
 $e = 0.4$ $e = 0$

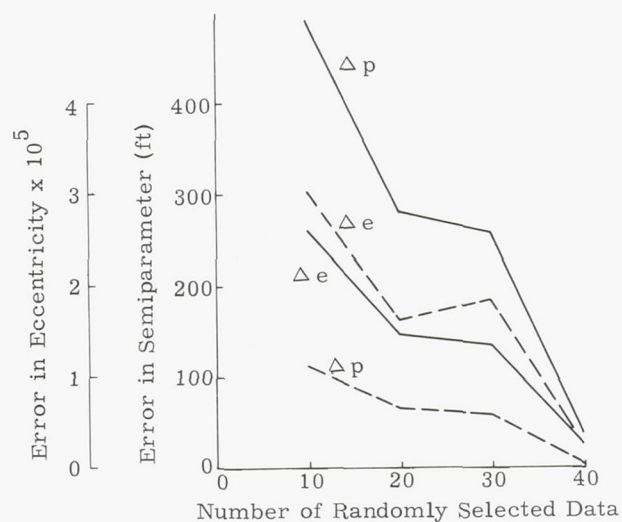


Fig. 7. Effect of a Limited Number of Data on Accuracy of Orbit Determination

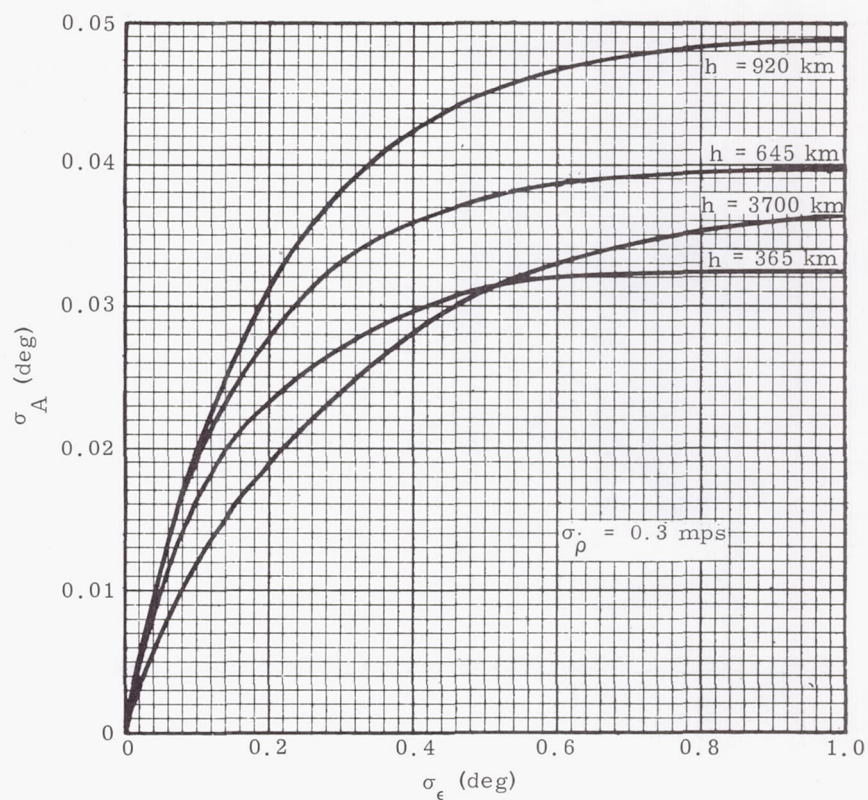


Fig. 8. Angular Observation Errors, σ_A Versus σ_ϵ

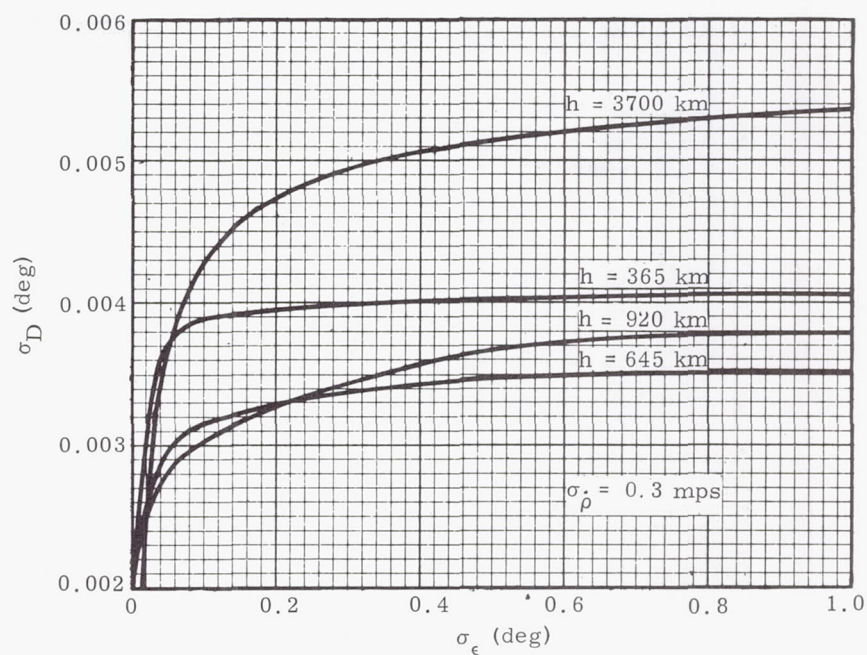


Fig. 9. Angular Observation Errors, σ_D Versus σ_ϵ

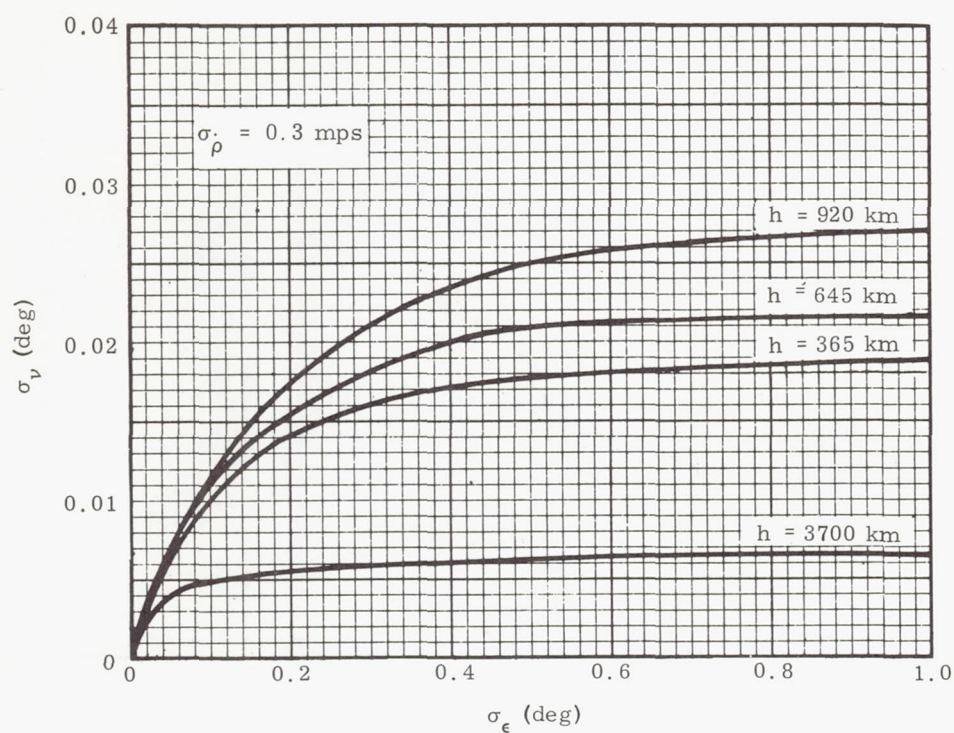


Fig. 10. Angular Observation Errors, σ_v Versus σ_ϵ

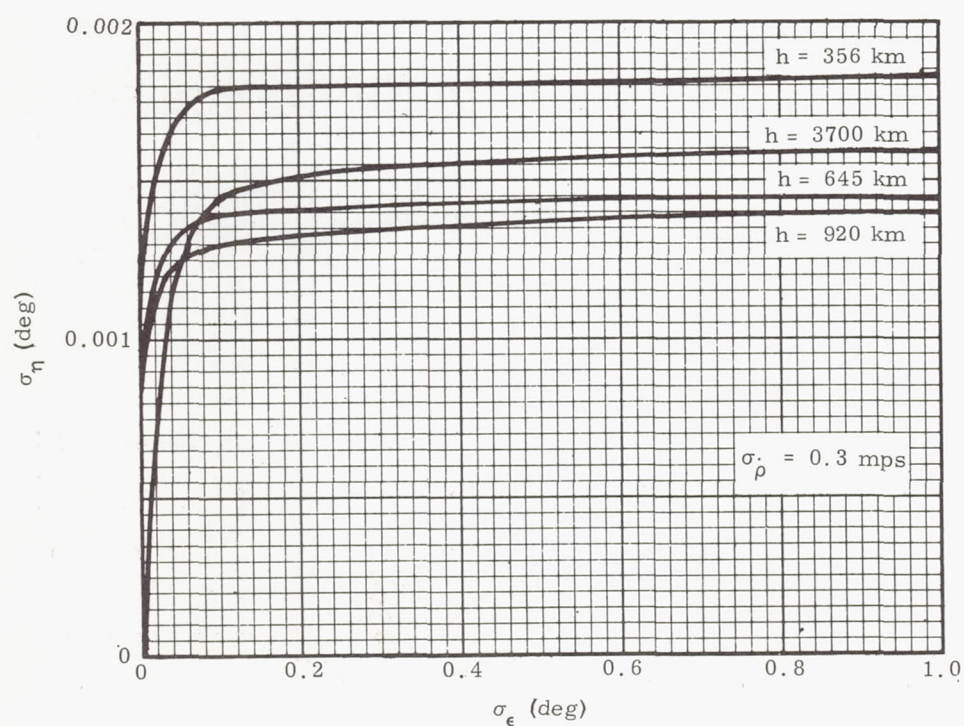


Fig. 11. Angular Observation Errors, σ_η Versus σ_ϵ

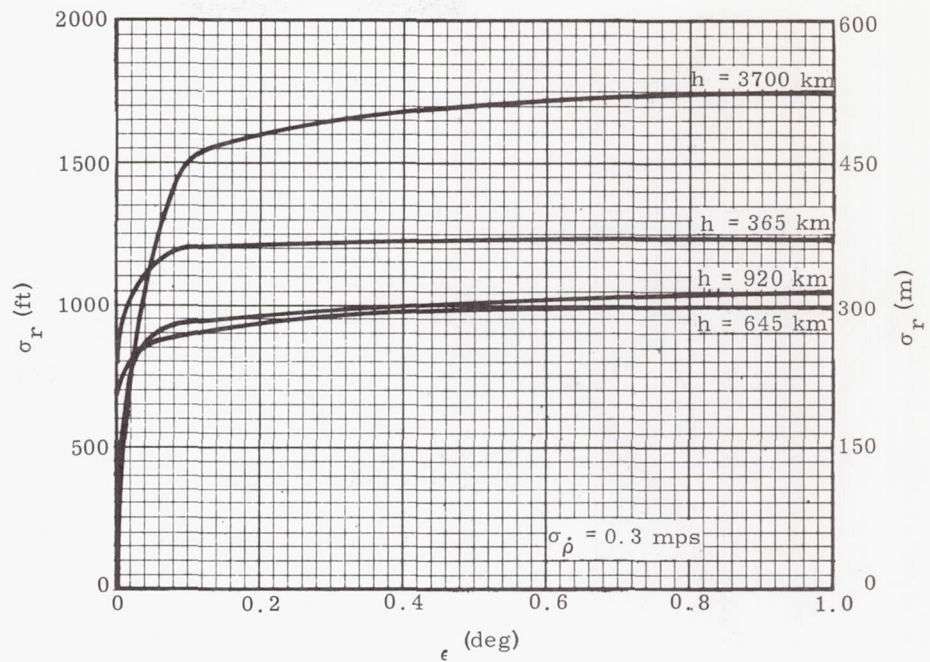


Fig. 12. Angular Observation Errors, σ_r Versus σ_ϵ

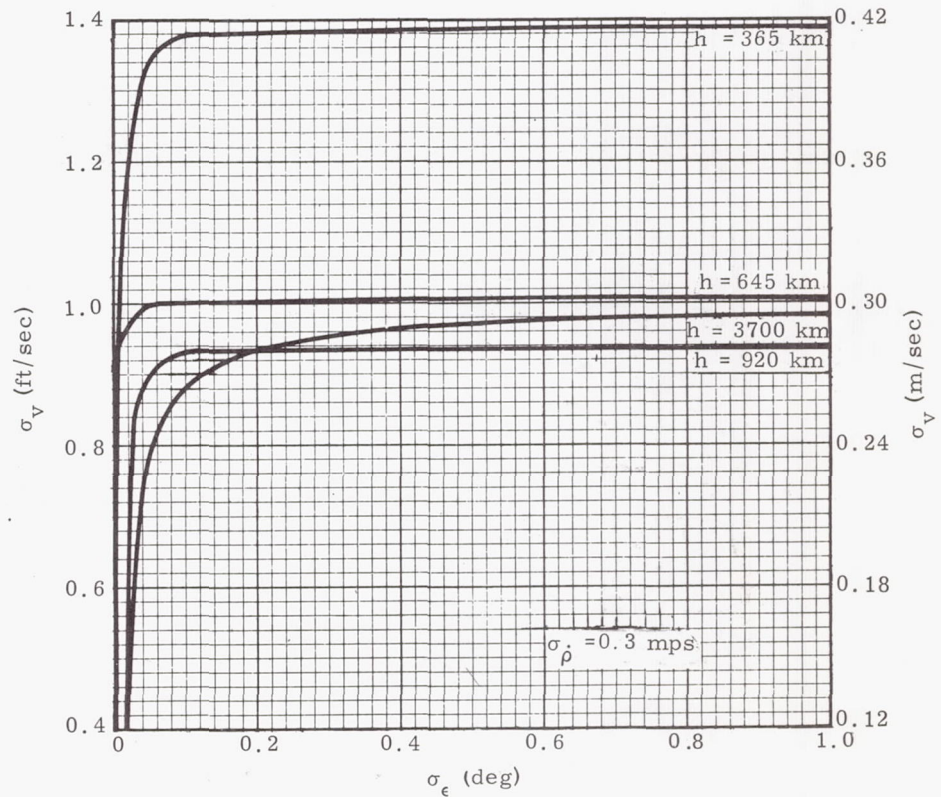


Fig. 13. Angular Observation Errors, σ_v Versus σ_ϵ

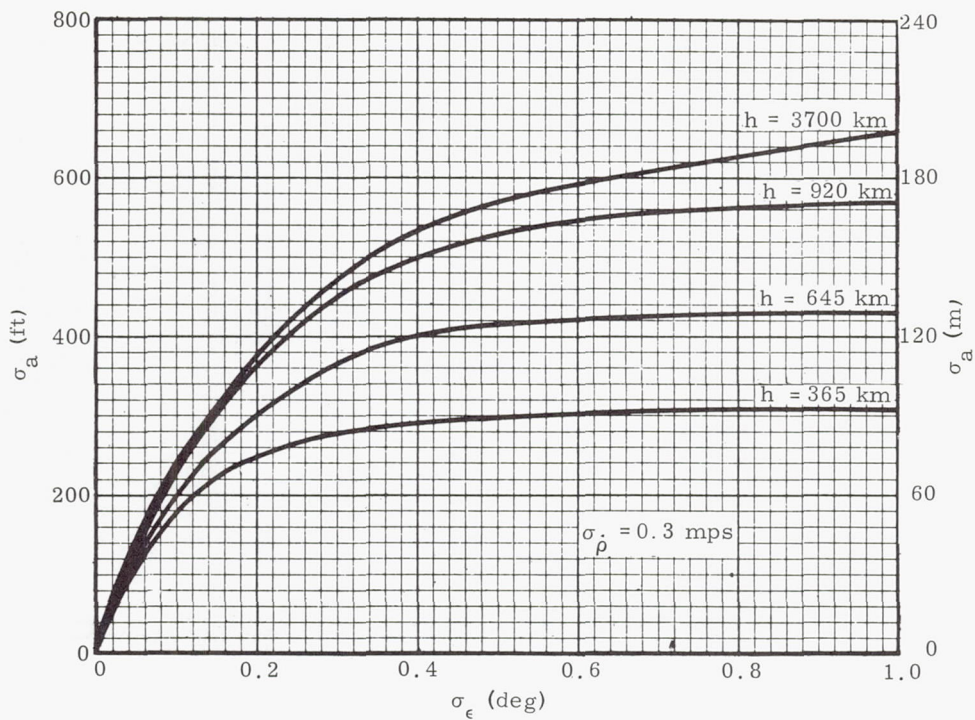


Fig. 14. Angular Observation Errors, σ_a Versus σ_ϵ

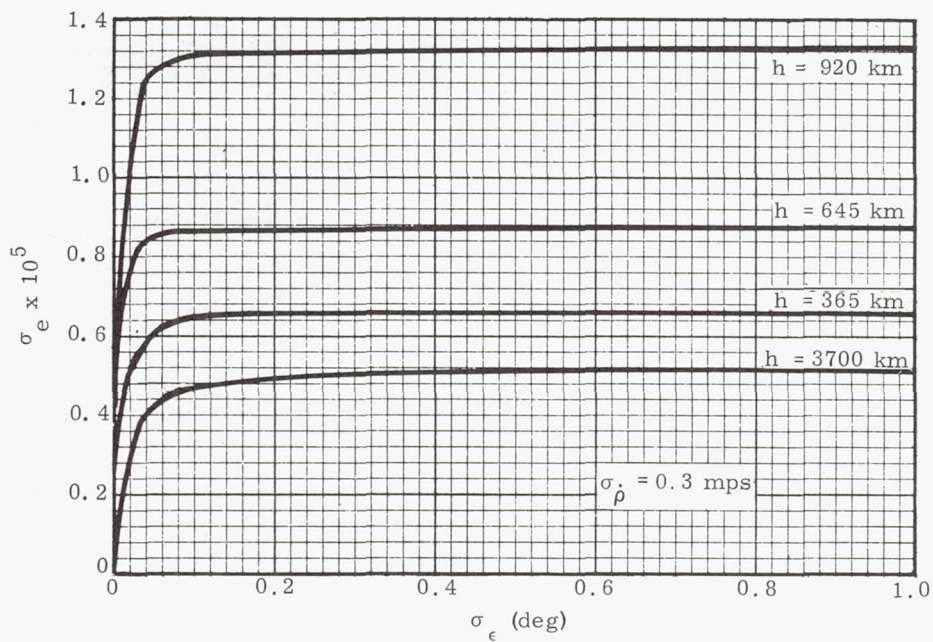


Fig. 15. Angular Observation Errors, σ_e Versus σ_ϵ

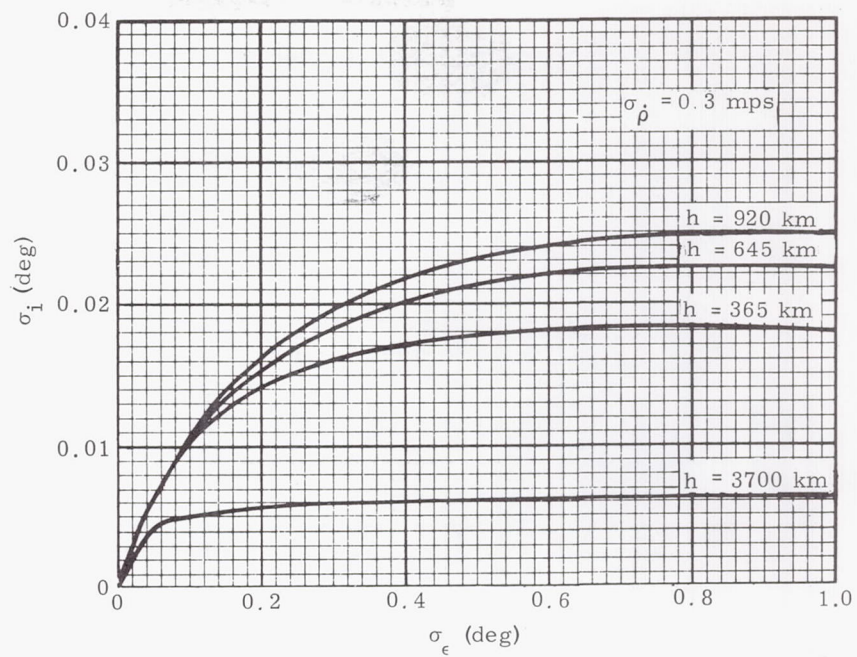


Fig. 16. Angular Observation Errors, σ_i Versus σ_ϵ

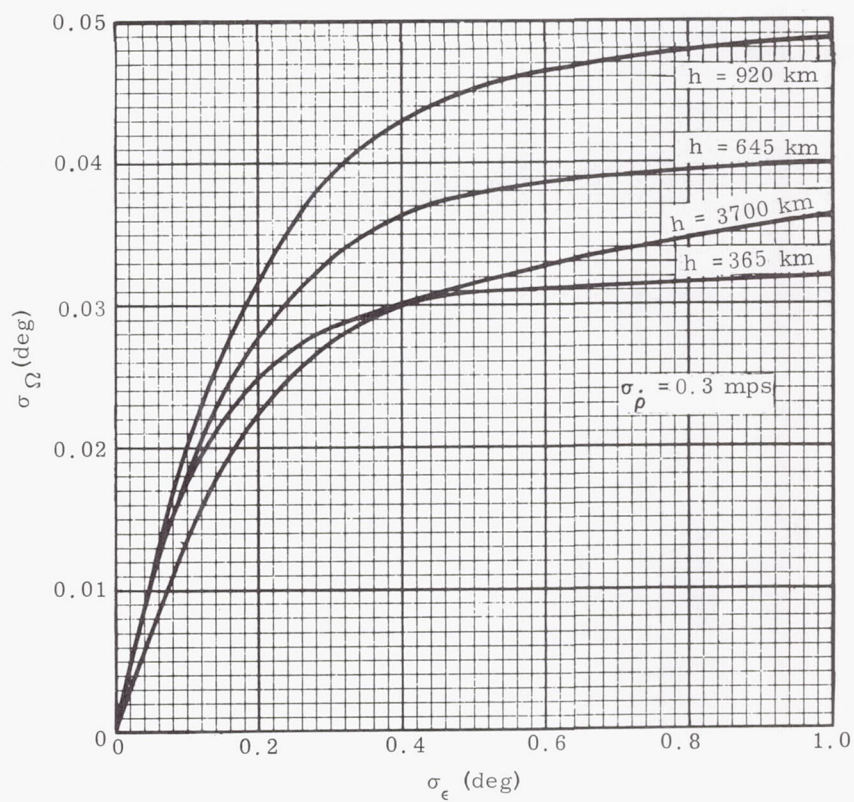


Fig. 17. Angular Observation Errors, σ_Ω Versus σ_ϵ

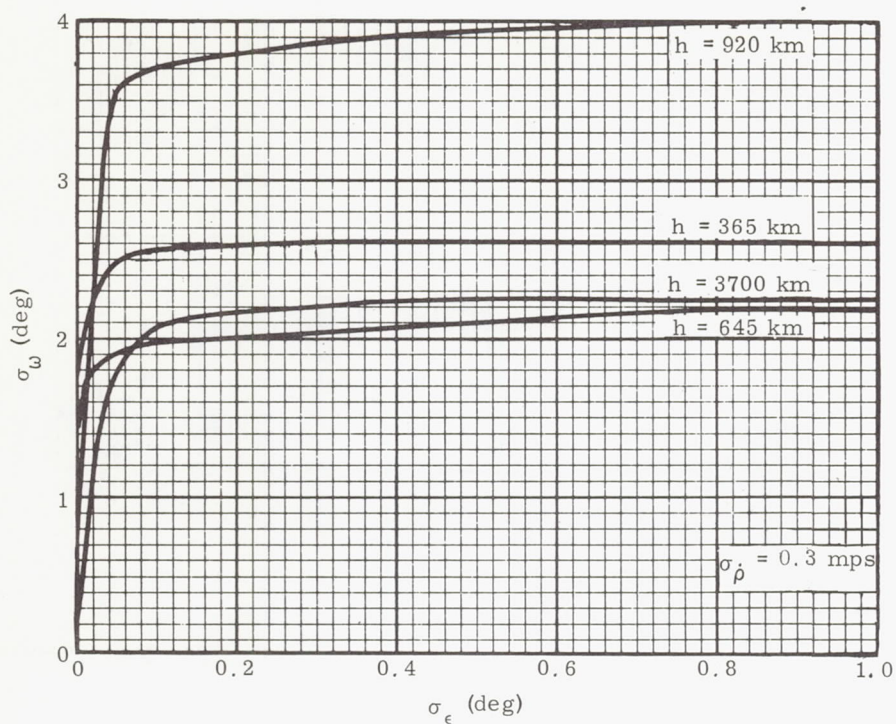


Fig. 18. Angular Observation Errors, σ_ω Versus σ_ϵ

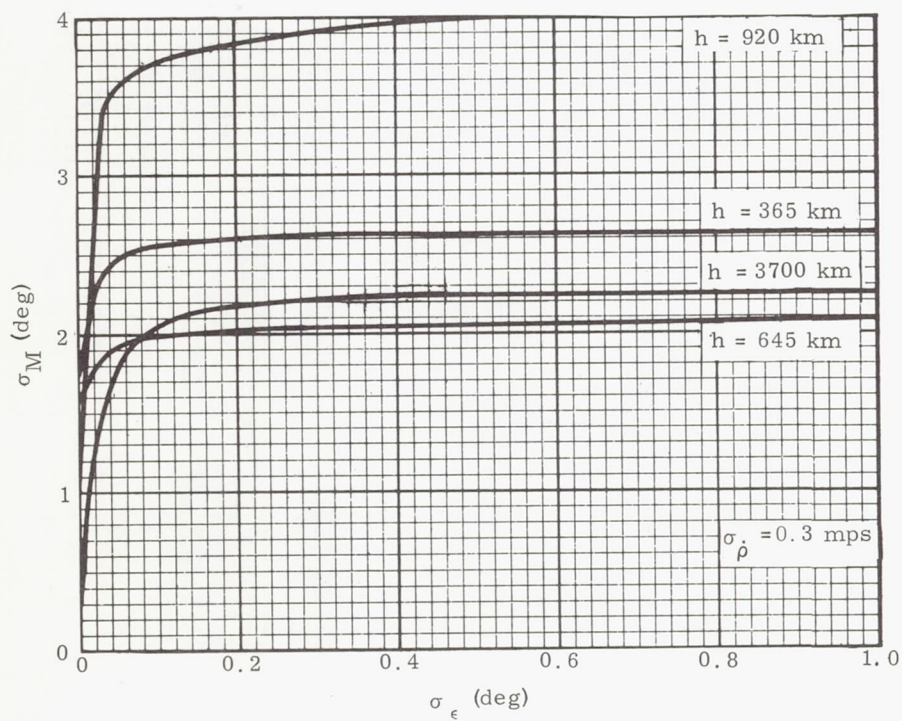


Fig. 19. Angular Observation Errors, σ_M Versus σ_ϵ

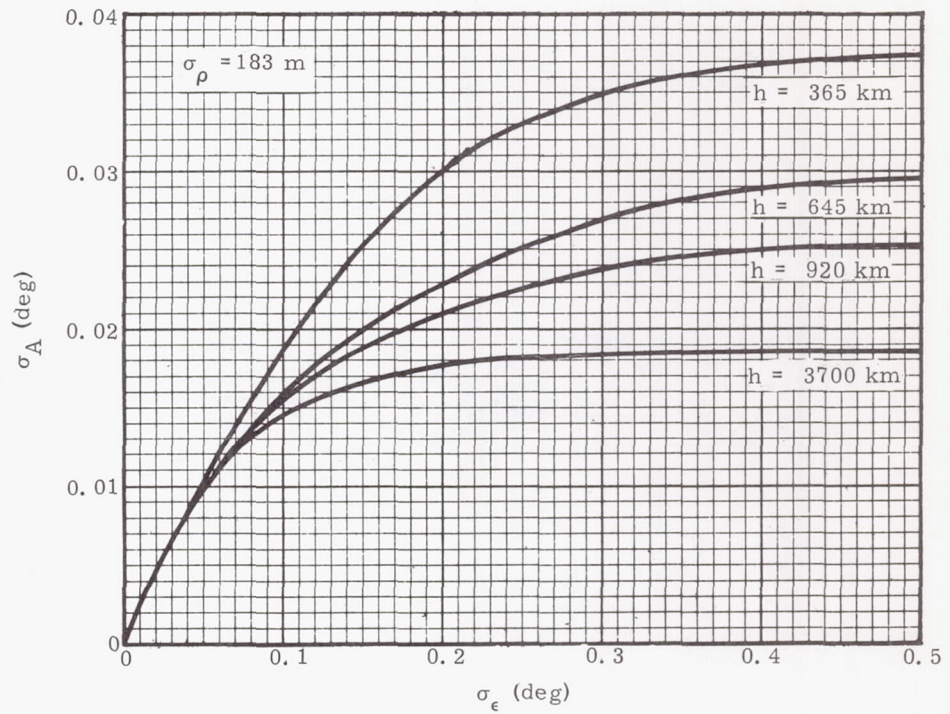


Fig. 20. Angular Observation Errors, σ_A Versus σ_ϵ

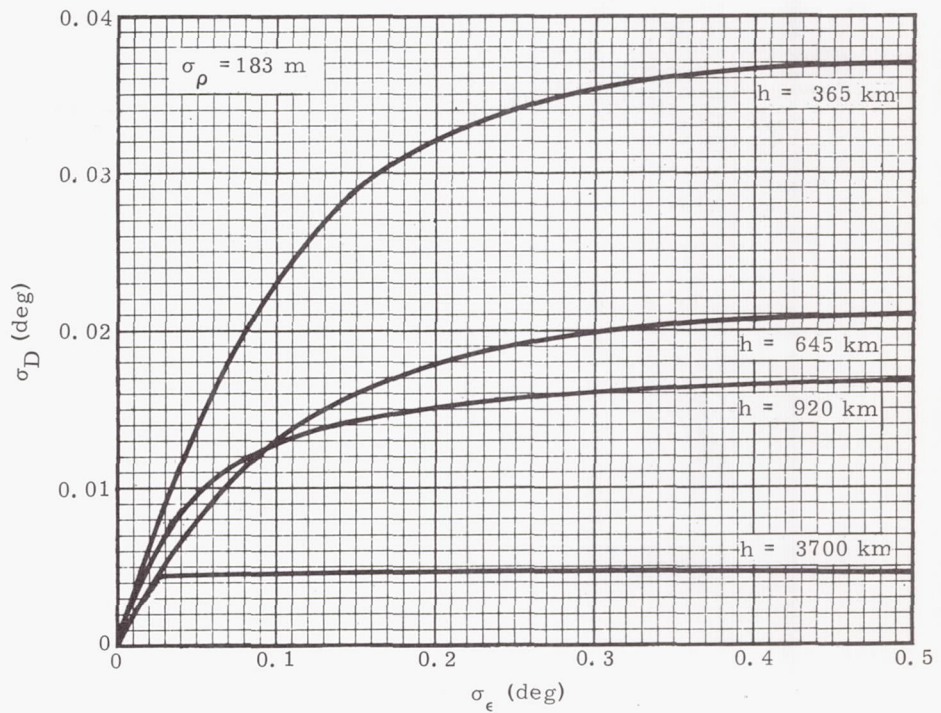


Fig. 21. Angular Observation Errors, σ_D Versus σ_ϵ

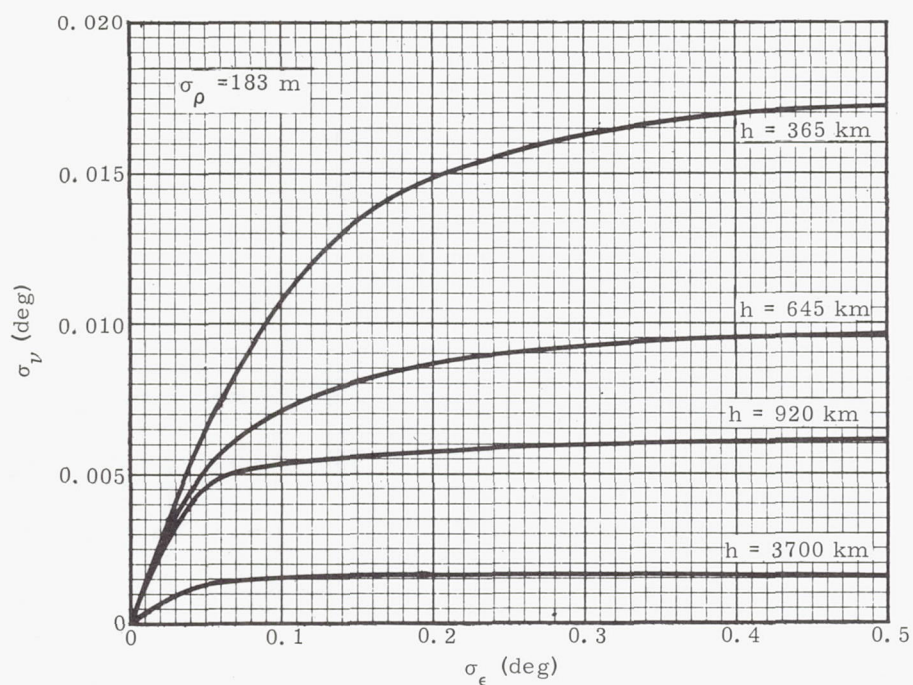


Fig. 22. Angular Observation Errors, σ_v Versus σ_ϵ

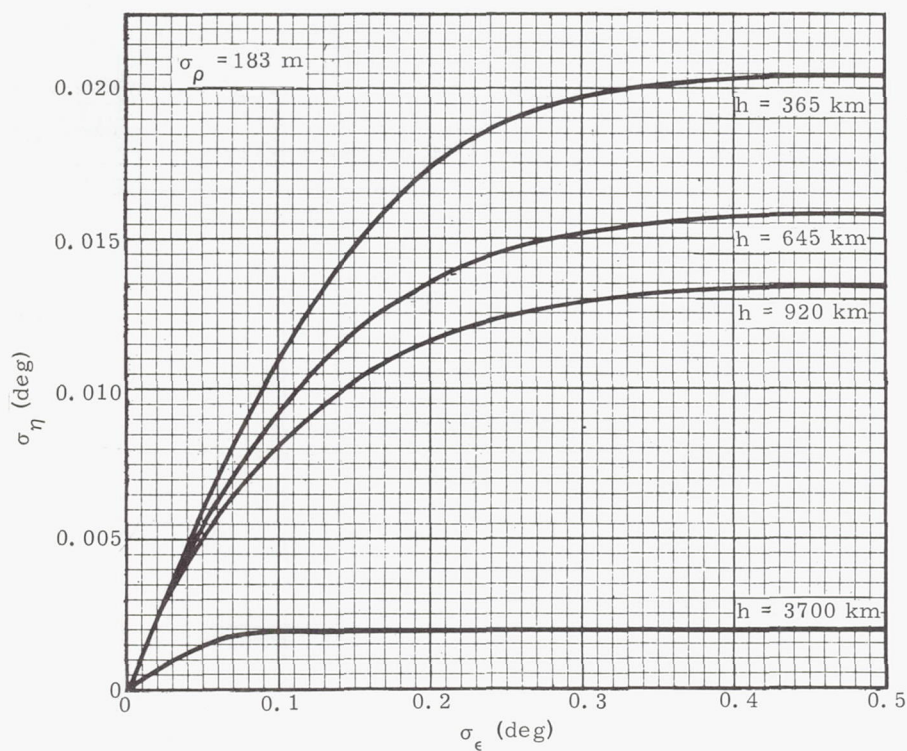


Fig. 23. Angular Observation Errors, σ_η Versus σ_ϵ

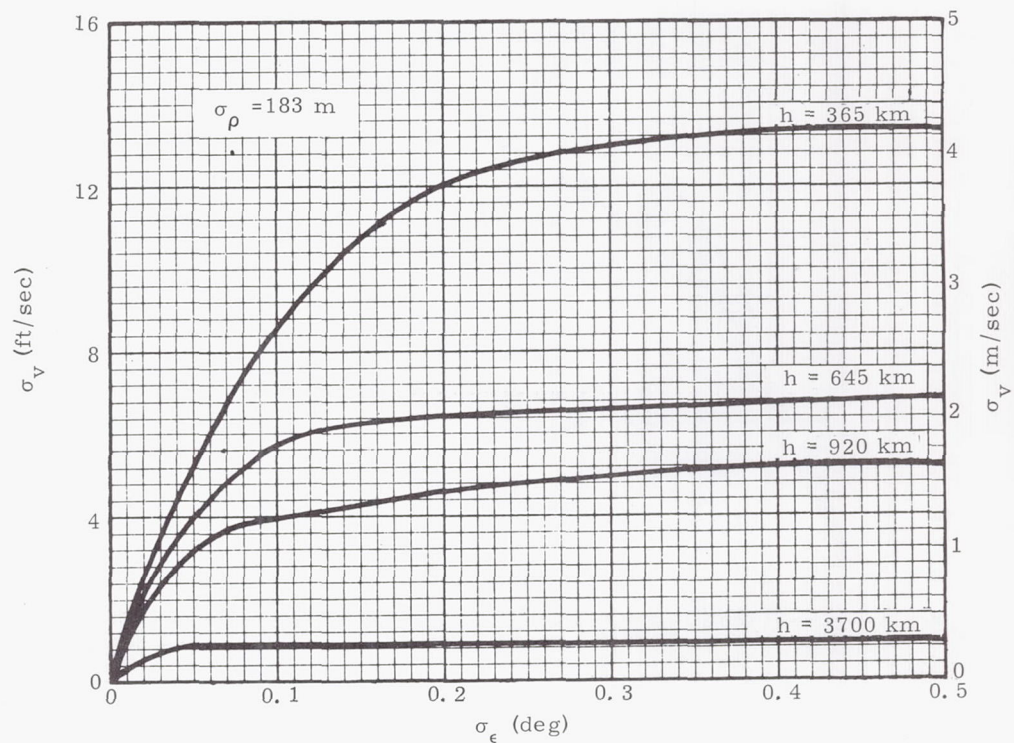


Fig. 24. Angular Observation Errors, σ_v Versus σ_ϵ

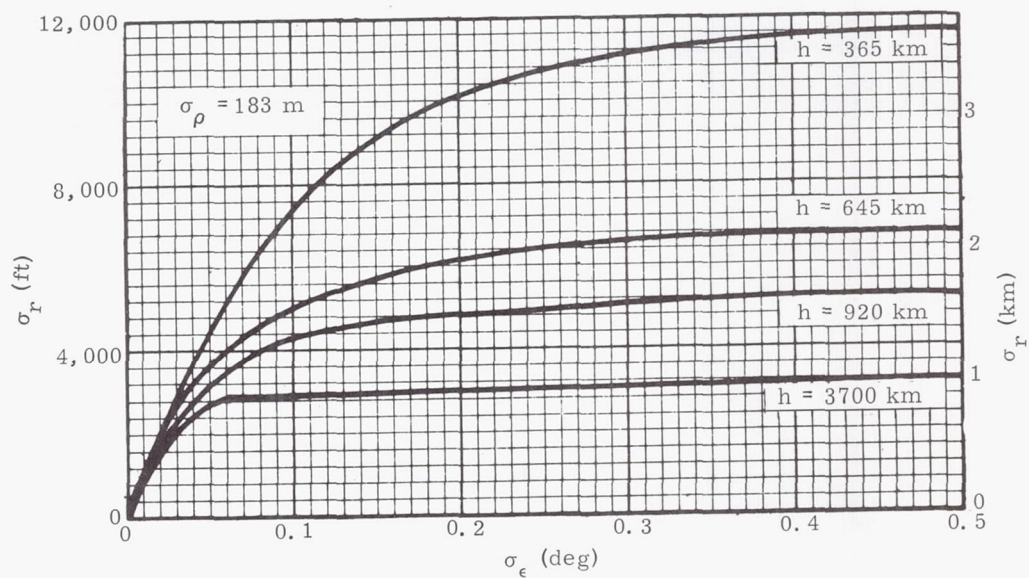


Fig. 25. Angular Observation Errors, σ_r Versus σ_ϵ

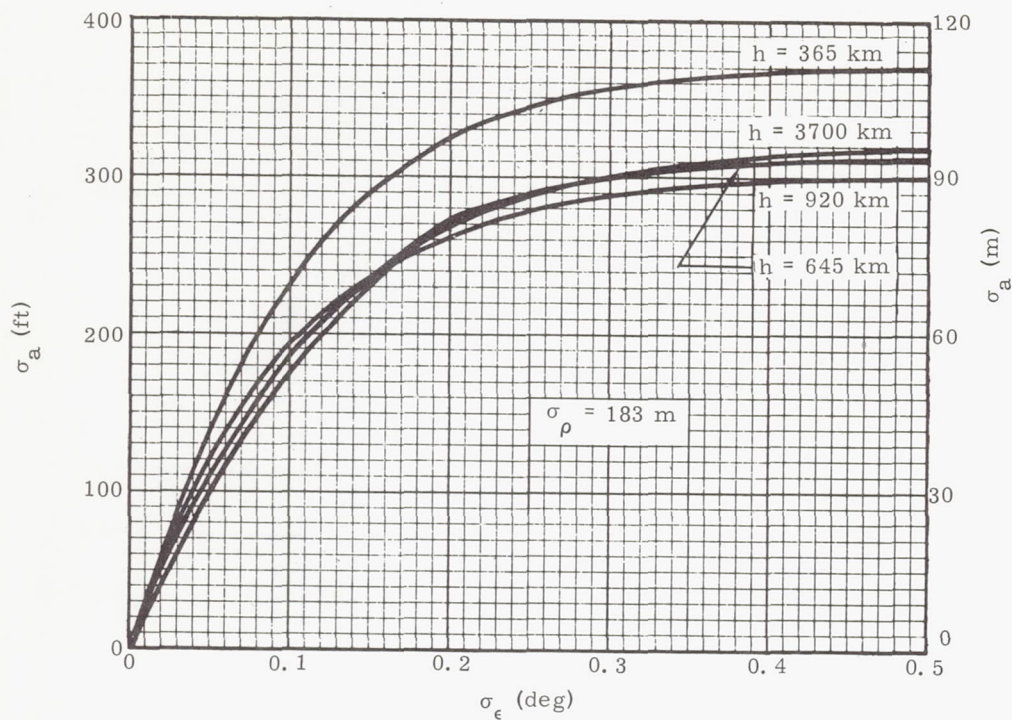


Fig. 26. Angular Observation Errors, σ_a Versus σ_ϵ

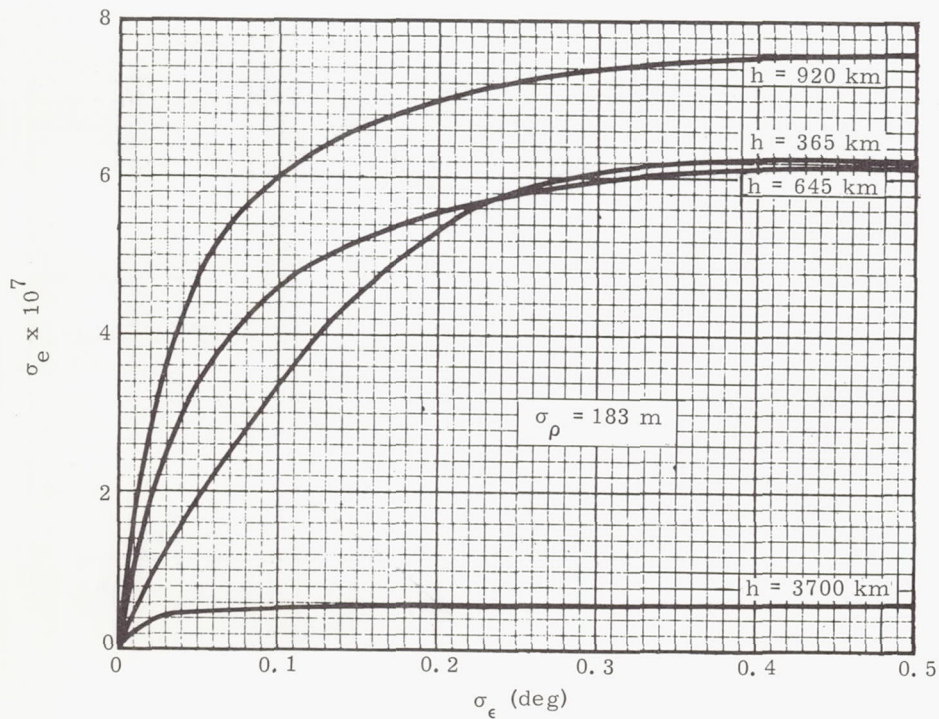


Fig. 27. Angular Observation Errors, σ_e Versus σ_ϵ

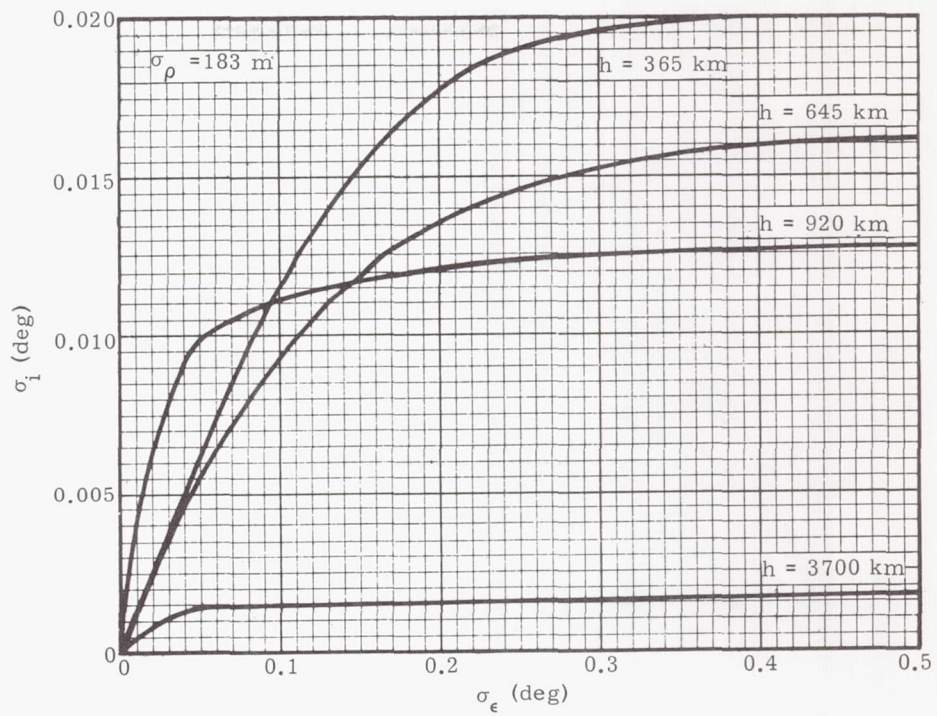


Fig. 28. Angular Observation Errors, σ_i Versus σ_ϵ

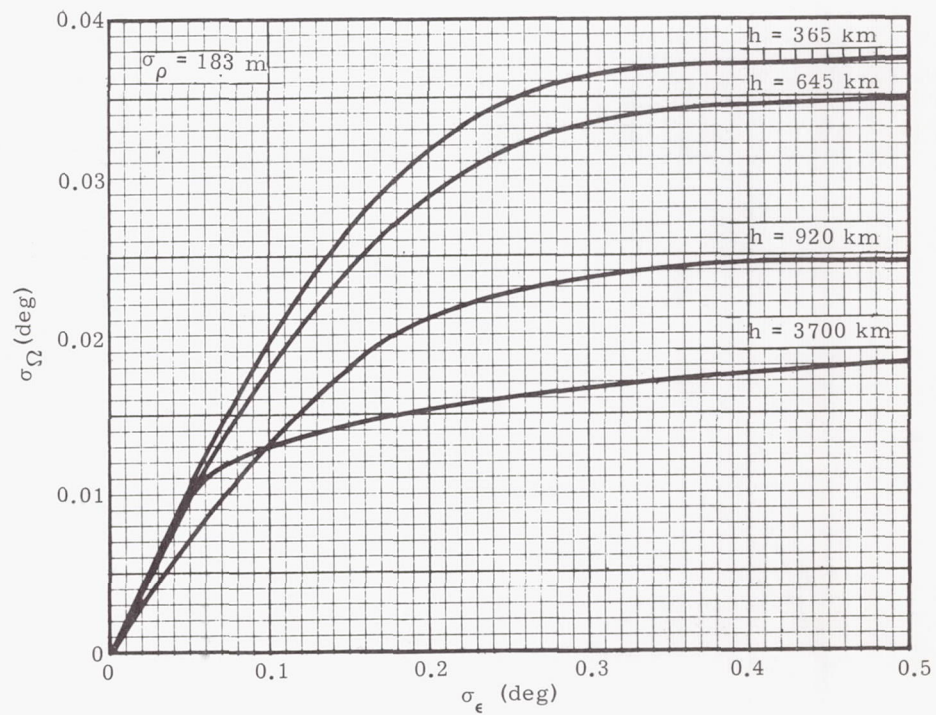


Fig. 29. Angular Observation Errors, σ_Ω Versus σ_ϵ

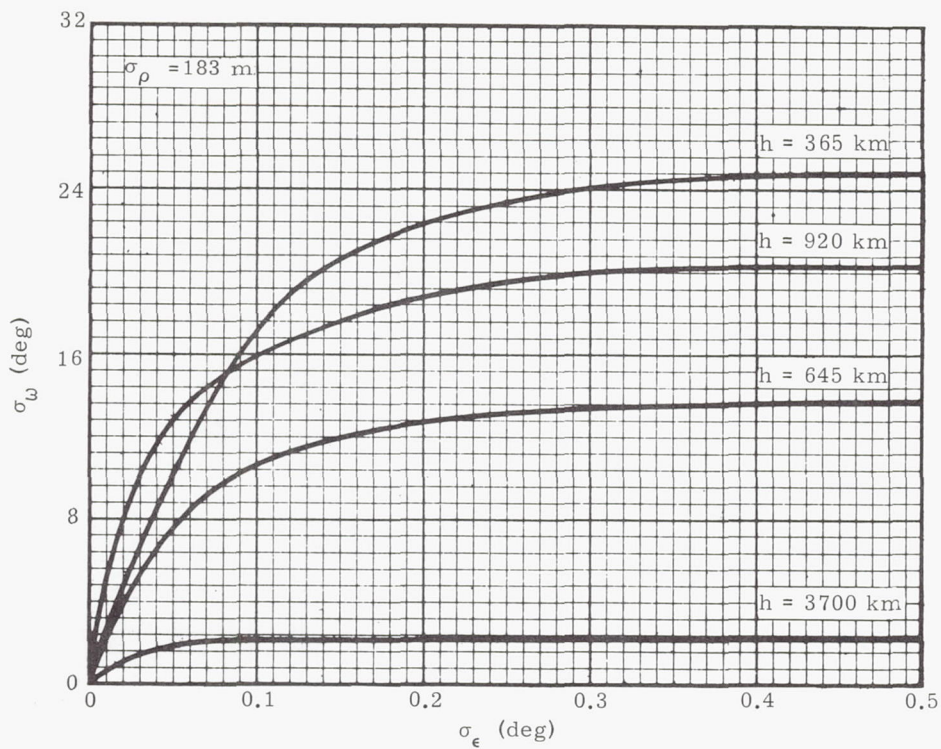


Fig. 30. Angular Observation Errors, σ_ω Versus σ_ϵ

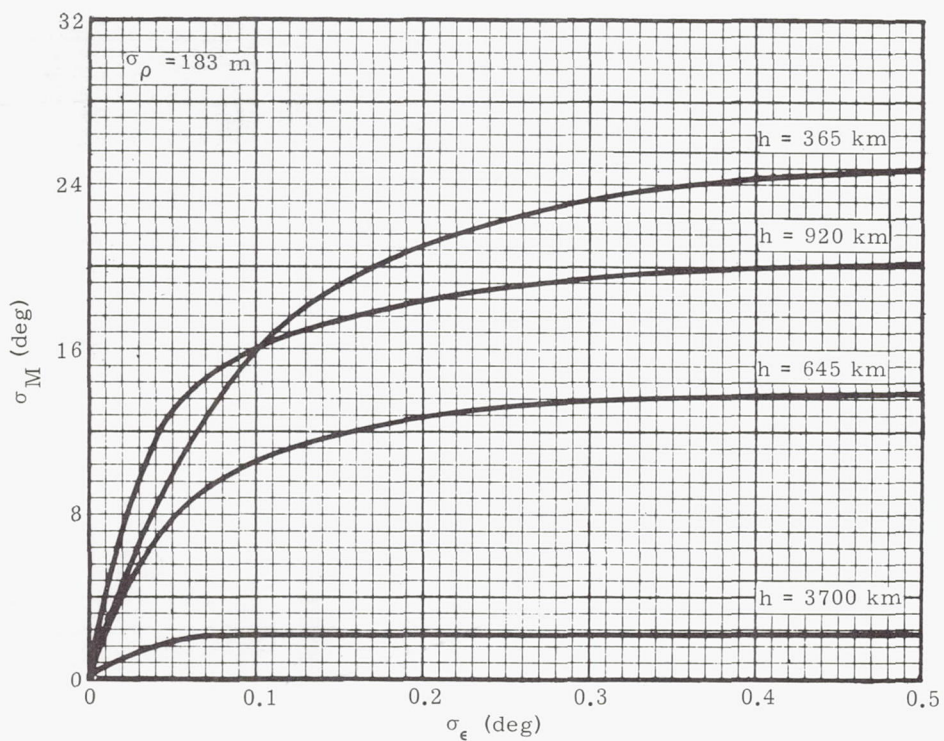


Fig. 31. Angular Observation Errors, σ_M Versus σ_ϵ

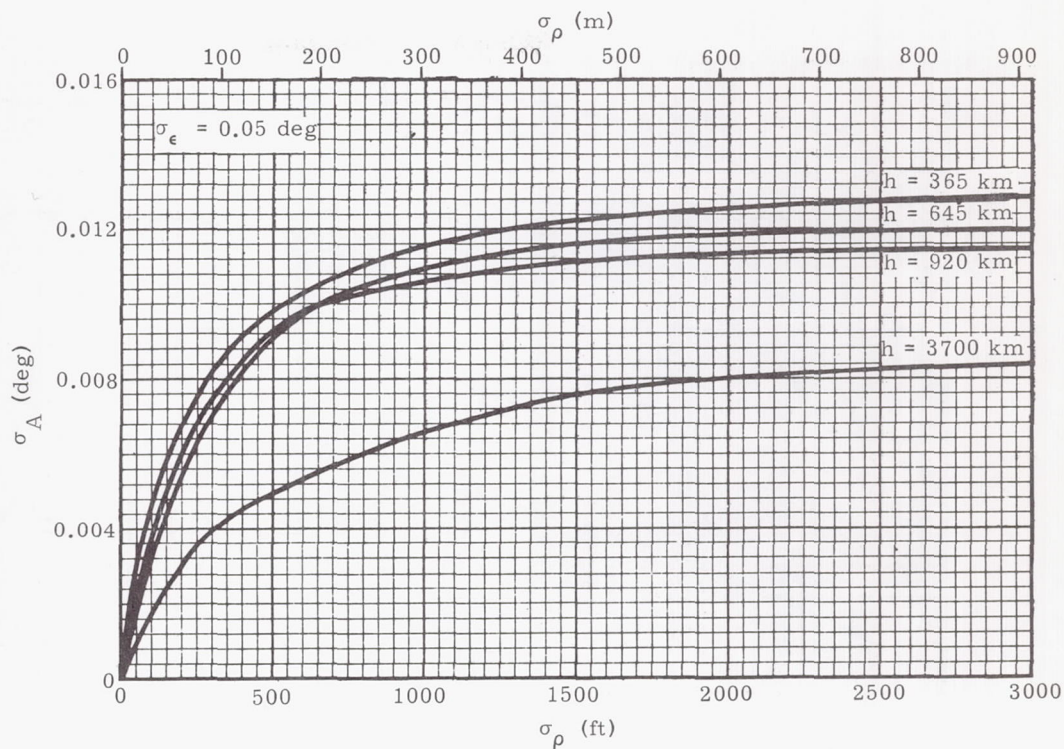


Fig. 32. Range Observation Errors, σ_A Versus σ_ρ

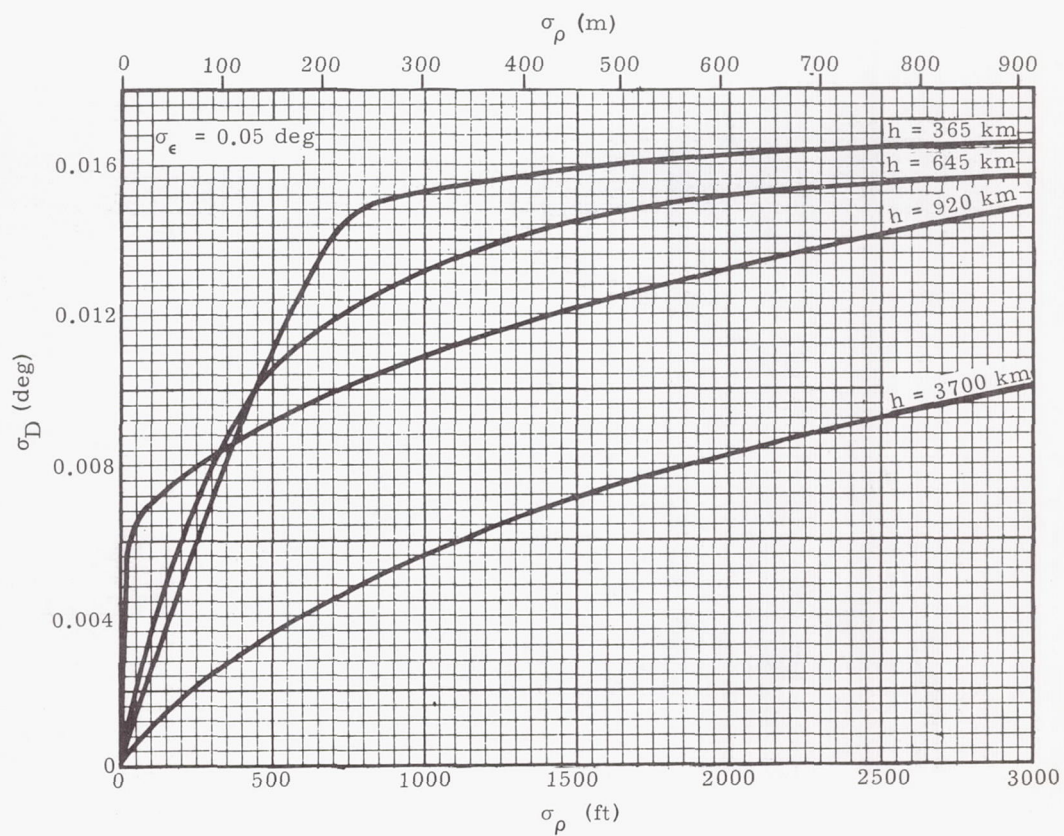


Fig. 33. Range Observation Errors, σ_D Versus σ_ρ

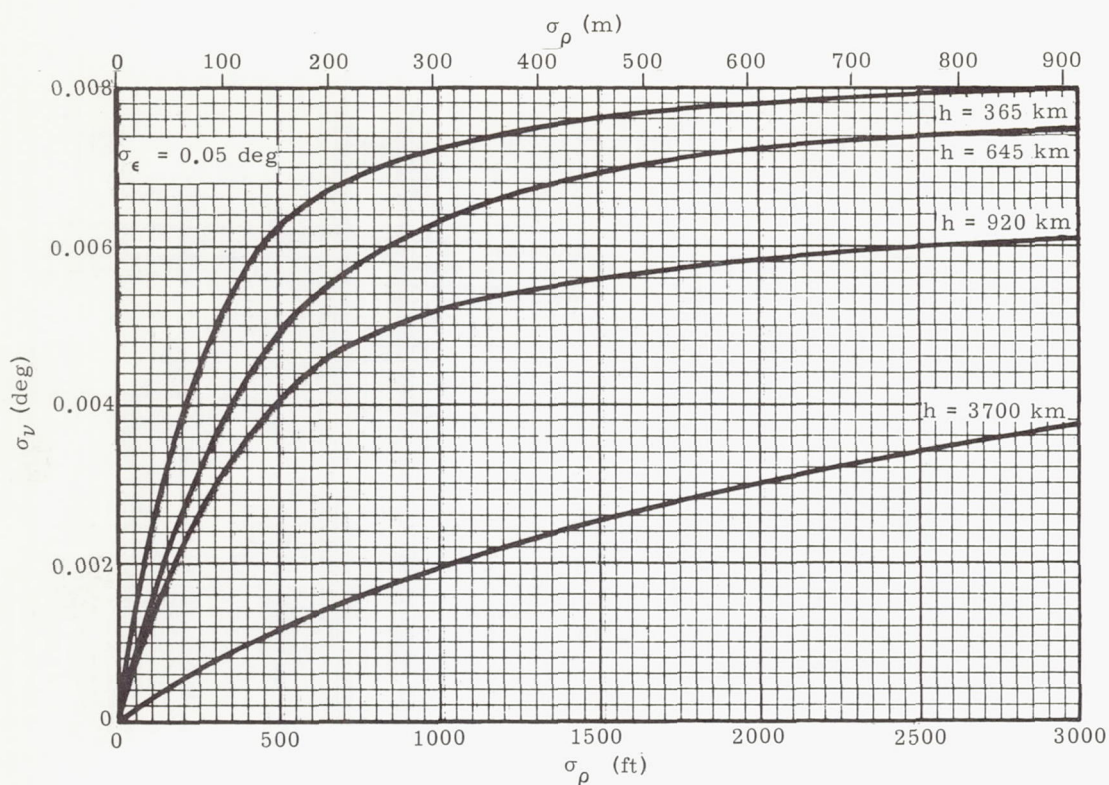


Fig. 34. Range Observation Errors, σ_v Versus σ_ρ

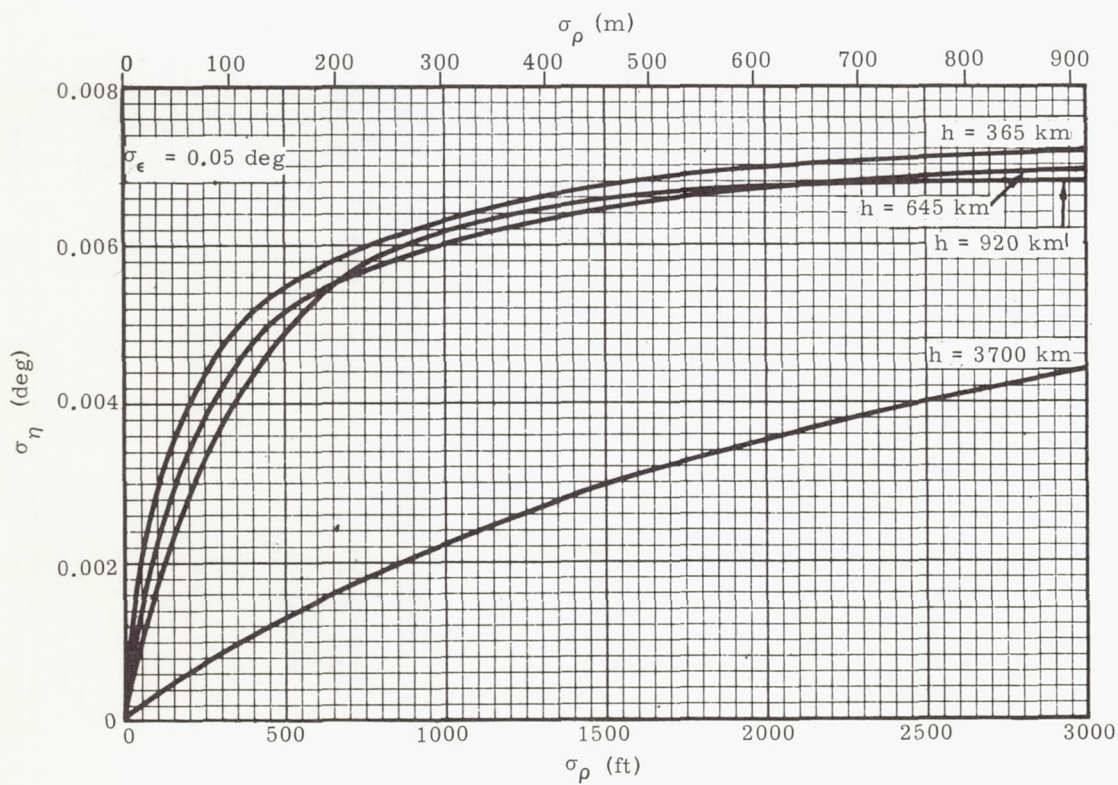


Fig. 35. Range Observation Errors, σ_η Versus σ_ρ

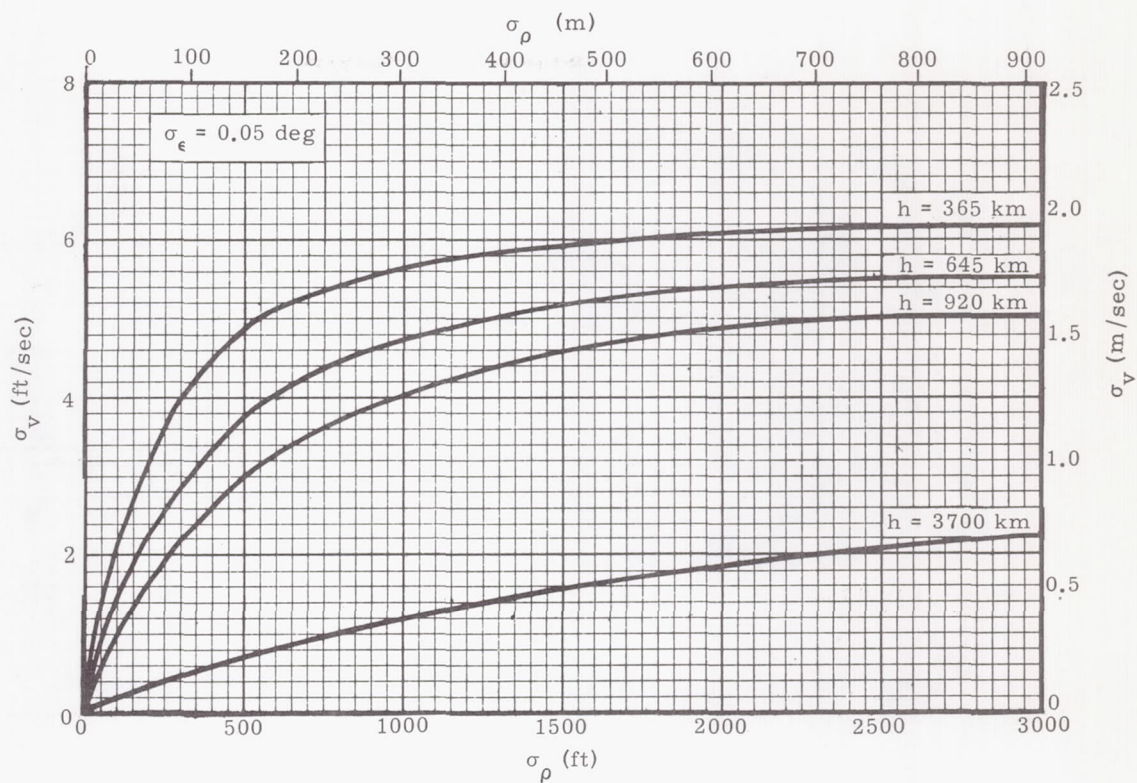


Fig. 36. Range Observation Errors, σ_v Versus σ_ρ

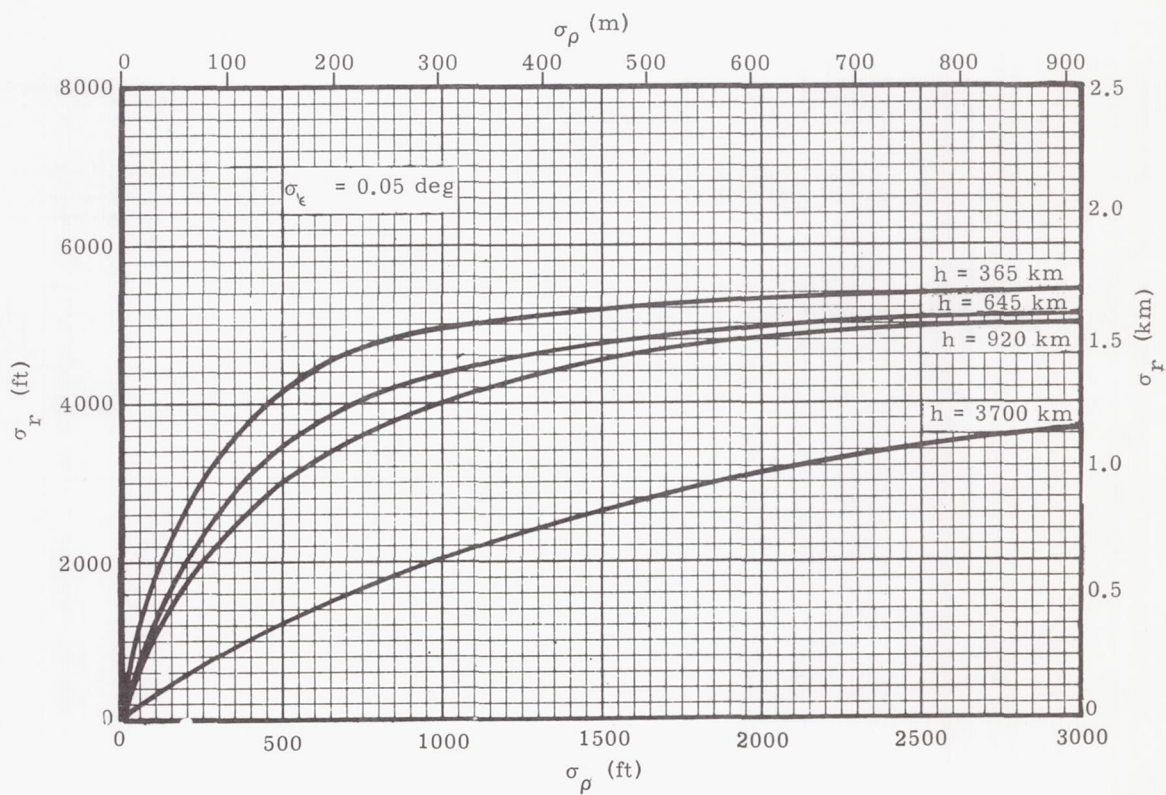


Fig. 37. Range Observation Errors, σ_r Versus σ_ρ

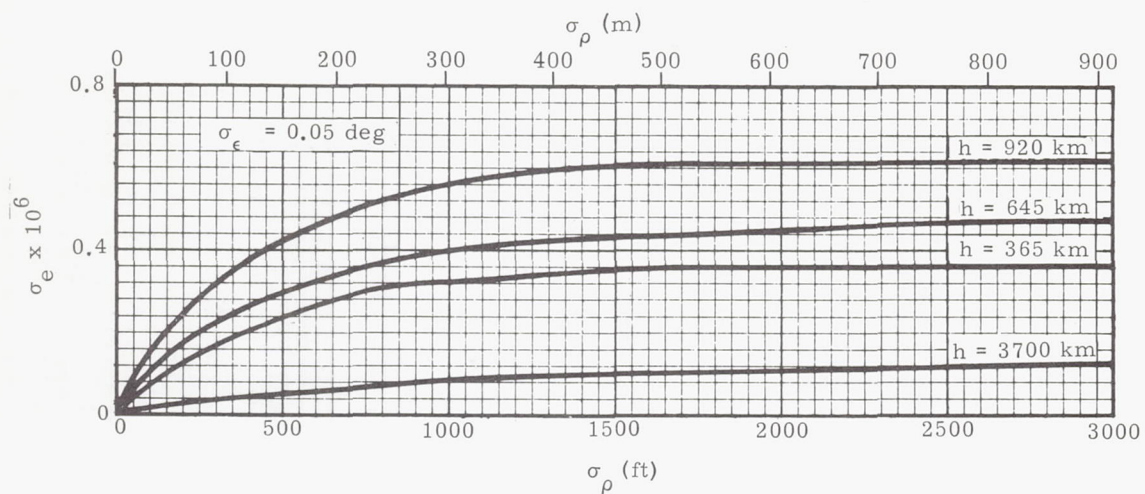


Fig. 38. Range Observation Errors, σ_e Versus σ_ρ

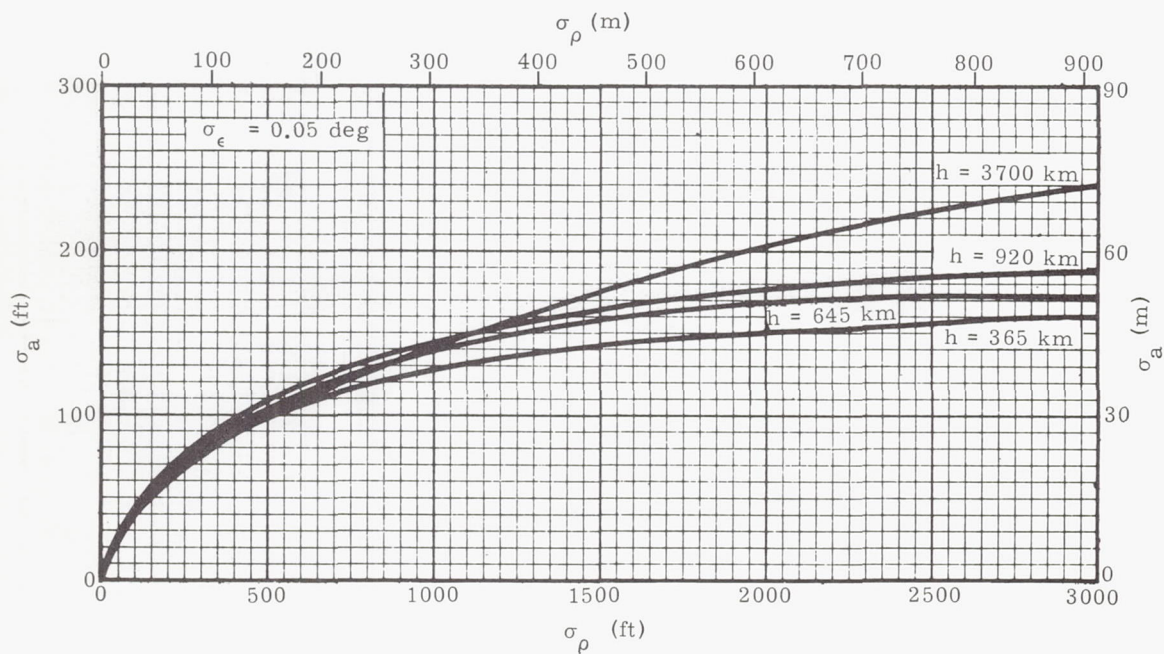


Fig. 39. Range Observation Errors, σ_a Versus σ_ρ

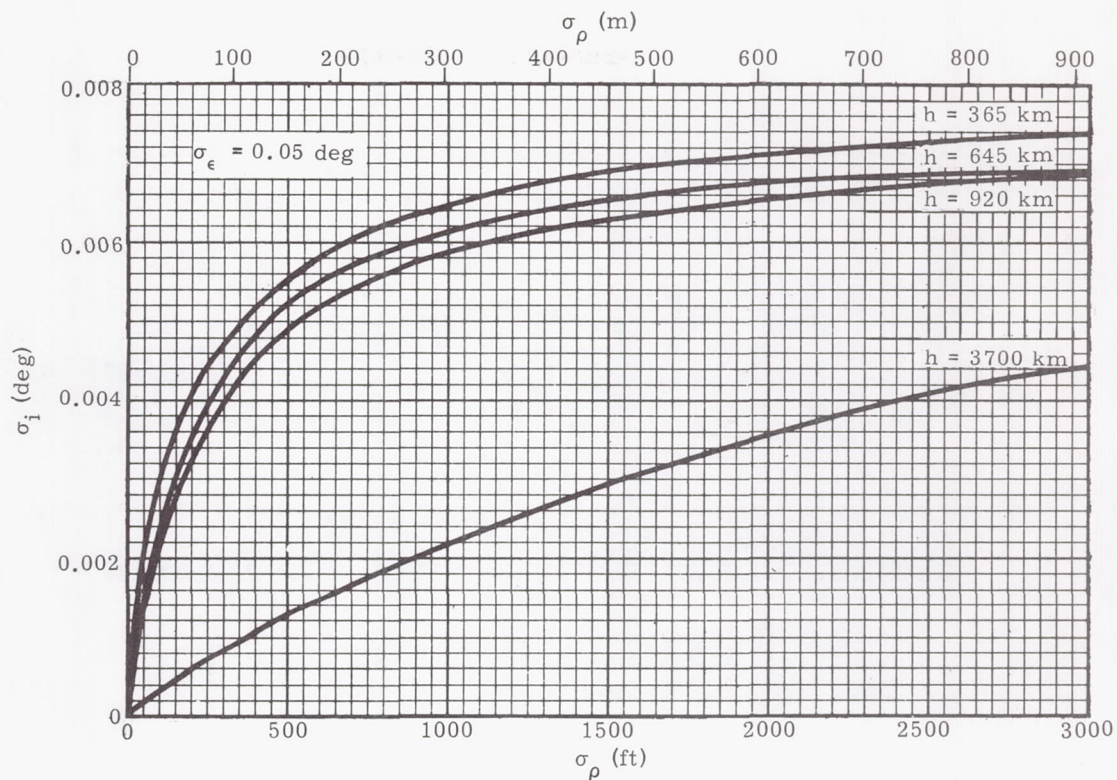


Fig. 40. Range Observation Errors, σ_i Versus σ_ρ

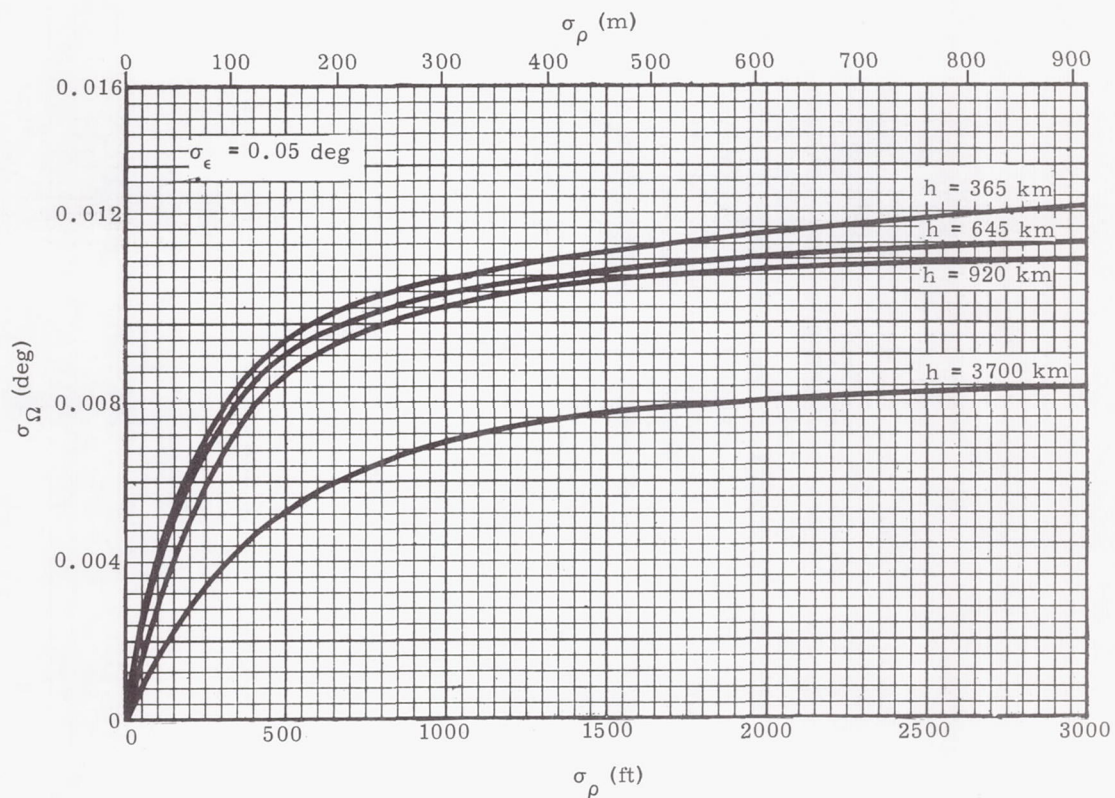


Fig. 41. Range Observation Errors, σ_Ω Versus σ_ρ

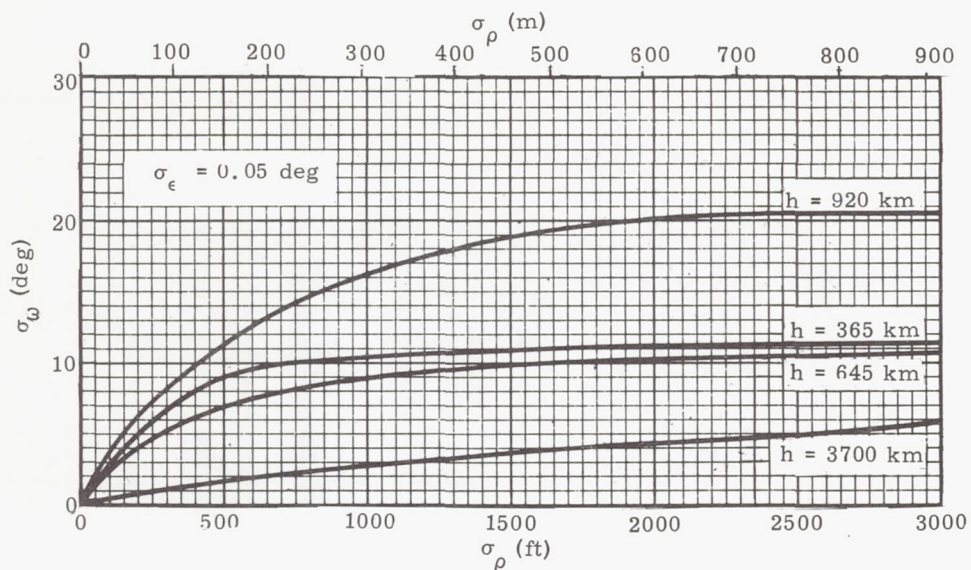


Fig. 42. Range Observation Errors, σ_ω Versus σ_ρ

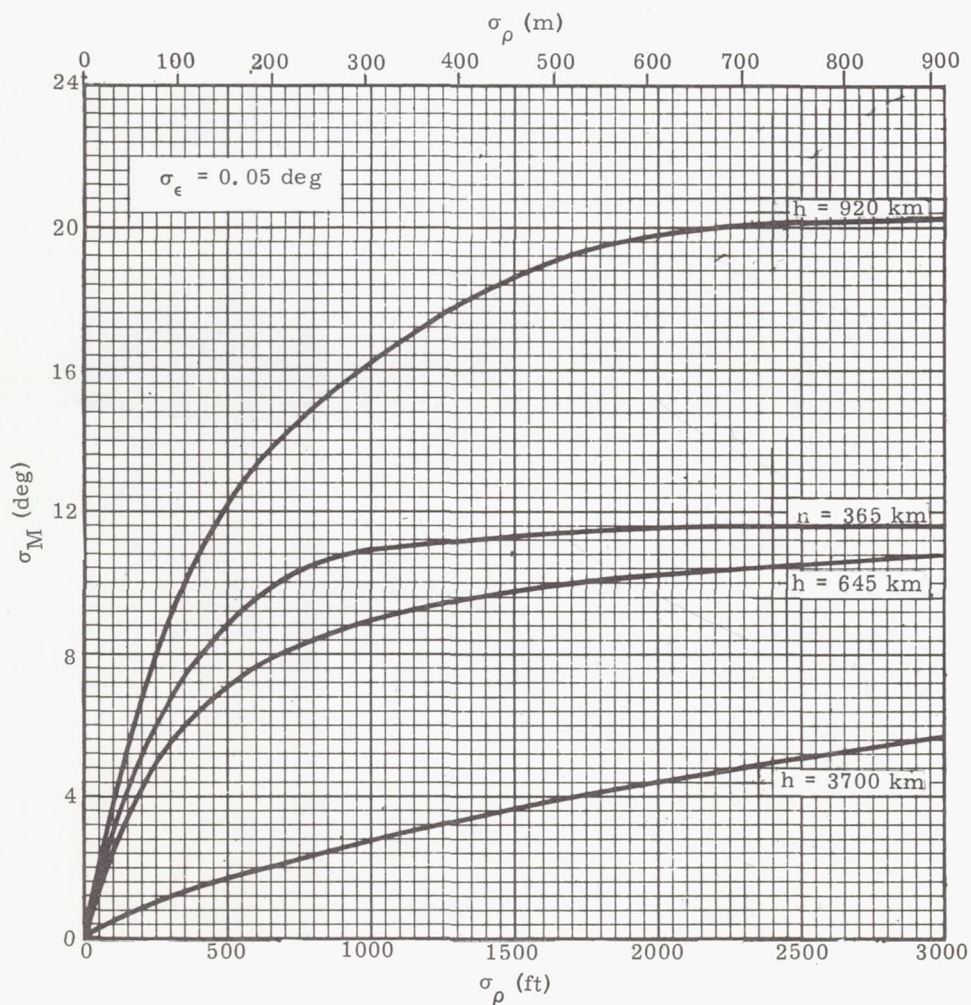


Fig. 43. Range Observation Errors, σ_M Versus σ_ρ

CHAPTER XII
GUIDANCE AND CONTROL

Prepared by:

J. D. Kraft
Martin Company (Baltimore)
Aerospace Mechanics Department
March 1963

| | Page |
|---|--------|
| Symbols | XII-1 |
| A. Introduction | XII-2 |
| B. Guidance and Control Requirements | XII-2 |
| C. Space Vehicle Guidance Techniques | XII-28 |
| D. Design of Attitude Control Systems for Earth Satellites | XII-31 |
| E. References | XII-56 |
| F. Bibliography | XII-56 |
| Illustrations | XII-63 |

LIST OF ILLUSTRATIONS

| Figure | | Page |
|--------|--|--------|
| 1 | Results of Optimization for Equal σ in Pitch and Yaw Equal to $\sigma_{\Delta}^{\epsilon_0}$ | XII-65 |
| 2 | Normalized Density Function of Δv (Equation 110) | XII-65 |
| 3 | Vacuum Ballistic Trajectory Error Analysis (velocity and radius, cutoff to apogee, partials) | XII-66 |
| 4 | Vacuum Ballistic Trajectory Error Analysis (velocity and radius partials, expanded scale) | XII-67 |
| 5 | Vacuum Ballistic Trajectory Error Analysis (correction for $r_0/r_f = 1.02$) | XII-68 |
| 6 | Vacuum Ballistic Trajectory Error Analysis (correction for $r_0/r_f = 1.04$) | XII-69 |
| 7 | Vacuum Ballistic Trajectory Error Analysis (radius partial, apogee to r_f , $r_f = r_0$ | XII-70 |
| 8 | Vacuum Ballistic Trajectory Error Analysis (radius partial, apogee to r_f , $r_f = r_0/1.02$) | XII-71 |
| 9 | Vacuum Ballistic Trajectory Error Analysis (radius partial, apogee to r_f , $r_f = r_0/1.04$) | XII-72 |
| 10 | Vacuum Ballistic Trajectory Error Analysis (flight path angle partial, $r_0/r_f = 1.00$) | XII-73 |
| 11 | Vacuum Ballistic Trajectory Error Analysis (flight path angle partial, extended velocities, $r_0/r_f = 1.00$) | XII-74 |
| 12 | Vacuum Ballistic Trajectory Error Analysis (flight path angle partial, $r_0/r_f = 1.02$) | XII-75 |
| 13 | Vacuum Ballistic Trajectory Error Analysis (flight path angle partial, extended, $r_0/r_f = 1.02$) | XII-76 |
| 14 | Vacuum Ballistic Trajectory Error Analysis (flight path angle partial, $r_0/r_f = 1.04$) | XII-77 |

LIST OF ILLUSTRATIONS (continued)

| Figure | | Page |
|--------|--|--------|
| 15 | Vacuum Ballistic Trajectory Error Analysis (flight path angle partials, extended velocities $r_0/r_f = 1.04$) | XII-78 |
| 16 | Vacuum Ballistic Trajectory Error Analysis (circular velocity as a function of altitude) | XII-79 |
| 17 | Vacuum Ballistic Trajectory Error Analysis (r_0/r_f as a function of h_0 and h_f) | XII-80 |
| 18 | Altitude and Velocity Influence Coefficients Versus Range (for values of elevation angle γ_0) . . . | XII-81 |
| 19 | Elevation Angle Influence Coefficient Versus Range (for values of elevation angle γ_0) | XII-81 |
| 20 | Time of Flight Versus Range | XII-82 |
| 21 | Overall Control System Block Diagram with Radio Guidance Loop | XII-83 |
| 22 | Functional Block Diagram for a Radio-Inertial System | XII-83 |
| 23 | Actual Antenna Radiation Pattern Showing Important Trajectory Steering Constraints | XII-84 |
| 24 | Gravity Computer. | XII-84 |
| 25 | Steering Computer | XII-85 |
| 26 | Motor Shutoff Computer | XII-85 |
| 27 | Torque from Solar Radiation as a Function of Area and Lever Arm | XII-86 |
| 28a | Field Intensity Versus Altitude for Earth's Magnetic Field | XII-86 |
| 28b | Maximum Torque per Ampere-Turn for a 0.3 m Radius Coil Versus Altitude over the Magnetic Equator. | XII-86 |

LIST OF ILLUSTRATIONS (continued)

| Figure | | Page |
|--------|---|--------|
| 29 | Flux Density in Inertial Space Versus Position in 400-Naut Mi (741 km) Orbit | XII-87 |
| 30 | Component of Flux Density Along Earth's Local Vertical in 400-Naut Mi(741 km) Orbit for Several Orbit Inclinations | XII-88 |
| 31 | Magnitude of Earth's Magnetic Field at 400-Naut Mi (741 km) as a Function of Latitude Assuming the Magnetic Dipole Is Along the Earth's Spin Axes | XII-88 |
| 32 | Typical Conical Earth Scanning System | XII-89 |
| 33 | Geometry for Using Edge Tracking to Generate Attitude Information | XII-90 |
| 34 | A Wide Angle Passive Scanner | XII-90 |
| 35 | A Possible Yaw and Array Sun Sensor Arrangement | XII-91 |
| 36 | T Shadow Bar Sun Sensor | XII-91 |
| 37 | Coordinate System for Computation of Yaw and Solar Array Laws | XII-92 |
| 38 | Yaw and Solar Array Control Laws | XII-92 |
| 39a | Torque in Body Coordinates Due to Solar Radiation Pressure for One Orbit | XII-93 |
| 39b | Momentum Change in Inertial Coordinates Due to Solar Radiation Pressure for One Orbit | XII-93 |
| 40 | Total Stored Momentum During One Orbit Due to Gravity Gradient | XII-93 |
| 41 | Block Diagram of Simple On-Off Control System . . | XII-94 |
| 42 | Phase Plane Portrait of a Contractor Control System | XII-94 |

LIST OF ILLUSTRATIONS (continued)

| Figure | | Page |
|--------|---|--------|
| 43 | Block Diagram of Gas Jet Reaction Wheel Dual Mode System | XII-94 |
| 44 | Typical Phase Portrait Dual Mode System with Constant Disturbance Torque | XII-95 |
| 45 | Example Attitude Control System Block Diagram for Acquisition Mode | XII-95 |
| 46 | Phase Portrait of Roll Error and Roll Error Phase of Acquisition | XII-96 |
| 47 | Angle and Angular Rate at First Switching Line Versus Acceleration for Initial Conditions of $1^\circ/\text{sec}$ and 180° Error | XII-96 |
| 48 | Angle and Angular Rate Versus Time of Acqui- sition | XII-97 |
| 49 | Basic Attitude Control System Block Diagram for Normal Mode | XII-97 |

XII. GUIDANCE AND CONTROL

| SYMBOLS | | | |
|----------|--|------------|--|
| a | Semimajor axis | μ | Gravitational constant of the earth; also, mean value in statistical discussions |
| e | Orbit eccentricity | ν | Angle from the ascending node to the projection of the radius to the vehicle on the equatorial plane |
| E | Eccentric anomaly | ρ | Range; also, correlation |
| g | Acceleration due to gravity | σ^2 | Variance |
| i | Orbit inclination | τ | Orbit period |
| L | Geocentric latitude | ϕ | Earth central angle in the orbit plane from ascending node to the vehicle position |
| M | Mean anomaly | ψ | Earth central angle normal to the orbit plane |
| r | Orbit radius | ω | Argument of perigee |
| R | Radius of the earth | Ω | Longitude or right ascension of the ascending node. |
| t | Time | | |
| t_p | Time of perigee passage | | |
| v | Magnitude of vehicle velocity | | |
| α | Azimuth of velocity vector relative to nominal | | |
| β | Azimuth of the orbit path relative to the north point on the horizon | | |
| γ | Flight path angle relative to local horizontal | | |
| θ | True anomaly | | |
| | | | Subscripts |
| | | a | Apogee value |
| | | p | Perigee value |

A. INTRODUCTION

The purpose of this chapter is threefold.

- (1) Develop the guidance and control requirements as functions of the tolerances imposed on the trajectory.
- (2) Introduce the subject of satellite guidance with a discussion of guidance techniques.
- (3) Introduce the subject of attitude control.

The first item can generally be discussed by developing an error analysis relating the errors in a specified set of orbit parameters, or, analogously, in position and velocity at a specified time, to errors occurring at injection and then by relating errors at injection to errors in the powered ascent phase. The first analysis is presented in Section B of this chapter (powered ascent trajectories are not covered in this manual) in a general form obtained without sacrifice or assumption. The remaining discussions will be of a more qualitative nature. The difference in emphasis is due to the fact that the field of guidance and control involves studies both of techniques and hardware to implement the desired changes; however, discussions of hardware have been omitted from this text due to its constantly changing nature. These discussions are presented in Sections C and D.

B. GUIDANCE AND CONTROL REQUIREMENTS

Since the goal of a guidance and control system is generally to bring the vehicle to a certain position with a certain velocity, the first step in design of such a system is generally ascertaining the accuracy in this position and velocity required by the mission. The mission requirements are usually expressed in terms of allowable tolerances in orbit elements or required position and velocity accuracies at some terminal point in the trajectory. Therefore, the designer must be able to relate these mission tolerances to tolerances in the final position and velocity of the trajectory phase in which the guidance system is operational. Relations between these tolerances are derived in this section. Errors in elliptic orbits are considered in Subsection 1, and errors in powered flight trajectories are considered in Subsection 2.

1. Error Analysis of Elliptic Orbits

An elliptic orbit can be completely specified by assigning six independent parameters. Of particular interest are the classical elements (semimajor axis (a), eccentricity (e), argument of perigee (ω), time of perigee (t_p), inclination of the orbit plane to the equatorial plane (i) and the celestial longitude or right ascension of the ascending node (Ω) and the polar position and velocity components (radial distance of the vehicle from the center of the earth (r), central angle in the orbit plane from ascending node to vehicle position (ϕ), position angle normal to the orbit plane ($\psi = 0$ nominally), vehicle velocity magnitude

(v), flight path angle in the vertical plane relative to local horizontal (γ) and flight path angle in the horizontal plane (azimuth angle) with respect to north (β)). Differentiation of the equations relating these two systems provides a set of error formulas which serves as a basis for specification of guidance system requirements.

a. General differential analysis

Since the equations relating the planar parameters (a , e , ω , t_p and r , ϕ , v , γ) are not coupled with the equations relating the parameters defining planar orientation, the derivation can be conveniently considered in two parts.

(1) Planar parameters

Generation of the four error equations

$$da = f_1 (dr, d\phi, dv, d\gamma)$$

$$de = f_2 (dr, d\phi, dv, d\gamma)$$

$$d\omega = f_3 (dr, d\phi, dv, d\gamma)$$

$$dt_p = f_4 (dr, d\phi, dv, d\gamma)$$

must be based upon four independent relations between the variables (a , e , ω , t_p) and (r , ϕ , v , γ):

$$v^2 = \mu \left(\frac{2}{r} - \frac{1}{a} \right) \quad (1)$$

$$r^2 v^2 \cos^2 \gamma = \mu a (1 - e^2) \quad (2)$$

$$r = \frac{a(1 - e^2)}{1 + e \cos(\phi - \omega)} \quad (3)$$

$$\begin{aligned} t_p - t &= -\sqrt{\frac{a^3}{\mu}} (E - e \sin E) \\ &= -\sqrt{\frac{a^3}{\mu}} M \end{aligned} \quad (4)$$

where

$$E = \cos^{-1} \left(\frac{a - r}{ea} \right)$$

These equations are, respectively, the energy equation, the law of areas (Kepler's second law), the equation of conic form (Kepler's first law) and Kepler's equation. The establishment of these laws is considered in Chapter III. Taking differentials of Eq (1) gives the required linear error formula for the semimajor axis.

$$da = 2 \frac{a^2}{r^2} dr + \frac{2a^2 v}{\mu} dv \quad (5)$$

This equation is most conveniently expressed in normalized form with coefficients written in terms of only one variable, either r or $\theta = \phi - \omega$. From Eqs (1) and (3)

$$da = 2 \frac{a^2}{r^2} dr + 2a^2 \sqrt{\frac{1}{\mu} \left(\frac{2}{r} - \frac{1}{a} \right)} dv \quad (6)$$

$$= 2 \frac{(1 + e \cos \theta)^2}{(1 - e^2)^2} dr + 2a \sqrt{\frac{a}{\mu}} \sqrt{\frac{1 + 2e \cos \theta + e^2}{1 - e^2}} dv \quad (7)$$

or

$$\frac{da}{a} = 2 \left(\frac{a}{r} \right) \frac{dr}{r} + 2 \left(2 \frac{a}{r} - 1 \right) \frac{dv}{v} \quad (8)$$

$$= 2 \frac{1 + e \cos \theta}{1 - e^2} \frac{dr}{r} + 2 \left(2 \frac{1 + e \cos \theta}{1 - e^2} - 1 \right) \frac{dv}{v} \quad (9)$$

(Also, since the orbit period $\tau = 2\pi \sqrt{\frac{a^3}{\mu}}$, $\frac{d\tau}{\tau} = \frac{3}{2} \frac{da}{a} = 3 \frac{a}{r} \frac{dr}{r} + 3 \left(2 \frac{a}{r} - 1 \right) \frac{dv}{v}$.) Differentials of eccentricity may be determined from Eq (2).

$$de = \frac{v^2 \cos^2 \gamma}{\mu e a} (a - r) dr + \frac{2rv \cos^2 \gamma}{\mu e a} (a - r) dv + \frac{r^2 v^2 \sin \gamma \cos \gamma}{\mu e a} d\gamma \quad (10)$$

Substitution of Eqs (1), (2) and (3) and simplification gives

$$de = \frac{1 - e^2}{er} \left(\frac{a}{r} - 1 \right) dr + 2 \frac{1 - e^2}{er} (a - r) dv + \frac{1}{e} \sqrt{(1 - e^2) \left[\left(\frac{r}{a} - 1 \right)^2 - e^2 \right]} d\gamma \quad (11)$$

$$= \frac{(e + \cos \theta)(1 + e \cos \theta)}{a(1 - e^2)} dr + 2(e + \cos \theta) \left[\frac{a(1 - e^2)}{\mu(1 + 2e \cos \theta + e^2)} \right]^{1/2} dv + (1 - e^2) \frac{\sin \theta}{1 + e \cos \theta} d\gamma \quad (12)$$

or, in normalized form,

$$de = \frac{1 - e^2}{e} \left(\frac{a}{r} - 1 \right) \frac{dr}{r} + 2 \frac{1 - e^2}{e} \left(\frac{a}{r} - 1 \right) \frac{dv}{v} + \frac{1}{e} \sqrt{(1 - e^2) \left[\left(\frac{r}{a} - 1 \right)^2 - e^2 \right]} d\gamma \quad (13)$$

$$= (e + \cos \theta) \frac{dr}{r} + 2(e + \cos \theta) \frac{dv}{v} + (1 - e^2) \frac{\sin \theta}{1 + e \cos \theta} d\gamma \quad (14)$$

From Eq (3),

$$\cos(\phi - \omega) = \frac{a(1 - e^2) - r}{er},$$

differentials of the argument of perigee may be written.

$$-\sin(\phi - \omega)(d\phi - d\omega) = \frac{1 + e \cos \theta}{e} \frac{da}{a} - \left(\frac{\cos \theta}{e} + 2 \frac{1 + e \cos \theta}{1 - e^2} \right) de - \frac{1 + e \cos \theta}{e} \frac{dr}{r}$$

Substitution for da and de from Eqs (5) through (14) gives $d\omega$.

$$d\omega = \pm \frac{1}{e} \sqrt{1 - \left[\frac{a(1 - e^2) - r}{er} \right]^2} \frac{dr}{r} + \frac{2}{e} \sqrt{1 - \left[\frac{a(1 - e^2) - r}{er} \right]^2} \frac{dv}{v} - \frac{1}{e^2} \left[1 + e^2 - \frac{r}{a} \right] d\gamma + d\phi \quad (15)$$

$$d\omega = \frac{\sin \theta}{e} \frac{dr}{r} + 2 \frac{\sin \theta}{e} \frac{dv}{v} - \frac{2e + (1 + e^2) \cos \theta}{e(1 + e \cos \theta)} d\phi \quad (16)$$

The linear error relation for the final planar element, t_p , is obtained from Eq (4).

$$\frac{d(t_p - t)}{t_p - t} = \frac{3}{2} \frac{da}{a} - \frac{\sin E}{E - e \sin E} de + \frac{1 - e \cos E}{E - e \sin E} dE \quad (17)$$

$$dE = -\frac{1}{e \sin E} \left[\frac{r}{a} \frac{da}{a} - \left(1 - \frac{r}{a}\right) \frac{de}{e} - \frac{dr}{a} \right]. \quad (18)$$
$$\begin{aligned} \frac{d(t_p - t)}{t_p - t} = & \left\{ 3 \frac{a}{r} \pm \frac{1}{M} \left[2 \frac{a}{r} - 1 - \left(\frac{a}{r} \right)^2 (1 \right. \right. \\ & \left. \left. - e^2) \right]^{-1/2} \left[-2 + \frac{r}{a} \right. \right. \\ & \left. \left. + \left(\frac{a}{r} - 1 \right) \left(\frac{1 - e^2}{e^2} \right) \left(\frac{a}{r} (1 - e^2) \right. \right. \right. \\ & \left. \left. - 1) \right] \right\} \frac{dr}{r} + \left\{ 3 \left(2 \frac{a}{r} - 1 \right) \right. \\ & \left. \mp \frac{2}{M} \left[e^2 - \left(1 - \frac{r}{a} \right)^2 \right]^{1/2} \left[1 \right. \right. \\ & \left. \left. + \frac{a}{r} \left(\frac{1 - e^2}{e^2} \right) \right] \right\} \frac{dv}{v} \\ & + \frac{1}{M} \frac{(1 - e^2)^{3/2}}{e^2} \left[1 - \frac{r}{a} \left(\frac{1}{1 - e^2} \right) \right] d\gamma \end{aligned} \quad (19)$$

$$\begin{aligned}
= & \left\{ \frac{3(1 + e \cos \theta)}{1 - e^2} + \frac{1}{M} \frac{\sqrt{1 - e^2}}{e \sin \theta} \left[-2 \right. \right. \\
& + (e + \cos \theta) \cos \theta + \frac{1 - e^2}{1 + e \cos \theta} \left. \left. \right] \right\} \frac{dr}{r} \\
& + \left[3 \frac{1 + 2e \cos \theta + e^2}{1 - e^2} \right. \\
& - \frac{2}{M} \frac{\sqrt{1 - e^2}}{e} \sin \theta \frac{1 + e \cos \theta + e^2}{1 + e \cos \theta} \left. \right] \frac{dv}{v} \\
& + \frac{1}{M} \frac{(1 - e^2)^{3/2}}{e} \frac{\cos \theta}{1 + e \cos \theta} d\gamma \quad (20)
\end{aligned}$$

(2) Orientation parameters

$$d\mathbf{i} = \frac{\partial \mathbf{i}}{\partial \psi} d\psi + \frac{\partial \mathbf{i}}{\partial \beta} d\beta$$

$$d\Omega = \frac{d\Omega}{d\psi} d\psi + \frac{\partial \Omega}{\partial \beta} d\beta$$

$$\cos (i_0 + \Delta i) = \cos (L_0 + \Delta L) \sin (\beta_0 + \Delta \beta)$$
$$\begin{aligned} \cos i_0 - \sin i_0 \Delta i &\approx \cos L_0 \sin \beta_0 \\ &+ \cos L_0 \cos \beta_0 \Delta \beta \\ &- \sin L_0 \sin \beta_0 \Delta L \end{aligned}$$
$$\Delta i \approx - \frac{\cos L_0 \cos \beta_0}{\sin i_0} \Delta \beta + \frac{\sin L_0 \sin \beta_0}{\sin i_0} \Delta L. \quad (21)$$
$$\Delta L = f(\Delta\psi, \Delta\beta)$$
$$\cos (90^{\circ} - L_0 - \Delta L) = \cos (90^{\circ} - L_0) \cos \Delta \psi$$

$$+ \sin (90^\circ - L_0) \sin \Delta \psi \cos (90^\circ + \beta_0)$$

$$\Delta L \approx -\sin \beta_0 \Delta \psi.$$
$$di = -\frac{\cos L_0 \cos \beta_0}{\sin i_0} \Delta\beta - \frac{\sin L_0 \sin^2 \beta_0}{\sin i_0} \Delta\psi.$$
$$\cos (\nu_0 + \Delta A - \Delta \Omega) = \frac{\cos (\beta_0 + \Delta \beta)}{\sin (i_0 + \Delta i)}$$
$$\frac{\sin \Delta A}{\sin \Delta \psi} = \frac{\sin (90^\circ + \beta_0)}{\sin (90^\circ - L_0 - \Delta L)}$$
$$\tan \nu_0 (\Delta A - \Delta \Omega) \approx \tan \beta_0 \Delta \beta + \cot i_0 \Delta i$$

$$\Delta A \approx \frac{\cos \beta_0}{\cos L_0} \Delta \psi.$$

$$\begin{aligned} d\Omega = & \left[-\frac{\tan \beta_0}{\tan \nu_0} + \frac{\cot i_0 \cos L_0 \cos \beta_0}{\tan \nu_0 \sin i_0} \right] \Delta\beta \\ & + \left[\frac{\cos \beta_0}{\cos L_0} + \frac{\cot i_0 \sin L_0 \sin^2 \beta_0}{\tan \nu_0 \sin i_0} \right] \Delta\psi. \end{aligned}$$
$$d\mathbf{i} = - \frac{\sin L_0 \cos^2 i_0}{\sin i_0 \cos^2 L_0} d\psi \mp \sqrt{1 - \frac{\sin^2 L_0}{\sin^2 i_0}} d\beta \quad (22)$$

$$d\Omega = \pm \frac{1}{\cos^2 L_0 \sin i_0} \sqrt{1 - \frac{\sin^2 L_0}{\sin^2 i_0}} d\psi - \frac{\sin L_0}{\sin^2 i_0} d\beta \quad (23)$$

$$\cos (i_0 + \Delta i) = \cos L' \sin (\beta' + \Delta \psi)$$

$$\Delta i \approx - \frac{\cos L' \cos \beta'}{\sin L_0} \Delta \psi.$$
$$\tan \beta' = \frac{\cot i_0}{\cos (90 - \phi_0)}$$
$$\phi_0 = \arccos N_0 S_0$$
$$\sin \beta' = \frac{\cos i_0}{\cos L'}$$

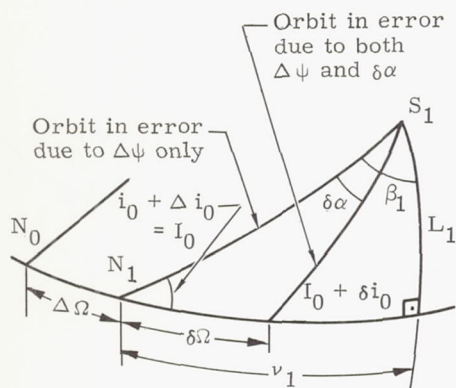
$$\Delta i = -\sin \phi_0 \Delta \psi = -\frac{\sin L_0}{\sin i_0} \Delta \psi.$$

$$\tan (\nu' + \Delta \Omega) = \sin L' \tan (\beta' + \Delta \psi)$$
$$\Delta\Omega = \arccos \frac{\mathbf{N}_0 \cdot \mathbf{N}_1}{|\mathbf{N}_0| |\mathbf{N}_1|}$$

$$\Delta\Omega \approx \frac{\sin L' \cos^2 \nu'}{\cos^2 \beta'} \Delta\gamma$$

$$\Delta\Omega \approx \frac{\cos \phi}{\sin i_0} \Delta\gamma = \frac{1}{\sin i_0} \sqrt{1 - \frac{\sin^2 L_0}{\sin^2 i_0}} \Delta\gamma.$$

Now consider an error due to $\delta\alpha$ superimposed on the previously considered incorrect orbit as shown in the accompanying sketch. The additional errors due to $\delta\alpha$ will be denoted by $\delta(\)$.



$$\sin(\beta_1 - \delta\alpha) = \frac{\cos(I_0 + \delta i_0)}{\cos L_1}$$

where

$$I_0 = i_0 + \Delta i_0$$

or

$$\begin{aligned} \delta i_0 &\approx \frac{\cos \beta_1 \cos L_1}{\sin I_0} \delta\alpha \\ &\approx \frac{\cos \beta_0 \cos L_0}{\sin i_0} \delta\alpha \end{aligned}$$

Also, from

$$\cos(\nu_1 - \delta\Omega) = \frac{\cos(\beta_1 - \delta\alpha)}{\sin(I_0 + \delta i_0)}$$

$$\begin{aligned} \delta\Omega &\approx -\frac{\cos \beta_1}{\sin I_0} - \frac{\cos \beta_1}{\sin I_0} \cot I_0 \delta i_0 + \frac{\sin \beta_1}{\sin I_0} \delta\alpha \\ &\approx \frac{\sin L_0}{\sin^2 i_0} \delta\alpha \end{aligned}$$

The the total error formulas, analogous to Eqs (22) and (23), are obtained by adding the contributions due to $\Delta\psi$ and $\delta\alpha$ (that is, forming $\Delta i + \delta i$ and $\Delta\Omega + \delta\Omega$).

$$di = -\frac{\sin L_0}{\sin i_0} d\psi + \cos \phi_0 d\alpha \quad (24)$$

$$d\Omega = \frac{\cos \phi_0}{\sin i_0} d\psi + \frac{\sin L_0}{\sin^2 i_0} d\alpha \quad (25)$$

The differential error expressions derived in this section (Eqs (8), (9), (13) through (16), (19), (20), (24) and (25)) are presented concisely for reference in Table 1.

The inverses of the relations expressed in Table 1 (that is, the errors in polar position and velocity components as functions of errors in the classical elements) are also useful error formulas. These formulas can be generated simply by inverting the matrix of coefficients given in Table 1. If Table 1 is expressed as

$$\begin{Bmatrix} p_i \end{Bmatrix} = \begin{bmatrix} a_{ij} \end{bmatrix} \begin{Bmatrix} q_j \end{Bmatrix}$$

where

$$\begin{Bmatrix} p_i \end{Bmatrix} = \left\{ \frac{da}{a}, de, d\omega, \frac{d(t_p - t)}{t_p - t}, di, d\Omega \right\}$$

= the six vector of nondimensional orbit parameter differentials

$$\begin{Bmatrix} q_j \end{Bmatrix} = \left\{ \frac{dr}{r}, \frac{dv}{v}, d\gamma, d\phi, d\psi, d\beta \right\}$$

= the six vector of nondimensional polar coordinates

$$\begin{bmatrix} a_{ij} \end{bmatrix} = \begin{bmatrix} a_{11} & a_{12} & 0 & 0 & 0 & 0 \\ a_{21} & a_{22} & a_{23} & 0 & 0 & 0 \\ a_{31} & a_{32} & a_{33} & 1 & 0 & 0 \\ a_{41} & a_{42} & a_{43} & 0 & 0 & 0 \\ 0 & 0 & 0 & 0 & a_{55} & a_{56} \\ 0 & 0 & 0 & 0 & a_{65} & a_{66} \end{bmatrix}$$

Then the required inverse matrix is

$$\begin{bmatrix} a_{ij} \end{bmatrix}^{-1} = \frac{\begin{bmatrix} \tilde{a}_{ij} \end{bmatrix}}{|a_{ij}|}$$

where

$$\begin{bmatrix} \tilde{a}_{ij} \end{bmatrix} = \text{adjoint of } \begin{bmatrix} a_{ij} \end{bmatrix} \text{ (transpose the cofactor matrix)}$$

$$|a_{ij}| = \text{determinant with elements } a_{ij}.$$

Inversion is most conveniently accomplished if the 4 x 4 submatrix of planar parameter coefficients and the 2 x 2 submatrix of orientation parameter coefficients are inverted separately. The process is also simplified by noting that

$$\begin{vmatrix} a_{11} & a_{12} & 0 & 0 \\ a_{21} & a_{22} & a_{23} & 0 \\ a_{31} & a_{32} & a_{33} & 1 \\ a_{41} & a_{42} & a_{43} & 0 \end{vmatrix} = - \begin{vmatrix} a_{11} & a_{12} & 0 \\ a_{21} & a_{22} & a_{23} \\ a_{41} & a_{42} & a_{43} \end{vmatrix}$$

$$= - \frac{2(1 - e^2)^{3/2}}{M} \frac{(1 + e^2 + 2e \cos \theta)}{e(1 + e \cos \theta)^2}$$

The resulting inverse matrix is presented in Table 2.

With the relations of Tables 1 and 2, errors in one phase of an orbit can be determined as functions of errors several phases prior to or subsequent to that phase. For example, errors in position and velocity at orbit injection can be used to solve for errors in the orbit elements, which can in turn be used to determine by the inverse relations, errors in position and velocity at any future time.

b. Errors in orbit extrema

Orbit tolerances are frequently specified in terms of allowable errors in apogee or perigee conditions. For example, in establishment of a low-altitude orbit, a perigee altitude tolerance may be specified in order to assure a long orbit lifetime. Equations for these errors in apogee and perigee conditions can be easily determined as a special case of the previous general analysis (Section B.1.a.).

From Eqs (1) and (3)

$$r_a = a(1 + e) \quad (26)$$

$$r_p = a(1 - e) \quad (27)$$

$$v_a = \sqrt{\frac{\mu}{a} \frac{1 - e}{1 + e}} \quad (28)$$

$$v_p = \sqrt{\frac{\mu}{a} \frac{1 + e}{1 - e}} \quad (29)$$

where subscripts a and p denote apogee and perigee conditions, respectively. These equations yield the following differentials.

$$dr_a = (1 + e) da + ade \quad (30)$$

$$dr_p = (1 - e) da - ade \quad (31)$$

$$dv_a = -\frac{v_a}{2a} da - \frac{v_p}{(1 + e)^2} de \quad (32)$$

$$dv_p = -\frac{v_p}{2a} da + \frac{v_a}{(1 - e)^2} de \quad (33)$$

These equations may be expressed in nondimensional form as follows.

$$\frac{dr_a}{r_a} = \frac{da}{a} + \frac{de}{1 + e} \quad (34)$$

$$\frac{dr_p}{r_p} = \frac{da}{a} - \frac{de}{1 - e} \quad (35)$$

$$\frac{dv_a}{v_a} = -\frac{1}{2} \frac{da}{a} - \frac{de}{1 - e^2} \quad (36)$$

$$\frac{dv_p}{v_p} = -\frac{1}{2} \frac{da}{a} + \frac{de}{1 - e^2} \quad (37)$$

Then

$$\begin{bmatrix} \frac{dr_a}{r_a} \\ \frac{dr_p}{r_p} \end{bmatrix} = \begin{bmatrix} 1 & \frac{1}{1 + e} \\ 1 & \frac{-1}{1 - e} \end{bmatrix} \begin{bmatrix} \frac{da}{a} \\ de \end{bmatrix} = \begin{bmatrix} 1 & \frac{1}{1 + e} \\ 1 & \frac{-1}{1 - e} \end{bmatrix} \begin{bmatrix} a_{11} & a_{12} & 0 \\ a_{21} & a_{22} & a_{23} \end{bmatrix} \begin{bmatrix} \frac{dr}{r} \\ \frac{dv}{v} \\ d\gamma \end{bmatrix}$$

and

$$\begin{bmatrix} \frac{dv_a}{v_a} \\ \frac{dv_p}{v_p} \end{bmatrix} = \begin{bmatrix} -\frac{1}{2} & \frac{-1}{1 - e^2} \\ -\frac{1}{2} & \frac{1}{1 - e^2} \end{bmatrix} \begin{bmatrix} \frac{da}{a} \\ de \end{bmatrix} = \begin{bmatrix} -\frac{1}{2} & \frac{-1}{1 - e^2} \\ -\frac{1}{2} & \frac{1}{1 - e^2} \end{bmatrix} \begin{bmatrix} a_{11} & a_{12} & 0 \\ a_{21} & a_{22} & a_{23} \end{bmatrix} \begin{bmatrix} \frac{dr}{r} \\ \frac{dv}{v} \\ d\gamma \end{bmatrix}$$

Substitution of the a_{ij} from Table 1 gives the differentials of the apogee and perigee values.

$$\begin{aligned} \frac{dr_a}{r_a} &= \frac{a}{r} \left[2 + \frac{1 - e}{e} \left(1 - \frac{r}{a} \right) \right] \frac{dr}{r} \\ &+ 2 \frac{a}{r} \left[1 + \frac{1}{e} \left(1 - \frac{r}{a} \right) \right] \frac{dv}{v} \\ &\pm \frac{1 - e}{e} \sqrt{\left(\frac{r}{a} \right)^2 \frac{\left(2 \frac{a}{r} - 1 \right)}{(1 - e^2)^2} - 1} d\gamma \end{aligned} \quad (38)$$

$$\begin{aligned} \frac{dr_p}{r_p} &= \frac{a}{r} \left[2 - \frac{(1 + e)}{e} \left(1 - \frac{r}{a} \right) \right] \frac{dr}{r} \\ &+ 2 \frac{a}{r} \left[1 - \frac{1}{e} \left(1 - \frac{r}{a} \right) \right] \frac{dv}{v} \\ &\mp \frac{1 + e}{e} \sqrt{\left(\frac{r}{a} \right)^2 \frac{\left(2 \frac{a}{r} - 1 \right)}{(1 - e^2)^2} - 1} d\gamma \end{aligned} \quad (39)$$

$$\begin{aligned} \frac{dv_a}{v_a} &= \left[-\frac{a}{r} + \frac{1}{e} \left(1 - \frac{a}{r} \right) \right] \frac{dr}{r} + \left[1 - 2 \frac{a}{r} \right. \\ &\left. + \frac{2}{e} \left(1 - \frac{a}{r} \right) \right] \frac{dv}{v} \mp \frac{1}{e} \sqrt{\left(\frac{r}{a} \right)^2 \frac{\left(2 \frac{a}{r} - 1 \right)}{1 - e^2} - 1} d\gamma \end{aligned} \quad (40)$$

TABLE 1
Error Analysis Equations

| | | | | | | | |
|--|--|--|---|--|---|--|--|
| $\left[\begin{array}{c} \frac{da}{a} \\ de \\ d\omega \\ \frac{d(t_p - t)}{t_p - t} \\ di \\ d\Omega \end{array} \right]$ | $\left[\begin{array}{c} \frac{2(1+e \cos \theta)}{1-e^2} \\ e + \cos \theta \\ \frac{\sin \theta}{e} \\ \frac{3(1+e \cos \theta)}{1-e^2} + \frac{1}{M} \frac{\sqrt{1-e^2}}{e \sin \theta} \left[-2 \right. \\ \left. + (e + \cos \theta) \cos \theta + \frac{1-e^2}{1+e \cos \theta} \right] \\ 0 \\ 0 \end{array} \right]$ | $\left[\begin{array}{c} 2 \frac{1+2e \cos \theta + e^2}{1-e^2} \\ 2(e + \cos \theta) \\ 2 \frac{\sin \theta}{e} \\ 3 \frac{1+2e \cos \theta + e^2}{1-e^2} \\ - \frac{2}{M} \frac{\sqrt{1-e^2}}{e} \sin \theta \frac{1+e \cos \theta + e^2}{1+e \cos \theta} \\ 0 \\ 0 \end{array} \right]$ | $\left[\begin{array}{c} 0 \\ (1-e^2) \frac{\sin \theta}{1+e \cos \theta} \\ - \frac{2e + (1+e^2) \cos \theta}{e(1+e \cos \theta)} \\ 0 \\ \frac{1}{M} \frac{(1-e^2)^{3/2}}{e} \frac{\cos \theta}{1+e \cos \theta} \\ 0 \\ 0 \end{array} \right]$ | $\left[\begin{array}{c} 0 \\ 0 \\ 1 \\ 0 \\ 0 \\ 0 \end{array} \right]$ | $\left[\begin{array}{c} 0 \\ 0 \\ 0 \\ 0 \\ - \frac{\sin L_0 \sin^2 \beta_0}{\sin i_0} \\ \frac{\cos \beta_0}{\cos L_0} + \frac{\cos i_0 \sin \beta_0 \cos \beta_0}{\sin^2 i_0} \end{array} \right]$ | $\left[\begin{array}{c} 0 \\ 0 \\ 0 \\ 0 \\ - \frac{\cos L_0 \cos \beta_0}{\sin i_0} \\ \frac{1}{\sin L_0} [\cot^2 i_0 \cot^2 \beta_0 - 1] \end{array} \right]$ | $\left[\begin{array}{c} \frac{dr}{r} \\ \frac{dv}{v} \\ dy \\ d\phi \\ d\psi \\ d\beta \end{array} \right]$ |
| $\left[\begin{array}{c} \frac{da}{a} \\ de \\ d\omega \\ \frac{d(t_p - t)}{t_p - t} \\ di \\ d\Omega \end{array} \right]$ | $\left[\begin{array}{c} 2 \frac{a}{r} \\ \frac{1-e^2}{e} \left(\frac{a}{r} - 1 \right) \\ \pm \frac{1}{e} \sqrt{1 - \left[\frac{a(1-e^2) - r}{er} \right]^2} \\ 3 \frac{a}{r} \pm \frac{1}{M} \left[2 \frac{a}{r} - 1 - \left(\frac{a}{r} \right)^2 (1-e^2) \right]^{-1/2} \left[-2 \right. \\ \left. + \frac{r}{a} + \left(\frac{a}{r} - 1 \right) \frac{(1-e^2)}{e^2} \left\{ \frac{a}{r} (1-e^2) - 1 \right\} \right] \\ 0 \\ 0 \end{array} \right]$ | $\left[\begin{array}{c} 2 \left(2 \frac{a}{r} - 1 \right) \\ 2 \frac{1-e^2}{e} \left(\frac{a}{r} - 1 \right) \\ \pm \frac{2}{e} \sqrt{1 - \left[\frac{a(1-e^2) - r}{er} \right]^2} \\ 3 \left(2 \frac{a}{r} - 1 \right) \mp \frac{2}{M} \left[e^2 \right. \\ \left. - \left(1 - \frac{r}{a} \right)^2 \right]^{1/2} \left[1 + \frac{a}{r} \frac{(1-e^2)}{e^2} \right] \\ 0 \\ 0 \end{array} \right]$ | $\left[\begin{array}{c} 0 \\ \pm \frac{1}{e} \sqrt{(1-e^2) \left[\left(\frac{r}{a} - 1 \right)^2 - e^2 \right]} \\ - \frac{1}{e^2} \left[1 + e^2 - \frac{r}{a} \right] \\ \frac{1}{M} \frac{(1-e^2)^{3/2}}{e^2} \left[1 - \frac{r}{a} \frac{1}{1-e^2} \right] \\ 0 \\ 0 \end{array} \right]$ | $\left[\begin{array}{c} 0 \\ 0 \\ 1 \\ 0 \\ 0 \\ 0 \end{array} \right]$ | $\left[\begin{array}{c} 0 \\ 0 \\ 0 \\ 0 \\ - \frac{\sin L_0 \cos^2 i_0}{\sin i_0 \cos^2 L_0} \\ \pm \frac{1}{\cos^2 L_0 \sin i_0} \sqrt{1 - \frac{\sin^2 L_0}{\sin^2 i_0}} \end{array} \right]$ | $\left[\begin{array}{c} 0 \\ 0 \\ 0 \\ 0 \\ \sqrt{1 - \frac{\sin^2 L_0}{\sin^2 i_0}} \\ - \frac{\sin L_0}{\sin^2 i_0} \end{array} \right]$ | $\left[\begin{array}{c} \frac{dr}{r} \\ \frac{dv}{v} \\ dy \\ d\phi \\ d\psi \\ d\beta \end{array} \right]$ |

$$\begin{aligned} \frac{dv_p}{v_p} = & \left[-\frac{a}{r} + \frac{1}{e} \left(\frac{a}{r} - 1 \right) \right] \frac{dr}{r} \\ & + \left[1 - 2 \frac{a}{r} + \frac{2}{e} \left(\frac{a}{r} - 1 \right) \right] \frac{dv}{v} \\ & \pm \frac{1}{e} \sqrt{\left(\frac{r}{a} \right)^2 \frac{(2 \frac{a}{r} - 1)}{1 - e^2} - 1} d\gamma \end{aligned} \quad (41)$$

upper sign for + γ , lower sign for - γ

With coefficients expressed in terms of the variable θ , Eqs (38) through (41) become

$$\begin{aligned} \frac{dr_a}{r_a} = & \frac{1}{1-e} (2 - e + \cos \theta) \frac{dr}{r} \\ & + \frac{2}{1-e} (1 + \cos \theta) \frac{dv}{v} \\ & + (1 - e) \frac{\sin \theta}{1 + e \cos \theta} d\gamma \end{aligned} \quad (42)$$

$$\begin{aligned} \frac{dr_p}{r_p} = & \frac{1}{1+e} (2 + e - \cos \theta) \frac{dr}{r} \\ & + \frac{2}{1+e} (1 - \cos \theta) \frac{dv}{v} \\ & - (1 - e) \frac{\sin \theta}{1 + e \cos \theta} d\gamma \end{aligned} \quad (43)$$

$$\begin{aligned} \frac{dv_a}{v_a} = & \frac{-1}{1-e} (1 + \cos \theta) \frac{dr}{r} \\ & - \frac{1}{1-e} (1 + e + 2 \cos \theta) \frac{dv}{v} \\ & - \frac{\sin \theta}{1 + e \cos \theta} d\gamma \end{aligned} \quad (44)$$

$$\begin{aligned} \frac{dv_p}{v_p} = & -\frac{1}{1+e} (1 - \cos \theta) \frac{dr}{r} \\ & - \frac{1}{1+e} (1 - e - 2 \cos \theta) \frac{dv}{v} \\ & + \frac{\sin \theta}{1 + e \cos \theta} d\gamma \end{aligned} \quad (45)$$

Eqs (38) through (45) are collected in Table 3.

c. Evaluation of critical cases ($e \approx 0$, $i \approx 0^\circ$)

Many of the error formula coefficients involved in transformation from polar coordinate errors to orbit element errors (Table 1) are indeterminate or inaccurate for $e \approx 0$ or $i \approx 0^\circ$. Error formulas for these special cases may be developed by a Taylor series approach, as used in Ref. (1). If $a = a_0 + \Delta a$, $r = r_0 + \Delta r$, $v = v_0 + \Delta v$ are substituted in Eq (1),

$$a_0 + \Delta a = \left[\frac{2}{r_0 + \Delta r} - \frac{(v_0 + \Delta v)^2}{\mu} \right]^{-1}$$

Since $a_0 = r_0$ and $v_0 = \sqrt{\frac{\mu}{r_0}}$ for nominally circular orbits,

$$1 + \frac{\Delta a}{r_0} = \left[\frac{2}{1 + \frac{\Delta r}{r_0}} - \left(1 + \frac{\Delta v}{v_0} \right)^2 \right]^{-1} \quad (46)$$

Neglecting terms of second order and higher in the Maclaurin series expansion

$$\begin{aligned} (1 + \epsilon)^n = & 1 + n\epsilon + \frac{n(n-1)\epsilon^2}{2!} \\ & + \frac{n(n-1)(n-2)\epsilon^3}{3!} + \dots \end{aligned} \quad (47)$$

$$(\epsilon^2 \ll 1)$$

of the various terms of Eq (46) gives

$$\frac{\Delta a}{r_0} \approx 2 \frac{\Delta r_0}{r_0} + 2 \frac{\Delta v_0}{v_0} \quad (1 \gg \epsilon^2) \quad (48)$$

which checks with Eq (8) for nominally circular orbits ($a_0 = r_0$ in the coefficients). However, similar evaluation of Δe from Eq (2) (that is, letting $r = r_0 + \Delta r$, $v = v_0 + \Delta v$, $\gamma = \Delta \gamma$ in

$$e^2 = 1 + \frac{1}{2} r^2 v^4 \cos^2 \gamma - \frac{2}{\mu} r v^2 \cos^2 \gamma$$

requires retaining second order terms in approximations by Eq (47) since the first order terms vanish. The resulting solution is

$$\begin{aligned} e^2 \approx & \left(2 \frac{\Delta v}{v_0} + \frac{\Delta r}{r_0} \right)^2 + \gamma^2 \cdot \\ & (1 \gg e^2) \end{aligned} \quad (49)$$

TABLE 2
Error Analysis Equations

$$\begin{bmatrix} \frac{dr}{r} \\ \frac{dv}{v} \\ d\gamma \\ d\phi \\ d\psi \\ d\beta \end{bmatrix} = \begin{bmatrix} 1 - \frac{3}{2} \frac{e M \sin \theta}{(1-e)^{3/2}} (1+e \cos \theta) & -\frac{1}{1-e^2} \cos \theta (1+e \cos \theta) & 0 & \frac{M e \sin \theta}{(1-e^2)^{3/2}} (1+e \cos \theta) & 0 & 0 \\ \frac{1}{2} \left[-1 + 3 \frac{e M \sin \theta (1+e \cos \theta)^2}{(1-e^2)^{3/2} (1+e^2+2e \cos \theta)} \right] & \frac{1}{(1-e^2)} \frac{\cos \theta (1+e \cos \theta)^2}{(1+e^2+2e \cos \theta)} & 0 & 2 \sin \theta & 0 & 0 \\ -\frac{3 e M (e+\cos \theta) (1+e \cos \theta)^2}{2 (1-e^2)^{3/2} (1+e^2+2e \cos \theta)} & \frac{\sin \theta (1+e^2+e \cos \theta) (1+e \cos \theta)}{(1-e^2) (1+e^2+2e \cos \theta)} & 0 & \frac{M e (1+e \cos \theta)^2 (e+\cos \theta)}{(1-e^2)^{3/2} (1+e^2+2e \cos \theta)} & 0 & 0 \\ -\frac{3}{2} M \frac{(1+e \cos \theta)^2}{(1-e^2)^{3/2}} & \frac{1}{1-e^2} \sin \theta (2+e \cos \theta) & 1 & \frac{M (1+e \cos \theta)^2}{(1-e^2)^{3/2}} & 0 & 0 \\ 0 & 0 & 0 & 0 & \frac{\sin i_0}{\sin L_0} (\cot^2 i_0 \cot^2 \beta_0 - 1) & \cos L_0 \cos \beta_0 \\ 0 & 0 & 0 & 0 & -\cos \beta_0 \left[\frac{\sin i_0}{\cos L_0} + \frac{\cos i_0 \sin \beta_0}{\sin i_0} \right] & -\sin L_0 \sin^2 \beta_0 \end{bmatrix} \begin{bmatrix} \frac{da}{a} \\ de \\ d\omega \\ \frac{d(t_p - t)}{t_p - t} \\ di \\ d\Omega \end{bmatrix}$$

TABLE 3
Error Analysis Equations

$$\begin{bmatrix} \frac{dr_a}{r_a} \\ \frac{dr_p}{r_p} \\ \frac{dv_a}{v_a} \\ \frac{dv_p}{v_p} \end{bmatrix} = \begin{bmatrix} \frac{1}{1-e} (2-e+\cos \theta) & 2 \frac{1}{1-e} (1+\cos \theta) & (1-e) \frac{\sin \theta}{1+e \cos \theta} \\ \frac{1}{1+e} (2+e-\cos \theta) & 2 \frac{1}{1+e} (1-\cos \theta) & -(1+e) \frac{\sin \theta}{1+e \cos \theta} \\ -\frac{1}{1-e} (1+\cos \theta) & -\frac{1}{1-e} (1+e+2 \cos \theta) & -\frac{\sin \theta}{1+e \cos \theta} \\ -\frac{1}{1+e} (1-\cos \theta) & -\frac{1}{1+e} (1-e-2 \cos \theta) & \frac{\sin \theta}{1+e \cos \theta} \end{bmatrix} \begin{bmatrix} \frac{dr}{r} \\ \frac{dv}{v} \\ d\gamma \end{bmatrix}$$

$$\begin{bmatrix} \frac{dr_a}{r_a} \\ \frac{dr_p}{r_p} \\ \frac{dv_a}{v_a} \\ \frac{dv_p}{v_p} \end{bmatrix} = \begin{bmatrix} \frac{a}{r} \left[2 + \frac{(1-e)}{e} \left(1 - \frac{r}{a} \right) \right] & 2 \frac{a}{r} \left[1 + \frac{1}{e} \left(1 - \frac{r}{a} \right) \right] & \pm \frac{1-e}{e} \left[\left(\frac{r}{a} \right)^2 \frac{2 \frac{a}{r} - 1}{1-e^2} - 1 \right]^{1/2} \\ \frac{a}{r} \left[2 - \frac{1+e}{e} \left(1 - \frac{r}{a} \right) \right] & 2 \frac{a}{r} \left[1 - \frac{1}{e} \left(1 - \frac{r}{a} \right) \right] & \mp \frac{1+e}{e} \left[\left(\frac{r}{a} \right)^2 \frac{2 \frac{a}{r} - 1}{1-e^2} - 1 \right]^{1/2} \\ -\frac{a}{r} + \frac{1}{e} \left(1 - \frac{a}{r} \right) & 1 - 2 \frac{a}{r} + \frac{2}{e} \left(1 - \frac{a}{r} \right) & \mp \frac{1}{e} \left[\left(\frac{r}{a} \right)^2 \frac{2 \frac{a}{r} - 1}{1-e^2} - 1 \right]^{1/2} \\ -\frac{a}{r} + \frac{1}{e} \left(\frac{a}{r} - 1 \right) & 1 - 2 \frac{a}{r} + \frac{2}{e} \left(\frac{a}{r} - 1 \right) & \pm \frac{1}{e} \left[\left(\frac{r}{a} \right)^2 \frac{2 \frac{a}{r} - 1}{1-e^2} - 1 \right]^{1/2} \end{bmatrix} \begin{bmatrix} \frac{dr}{r} \\ \frac{dv}{v} \\ d\gamma \end{bmatrix}$$

Similarly the series approximation of Eq (47) gives, from Eqs (26) and (27),

$$\frac{\Delta r_a}{r_0} \approx \frac{\Delta a}{r_0} + e \quad (50)$$

$$\frac{\Delta r_p}{r_0} \approx \frac{\Delta a}{r_0} - e \quad (51)$$

$$(1 > e^2)$$

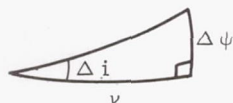
Substitution of Eqs (48) and (49) in Eqs (50) and (51) gives

$$\frac{\Delta r_a}{r_0} \approx 2 \frac{\Delta r_0}{r_0} + 2 \frac{\Delta v_0}{v_0} + \sqrt{\left(2 \frac{\Delta v}{v_0} + \frac{\Delta r}{r_0}\right)^2 + \gamma^2} \quad (52)$$

$$\frac{\Delta r_p}{r_0} \approx 2 \frac{\Delta r_0}{r_0} + 2 \frac{\Delta v_0}{v_0} - \sqrt{\left(2 \frac{\Delta v}{v_0} + \frac{\Delta r}{r_0}\right)^2 + \gamma^2} \quad (53)$$

The elements ω and t_p are not defined in the circular orbit case and, therefore, will not be considered. However, di and $d\Omega$ are indeterminate for $i = 0^\circ$. For this case, from spherical trigonometry,

$$\cos \Delta i = \cos \Delta \psi \sin (90 + \Delta \beta).$$



The Maclaurin series approximation gives

$$1 - \frac{\Delta i^2}{2} = \left(1 - \frac{\Delta \psi^2}{2}\right) \left(1 - \frac{\Delta \beta^2}{2}\right)$$

or

$$\Delta i^2 = \Delta \psi^2 + \Delta \beta^2 \quad (54)$$

The error in Ω is not defined (since, for the nominally equatorial orbit, the ascending node is not defined). However, the node of the incorrect orbit can be determined from

$$\sin \nu = \frac{\tan \Delta \psi}{\tan \Delta i} \approx \frac{\Delta \psi}{\Delta i} \quad (55)$$

The case of near circular orbits is also considered for the inverse transformation (errors in polar coordinates as functions of orbit element errors) in Ref. (1). For the small eccentricities of this special case, the planar variables can be expressed by the following series expansions, as given in Chapter III.

$$\frac{r}{a} = 1 - e \cos M - \frac{e^2}{2} (\cos 2M - 1)$$

(continued)

$$- \frac{e^3}{2! 2^2} (3 \cos 3M - 3M) - \dots$$

$$\sqrt{\frac{\mu}{a}} = 1 + e \cos \theta + \frac{e^2}{4} (3 - \cos 2\theta) + \frac{e^3}{8} (4 \cos \theta - \cos 3\theta - 7) + \dots$$

$$\theta = M + 2e \sin M + \frac{5e^2}{4} \sin 2M$$

$$+ \frac{e^3}{12} (13 \sin 3M - 3 \sin M)$$

$$\gamma = e \sin \theta - \frac{e^2}{2} \sin 2\theta + \frac{e^3}{3} \sin 3\theta - \dots$$

$$M = \text{mean anomaly} = \sqrt{\frac{\mu}{a^3}} (t - t_p) \quad (56)$$

For $e^2 \ll 1$, approximate relations can be written.

$$r \approx a (1 - e \cos M) \quad (57)$$

$$v \approx \sqrt{\frac{\mu}{a}} (1 + e \cos M) \quad (58)$$

$$\theta \approx M + 2e \sin M \quad (59)$$

$$\gamma \approx e \sin M \quad (60)$$

From Eq (56)

$$M = M_0 + \Delta M = \left[\frac{\mu}{r_0^3 \left(1 + \frac{\Delta a}{r_1}\right)^3} \right]^{1/2} (t - t_{p0} - \Delta t_p)$$

or

$$\Delta M = -\frac{3}{2} \frac{\Delta a}{r_0} M_0 - \sqrt{\frac{\mu}{r_0^3}} \Delta t_p \quad (61)$$

The errors at any later time Δr_2 , Δv_2 , $\Delta \gamma_2$ and $\Delta \theta_2$ will be determined as functions of Δr_1 , Δv_1 , and $\Delta \gamma_1$ by varying one injection parameter at a time and assuming a linear combination of the individual errors.

$$\text{Case (1)} \quad [\Delta r_1 = 0, \Delta v_1 = 0, \Delta \gamma_1 \neq 0]$$

If γ_1 is the only launch parameter which is in error, $\Delta r_1 = 0$, $\Delta v_1 = 0$, $\gamma_1 = \Delta \gamma_1$, and from Eq (49), $e \approx |\Delta \gamma_1|$, where $\Delta \gamma_1$ is an error due to a velocity component normal to the desired circular orbit velocity at launch. For the circular orbit, M and t_p are referenced to the perigee direction in the incorrect orbit. Since the semimajor axis a is a function of r and v but not γ , $\Delta a = 0$ for this case. Then, from Eqs (57) through (61),

$$\Delta r_{(1)} \approx -e r_0 \cos M_0 \approx -r_0 |\Delta \gamma_1| \cos M_0$$

$$\frac{\Delta v_{(1)}}{v_0} \approx |\Delta \gamma_1| \cos M_0$$

$$\Delta \theta_{(1)} \approx - \sqrt{\frac{\mu}{r_0^3}} \Delta t_p + 2 \left| \Delta \gamma_1 \right| \sin M_0$$

$$\Delta \gamma_{(1)} \approx \left| \Delta \gamma_1 \right| \sin M_0$$

From the $\Delta r_{(1)}$ equation, $\Delta r = 0$ when $\cos M_0 = 0$. Therefore, for case (1), $M_0 = 90^\circ$ (for γ_1 positive) or $M_0 = 270^\circ$ (for γ_1 negative). The absolute magnitudes in these equations may be removed by defining a mean anomaly M_0 , referenced to the initial point. Then $\mathcal{M}_0 = M_0 - 90^\circ$ for positive $\Delta \gamma_1$, and $\mathcal{M}_0 = M_0 + 90^\circ$ for negative $\Delta \gamma_1$. Substitution in the previous equations gives, for either positive or negative $\Delta \gamma_1$,

$$\frac{\Delta r_{(1)}}{r_0} \approx \Delta \gamma_1 \sin \mathcal{M}_0 \quad (62)$$

$$\frac{\Delta v_{(1)}}{v_0} \approx - \Delta \gamma_1 \sin \mathcal{M}_0 \quad (63)$$

$$\Delta \theta_{(1)} \approx 2 \Delta \gamma_1 (\cos \mathcal{M}_0 - 1) \quad (64)$$

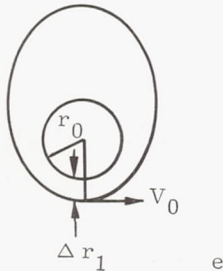
$$\Delta \gamma_{(1)} \approx \Delta \gamma_1 \cos \mathcal{M}_0 \quad (65)$$

In derivation of Eq (64) use is made of the fact that $\Delta \theta_{(1)} = 0$ at $\mathcal{M}_0 = 0$ since the correct and incorrect orbits intersect at the initial point.

$$\text{Case (2)} \left[\Delta \gamma_1 = 0, \Delta v_1 = 0, \Delta r_1 \neq 0 \right]$$

For $\Delta \gamma_1 = 0, \Delta v_1 = 0, \Delta r_1 \neq 0$, Eqs (48) and (49) give

$$\begin{aligned} \frac{\Delta a_{(2)}}{r_0} &\approx 2 \frac{\Delta r_1}{r_0} \\ e_{(2)} &\approx \frac{|\Delta r_1|}{r_1} \end{aligned}$$



Then, from Eqs (57) through (61)

$$\frac{\Delta r_{(2)}}{r_0} \approx 2 \frac{\Delta r_1}{r_0} - \frac{|\Delta r_1|}{r_0} \cos M_0$$

$$\frac{\Delta v_{(2)}}{v_0} \approx - \frac{\Delta r_1}{r_0} + \frac{|\Delta r_1|}{r_0} \cos M_0$$

$$\begin{aligned} \Delta \theta_{(2)} &\approx -3 \frac{\Delta r_1}{r_0} M_0 - \sqrt{\frac{\mu}{r_0^3}} \Delta t_p \\ &\quad + 2 \frac{|\Delta r_1|}{r_0} \sin M_0 \end{aligned}$$

$$\Delta \gamma_{(2)} \approx \frac{|\Delta r_1|}{r_0} \sin M_0$$

But $M_0 = 0^\circ$ for Δr_1 positive, and $M = 180^\circ$ for Δr_1 negative. Then, for $\mathcal{M}_0 = 0^\circ$ at launch,

$$\frac{\Delta r_{(2)}}{r_0} \approx \frac{\Delta r_1}{r_0} (2 - \cos \mathcal{M}_0) \quad (66)$$

$$\frac{\Delta v_{(2)}}{v_0} \approx \frac{\Delta r_1}{r_0} (\cos \mathcal{M}_0 - 1) \quad (67)$$

$$\Delta \theta_{(2)} \approx \frac{\Delta r_1}{r_0} (2 \sin \mathcal{M}_0 - 3 \mathcal{M}_0) \quad (68)$$

$$\Delta \gamma_{(2)} \approx \frac{\Delta r_1}{r_0} \sin \mathcal{M}_0 \quad (69)$$

$$\text{Case (3)} \left[\Delta r_1 = 0, \Delta \gamma_1 = 0, \Delta v_1 \neq 0 \right]$$

For the remaining case, where $\Delta r_1 = 0$, $\Delta \gamma_1 = 0$ and $\Delta v_1 \neq 0$, Eqs (48) and (49) gives

$$\frac{\Delta a_{(3)}}{r_0} \approx 2 \frac{\Delta v_1}{V_0}$$

$$e_{(3)} \approx 2 \frac{|\Delta v_1|}{V_0}$$

A procedure similar to that used in cases (1) and (2) gives

$$\frac{\Delta r_{(3)}}{r_0} \approx 2 \frac{\Delta v_1}{v_0} (1 - \cos \mathcal{M}_0) \quad (70)$$

$$\frac{\Delta v_{(3)}}{v_0} \approx \frac{\Delta v_1}{v_0} (2 \cos \mathcal{M}_0 - 1) \quad (71)$$

$$\begin{aligned} \Delta \theta_{(3)} &\approx -3 \mathcal{M}_0 \frac{\Delta v_1}{v_0} + 4 \frac{\Delta v_1}{v_0} \sin \mathcal{M}_0 \\ &\quad (72) \end{aligned}$$

$$\Delta \gamma_{(3)} \approx 2 \frac{\Delta v_1}{v_0} \sin \mathcal{M}_0 \quad (72)$$

The total error solutions are obtained by combining the effect of all three errors linearly (adding Eqs (62), (66) and (70); Eqs (63), (67) and (71); etc.).

$$\frac{\Delta r}{r_0} \approx \sin \mathcal{M}_0 \Delta \gamma_1 + (2 - \cos \mathcal{M}_0) \frac{\Delta r_1}{r_0} + 2 (1 - \cos \mathcal{M}_0) \frac{\Delta v_1}{v_0} \quad (74)$$

$$\frac{\Delta v}{v_0} \approx -\sin \mathcal{M}_0 \Delta \gamma_1 + (\cos \mathcal{M}_0 - 1) \frac{\Delta r_1}{r_0} + (2 \cos \mathcal{M}_0 - 1) \frac{\Delta v_1}{v_0} \quad (75)$$

$$\Delta \phi \approx \Delta \omega_1 + 2 (\cos \mathcal{M}_0 - 1) \Delta \gamma_1 + (2 \sin \mathcal{M}_0 - 3 \mathcal{M}_0) \frac{\Delta r_1}{r_0} + (4 \sin \mathcal{M}_0 - 3 \mathcal{M}_0) \frac{\Delta v_1}{v_0} \quad (76)$$

$$\Delta \gamma \approx \cos \mathcal{M}_0 \Delta \gamma_1 + \sin \mathcal{M}_0 \frac{\Delta r_1}{r_0} + 2 \sin \mathcal{M}_0 \frac{\Delta v_1}{v_0} \quad (77)$$

$$e^2 \ll 1$$

d. Statistical analysis

The error formulas developed in previous sections serve to convert a specific set of errors from one system of orbit determining variables to another. However, in preliminary design work, specific sets of errors are frequently not of interest. Rather, the design engineer must determine the probability that a certain error will be less than the tolerable limit. That is, he requires a probabilistic relation rather than an algebraic relation between the errors. This section concerns the determination of the error probabilities from the previously determined error formulas.

(1) Probability of Linear Error Functions

The majority of these error formulas are linear differential approximations of the form.

$$u = \sum_i a_i x_i, \quad i = 1, 2, \dots, k$$

where the a_i are constants. If the x_i (the errors to be transformed) are independently and normally distributed with means μ_i and variances σ_i^2 , then the moment generating function $\mu(t)$ for the distribution of the variate u is given as follows:

$$m(t) = \left(\frac{1}{2\pi}\right)^{\frac{k}{2}} \left(\prod_{i=1}^k \frac{1}{\sigma_i}\right) \int_{-\infty}^{\infty} \int_{-\infty}^{\infty} \dots \int_{-\infty}^{\infty} \exp \left[t \sum_i a_i x_i - \frac{1}{2} \sum_i \left(\frac{x_i - \mu_i}{\sigma_i} \right)^2 \right] dx_1 dx_2 \dots dx_k$$

Transformation to the standard form is convenient.

Let

$$y_i = \frac{x_i - \mu_i}{\sigma_i}$$

Then

$$\begin{aligned} m(t) &= \left(\frac{1}{2\pi}\right)^{k/2} \prod_i \left(\int_{-\infty}^{\infty} \exp(t a_i \mu_i) \exp(t a_i y_i \sigma_i - \frac{1}{2} y_i^2) dy_i \right) \\ &= \left(\frac{1}{2\pi}\right)^{k/2} \prod_i \left(\exp(t a_i \mu_i) \exp\left(\frac{1}{2} t^2 a_i^2 \sigma_i^2\right) \cdot \int_{-\infty}^{\infty} \exp\left(-\frac{1}{2} \left[y_i^2 - 2 t a_i y_i \sigma_i + t^2 a_i^2 \sigma_i^2\right]\right) dy_i \right) \\ &= \exp \left[t \sum_i a_i \mu_i + \frac{t^2}{2} \sum_i a_i^2 \sigma_i^2 \right] \quad (78) \end{aligned}$$

However, the moment generating function for the normal distribution is

$$m_n(t) = \exp(t\mu + \frac{1}{2} t^2 \sigma^2)$$

Therefore, Eq (78) is the moment generating function for a normal distribution

$$n(u) = \frac{1}{\sqrt{2\pi}\sigma} \exp \left[-\frac{1}{2} \left(\frac{u - \mu}{\sigma} \right)^2 \right]$$

with mean and variance given by

$$\mu = \sum_i a_i \mu_i \quad (79)$$

$$\sigma^2 = \sum_i a_i^2 \sigma_i^2 \quad (80)$$

Similarly, if the x_i are correlated instead of being independently distributed, u is distributed normally with

$$\mu = \sum_i a_i \mu_i \quad (81)$$

$$\sigma^2 = \sum_i a_i^2 \sigma_i^2 + \sum_{i,j} a_{ij} \sigma_{ij} \quad (82)$$

The covariance, σ_{ij} , is sometimes written $\rho_{ij} \sigma_i \sigma_j$ where ρ_{ij} is the correlation. These results (Eq (79) and (80) or (81) and (82)) then describe the probability distributions of the left-hand column vectors of Tables 1, 2 and 3 if the distributions of the right-hand column vectors are assumed to be normal. For example, from Eq (48), if Δr and Δv are normally distributed with zero means, then Δa is normally distributed with zero mean and variance

$$\frac{\sigma_{\Delta a}^2}{r_0^2} = 4 \left[\frac{\sigma_{\Delta v}^2}{v_0^2} + \frac{\sigma_{\Delta r}^2}{r_0^2} + 2 \frac{\rho_{\Delta v \Delta r} \sigma_{\Delta v} \sigma_{\Delta r}}{v_0 r_0} \right].$$

(nominally circular orbits)

Once the distribution of the transformed error is determined, the probability that u will lie between two given values u_1 and u_2 is given by

$$P \left[u_1 < u < u_2 \right] = \int_{u_1}^{u_2} n(u) du.$$

Since areas under the normal error distribution curve are widely tabulated, the probability that the error u will be less than a specified tolerable limit u^* ,

$$P \left[|u| < u^* \right] = \int_0^{u^*} n(u) du, \quad (83)$$

may be readily evaluated from tables. The solution for error probabilities has thus been obtained in all cases in which the error formula can be approximated by a linear function.

(2) Probability of Nonlinear Error Functions

Although most of the error formulas are linear, certain formulas for nominally circular orbits (for example, Eqs (49), (52), (53) and (54)) involve nonlinear relations of the form

$$u = \sqrt{x_1^2 + x_2^2} \quad (84)$$

Determination of the probability distribution of the function of Eq (84) is not so simple as in the case of the linear error formula, and the resulting distribution is not normal. If x_1 and x_2 are assumed normally and independently distributed, their joint distribution is simply the product of the individual distributions,

$$n(x_1, x_2) = \frac{1}{2\pi \sigma_{x_1} \sigma_{x_2}} \exp \left\{ -\frac{1}{2} \left[\left(\frac{x_1}{\sigma_{x_1}} \right)^2 + \left(\frac{x_2}{\sigma_{x_2}} \right)^2 \right] \right\}.$$

The distribution of u may be obtained by eliminating either x_1 or x_2 in terms of u to obtain a density

$$g(u, x_2) = \sum_i n \left[x_1(u, x_2), x_2 \right] \left| \frac{\partial x_1}{\partial u} \right|_i$$

where each term in the summation represents one branch of a possibly nonmonotone function $u(x_1)$. The desired distribution, $g(u)$, may then be obtained by integrating over the x_2 in $g(u, x_2)$.

$$g(u) = \int_{-\infty}^{\infty} g(u, x_2) dx_2$$

In particular, for $u = \sqrt{x_1^2 + x_2^2}$

$$x_1 = \pm \sqrt{u^2 - x_2^2}$$

$$\left| \frac{\partial x_1}{\partial u} \right| = \frac{u}{\sqrt{u^2 - x_2^2}}$$

$$g(u, x_2) = 2 \left\{ \frac{1}{2\pi \sigma_{x_1} \sigma_{x_2}} \exp \left[-\frac{1}{2} \left(\frac{u^2 - x_2^2}{\sigma_{x_1}^2} + \frac{x_2^2}{\sigma_{x_2}^2} \right) \right] \frac{u}{\sqrt{u^2 - x_2^2}} \right\}$$

Thus,

$$g(u) = \frac{u \exp \left[-\frac{1}{2} \frac{u^2}{\sigma_{x_1}^2} \right]}{\pi \sigma_{x_1} \sigma_{x_2}} \int_{-\infty}^{\infty} \frac{1}{\sqrt{u^2 - x_2^2}} \cdot \exp \left\{ -\frac{1}{2} \left[x_2^2 \left(\frac{1}{\sigma_{x_2}^2} - \frac{1}{\sigma_{x_1}^2} \right) \right] \right\} dx_2$$

$$\left[= \int_{-\infty}^{\infty} g(u, x_2) dx_2 \right]$$

After the transformation

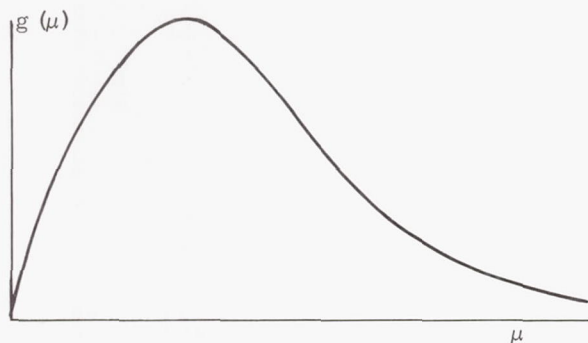
$$t = x_2^2$$

this expression may be integrated to yield the required distribution

$$g(u) = \frac{u}{\sigma_{x_1} \sigma_{x_2}} \exp \left[-\frac{u^2}{4} \left(\frac{1}{\sigma_{x_1}^2} + \frac{1}{\sigma_{x_2}^2} \right) \right] I_0 \left[\frac{u^2}{4} \left(\frac{1}{\sigma_{x_2}^2} - \frac{1}{\sigma_{x_1}^2} \right) \right], \quad 0 < x_2^2 < u^2, \quad (85)$$

$$= 0, \quad x_2^2 > u^2$$

This $g(u)$ (and, in particular, the distribution of corrected orbit eccentricity error) is a skewed, single-sided distribution with positive mean and a shape similar to that of the gamma distribution.



In manipulation of the distribution $g(u)$ the following definitions are convenient.

$$K_1 \equiv \frac{1}{\sigma_{x_1} \sigma_{x_2}}$$

$$K_2 \equiv \frac{1}{4} \left[\frac{1}{\sigma_{x_1}^2} + \frac{1}{\sigma_{x_2}^2} \right]$$

$$K_3 \equiv \frac{1}{4} \left[\frac{1}{\sigma_{x_2}^2} - \frac{1}{\sigma_{x_1}^2} \right]$$

The distribution is then

$$g(u) = K_1 u e^{-K_2 u^2} I_0(K_3 u^2)$$

Quantities of some significance in describing the properties of the distribution (e.g., central values, spread, skewness, etc.) are the moments of the distribution. The r th moment of $g(u)$ is

$$\begin{aligned} \bar{\mu}_r &= \int_{-\infty}^{\infty} u^r g(u) du \\ &= K_1 \int_{-\infty}^{\infty} u^{r+1} \exp(-K_2 u^2) I_0(K_3 u^2) du \end{aligned}$$

After the transformation $t = u^2$, the integral can be evaluated in various forms.

$$\begin{aligned} \int_0^{\infty} t^n e^{-K_2 t} I_{\nu}(K_3 t) dt &= \Gamma(n + \nu + 1) (K_2)^{-n-\nu-1} \\ &\quad \cdot (K_3)^{-\nu} P_n^{-\nu} \left(\frac{K_3}{\sqrt{K_2^2 - K_3^2}} \right) \end{aligned}$$

$$K_2 > |K_3|$$

where the generalized Legendre function is given by

$$P_n^m(z) = \frac{1}{\Gamma(1-m)} \left(\frac{z+1}{z-1} \right)^{m/2} {}_2F_1(-n, n+1; 1 - m; \frac{1}{2} - \frac{1}{2}z)$$

and the hypergeometric series is given by

$$\begin{aligned} {}_mF_n(a_1, \dots, a_m; \gamma_1, \dots, \gamma_n; z) \\ = \sum_{i=0}^{\infty} \frac{(a_1)_i \dots (a_m)_i}{(\gamma_1)_i \dots (\gamma_n)_i} \frac{z^i}{i!} \end{aligned}$$

Then

$$\begin{aligned} \bar{\mu}_r &= \frac{K_1}{2} \frac{\Gamma(\frac{r}{2} + 1)}{K_2^{r/2+1}} {}_2F_1 \left[\frac{r+2}{4}, \frac{r+4}{4}, 1; \left(\frac{K_3}{K_2} \right)^2 \right] \\ &= \frac{K_1}{2} \frac{\Gamma(\frac{r}{2} + 1)}{K_2^{r/2+1}} \sum_{i=0}^{\infty} \frac{(\frac{r+2}{4}; 1; i) (\frac{r+4}{4}; 1; i)}{i! (1; 1; i)} \left(\frac{K_3}{K_2} \right)^{2i} \end{aligned}$$

In particular, the mean of the distribution $g(u)$ is given by

$$\begin{aligned} \bar{\mu}_1 &= \frac{K_1}{2K_2^{3/2}} {}_2F_1 \left[\frac{3}{4}, \frac{5}{4}, 1; \left(\frac{K_3}{K_2} \right)^2 \right] \\ &= \frac{K_1}{4K_2^{3/2}} \left[1 + \frac{3}{4} \cdot \frac{5}{4} \left(\frac{K_3}{K_2} \right)^2 + \frac{3}{4} \cdot \frac{7}{4} \cdot \frac{5}{4} \cdot \frac{9}{4} \left(\frac{K_3}{K_2} \right)^4 \right. \\ &\quad \left. + \frac{3}{4} \cdot \frac{7}{4} \cdot \frac{11}{4} \cdot \frac{5}{4} \cdot \frac{9}{4} \cdot \frac{13}{4} \left(\frac{K_3}{K_2} \right)^6 + \dots \right] \end{aligned}$$

The second moment is of interest in determination of the variance of $g(u)$.

$$\begin{aligned} \bar{\mu}_2 &= \frac{K_1}{2} \frac{\Gamma(2)}{K_2^2} {}_2F_1 \left[1, \frac{3}{2}, 1; \left(\frac{K_3}{K_2} \right)^2 \right] \\ &= \frac{K_1}{2K_2^2} \left[1 + \frac{3}{2} \left(\frac{K_3}{K_2} \right)^2 + \frac{1}{2!} \cdot \frac{3}{2} \cdot \frac{5}{2} \left(\frac{K_3}{K_2} \right)^4 \right. \\ &\quad \left. + \frac{1}{3!} \cdot \frac{3}{2} \cdot \frac{5}{2} \cdot \frac{7}{2} \left(\frac{K_3}{K_2} \right)^6 + \dots \right] \end{aligned}$$

Then the variance is

$$\sigma_u^2 = \bar{\mu}_2 - (\bar{\mu}_1)^2$$

Thus, the probability distributions of errors given by nonlinear equations of the form of Eq

(84) are rather complex. Therefore, the probability that the error u will be less than a specified tolerable limit u^* must be computed by numerical integration or by the Monte-Carlo technique. The probability could be computed, for the case of Eq (84) by numerical integration.

$$P[u < u^*] = \int_0^{u^*} g(u) du,$$

where $g(u)$ is defined in Eq (85). However, in general, this probability may be more readily computed from

$$P[u < u^*] = \int \int \dots \int_{u < u^*} f(x_1, x_2, \dots, x_n) dx_1 dx_2 \dots dx_n \quad (86)$$

where $f(x_1, x_2, \dots, x_n)$ is the multivariate distribution of the errors x_1, x_2, \dots, x_n and the integration limits are defined from the region in which $u < u^*$. If the number of random variables x_i is larger than five, the Monte-Carlo method is a convenient alternative solution for the probability P that a multivariate normal variable lies in a region R . These methods of evaluating the probabilities are considered in the following section.

The determination of the surface defining the region $u < u^*$ (that is, the limits of integration) is generally not difficult. In some cases, however, this surface may be difficult to construct. In this eventuality a more general technique may be employed. Consider for example an error function which is expressible as a sum of a normally distributed error Δp_n and an arbitrary known function $f(\Delta q)$ of a second normally distributed variable, Δq .

$$\Delta p = \Delta p_n + f(\Delta q)$$

For a complicated function $f(\Delta q)$, the determination of constant Δp surfaces in the $\Delta q, \Delta p_n$ space become unwieldy. The individual density functions of Δp_n and $f(\Delta q)$ are readily obtainable, the latter by dividing the Gaussian density of Δq by $\frac{df(\Delta q)}{d\Delta q}$. Hence, $f(\Delta p)$, the density function of Δp , can be formulated as a convolution integral of the individual density functions

$$f(\Delta p) = \int_{-\infty}^{\infty} g(\Delta p - \xi) z(\xi) d\xi \quad (87)$$

where

$$\begin{aligned} g(\Delta p_n) &= \text{density function of } \Delta p_n \\ z[f(\Delta q)] &= \text{density function of } f(\Delta q) \end{aligned}$$

(3) Evaluation of Multivariate Normal Probabilities (Ref. 2)

Error analyses and success probability determination for space missions (as well as other

areas) frequently require the integration of a multivariate normal distribution over some appropriate region. In some instances, it is possible to use special computational routines to obtain this integral. In other situations, the Monte-Carlo method may have to be used. A general formulation and an illustration of both methods follow.

Theoretical discussion and special computational routines. The probability P is sought where

$$P = \int_{L'_1}^{U'_1} \int_{L'_2}^{U'_2} \dots \int_{L'_{n-1}}^{U'_{n-1}} \int_{L'_n}^{U'_n} f(x_1, \dots, x_n) dx_n \dots dx_1 \quad (88)$$

with $f(x_1, \dots, x_n)$ the multivariate normal distribution with mean vector (μ_1, \dots, μ_n) and variance-covariance matrix

$$\Sigma = (\sigma_{ij}), \quad i, j = 1, \dots, n, \quad \sigma_{ij} = \sigma_{ji}.$$

That is,

$$f(x_1, \dots, x_n) = \frac{1}{(2\pi)^{n/2} |\Sigma|^{1/2}} \exp \left[-\frac{1}{2} \sum_{j=1}^n \sum_{i=1}^n \sigma^{ij} (x_i - \mu_i) (x_j - \mu_j) \right] \quad (89)$$

with σ^{ij} the (i, j) element in the matrix Σ^{-1} and $|\Sigma|$ denoting the determinant of the matrix Σ , and where

$$\begin{aligned} U'_n &= U'_n(x_1, \dots, x_{n-1}), \quad L'_n = L'_n(x_1, \dots, x_{n-1}) \\ U'_{n-1} &= U'_{n-1}(x_1, \dots, x_{n-2}), \\ L'_{n-1} &= L'_{n-1}(x_1, \dots, x_{n-2}) \\ U'_2 &= U'_2(x_1), \quad L'_2 = L'_2(x_1) \\ U'_1 &= \text{constant}, \quad L'_1 = \text{constant} \end{aligned} \quad (90)$$

In order to obtain the number P via the computational routines, a transformation must be made to new variables z_1, \dots, z_n which have mean vector $(0, \dots, 0)$ and variance-covariance matrix I_n , the unit matrix of size n . That is, the distribution of (z_1, \dots, z_n) is

$$\frac{1}{(2\pi)^{n/2}} \exp \left[-\frac{1}{2} (z_1^2 + z_2^2 + \dots + z_n^2) \right] \quad (91)$$

Of course, when a transformation is made to these new variables (z_1, \dots, z_n), the limits of integration change as well as the integrand. Therefore, among all the possible transformations, one must be chosen which will render the limits in a suitable form for the computational routines. Such a transformation is

$$x_i = \mu_i + \sum_{j=1}^i c_{ij} z_j, \quad i = 1, \dots, n \quad (92)$$

with the coefficients c_{ij} defined recursively by

$$\begin{aligned} c_{i1} &= \frac{\sigma_{i1}}{\sqrt{\sigma_{11}}}, \quad 1 \leq i \leq n \\ c_{ii} &= \sqrt{\sigma_{ii} - \sum_{k=1}^{i-1} c_{ik}^2}, \quad 1 < i \leq n \\ c_{ij} &= \frac{\sigma_{ij} - \sum_{k=1}^{j-1} c_{ik} c_{jk}}{c_{jj}}, \quad n \geq i > j > 1 \\ c_{ij} &= 0, \quad 1 \leq i < j \leq n. \end{aligned} \quad (93)$$

Now the integral of Eq (88), giving the probability P , is

$$P = \frac{1}{(2\pi)^{n/2}} \int_{L_1}^{U_1} \int_{L_2}^{U_2} \dots \int_{L_{n-1}}^{U_{n-1}} \int_{L_n}^{U_n} \exp \left[-\frac{1}{2} (z_1^2 + \dots + z_n^2) \right] dz_n \dots dz_1 \quad (94)$$

with

$$\begin{aligned} U_n &= U_n(z_1, \dots, z_{n-1}), \quad L_n = L_n(z_1, \dots, z_{n-1}) \\ U_{n-1} &= U_{n-1}(z_1, \dots, z_{n-2}), \\ L_{n-1} &= L_{n-1}(z_1, \dots, z_{n-2}) \\ U_2 &= U_2(z_1), \quad L_2 = L_2(z_1) \\ U_1 &= \text{constant}, \quad L_1 = \text{constant} \end{aligned} \quad (95)$$

where the limits U_k and L_k are obtained from U'_k and L'_k by substituting into the relations $L'_k \leq x_k \leq U'_k$ expressions (92) for the x 's in terms of z 's.

The following example may illuminate the preceding generalities. Let the requirement for a successful orbit be

$$-B \leq \delta r_p \leq \delta r_a \leq A \quad (96)$$

for given positive numbers A and B . Equations (52) and (53) can be written more concisely in the following form:

$$\delta r_p = t_3 - \sqrt{t_1^2 + t_2^2} \quad (97)$$

$$\delta r_a = t_3 + \sqrt{t_1^2 + t_2^2} \quad (98)$$

where (t_1, t_2, t_3) has the multivariate normal distribution with mean vector (μ_1, μ_2, μ_3) and variance-covariance matrix

$$\Sigma = \begin{bmatrix} \sigma_{11} & \sigma_{12} & \sigma_{13} \\ \sigma_{21} & \sigma_{22} & \sigma_{23} \\ \sigma_{31} & \sigma_{32} & \sigma_{33} \end{bmatrix}$$

The numbers A and B are specified in the mission requirements; and $\mu_1, \mu_2, \mu_3, \sigma_{11}, \sigma_{12}, \sigma_{13}, \sigma_{22}$, and σ_{33} ($\sigma_{ij} = \sigma_{ji}$) may be computed from the definitions of the t_i (Eqs (52) and (53)), the linear error analysis of Section B.1.d.(1) and given values of $\sigma_{\Delta r}, \sigma_{\Delta v}, \sigma_\gamma$. To obtain the probability P that Eq (96) holds, Eqs (97) and (98) are substituted into Eq (96) and the condition for success is symmetrized by making the preliminary change of variable $x_1 = t_1, x_2 = t_2, x_3 = t_3 - 1/2 (A - B)$. Then the criterion for success becomes

$$\begin{aligned} -1/2 (A + B) \leq x_3 - \sqrt{x_1^2 + x_2^2} \leq x_3 \\ + \sqrt{x_1^2 + x_2^2} \leq 1/2 (A + B) \end{aligned} \quad (99)$$

where (x_1, x_2, x_3) has mean vector $\mu_1, \mu_2, \mu_3 - 1/2 (A - B)$ and unchanged variance-covariance matrix Σ .

The region in the (x_1, x_2, x_3) space is composed of two conical segments, as shown in the following sketch.

It is desired to integrate the distribution of (x_1, x_2, x_3) over the region determined by Eq (99). The resulting probability, analogous to Eq (88) is the desired result. The upper and lower limits analogous to Eq (90) are

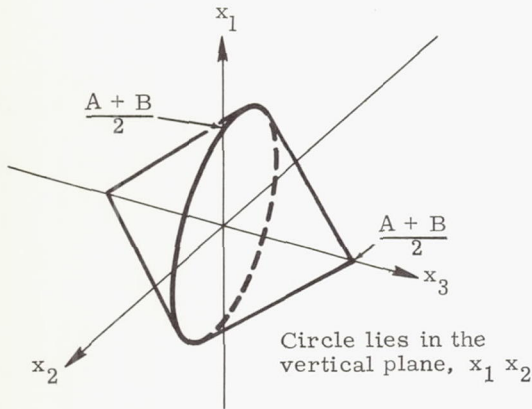
$$U'_3 = 1/2 (A + B) - \sqrt{x_1^2 + x_2^2}$$

$$L'_3 = -1/2 (A + B) + \sqrt{x_1^2 + x_2^2}$$

$$U'_2 = \sqrt{1/2 (A+B)^2 - x_1^2},$$

$$L'_2 = -\sqrt{1/2 (A+B)^2 - x_1^2} \quad (100)$$

$$U'_1 = 1/2 (A+B), \quad L'_1 = -1/2 (A+B).$$



In this instance, the transformation of Eq (92) to the variables (z_1, z_2, z_3) is given by

$$\begin{aligned} x_1 &= \mu_1 + c_{11} z_1 \\ x_2 &= \mu_2 + c_{21} z_1 + c_{22} z_2 \\ x_3 &= \mu_3 - 1/2 (A-B) + c_{31} z_1 + c_{32} z_2 + c_{33} z_3 \end{aligned} \quad (101)$$

with the coefficients c_{ij} given explicitly by

$$\begin{aligned} c_{11} &= (\sigma_{11})^{1/2}, \quad c_{21} = \frac{\sigma_{21}}{(\sigma_{11})^{1/2}}, \quad c_{31} = \frac{\sigma_{31}}{(\sigma_{11})^{1/2}} \\ c_{22} &= \sqrt{\sigma_{22} - \frac{\sigma_{21}^2}{\sigma_{11}}}, \quad c_{32} = \frac{\sigma_{32} - c_{31} c_{21}}{c_{22}} \\ c_{33} &= \sqrt{\sigma_{33} - \frac{\sigma_{31}^2}{\sigma_{11}} - \frac{\sigma_{32}^2}{c_{22}^2}} \end{aligned} \quad (102)$$

Introducing these c 's into Eq (101) and the x 's from Eq (101) into the relations $L'_k \leq x_k \leq U'_k$ ($k = 1, 2, 3$) yields, analogous to Eq (95),

$$\begin{aligned} U_3 &= \frac{1}{c_{33}} \left[-\mu_3 + A - c_{31} z_1 - c_{32} z_2 \right. \\ &\quad \left. - \sqrt{(\mu_1 + c_{11} z_1)^2 + (\mu_2 + c_{21} z_1 + c_{22} z_2)^2} \right] \\ L_3 &= \frac{1}{c_{33}} \left[-\mu_3 - B - c_{31} z_1 - c_{32} z_2 \right. \\ &\quad \left. + \sqrt{(\mu_1 + c_{11} z_1)^2 + (\mu_2 + c_{21} z_1 + c_{22} z_2)^2} \right] \end{aligned}$$

$$U_2 = \frac{1}{c_{22}} \left\{ -\mu_2 - c_{21} z_1 + \left[1/4 (A+B)^2 - (\mu_1 + c_{11} z_1)^2 \right]^{1/2} \right\}$$

$$L_2 = \frac{1}{c_{22}} \left\{ -\mu_2 - c_{21} z_1 - \left[1/4 (A+B)^2 - (\mu_1 + c_{11} z_1)^2 \right]^{1/2} \right\} \quad (103)$$

$$U_1 = \frac{1}{c_{11}} \left[-\mu_1 + 1/2 (A+B) \right]$$

$$L_1 = \frac{1}{c_{11}} \left[-\mu_1 - 1/2 (A+B) \right].$$

Now the probability

$$P = \frac{1}{(2\pi)^{3/2}} \int_{L_1}^{U_1} \int_{L_2}^{U_2} \int_{L_3}^{U_3} \exp \left[-1/2 (z_1^2 + z_2^2 + z_3^2) \right] dz_3 dz_2 dz_1$$

can be obtained from a suitable computational routine.

Monte-Carlo method. Consider again the problem of obtaining the probability P that a multivariate normal variable lies in a region R . The Monte-Carlo method may be used, for example, in situations where the number of components of the random variable is larger than five (the routines previously described are no longer applicable).

The method proceeds as follows. Select a sample of size N of the random variable of interest. Count the number N_0 of these sample values which lie in the region R . The fraction N_0/N is an estimate of P .

The question arises: how to choose the sample size N so as to estimate P with assigned precision. An answer can be given if the problem is formulated this way. Choose N large enough for the probability that $|N_0/N - P| < d$ to equal a for preassigned d and a . Then if a "guess" for P is available, choose

$$N = \frac{P(1-P) z_a^2}{d^2} \quad (104)$$

where z_a is defined by

$$\frac{1}{\sqrt{2\pi}} \int_{-z_a}^{z_a} \exp(-1/2 t^2) dt = a$$

and is obtained from tables of the normal distribution. If no "guess" for P is available,

an upper bound on the choice of N is $\frac{z_a^2}{4d^2}$.

Thus, to estimate P within 0.1 with a probability of 0.95, a conservative choice for N is

$$\frac{(1.96)^2}{4(0.10)^2} = 96.04$$

To estimate P to within 0.01 with a probability of 0.95, N must be 9,604 at most. To estimate P to within 0.01 with a probability of 0.95, if there is reason to suppose that P is near 0.9, Eq (104) yields

$$N \approx \frac{(0.9)(0.1)(1.96)^2}{4(0.01)^2} = 864.4.$$

Thus, a reduction of almost 9000 in the sample size necessary to meet a certain criterion has been achieved by using additional information known to the experimenter.

In conclusion, a remark should be made on the usefulness of the Monte-Carlo method in evaluating probabilities when the random variables of interest are not necessarily normally distributed. The estimate of the sample size required given above does not depend on the normality of the variables under consideration. It is valid no matter what their distribution is. (The fact that z_a in the formulas is obtained from tables of the normal distribution is incidental.)

(4) Probability Analysis of Vehicle Position and Velocity (Ref. 1)

By means of the previously considered statistical theories and the equations of Table 2, the probability distribution of the position and velocity of an orbiting vehicle can be determined at any time. This section deals with a convenient method of analysis for the problem. Let

$$\{p_i\} = [a_{ij}(\theta)] \{q_j\}$$

represent the relation between the position and velocity errors p_i and the orbit injection errors q_j . If the q_j are normally and independently distributed without biases, their multivariate distribution is given by

$$f(q_1, q_2, \dots, q_6) = \prod_{i=1}^6 \left\{ \left(\frac{1}{2\pi\sigma_i} \right)^{1/2} \exp \left[-\frac{1}{2} \left(\frac{q_i}{\sigma_i} \right)^2 \right] \right\} \quad (105)$$

Then the multivariate distribution of the transformed errors is

$$g(p_1, p_2, \dots, p_6) = f(q_1, q_2, \dots, q_6) \left| \frac{\partial(q_1, q_2, \dots, q_6)}{\partial(p_1, p_2, \dots, p_6)} \right| \quad (106)$$

The region $g(p_1, p_2, \dots, p_6) = \text{constant}$ is a six-dimensional ellipsoidal surface of equal probability.

This time-varying hypersurface provides a convenient definition of the region of occurrence of the vehicle position and velocity with given probability.

For example, consider the simple case of only two orbit injection errors.

$$p_1 = a_{11} q_1 + q_{12} q_2$$

$$p_2 = q_{21} q_1 + q_{22} q_2$$

Then if

$$f(q_1, q_2) = \frac{1}{2\pi\sigma_{q1}\sigma_{q2}} \exp \left[-\frac{1}{2} \left(\frac{q_1^2}{\sigma_{q1}^2} + \frac{q_2^2}{\sigma_{q2}^2} \right) \right],$$

$$g(p_1, p_2) = \frac{1}{2\pi\sigma_{q1}\sigma_{q2} |a_{11}a_{22} - a_{12}a_{21}|} e^{-\frac{1}{2} Q^2} \quad (107)$$

where the quadratic form is

$$Q^2 = \frac{1}{(a_{11}a_{22} - a_{12}a_{21})^2} \left[\left(\frac{a_{22}^2}{\sigma_{q1}^2} + \frac{a_{21}^2}{\sigma_{q2}^2} \right) p_1^2 - 2 \left(\frac{a_{22}a_{12}}{\sigma_{q1}^2} + \frac{a_{11}a_{21}}{\sigma_{q2}^2} \right) p_1 p_2 + \left(\frac{a_{12}^2}{\sigma_{q1}^2} + \frac{a_{22}^2}{\sigma_{q2}^2} \right) p_2^2 \right] \quad (108)$$

Since the coefficients a_{ij} are functions of time, the distribution changes with time. In this two-variable case, $g = \text{constant}$ defines an ellipse. Equations (107) and (108) can be written in simplified notation as

$$g(p_1, p_2) = K \exp \left[-\frac{1}{2} (Ap_1^2 + 2Bp_1 p_2 + Cp_2^2) \right]$$

If the axis of the $p_1 - p_2$ coordinate system is rotated through an angle $\frac{1}{2} \tan^{-1} \left(\frac{2B}{A-C} \right)$, the cross product term is eliminated.

$$g(p'_1, p'_2) = K' e^{-\frac{1}{2} [p_1'^2 + D^2 p_2'^2]} \quad (109)$$

where p'_1 and p'_2 are the new coordinates. Also, D can be absorbed by defining new coordinates $p''_1 = p'_1$ and $p''_2 = Dp'_2$.

$$g(p''_1, p''_2) = \frac{K'}{D} \exp \left[-\frac{1}{2} (p_1''^2 + p_2''^2) \right] \quad (110)$$

Again, variables can be changed to polar coordinates so that the polar angle can be integrated from 0 to 2π and the radius ($R^2 = p_1''^2 + p_2''^2$) from 0 to R. The probability of a vehicle being within R is then

$$P(R) = 1 - e^{-\frac{R^2}{2}} \quad (111)$$

because $\frac{2\pi K_1}{D} = 1$ for the normalized distribution.

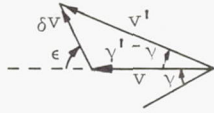
2. Error Analysis of Powered Trajectories

Typical trajectory sequences consist of alternating powered and free-flight phases. The final mission errors are functions of errors occurring in all such phases. This section considers the contribution of errors in the powered phases just as Section B.1. considered errors in the free-flight phases. If the powered phases are short so that the impulse maneuver theories are reasonably accurate, approximate analytic relations can be developed. However, the increased complexity of motion in powered flight generally requires numerical analysis.

a. Impulse analysis

(1) General case

The equations describing addition of a vector impulse δv are the laws of cosines and sines:



$$f_1 = -\delta v^2 + v^2 + v'^2 - 2vv' \cos(\gamma' - \gamma) = 0 \quad (112)$$

$$f_2 = \delta v \sin \epsilon + v' \sin(\gamma' - \gamma) = 0 \quad (113)$$

Symbols are consistent with previous notation and are further defined in the sketch. Errors in v' and γ' are to be determined as functions of errors in v , γ , ϵ and δv . From Eqs (112) and (113) the error relationships, approximated by linear differentials, can be expressed as follows.

$$-\delta v d(\delta v) + v' dv + vv' \sin(\gamma' - \gamma) (d\gamma' - d\gamma)$$

$$- \cos(\gamma' - \gamma) (v dv' + v' dv) + v dv = 0$$

and

$$-\sin \epsilon d(\delta v) - \delta v \cos \epsilon d\epsilon + \sin(\gamma' - \gamma) dv'$$

$$+ v' \cos(\gamma' - \gamma) (d\gamma' - d\gamma) = 0$$

Terms may be collected, and the resulting expressions solved by application of Cramer's rule for the errors dv' and $d\gamma'$. In this solution the Jacobian

$$\frac{\partial(f_1, f_2)}{\partial(v', \gamma')} = 2 \begin{vmatrix} v' - v \cos(\gamma' - \gamma) & vv' \sin(\gamma' - \gamma) \\ \sin(\gamma' - \gamma) & v' \cos(\gamma' - \gamma) \end{vmatrix}$$

$$= 2v' [v' \cos(\gamma' - \gamma) - v]$$

is useful. The results are

$$dv' = \left[\frac{\delta v \cos(\gamma' - \gamma) - \frac{vv'}{\delta v} \sin^2(\gamma' - \gamma)}{v' \cos(\gamma' - \gamma) - v} \right] d(\delta v) + \cos(\gamma' - \gamma) dv - v \sin(\gamma' - \gamma) d\epsilon$$

$$d\gamma' = \frac{\sin(\gamma' - \gamma) \left[\left\{ v' - v \cos(\gamma' - \gamma) \right\} \frac{v'}{\delta v} - \delta v \right]}{v' [v' \cos(\gamma' - \gamma) - v]} d(\delta v) - \frac{\sin(\gamma' - \gamma)}{v'} dv + \left[1 - \frac{v}{v'} \cos(\gamma' - \gamma) \right] d\epsilon + d\gamma$$

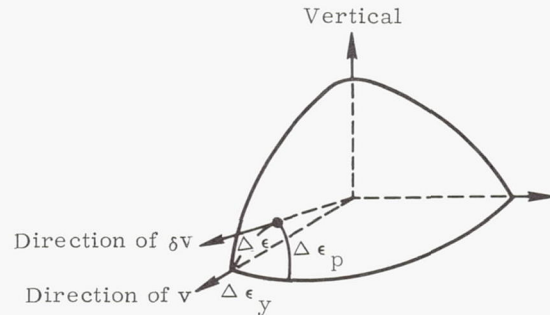
In terms of $(\gamma' - \gamma)$ or, in terms of ϵ ,

$$dv' = \left[\frac{\delta v}{v'} + \frac{v}{v'} \cos \epsilon \right] d(\delta v) + \left[\frac{\delta v}{v'} \cos \epsilon + \frac{v}{v'} \right] dv - v \frac{\delta v}{v'} \sin \epsilon d\epsilon \quad (114)$$

$$d\gamma' = \frac{v}{v'^2} \sin \epsilon d(\delta v) - \frac{\delta v}{v'^2} \sin \epsilon dv + \frac{\delta v}{v'^2} (\delta v + v \cos \epsilon) d\epsilon + d\gamma \quad (115)$$

(2) Nominally Tangential Impulses ($\epsilon = 0$) (Ref. 2)

In many missions a velocity increment, δv , is added at the apogee of a coast period in a direction nominally parallel to the existing coast velocity, v . An attitude error, $\Delta \epsilon$, during the apogee burning causes a nonlinear speed error in the system, in addition to a speed error representing a linear transformation of the other Gaussian sources. The geometry is shown in the accompanying sketch. The resulting speed error, Δv_1 , due to this source is



$$\Delta v_1 = v + \delta v - \sqrt{(\delta v)^2 + v^2 + 2\delta v v \cos \Delta \epsilon} \quad (116)$$

For small $\Delta \epsilon$, Eq (116) becomes

$$\Delta v_1 \approx \frac{\delta v}{2 \left(1 + \frac{\delta v}{v} \right)} (\Delta \epsilon)^2 \quad (117)$$

where terms up to second order have been retained.

The $\Delta \epsilon$ in Eq (117) is actually composed of two components in directions normal to v . These are typically a yaw attitude error, $\Delta \epsilon_y$, and a pitch attitude error, $\Delta \epsilon_p$, as shown in the sketch.

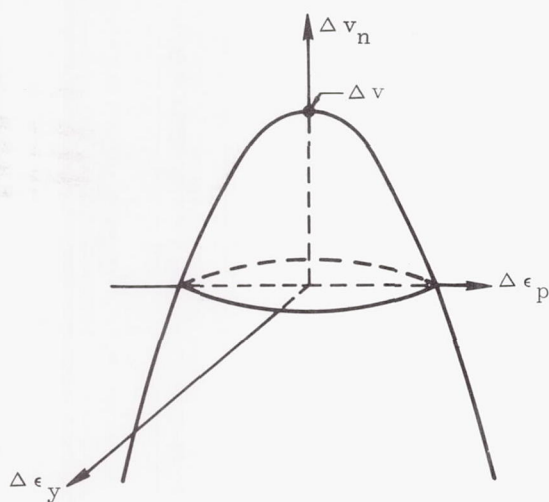
Thus Eq (117) becomes

$$\Delta v_1 = \frac{\delta v}{2 \left(1 + \frac{\delta v}{v}\right)} \left[(\Delta \epsilon_y)^2 + (\Delta \epsilon_p)^2 \right] \quad (118)$$

To this must be added the Gaussian speed error, Δv_n , due to a linear transformation from the other sources (see previous section). The total speed error, Δv , then becomes

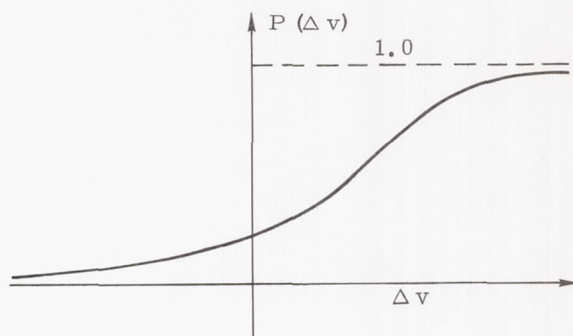
$$\Delta v = \frac{\delta v}{2 \left(1 + \frac{\delta v}{v}\right)} \left[(\Delta \epsilon_y)^2 + (\Delta \epsilon_p)^2 \right] + \Delta v_n \quad (119)$$

The statistics of Eq (119) are non-Gaussian though $\Delta \epsilon_y$, $\Delta \epsilon_p$, Δv_n are Gaussian. It is again convenient to consider the space of $\Delta \epsilon_y$, $\Delta \epsilon_p$, Δv_n which represents a trivariate normal density. In this space, surfaces of constant Δv are paraboloids of revolution parallel to the axis Δv_n as shown in the sketch. An analogous procedure is described in Section B.1. d(3). Hence integration of the trivariate normal distribution of $\Delta \epsilon_y$, $\Delta \epsilon_p$, Δv_n within the paraboloid (from $\Delta v_n = -\infty$ to Δv) yields the probability that Δv is less than some specified value. Integration for different values of Δv yields the entire statistics of Δv .

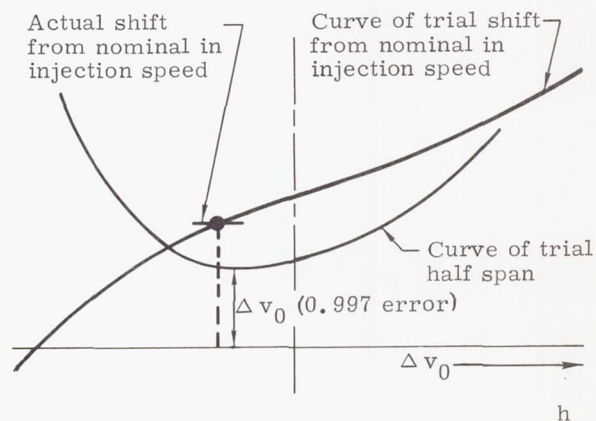


An interesting optimization theory is often applicable, once the complete statistics of Δv are obtained. It may be desirable to modify the nominal value of v in the trajectory such that it is assured to any given probability (say 0.997 or 3σ) that the magnitude of the resulting speed error is less than Δv_0 , where it is desirable to minimize Δv_0 . This might be the case for example in a satellite which employs orbit corrections after injection, where minimization of the speed error at injection, Δv_0 , minimizes the propulsion capability required in the payload. This optimization is carried out as follows.

The cumulative distribution function $P(\Delta v)$ is obtained as described above. The above optimization requirement can be interpreted as a selection of the minimum continuous span in Δv over which the $P(\Delta v)$ function changes by 0.997. Designation of the center of that span as the shift in nominal injection speed would then complete the required optimization.



The foregoing is easily carried out by choosing a running variable Δv_0 as a trial smaller extreme of the 0.997 span of Δv , and reading off in the figure the associated span of Δv which contains the necessary 0.997 change in $P(\Delta v)$. Plotting as a continuous function of Δv_0 the quantities, half the span and the center of the span, permits determination of the optimum operating point as that value of Δv_0 which has the minimum half span. This is shown in the following sketch. The corresponding change in the nominal injection speed and the 0.997 error in speed, Δv_0 , are determined from the figure for this optimum Δv_0 .



This optimization procedure for nonlinear speed errors has been carried out for equal variances in $\Delta \epsilon_y$ and $\Delta \epsilon_p$, and the results are presented in Fig. 1. The reason that the optimization procedure is useful is the skewed and biased nature of the density function of Δv given by Eq (119), which is shown in Fig. 2. This suggests a shift in nominal operating value of speed as was formally carried out.

The technique Eq (87) could have been employed as an alternative method of solution in Eq (119). Note that $y(\Delta\epsilon)$, the density function of $\Delta\epsilon$ in Eq (119), is a Rayleigh distribution, if the standard deviations of $\Delta\epsilon_y$ and $\Delta\epsilon_p$ are the same, $\Delta\epsilon_0$.

$$y(\Delta\epsilon) = \frac{\Delta\epsilon}{\sigma_{\Delta\epsilon_0}^2} e^{-\frac{(\Delta\epsilon)^2}{2\sigma_{\Delta\epsilon_0}^2}} \quad 0 < \Delta\epsilon < \infty \quad (120)$$

or

$$z[f(\Delta\epsilon)] = \frac{1}{k} e^{-\frac{f(\Delta\epsilon)}{k}} \quad 0 < (\Delta\epsilon) < \infty \quad (121)$$

where

$$k = \frac{\delta v}{1 + \frac{\delta v}{v}} \sigma_{\Delta\epsilon_0}^2 \quad (122)$$

and where $f(\Delta\epsilon)$ is the non-Gaussian part of Eq (119). Hence, using Eqs (87) and (121) in (119) yields

$$p(\Delta v) = \int_0^\infty \frac{1}{k} e^{-\frac{\xi}{k}} \frac{e^{-\frac{(\Delta v - \xi)^2}{2\sigma_{\Delta v_n}^2}}}{\sqrt{2\pi\sigma_{\Delta v_n}^2}} d\xi \quad (123)$$

Equation (123) can be expressed in terms of tabulated functions:

$p(\Delta v)$ = density function of Δv

$$= \frac{e^{\left[-\frac{\Delta v}{k} + \frac{1}{2} \left(\frac{\sigma_{\Delta v_n}}{k}\right)^2\right]}}{k} \left[1 - R\left(\frac{\sigma_{\Delta v_n} - \Delta v}{k}\right)\right] \quad (124)$$

where

$$R(u) = \int_{-\infty}^u \frac{\exp(-t^2/2)}{\sqrt{2\pi}} dt \quad (125)$$

= a tabulated function

Also the cumulative distribution $P(\Delta v)$ can be found by integrating Eq (124)

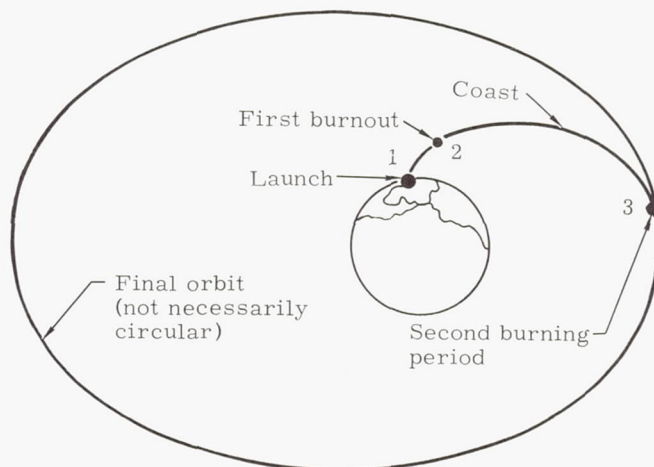
$P(\Delta V)$ = cumulative distribution of ΔV

$$= R \frac{\Delta V}{\sigma_{\Delta V_n}} - \left\{ \exp \left[\frac{1}{2} \left(\frac{\sigma_{\Delta V_n}}{k} \right)^2 - \frac{\Delta V}{k} \right] \right. \\ \left. \cdot \left[1 - R \left(\frac{\sigma_{\Delta V_n}}{k} - \frac{\Delta V}{\sigma_{\Delta V_n}} \right) \right] \right\} \quad (126)$$

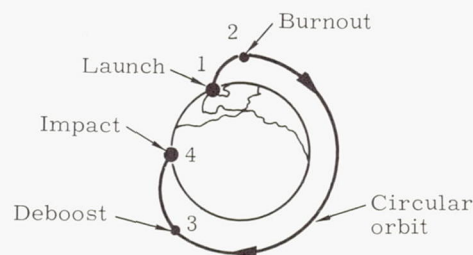
b. General guidance error analysis (Ref. 2)

The guidance error analysis procedure to be described is a universal one for satellite missions. It can be applied to any type of trajectory, with guidance provided by an arbitrary type of guidance system, and with an arbitrary criterion employed for error in final orbit.

The type of powered flight trajectory that can be handled is perfectly general, although two or three discrete burns, each followed by a coast period, are the most common. The following sketches show some typical trajectories. Continuous low-thrust burning, characteristic of nuclear stages, can also be accommodated within the error analysis procedure. Also of arbitrary assignment are the nominal orbit parameters at the end of each burning phase.



(a) Injection into Arbitrary Orbit Using a Coast Period Between Burns



(b) Re-entry from Orbit

The error analysis procedure is capable of treating any type of guidance system, whether it be an inertial platform, a radio guidance system, an open loop autopilot system, or combinations thereof on the different stages.

Finally, the statistical quantities of interest in the final orbit may be the elliptic elements (such as eccentricity, period, etc.) or the band of altitudes within which the orbit should be confined according to some assigned statistical probability; or the impact error associated with a re-entry vehicle; or some other criterion.

Basically, the approach may be considered as consisting of four steps:

- (1) Determination of the B matrix which relates the injection error vector X to system error S
- $$X = BS$$
- (2) Determination of the covariance matrix which contains error-interrelations and is normalized to the one-sigma error values.
 - (3) Determination of boundaries in Gaussian space along which quantities of interest are constant.
 - (4) Integration over this boundary (if one variable is of interest) or over the inter-sections of several boundaries (if several variables are of interest).

(1) Determination of the B matrix

The linearity assumption is made that each of the N statistically independent error sources produces a proportional error in each component of the six-dimensional error vector at end of powered flight, X . Hence, there exists a $6 \times N$ matrix B which relates the N -dimensional vector error source, S , to the six-dimensional vector, X . The element B_{ij} in this matrix is the partial derivative of the i th component of X with respect to the one-sigma value of the j th component of the error source, S (thus each component of S is normalized by its standard deviation for convenience, as defined below). The assumption of linearity is very good in nearly all cases. The notable exceptions and method of treatment have been noted (Section B-1-c).

In the following analysis the basic error sources, S , are assumed statistically independent and unbiased. The above definition is stated explicitly as

$$X = BS \quad (127)$$

where each component S_i is expressed in units of its standard deviation, σ_i . Table 4 shows the error sources that usually are most significant for each type of guidance system.

TABLE 4
Sources of Error for Various Guidance Systems

| Guidance System | Inertial Platform Guidance System | Radio Guidance System | Autopilot or Open Loop Guidance System |
|-------------------------------------|---|---|---|
| Internal and external error sources | Platform and component initial alignment errors. Gyro drift. Accelerometer errors: scale factor, bias, cross coupling, etc. Airborne computer errors. Engine shutdown errors. | Errors in measurement of position and velocity coordinates due to basic measurement devices and due to propagation refraction through the medium. Ground based computer errors. Engine shutdown errors. | Initial alignment errors of engine and inertial elements. Gyro drift. Gyro torquing error, due to power supply and gyro itself. Vehicle center of gravity offset. Accelerometer errors. Propulsion system errors: I_{sp} and weight flow. Engine shutdown errors. Timing errors. |

The method in determination of the B matrix is to take each independent error source, one at a time, and find the six-dimensional error in X due to this, thereby yielding one column in the 6 x N matrix. This is done most expediently by using the same digital computer program which has previously been used in determination of the complete powered flight trajectory. N + 1 machine runs are made using this program, each one carried out from liftoff through each burning phase and coast phase until the end of the last burning period. On the first of these runs, all input conditions are nominal, and, of course, X is zero. On the second and each subsequent run, one input is perturbed, that being the error source under consideration for that run. As stated above, the amount of the perturbation is taken for convenience as the one-sigma value. The difference from nominal of the resultant output is X, which is the desired column in the B matrix, from Eq (127).

(2) Determination of covariance matrix, Λ

The vector X is a six-dimensional Gaussian density function since each of its components is a linear transformation of Gaussian error sources from Eq (127). The complete statistics of X are therefore given by the covariance matrix, A, defined by

$$\Lambda = E(X X^T)$$

where X^T is the transpose of the column vector and E is the statistical expectation operator defined by

$$E[h(x)] = \int_{-\infty}^{\infty} h(x) f(x) dx$$

where h(x) is any function of a variable of distribution f(x). Inserting Eq (127) in the equation for Λ yields

$$\Lambda = E(BSS^T B^T) \quad (128)$$

$$= BB^T \quad (129)$$

= 6 x 6 matrix

In deriving Eq (130), the following fact was used.

$$E(SS^T) = \text{unit matrix} \quad (130)$$

This follows because of the statistical independence of the error sources in S, and because of the way B was defined in Eq (127).

In unusual circumstances where the assumptions given for Eq (127) are invalid, the same theory applies, but the expressions previously developed have additional terms. Such a situation might physically arise, for example, in a radio guidance system, if uncertainty in refraction causes a correlated (though unbiased) error in several basic measurements such as range, angle and their derivatives. The only change in the equations derived in this section caused by such a correlation between the components of S occurs in Eq (129), which becomes

$$\Lambda = BE(SS^T)B^T \quad (131)$$

where the matrix $E(SS^T)$ is no longer a unit matrix, but contains the correlation coefficients as off-diagonal terms. Equation (131) then becomes the basic 6 x 6 matrix defining completely the statistics at final burnout, with all other equations remaining the same.

If an error source is biased and the value is known (which is really necessary if it is to be included in the error analysis) then the true system error can be reduced by inserting a compensating offset.

3. Error Analysis of Various Trajectory Sequences (Ref. 2)

As noted in the previous sections, the error analysis procedure generally requires machine computation, although the transformation of errors in free-flight can be expressed analytically. These analytic expressions are useful, especially in cases where the errors at end of first burning can also be obtained analytically (for example, in a radio guidance system). Thus, in these cases, the complete error analysis may be carried out analytically without machine computation.

Table 5 gives the in-plane errors for a fairly general trajectory, which invokes only the usual constraint that second burn occur at apogee of the coast ellipse. These equations become greatly simplified for a Hohmann transfer ellipse, as shown in Table 6. Table 7 is the transformation of errors in a nominally circular orbit. Table 8 gives out-of-plane errors.

The in-plane equations given in Tables 5, 6 and 7 are derived by taking first order perturbations in the two basic equations of motion in a central force field given below. These are:

$$\begin{aligned} \frac{r_0}{r_f} &= \frac{1 - \cos \phi_f}{\lambda_0 \cos^2 \gamma_0} + \frac{\cos(\gamma_0 + \phi_f)}{\cos \gamma_0} \\ &= \frac{1 + e \sin(\phi - \alpha)}{\lambda_0 \cos^2 \gamma_0} \end{aligned} \quad (132)$$

$$t = \frac{\lambda_0^2 r_0 \cos^3 \gamma_0}{v_0} \int_0^{\phi_f} \left[1 + e \sin(\phi - \alpha) \right]^{-2} d\phi \quad (133)$$

where the zero subscript refers to conditions at beginning of coast, and the f subscript refers to quantities at apogee.

TABLE 5

In-Plane Errors at Injection in Terms of Errors Introduced During Each of Two Burns Separated by a Coast Time, t^*

Subscript 0 represents beginning of coast
Subscript c represents end of coast
Subscript f represents injection
 $\Delta\eta$ represents pitch attitude error in second burn
 δv = velocity increment in second burn
 μ = gravitational constant times mass of earth
 λ = ratio of twice kinetic to potential energy at burnout

1. Altitude Error

$$\Delta r_f = \left(\frac{\partial r}{\partial r_0} \right)_t \Delta r_0 + \left(\frac{\partial r}{\partial v_0} \right)_t \Delta v_0 + \left(\frac{\partial r}{\partial \gamma_0} \right)_t \Delta \gamma_0$$

$$\left(\frac{\partial r}{\partial r_0} \right)_t = \frac{r_f}{r_0} \left[1 + \frac{r_f}{r_0} \frac{(1 - \cos \phi_f)}{\lambda_0 \cos^2 \gamma_0} \right]$$

$$\left(\frac{\partial r}{\partial v_0} \right)_t = 2 \frac{r_f}{v_0} \frac{r_f}{r_0} \frac{1 - \cos \phi_f}{\lambda_0 \cos^2 \gamma_0}$$

$$\left(\frac{\partial r}{\partial \gamma_0} \right)_t = \frac{r_f}{r_0} \frac{r_f}{\cos^2 \gamma_0} \left[\frac{2(1 - \cos \phi_f)}{\lambda_0 \tan \beta_0} - \sin \phi_f \right]$$

2. Velocity Error

$$\delta v_f = \left(\frac{\partial v}{\partial r_0} \right)_t \Delta r_0 + \left(\frac{\partial v}{\partial v_0} \right)_t \Delta v_0 + \left(\frac{\partial v}{\partial \gamma_0} \right)_t \Delta \gamma_0$$

$$\left(\frac{\partial v}{\partial r_0} \right)_t = \left[\frac{\mu}{v r_0^2} - \frac{\mu}{v_c r_f^2} \left(\frac{\partial r}{\partial r_0} \right)_t \right]$$

$$\left(\frac{\partial v}{\partial v_0} \right)_t = \left[\frac{v_0}{v_c} - \frac{\mu}{v_c r_f^2} \left(\frac{\partial r}{\partial v_0} \right)_t \right]$$

$$\left(\frac{\partial v}{\partial \gamma_0} \right)_t = - \frac{\mu}{v_c r_f^2} \left(\frac{\partial r}{\partial \gamma_0} \right)_t \quad (\text{continued})$$

TABLE 5 (continued)

3. Flight Path Angle

$$\delta \gamma_f = \frac{v_c}{v_f} \left[\left(\frac{\partial \gamma}{\partial r_0} \right)_t \Delta r_0 + \left(\frac{\partial \gamma}{\partial v_0} \right)_t \Delta v_0 + \left(\frac{\partial \gamma}{\partial \gamma_0} \right)_t \Delta \gamma_0 \right]$$

$$+ \left(\frac{\partial \gamma}{\partial t} \right)_t \Delta t + \frac{\Delta v}{v_f} (\Delta \eta - \Delta \phi_f)$$

$$\left(\frac{\partial \gamma}{\partial r_0} \right)_t = - \frac{v_0}{v_c r_0} \frac{\sin \phi_f}{\lambda_0 \cos \gamma_0} - \frac{v_0}{v_c} \left[\frac{\cos \phi_f}{\lambda_0 \cos \gamma_0} - \cos(\gamma_0 + \phi_f) \right] \left(\frac{\partial \phi}{\partial r_0} \right)_t$$

$$\left(\frac{\partial \phi}{\partial r_0} \right)_t = - (1 - e)^2 \left[\frac{3}{r_0} k_1 + \frac{4 \sin^2 \phi_f}{\lambda_0 r_0 \cos^2 \gamma_0} k_2 - \frac{2 \lambda_0 (\lambda_0 - 1) \cos^2 \gamma_0}{e r_0} k_3 \right]$$

$$\left(\frac{\partial \gamma}{\partial v_0} \right)_t = \frac{2}{v_c} \frac{\sin \phi_f}{\lambda_0 \cos \gamma_0} - \frac{v_0}{v_c} \left[\frac{\cos \phi_f}{\lambda_0 \cos \gamma_0} - \cos(\gamma_0 + \phi_f) \right] \left(\frac{\partial \phi}{\partial v_0} \right)_t$$

$$\left(\frac{\partial \phi}{\partial v_0} \right)_t = - (1 - e)^2 \left[\frac{3}{v_0} k_1 + \frac{8 \sin^2 \phi_f}{\lambda_0 v_0 \sin^2 \gamma_0} k_2 - \frac{4 \lambda_0 (\lambda_0 - 1) \cos^2 \gamma_0}{e v_0} k_3 \right]$$

(continued)

* Tables 5 to 8 are analytic expressions for determining B matrix. The only constraint on the trajectory is that the end of coast be apogee of the transfer ellipse. Gyro reference is assumed for apogee burn.

TABLE 5 (continued)

$$\left(\frac{\partial \gamma}{\partial \gamma_0}\right)_t = \frac{v_0}{v_c} \left[\frac{-\sin \phi_f \sin \beta_0}{\lambda_0 \cos^2 0} + \cos(\gamma_0 + \phi_f) \right] - \left\{ \frac{v_0}{v_c} \left[\frac{\cos \phi_f}{\lambda_0 \cos \gamma_0} - \cos(\gamma_0 + \phi_f) \right] \cdot \left(\frac{\partial \phi_f}{\partial \gamma_0}\right)_t \right\}$$

$$\left(\frac{\partial \phi}{\partial \gamma_0}\right)_t = (1-e)^2 \left[3 \tan \gamma_0 k_1 + 2 \left(-\frac{4 \cos 2\gamma_0 \sin^2 \phi_f}{\lambda_0 \sin^2 2\gamma_0} + \frac{\sin^2 \phi_f}{\sin^2 \beta_0} \right) k_2 - \frac{\lambda_0 (2 - \lambda_0) \sin 2\gamma_0}{e} k_3 \right]$$

$$\alpha = \phi_f + \frac{\pi}{2}$$

$$k_1 = \int_0^{\phi_f} \frac{d\phi}{[1 + e \sin(\phi - \alpha)]^2} = \frac{e}{1-e^2} \frac{\sin \phi_f}{1 - e \cos \phi_f} + \frac{1}{1-e^2} k_4$$

$$k_2 = \int_0^{\phi_f} \frac{e \cos(\phi - \alpha) d\phi}{[1 + e \sin(\phi - \alpha)]^3} = \frac{1}{2} \left[\frac{1}{(1 - e \cos \phi_f)^2} - \frac{1}{(1 - e)^2} \right]$$

$$k_3 = \int_0^{\phi_f} \frac{\sin(\phi - \alpha) d\phi}{[1 + e \sin(\phi - \alpha)]^3} = \frac{1}{2} \frac{1}{(1 - e^2)} \frac{\sin \phi_f}{(1 - e \sin \phi_f)^2} + \frac{1}{2} \frac{2e^2 + 1}{(1 - e^2)^2} \frac{\sin \phi_f}{(1 - e \cos \phi_f)} + \frac{\frac{3}{2}e}{(1 - e^2)^2} k_4$$

$$k_4 = \int_0^{\phi_f} \frac{d\phi}{1 + e \sin(\phi_f - \alpha)} = \left\{ \frac{2}{\sqrt{1 - e^2}} \tan^{-1} \left(\sqrt{\frac{1 - e}{1 + e}} \tan \frac{\phi_f}{2} \right) \right\}$$

TABLE 6

In-Plane Errors at Injection in Terms of Errors Introduced During Each of Two Burns Separated by a Coast Time, t , $\gamma_0 = 0^\circ$ (Hohmann Transfer)

$$\frac{\Delta r_f}{r_f} = \frac{\Delta r_0}{r_0} \left(2 + \frac{r_f}{r_0} \right) + 2 \frac{\Delta v_0}{v_0} \left(1 + \frac{r_f}{r_0} \right)$$

$$\Delta v_f = -\frac{\Delta r_0}{r_0} \frac{2}{\lambda_0} v_0 - \Delta v_0 \left(2 + \frac{r_0}{r_f} \right) + \Delta(\delta v)$$

$$\Delta \phi_f = \frac{4}{\lambda_0} \Delta \gamma_0 - k_5 \left(\frac{\Delta r_0}{\lambda_0 r_0} + \frac{\Delta v_0}{v_0} \right) + \Delta t \frac{v_c}{r_f}$$

where

$$k_5 = \frac{3\pi}{\lambda_0} \left(\frac{r_f}{r_0} \right)^{1/2}$$

$$\Delta \gamma_f = -\Delta \gamma_0 \left[\frac{r_0}{r_f} \frac{v_c}{v_f} + \left(\frac{\delta v}{v_f} \frac{4}{\lambda_0} \right)^* \right] - \Delta \eta \frac{\delta v}{v_f} + \left\{ \left[\frac{\Delta r_0}{r_0 \lambda_0} + \frac{\Delta v_0}{v_0} \right] \cdot \left[k_5 \frac{(\lambda_0 - 1)}{\lambda_0} \frac{v_0}{v_f} + \left(\frac{\delta v}{v_f} k_5 \right)^* \right] + \delta t \left[\frac{v_0 (\lambda_0 - 1)}{v_f \lambda_0} - \left(\frac{\delta v}{v_f} \right)^* \right] \frac{v_c}{r_f} \right\}$$

* The terms encircled are eliminated when a horizon scanner reference is used for apogee.

TABLE 7

Coast Phase Transformation of In-Plane Initial Errors Δr_0 , Δv_0 , $\Delta \gamma_0$ Into Final Errors δr_f , δv_f , $\delta \beta_f$, $\delta \phi_f$ After Traversing an Angle ϕ_f in a Nominally Circular Orbit

$$\begin{bmatrix} \frac{\Delta r_f}{r_0} \\ \frac{\Delta v_f}{v_0} \\ \Delta \gamma_f \\ \Delta \phi_f \end{bmatrix} = \begin{bmatrix} 2 - \cos \phi_f & 2(1 - \cos \phi_f) & -\sin \phi_f \\ -(1 - \cos \phi_f) & (-1 + 2 \cos \phi_f) & \sin \phi_f \\ -\sin \phi_f & -2 \sin \phi_f & \cos \phi_f \\ -3 \phi_f + 2 \sin \phi_f & -3 \phi_f + 4 \sin \phi_f & 2(1 - \cos \phi_f) \end{bmatrix} \begin{bmatrix} \frac{\Delta r_0}{r_0} \\ \frac{\Delta v_0}{v_0} \\ \Delta \gamma_0 \end{bmatrix}$$

TABLE 8

Coast Phase Transformation
for Out-of-Plane Errors

Out-of-plane error α and ψ in terms of initial errors, α_0 , ψ_0 and ϕ_f . ψ and α are defined in Section B.

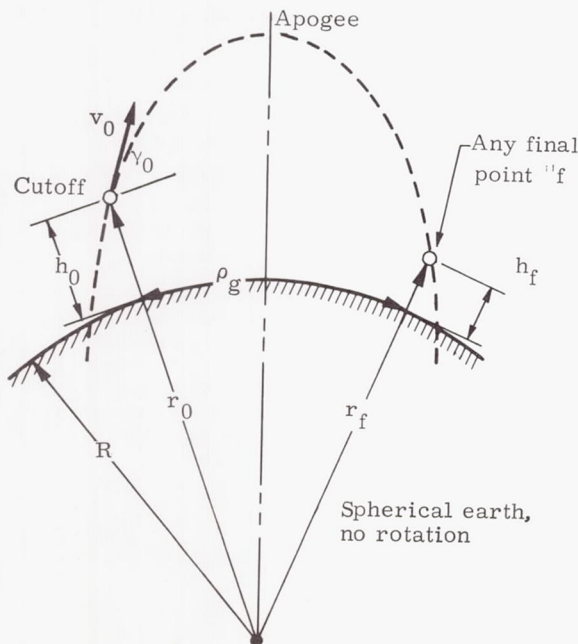
$$\begin{bmatrix} \delta\alpha \\ \delta\psi \end{bmatrix} = \begin{bmatrix} \cos \phi_f & -\sin \phi_f \\ \sin \phi_f & \cos \phi_f \end{bmatrix} \begin{bmatrix} \delta\alpha_0 \\ \delta\psi_0 \end{bmatrix}$$

4. Ballistic Trajectory Error Analysis (Ref. 3)

The ground range over a nonrotating earth achieved by a ballistic missile is given by

$$\begin{aligned} \rho_g &= R \tan^{-1} \frac{\sin \gamma_0 \cos \gamma_0}{\frac{\mu}{r_0 v_0^2} - \cos^2 \gamma_0} \\ &+ R \tan^{-1} \cos \gamma_0 \left[1 - \left(\frac{r_0}{r_f} \right)^2 \cos^2 \gamma_0 \right. \\ &\left. + \frac{2\mu}{r_0 v_0^2} \left(\frac{r_0}{r_f} - 1 \right) \right] \left[\frac{\mu}{r_0 v_0^2} - \frac{r_0}{r_f} \cos^2 \gamma_0 \right]^{-1} \end{aligned} \quad (134)$$

where subscript 0 indicates a cutoff condition, and subscript f indicates a final condition, and R is the radius of the earth, as shown in the accompanying sketch. Differentiation of Eq (134) yields the following error partials.



$$v_0 \frac{\partial r}{\partial v_0} = 2 K_1 K_2 \quad (135)$$

$$\begin{aligned} r_0 \frac{\partial r}{\partial r_0} &= K_1 + \left\{ R \cos \gamma_0 \left[\left(\frac{v_c}{v_0} \right)^4 \left(2 \frac{r_0}{r_f} - 1 \right) \right. \right. \\ &+ \left(\frac{v_c}{v_0} \right)^2 \left(1 - 3 \frac{r_0}{r_f} \cos^2 \gamma_0 \right) \\ &+ \left. \left. \frac{r_0}{r_f} \cos^2 \gamma_0 \right] \left[\left\{ \left[\frac{v_c}{v_0} \right]^2 - \cos^2 \gamma_0 \right\}^2 \right. \right. \\ &+ \left. \left. \sin^2 \gamma_0 \cos^2 \gamma_0 \right\} \right. \\ &\left. \left. \sqrt{1 - \frac{r_0}{r_f} \cos^2 \gamma_0 + 2 \left(\frac{v_c}{v_0} \right)^2 \left(\frac{r_0}{r_f} - 1 \right)} \right] \right\}^{-1} \end{aligned} \quad (136)$$

$$K_1 = \left\{ R \left(\frac{v_c}{v_0} \right)^2 \sin \gamma_0 \cos \gamma_0 \left[\left[\frac{v_c}{v_0} \right]^2 - \cos^2 \gamma_0 \right] \right. \\ \left. + \sin^2 \gamma_0 \cos^2 \gamma_0 \right\}^{-1}$$

$$K_2 = 1 + \left\{ 1 - \frac{r_0}{r_f} \cos^2 \gamma_0 + \left(\frac{v_c}{v_0} \right)^2 \left(\frac{r_0}{r_f} - 1 \right) \right\} \\ \cdot \left\{ \sin \gamma_0 \sqrt{1 - \frac{r_0}{r_f} \cos^2 \gamma_0 + 2 \left(\frac{v_c}{v_0} \right)^2 \left(\frac{r_0}{r_f} - 1 \right)} \right\}^{-1}$$

$$\begin{aligned} \frac{\partial r}{\partial v_0} &= - \left\{ R \left[\left(\frac{v_c}{v_0} \right)^2 \left(1 - 2 \cos^2 \gamma_0 \right) + \cos^2 \gamma_0 \right] \right. \\ &\cdot \left[\left(\frac{v_c}{v_0} \right)^2 - \cos^2 \gamma_0 \right]^2 + \sin^2 \gamma_0 \cos^2 \gamma_0 \left. \right\}^{-1} \\ &- \left\{ R \sin \gamma_0 \left[\left(\frac{v_c}{v_0} \right)^2 \left(1 - 2 \frac{r_0}{r_f} \cos^2 \gamma_0 \right) \right. \right. \\ &+ \left. \left. \frac{r_0}{r_f} \cos^2 \gamma_0 + 2 \left(\frac{v_c}{v_0} \right)^4 \left(\frac{r_0}{r_f} - 1 \right) \right] \right. \\ &\cdot \left[\left[\left(\frac{v_c}{v_0} \right)^2 - \cos^2 \gamma_0 \right]^2 + \sin^2 \gamma_0 \cos^2 \gamma_0 \right] \\ &\cdot \left. \left. \sqrt{1 - \frac{r_0}{r_f} \cos^2 \gamma_0 + 2 \left(\frac{v_c}{v_0} \right)^2 \left(\frac{r_0}{r_f} - 1 \right)} \right] \right\}^{-1} \end{aligned} \quad (137)$$

where

v_c = circular orbit velocity at cutoff altitude.

These error sensitivities are plotted in Figs. 3 through 17. The quantity K_1 , which arises from the first term (cutoff to apogee term) of Eq (134), and which appears as the first term of Eq (136) and as a factor of Eq (135), is plotted in Figs. 3 and 4. The multiplying factor K_2 is shown in

Figs. 5 and 6. The second term of Eq (136) (that is, the part of the error partial $\frac{\partial \rho}{\partial r_0} \frac{g}{g_0}$ arising

during that portion of the trajectory between apogee and the final point) is given by Figs. 7,

8 and 9. The first term of $\frac{\partial \rho}{\partial y} \frac{g}{g_0}$ (cutoff to apogee) is shown in Figs. 10 and 11. The second term is shown in Figs. 10 through 15. Figures 16 and 17 are useful auxiliary graphs in using Figs. 3 through 15. The error sensitivities are also given (Ref. 4) in Figs. 18 and 19 as functions of range and Fig. 20 gives flight time as a function of range.

C. SPACE VEHICLE GUIDANCE TECHNIQUES (Ref. 2)

Once the requirements imposed by the mission on the guidance system have been appraised by the methods of Section B, a guidance philosophy may be selected to meet that requirement. Guidance may be defined as the processes of measurement, data extraction and smoothing, computation and control which are required to assure that a space vehicle reaches a desired destination from a given launch point. For the present purposes, the destination may be a point for injection into an arbitrary parking orbit from a direct ascent trajectory to a point in space, with the proper six-initial conditions to place the vehicle on a coast ellipse (for a transfer maneuver), parabola or hyperbola to establish a lunar or interplanetary trajectory, or some other final-value condition. Thus, it is customary to classify the problem by:

- (1) Launch guidance
- (2) Midcourse guidance
- (3) Terminal guidance

and to further classify the guidance problem by the form of the mechanization and constraints, as:

- (1) Radio supervised (maximum radar range, minimum elevation angle, required look-angles for antenna patterns, maximum slewing rates, etc.).
- (2) Inertial (platform stability, linearity, threshold levels and dynamic range, integration accuracy, etc.).

- (3) Radio-inertial (combination systems where position may be derived from radar with inherent radar constraints, and velocity from inertial measurement with inherent inertial system constraints).

The literature is now becoming extensive on these more specialized problems of theory and mechanization. It is nearly impossible within the span of the handbook to do more than suggest different approaches to the guidance problem insofar as specific mechanizations are concerned. The chief emphasis will be on providing the mission analyst with general methods of guidance analysis applicable to any class of guidance system.

1. Formulation of Guidance Equations

The formulation of the guidance equations for the launch guidance phase may take the form of, (1) explicit guidance, (2) delta guidance, or (3) Q-guidance.

Explicit guidance. The required velocity vector, \vec{v}_r , is obtained in closed form as a function of position and time. The velocity-to-be-gained, \vec{v}_g , is then obtained as

$$\vec{v}_g = \vec{v}_r - \vec{v} \quad (138)$$

where \vec{v} is the instantaneous velocity of the vehicle. The vehicle is then steered in an efficient manner until $\vec{v}_g = 0$, at which time the engines are shut off.

Delta guidance. In delta guidance, the required velocity vector is approximated by a functional expansion about the nominal expected burnout position and time (x_n, y_n, z_n, t_n) as

$$\begin{aligned} \vec{v}_r = \vec{v}_{rn} + \vec{A}(x_n - x) + \vec{B}(y_n - y) + \vec{C}(z_n - z) \\ + \vec{D}(t_n - t) + \text{second order terms} \end{aligned} \quad (139)$$

where \vec{v}_{rn} , \vec{A} , \vec{B} , \vec{C} , \vec{D} are constant vectors and x, y, z denote the platform coordinate system. Several second-order difference terms such as $(x_n - x)(z_n - z)$ may be required to obtain the desired accuracy. The advantage of the above method is that only simple arithmetic operations rather than the square roots and divisions required for explicit guidance need be performed by the airborne digital computer. The disadvantages result from the larger number of constants that must be precalculated and inserted into the onboard digital computer.

Q-guidance. Another method of guidance is referred to as Q-guidance. This method gives the velocity-to-be-gained directly by integration of

$$\dot{\vec{v}}_g^i = \vec{A}_t^i - \sum_j^3 Q_j^i \vec{v}_g^i \quad (140)$$

where $i, j = 1, 2, 3$ refer to x, y and z components, A_t^i are the components of thrust-drag acceleration as measured by the accelerometers; and the matrix Q_j^i is defined as

$$Q_j^i = \frac{\partial v^i}{\partial x^j}$$

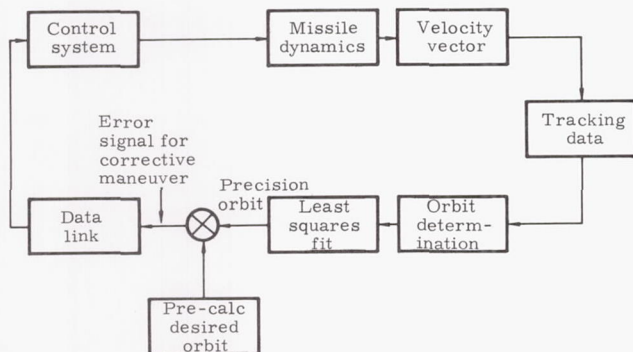
In explicit and delta guidance, it is necessary to perform a gravity computation, which is not required for Q-guidance. The only guidance constants required for Q-guidance are the components of the Q-matrix and three initial values for \vec{v}_g .

The components of the Q-matrix will contain about 10 trajectory-dependent constants. The disadvantage of Q-guidance is that the computer does not evaluate instantaneous position or velocity. These quantities are useful in orienting the body attitude during the coast period and for resetting the digital computer prior to the later burning periods.

2. Launch Guidance

a. Radio launch guidance

A radio guidance mechanization of a spacecraft steering loop may proceed along the most general lines as shown in the sketch where the guidance complexity is placed in the ground equipment. An entire tracking network may be involved in gathering the tracking data. Depending on the nature of the tracking data (range-only, range-azimuth-elevation, angle-only) and the number of participating stations, an initial and then precision orbit is calculated by, say, an IBM 7990 computer; the actual orbit is compared to the desired orbit, and pitch and yaw steering commands or discrete commands are generated and sent to the control system of the spacecraft for thrust vector control.



A single semispecial purpose guidance computer located at the launch site may be schematically represented as in Fig. 21.

The missile dynamics for either a symmetric or nonsymmetric shape are given, together with all equations of motion reduced to a form suitable for digital computer calculation. Finally, a functional block diagram is shown in Fig. 22 for a combination CW and pulse radio guidance system. One of the most severe constraints in a radio-inertial system is due to the antenna radiation pattern (see Fig. 23) and signal sensitivities of the spacecraft receivers. One way of overcoming such problems (though introducing other perhaps more flexible constraints) is to consider the usual inertial guidance mechanization.

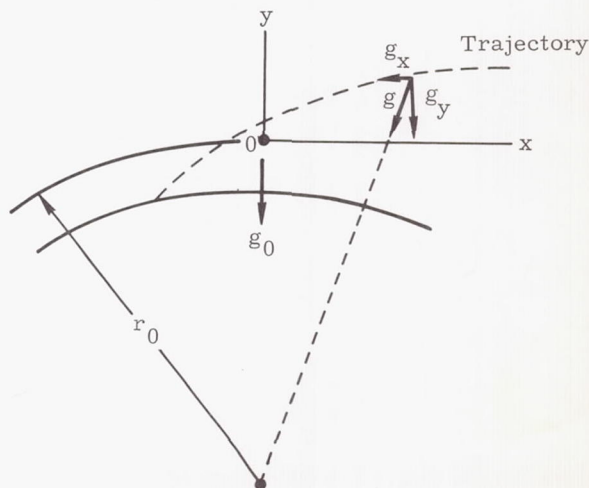
b. Inertial launch guidance (Ref. 5)

To accomplish inertial navigation in a region containing gravity fields some method must be used for calculating gravity acceleration. If the path of the vehicle can be accurately predicted, the effects of gravity can be precalculated. In this case, guidance during flight would be done in terms of thrust acceleration and its time integrals only. As the path of a specific vehicle becomes difficult to predict (relative to the accuracy requirement), it becomes necessary to make a gravity computation during flight.

The following sketch shows, with an exaggerated scale, the powered flight trajectory of a space vehicle. A rectangular coordinate system with origin in the vicinity of the trajectory and with the y -axis vertical can be used to express the components of gravity relative to a free-fall reference frame at the center of the earth as follows:

$$g_x = -g \frac{x}{r} = \frac{-g_0 r_0^2 x}{[x^2 + z^2 + (r_0 + y)^2]^{3/2}} \quad (141)$$

$$g_y = -g \frac{y + r_0}{r} = \frac{-g_0 r_0^2 (y + r_0)}{[x^2 + z^2 + (r_0 + y)^2]^{3/2}} \quad (142)$$



The g_z term is similar to g_x , but for simplicity will be omitted here. x can be taken in the nominal plane of the trajectory and the problem considered in two dimensions. These equations are nonlinear and their mechanization requires considerable computer complexity. Simple linear approximations which are valid near the origin of coordinates are

$$g_x = -\frac{g_0}{r_0} x \quad (143)$$

$$g_y = -g_0 \left(1 - \frac{2y}{r_0}\right). \quad (144)$$

The acceleration equations in component form are

$$\ddot{x} = a_{tx} + g_x \quad (145)$$

$$\ddot{y} = a_{ty} + g_y \quad (146)$$

Block diagrams for the solution of these linear equations are shown in Fig. 24. The x channel has negative feedback and two integrations and thus has a sinusoidal response to an input disturbance. The y channel has positive feedback and an input disturbance leads to a diverging value of y .

The effect of the approximation in the gravity computer can, of course, be calculated for a given trajectory. Additional terms to include the non-spherical gravity field of the earth can be included as necessary. If the acceleration free-fall reference frame is located in a satellite, for example, then the gravity components which give the difference in gravity between the location of the accelerometer and the reference frame, would differ from those given in Eqs (141) and (142). Because the satellite moves through the earth's gravity field, the gravity components would vary with time.

The effect of the gravity computation upon position and velocity error buildup caused by accelerometer or initial condition errors is of considerable interest. It can be investigated analytically in terms of perturbation equations of the form

$$\Delta \ddot{x} = \Delta a_{tx} + \Delta g_x = \Delta a_{tx} + \frac{\partial g_x}{\partial x} \Delta x + \frac{\partial g_x}{\partial y} \Delta y \quad (147)$$

$$\Delta \ddot{y} = \Delta a_{ty} + \Delta g_y = \Delta a_{ty} + \frac{\partial g_y}{\partial x} \Delta x + \frac{\partial g_y}{\partial y} \Delta y \quad (148)$$

The differential coefficients are functions of space which can be obtained from Eqs (141) and (142). They should be evaluated along the unperturbed path of the vehicle. However, this leads to differential equations with time varying coefficients which cannot be solved in closed form. For flights in a region of a few hundred miles breadth, the coefficients can be evaluated at one point in the vicinity of the trajectory with adequate accuracy for the purposes here. This gives the following equations for the perturbation in position

caused by thrust acceleration perturbation or accelerometer error.

$$\Delta \ddot{x} + \frac{g_0}{r_0} \Delta x = \Delta a_{tx} \quad (149)$$

$$\Delta \ddot{y} - \frac{2g_0}{r_0} \Delta y = \Delta a_{ty}. \quad (150)$$

The physical meaning of these equations is easy to see. For example, a positive error in vertical position leads to a calculated value of gravity acceleration which is too small and thus to a calculated value of true acceleration which is too large. This in turn integrates into an even larger positive position error.

The solution to Eqs (149) and (150) for constant values of thrust acceleration perturbations (accelerometer bias or zero offset) are

$$\Delta x = \frac{\Delta a_{tx}}{g_0/r_0} \left[1 - \cos \sqrt{\frac{g_0}{r_0}} t \right] \quad (151)$$

$$\Delta y = \frac{\Delta a_{ty}}{2g_0/r_0} \left[\cosh \sqrt{\frac{2g_0}{r_0}} t - 1 \right] \quad (152)$$

The terms for initial condition perturbations are similar to these. Near the surface of the earth, the sinusoidal oscillation has a period of about 84 min, that is,

$$2\pi \sqrt{r_0/g_0} \approx 84 \text{ min.}$$

Position errors caused by accelerometer errors other than a constant bias can be calculated by well known methods. An offset in the attitude reference will cause a cross coupling error, thus $\Delta a_{tx} = \beta a_{ty}$, where β is the attitude reference error. A gyro drift rate thus gives an increasing position error.

These perturbations or error equations illustrate a basic limitation of inertial guidance for long times of flight, namely, that errors in the vertical direction increase exponentially with time. However, errors in the horizontal direction caused by accelerometers are oscillatory with a period of 84 min. This makes practical two-dimensional inertial systems for aircraft and ships which can employ altimeters to measure altitudes. For flight times less than about 10 min, Eqs (151) and (152) can be approximated by the simple equations

$$\Delta x = \Delta a_{tx} \frac{t^2}{2}; \quad \Delta \dot{x} = \Delta a_{tx} t \quad (153)$$

$$\Delta y = \Delta a_{ty} \frac{t^2}{2}; \quad \Delta \dot{y} = \Delta a_{ty} t \quad (154)$$

which are those that would be obtained by ignoring the feedback error from the gravity calculation. They would also be those obtained for navigation in a constant gravity field.

Associated with the concept of this guidance is that of the standard or reference trajectory. Such

a trajectory is one which a standard or nominal missile would follow under standard or nominal aerodynamic conditions. The path of any specific missile should follow the standard trajectory quite closely. In general, the specific paths will be statistically distributed about the standard which in some sense will be a mean of the distribution.

A schematic of a steering computer is given in Fig. 25. The angle commanded by the pitch programmer is compared with the gimbal pitch angle to give a pitch steering command to the missile control system. The overall guidance loop is illustrated in Fig. 25 by the feedback from the missile control system through missile dynamics to the inertial measurement unit.

Lateral and pitch steering having been accomplished, the remaining problem is to terminate the missile thrust at the proper time so that the spacecraft will hit the intended aiming point. The proper combination of burnout values can be obtained by considering the effects on target miss of small changes in the horizontal and vertical components of position and velocity. To express this analytically, the range of the missile is expanded as a function of position and velocity components about the standard burnout point.

$$\begin{aligned} \rho - \rho_s = & \frac{\partial \rho}{\partial x} (x - x_s) + \frac{\partial \rho}{\partial y} (y - y_s) \\ & + \frac{\partial \rho}{\partial \dot{x}} (\dot{x} - \dot{x}_s) + \frac{\partial \rho}{\partial \dot{y}} (\dot{y} - \dot{y}_s) + \dots \end{aligned} \quad (155)$$

ρ designates range, the subscript s designates standard conditions, and the partial derivative coefficients are evaluated at the standard burnout point, $\partial \rho / \partial x \equiv C_x$, etc. A computer which continuously calculates the downrange miss at the aiming point is shown in Fig. 26. Prior to the start of the flight, values of the standard burnout conditions, x_s , etc., are fed into the computer along with values of the coefficients, C_x , etc., which are calculated for the particular range desired. At some zero time for guidance (which should be within a few seconds of the actual lift-off time of the missile) the accelerometers are connected to the computer and torquing of the gyros at earth rate is stopped. Position and velocity components relative to the launch point then appear in the channels indicated in the figure and the computer calculates the downrange miss, M_r . Early in the flight, the calculated value will be grossly in error because only linear terms are used in the expansion. Near burnout, however, the computation will be quite accurate. The thrust of the missile is terminated when the computed miss becomes zero. This will always occur because the missile is flying toward the impact point with an increasing velocity.

The inertial guidance scheme should be evaluated from several standpoints. For example, the need for the gravity computer should be investigated. If the actual missile flight is sufficiently close to the nominal flight, the effect of gravity can be precalculated with sufficient accuracy and no gravity computer is necessary. On the other

hand, and especially for extreme accuracy, additional terms in the gravity expansion might be necessary. If the variation in missile thrust is large, higher order terms might be needed in the expansion of the motor shutoff, Eq (155). Refinements in the guidance scheme would include means of compensation for time of flight variations. The design of the system should include an error analysis of all of the principal components so that a proper balance in design complexity can be obtained. For example, high accuracy in the cutoff expansion is meaningless if the accelerometers are low accuracy devices. A thorough error analysis including the effects of inertial component tolerances is presented in Ref. 6.

3. Midcourse Guidance

Guidance principles applied to launch guidance have been discussed in the earlier sections. The spacecraft may be assumed to travel along a free flight path to its destination without further application of thrust or guidance. This type of guidance is accurate enough in general for establishing earth satellite orbits, and possibly in more refined operations. However, for precise navigation to the moon, to establish satellite orbits about the moon, or for interplanetary orbits midcourse and terminal guidance will be needed. Midcourse corrections for lunar trajectories are considered in detail in the companion work, Lunar Flight Handbook, Ref. 7. Differential corrections are considered in Chapter VI of this manual.

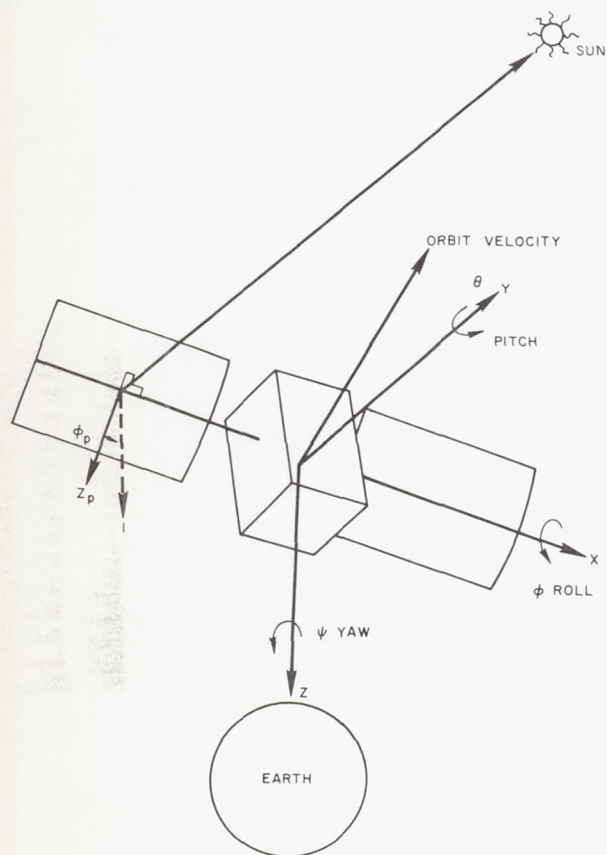
D. DESIGN OF ATTITUDE CONTROL SYSTEMS FOR EARTH SATELLITES (Ref. 2)

The design of a spacecraft attitude control system is a complex problem. The specific stabilization and orientation requirements must be met, and compatibility with other spacecraft subsystems must be ensured. The early spacecraft, which were designed for long term operation, were spin stabilized. More stringent requirements of present experimental, communications, interception or reconnaissance missions have demanded more precise or more complex control. The purpose of this part of the Handbook is to present several important problems which must receive attention in the design of the attitude control system. Tradeoff and systems problems, considerations involved in a particular choice of an attitude control system, and design data which may be helpful for preliminary calculations are presented. The scope of the section is, by and large, limited to consideration of the attitude control of earth-orbiting satellites.

The designer is confronted with the problem of choosing among a number of possible solutions for a particular attitude control system. Since no attitude control system can be broadly classed as optimal for every mission, a range of the possible control system selections must be reviewed in the preliminary design as each relates to both the required control system performance and the design of other subsystems. Often, the number of solutions can be quickly narrowed to one or two

logical choices. The designer must define the flight sequence, particular modes of control, and control laws, evaluate the effects of disturbing forces during operation, and assess the control system reliability to provide an optimum correction technique for fine position and time control.

To aid the designer and mission analyst in this task, the Handbook treats important system considerations of the mission and control specifications; methods of obtaining control orientation; control system sensors and control modes. One typical satellite configuration is shown in the following sketch.



1. Mission and Control Configuration

The purpose of this section is to survey the various types of spacecraft attitude control systems which might be used for various missions. It is important to begin with a general discussion of the broad specifications which are important in the preliminary design. Because control system specifications for the spacecraft often differ depending on the mission, this section treats only broad requirements. Once the mission is determined, the designer can look at various control schemes for the particular payload or range of payloads that can be launched by the available boosters. This means that for some missions, studies involving the tradeoff between booster capability, weight of payload in a particular orbit or set of orbits, costs, reliability, the basic requirements of the mission, and other system interrelations are required. Pointing accuracy,

maximum attitude rates, system lifetime, reliability, allowable weight, cost, state of hardware development, orbital requirements, boost environment, etc., are typical inputs to the control system design.

a. Mission

A limited set of possible missions will indicate the range of similarities and differences of probable attitude control system requirements. Broadly, the missions have been categorized into experimental spacecraft, reconnaissance satellites, communication satellites and missions requiring orbital docking.

(1) Experimental spacecraft. The satellites and interplanetary probes launched to date have wide and varied stabilization requirements. Satellites containing equipment for detailed solar or stellar observations may need to stabilize with respect to the sun or star under observation to within a very few seconds of arc with very low rates (Orbiting Astronomical Observatory). To obtain information concerning the earth's magnetic field, cosmic radiation, and the like, a satellite may need stabilization within the limits of only 1° or 2° (Orbiting Geophysical Observatory). Spacecraft for investigating various aspects of the moon, Venus and Mars, may require control during a landing operation as well as stabilization during space transit. The mid-course orientation requirements may be similar to those of a satellite, but as the vehicle approaches the planet, separate terminal control and guidance schemes are generally required. The lifetime of experimental satellites must be considered.

(2) Reconnaissance satellite. Two types of vehicles to perform reconnaissance missions may be distinguished. The first is similar to the earth-pointing experimental satellite in that the mission function is to obtain pictures or data concerning earth topography or activities on the earth. Basically, this system will have control requirements which will be a direct function of the resolution capability of the reconnaissance equipment aboard; good absolute pointing accuracy, and very low pointing error rates are required. A second type of reconnaissance vehicle is one for inspection in orbit of other satellites and space vehicles. Such inspection will probably require accurate orientation with respect to some other object, like the earth or sun.

(3) Communication satellite. Various forms of control systems will be required to meet the needs of varying orbits, synchronism requirements and antenna pointing. An oriented antenna may increase the antenna gain by as much as 10 db. This could simplify the communication system at the expense of additional control system complexity. The number of communication satellites depends on the orbit and coverage requirements. While more low altitude satellites are required for the same coverage as higher altitude satellites, the booster capability will allow more to be launched at lower cost, or alternatively, lower cost may be achieved through the use of simpler, more reliable boosters. The altitude also affects the control system design through

altitude-dependent environmental characteristics such as aerodynamics, gravity gradient, radiation and other phenomena. The number of satellites with synchronized orbits which require the additional complexity of a synchronizing or indexing system must be compared with those required in "random" orbits where such a system is not required. For example, 18 satellites in a 6-hour synchronized circular orbit are required for continuous coverage between New York and Paris, whereas approximately 21 are required in "random" orbits for 99% coverage.

(4) Orbital docking. Studies have indicated that the physical mating of two satellites in orbit is feasible. This system would permit the transfer of fuel to provide additional velocity to one of the vehicles (target vehicle) in orbit, essentially yielding an increase in booster capability. The actual mechanics and dynamics of the docking process and the problems of terminal guidance will require detailed attention by the mission analyst. For search, preterminal and terminal modes, the attitude control may require an earth or sun reference in addition to the target vehicle reference.

b. Control configuration

The limitations on size and shape which arise from the limited booster capabilities immediately constrain the configuration. The shape and particularly the moments of inertia are significant. If, for example, the spacecraft is to be spin stabilized, then for internal energy dissipation to provide stable damping, the moment of inertia about the desired spin axis must be larger than that about the other two axes. If, however, the vehicle is to be a low altitude, fully oriented satellite, the inertia configuration will determine whether or not the spacecraft is stable with respect to the torques generated by the earth's gravity field. In fact, the designer may choose configurations so that there is sufficient control moment to stabilize the vehicle from this effect alone.

If the center of aerodynamic pressure does not coincide with the spacecraft's center of gravity, there may be large aerodynamic overturning moments for the low altitude satellite which can affect the control system design and methods for generating countertorques. Principal axis/control axis alignment, difference in inertias, may be significant in the spacecraft dynamic response. In the design of momentum storage and mass expulsion systems, minimizing the moments of inertia about the axes will help reduce the weight of the momentum storage and mass expulsion device. Unfortunately, the other subsystems, particularly the power supply and temperature control, may have a predominant effect on the configuration.

(1) Power supply system. It is anticipated that power supplies for earth satellites requiring long life will continue to use the sun's energy to provide primary power. Rechargeable batteries will be provided to supply the power during periods of eclipse. The solar array size must meet the electrical power requirements of the system and recharge the batteries during periods of sunlight.

The power supply efficiency is maximum if the control system is capable of orienting the faces containing the solar cells toward the sun throughout the lifetime of the satellite--except, of course, during periods of eclipse (see Chapter XIII). If, however, a spin stabilized satellite is chosen, a maximum of only 25% of this power can be realized for a spherical satellite covered with solar cells in any orbit. Two particular spin axis orientations will provide more efficiency: (1) where the spin axis is continually aligned along the sun line, the efficiency is equivalent to that of the oriented array; and (2) where the spin axis is oriented normal to the sun line, an efficiency of approximately 32% of that of the fully oriented array is achieved.

The cyclic life of the batteries is affected by several things, including temperature, depth of discharge and height of charge. The control system response characteristics during acquisition of the sun can effectively reduce the depth of discharge required for a particular orbit through minimizing the time required for the solar array to reacquire the sun after an eclipse. The longer this takes, the more the batteries will be discharged and the less time there will be for recharge before entering eclipse again. This problem is particularly significant in orbits with eclipse periods which exist for a significant period of time.

During orbits with extremely long periods of sunlight compared to eclipse time, it may be desirable to include in the solar array control laws a provision for charge-control to prevent overcharging the battery. Since both continuous sun and earth orientation are impossible without an extra degree of freedom (except for special orbits and during particular periods in each orbit) systems which do not have a rotatable solar array have a reduced efficiency. However, if the power requirements are not extreme, it may be more reliable to have an unoriented rather than oriented array. This is an important tradeoff study to perform.

The electrical power obtained from rotatable solar arrays must be transmitted from the array to the body. The control system, as will be shown later, can be used to eliminate the need for providing complete rotational freedom which would suggest the need of slip-rings for power transmission. Control laws can be used which limit the required solar array travel to $\pm 90^\circ$.

There are a number of other possible array configurations for which specific control laws can be generated. The problems associated with continuous but very slow drives may indicate that stepping the array or providing a set of multiple-fixed positions is an easier and more reliable approach.

(2) Temperature control. A number of active and passive temperature control systems are possible for satellite application. One system which has a great effect on both the control system design and the configuration is one in which the main body is attitude controlled, so that the two surfaces perpendicular to solar array axis

never see the sun. The temperature is controlled by insulating those four surfaces which sometime during the satellite lifetime will see the sun, thus preventing heat absorption. The other two surfaces contain shutters which are actuated to control the emissivity or radiation of internally generated heat into free space. These shutters will not be exposed to direct sunlight for long periods of time if the control system is working properly. If the satellite is earth oriented, sun control about the axis along the local vertical (yaw) will prevent direct sunlight from impinging on these surfaces suggesting four design considerations for the control system. These are:

- (1) Quick acquisition must be made to the sun orientation following separation from the boost vehicle to avoid long periods of unoriented attitude.
- (2) Special methods of control may be required by the temperature control systems. The time required to acquire the sun when the spacecraft emerges from the eclipse must be controlled. The effect of low control gain during periods of high noon (i. e., a condition obtained when the sun is in or nearly in the orbit plane) must be reviewed to keep from exposing these surfaces to the sun for long periods of time.
- (3) Any other modes such as rotation out of the required plane for velocity corrections must take into consideration the possible exposure of these surfaces.
- (4) The sun-pointing accuracy during periods of normal control must satisfy the temperature requirements.

(3) Orbit control system. For many earth oriented satellites, a system to provide change in the satellite's velocity during its time in orbit will be necessary. The indexing into a synchronous orbit of a communication satellite, the terminal guidance of a docking satellite, or the deboost of a vehicle for re-entry, are examples of systems which will utilize a propulsion system to change the spacecraft velocity while in orbit. The control system must be capable of properly reorienting the vehicle in space so the nozzle or rocket thrust will have the correct spatial attitude when the rocket is fired. Furthermore, since the thrust of this rocket will probably not pass exactly through the spacecraft center of gravity, an overturning moment will occur. Sufficient control authority must be available to correct for these moments. In addition, most orbit control systems will have a fine or precise vernier correction and/or a station-keeping mode that could easily use the control system nozzles and obtain energy from the attitude control system. Some simplification in hardware design will be obtained through integration of these systems.

(4) Data link. Earth satellites will be required to communicate with earth based stations. For many systems specific antenna pointing is required. Antenna gain and beamwidth, communication security, ground receiver flexibility and coverage are areas which affect the system design. For earth satellites, pointing accuracy

of a few degrees is sufficient to retain most of the power in the transmitted signal. With proper orientation of antennas for interplanetary probes, increased data transmission rate may be possible.

The data link, or communication system, can also be used to command special modes of control. For example, through analysis of telemetry data it may be learned that a component has failed. The communications system may then send a command to switch in a redundant component.

(5) Control configuration environment and reliability. The environment in which the attitude control system will be required to operate is of extreme importance. Control and disturbance torque generation and sensing requirements are discussed later. The principal considerations which affect the control system reliability and equipment design may be itemized as follows:

Boost environment. The control system in the satellite must meet the requirement that it be operable after boost into orbit. During the first seconds of boost, the high accelerations (say 10 g), vibration, and heat environment impose severe restrictions on all components.

Vacuum. The pressure at 100 naut mi or 185 km is approximately 10^{-5} mm Hg, decreasing rapidly to 10^{-10} mm at 1000 naut mi (1850 km) and to 10^{-13} mm at 100,000 naut mi (18,500 km). In vacuum, there is no resistance to sublimation and evaporation of molecules of surface materials. There is a tendency for systems to "out-gas," creating additional control system torques and reducing the supply required for control torque generation. Substances with a low vapor pressure should be used to reduce the evaporation. The positive elimination or proper sealing of rubbing surfaces can reduce the problem to negligible proportions. As an example, slip rings for transferring power from the solar array to the main body can be eliminated by employing special yaw and solar array control laws (described later) which limit the solar array travel to $\pm 90^\circ$. If motor-driven sensors, inertial wheels, and servos are used, they must be sealed to prevent the evaporation of lubricants from reducing the lifetime of the bearings.

Micrometeoroids. The average control system torque caused by this effect is small and can generally be ignored in comparison with other torques experienced in space. Chapter II considers the quantity and energy distribution of micrometeoroids in space. Two additional considerations are the possible puncture of the gas tank by a large micrometeoroid, and the general effect of bombardment on control system sensors and other components which are directly exposed.

Particle radiation. Shielding is necessary to protect such components or surfaces as are exposed to the bombardment of high energy protons and neutrons. Radiation damage can occur to sun sensors using solar cells, horizon scanners utilizing susceptible optical and detector materials, solid-state electronics, etc. Radiation damage depends on orbit altitude and inclination and must be evaluated.

Other considerations. Other environmental considerations include ultraviolet rays which serve only to increase the rate of sublimation; X-rays and gamma rays which are only significant during solar storms and can be essentially eliminated by the same mechanisms that protect against high energy protons and neutrons; and cosmic flux which appears to be of insignificant consequence in ionization.

Reliability. The degradation of system reliability due to space environment is difficult to predict. The use of failure rate data to assess the reliability of the control system is an important design tool and warrants further consideration. The number of components in the preliminary control configuration can usually be estimated. These estimates then form the basis for a reliability study.

Assume that the failure of a single component will cause the entire system to fail and that the extrapolation from a laboratory environment to an operating space environment can be performed realistically. Even in the event of errors in extrapolation, the relative reliability of different design approaches can still be evaluated.

The failure rate data for some commonly used components are given in Table 9. These data refer to a laboratory environment with an ambient temperature of 30° C and applied electrical stresses of approximately 25% of the rated. In the period between "infant mortality" and "wear out," most components experience a constant percentage random failure rate, λ_c . The probability of a system operating successfully for time, t_1 , is defined by

$$P_s = e^{-\lambda t_1} \quad (156)$$

where

λ = composite system failure rate in space environment

t_1 = length of operating time.

TABLE 9

Some Commonly Used Failure Rates

| Component | Inherent Laboratory Failure Rate Per 10 ⁹ Hours |
|-----------------------------------|--|
| Silicon transistors | 153 |
| Silicon diodes | 51 |
| Resistors (film) | 8 |
| Pots (composition) | 38 |
| Capacitors (paper) | 3 |
| Capacitors (solid tantalum) | 40 |
| Transformer/winding (low voltage) | 10 |
| Relays (DPDT) | 296 |
| Motors and tachometers (ac) | 200 |
| Magnetic amplifiers | 30 |
| Control windings | 10 |

The failure rate data is often expressed in units of frits which are defined as the number of failures in 10⁹ hr. If there is a requirement for a 1-year operation and the system in space environment is assumed to be degraded over the laboratory environment by a factor of 3, the probability of one year's successful operation is then

$$P_{1 \text{ year}} = \frac{\sum \text{frits} \times 3 \times 8760 \text{ hours}}{10^9} \quad (157)$$

2. Control Orientation Methods

This and the succeeding sections define some of the methods, techniques, and problems associated with the design of the attitude control orientation and stabilization system. A most important choice in the early design is the method of obtaining attitude control torques. This section provides brief discussions of the important methods for providing control orientation.

Each method is specifically concerned with the effects of space environment and other changes of momentum the spacecraft may experience. It is important to remember the fundamental differences between torques which are constant in inertial space, always resulting in additional momentum to the system, and torques which are constant with respect to body coordinates and are in many cases cyclic in inertial space. Such cyclic torques do not necessarily require the removal of momentum from the system.

The following items and combinations of them are briefly discussed: (1) methods such as inertial orientation (spin stabilization); (2) the manipulation of the natural forces of space, such as gravity gradient, solar pressure, earth magnetic field, and aerodynamics; (3) the merits of internal rotating momentum storage and mass expulsion. A choice from among the several possible approaches is generally necessary quite early in the design. Special modes, such as separation rate control, acquisition, eclipse, indexing, terminal guidance, etc., may dictate special control requirements. These modes are discussed separately in a later section.

a. Inertial orientation

The simplest means of obtaining control is to spin the vehicle about a known axis. If this axis is either the minimum or maximum principal axis of inertia, the momentum imparted by the spin rate will cause (without the influence of external disturbances) the spin axis to remain fixed in inertial space. If there is no need to orient a particular axis or antenna on the vehicle to the earth and if sufficient energy can be obtained from the sun for electrical power, this method is the simplest. Pioneer V, Explorer VI, Courier, and others have been stabilized in such a manner. The final orientation of the spin axis in space will be the inertial orientation which exists at the time the spacecraft is spun. If there is initial momentum not along the spin axis, the system is stable only if the spin axis is also the axis of maximum inertia. Mercury ring

dampers are sometimes utilized to remove the wobble which occurs due to separation rates and dynamic unbalance effects.

There are several possible control orientations that might be required. Some of the more usual ones are sun orientation and stellar orientation:

(1) Sun orientation. It is possible to orient the spin axis toward the sun. This orientation gives the same power efficiency as an oriented solar array but it could complicate a communication system because of the time-dependent orientation of a body-fixed antenna with respect to the earth. To maintain the spin axis orientation to the sun will require precession of the spin axis at the rate of one revolution per year plus that required to compensate for the regression of the orbit line of nodes. A very simple attitude system can be used to obtain this orientation, if the pointing requirements are not too stringent.

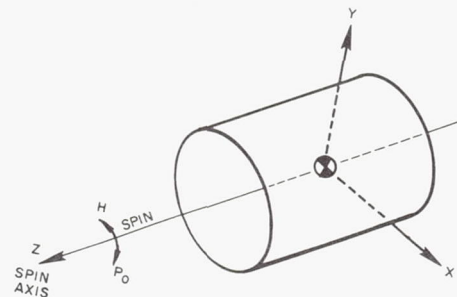
(2) Orbit plane orientation. A spin stabilized satellite with its spin axis normal to the orbit plane can be used for a number of applications, for example, satellites required to photograph or otherwise survey the earth's surface and communication satellites where the antenna provides a toroidal pattern about the spin axis. If the earth-sun line remains normal to the orbit plane, then a high efficiency solar array can be mounted normal to the spin axis. If the inclination of the orbital plane to the ecliptic plane is small, solar cells mounted on a cylindrical surface about the spin axis will operate for the satellite lifetime but provide a maximum power per cell of only $1/\pi \times$ the power per cell that would be achieved with cells in a comparable fully oriented array. If the orbit is unrestricted, then on the average each solar cell on the spinning vehicle will provide only $1/4$ the power per cell of cells in the comparable fully oriented array.

(3) Other orientations. Spin stabilized satellites can conceivably be employed to maintain other orientations than those discussed above. Such tasks as pointing telescopes at fixed stars can easily be performed; however, such requirements are often associated with scientific missions where data transmission considerations require earth oriented antennas for communication, and an oriented solar array for power. These auxiliary tasks cannot easily be performed with a spin stabilized satellite.

Spin stabilization does not appear to be a satisfactory control scheme for earth orientation of an axis of an earth orbiting satellite. Either large torques (large energy expenditure) are required to maintain this spin axis rotation, or internal moving parts such as reaction wheels are required. Torque impulse, if applied properly, will require an energy expenditure of $H\omega$ per revolution where H is the total momentum of the satellite and ω is the average satellite orbital rate. If wheels are used, they must be capable of storing momentum at least equal to the spin momentum; for this reason they introduce significant stability problems and require complex implementation. Other problems, such as achieving the proper initial orientation and devices for damping the nutation must be considered. The spacecraft de-

sign yielding maximum flexibility will not, for most cases, rely on spin momentum for stabilization and orientation.

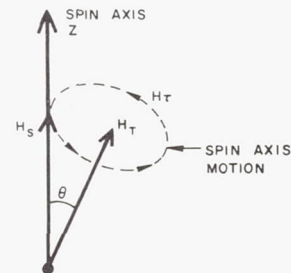
A symmetric body spinning at an angular velocity, p_0 , about either maximum or minimum principal axes of inertia will, in the absence of any external moments, maintain its initial orientation constant in inertial space. If the body total angular momentum vector initially coincides with the spin axis, and if an impulse angular momentum is now added normal to the spin axis, the body spin axis will precess about the new system total angular momentum vector. The rigid body axes are defined in the sketch. The body is considered to be symmetrical about the spin axis.



The motion of the satellite spinning at a constant spin rate in the absence of any external torques will generally be periodic about the spin axis. To simplify the solution of the equations of motion, a complex angular velocity, ω_n , is defined as

$$\omega_n = \omega_x + i\omega_y \quad (158)$$

Substituting this equation into Euler's equations of motion for a rigid body, the solution which defines the frequency of angular nutation is obtained in body coordinates. This means if the total body angular momentum, H_t , is about some other axis than the spin axis, the spin axis will experience nutation (free precession) about the total momentum vector. The following sketch shows the trace of the tip of the body spin axis under such an influence.



A point on the nutating body rotates at a frequency, given by

$$\Omega = \left(\frac{I_z}{I_x} - 1 \right) p_0 \quad (159)$$

where I_z is the moment of inertia about the spin axis and I_x is the moment of inertia about a transverse axis. For an inertial observer watching a fixed point on the body, this frequency is simply

$$\Omega_1 = \frac{I_z p_0}{I_x} \text{ for small } \theta. \quad (160)$$

The half angle cone, θ , for the motion of z is given by

$$\tan \theta = \frac{I_z p_0}{I_x \omega_n}. \quad (161)$$

Passive dampers dissipate energy to remove the nutation (but do not change the system angular momentum) causing the z -axis to be aligned with H_t . Precession of the vehicle angular momentum vector is obtained by application of a moment impulse applied normal to the momentum vector. Any nutation that results from momentum vector reorientation can be damped passively by several schemes and it can also be prevented by proper application of another impulse also normal to the z -axis.

If an impulse is applied normal to the spin axis to cause a precession, then the application of another moment impulse (equal to the first and also normal to the spin axis), after the body has rotated through an angle ϕ given by

$$\phi = \frac{I_x}{I_z} \pi \text{ radians} \quad (162)$$

will eliminate the nutation and will have caused the z -axis to precess through an angle of 2θ . Energy considerations will show that, for passive damping schemes, the moment of inertia about the spin axis must be greater than that about a transverse axis.

The advantages and disadvantages of spin stabilization as contrasted with control of non-spin configurations are presented below.

Advantages. (1) Fixed inertial orientation with limited accuracy can be achieved with a completely passive system; (2) accurate orientation with respect to a fixed star or slowly rotating line of sight can generally be achieved with a fairly simple, lightweight system; and (3) most disturbances including torques from velocity correction jet misalignments have only a small effect on the accuracy of a spin stabilized body.

Disadvantages. (1) Only one axis can be controlled; (2) a complex control system is required to point the spin axis along a rapidly rotating line of desired orientation; and (3) spin speed control may be required on systems where disturbance torques may cause large changes in the spin momentum of the system.

b. Use of natural forces of space environment

This section discusses the major sources of torques which will be experienced by the vehicle

during its lifetime in orbit. These torques may be harnessed for control purposes or treated simply as disturbing influences for which control moments from other sources must be provided. Four major sources of torque which might be used for control are solar radiation pressure, gravity gradient, earth's magnetic field and aerodynamics. Gravity gradient, aerodynamics and earth's magnetic field have their greatest effect at low altitudes; solar radiation pressure is largely independent of altitude, and depends on the spacecraft surface area facing the sun.

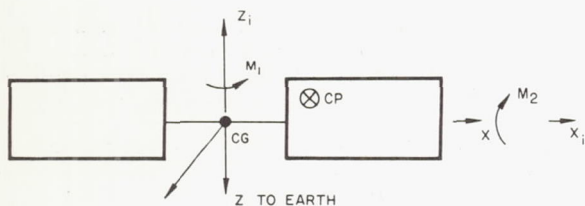
(1) **Solar radiation torque.** The torque due to solar radiation pressure forces acting on a satellite vehicle is significant and must be evaluated. The combined equations necessary to express these torques in the general equations of motion of the vehicle are highly nonlinear. The purpose here will be to discuss briefly the cause of solar radiation torque and its effect on spin stabilized spacecraft and satellites with active attitude control orientation in an earth-sun reference.

Every satellite vehicle is composed of a number of distinct surfaces, each with particular surface reflective properties and characteristics. The bombardment of these surfaces by photons emanating from the sun will create forces on the spacecraft. The magnitude and direction of these forces are determined by the reflective properties of the surface. If the center of radiation pressure through which these forces act is not coincident with the vehicle center of mass, then a torque acting on the vehicle will be developed. This torque may be of sufficient magnitude to affect the control system design.

The radiation power in the vicinity of the earth is $1.94 \text{ cal/cm}^2\text{-min}$ corresponding to a pressure of $9.4 \times 10^{-8} \text{ psf}$ ($4.48 \times 10^{-6} \text{ n/m}^2$) for complete absorption. In preliminary design it is necessary to calculate an upper bound on the radiation torque in order to determine the spacecraft momentum storage requirements for control system design.

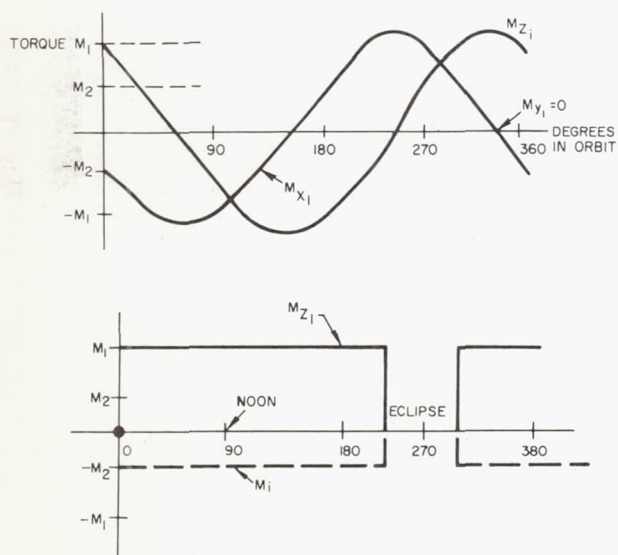
The effect of the solar radiation torque on a spin stabilized satellite depends on the orientation of the spin axis with respect to the earth-sun line and the vehicle projected area facing the sun. The force parallel to the spin axis during one spin cycle will have no net effect on the vehicle. That force perpendicular to the spin axis can create precession of the spacecraft if it does not pass through the center of mass. The nature of the momentum change will depend on the orbit. For example, in a polar orbit (where there is no orbit plane regression) the net momentum caused by this torque will average to zero in one year.

For a fully oriented satellite with sun-earth orientation the torques will depend on the control laws and the inclination of the orbit with respect to the sun. Where the sun lies in the plane of the orbit, the torques in two axes will be cyclic in inertial space except for any rectification because of the constraint of earth orientation. Consider the example where the solar radiation torques are due solely to a solar array, as shown in the following sketch.



The radiation force acts through the center of pressure (CP) and creates constant moments about the z- and x-body axes, M_1 and M_2 respectively. If the z-axis is continuously oriented toward the earth and the sun is perpendicular to the orbit plane, the torques are cyclic in inertial space. For the sun in the orbit plane the moment is constant in inertial space. A plot of these torques in inertial space for orbits possessing inclination with respect to the sun of 90° and 0° is shown in the following sketches.

The solar radiation torque may also be used to provide useful control system torques. It has been proposed to equip the spacecraft with a large weather-vane type of reflective sail and control the vehicle by actuating this sail to create control torques. Such a scheme is difficult to implement and requires special control during eclipse and some form of momentum storage during periods when control torques about required axes cannot be obtained. Figure 27 presents the torque from solar radiation as a function of area and radiation pressure lever arm for total absorption.



(2) Gravity gradient. The earth's gravitational potential varies with altitude. For this reason the center of gravity and the center of mass of a satellite are not exactly coincident. Unless the force of gravity, applied at the center of gravity, acts along a line passing through the center of mass, a torque tending to rotate the satellite will result. This torque can be employed to stabilize a satellite with respect to the earth's gravitational field. The gravitational torque may represent a disturbing input which must be overcome by the satellite control system.

The force due to gravity on a unit mass can be expressed in terms of the negative gradient of the gravitational potential as

$$\vec{F} = -\nabla\left(\frac{-\mu}{r}\right) \quad (163)$$

where

- r = the magnitude of \vec{r} , a radius vector from the earth's center to the unit mass
- μ = the product of the universal gravitational constant and the mass of the earth
- $-\mu/r$ = the gravitational potential, a representation sufficiently accurate for the purpose here.

The torque \vec{M}_g tending to rotate the satellite about its center of mass is then

$$\vec{M}_g = -\int \vec{\rho} \times \nabla\left(\frac{-\mu}{r}\right) dm \quad (164)$$

where $\vec{\rho}$ is a radius vector from the satellite center of mass to the differential mass dm and the integration includes all mass of the satellite. For conditions where ρ is very small with respect to r , a condition always satisfied for earth satellites, the preceding integral expression for torque can be evaluated to yield

$$M_{g_x} = \frac{3\mu}{r_0^3} (\vec{u}_r \cdot \vec{j}) (\vec{u}_r \cdot \vec{k}) (I_{yy} - I_{zz}) \quad (165)$$

$$M_{g_y} = \frac{3\mu}{r_0^3} (\vec{u}_r \cdot \vec{i}) (\vec{u}_r \cdot \vec{k}) (I_{zz} - I_{xx}) \quad (166)$$

$$M_{g_z} = \frac{3\mu}{r_0^3} (\vec{u}_r \cdot \vec{i}) (\vec{u}_r \cdot \vec{j}) (I_{xx} - I_{yy}) \quad (167)$$

where

$$\vec{M}_g = M_{g_x} \vec{i} + M_{g_y} \vec{j} + M_{g_z} \vec{k} \quad (168)$$

and

- $\vec{i}, \vec{j}, \vec{k}$ = unit vectors along satellite principal axes of inertia
- \vec{u}_r, r_0 = unit vector for and magnitude of radius vector from the center of the earth to the satellite center of mass, respectively

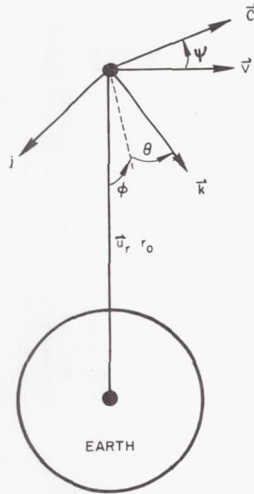
$$I_{xx}, I_{yy}, I_{zz} = \text{moments of inertia about } \vec{i}, \vec{j}, \vec{k} \text{ respectively}$$

Examination of these torque equations shows that all three torque components will be zero when \vec{u}_r is aligned with a principal axis of inertia.

However, a stable torque-free orientation will exist only when the principal axis with minimum

moment of inertia is aligned with \vec{u}_r . Complete stable orientation is possible only for the above condition when, in addition, the axis of maximum moment of inertia is aligned perpendicular to the satellite orbit plane. Gravity gradient torques provide the vertical orientation of the axis of minimum moment of inertia and result in a satellite rotation of the orbit rate. Gyroscopic action tends to orient the axis of maximum moment of inertia perpendicular to the orbit plane and thus along the angular rotation vector.

To establish more clearly the effects of gravity gradient on a satellite it is convenient to consider the satellite in a circular orbit shown in the following sketch. If all error angles are small, then the torque components due to gravity gradient are



$$M_{g_x} = -3\omega_0^2 (I_{yy} - I_{zz}) \phi \quad (169)$$

$$M_{g_y} = -3\omega_0^2 (I_{xx} - I_{zz}) \theta \quad (170)$$

$$M_{g_z} = 0 \quad (171)$$

where ω_0 is the orbit rate. The time rate of change of angular momentum of the system is equal to the applied torque and for small error angles, the angular velocity vector $\vec{\Omega}$, is given by

$$\vec{\Omega} = \vec{i} (\dot{\phi} - \omega_0 \psi) + \vec{j} (\dot{\theta} - \omega_0) + \vec{k} (\dot{\psi} + \omega_0 \phi) \quad (172)$$

The linearized equations of motion for the system become

$$I_{xx} \ddot{\phi} + 4\omega_0^2 (I_{yy} - I_{zz}) \phi = 0 \quad (173)$$

$$I_{yy} \ddot{\theta} + 3\omega_0^2 (I_{xx} - I_{zz}) \theta = 0 \quad (174)$$

$$I_{zz} \ddot{\psi} + \omega_0^2 (I_{yy} - I_{xx}) \psi = 0 \quad (175)$$

where cross-coupling terms have been neglected.

An undamped motion will occur about the orientation where all three error angles are zero if $I_{yy} > I_{xx} > I_{zz}$. In order to stabilize a satellite by use of gravity gradient torque some auxiliary damping system is required. Such damping can be provided by reaction wheels driven from sensors within the satellite.

A more attractive scheme is to provide the necessary damping by passive means such as body flexure, liquid dampers, or passive interactions with the earth's magnetic field. Unfortunately, such passive techniques are not yet completely understood, and at present their design is difficult unless very small damping factors can be tolerated.

The limitations of the usefulness of gravity gradient torque for stabilizing a satellite with respect to local vertical and the orbit plane are:

- (1) Gravity gradient torques decrease with altitude while some disturbance torques (notably solar radiation pressure torques) are invariant with altitude, thus it is difficult to design high altitude satellites to operate primarily with gravity gradient stabilization.
- (2) Orbit eccentricity introduces disturbances in the gravity gradient control which preclude the use of this type of control for highly eccentric orbits.
- (3) At low altitudes aerodynamic torques are encountered which greatly complicate the design of a gravity gradient controlled satellite.
- (4) Satellite requirements such as solar arrays to collect solar energy, communication antenna placement, booms for experiments, and restrictions on configuration for compatibility with the boost vehicle may so constrain the satellite configuration that gravity gradient stabilization cannot be achieved.
- (5) Highly accurate orientation is difficult to achieve since attitude errors must be developed to provide gravity gradient torques to counter disturbance torques.

Gravity gradient torques become disturbance torques when other than local vertical orientation is desired, or when control is accomplished primarily with other techniques such as gas expulsion systems operated from a horizon scanner. In the latter case, gravity gradient torques will generally constitute system disturbances even when the desired orientation is apparently the stable gravity gradient orientation. The active control system will always attempt to align with respect to the control axes, which will coincide with the principal axes of inertia only in the case

of perfect alignment. Furthermore, if a solar array that rotates with respect to the satellite proper is used to generate electrical energy, the principal axis of inertia will rotate with respect to the control axes and an additional system disturbance will result.

(3) Earth's magnetic field. The magnetic field of the earth can be used in conjunction with magnetic rods or current carrying coils to provide control torques. The earth's magnetic field has already been used with magnetic rod arrays to provide "despin systems" on Transit 1B and 2A satellites. It is now evident that a complete control system is feasible based on obtaining control moments from the energizing of satellite-fixed, current-carrying coils. For lower altitudes, the torque obtained from the coils can offset the effects of disturbance torques without large expenditures of power or extremely weighty coils. For designs utilizing other torquing schemes it is imperative that care be taken to reduce the magnetic moment of the spacecraft so that magnetically induced disturbance torques are not significant.

All the factors contributing to the earth's magnetic field are not well understood, but it is clear that for satellites greater than 100 mi above the surface of the earth, circulating currents in the atmosphere and surface field irregularities do not significantly affect the approximation of a field which will be produced by assuming a simple magnetic dipole at the center of the earth.

The axis of this dipole, which best represents the magnetic field, is skewed at an angle of approximately 18° with respect to the earth's spin axis. The North Magnetic Pole is at approximately 70° N Latitude, 97° W Longitude. The South Magnetic Pole is at approximately 73.5° S Latitude and 155° E Longitude. This means that the axis of the dipole, and hence the field, precesses around the earth's spin axis. This precession is significant and means that only in orbits which are synchronous with respect to the earth's spin will the effects of the magnetic field be the same during successive orbits or sets of orbits (depending on the synchronous period). Only in a 24-hour orbit which contains the dipole is it impossible to generate torques for complete three-axis control. In general, the field will vary constantly with respect to system axes. In any one day (due to the field's precession about the earth's spin axis) it appears possible to generate control torques about all of the required control axes. These torques may not be available at the instant they are required, suggesting the requirement for momentum storage. Further, the magnitude of the field is different on each successive orbit, depending on the altitude, inclination, eccentricity, time of launch, point of injection, control axis orientation (control laws) etc. Knowledge of the field magnitude and direction is essential to the proper energizing of coils and must be supplied either by computation or measurement. The data essential to the preliminary designer is the magnitude of the field as a function of altitude and variations typical of those which will be experienced in the particular orbit. Figure 28 shows the total magnetic field as a function of altitude for the dipole representation.

A current carrying coil in the magnetic field tends to assume a position that will result in the largest possible flux through it in a positive sense. That is, the force F on an element of wire in a flux field, B , is given by

$$\vec{F} = i \, d\vec{l} \times \vec{B} \quad (176)$$

or a coil whose center is along the spacecraft z-axis would cause the spacecraft to experience a torque, \vec{M}_m in dyne-centimeters of

$$\vec{M}_m = \frac{\pi r_c^2}{10} n (\vec{u}_x B_y + \vec{u}_y B_x) \quad (177)$$

where

\vec{u}_x and \vec{u}_y = unit vectors along x and y spacecraft axes respectively

r_c = the radius of the coil in centimeters

i = the current in amperes

B = the flux density in gauss

n = the number of turns.

It is interesting to note that 0.1 gauss acting normal to a 10-turn coil of No. 14 (standard household wiring) copper wire 1 ft in (0.3 m) radius (weight less than 1 lb (4.4 newtons) without supports) when energized with 1 w will produce a torque approximately 5.8×10^{-5} ft-lb. (7.9×10^{-5} m-newtons) This is potentially an extremely attractive torque for control. This torque is about an order of magnitude above that anticipated for either solar radiation or gravity gradient with reasonable design practices. The magnitude of the control torque obtainable for a coil with a 1-ft (0.3 m) radius over the magnetic equator is plotted in Fig. 28 as a function of altitude.

There are some interesting tradeoff studies between weight, power, wire size, and the use of materials that can be considered. For example, for a circular coil the torque in a constant field is equivalent to

$$\text{Torque} = k_1 P^{1/2} W^{1/2} R \rho^{-1/2} \quad (178)$$

k_1 = constant of proportionality ($i = 1, 2, 3$)

P = applied power

W = weight of the coil

R = radius of the coil

ρ = relative resistivity of the material.

The most significant increase in torque is obtained with larger radius coils. Larger coils of the same size wire with the same power show

$$W = k_2 R$$

$$T = k_3 R^{3/2}$$

A knowledge of the variations of the earth's magnetic field along the orbit is important. The combination of nodal regression, dipole axis precession, and orbit period means that the flux will vary each revolution and is different from time to time, except for those that have a period which is a multiple of the earth's spin rate. The variations of the flux density in an inertial coordinate system are plotted as a function of time for orbit inclinations of 0°, 30°, 60° and 90° for two consecutive orbits of 400 naut mi (741 km) in Fig. 29. The inertial coordinate system for these plots has the x-axis along the earth-sun line at the vernal equinox, the z-axis essentially along the positive earth spin vector, and the y-axis to form the right-handed set. To see the effectiveness of control, the component of flux density along the earth's local vertical is plotted as a function of time for the 400-naut mi orbit in Fig. 30.

For the purposes of calculation, the earth's field can be simply expressed in terms of the axial and normal component from the earth's magnetic dipole. The equations are

$$H_{\text{axial}} = 0.308 \frac{(1 - 3 \cos^2 \delta)}{(r/R)^3} \quad (179)$$

$$H_{\text{normal}} = 0.461 \frac{\sin 2 \delta}{(r/R)^3} \quad (180)$$

where

H_{axial} and H_{normal} = the components of field intensity in oersteds

δ = the angle between the earth's magnetic dipole axis and the radius vector to the satellite

r = the radius vector to the satellite from the center of the earth in centimeters

R = the radius of the earth (6.371×10^8 cm)

If the dipole is aligned along the earth's spin axis (a reasonable assumption for preliminary calculations), then the latitude, L , is equal to $(90 - \delta)^\circ$. Figure 31 shows the total magnetic field $(H_{\text{axial}}^2 + H_{\text{normal}}^2)^{1/2}$ as a function of latitude for this assumption.

Some of the limitations and considerations on the usefulness of earth's magnetic field for stabilizing a satellite are:

- (1) Since the torque generated is always about an axis perpendicular to the earth's field, only two axes can be controlled at once. It is necessary to add devices such as inertia flywheels or gyros to store the momentum along the axis which cannot be controlled until the spacecraft reaches an orbit position where the momentum may be magnetically transferred from that axis.
- (2) The magnitude of the control torque must be greater than the sum of the internal and external disturbance

torques. It is not difficult to achieve fairly significant control torques at altitudes up to 10,000 mi. (16,000 km)

- (3) The earth's field in body coordinates is continually changing. In-flight computation based on this field must be performed or the direction of the field must be sensed in order to determine proper current patterns required by the coils. This might be done using magnetometers as magnetic field sensors and primary orientation signals obtained from earth local vertical sensors, sun sensors, or star trackers and others.
- (4) The stability of a system using body-fixed coils in the earth's magnetic field is questionable because of the difficulty imposed by the inherent cross-coupling torques due to the action of the magnetic field on the coil. Current carrying rods or sheets may provide one solution. Another possible solution would be to use the magnetic field to induce momentum in a controlled way by providing eddy current damping to the momentum wheels. Unfortunately the amount of momentum imparted to the body by this method is, for practical purposes, quite low.

(4) Aerodynamic torques. The earth satellite in a low altitude orbit, or with a low altitude perigee, will experience aerodynamic forces during its lifetime. The nature of these forces, depending on the orientation of the vehicle and its altitude, may be of consequence and may require an expenditure of a significant amount of control system momentum. In fact, for some extremely low altitude satellites, certain proposals have been made to use the aerodynamic torques through a large rudder or actuating trailing drag device to obtain control torques. Since somewhat higher altitude satellites are being considered here, the aerodynamic torque will be treated as a disturbance torque with simplified methods for computing its effects.

Knowledge of the density of the upper atmosphere is constantly improving. The ARDC 1959 Atmosphere, which is frequently used, represents the average density when perigee is in twilight near the time of a sunspot maximum. The density can vary considerably from the ARDC 1959 model.

"Hyperthermal free molecule" flow theory is generally used to obtain the shearing and normal stresses on the various flat surfaces of a space vehicle. Although this theory has been adequately described, two important criteria associated with it are worthy of note.

- (1) The mean free path of the air molecules must be many times greater than the size of the body moving through the air. In the vicinity of the body, the frequency of collisions between air molecules is negligible relative to the frequency of collisions between the molecules and the body surface. The above condition

is realized for most spacecraft since at an altitude of 150 mi (280 km), the mean free path of free stream molecules is approximately 1000 ft (300 m) whereas the largest body dimension is usually less than 15 ft. (5 m)

- (2) The term "hyperthermal" implies a vehicle speed much greater than the mean free stream molecular speed. The orbital speed of spacecraft at 150 mi (280 km) is roughly an order of magnitude greater than the mean molecular speed, and hence, the hyperthermal condition is deemed acceptable.

The equations which describe the pressure, P , and the shearing stress, S , are

$$P = 2(2 - \sigma') q \sin^2 \beta \quad (181)$$

$$S = 2\sigma q \sin \beta \cos \beta \quad (182)$$

where the pressure, P , acts normal to the surface and the shearing stress, S , tangent to the surface in the direction of the normal projection of the velocity vector on the surface. The angle of attack, β , may be expressed in terms of the yawing angle, ψ , for the body surface. Hence, $\beta = \psi$ and $\beta = 90^\circ - \psi$ for surfaces whose normals are along the y - and x -body-axes, respectively (see sketch Section D.1.). It can be shown for the solar array that $\sin \beta = \sin \psi \cos \phi_p$. The previous angle

relations are valid only when the velocity vector lies in the x_b, y_b plane. Computation of force on the body and array surfaces as a function of β or ψ and ϕ_p is a straightforward process provided the surface area is known. The question of surface area arises when it is realized that at most yaw angles the leading paddle partially shades the body and portions of the body partially shade the trailing paddle from possible molecular collisions. As a result, shading factors must be calculated. Since for this type of flow the center of pressure is essentially at the center of the exposed surfaces, it is necessary to calculate the latter in conjunction with the shading factors.

The two quantities, σ and σ' , respectively, defined as the surface reflection coefficients for tangential and normal momentum exchange, have a significant influence on the magnitude of the pressure and shearing stress. The nature of the molecular re-emission, and hence the value of σ and σ' , are functions of the type of surface material, the velocity angle of incidence, and the wall temperature. The value of σ and σ' can vary between 0 and 1. The few measurements made on typical engineering surfaces indicate values of σ between 0.8 and 1.0. For low angles of attack it appears that the characteristic of re-emission may be altered sufficiently to cause considerable deviations of σ' from these values. The quantity, σ' , had not yet been measured experimentally; however, the values of σ and σ' should not differ greatly. The surface interaction experiments which have been conducted imply that most molecules do not rebound in billiard-ball fashion, i.e., with the angles of incidence and reflection equal, but that they are diffusely scattered due to

- (1) physical roughness of the surface, and (2) temporary trapping on the surface. The effect of changes of these coefficients on the maximum disturbing moments must also be considered in the design until better data are available.

For preliminary design, an approximate maximum moment due to aerodynamics for a spacecraft similar to that shown in the sketch of Section D.1. can be computed quickly. Compute the offset of the center of area from the center of mass and the exposed area for the β or b 's which appear critical. The torque due to drag is simply

$$M_D = C_D L_D A q \quad (183)$$

where

C_D = the drag coefficient or $2(2 - \sigma')$

L_D = the assumed center of area offset from the center of gravity

A = the total area bombarded by molecules

q = dynamic pressure at the spacecraft altitude equal to $1/2 \rho v^2$.

If aerodynamic torques are a problem, the length, L_D , which is determined by the center of area normal to the airstream, must be closely controlled.

If the yaw angle is such that the spacecraft does not shade impinging molecules from one paddle, then no net equivalent lift torque is experienced. However, there will be a torque if the yaw angle is such that one of the paddles is shaded. The moment which tends to rotate the body about the axis is given approximately by

$$M_L = C_L (1 - f) L_L A_p q \sin^2 \psi \cos^2 \phi_p \sin \phi_p \quad (184)$$

where

C_L = lift coefficient or $2(2 - \sigma' - \sigma)$

L_L = the distance of center of solar paddle area from center of vehicle mass

f = the shading factor on one paddle

A_p = the area of one solar paddle

ψ = the angle with respect to the velocity vector (yaw angle)

ϕ_p = the solar array angle.

This expression is not evaluated since the shading factor is also a function of ψ and possibly ϕ_p . The equations presented for these torques are approximate and are presented only to allow a rough determination. Different equations, of course, must be derived for other configurations and, in any event, a more refined analysis of these torques should be performed if a problem area is suspected.

c. Use of momentum storage devices

The use of rotating devices to provide momentum storage in a spacecraft has been described extensively in the literature. Such devices are generally used to continuously absorb the effect of disturbance torques, to store momentum due to orbital rate, and to perform special control maneuvers. Constant speed rotating inertial devices may be used to change the gyroscopic coupling torques about a particular axis or axes. In designing a system for momentum storage, it must be remembered that the momentum storage requirements are determined by inertial torques as they appear in body axes. A constant external torque with respect to inertial space will change the total momentum of the system, and hence the storage requirements will increase with time. However, disturbance torques which are fixed in the body may require momentum storage that is cyclic in inertial space, dependent on the orientation of the body axes with respect to inertial space. Understanding the relationship of the inertial and body reference frames is a fundamental point in determining how stored momentum must be handled. For example, assume a spacecraft is to rotate uniformly in such a way as to point to the earth as it progresses in orbit; to do so requires a rotation of 360° per orbit. In the absence of any applied torques, the stored momentum of the system will remain constant with respect to inertial space. In general, at any point in orbit, the momentum can be considered to be stored in three-body-fixed wheels whose axes may not coincide with the inertial frame. In such an instance the wheels will change speed continuously in order to transfer momentum from one body axis to another (although the momenta are fixed in inertial space) in order that at every instant the sum of the individual momenta will equal the total constant momentum.

The effectiveness of reaction wheels is based on the law that the time rate of change of wheel momentum is equal to the torque. The attitude error signal is used with filtering to control the wheel speed, meaning that for nonzero constant momentum storage there must be an angular pointing error. Integral control can be used to alleviate this problem in the steady state. Since most momentum storage devices are limited in their storage capability, momentum storage may be used in conjunction with momentum expulsion devices to allow operation beyond the capability of the storage device for removing the momentum. Such systems then combine the most useful function of the momentum storage (to absorb continuously without extreme energy expenditure the momentum imparted by disturbance torques and orbital maneuvers) and that of the mass expulsion system (to remove momentum from the system only when it saturates the storage device).

The momentum storage system adds complexity to the system. If the problem of coupling between axes is significant, careful design will be required. Methods proposed for obtaining momentum storage include rotating inertia (a motor-driven inertial flywheel, gyro stabilizer gimbaled gyroscopes) and the control of the motion of a fluid moving in an enclosed circuit. In an attempt to reduce the cross-coupling terms, a free sphere has been

proposed. The present satellite designs generally use the single-axis, motor-driven flywheels.

d. Use of mass expulsion devices

The attitude control of a spacecraft with initial rates in the presence of an external torque field can be simply achieved through the use of a variety of mass expulsion devices. The actuation of such devices will be controlled by the output of a sensor and used to change the angular rate of the spacecraft to keep it within some attitude error limit or to precess the spin axis of a spin stabilized spacecraft. The mass expulsion system may either produce a torque proportional to the error signal or produce quantized torque levels for controlled periods of time to maintain the vehicle angular momentum below some prescribed limit.

The governing problem in design is the trade-off between weight and reliability. The simplest system is the single level thrust, on-off system used to maintain the spacecraft attitude error and error rate within certain limits. The impulse required for such systems is a direct function of the limit cycle rate, the lowest value of which is determined by such parameters as rate gain, position gain, filtering, sensor noise, valve actuation hysteresis, valve time delay, thrust build-up and decay characteristics, design thrust level, etc.

The use of cold gas such as dry nitrogen with nozzles and regulators designed to produce thrusts of the order of 0.1 to 0.001 lb (.4 to .004 newtons) is acceptable for most present spacecraft weights and lifetimes. Of course, larger thrusts will be required to provide control moments for large satellites or during periods when the booster stage is attached to the spacecraft or when misalignments of the thrust used for midcourse corrections require a larger control authority to overcome overturning moments. Hot gas systems will have a specific impulse considerably greater than that of the cold gas; however, problems associated with multiple starts, obtaining the low-thrust level, and thrust characteristics may not make such a system attractive except where larger thrust levels are required.

The on-off system, when used as the only means of obtaining control torques, requires a significant amount of impulse for long-term operation. If thrust is made proportional to the attitude error (such as is possible with proportional jets) it will react to disturbance torques continuously except when operation is within the low signal nonlinearities of the valve. The continuous operation in response to cyclic disturbance torques will also require a large expenditure of impulse over a significant lifetime. A more suitable design for long lifetime missions will be to expend electrical power (which can be replenished easily using solar cells) to control body-fixed reaction wheels in response to the angular momentum changes. The mass expulsion system would only be used to remove the effects of secular torques.

The development of more efficient, higher impulse systems such as plasma, ion and vapor propulsion is necessary for propulsive systems

in satellites which must achieve the longer lifetimes of several years--probably a requirement of the near future. With these systems, a significant weight advantage will be obtained if their reliability is acceptable.

Proportional and simple on-off controls have been mentioned as possible means of obtaining control torques without any additional torque-producing requirements. Other schemes have been proposed. One reduces the gas required by a simple on-off single level thruster by using the flexibility of a two-level thrusting system. Such a system, if properly designed, does not require rate information for stable operation. Another method with some advantages is modulation of the pulse duration applied by a single level jet as a function of the error signal. This system is also stable without rate information.

e. Combination systems

Momentum expulsion and momentum storage devices can be designed to complement one another. The storage device will control or store momentum due to cyclical torques on the spacecraft without gas expulsion and the jets will overcome long-term constant disturbance torques by periodically desaturating the storage device by expelling mass from the spacecraft. The jets will be needed also to counter initial body attitude rates, when the vehicle is separated from its booster, and perhaps torques produced by rocket thrust misalignment during guidance maneuvers.

The desirability of such combined systems will be determined on the basis of the factors of weight (including power consumption) and reliability for a given lifetime.

3. Methods of Attitude Sensing

The purpose of this section is to examine important methods which could be used for sensing the attitude of spacecraft from which attitude error signals can be generated. Basically, the methods will include earth, sun and stellar sighting, the use of inertial instruments, and the use of ambient fields.

a. Earth horizon sensors

The achievement of many earth orbiting missions will require the spacecraft to point one axis along or at some preset fixed angle with respect to the earth's instantaneous local vertical. There are a number of earth sensing devices, generally referred to as horizon scanners, which may be employed for this purpose. Horizon scanner operation depends on the detection of the difference in radiation emitted or reflected by the earth and the earth's atmosphere, and the radiation emitted by free space. The radiation emitted by the earth and the earth's atmosphere approximates black body radiation at a temperature which varies from 220° K to 280° K. In addition to the emitted radiation, the earth reflects solar radiation dependent on the relative earth and sun positions. This discussion will be confined to devices which utilize only earth and earth's atmosphere emitted radiation and thus capable of both night and day operation.

A horizon scanner consists of four basic parts: an optical system; a scanning system; a radiation detector; and an information processing system. The optical system's principal function is to concentrate the energy in the optical field of view onto a suitable detector system. The scanning system moves the optical field of view in some precise manner relative to the spacecraft. The radiation detector may be a single element or system of elements which are sensitive to the radiation to be measured. The information processing system contains the logic circuitry necessary to provide proper error signals to the control system.

There are basic limitations to the accuracy of horizon scanners which are dependent on the altitude of the spacecraft relative to the earth. The limitations involve the shape of the earth, and the variations in the earth-space radiation difference. By proper selection of the radiation spectra used by the detector and scanning mechanism used to locate the earth, these inaccuracies may be minimized.

The most widely accepted detector for application in horizon scanners is the thermistor balometer. This device has substantially a flat spectral response from ultraviolet to the far infrared and, for uncooled detectors, exhibits the best detection in the infrared spectral range. The precise spectral range for detector operation is determined by the selection of elements in the optical system.

The method used for scanning depends upon the orbital parameters of the spacecraft mission, overall system accuracy, and the requirements for earth acquisition.

There are three principal types of scanning techniques: a fixed field of view continuously scanning in a cone; an edge tracker system which locates and tracks the horizon in a fixed plane; and a passive scanner which utilizes a wide field of view imaged on a detector array. There are other scanning systems which will not be discussed, such as a rosette scan pattern or the possible use of image tube techniques for electronic image plane scanning.

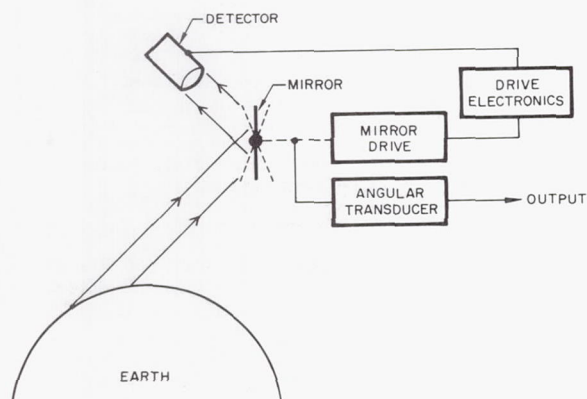
(1) Conical scanning. Figure 32 depicts a typical conical scanner system (two scanners) in normal operation. The optics for each scanner consists of a prism and lens system which causes the field of view, focused on the detector, to scan in a circle in some fixed half-angle cone by continuous rotation of the prism.

A schematic of the scanner optics is shown in Fig. 32b. The detector output signal for each revolution of the prism is shown in Fig. 32c. Each scanner controls one of the vehicle axes. The control signal is generated by sensing the width of the balometer output pulse on either side of a reference signal, which is aligned with the vehicle control axis. Referring to Fig. 32d, the vehicle is aligned in roll when A-C is equal to C-B. Control relative to two axes may also be obtained with the same type of scanners in alternate scan orientation. Referring to Fig. 32e, the vehicle is aligned in roll when A-C is equal to C-B, and aligned in pitch when A-B is equal to A'-B'. This

type of scan technique is best applied to spacecraft missions which have nearly circular orbits. Since the scanner is generally best designed for operation over a limited range of altitudes, the large variation in the ratio of earth-to-space return signals obtained in highly eccentric orbits will create a special design problem if accuracy is required.

The conical scanner can be designed also to operate with a half-angle cone equal to 90° . Two such scanners would control a spacecraft in two axes in the same manner as the scanner described above, where the axes of rotation of the prisms are normal to each other. The scan pattern would appear similar to Fig. 33 except the scans would intersect along the vehicle yaw axis, coincident with the local vertical when no spacecraft pitch or roll attitude error exists.

(2) Edge Tracking. The sketch shows a schematic of a single edge tracking horizon scanner. This scanner uses the detector output to drive a mirror. The field of view of the mirror is continuously oscillated through some small angle in a plane independent of the mirror drive. The mirror drive is nulled when the detector output is a square wave, which indicates that the mean position of the small oscillation of the field of view, and hence the mirror, coincides with the earth horizon.



The field of view of the mirror may be oscillated by many techniques--for example, by oscillating the mirror as shown in the figure, or by interrupting the incoming radiation with a shaped reticle. Figure 33 indicates how three-edge tracking scanners may be used to generate spacecraft pitch and roll control signals. The angle of each mirror is measured relative to a vehicle reference axis. The field of view of each scanner searches in a fixed plane relative to the spacecraft. The pitch and roll attitude error signal may be generated by processing the difference in the angles measured by trackers A and D, and the angles measured by trackers A and B. A fourth tracker, C, may be used to provide the redundant error signals.

(3) Passive scanner. A simple example of a passive scanner is shown in Fig. 34. A wide-angle lens system images the earth's radiation on a detector array. The control error signals are obtained by differencing the detector outputs. This system is only workable for spacecraft missions with near circular orbits, since the detector array must be sized for a near constant size earth image.

Other passive scanners might include electronic imaging tubes and simple shadow bar techniques for operation at extreme disturbances.

The scanners also suffer from the problem of sun interference. The presence of the sun with its high energy in the balometer field of view for extended periods will cause erroneous signals to be generated and may possibly damage the detector. Means of determining the sun's presence and eliminating its effect on the control signal must be provided. The passive scanner with its large field of view will contain the sun more during orbital life than the other scanners. During this time the scanner must not only be made inoperative but, in order to protect the detector system from damage due to solar radiation, some positive filtering of the sun's energy must be accomplished.

b. V/H technique

The V/H technique, as applied to attitude control, is described in Ref. (8). The V/H technique is also a potentially accurate navigation system for close orbits of a planet. From correlation of stored strip pictures of the expected track of the vehicle and real-time pictures taken from the satellite, deviations from the desired orbital position could be determined. Velocity information could be obtained by correlating two successive pictures taken with a fixed time delay.

Basically, the method consists of measuring the ratio of satellite velocity (V) to altitude (H) by the use of the following equation:

$$\frac{V}{H} = \frac{\dot{\alpha}}{\cos^2 \alpha} \cdot \frac{\dot{H}}{H} \tan \alpha$$

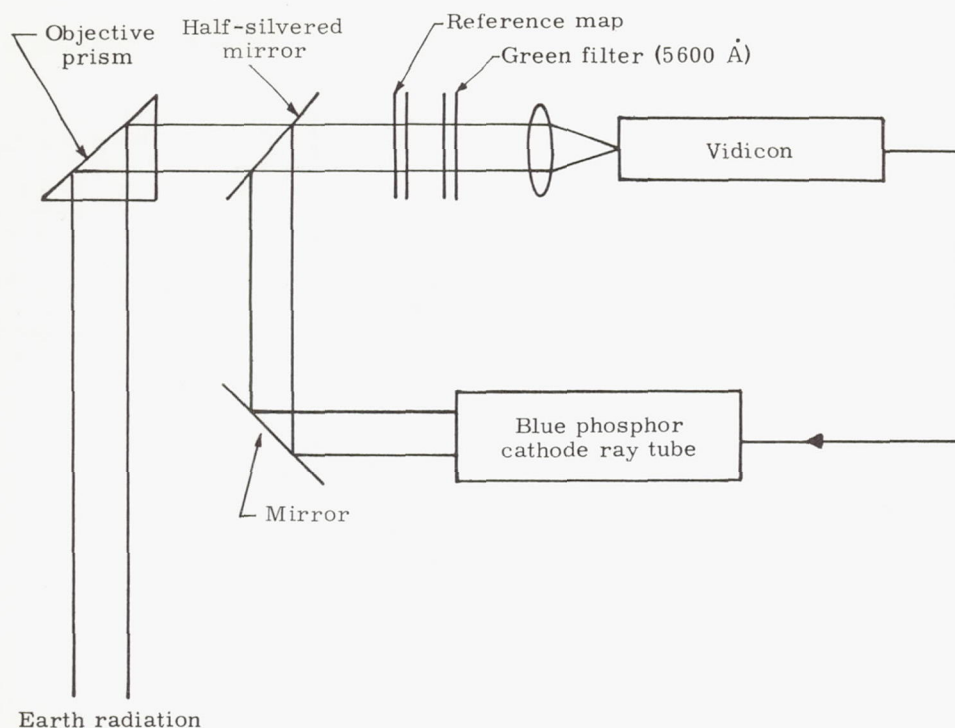
where α is the angle between some object on the ground and the vertical. This is mechanized by correlation of video signals from successive frames of a vidicon. Image velocity V' is directly proportional to V/H .

$$V' = H' \cdot \frac{V}{H}$$

where H' is the focal length of the instrument.

A mechanization diagram of the optical correlator for the V/H orbital guidance system is shown in the following sketch.

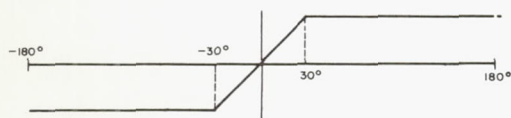
The reference map is formed electronically by exciting an optically thin CdS (cadmium sulfide) film by a long persistence blue phosphor light, thus creating a pattern of absorption. The blue phosphor light renders transparent object areas upon illumination. The CdS film must be of sufficient thickness to provide a volume absorption which would prevent obtaining false results. False results would be obtained if the film were not thick enough, and some unmatched part of the scene would have greater transmitted brightness than the correlation peak. The optimum film thickness should be obtained by experimentation. The green emission is eliminated by the green filter, and the transmitted light will have the characteristic of two patterns multiplied together. When this distribution is integrated, the correlation function is formed except that some background level will be transmitted. However, the peak will exist and can be detected.



c. Sun sensors

The sun is an excellent reference for many satellites in that fairly simple sensors can be used to attain both a measure of yaw orientation and, if a rotatable solar array is used, solar array orientation. Spacecraft for solar experiments will use such devices for orienting along the sun-line. The principal problem with sun sensors occurs when the vehicle is in eclipse and such sensors can no longer be used. As will be indicated later in the discussion of modes of attitude control, several steps may be taken to minimize effects of such a problem.

The simplest form of sun sensor employs photovoltaic solar cells. These cells can be used in a variety of ways to provide angular error information. For most applications the linear range is limited to ± 20 to 40° with a saturated output over the rest of the 360° . The following sketch illustrates such a characteristic.



If relatively high accuracy is required, a device similar to that indicated as yaw scanner in Fig. 35 will, by measuring dwell amplitude on the scanning mirror, give about 0.05° for linear ranges up to 10° . (A reduction in accuracy will be imposed if greater linear ranges are required.) If accuracies no better than about 0.5° to 1° are of interest, then the extremely simple shadowing array such as the array orientation sensor, one-half of which is shown in Fig. 35, or the T-bar arrangement shown in Fig. 36 may be employed. It should be noted that such devices are subject to null shifts and gain variation, due to the difference in thermal properties of the cells.

A relatively new method of sun sensing is the use of a spot position transducer. This device is a solid-state transducer whose output is sensitive to the position of a light spot on its surface. This transducer converts the light-spot x and y displacement into a pair of voltages V_x and V_y proportional to the displacement. The displacements are referred to the cell center where x , y , V_x and V_y are all zero. By using a simple lens, the sun may be imaged on the transducer. A function of the angular position of the sun is then obtained in the two axes normal to the position of optical axis of the system. The linearity and accuracy which may be obtained with this device are determined by the sophistication employed in the optics and the desired field of view.

Many systems are available for measuring deviations from the sun. The three presented here represent only a very small sample.

d. Gyro mechanisms

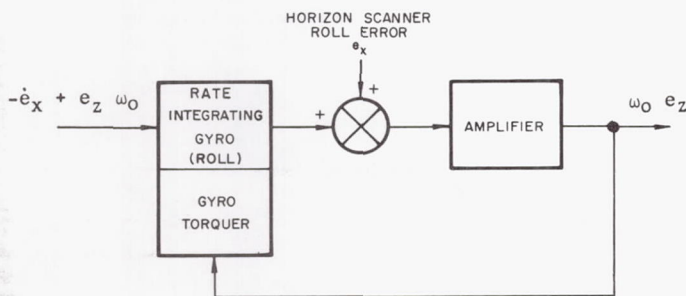
Error signals for control to an inertial reference can be provided by gyro mechanisms. Both single-degree-of-freedom and two-degree-of-freedom gyros could be used for this application. For long term operation, gyro drift will cause major attitude reference errors unless means for resetting the gyro and/or in-flight calibration to eliminate drift are incorporated. This might be done with information derived in the vehicle with relationship to stars, sun, etc., or on ground-command based on ephemeris or telemetry data.

One means of determining spacecraft error from the orbit plane is to operate a gyro whose input axis is to be aligned in the orbit plane in a rate mode. Such a gyro, if not oriented in the orbit plane, will sense some fraction of the orbital rate of the earth-oriented vehicle as it proceeds in its orbit around the earth. The use of this rate essentially provides a gyrocompass

scheme for determining orbit plane reference above very low altitude orbits where the orbital rate is high. Such a system has practical difficulties. Compensation will be required for the spacecraft rates in roll (or pitch) which will also appear in the output of the gyro. The drift characteristics and basic accuracy of the gyro limit the ultimate accuracy of the system. For a small input axis alignment error, e_z , the gyro output, \dot{e}_g , will be the component of pitch and roll rate, \dot{e}_h , along the axis plus the component of orbital rate, $\omega_0 e_z$.

$$\dot{e}_g = \dot{e}_h + \omega_0 e_z \quad (185)$$

By properly introducing the component of error due to input other than orbital rate, e_h , (see sketch) the output of a rate integrating gyro in a rate mode can be approximately that of the component of orbital rate. For convenience, the roll axis is to be aligned in the orbit plane. Thus e_h becomes e_x . Note that the noise introduced from the sensed motions about the roll axis may be significant, and if the orbital rate is too low (reduced as a function of altitude) the system is impractical.



The use of the gyrocompass technique as standard practice requires additional power for temperature control, and is subject to the long term reliability problems generally associated with most gyros.

Other schemes for orienting the body with respect to the orbit plane should be studied. It is possible to use ephemeris data, from which sun/orbit plane orientation with respect to one another can be predicted. This, combined with the control laws, will provide knowledge of the satellite yaw attitude with respect to the orbit plane. Sun sensors can be used to determine when the spacecraft is in the noon, or near-noon, condition (that is, when the solar array goes through 0°). At this time the vehicle yaw angle is known and can be used. A gyro will maintain inertial orientation about the yaw axis and additional commands are necessary only to remove the errors due to gyro drift and to the regression of nodes.

e. Celestial observations

The star field may be used in two ways for the orientation of the satellite. First, a particular star might be used as the sun or the earth are used to maintain a fixed orientation with respect

to that star. (In the case of complete star orientation perhaps two or more stars may be chosen for such an orientation.) Secondly, the star field of motion as observed in the vehicle can be used to measure the rate of change of the vehicle.

(1) Attitude. Sighting on distant stars may be used with an inertially established frame of reference to achieve initial alignment of the references or to prevent long term drift, if necessary. It is possible to use optical sightings, such as a telescope, or even the radio frequency noise sensed by a radio-telescope. The two severe problems encountered in the use of celestial sensing are the acquisition of the star, and the amount of computation required to transform the star reference set of axes into the appropriate vehicle control error signals. One excellent way in which a star may be used to obtain continuous or intermittent information without complicated computation is in orbits where a pole star is available. A very good application of this method is in an earth equatorial orbit. Actually, any inclined orbit about a spherical body with a pole star would be acceptable, but, because of the regression of the line of nodes due to the earth's oblateness, computation is required for most earth-orbiting vehicles. The tracking of stars with high precision telescopes and very accurate telescopic drives is necessary to obtain exceptional accuracy. Of particular interest is the Orbiting Astronomical Observatory which is under development by NASA, in which absolute sensor accuracies on the order of seconds of arc are required.

(2) Attitude rate. Considerable interest has been expressed in what are often called "celestial driftometers." A telescope or some other optical means is fixed relative to the axes of the satellite and drift velocities of the stars across the field are measured. From this, one can obtain a component of the angular velocity of the star field relative to the vehicle which is then a component of the angular velocity in inertial space. The main purpose for this device is to provide rate measurements for precise control with respect to the orbital rate vector.

f. Other ambient field sensors

It is possible to obtain certain information about the vehicle's orientation in space through the use of ambient fields other than those previously discussed. Fields which can be used appear to be the gravity field, the magnetic field, and, for extremely low altitude orbits, the atmosphere. It has been suggested that if cosmic rays are directional in space, the gradient in its intensity may be used as a sensor.

(1) Gravity gradient. A vehicle will tend to align its axis of minimum inertia along the local vertical to the earth, and its axis of maximum inertia normal to the orbit plane, due to the effect of the gravitational field. This effect acts as a torque which provides control, and also as a sensor of direction of the gravitational potential. In other words, the restoring torque appears in the equations of motion as if it had been introduced by an independent control system operating on

external information. It is also impossible to imagine instruments constructed such that they would operate independently on the gravity field to determine the direction of the local vertical. Such instruments have been mentioned as possibilities, but none have been given serious consideration. The two possible types are the pendulum type, utilizing two pendulums forming a dumb-bell free to turn about one axis, and the other involving the use of accelerometers operating differently to provide a direct measure of the gravity gradient.

(2) Magnetic fields. The earth's magnetic field could conveniently be used as an orientation reference for satellites in near-earth orbits. This is reported to have been done in Sputnik III. Moreover, it seems that the magnetometers could be put to good advantage measuring the magnitude of the earth's magnetic field. The primary difficulty is not so much one of the inherent measuring capability of the instrument itself, but of measuring the precise direction of the magnetic field with respect to the vehicle in its orbit because of heterogeneities in the earth's field, ionospheric currents, geomagnetic storms, and fields present in the spacecraft itself. However, if magnetic torques are to be used to advantage, some measure of at least the direction of the magnetic field must be obtained.

(3) Atmosphere. In any low altitude orbit it may be possible to use such devices as are employed in airplanes, missiles, etc., which are most sensitive to the very nearly negligible atmosphere. For example, a weather vane might provide information about the relative winds for one set of axes. Using an extremely sensitive pressure device would allow the nulling of such pressures to achieve appropriate orientation. However, the pressure at the altitudes above 100 mi suggests that, at present, this is an impractical approach.

(4) Other ambient fields. Natural radiation such as cosmic rays, micrometeoroids and ion streams could be exploited for the use of attitude control system sensors. Most of these devices, however, appear to present no advantage over those being used and are not receiving a great deal of consideration. For example, the direction of the spacecraft velocity can be determined by the relative bombardment of charged particles with respect to the body axis. Ion "traps" flown on Explorer VIII have indicated that sufficient current can be obtained to orient the vehicle relative to the velocity vector. The accuracy of a system using ion traps will probably be below that of optical systems, but it may find application when other sensors are inoperative due to occulting of the sensed body.

Another potential method would include the use of radio techniques wherein the difference between the received signals of two antennas would be a measure of the attitude error in a plane containing the two antennas. This differencing could be obtained electrically in the spacecraft or through the use of interference techniques. An additional method might be the use of return signals from a body which is receiving the output of a satellite-contained radar. Such schemes

have been proposed for the landing of spacecraft on distant planets, as well as for achieving some measure of stabilization information at low altitudes.

4. Modes of Attitude Control

This section will discuss some primary modes of operation that are generally necessary in order that the spacecraft mission can be performed.

In general, the spacecraft will be separated from its booster with potentially sizable errors with respect to the final orientation requirements in both attitude and attitude rate. An initial mode of operation will be to control the initial rates and provide the proper attitude orientation. The process which describes the acquisition from separation to the final orientation is often called "acquisition" and generally consists of at least three separate modes--initial rate adjustment, search, and final acquisition. The actual switching and sequencing for achieving acquisition will vary between spacecraft systems, depending on the orientation requirements, sensor limitations, methods of obtaining control orientation, etc.

The second major control mode will be the mode of operation required to maintain the proper attitude orientation and stabilization. This mode is often referred to as the "normal" operating mode. Special operating provisions may be required when the normal control system operation is not possible; this occurs, for example, when the sun or star sensors are occulted by the earth, or when the spacecraft axis about which sun sensor information is used lies along the sun lines. Each orientation requirement defines a set of operating requirements, for example, control laws associated with solar array orientation, orbit plane orientation, and the like must be implemented. Other modes of control might include providing proper orientation of the spacecraft during velocity corrections required for orbit control, terminal maneuvering for docking, and deboost preparatory to re-entry.

a. Acquisition

During the separation of the spacecraft from its booster, angular impulses will be imparted to the spacecraft, resulting in initial rates which cannot be ignored. The first step after the control system has been electrically activated will be to control or null these rates with respect to some reference axes. For a spacecraft which uses a solar array, it is often desirable to null the rates in two axes about the earth-sun line by immediately orienting the solar array (held fixed with respect to the spacecraft during acquisition) to the sun. In the case of systems using the manipulation of the forces of space such as gravity gradient, earth's magnetic field, etc., momentum storage and/or mass expulsion devices are generally needed to reduce initial body rates to an acceptable level. Body-fixed rate measuring instruments providing attitude rate signals to momentum transfer devices can be used to reduce these rates before orientation of the body axes is achieved.

Once the body rates are reduced to small magnitudes, a search mode of operation will generally

be required. During this mode the sensors are caused to perform a search for those objects which they will sense to provide attitude error signals. There are many alternative approaches to the search mode. The selection of the approach is often dependent on a tradeoff between the dynamic range of the sensor, orbit conditions for acquisition, operational launch time requirements, etc. Depending on the sensor and the control system, either the entire spacecraft is rotated or it may be desirable to perform the search by articulating the sensor (like a radar dish, star tracker, etc.) with respect to the body.

Acquisition of proper orientation when the control torques are generated by essentially passive means is generally simpler than acquisition with active control systems. In the case of spinning satellites, lateral impulses at separation of satellite and booster will produce a free precession or nutation of the vehicle. An inertially fixed orientation is established by this satellite as soon as the nutation of the vehicle about its momentum vector has been damped. Such damping, as indicated previously, may be provided by a simple device like an annular ring of mercury located about the spin axis. A new inertial orientation of the spinning body is achieved by a controlled precession of the spin axis in a plane containing the initial momentum vector and the final desired orientation of the spin axis.

With the use of gravity gradient, once the initial rates have been stopped and sufficient damping has been added, the system will automatically acquire the earth's local vertical with the principal axis of minimum inertia and have the principal axis of maximum inertia normal to orbit plane. The angular error associated with the acquisition will depend on the relative magnitude of the disturbance and control torques and the misalignment of the control axis with the local vertical. The time required for acquisition depends on the capability of the damping devices and the initial conditions.

In the design of the acquisition mode, any requirements which severely limit the time to "acquire" must be carefully reviewed. Such limitations are significant in the determination of the amount of gas used, size of the pneumatic jets, torque requirements of the reaction wheel, etc. For example, the gas jet control moment may have been determined to provide a certain factor of desaturation to a set of reaction wheels operating in dual mode operation. However, the jet control moment that is determined for desaturation is usually not the best size to meet the rate nulling requirements. If this is true, a compromise solution will be necessary. The sensors used for acquisition may significantly affect the gas consumption. It may be desirable, for example, to add an auxiliary rate gyro and/or provide a sensor with a wider dynamic range. Neither of these requirements is necessary for normal operation. Additional electronics are required to perform the switching and logic functions required in this mode.

Final operational steps of acquisition, consisting of separate and successively more accurate modes of control, each operating over the

dynamic range consistent with the devices which are used for control sensing and orientation may be necessary. To obtain extremely precise accuracies, several of these modes of operation, each successively more accurate than the previous one, could be used.

b. Normal control

The orientation requirements of the spacecraft are mission-dependent. Those satellites oriented with a particular axis to be aligned along the earth's local vertical will have simple control in pitch and roll, generally nulling the outputs of earth horizon scanners. The control about the axis aligned along the local vertical (yaw axis) may depend on the orientation requirements with respect to the sun or other bodies. The yaw control may involve: orientation of the roll axis in the orbit plane; orientation of the solar array about the roll axis when the yaw axis points to the earth; special star orientation; or be simply unspecified.

The essential modes of control within the normal control for a nonspin earth-oriented satellite follow.

(1) Pitch/roll control. For purposes of discussion, the yaw axis is to be pointed along the earth's local vertical. Angular deviations from the local vertical can be determined by horizon scanners, processed and used directly for attitude control error signals.

(2) Yaw control. The yaw control problem is significant and depends on the spacecraft control requirements. The three most interesting cases are yaw orientation with respect to the orbit plane, yaw orientation to provide maximum solar energy on rotatable or nonrotatable solar cells, and no yaw requirements.

(a) Orbit plane orientation. Orientation with respect to the orbit plane is often a difficult control problem. The difficulty is primarily one of sensing rather than the need for any unique control laws. Gyrocompassing provided by the orbit rate coupling either through the use of gravity gradient or by mulling to the output of an orbital rate sensor are excellent schemes if there is sufficient orbital rate.

(b) Solar array/yaw orientation. Since the orbit plane can have any inclination with respect to the earth-sun line, it is necessary to provide two degrees of freedom to maintain a flat plate oriented normal to the sun line. In addition to solar array rotation, yaw orientation must be performed for maximum efficiency. If the solar array is not oriented, then yaw control with respect to the sun will in general improve efficiency over control with respect to the orbit plane or no control.

If the coordinate system shown in Fig. 37 is used, the following control laws indicate the yaw motion of the spacecraft (zero yaw angle occurs when the roll axis is in the orbit plane, and zero array angle when the sun is perpendicular to the earth satellite line). From the figure it follows that

$$\vec{u}_r = \vec{i} (\sin \alpha) + \vec{j} (\cos \alpha) \quad (186)$$

$$\vec{u}_s = \vec{j} (\cos \xi) + \vec{k} (\sin \xi) \quad (187)$$

$$\vec{u}_r \times \vec{u}_s = \vec{u}_p \sin \left(\frac{\pi}{2} - \phi_p \right) \quad (188)$$

$$\sin \psi = \vec{u}_p \cdot \vec{k} \quad (189)$$

$$\sin \phi_p = \vec{u}_r \cdot \vec{u}_s \quad (190)$$

combining Eqs (186), (187) and (190), the ideal array angle is given by

$$\sin \phi_p = \cos \alpha \cdot \cos \xi \quad (191)$$

combining Eqs (186), (187), (188) and (189)

$$\sin \psi = \frac{\sin \alpha \cos \xi}{\cos \phi_p} \quad (192)$$

and

$$\cos \psi = \frac{\sin \xi}{\cos \phi_p} \quad (193)$$

combining Eqs (192) and (193), the ideal yaw angle is given by

$$\tan \psi = \frac{\sin \alpha}{\tan \xi} \quad (194)$$

In order to eliminate the need for slip rings, the array angle and hence the yaw angle may be restricted to $\pm 90^\circ$. Figure 38 shows variation of array angle and yaw angle, respectively, with satellite location in orbit.

(c) Unspecified yaw orientation. For some missions there may be no specific requirements for orientation about the yaw axis. However, a requirement to maintain low yaw rates may exist due to requirements of on-board equipment or experiments. Even when such is not the case, it will generally be necessary to reduce yaw rates to within limits tolerable to the other axes controls before acquisition is complete.

(3) Eclipse. On systems where the sun information is used to determine yaw attitude error, the mode of operation during eclipse of the sun must be carefully reviewed. Often, yaw control is not required during eclipse. In such instances reacquisition of the sun when the spacecraft emerges from eclipse is necessary. If yaw control is required during occulting, then a special sensor or sensors must be provided in order to obtain appropriate attitude error signals. Yaw orientation might be maintained inertially with a programmed angle with respect to the orbit plane in order to have proper orientation at the time of emerging. A simpler scheme would be to maintain the spacecraft rate about the yaw axis below a known low value. In this case, reacquisition of the sun is still required upon emergence from eclipse, but may not require expenditure of as much impulse as the uncontrolled method.

It is interesting to note that, unless special provisions are incorporated, when the eclipse

region is entered, the momentum stored in the yaw inertia wheel will be dumped into the vehicle, creating an uncontrolled rotation. This occurs because the yaw loop is essentially opened, resulting in a zero wheel speed command. It may be desirable in some systems to damp the initial yaw wheel speed during eclipse to avoid the momentum transfer. For a sun-oriented, spin-stabilized spacecraft the problem of eclipse is not serious since the sun is essentially fixed in inertial space during the time of eclipse.

(4) Noon control. An additional control problem arises when the axis for which control information is being obtained is aligned along the line of sight of the sensed object providing that information. A sun-oriented spacecraft requires special control system operating provisions to maintain proper attitude orientation during periods in some orbits where the angle of the control axis with respect to the line of sight is not sufficient to obtain useful attitude angle information. For an earth-oriented satellite with a solar array, this condition occurs when the sun is in the orbit plane ($\xi = 0$) and the satellite yaw axis lies along the earth-sun line. This situation is often referred to as "high noon." If a sun sensor is used, the gain in the yaw axis will go to zero at this point again causing the momentum in the yaw wheel to be dumped into the body. For the control laws shown in Fig. 38, a 180° yaw rotation of the spacecraft is required at this time ($\alpha = 0$). This is often referred to as the "yaw-turn" and can be performed in a variety of ways. If there is a gyro present in the yaw axis, it can be used to provide stabilization during the maneuver. In many cases, the turn can be adequately performed by programming yaw reaction wheel speed in a manner which will cause the vehicle to rotate. In any case, precautions must be taken to minimize expenditure of impulse for eclipse and noon control.

c. Orbit control

Frequently velocity changes are required for orbit control or midcourse correction. The control system must have sufficient control authority to offset the disturbing torques caused by thrust misalignments from the propulsive devices used to correct the velocity. For system design simplicity it is usually desirable to have only one thrust nozzle on the vehicle. The control system is then required to orient the vehicle to allow the nozzle thrust to be applied in the correct direction. This will require a special orientation mode and perhaps a special sensor, depending on the orientation accuracy required. Large propulsive devices will be used for coarse orbit corrections. If precise corrections are required, it is likely that low thrust (probably cold gas) devices will be used to perform vernier indexing and long term station keeping. The required design of the vernier system in terms of the nozzles, gas supply, etc., should be integrated with the pneumatic system used for attitude control.

d. Other modes

The flight sequence must be determined early in the preliminary design. Such a sequence, if properly conceived, will define the operational requirements for the control system and, hence, the

major modes of control. This, coupled with a failure analysis, will be used to completely determine the primary and various alternate or backup modes of operation. A major number of modes of control beyond those described above are possible. Most of these modes are purely mission-dependent and must be considered for each particular mission.

The terminal mode of operation involved in the orbital docking maneuver of two satellites in orbit will be based on the particular design of the terminal sensors and the terminal guidance equipment that is used. A large number of possible modes exist with manned spacecraft wherein the primary motive is to recover the pilot (or crew) and allow him to participate in the navigation and control of the spacecraft. Clearly, modes of control covering such flight phenomenon as abort, re-entry, orbit maneuvering, etc., each using a combination of ground-based, on-board and manual sensing and torquing, may be required to achieve a well-integrated guidance and control design. In addition, special modes of unmanned vehicles such as a picture-taking mode, a mode for obtaining a star fix, etc., are conceivable.

5. Design of Spacecraft Control Systems

An example is provided to show specific design procedures for attitude control systems. From a given vehicle configuration and for a 400-naut mi (740 km) orbit, a reaction wheel/gas jet dual mode system is to be designed. Consider the following problem.

Example

a. Problem statement

Given the following control and spacecraft configuration specifications, design a dual mode reaction wheel/gas jet attitude control system.

| | Specifications |
|--------------------------|---|
| Orbit | 400-naut mi, (740 km) circular |
| Lifetime | One year |
| Orientation requirements | Yaw axis pointed to earth local vertical to $\pm 1^\circ$, solar array face perpendicular to sun line within $\pm 5^\circ$ |
| No slip rings | |
| Acquisition | Thirty min after separation from booster, maximum initial body rate $1^\circ/\text{sec}$ in all axes. |

Vehicle Configuration

The vehicle configuration will be the same as shown in the sketch of Section D-1, with the following specific properties. Vehicle inertias for two solar array angles

| | I_{xx} | I_{yy} | I_{zz} |
|-------------------------|--|----------|----------|
| For $\phi_p = 0^\circ$ | 100 | 160 | 115 |
| For $\phi_p = 90^\circ$ | 100 | 150 | 125 |
| Solar array area | 50 ft ² or (5 x 5 ft each paddle) 4.65 m ² | | |
| Gas jet lever arms | 2.5 ft all axes (7.63 m) | | |
| Vehicle dimension | 4 x 4 x 5 ft (1.2 x 1.2 x 1.5 m) | | |

b. Control laws

The requirement for elimination of slip-rings on the solar array means that the laws derived in Section C-4 are applicable. These laws are shown in Fig. 38.

c. Disturbance torques and momentum storage requirements

The calculation of disturbance torques for this example is limited to those due to solar radiation and gravity gradient. Other torques are considered negligible in comparison. In practice, all torques must be estimated.

(1) Solar radiation torque. We will assume a 0.5-ft (0.5 m) offset between the center of gravity, and a 50% reflectivity yielding an effective radiation pressure 1.5 times that for total absorption.

The projected areas are 50 sq ft (4.65 m²) for solar array, 20 sq ft (1.86 m²) as seen along the pitch or roll axis, and 16 sq ft (1.49 m²) as seen along the yaw axis.

In the case where the sun lies in the plane of the orbit the torques will be cyclic except for rectification which occurs because of eclipse and yaw control law (see Fig. 39a). In the case where the sun is perpendicular to the plane of the orbit where no eclipses occur, the torque will be periodic in inertial space. Then, the net momentum change per cycle will be zero. The component of momentum in inertial space is shown for sun inclination of 0° in Fig. 39b.

(2) Gravity gradient torques. The torques due to the gravity potential have been treated in Section D-2. By applying the vehicle parameters to the equations for determining gravity gradient torques, the total momentum change per orbit can be determined and is plotted in Fig. 40. Since the rotation of the solar array changes the spacecraft inertia, the momentum change is a function of the inclination of the sun with respect to the orbit plane. The stored momentum is plotted for three sun inclinations. As expected, the spacecraft is unstable with respect to gravity torques since the z-axis is not the axis of principal inertia.

(3) Total momentum requirement. The cyclical value of momentum shown in Figs. 39a and 39b will be used to provide information for the sizing of the inertia wheel. A conservative value of cyclical momentum would be 0.02 ft-lb/sec (0.27 $\frac{\text{m-newtons}}{\text{sec}}$) gravity gradient (height in Fig. 40) and

0.006 ft-lb/sec ($0.008 \frac{\text{m-newtons}}{\text{sec}}$) for solar radiation (height in Fig. 39). These are crude estimates for the preliminary design, but fortunately, as will be seen, turn out to be of secondary importance to the total storage requirements.

Over each orbit the momentum added to the system will be that which is not cyclical. Gravity gradient for $\xi = 45^\circ$ will add about 0.052 ft-lb/sec (0.071 m-n/s) and solar radiation for $\xi = 0$ will add 0.008 ft-lb/(0.011 m-n/s) sec per orbit. The inclination of $\xi = 0$ is the worst case for solar radiation since the maximum eclipse time occurs at this inclination. The gravity gradient dictates the most stringent requirement. Integrating 0.06 ft-lb/sec (0.08 m-n/s) over the 5250 orbits in one year, an impulse of approximately 125 lb-sec (557 n-s) is obtained.

(4) Design of a torque-producing system. The torque-producing system must provide sufficient impulse to overcome the secular effects of disturbance torques and must be designed to provide the minimum system weight while not appreciably reducing system reliability. Only two of these several approaches will be compared. These are the simple on-off (or contractor) mass expulsion control system using gas jets, and the dual mode system utilizing thrust devices (gas jets) and momentum storage (motor driven inertial flywheels).

The simple on-off or contractor control system will be acceptable if the resultant body rates are not too high and if the gas consumption over the required lifetime does not appreciably exceed the equivalent weight required for the momentum storage system. A block diagram of such a system is shown in Fig. 41; the system produces a limit cycle in attitude error with error rates as shown in the phase portrait of Fig. 42.

The design of these systems is well-known. The choice of acceleration (torque-to-inertia ratio) depends on the initial acquisition conditions and the characteristics of the sensor. A total thrust per axis of 0.02 lb (0.09 n) adequately satisfies the acquisition requirement. A jet lever arm of 2.5 ft (0.61 m) an attitude error dead zone of 0.5° , hysteresis of 1%, rate-to-position gain of 10, and negligible time delay were chosen for sample calculation. The resulting limit cycle period was 800 sec with a limit cycle rate of approximately $0.0025^\circ/\text{sec}$. For three channels of operation the total impulse requirements for one year will be approximately 3000 lb-sec (13,400 n-s), or for a cold gas pneumatic system like nitrogen or argon, approximately 120 lb (535 n) are required for the gas and tankage weight. This weight represents a large fraction of the total satellite weight and should be reduced, if possible. For low body rates such as this system produces, the most significant term is hysteresis. Since this example uses 1% hysteresis, considered a present state-of-the-art limit, and ignores time delay, which is also significant, a practical design would probably result in increased gas consumption for the on-off system.

(5) Design of dual mode system. The block diagram shown in Fig. 43 is that of a dual mode system and represents the addition to the gas jet system of motor-driven flywheels, which provides the capability of storing the cyclical momentum. Since the gas jets are not used to force

the system into a hard limit cycle, the only gas required is that to remove stored momentum due to secular torques and that necessary for initial sun-earth acquisition and special modes requiring the use of gas jets. Figure 44 shows the typical error angle-angular rate plot for the system under the effect of a constant disturbance torque.

(a) Momentum storage system. The first job to be treated in the design of the system will be to size the inertia wheels and determine the torque requirements on the drive motor. The requirements for pitch and roll reaction wheels are determined separately from those for the yaw wheel.

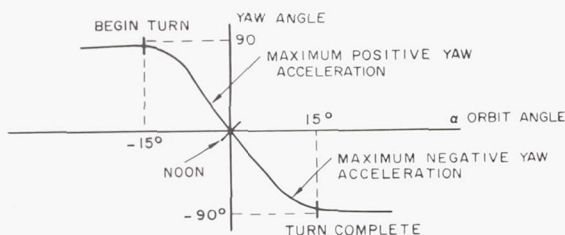
Pitch/roll wheel sizing. The pitch and roll wheels will be required to store the momentum due to torques which are cyclical in inertial space and to store the momentum which must be transferred from another axis to that body axis as the vehicle rotates in inertial space. In the disturbance torque calculations a peak cyclical momentum storage requirement of 0.026 ft-lb/sec (0.035 m-n/s) was determined, including the effects of both gravity gradient and solar radiation. In general, the wheels must also be capable of storing the body momentum required for the spacecraft orbital rate which is 1.05×10^{-3} rad/sec of 0.17 ft-lb/sec (0.23 m-n/s) if it occurs in the pitch axis or 0.105 ft-lb/sec (0.143 m-n/s) in the roll axis. Combining this with the disturbance torque requirements, momentum storage of 0.250 ft-lb/sec (0.341 m-n/s) will be chosen. If we choose the maximum allowable speed of the motor to be 500 rad/sec, the flywheel inertia then must be 0.5×10^{-3} slug-ft² (0.68×10^{-3} kg-m²). Since the orbital momentum in any one axis can be transferred to any other axis, during orbital maneuvers, a wheel of this size will be used in both the pitch and roll axes. This represents a solid steel wheel approximately 4 in. (10.2 cm) in diameter, 1/2-in. (1.2 cm) thick and weighing approximately 2 lb (8.9 n).

It is well to review the pitch and roll momentum storage capability from the standpoint of acquisition. Generally wheels will not have sufficient momentum storage capability to continue the initial rates. During acquisition the body rates must be reduced to a sufficiently low magnitude so that the wheel is able to store the residual momentum in the body. In many cases this will correspond to the contractor servo limit cycle rates. For the acquisition system design, which is discussed later, a torque-to-inertia ratio of approximately 3.5×10^{-4} rad/sec² will be determined to meet the acquisition system requirements. If an equivalent hysteresis of 5% is used for the design, a limit cycle rate of approximately $0.05^\circ/\text{sec}$ will exist. This rate dictates wheel momentum storage capability of at least 0.05 ft-lb/sec (0.08 n-m/s), well within our previously determined wheel storage capability. Further, it might be required that under normal operation the momentum storage capability be such as to maximize the time between gas jet firings. Note from Fig. 44 that, after gas is fired, it appears that the most desirable attitude would be at zero error signal or that represented by complete wheel desaturation (a). If the wheel momentum is not completely removed or if too much is added by the gas system, the final attitude

will occur at (b) or (c), respectively. With a torque-to-inertia ratio of 3.5×10^{-4} rad/sec², a rate-to-position gain of 11.25 and a hysteresis of 5%, a gas jet firing will remove approximately 30% of the wheel's saturation momentum.

If the jet firing is required to completely desaturate the wheel, a spacecraft angular rate at the time the jet is turned off, approximately 0.0015 rad/sec is necessary. For a system with the same gain ratio and hysteresis, a torque-to-inertia ratio of 3.8×10^{-3} rad/sec is required to completely desaturate the wheel. The presently chosen 3.5×10^{-4} rad/sec² will remove only 30% of the stored momentum.

Yaw wheel size and motor torque. The yaw wheel must not only be able to store the same momentum as the pitch and roll wheel but it must help to perform the yaw turn required at high noon. If it is assumed that the yaw turn is to be performed within 15° of high noon (solar array angle equal to 75°) and if it is assumed that the turn is to be performed strictly on wheels (i.e., no gas is to be fired), it is possible to determine the yaw wheel and motor torque requirements. The time for the satellite to move 15° in its orbit is 250 sec. Then for a maximum effort turn (constant torque) as shown in the following sketch, the motor torque required is 1.25 in. oz (0.0089 m-z). At the maximum spacecraft rate, the momentum which must be stored is approximately 1.56 ft-lb/sec (2.13 n-m/s). Since in a practical motor it is not possible to attain full torque as the speed increases, a 2-in. oz (0.014 m-n) motor is chosen. The momentum to be stored is 1.56 ft-lb/sec (2.13 m-n/s) for the turn, plus the 0.25 ft-lb/sec (0.34 m-n/s) (storage requirement capability necessary for momentum transfer from pitch and/or roll wheels). The yaw wheel inertia will be 3.2×10^{-3} slug-ft² (4.3×10^{-3} kg-m²) for the 500 rad/sec top motor speed. About a 6-in. diameter by 1-in. (2.5 cm) thick solid steel wheel weighing approximately 7 lb (31 n) is necessary.



Yaw Angle During Noon Turn

Pitch and roll motor torque requirements. The torque requirement for the pitch and roll motors may be based either on the "high noon" turn requirement or on the cancellation of spacecraft momentum before the phase plane trajectory reaches the opposite switching line (trajectory d in Fig. 44 is such an example) thus causing unnecessary gas to be fired. Each time a jet fires, about 0.5 in. -oz (0.0036 m-n) of torque is required to provide a trajectory to keep the other gas jet from firing. For this example, it has been assumed that the yaw turn maneuver

must occur within $\pm 15^\circ$ of the noon condition. This means that the pitch and roll wheels must be capable of transferring the maximum momentum stored by each to the other in 250 sec. For the maximum effort turn as shown in the previous sketch, the torque required to accomplish the transfer of the maximum momentum (0.250 ft-lb/sec) (0.34 m-n/s) is 0.71 in. -oz (0.0051 m-n) in pitch and 0.82 in. -oz (0.0058 m-n) in roll. Commercially available 1 in. -oz (0.00711 m-n) motors are chosen for the pitch and roll motors.

(b) Mass expulsion system. The mass expulsion system is designed on the basis of three requirements: first, the torque level is determined in concert with the sun sensor linear range and to obtain acquisition within the required time with minimum gas consumption; second, the total impulse requirements are equal to the sum of separate impulses required for acquisition, removal of secular disturbance torques, reacquisition, redundancy and contingency and; third, the design parameters are determined on the basis of practical values of equivalent hysteresis, dead zone, valve dynamics, etc. For a 1° limitation in local vertical, if the maximum orientation pitch occurs at the same instant that the roll error is maximum, then the errors in individual axes must be no greater than the 0.707° to meet the 1° requirement. The maximum dead zone in pitch and roll axes, for this example, will be designed to approximately 0.5° to allow for sensor errors, noise and misalignment.

As will be shown in the acquisition design, the thrust level per axis (usually two nozzles) will be about 0.02 lb (0.08 n). An impulse of 210 lb-sec (938 n-s) for 1 yr of operation will be required from the following sources.

| | (Lb-Sec) | (n-s) |
|--|----------|-------|
| Disturbance torques for 1 yr | 120 | 536 |
| Initial acquisition | 36 | 161 |
| Three reacquisitions | 3* | 13.4 |
| 20% contingency | 32 | 143 |
| Required because of pressure regulator limitations 10% | 19 | 85 |
| | 210 | 938.4 |

*Assuming that the maximum momentum of all the wheels is dumped into the body, the reacquisition requirement is still less than 1 lb-sec (1.4 n-s).

The pneumatic gas system including the tankage will weigh approximately 9 lb (40 n), assuming nitrogen with about 60 lb-sec of impulse (80 n-s) per pound (4.4 n) of weight, plus a nominal 140% allotment for tankage factor. The comparison of the two systems in weight for a year's operation finds the on-off system weighing a minimum of 120 lb (536 n) compared to the dual mode system weighing approximately 39 lb (173 n) including 20 lb (89 n) for the reaction wheels, motors, and circuitry plus 9 lb (40 n) for pneumatic system, plus the additional power supply required to drive the motors (estimated to be less than 10 lb).

(c) Acquisition sequence. For power supply requirements and temperature control it is necessary to cause either the yaw or pitch axes to lie along the sun line within 30 min of the time of separation from the booster vehicle. The spacecraft initial rates and initial attitude orientation will be assumed the most adverse, namely: $1^\circ/\text{sec}$ and 180° from desired orientation.

When separated from the booster, the spacecraft is misoriented and possesses booster separation-imparted body rates. The process of achieving normal control requires that the rates be nulled and that the sun and earth be acquired while the vehicle is in the sunlight. Of the several possible sequences the one chosen is as follows.

The rate null mode. During this mode the solar array is fixed at $+90^\circ$ and the yaw axis of the spacecraft is pointed at the sun, and rates about this axis are nulled. Information is provided by sun sensors and a yaw rate gyro. The array sun sensor provides roll signals and the yaw sun sensor provides pitch signals. By pointing the body at the sun initially, the power supply is immediately oriented for maximum charging and the orientation is proper for temperature control. In addition, the need for rate gyros in the pitch and roll axes is eliminated.

The orientation mode. During this mode the spacecraft is slowly rotated about the yaw axis to obtain horizon scanner returns from the earth. The solar array meanwhile maintains itself normal to the sun line. This method requires simple logic, little gas consumption, and ensures earth acquisition regardless of the position in orbit provided that the spacecraft is not in eclipse and that the scan angle coverage of the horizon scanner is sufficient.

The vehicle is now in its normal operating mode, the horizon scanners and sun sensors provide the information in pitch/roll and yaw to stabilize the spacecraft in the presence of disturbance torques, and the solar array is oriented so that the solar cells are facing the sun. If earth reference is lost, the vehicle will automatically return to the orientation of the rate null mode and reacquire the earth by repeating the above sequence. The block diagram of the acquisition mode is shown in Fig. 45.

(d) Design for acquisition. The following design is based on single axis computations which are considered adequate for preliminary design. All details of switching and choice of parameters must ultimately be determined by a three-axis study. The filter in the gas jet system is to be designed for rapid convergence from high rates to low limit cycle rates. The larger the rate gain, for a single axis at least, the lower the time and the less the gas that will be required to converge. For passive networks, practical upper limit for K_R is approximately

15. A filter $F(s)$ is assumed where

$$F(s) = \frac{12.5s + 1}{1.25s + 1} \quad (195)$$

The equivalent rate-to-position gain for the switching line is assumed to be 11.25.* Clearly one of the principal design parameters to be chosen will be angular acceleration (torque-to-inertia ratio). A decrease in torque will increase the gas consumption and the time required for sun acquisition. An increase in thrust will suggest an increase in sun sensor linear range in order to keep the gas consumption down.

Assume that the thrust is essentially the same for all axes and that yaw rates and error signal coupling between pitch and roll can be neglected. A conservative estimate of the total time for acquisition can be obtained by assuming consecutive pitch and roll system operation. The phase plane of Fig. 46 shows the operation in one axis, assuming the worst initial conditions. Figure 47 shows the maximum angular rate that the spacecraft will encounter versus torque-to-inertia ratio, assuming the initial condition of $1^\circ/\text{sec}$ and 180° attitude error. This curve is for the switching lines for the filter that is used. With a dead zone of about 1° about the yaw axes the rate at switching, if the sun sensor linear range is $\pm 30^\circ$, will be $2.6^\circ/\text{sec}$ and a torque-to-inertia ratio of $3.5 \times 10^{-4} \text{ rad/sec}^2$ will be required. It is next necessary to compute the time to acquire and the gas consumption. These can be determined approximately from the phase plot or from the rate diagram. An approximate closed form solution for the convergence in a single axis has been developed and is given by

$$t_{\text{acq}} = \frac{(\pi/180)^2 \omega_0^2}{2K_R F^2 r^2} \left[I_{xx}^2 + I_{yy}^2 (\phi_\rho = -90^\circ) \right] \quad (196)$$

where

ω_0 = initial crossover rate in degrees per second which is approximately $2.6^\circ/\text{sec}$

F = thrust per axis

R = thrust level arm

and since torque-to-inertia, λ , is given by

$$\lambda = \frac{Fr}{I} \quad (197)$$

$$t_{\text{acq}} = \frac{1.53 \times 10^{-4}}{11.25} \left(\frac{2.6}{3.5 \times 10^{-4}} \right)^2 \times 2 = 1720 \text{ sec} \quad (198)$$

which is slightly less than the specified 30 min. Here the torque-to-inertia ratio is assumed the

*In practice, the effect of acceleration and higher terms in the expansion $F(s) = 1 + 11.25s - 14.2s^2 + \dots$ must be considered. These terms may alter the limit cycle switching line, and hence gas consumption, significantly.

same in both axes. Figure 48 shows a few cycles of the settling transient for a similar system.

Because of the differences in inertia, and if $\lambda = 3.5 \times 10^{-4}$, the total thrust should be 0.014 lb (0.062 n) in the roll axis and 0.22 lb (0.98 n) in the pitch axis. We will use a thrust of 0.02 lb (0.089 n) per axis or nozzles acting in pairs with a thrust of 0.01 lb (0.044 n). (Some of the foregoing calculations could now be refined using the correct λ 's rather than the same λ for both axes.) A crude estimate of gas consumption for acquisition would be (assuming the jets are on at all times)

$$\begin{aligned} \text{Pitch and roll} & (1720)(0.02) \approx 35 \text{ lb-sec} \\ & \approx 156 \text{ n-s} \\ \text{Yaw} = \frac{I}{r} \omega & \frac{115}{2.5} (1/57.3) \approx 1 \text{ lb-sec} \\ & \approx 4.4 \text{ n-s} \\ \text{Total} & = 36 \text{ lb-sec} \\ & = 160 \text{ n-s} \\ & (199) \end{aligned}$$

If, instead of $\pm 30^\circ$, a linear range of $\pm 15^\circ$ is chosen for the sun sensor, the necessary λ to keep the solution in the linear range of the sensor would decrease by a factor of about 7 and the acquisition time would be increased by a factor of about 10. The resultant gas consumption would be up by only 40%. For the λ of 3.8×10^{-3} , which provides for perfect wheel desaturation (see Fig. 44), the sensor linear range should be at least 65° .

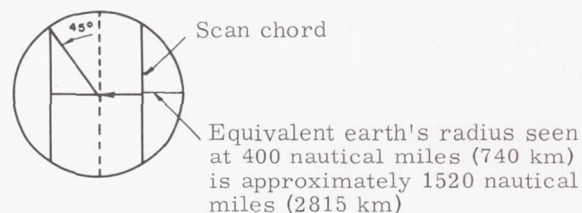
(6) Sensor design

(a) Sun sensor. The sun sensors located on the array for array error angles and on the body (or array) for yaw error angles will have a linear range of $\pm 30^\circ$. The operation around the null and the absolute linearity are not critical since accuracy to no better than $\pm 2^\circ$ is all that is required for the 5° pointing requirement, indicating that simple shadowing techniques can be used. Although the calculations of acquisition are based on a $\pm 1^\circ$ dead zone for yaw, they are crude and will not be seriously altered with the 2° dead zone.

(b) Horizon scanner. The scan angle, λ , (see sketch) for this system must be determined. Two requirements aid in the selection of this angle.

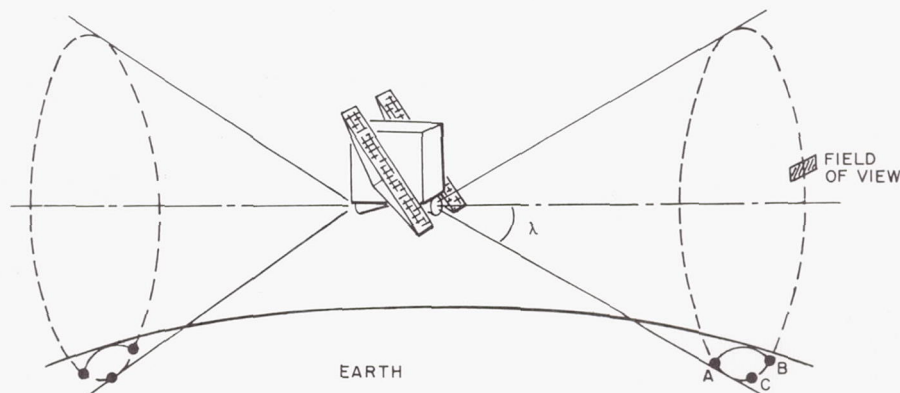
In order to ensure acquisition, the edge of the scan pattern must scan the earth for any spacecraft position. At 400 naut mi (740 km) the earth subtends approximately 135° at the satellite, indicating that a half angle cone of at least 24° is required to ensure acquisition. This, however, since it is at the very edge of the earth, will provide a very noisy signal.

From the linearity consideration of a change in pulse width per change in angle, a scan angle which normally crosses at 45° of the portion of the earth that is seen by the satellite is reasonable (see the following sketch).



The scan angle for this configuration then should be approximately 50° . The uncertainty due to ionospheric noise considered to be about 7 mi (13 km) indicates that a scanner error of about 0.27° in roll and pitch is possible. Other errors due typically to optical irregularities, mounting misalignment, thermistor balometer characteristics, etc., must also be considered. The proper scan rate would be determined on the basis of the tradeoff between inherent scanner signal-to-noise ratio and system bandwidth. This is not a significant problem for a 400-naut mi (740 km) orbit. Typical system bandwidth in excess of 3 cps is easily attained with a nominal scanner rate of 30 rps.

(7) System description. The system block diagram is shown in Fig. 49. The reaction wheel size has been selected and the torque requirements of the motor obtained, the gas jet has been determined and the impulse requirements per year established. The sun sensor and horizon scanner requirements have been briefly examined. To complete the study, a reliability analysis is necessary but has been excluded for this example. The acquisition noon-turn logic and solar array drive must, of course, be included. No special eclipse requirements are assumed. Reacquisition of sun must be studied and if only a small amount



of gas is required, it can probably be performed upon emergence from each eclipse. A simplified block diagram of the normal mode is shown in Fig. 49.

E. REFERENCES

1. Leach, R. and Townsend, G., "Guidance and Control Requirements," (Chapter XII of "Orbital Flight Manual") McGraw-Hill Book Company, Inc., 1962.
2. Wolverton, R. W. (editor), "Flight Performance Handbook for Orbital Operations," Space Technology Laboratories, Inc., September 1961.
3. Sparrow, W., and Bursey, C., "Vacuum Ballistic Trajectory Range Errors," Martin-Marietta Internal Report.
4. Air Force Technical Document USAFA/1-582.
5. Russell, W. T., "Inertial Guidance for Ballistic Vehicles," "Space Technology," edited by Seifert, H. S., John Wiley and Sons, New York, 1959.
6. Moore, R. A. and Meronek, D. F., "Generalized Inertial Guidance System Error Equations," Proceedings of the Third National Conference on Military Electronics, Washington, D. C., 29 June 1959.
7. Lunar Flight Handbook, Martin Company, ER 12685, Apr 1963.
8. Button, P. A., et al., "V/H Satellite Attitude Control," Radiation, Inc., Research Division.

F. BIBLIOGRAPHY

- Battin, R. H., "A Statistical Optimizing Navigation Procedure for Space Flight," ARS Journal, Vol. 32, No. 11, November 1962, p 1681.
- Bedford, L. H., "Guidance and Control," Journal of the Royal Aeronautical Society, May 1958, Vol. 62, pp 348 to 354.
- Bellman, R., Dreyfus, S. and Kalaba, R., "Applications of Dynamic Programming to Space Guidance, Satellites and Trajectories," The Rand Corporation, Santa Monica, California, August 1959.
- Blazek, H. F., "Performance of Inertial Components on an Unstabilized Base," American Rocket Society, May 1959, Preprint No. 775-59.
- Buglia, James J., Young, George R., Timmons, Jesse D. and Brinkworth, Helen S., "Analytical Method of Approximating the Motion of a Spinning Vehicle with Variable Mass and Inertia Properties Acted Upon by Several Disturbing Parameters," National Aeronautics and Space Administration, Report R-110, 1961.

Button, P. A., "Study of Satellite Guidance Sensors, Compendium of Technical Analysis," Radiation, Inc., Orlando, Florida, Final Report No. IR-1761-VI, 30 January 1961.

Cannon, R. H. Jr., "Some Basic Response Relations for Reaction-Wheel Attitude Control of Space Vehicles."

Cashmore, D. J. and Gordon, G. N., "Manned Navigation and Guidance in the Solar System," Journal of the British Interplanetary Society, March to April 1959, Vol. 17, No. 2.

Collins, O. C., "Determination of the Velocity Vector of a Space Vehicle from Apparent Changes in the Angular Separation of Stars," American Astronautical Society, Tenth Meeting, December 1960.

Crowley, J. C., Kolodkin, S. S. and Schneider, A. M., "Some Properties of the Gravitational Field and Their Possible Application to Space Navigation," Proceedings on the East Coast Conference on Aeronautical and Navigational Electronics, IRE, 1958.

Doolittle, J. H. and Pearson, J. R., "Study of Satellite Vehicle Orbital Guidance," Radiation, Inc., Orlando, Florida, Report No. RR 1188-59-01, February 1959.

Dow, P. C., Jr., "Re-entry Guidance at Escape Velocity," American Rocket Society, Preprint No. 2296-61, October 1961.

Draper, C. S., "Performance Requirements of Guidance Systems for Ballistic Missiles, Satellites and Space Vehicles," Cambridge, Massachusetts, Massachusetts Institute of Technology, MIT Instrumentation Laboratory, Report No. R-172, March 1958.

Drake, D. E. and Keown, E. R., "Programming of Digital Computers for Determination of Stability and Control Characteristics," WADC TR 59-290, July 1959.

Duncan, D. B., "Inertial Guidance and Space Navigation," Journal of the Institute of Navigation, Vol. 6, No. 1, p 30; "Analysis of an Inertial Guidance System," Jet Propulsion, Vol. 28, No. 2, pp 111 to 116, February 1958.

Dworetzky, L. H. and Edwards, A., "Principles of Doppler Inertial Guidance," ARS Journal, December 1959, Vol. 29, No. 12.

Ehrlicke, K. A., "Error Analysis of Keplerian Flights Involving a Single Central Force Field and Transfer Between Two Central Force Fields," Navigation Spring 1958, pp 5 to 23.

Fried, W. R., "Doppler Radars for Guidance, Design Techniques and Performance," ARS Journal, December 1959, Vol. 29, No. 12.

Frye, W. E., "Fundamentals of Inertial Guidance and Navigation," American Astronautical Society, Fourth Annual Meeting, January 1958.

Garber, T., "Ascent Guidance for Satellite Rendezvous," *Aerospace Engineering*, Vol. 19, May 1960.

Goetze, D., "Accuracy and Range of Infrared Horizon Sensors as Limited by Detector Noise," *ARS Journal*, Vol. 32, No. 7, July 1962, p 1039.

Gretz, R. W., "Error Sensitivities in Satellite Ascent and Orbital Transfer," *ARS Journal*, Vol. 32, No. 12, December 1962, p 1860.

Grube, R. H., "Optical Tracking for Terminal Guidance," *Automatic Control*, August 1960, Vol. 13, No. 2, pp 20 to 22.

Gurley, J. G., "On the Propagation of Errors in a Schuler-Type Inertial Navigation System," *American Rocket Society*, May 1960, Preprint No. 1173-60.

Harry, D. P. and Friedlander, A. L., "Exploratory Statistical Analysis of Planet Approach Phase Guidance Schemes," *NASA TN D-268*, March 1960.

Haeussermann, W., "Considerations About a Guidance and Control System for a 24-Hour Communication Satellite Launched with the Saturn Vehicle," *American Rocket Society*, December 1960, Preprint No. 1479-60.

Hayes, J. E. and Vander Velde, W. E., "Satellite Landing Control System Using Drag Modulation," *ARS Journal*, Vol. 32, No. 5, May 1962, p 722.

Hutchinson, R. C., "Geometrical and Astronomical Aspects of Employing a Star Tracker to Correct the Attitude of a Stable Platform," *Massachusetts Institute of Technology, Instrumentation Laboratory*, February 1961.

Ives, N. E., "Principles of Attitude Control of Artificial Satellites," *Farnborough, Great Britain, Royal Aircraft Establishment*, 1959, Report No. TN GW 534.

Jarmolow, K., "Dynamics of Spinning Rocket with Varying Inertial and Applied Moment," *Journal of Applied Physics*, March 1957, Vol. 28, No. 3, pp 208 to 213.

Juelich, O. C., "Passive Aerodynamic Attitude Stabilization of Near Earth Satellites," Vol. 3, *Mathematical Techniques and Computer Program*, North American Aviation, Inc., WADD TR 61-133, Aeronautical Systems Division, Flight Dynamics Laboratory, Columbus, Ohio, July 1961.

Karrenberg, H. K. and Roberson, R. E., "Guidance and Control of 24-Hour Communication Satellites," *Stockholm, XIth International Astronautical Congress*, 1960.
"Celestial Rate Sensing," *ARS Journal*, Vol. 31, No. 3, March 1961, pp 440 and 441.

Keeler, R. J., et al., "Injection Guidance," *Astronautics*, Vol. 6, No. 11, November 1961.

Ketchum, H. B.

"Navigational Calculations in Space Flight; Part I--Planetary Orbital Distances," *Journal of Space Flight*, April 1953, Vol. 5.

"Navigational Calculations in Space Flight; Part II--Planetary Orbital Velocities and Gravitational Fields," *Journal of Space Flight*, September 1953, Vol. 5.

"Navigational Calculations in Space Flight; Part III--Satellite Gravitational Field, Orbital Velocities and Elements of Orbits," *Journal of Space Flight*, December 1953, Vol. 5.

"Navigational Calculations in Space Flight; Part IV--The Effects of Atmospheric Friction," *Journal of Space Flight*, June 1954, Vol. 6.

Kooy, J. M. J., "On the Orbital Computations and the Guidance Problem of a Deep Space Rocket," *Amsterdam, Ninth International Astronautical Congress*, 1958.

Laning, J. H., Jr and Battin, R. H., "Theoretical Principle for a Class of Inertial Guidance Computers for Ballistic Missiles (U)," *Massachusetts Institute of Technology, Instrumentation Laboratory*, Cambridge, Massachusetts, Report No. R-125, June 21 and 22, 1956.

Lapaz, L., "On the Magnetic Damping of Rotation of Artificial Satellites of the Earth," *Journal of Geophysical Research*, Vol. 65, No. 7, July 1960, pp 2201 and 2202.

Larmore, L., "Celestial Observations for Space Navigation," *Aerospace Engineering*, January 1959, pp 37 to 42.

Lee, D. E., "Trajectory Control Development," *Los Angeles, Fourth Symposium on Ballistic Missiles and Space Technology*, August 1959.

Legalley, D. P., "Guidance, Navigation, Tracking and Space Physics," *Ballistic Missile and Space Technology*, New York, Academic Press, 1960, Vol. 3.

Longchamp, W. F., "Guidance Equipment Survey," *Los Angeles, Convair Astronautics*, Report No. AZP-095, April 1959.

Lorell, J., "Velocity Increments Required to Reduce Target Miss on Coasting Trajectories," *Advances in the Astronautical Sciences*, Vol. 6, The Macmillan Company, New York, 1960.

MacDonald, R. B. and Johnson, G. W., "Inertial Guidance for Hypersonic and Orbital Vehicles," *Institute of Aeronautical Sciences*, January 1957, Paper No. 59-33.

Mathews, K. C., "Orientation Errors in Command Guidance Systems," *ARS Journal*, January 1960, Vol. 30.

Miner, W. E. and Schmieder, D. H., "The Path-Adaptive Mode for Guiding Space Flight Vehicles," *American Rocket Society, George Marshall Space Flight Center*, for presentation at the *ARS Guidance, Control and Navigation Conference*, August 7 to 9, 1961, Stanford University.

Mueller, R. R., "Investigation of Possible Satellite Position-Sensing Methods," American Rocket Society, November 1959, Reprint No. 913-59.

Myers, G., "Guidance of Tiros 1," ARS Journal, Vol. 31, No. 5, 1961.

Newman, T. V., "Inertial Navigation and Space Flight," American Astronautical Society, New York, 4th Annual Meeting, January 1958.

Novak, D., "Inertial Guidance for Ascent and Injection into a Precise Orbit on a Predetermined Schedule," the Martin Company, Baltimore, Maryland, Engineering Report No. ER 11518, October 6, 1960.

Nyland, F., "Digital Computers for Control in Missiles and Space Vehicles," the Martin Company, Denver, Colorado, Report No. R-60-19, August 1960.

O'Mara, H. R. and Gabler, R. T., "The Propagation of Errors in Keplerian Orbits," The Rand Corporation, Santa Monica, California, Report No. P-1481, August 1958.

Palmer, R. R., et al., "Multiple Inertial System Operation in Long-Term Navigation," North American Aviation, Inc., for presentation at the ARS Guidance, Control and Navigation Conference, Stanford University, August 7 to 9, 1961.

Perret, E. E. and Corbin, J. L., "Effects of Small Changes in Position and Velocity at Burn-out on the Orbit of a Ballistic Missile," WADC TN 59-336, October 1959.

Pearson, J. R., "Technique Development of Orbital Guidance Equipment for Satellite Vehicles," Radiation, Inc., Orlando, Florida, Technical Note No. 1188-59-01, 17 April 1959.

Pfeiffer, C. G.
"Simple Guidance of Deep Space Booster Vehicles," *Astronautics*, Vol. 6, No. 11, November 1961.
"Rudimentary Launch Guidance Methods for Space Missions," American Rocket Society, Preprint No. 1172-60, 1960.

Reis, R. J., "Passive Detection of Lunar Features for Terminal Guidance," ITT Laboratories, Fort Wayne, Indiana, April 1959.

Reiss, M. H., "Systems Approach to Space Vehicle Guidance," WADC Report, September 1958.

Roberson, R. E.
"General Guidance and Control Concepts for Satellites and Space Vehicles," Amsterdam, 9th Congress of the International Astronautical Federation, August 1958.
"On Guidance and Control Requirements in Astronautics," *Journal of the Franklin Institute*, Vol. 269, pp 196 to 220, March 1960.
"Astronautical Guidance and Control in Space," *Journal of the Astronautical Sciences*, Vol. 7, No. 4, pp 87 to 95, Winter 1960.

Rosen, B. M., "Lunar Mission Guidance Requirements," *Sperry Engineering Review*, Vol. 12, June 1959.

Rosenstock, H. B., "The Effect of the Earth's Magnetic Field on the Spin of the Satellite," *Astronautica Acta*, Vol. 3, pp 215 to 221, 1957.

Russell, W. T., "Inertial Guidance for Rocket-Propelled Missiles," *Jet Propulsion*, Vol. 28, pp 17 to 24, January 1958.

Satyendra, K. N. and Bradford, R. E., "Self-Contained Navigational System for Determination of Orbital Elements of a Satellite," *ARS Journal*, Vol. 31, No. 7, pp 949 to 956, July 1961.

Savet, P. H., "Attitude Control of Orbiting Satellites at High Eccentricity," *ARS Journal*, Vol. 32, No. 10, p 1577, October 1962.

Savet, P. H. and Carroll, J., "Space Navigation and Exploration by Gravity Gradient Detection," Institute of Aeronautical Sciences, Los Angeles, National Summer Meeting, June 1959.

Schlitt, H., "Advanced Instrumentation Concepts in the Field of Inertial Navigation," Institute of Aeronautical Sciences, St. Louis, Midwestern Meeting on Guided Missiles, May 1958.

Schmaedeke, W. and Swanlund, G., "Optimizing Techniques for Injection Guidance," Minneapolis-Honeywell Regulator Company, presented at ARS Guidance, Control and Navigation Conference, Stanford University, August 7 to 9, 1961.

Scull, J. R., "Space Guidance," American Rocket Society, Preprint No. 2113-61, October 1961.

Seward, H. H., "Sunfinder for an Interplanetary Vehicle (U)," Massachusetts Institute of Technology, Instrumentation Laboratory, Cambridge, Massachusetts, December 1960.

Shepler, H. C., "Visual Tracking of Space Vehicles," American Astronautical Society, Preprint No. 60-51, 1960.

Shklovskii, I. S., "Optical Methods for Tracking Earth Satellites," *Planetary and Space Sciences*, Vol. 5, No. 3, pp 233 to 237, July 1961.

Sirri, N., "Space-Vehicle Attitude Control," California Institute of Technology, Jet Propulsion Laboratory, Pasadena, California, JPL Report No. TR 34-121, 1960.

Stubbs, H. E., "Investigation of Physical Phenomena for Space Navigation (U)," Geophysics Corporation of America, Bedford, Massachusetts, Report No. ASD TR 61-286, August 1961.

Swanlund, G. and Ito, W., "Analysis Techniques to Determine the Guidance Computer Requirements for Space Vehicles," American Rocket Society, Preprint No. 2292-61, October 1961.

Thompson, J. W., "Lunar Parrallax Method of Astro Navigation," The Rand Corporation, Santa Monica, California, Report No. P-181, December 1950.

Townsend, G. and Leach, R., "Guidance and Control Requirements," Design Guide to Orbital Flight, McGraw-Hill Book Company, New York, Chapter 12, 1962.

Townsend, G., Kork, J. and Kraft, D.
"Guidance Requirements for a 24-hr Satellite," the Martin Company, Baltimore, Maryland, Engineering Report No. ER 10718-6, October 1959.

"Orbital Guidance Systems Study," The Martin Company, Baltimore, Maryland, Engineering Report No. ER 11439-3, November 1960.

Tripp, C. N. and Boardman, W. P., "Attitude Control Rocket Requirements for Space Vehicles," Marquardt Corporation, presented at the National IAS-ARS Joint Meeting, Los Angeles, Calif., June 13 to 16, 1961.

Vertregt, M., "Orientation in Space," Journal of the British Interplanetary Society, Vol. 15, No. 6, pp 324 to 338, November and December 1956.

Wheelon, A. D., "Midcourse and Terminal Guidance," University of California, Engineering Extension, Berkeley, California, April 1958, Eng X461-AEC, Space Technology Lecture 12B. (Also, Space Technology, John Wiley & Sons, New York, 1959 (Siefert, H., ed.))

White, J. A.

"A Study of the Guidance of Space Vehicles Returning to a Braking Ellipse About the Earth," NASA TN D-191, January 1960.

"A Study of the Effect of Errors in Measurement of Velocity and Flight-Path Angle on the Guidance of a Space Vehicle Approaching the Earth," NASA TN D-957, October 1961.

Wing, W. G., "State of the Art: Inertial Guidance," Space/Aeronautics, Vol. 31, p 24, January 1959.

West, C. T. and Goodstein, R., "On the Simplification of the Attitude Equations of a Satellite," American Astronautical Society, Preprint No. 60-13, 1960.

Widrow, B., "Rate of Adaptation in Control Systems," ARS Journal, Vol. 32, No. 9, p 1378, September 1962.

Windeknecht, T. G., "A Simple System of Sun Orientation for a Spinning Satellite," Institute of Aerospace Sciences, Preprint No. 61-204-1898, June 1961.

Williams, O. S. and Wiseman, J. R., "Low-Thrust Bipropellant Pulse-Rockets for Satellite Attitude Control," American Rocket Society, Preprint No. 1503-60, 1960.

Williams, O. S., "Performance and Reliability of Rocket Attitude Control Systems," Thiokol Astronaut, Vol. 2, No. 1, pp 3 to 6, 1960.

Wilson, R. H., Jr., "Magnetic Field Effects on Artificial Satellites," Sky and Telescope, Vol. 20, No. 2, pp 77 to 79, August 1960.

Wisneski, M. L., "Error Matrix for a Flight on a Circular Orbit," ARS Journal, Vol. 32, No. 9, p 1416, September 1962.

Wolaver, L. E., "Derivation and Burnout Errors," "A Study of the Satellite Equations of Motion," WADC Aeronautical Research Laboratory, WCLJY Internal Memo 58-0, Part I, March 1958.

Zajac, E. E., "Damping of a Gravitationally Oriented Two-Body Satellite," ARS Journal, Vol. 32, No. 12, p 1871, December 1962.

"Analytical Investigation to Determine the Dynamic Requirements of Missile Flight Control Systems," Systems Technology, Inc., Report No. TN-3, 6 January 1959.

"Detection and Analysis of Missile Guidance Systems," ITT Laboratories, Fort Wayne, Indiana, August 1958 to February 1961.

1st Quarterly Report, August 1958.

2nd Quarterly Report 72001, March 1959.

3rd Quarterly Report 72027, October 1959.

4th Quarterly Report 72037, November 1959.

5th Quarterly Report 72042, November 1959.

6th Quarterly Report 72050, December 1959.

7th Quarterly Report 72082, May 1960.

8th Quarterly Report 72095, July 1960.

9th Quarterly Report 72143, January 1961.

10th Quarterly Report 72155, February 1961.

"Developmental Star Tracker Final Report," Santa Barbara Research Department, Santa Barbara, California, Report No. 1030-F, July 1956.

"Doppler Velocity for Space Navigation," General Precision Laboratory, New York, Interim Engineering Reports Nos. A18-3 and A18-4.

"First Quarterly Engineering Report on the Study of Electromagnetic Phenomena for Space Navigation," The Franklin Institute, Philadelphia, Pennsylvania, Report No. Q-A2183-1, 1 July to 30 September 1958.

"First Quarterly Technical Note on Study of Automatic Position Fixing," General Precision Laboratory, New York, Report No. A20-1, 1 December 1958.

"Guidance and Control; Trajectories; Radio Propagation," Transactions of Second Technical Symposium on Ballistic Missiles, Ramo-Woolbridge, AFBMD, ARDC, Vol. II, 12 to 14 June 1957.

"Proceedings of the National Specialists Meetings on Guidance of Aerospace Vehicles," Institute of the Aeronautical Sciences, New York, 1960.

Antes, L. L.

"Command and Data Link for an Astronomical Satellite."

Spradlin, L. W.

"The Long-Time Satellite Rendezvous Trajectory."

Lowry, J. H., Jr. and Buehrle, C. D.

"Guidance and Control of Point Return Vehicles,"

- Haywood, W. J., Jr.
"Application of Optical Techniques to Interplanetary Navigation."
Ormsby, R. D.
"A Free Reaction Sphere Satellite Attitude Control System."
Useller, J. W. and Algranti, J. S.
"Pilot Control of Space Vehicle Tumbling."
Alonso, R. L. and Laning, J. H., Jr.
"Design Principles for a Control Computer for Space Guidance."
Grube, R. H.
"Terminal Guidance for Lunar and Planetary Probes."
- "Study of Satellite Guidance Sensors," Radiation, Inc., Final Technical Report No. IR-1761-VI, Orlando, Florida, 2 Vols., January 1961.
- "Technique Development of Orbital Guidance Equipment for Satellite Vehicles," Radiation, Inc., Orlando, Florida, April 1959 to July 1960.
Quarterly Technical Note 1188-59-01, April 1959.
Quarterly Technical Note 1188-59-02, July 1959.
Quarterly Technical Note 1188-59-03, October 1959.
Quarterly Technical Note 1188-59-04, January 1960.
Quarterly Technical Note 1188-60-01, April 1960.
Quarterly Technical Note 1188-60-02, July 1960.
- Techniques of Indication and Control for Inertial Guidance of Ballistic Missiles," Massachusetts Institute of Technology, Cambridge, Massachusetts, Instrumentation Laboratory, February 1959.
- "Radio and Inertial Guidance," Transactions of the First Technical Symposium on Ballistic Missiles, Ramo-Wooldridge, Report No. GM 01.1-266, Vols. 1 and 2, 21 and 22 June 1956.
- "Radio and Inertial Guidance," Transactions of the Second Technical Symposium on Ballistic Missiles. Ramo-Wooldridge, Report No. GM TR 202, Vols. 1 and 2, 12 to 14 June 1957.
- "Radio and Inertial Guidance," Transactions of the Third Technical Symposium on Ballistic Missiles, Ramo-Wooldridge, Vols. 1 and 2, 14 to 15 July 1958.
- "USAF Symposium on Guidance of Ballistic Missiles and Space Vehicles," WADC TR 58-270, March 1958.
- Adams, J. J. and Chilton, R. E.
"A Weight Comparison of Several Attitude Control Systems for Satellites," NASA Memorandum 12-30-586, February 1959
- Arck, M. H. and Merlen, M. M.
"Horizon Sensors for Vertical Stabilization of Satellites and Space Vehicles," IAS Symposium, Boston, May 1960.
- Barnes, J. L., "Precision Position and Attitude Control for Synchronous Satellites," Stockholm, XIth International Astronautical Congress, Astrodynamics Colloquium, 1960.
- Chatkoff, M. and Lynch, G., "Attitude Control of a Space Vehicle by a Gyroscopic Reference Unit," Aero/Space Engineering, Vol. 19, May 1960.
- Davis, W. R., "Determination of a Unique Attitude for an Earth Satellite," American Astronautical Society, 4th Annual Meeting, New York, January 1958.
- DeLisle, J. E., et al., "Attitude Control of Spacecraft," Astronautics, Vol. 6, No. 11, November 1961.
- Freed, L. E., "Attitude Control System for a Spinning Body," Institute of Aerospace Sciences, Preprint No. 61-207-1901, June 1961.
- Gates, C. R., "Attitude Control of Space Vehicles," California Institute of Technology, Pasadena, California, Jet Propulsion Laboratory, JPL Report No. EP 795, February 5, 1960. (Presented at the National Automatic Control Conference, Dallas, Texas, November 4 to 6, 1959.)
- Gillespie, W., Jr., "Some Notes on Attitude Control on Earth Satellite Vehicles," NASA TN D-40, December 1959.
- Grasshoff, L., "Method for Controlling the Attitude of a Spin-Stabilized Satellite," ARS Journal, Vol. 31, No. 5, 1961.
- Haeussermann, W. E., "Recent Advances in Attitude Control of Space Vehicles," ARS Journal Vol. 32, No. 2, p 188, February 1962.
- Kalman, R. E. and Bertrom, J. E., "Control System Analyses and Design via the Second Method of Liapunov," RIAS, Inc., Baltimore, Maryland, Monograph 59-13. (Also, ASME Paper No. 59-NAC-2, 1959.)
- Levin, S. M. and Manusevich, L. G., "A Vector Method for Calculating One Class of Control Systems," Automation and Remote Control, Vol. 21, No. 10, pp 962 to 970, October 1960.
- Lillestrand, R. L., "Use of a Stellar Aberrator in Space Systems," XIth International Astronautical Congress, Astrodynamics Colloquium, Stockholm, 1960.
- Litovchenko, I. A., "On a Problem of Optimum Control," Automation and Remote Control, Vol. 21, No. 8, pp 791 to 798, August 1960.
- Mueller, H., "An Attitude Control System for Extremely Small Control Forces," XIth International Astronautical Congress, Astrodynamics Colloquium, Stockholm, 1960.
- Ormsby, R., "Capabilities and Limitations of Reaction Spheres for Attitude Control," ARS Journal, Vol. 31, No. 6, 1961.

Ormsby, R. and Smith, M. C., "A Reaction Spheres Attitude Control System," American Rocket Society, Preprint No. 1500-60, 1960.

Pistiner, J. S., "On-Off Control System for Attitude Stabilization of a Space Vehicle," ARS Journal, Vol. 29, No. 4, pp 283 to 289, April 1959.

Potter, N. S., "Orientation Sensing in Inertial Space by Celestial Pattern Recognition Techniques," American Rocket Society, Preprint No. 1482-60, 1960.

Ritchie, M. L., Hanes, L. F. and Hainsworth, T. C., "Some Display-Control Aspects of Manual Attitude Control in Space," American Astronautical Society, Preprint No. 60-14, January 1960.

Roberson, R. E.

"Optical Determination of Orientation and Position near a Planet," American Rocket Society, Preprint No. 643-58, 1958.

"Principle of Inertial Control of Satellite Attitude," 9th International Astronautical Congress, 1958.

"Gyroscopic Sensing of Satellite Yaw," International Congress on Automatic Control, Moscow, June 1960.

"Attitude Sensing and Control for a Satellite Vehicle," The Rand Corporation, Santa Monica, California, Research Memo No. RM-1050, January 1953.

"Gravitational Torque on a Satellite Vehicle," Journal of the Franklin Institute, Vol. 265, No. 1, January 1958.

"Control of Satellites," WADD TR 60-643, 31 July 1960.

"Methods of Attitude Sensing," Proceedings of the Manned Space Station Symposium, Los Angeles, April 1960.

"Gravity Gradient Determination of the Vertical," American Rocket Society, Preprint No. 1496-60, December 1960.

Roman, N. G., "Attitude Control and Stabilization Required for Satellite Telescopes," Proceedings of the Manned Space Station Symposium, Los Angeles, April 1960.

Sohn, R. L., "Attitude Stabilization by Means of Solar Radiation Pressure," ARS Journal, Vol. 29, No. 5, pp 371 to 373, May 1959.

Stalony-Dobrzanski, J. and Imai, O., "Attitude and Flight Path Control System for a Space Station Supply Vehicle," Aero/Space Engineering, Vol. 19, May 1960.

Thomson, W. T. and Reiter, G. S., "Attitude Drift of Space Vehicles," Journal of the Astronautical Sciences, Vol. 7, No. 2, pp 29 to 34, 1960.

Tripp, C. N., "Attitude Control Rocket Requirements for Space Vehicles," Institute of the Aerospace Sciences, Preprint No. 61-205-1899, 1961.

Von Pahlen, F., "An Accurate Determination of Attitude by Optical Means," IAS Symposium, Boston, May 1960.

ILLUSTRATIONS

Preceding Page Blank

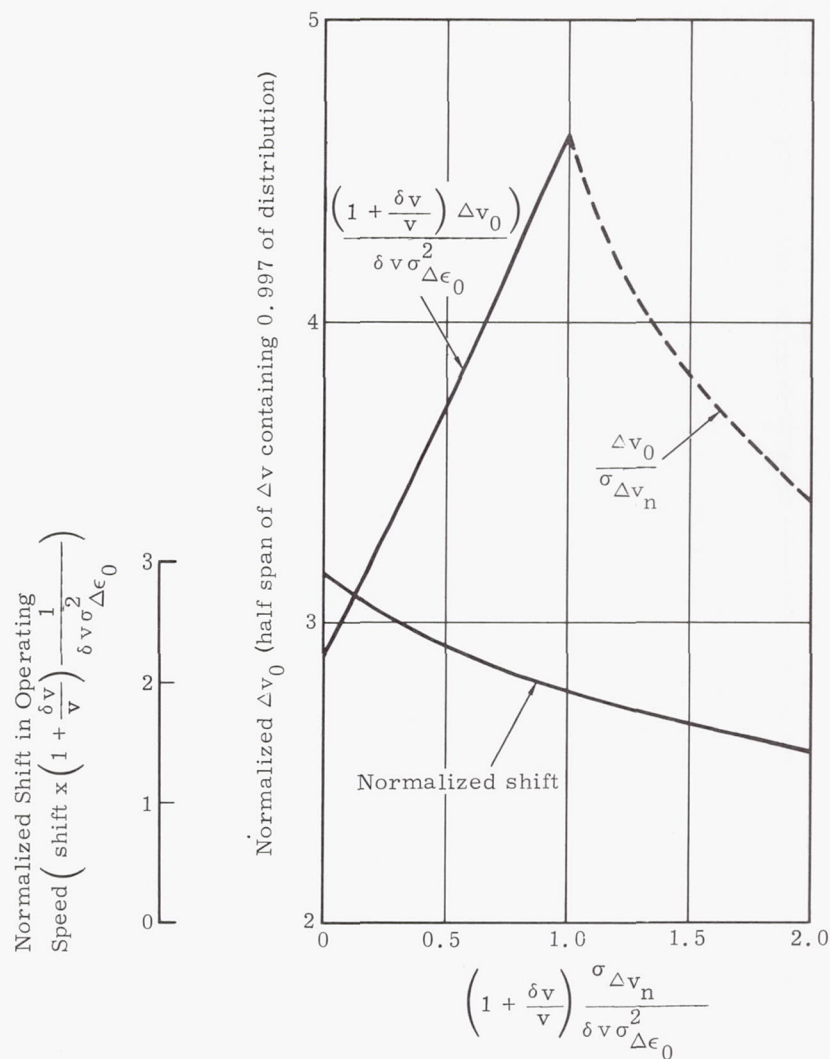


Fig. 1. Results of Optimization for Equal σ in Pitch and Yaw Equal to $\sigma_{\Delta \epsilon_0}$

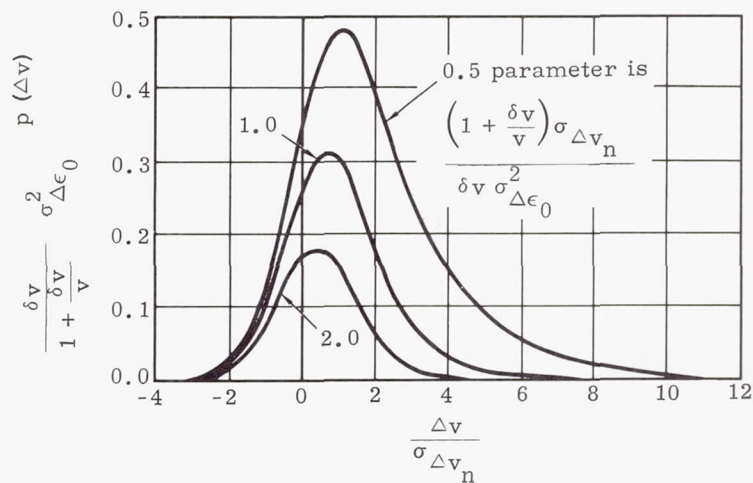


Fig. 2. Normalized Density Function of Δv (Equation 119)

Preceding Page Blank

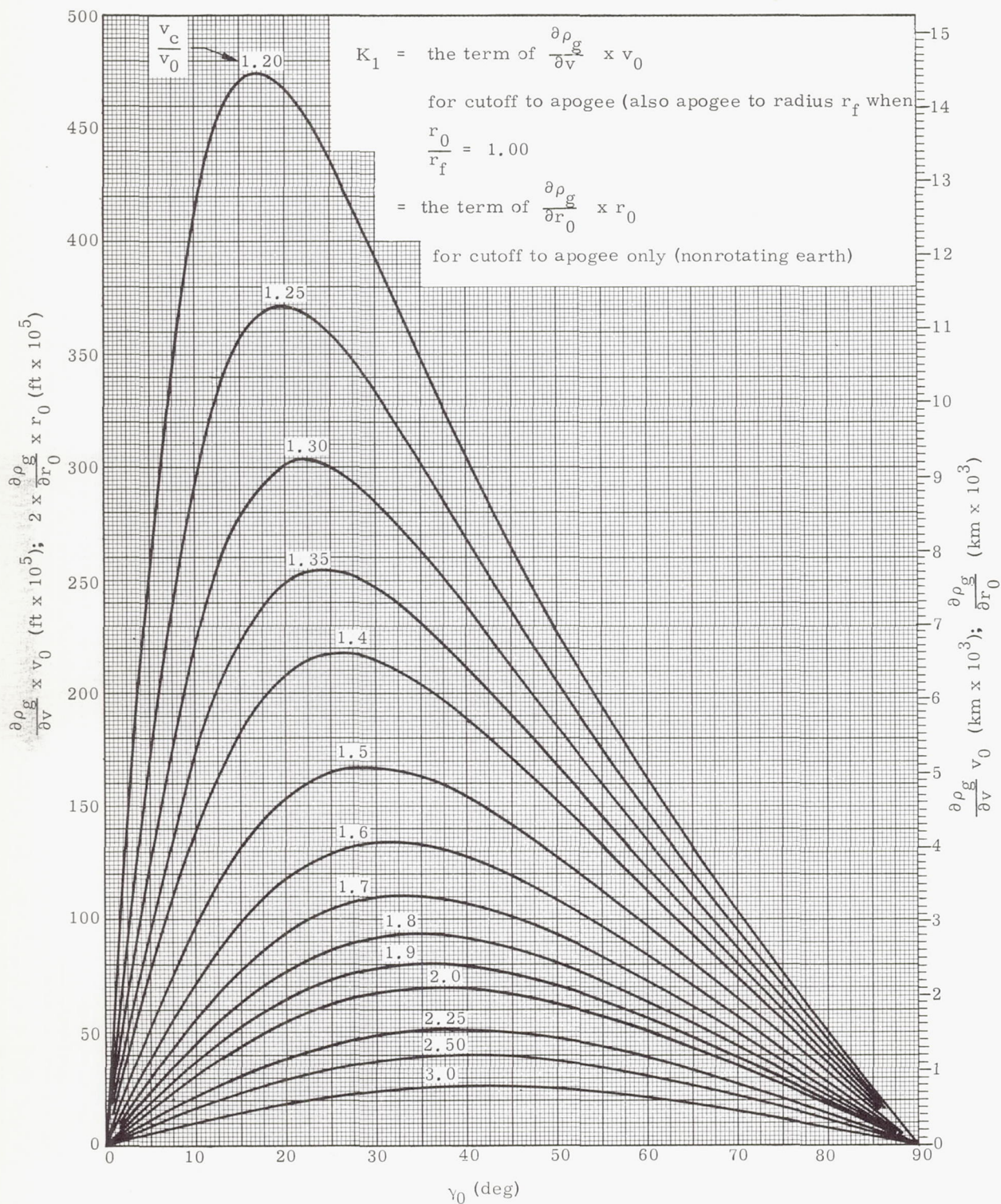


Fig. 3. Vacuum Ballistic Trajectory Error Analysis
(velocity and radius, cutoff to apogee, partials)

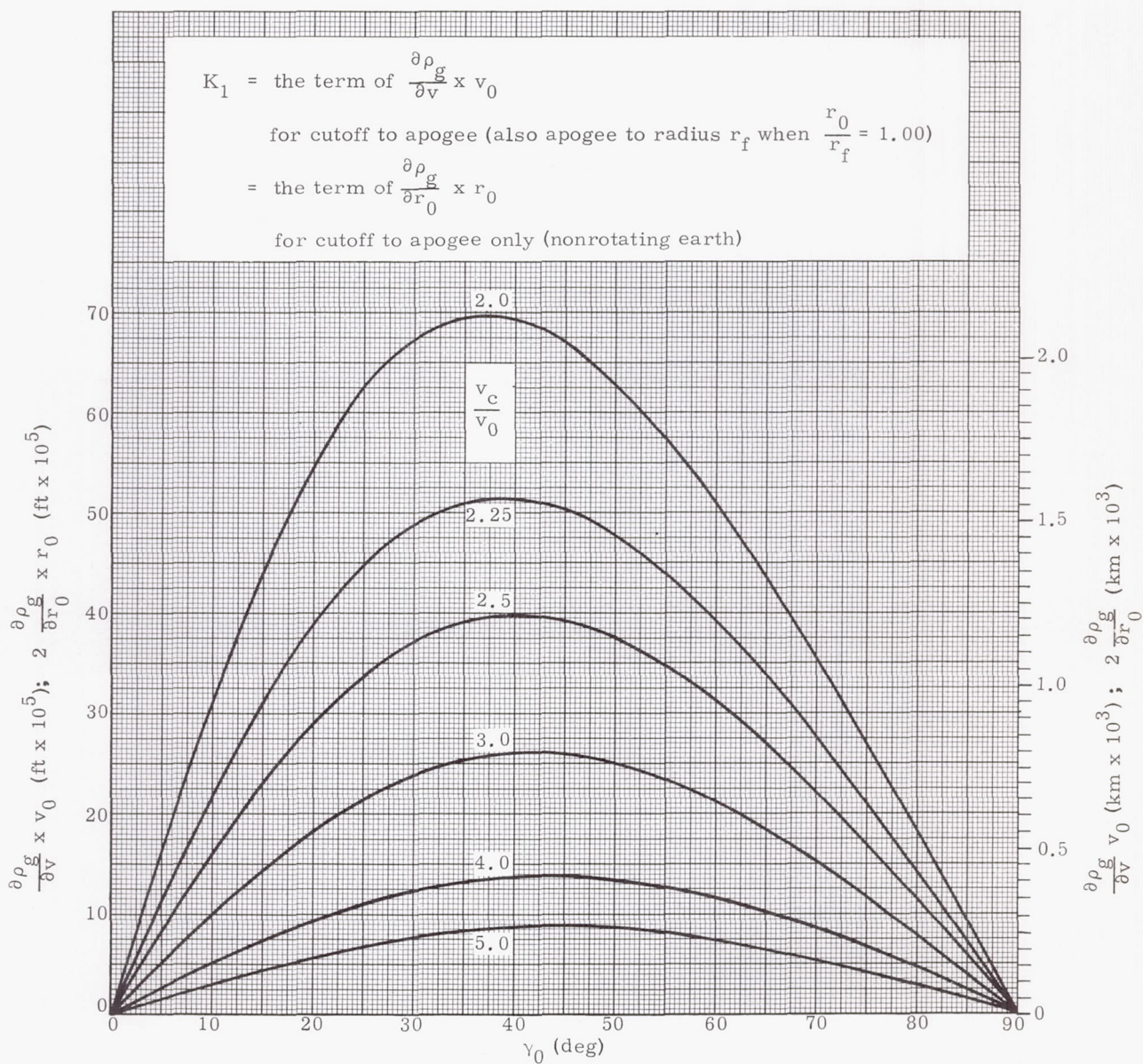


Fig. 4. Vacuum Ballistic Trajectory Error Analysis
(velocity and radius partials, expanded scale)

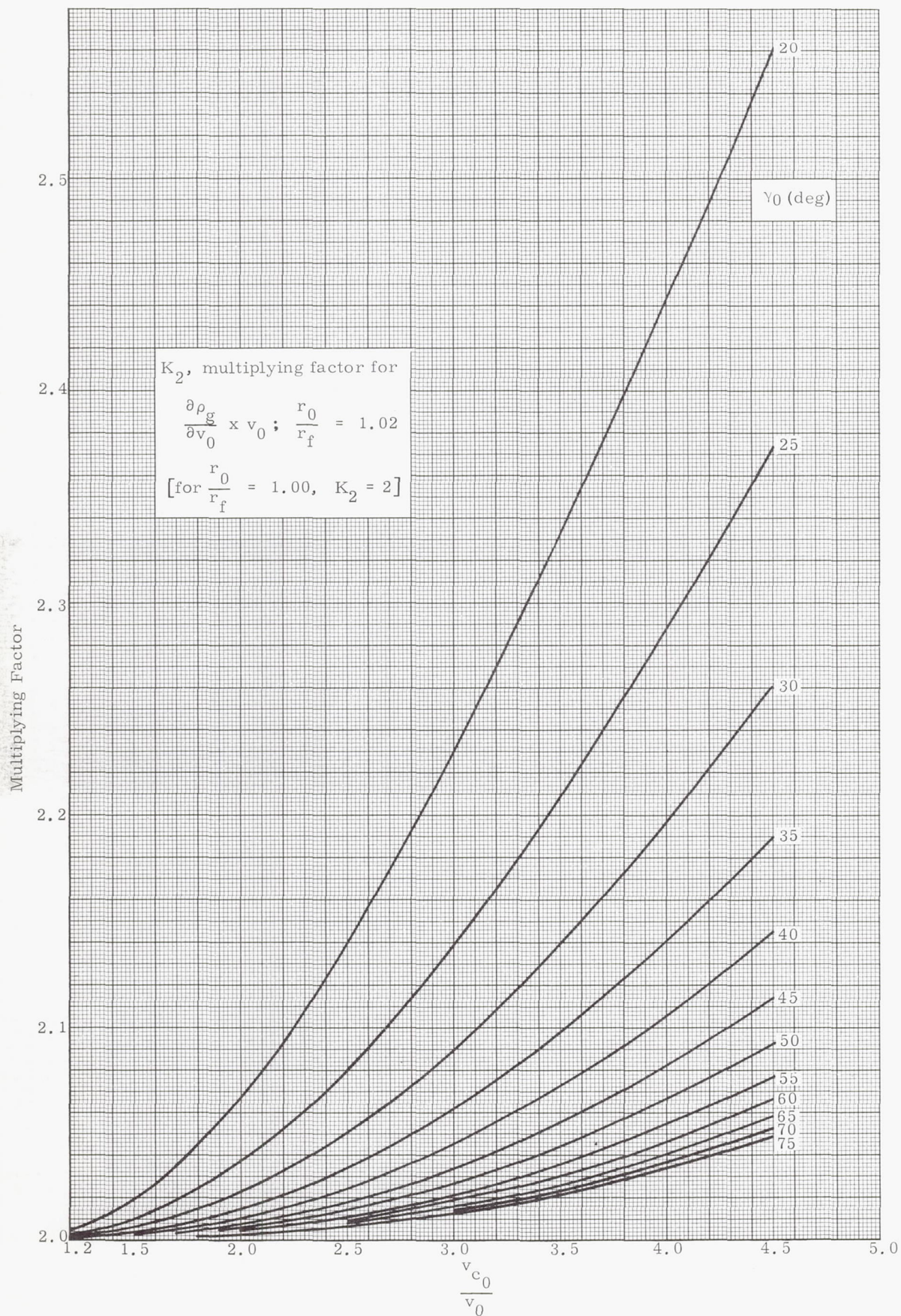


Fig. 5. Vacuum Ballistic Trajectory Error Analysis (correction for $r_0/r_f = 1.02$)

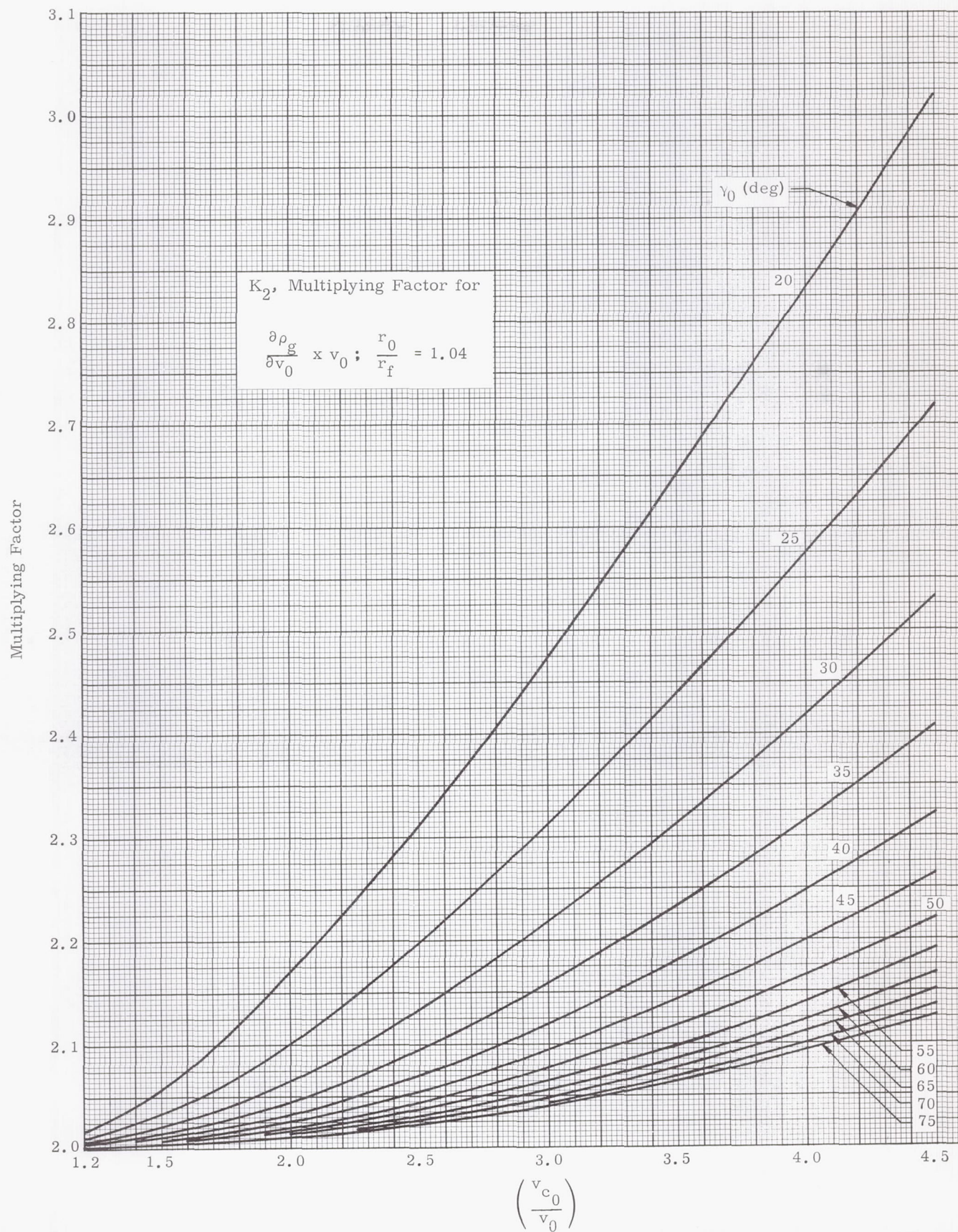


Fig. 6. Vacuum Ballistic Trajectory Error Analysis (correction for $r_0/r_f = 1.04$)

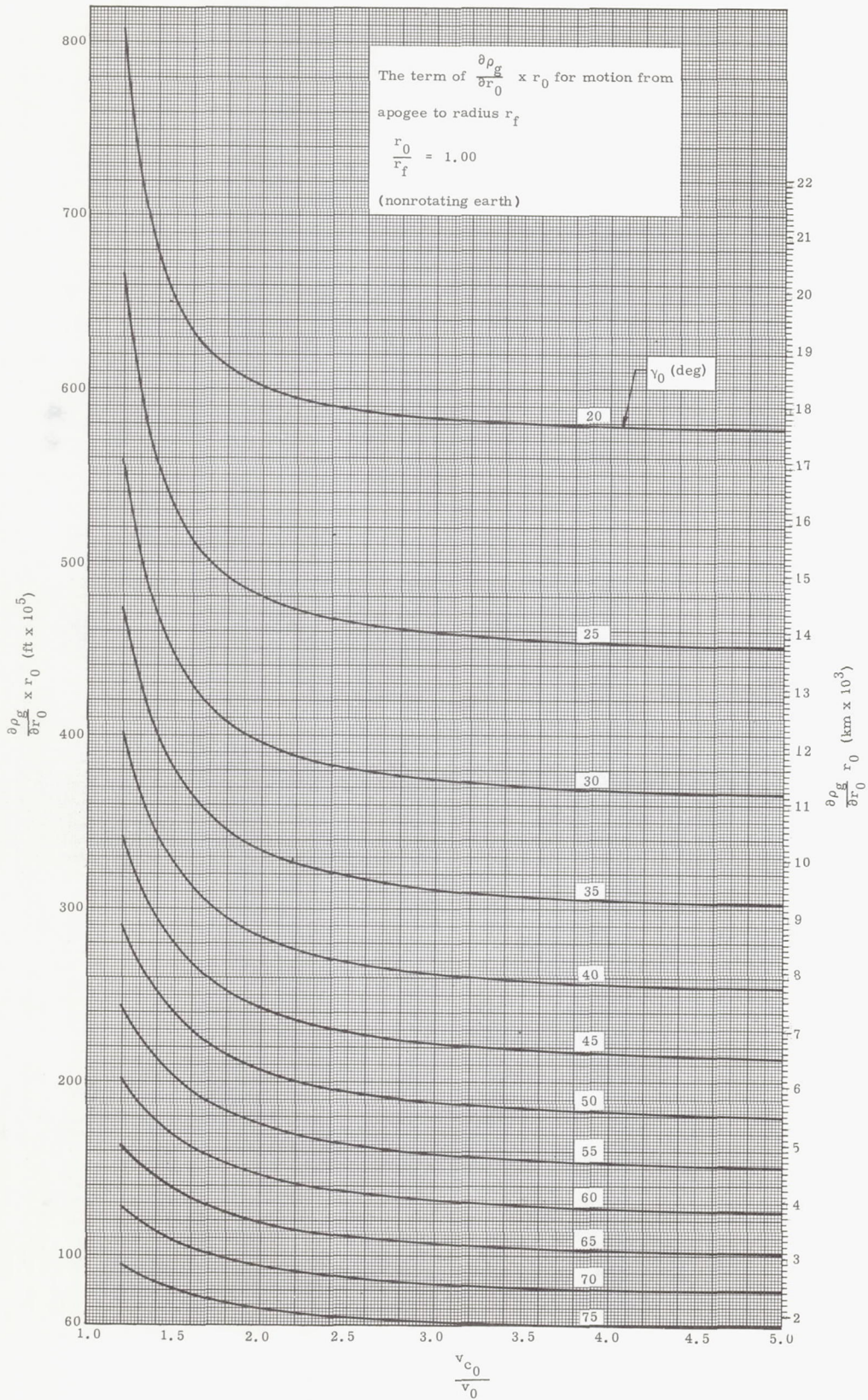


Fig. 7. Vacuum Ballistic Trajectory Error Analysis (radius partial, apogee to r_f , $r_f = r_0$)

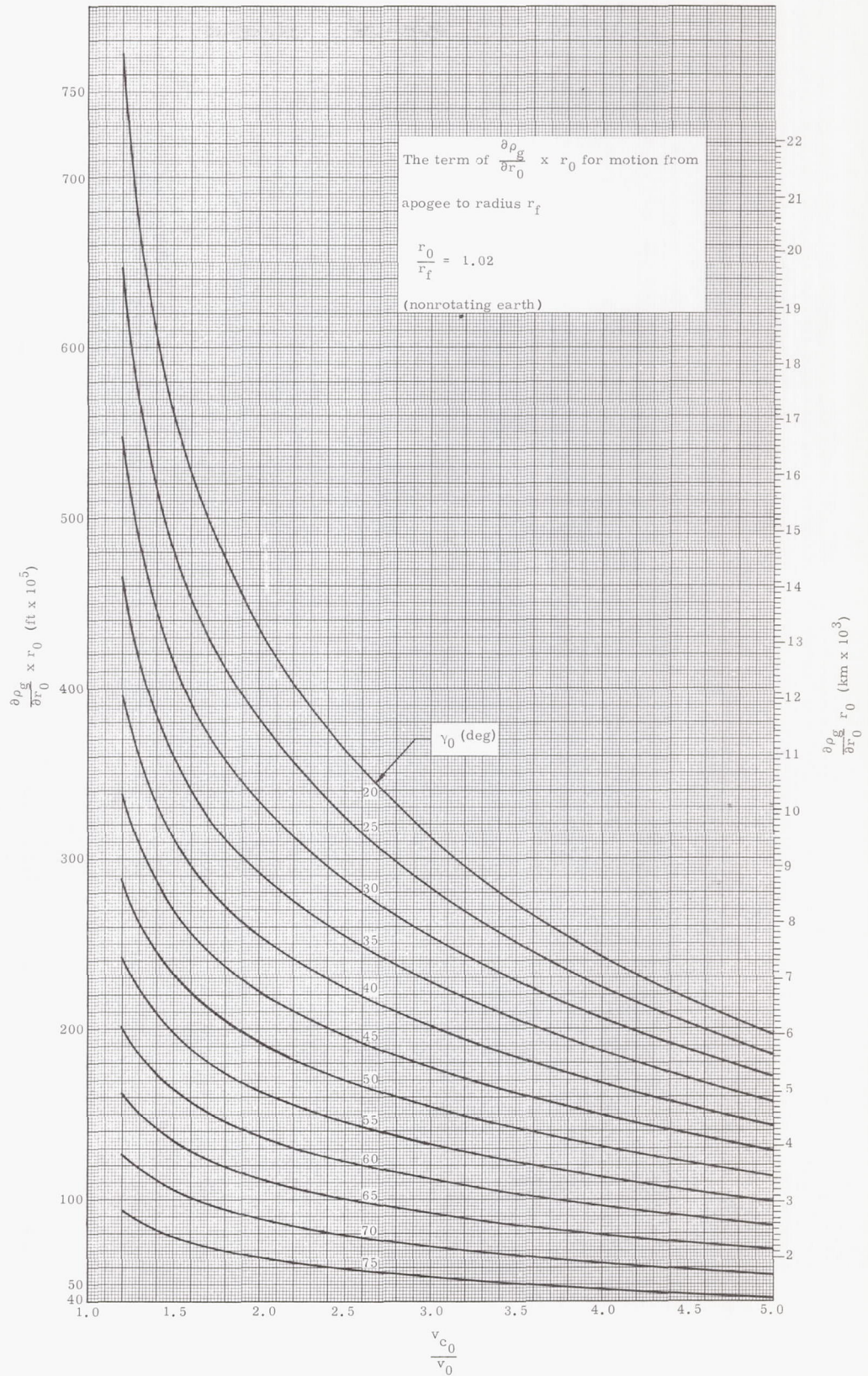


Fig. 8. Vacuum Ballistic Trajectory Error Analysis (radius partial, apogee to r_f , $r_f = r_0/1.02$)

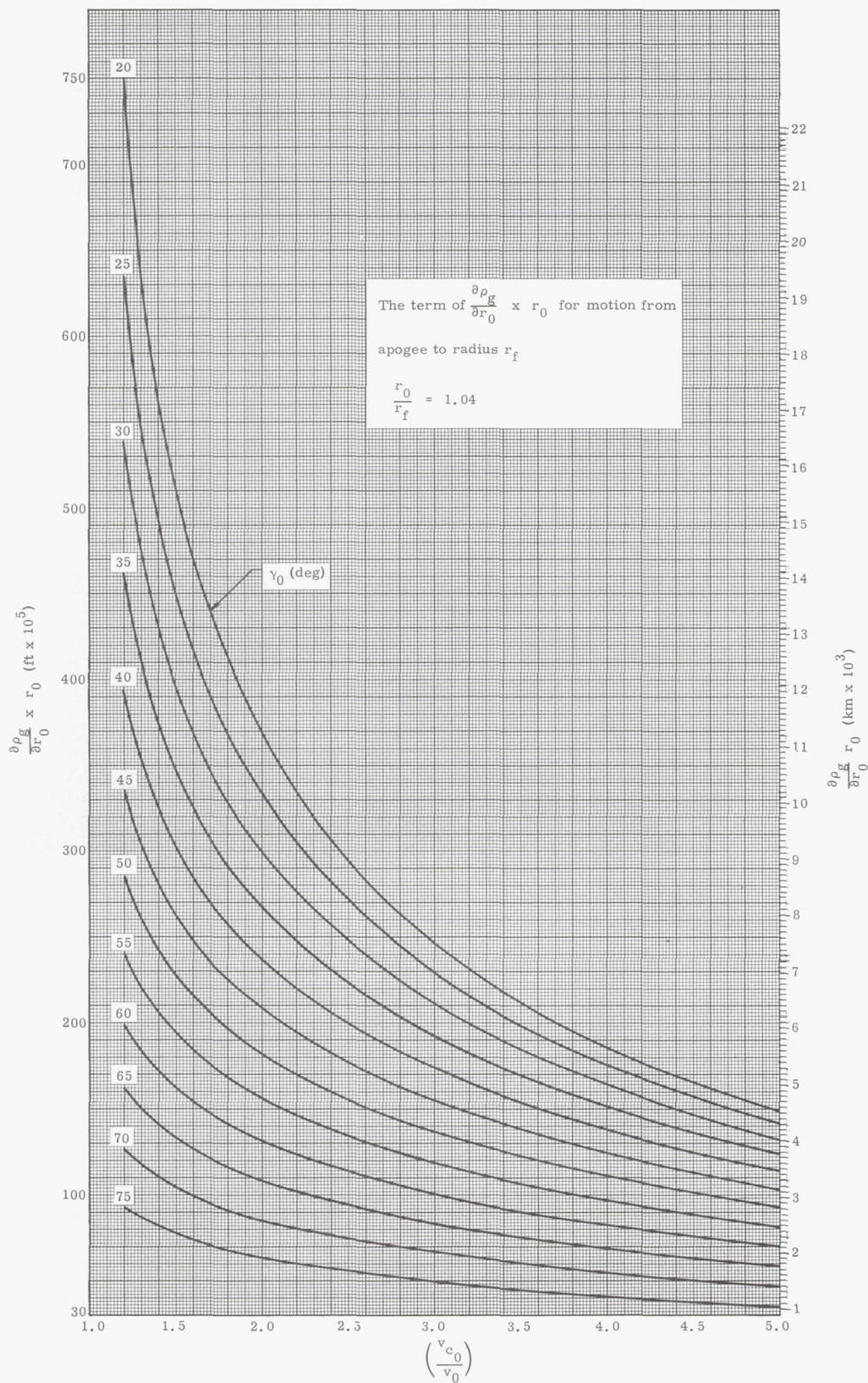


Fig. 9. Vacuum Ballistic Trajectory Error Analysis
(radius partial, apogee to r_f , $r_f = r_0/1.04$)

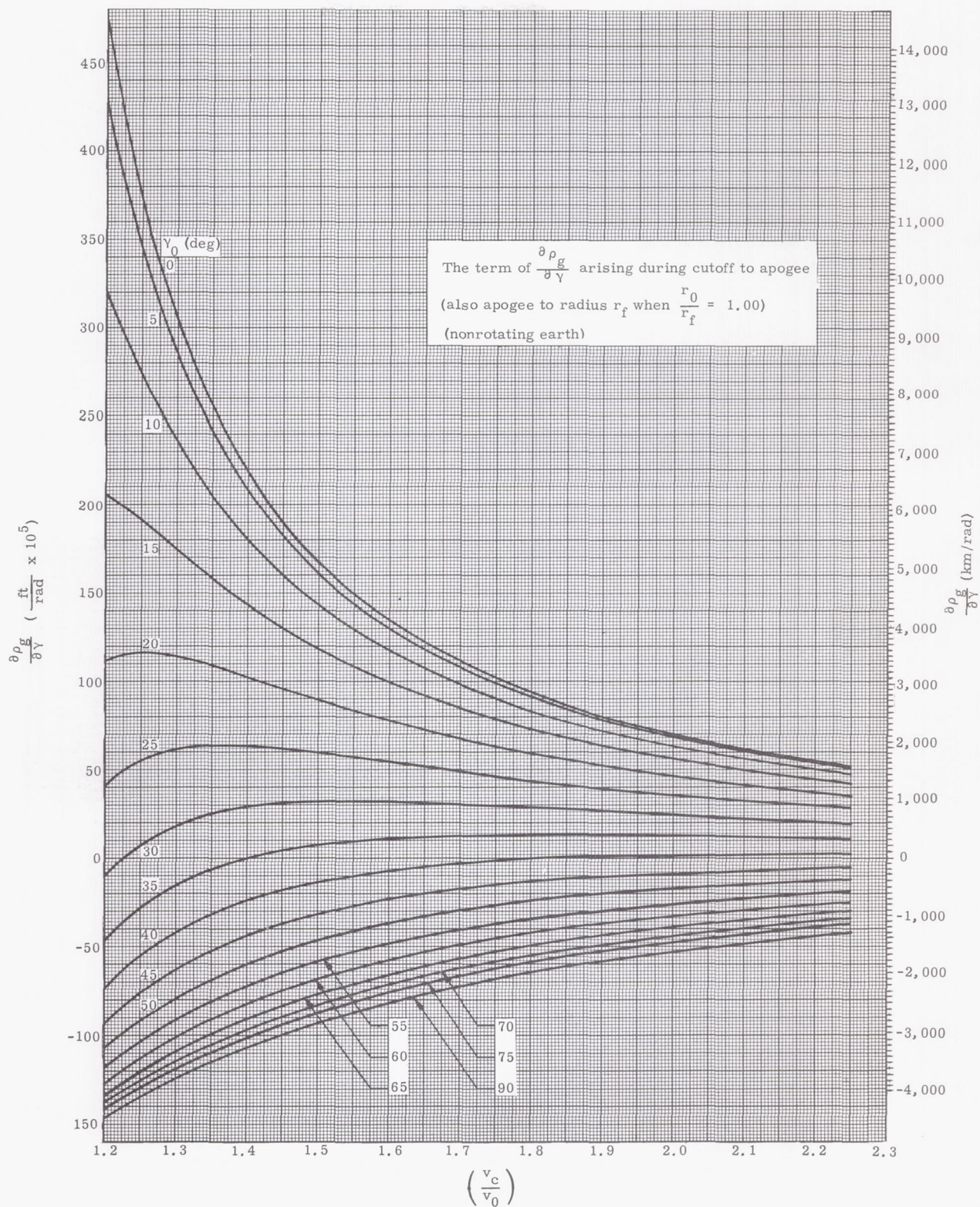


Fig. 10. Vacuum Ballistic Trajectory Error Analysis
(flight path angle partial, $r_0/r_f = 1.00$)

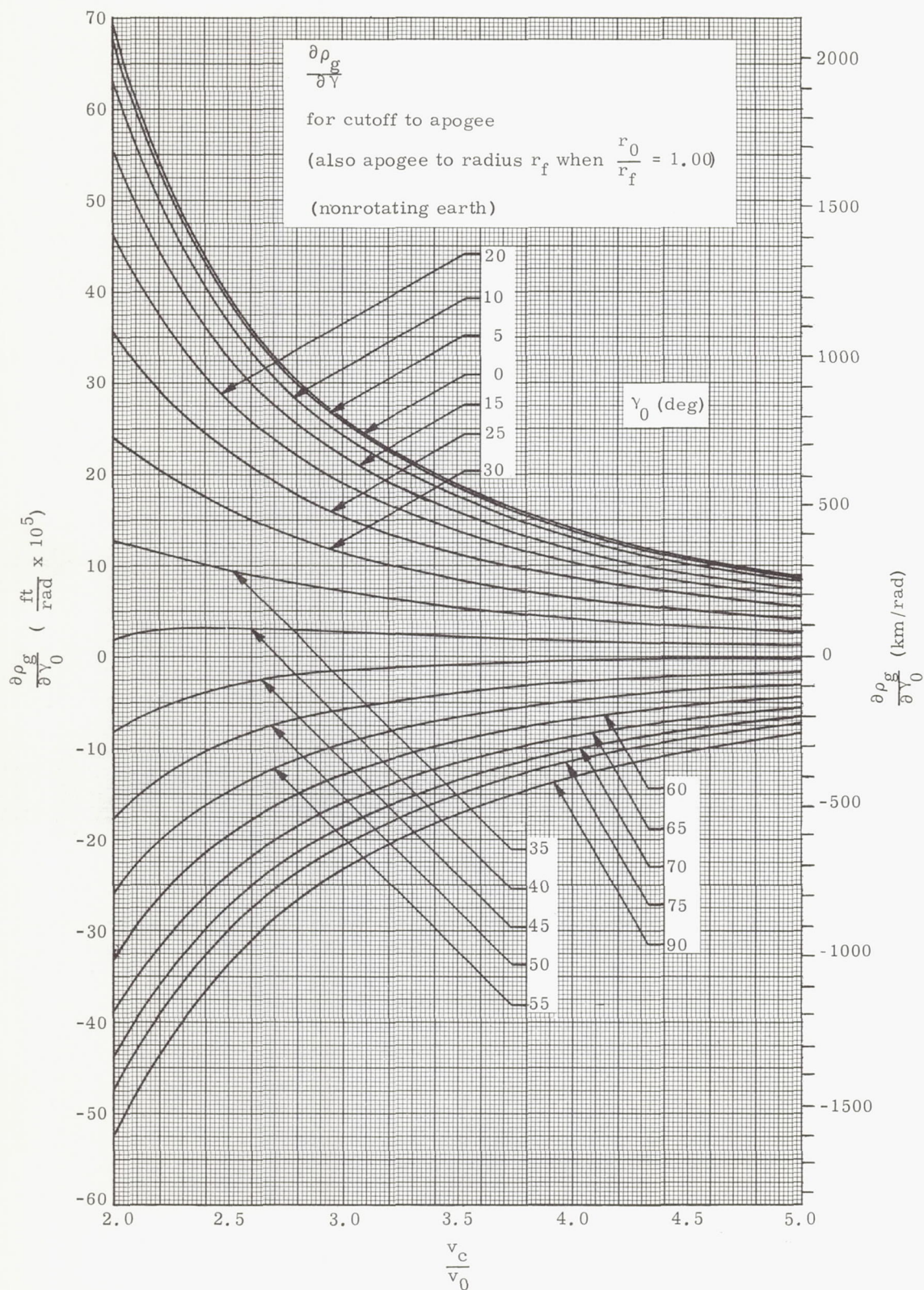


Fig. 11. Vacuum Ballistic Trajectory Error Analysis (flight path angle partial, extended velocities, $r_0/r_f = 1.00$)

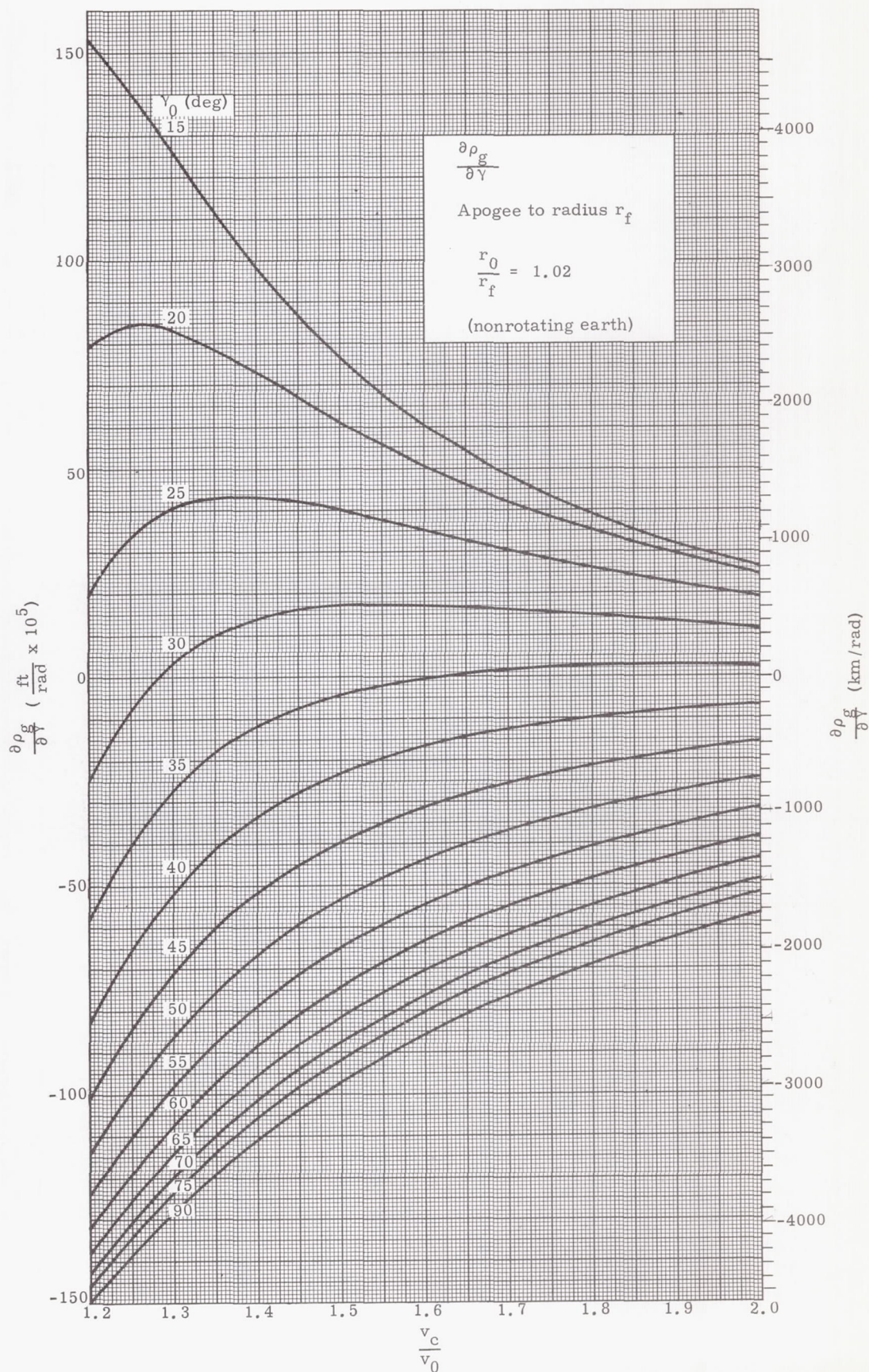


Fig. 12. Vacuum Ballistic Trajectory Error Analysis (flight path angle partial, $r_0/r_f = 1.02$)

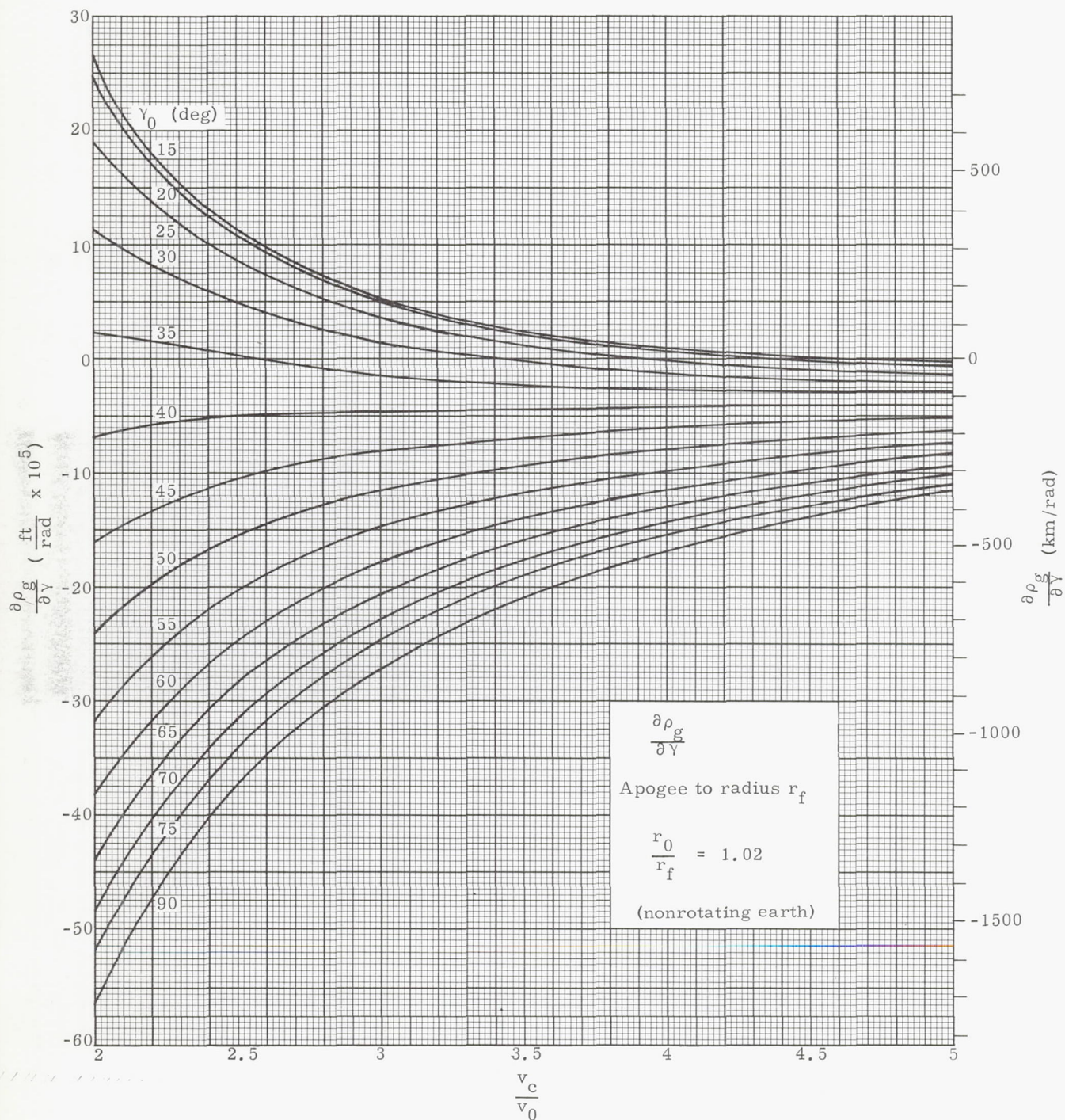


Fig. 13. Vacuum Ballistic Trajectory Error Analysis
(flight path angle partial, extended, $r_0/r_f = 1.02$)

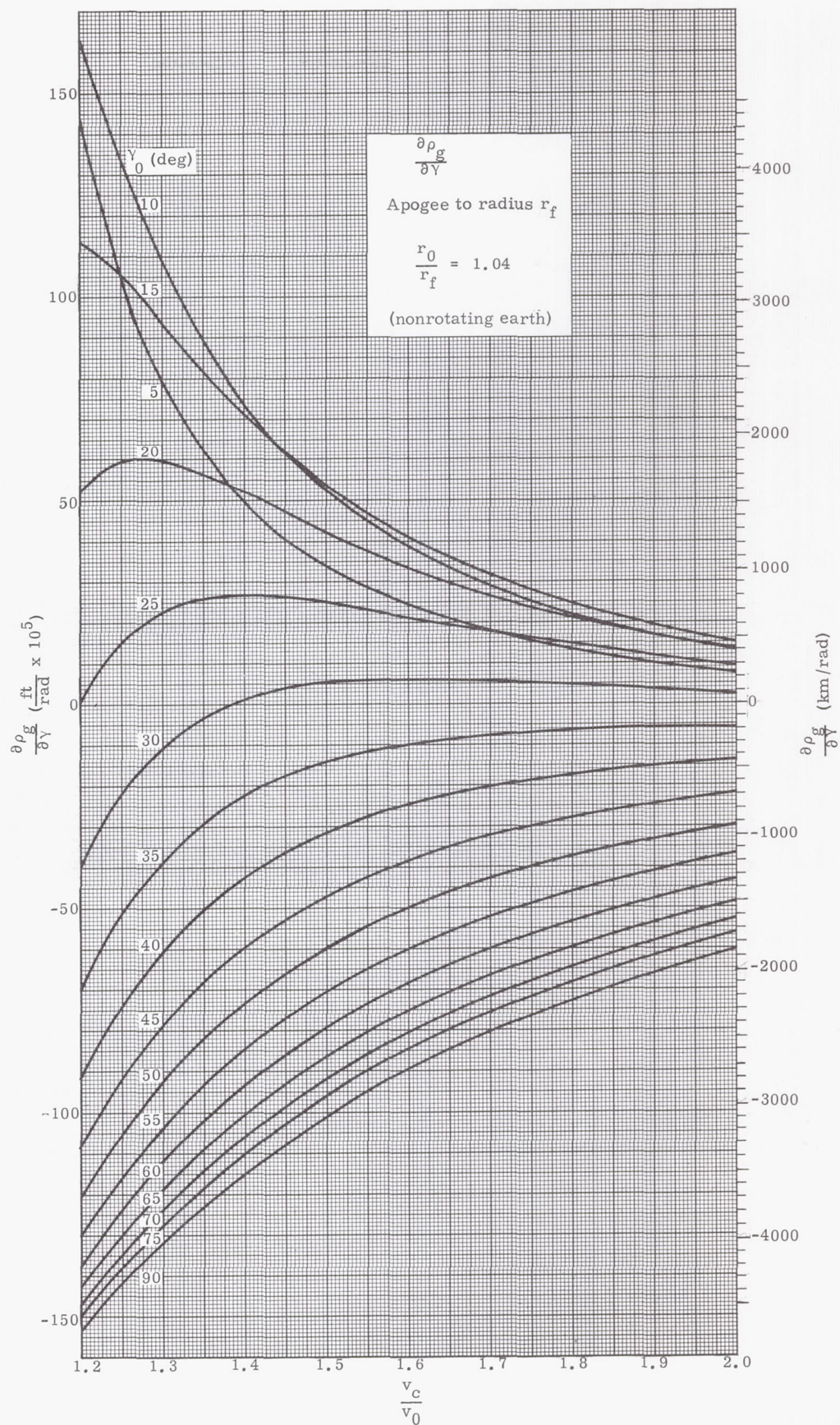


Fig. 14. Vacuum Ballistic Trajectory Error Analysis (flight path angle partial $r_0/r_f = 1.04$)

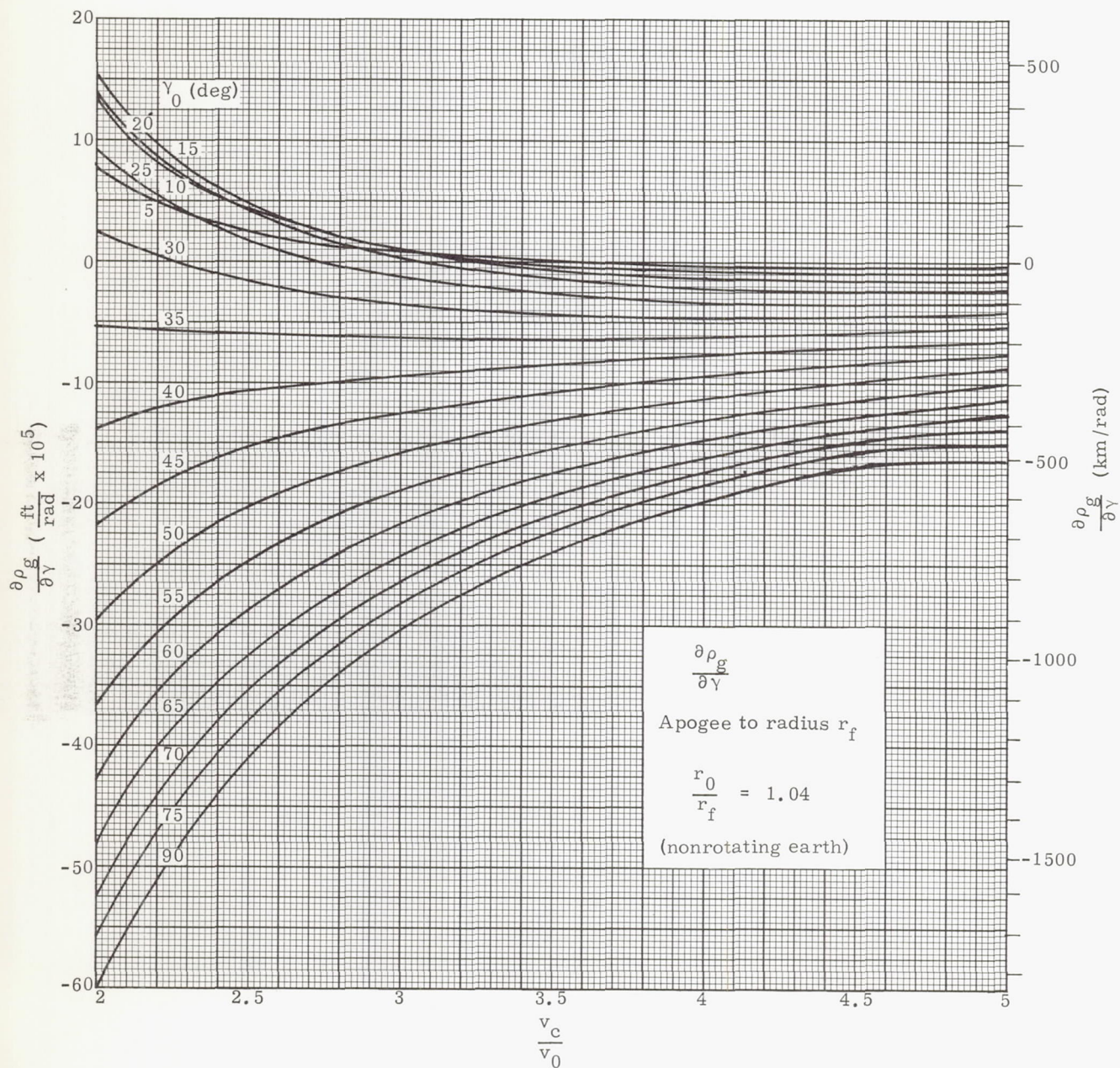


Fig. 15. Vacuum Ballistic Trajectory Error Analysis (flight path angle partials, extended velocities, $r_0/r_f = 1.04$)

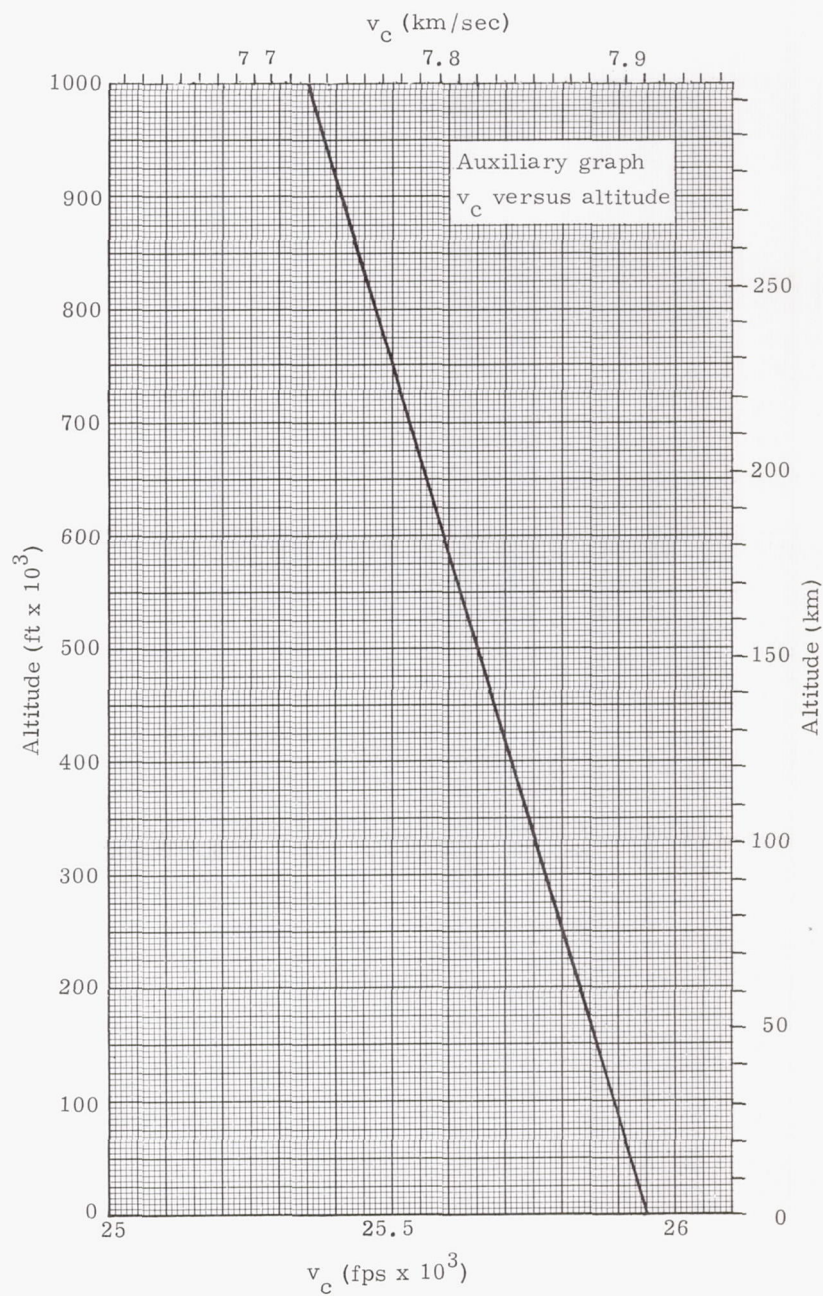


Fig. 16. Vacuum Ballistic Trajectory Error Analysis
 (circular velocity as a function of altitude)

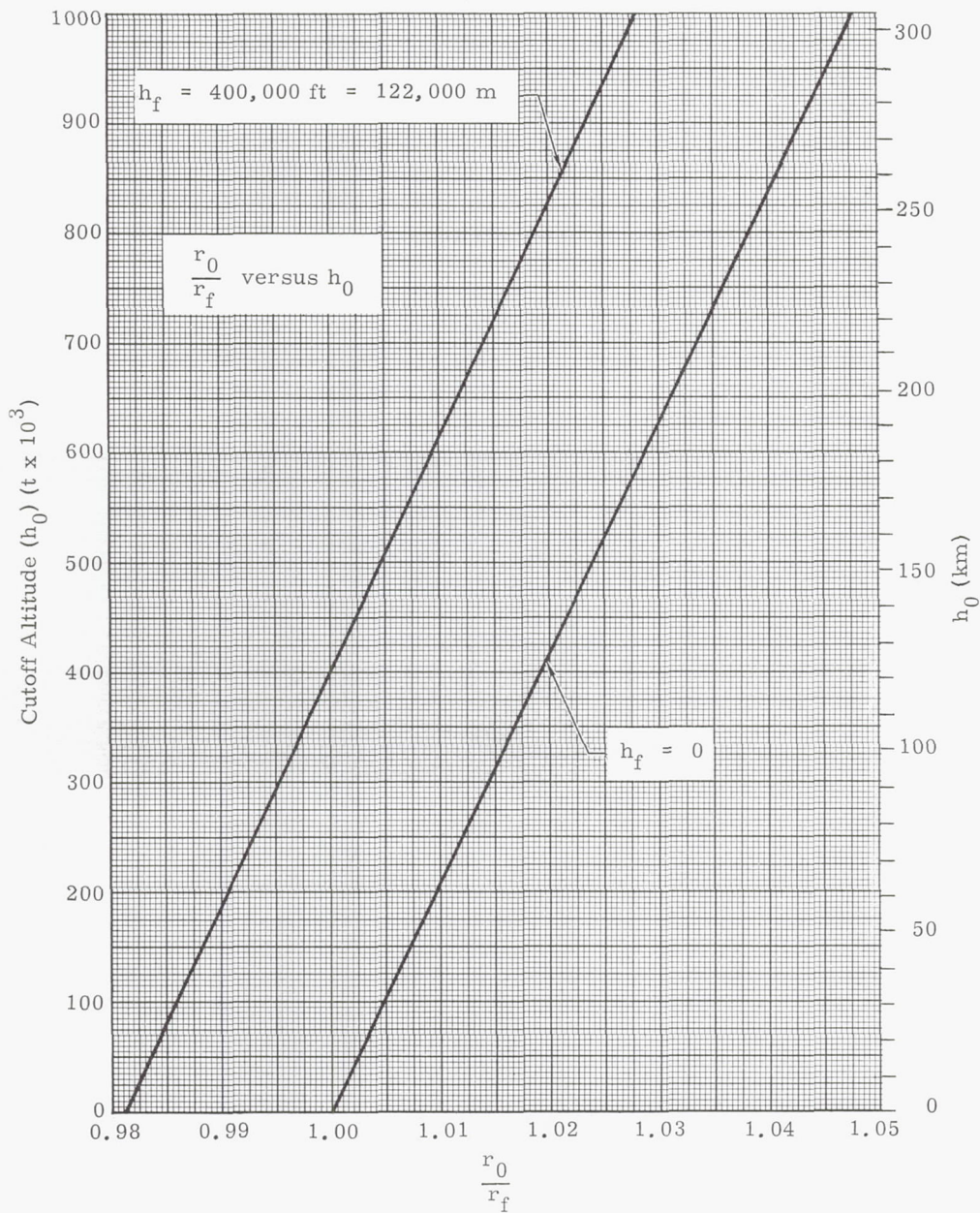


Fig. 17. Vacuum Ballistic Trajectory Error Analysis
 $(r_0/r_f$ as a function of h_0 and h_f)

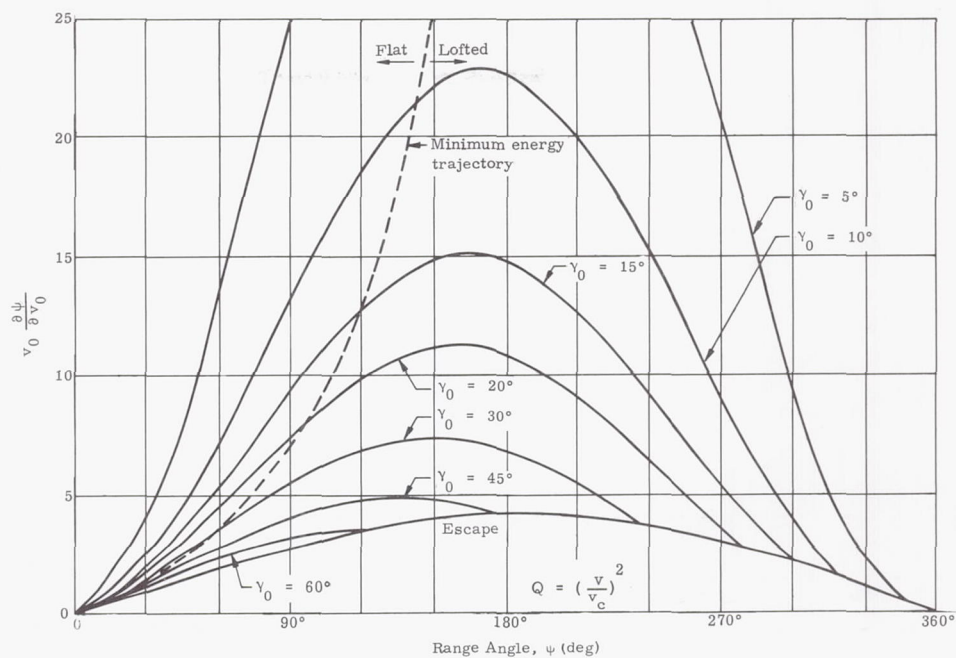


Fig. 18. Altitude and Velocity Influence Coefficients Versus Range (for values of elevation angle γ_0)

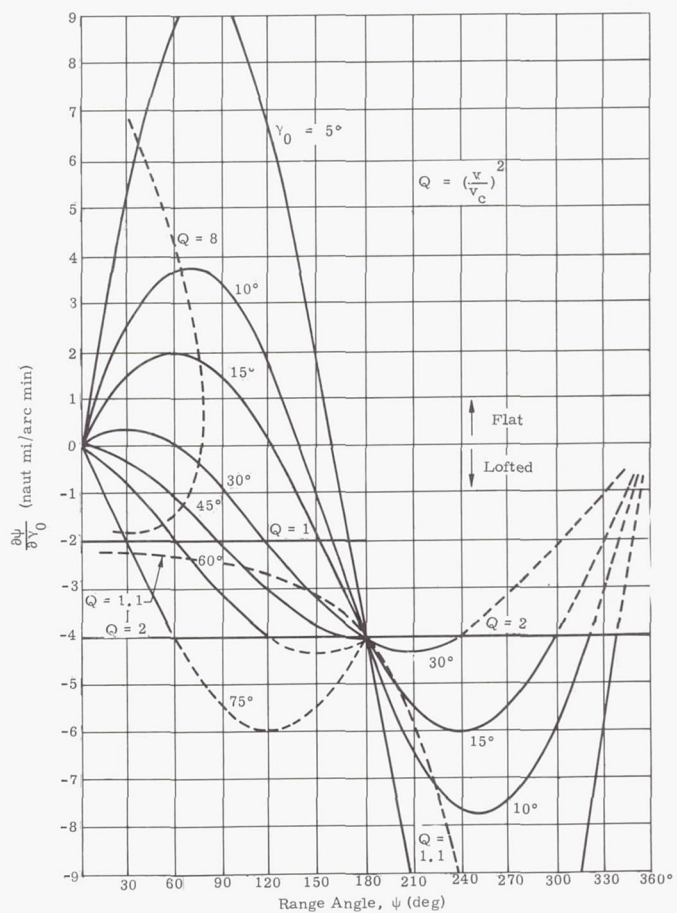


Fig. 19. Elevation Angle Influence Coefficient Versus Range (for values of elevation angle γ_0)

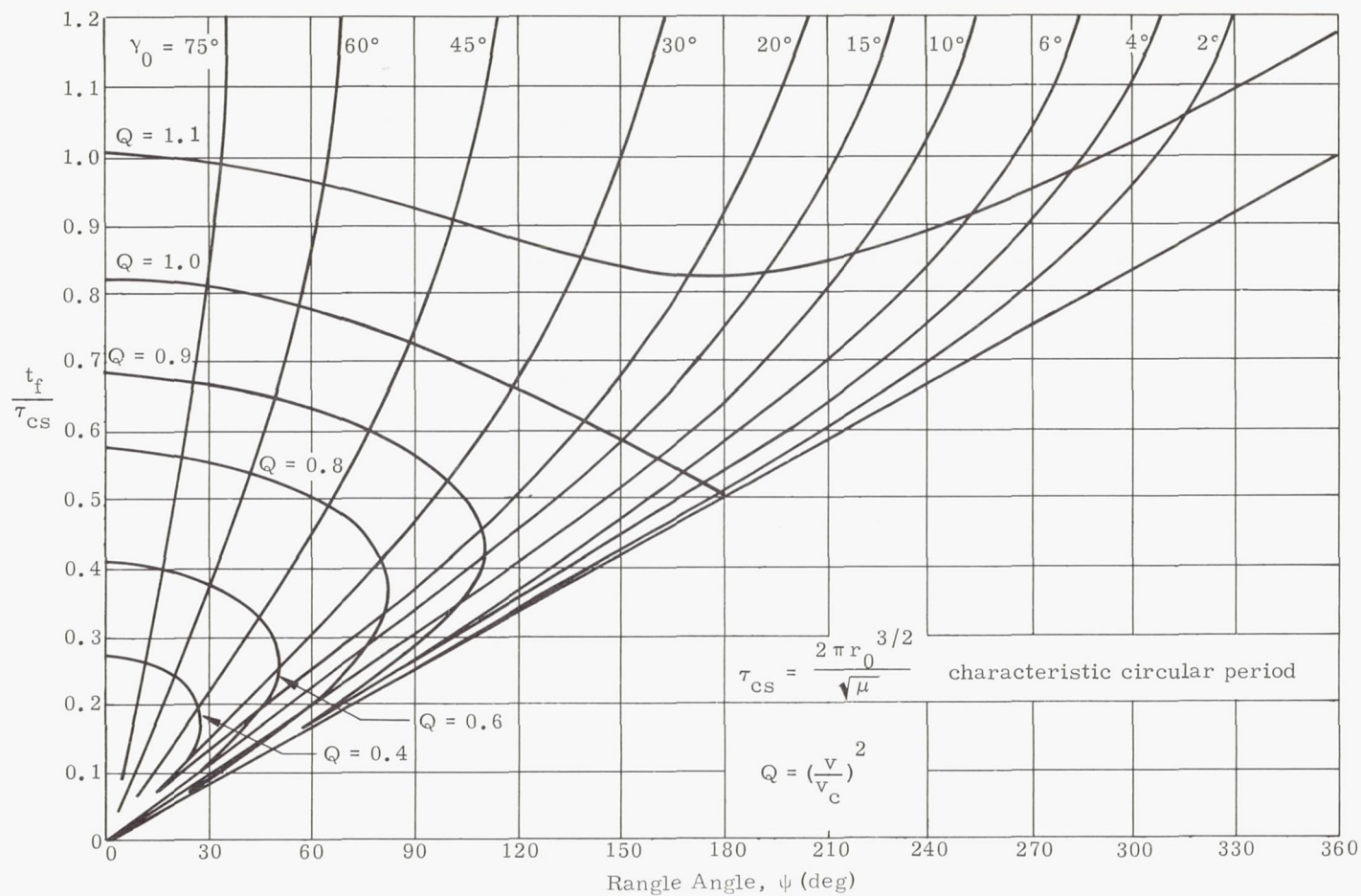


Fig. 20. Time of Flight Versus Range

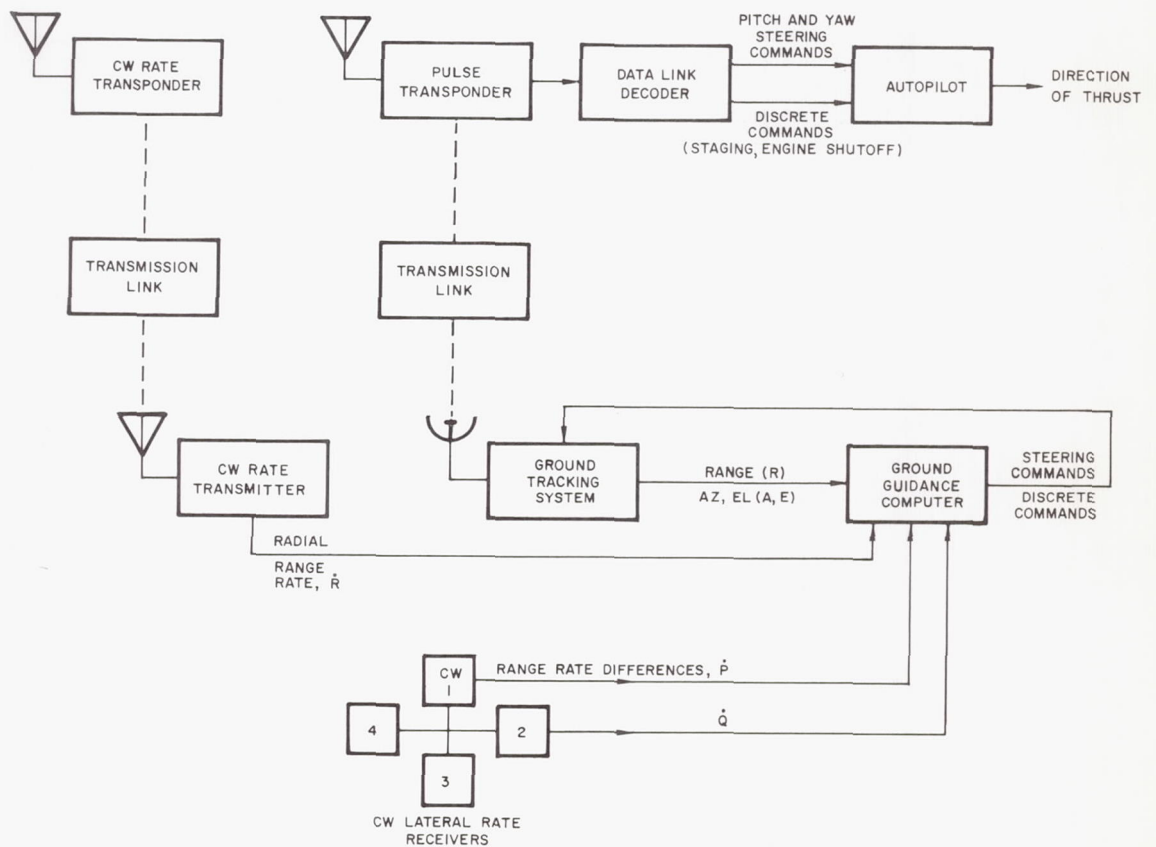
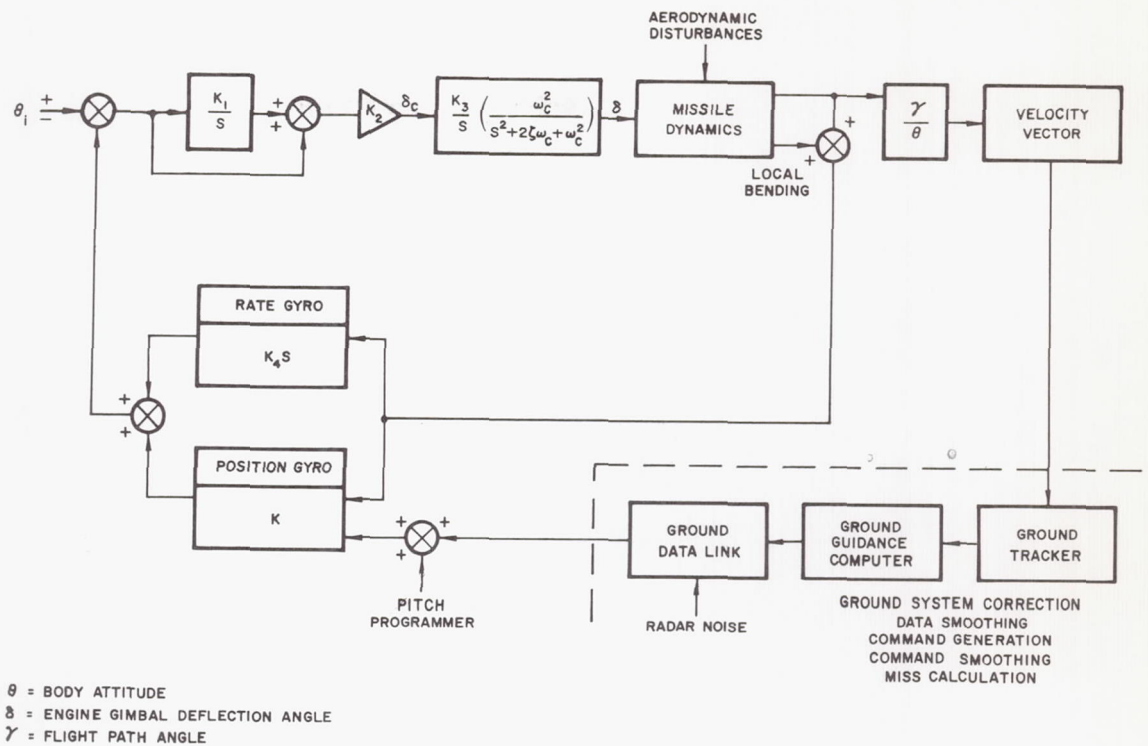


Fig. 22. Functional Block Diagram for a Radio-Inertial System

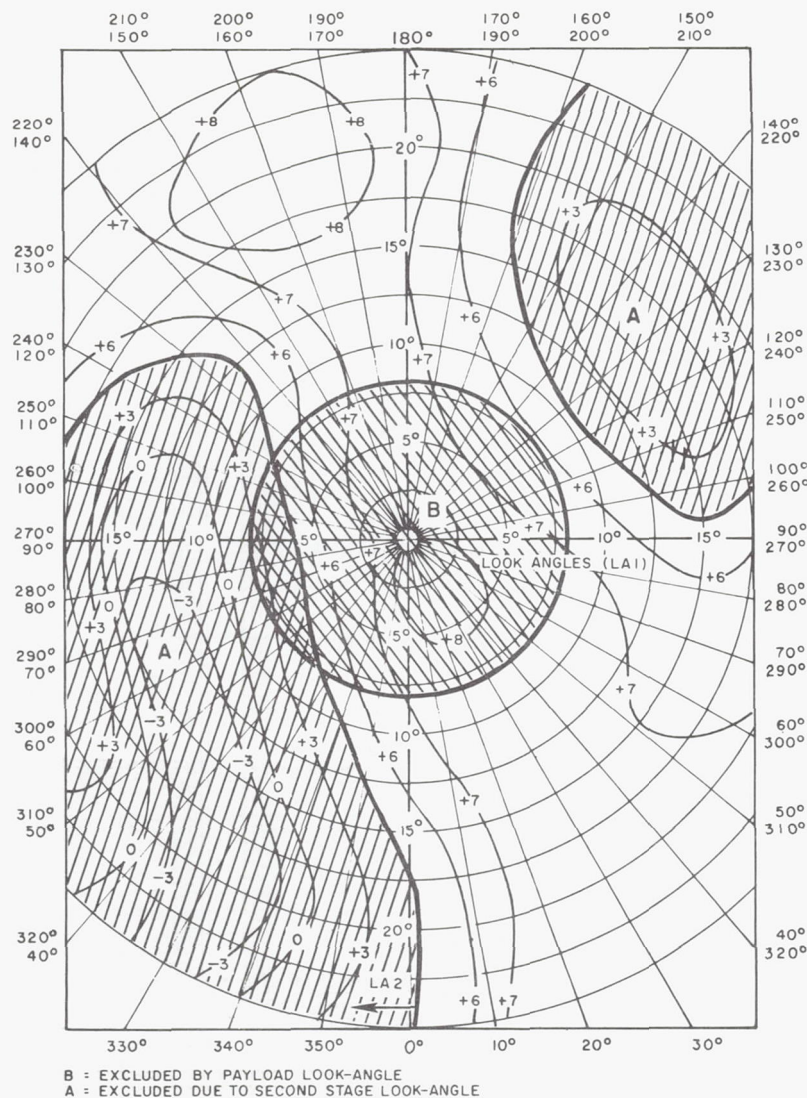


Fig. 23. Actual Antenna Radiation Pattern Showing Important Trajectory Steering Constraints

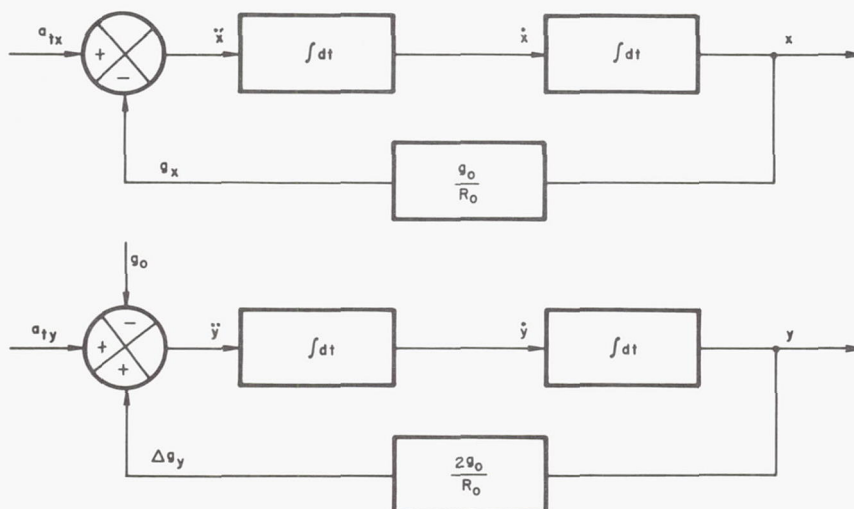


Fig. 24. Gravity Computer

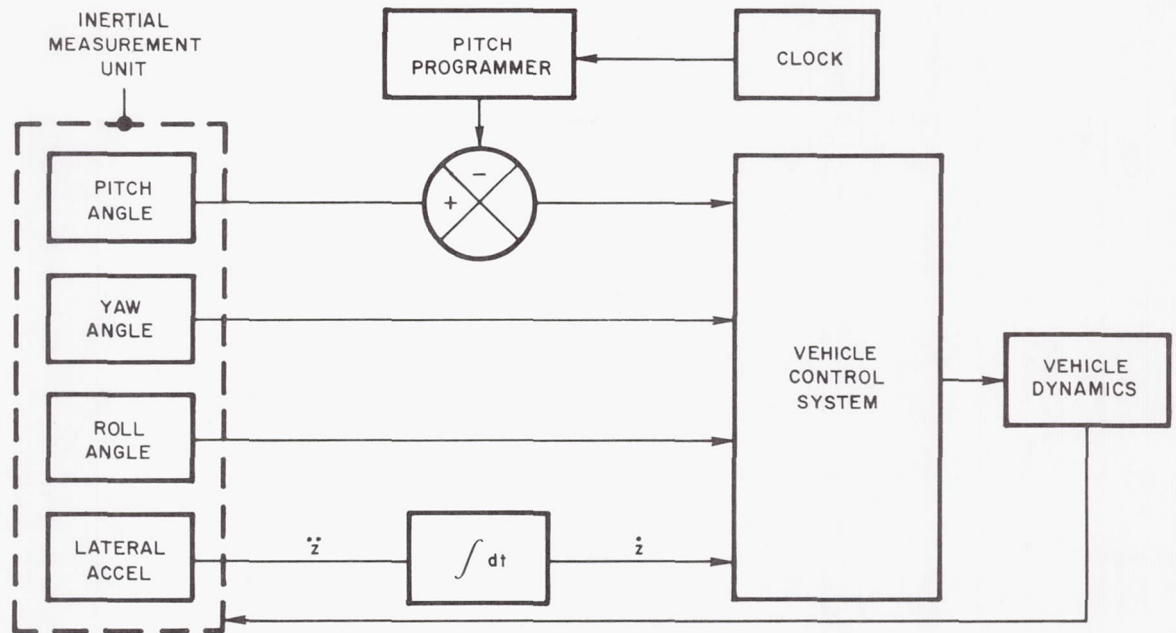


Fig. 25. Steering Computer

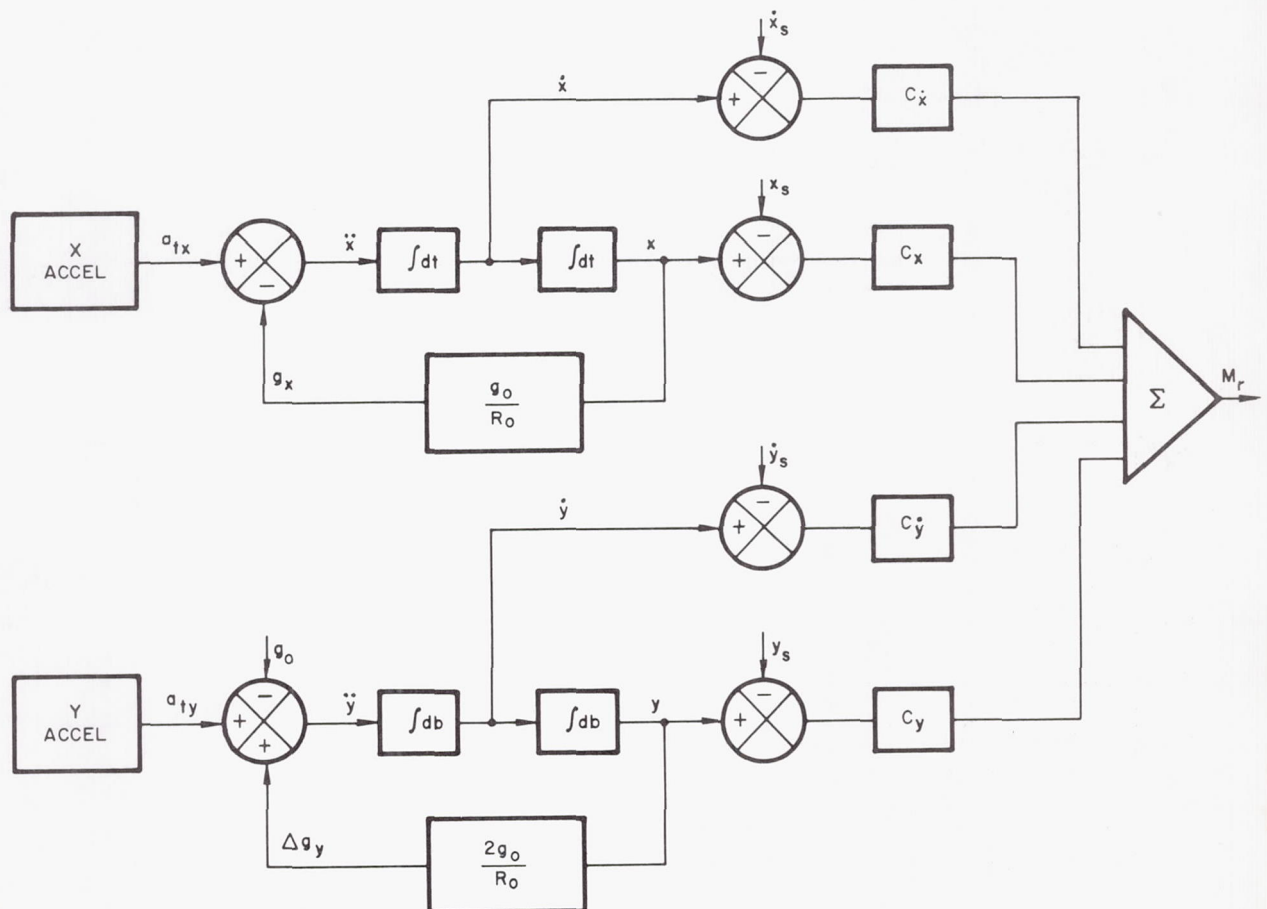


Fig. 26. Motor Shutoff Computer

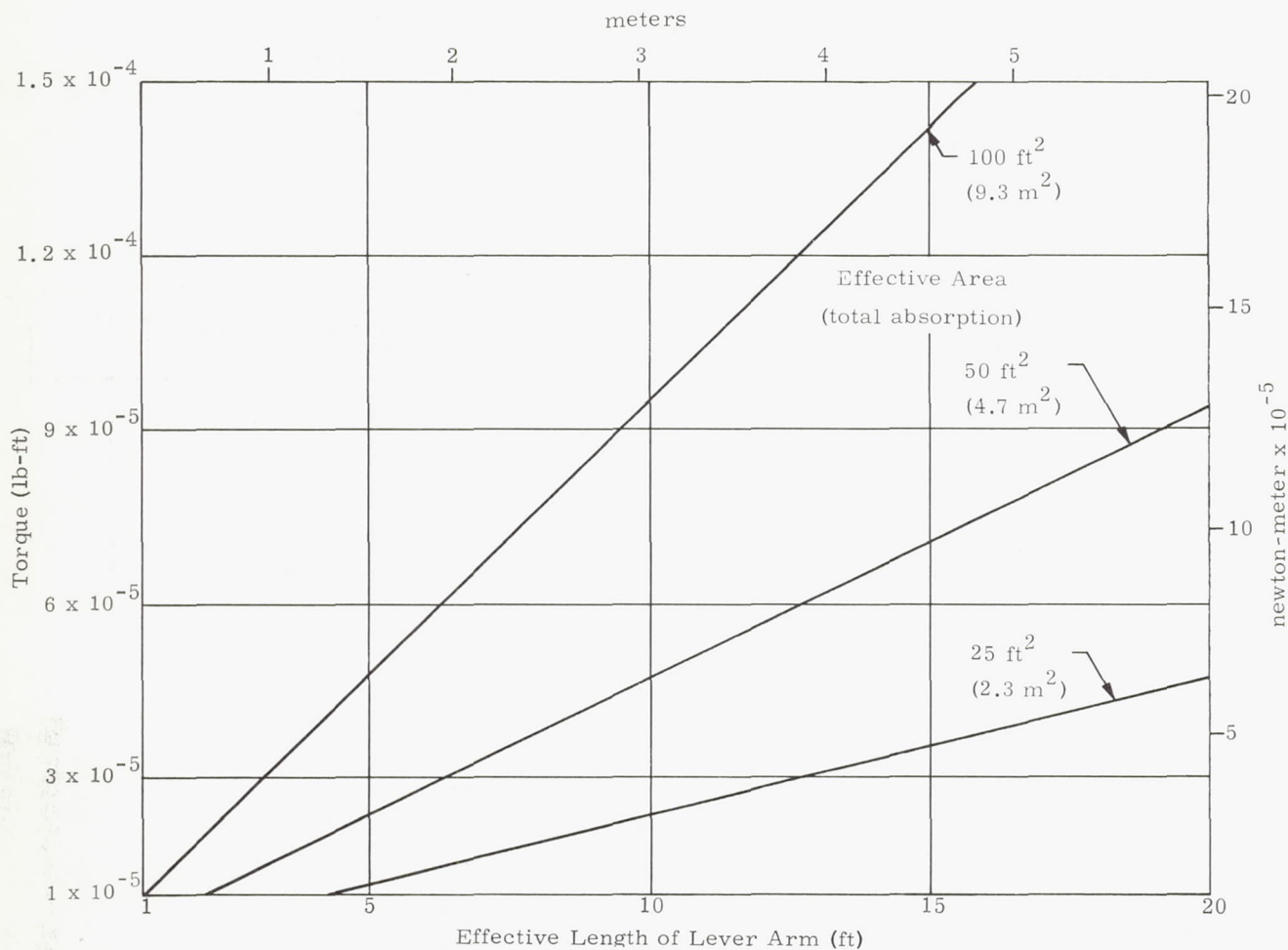


Fig. 27. Torque from Solar Radiation as a Function of Area and Lever Arm

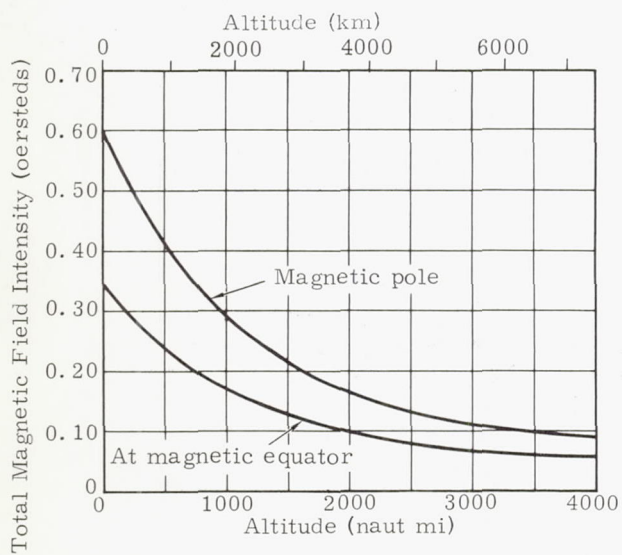


Fig. 28a. Field Intensity Versus Altitude for Earth's Magnetic Field

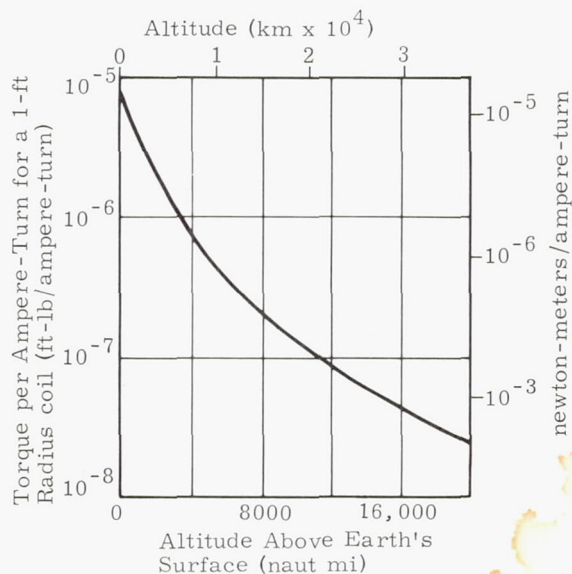


Fig. 28b. Maximum Torque per Ampere-Turn for a 1-ft Radius Coil Versus Altitude over the Magnetic Equator

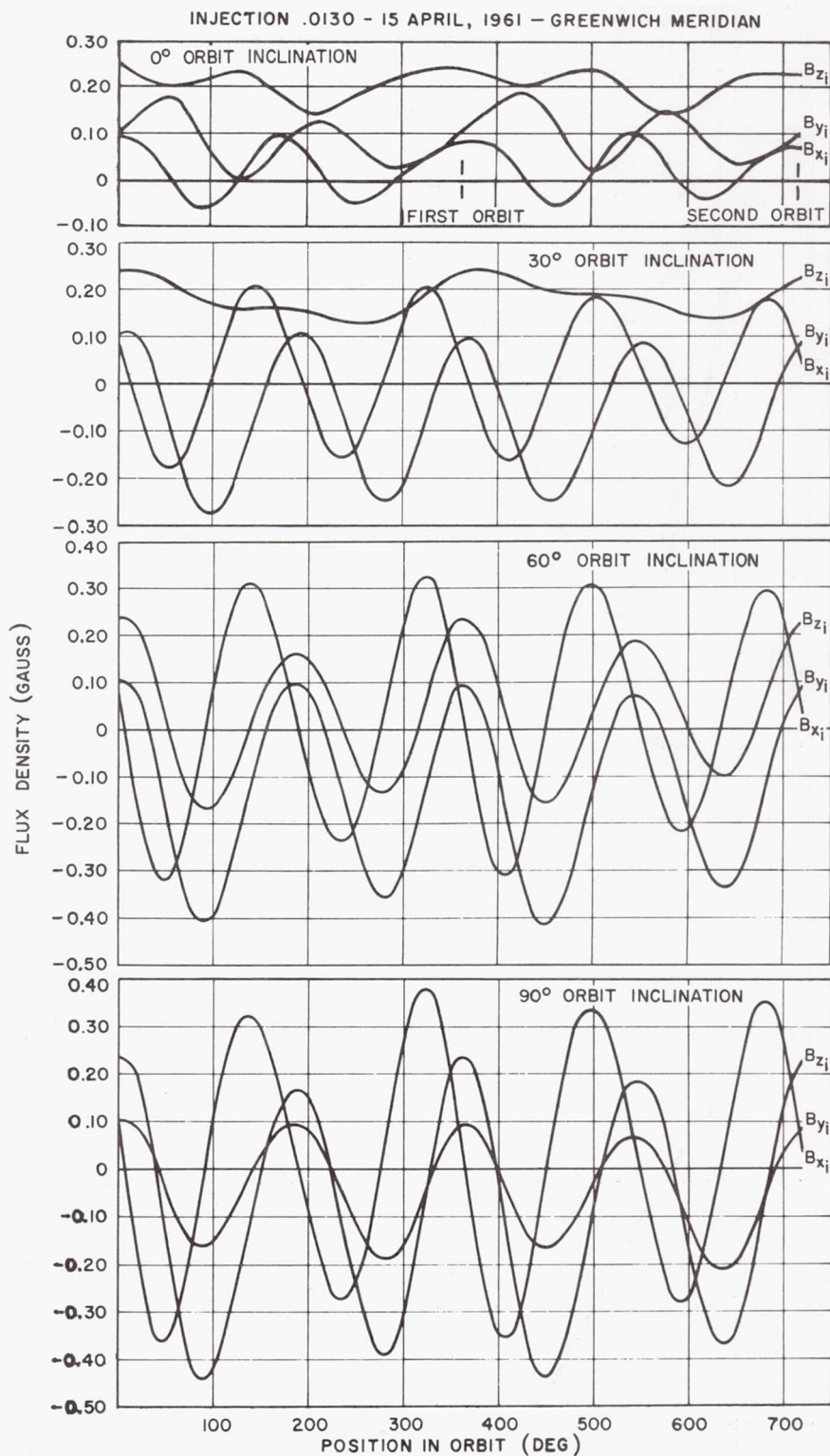


Fig. 29. Flux Density in Inertial Space Versus Position in 400-naut mi (741 km) Orbit

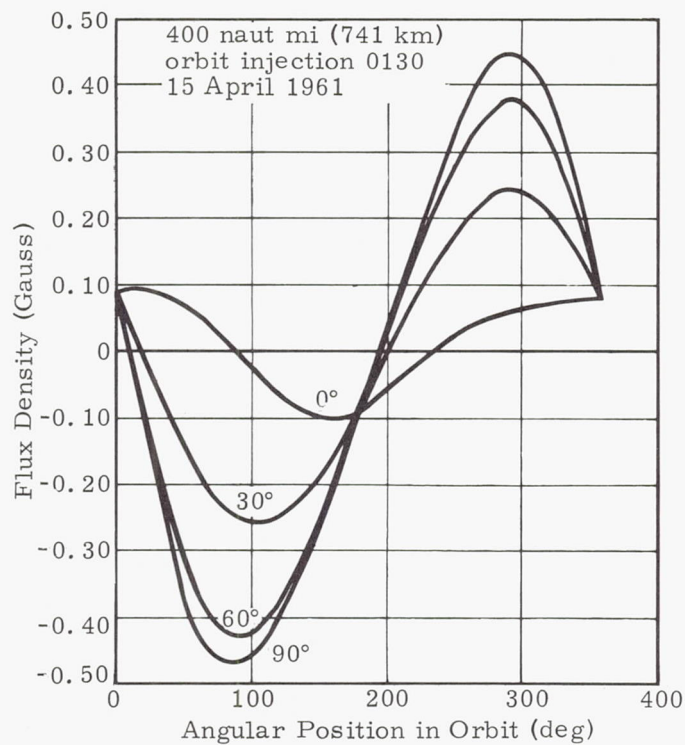


Fig. 30. Component of Flux Density Along Earth's Local Vertical in 400-naut mi Orbit for Several Orbit Inclinations (741 km)

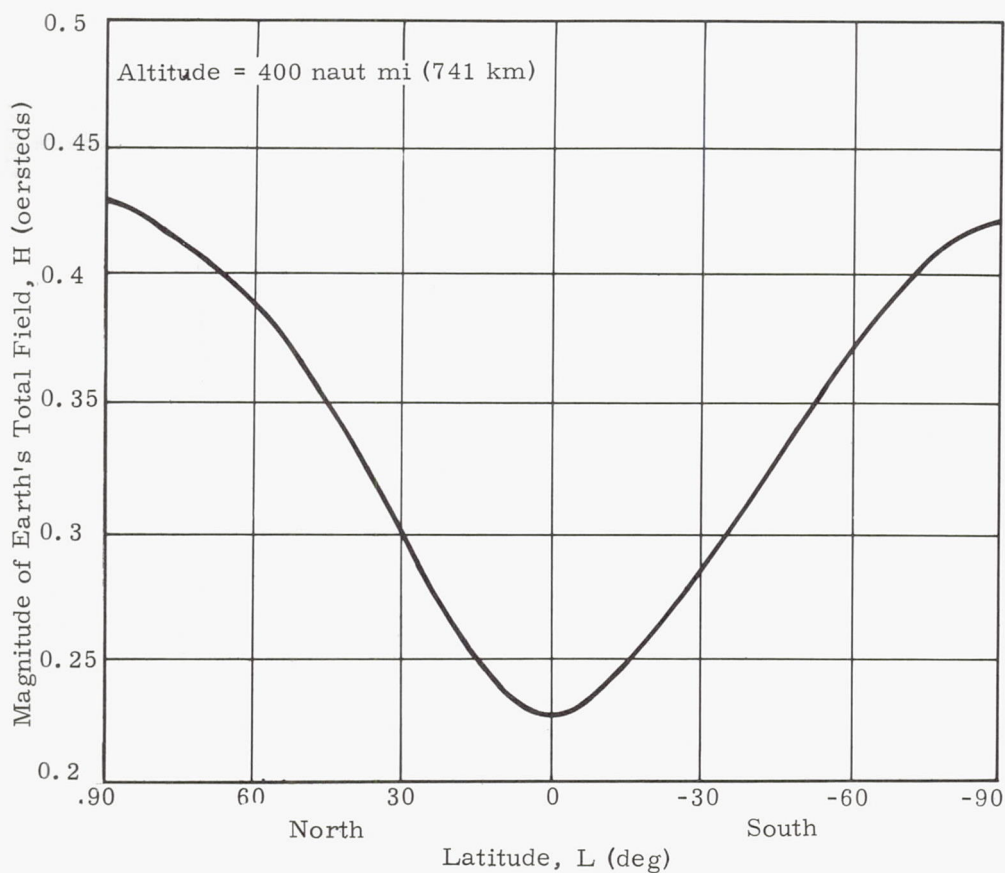


Fig. 31. Magnitude of Earth's Magnetic Field at 400 naut mi (741 km) as a Function of Latitude Assuming the Magnetic Dipole is Along the Earth's Spin Axis

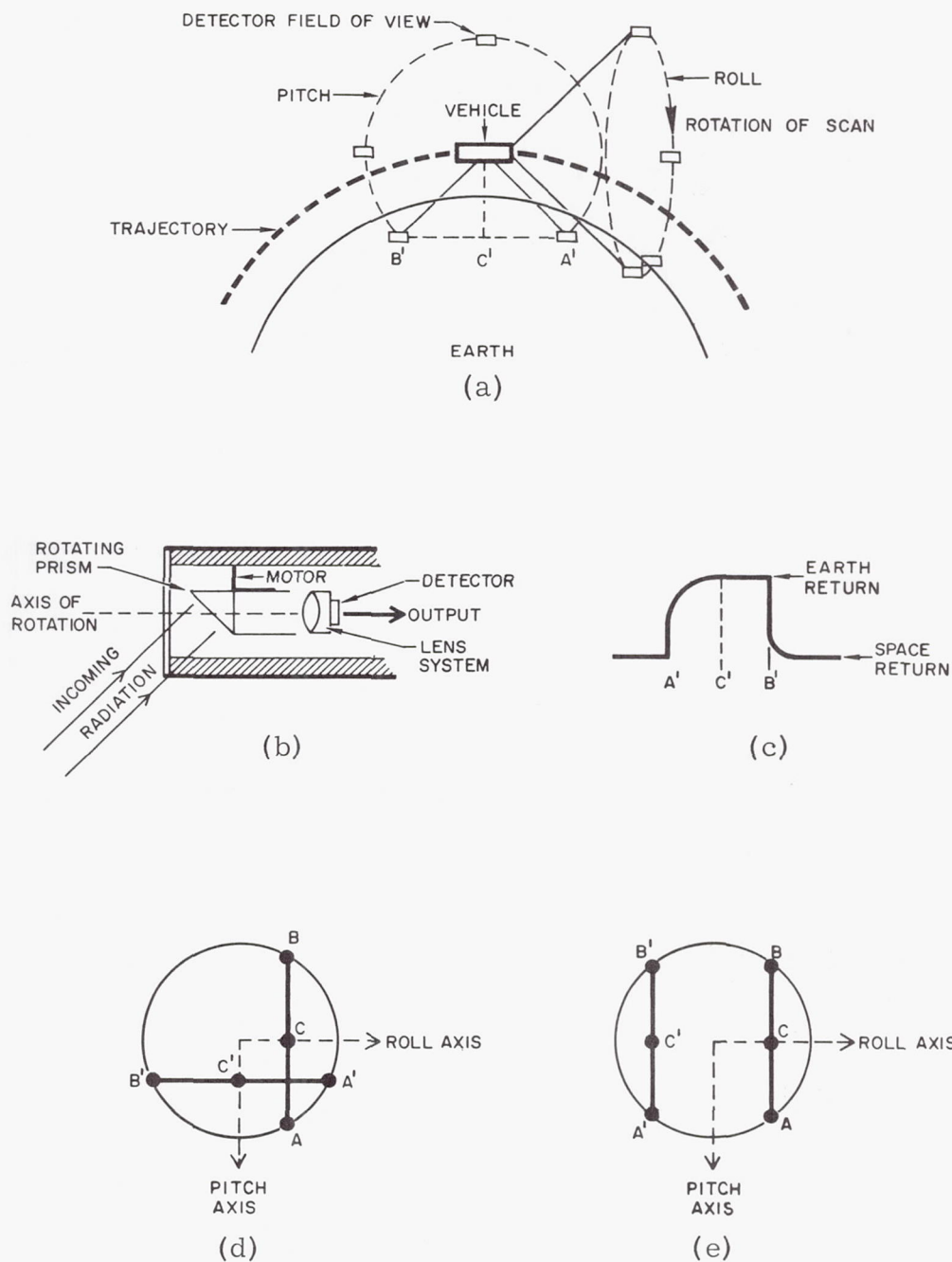


Fig. 32. Typical Conical Earth Scanning System

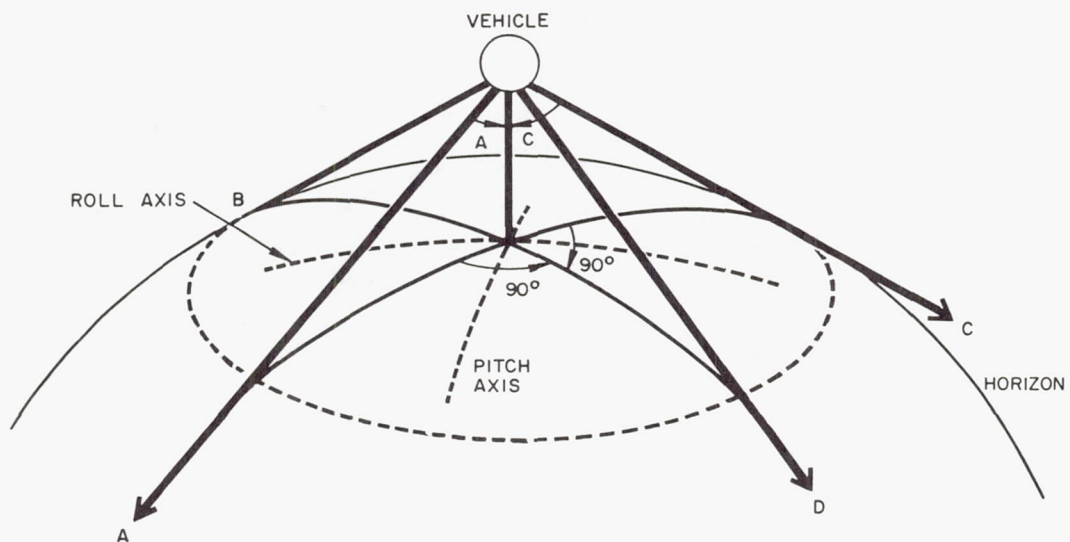


Fig. 33. Geometry for Using Edge Tracking to Generate Attitude Information

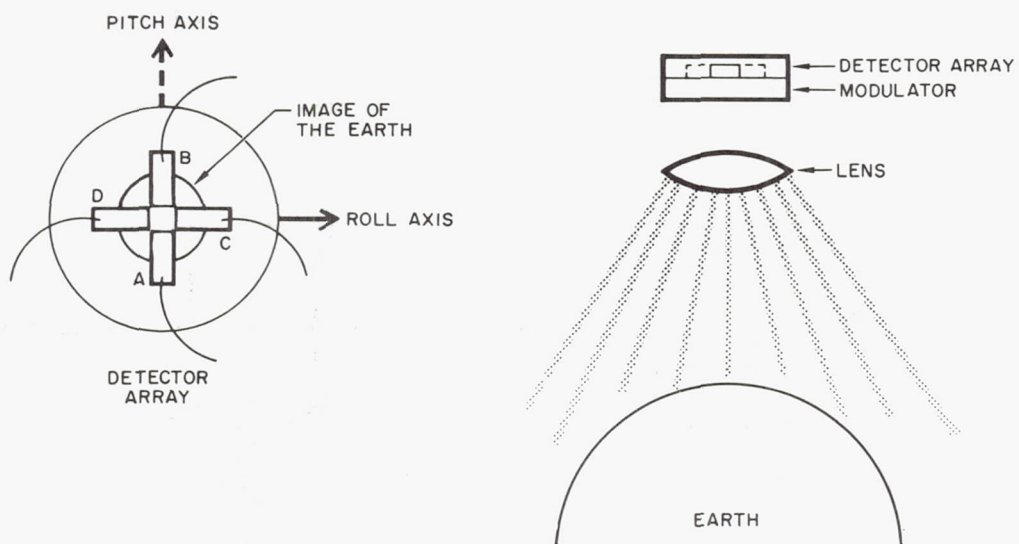


Fig. 34. A Wide Angle Passive Scanner

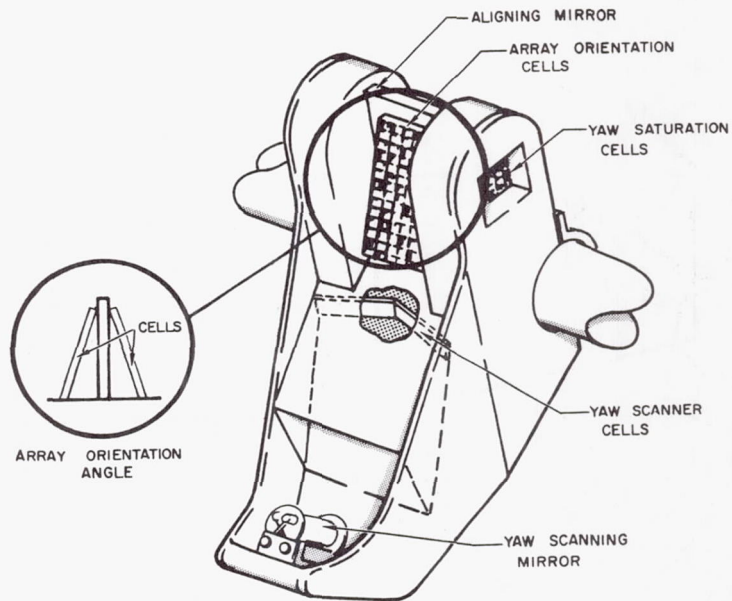


Fig. 35. A Possible Yaw and Array Sun Sensor Arrangement

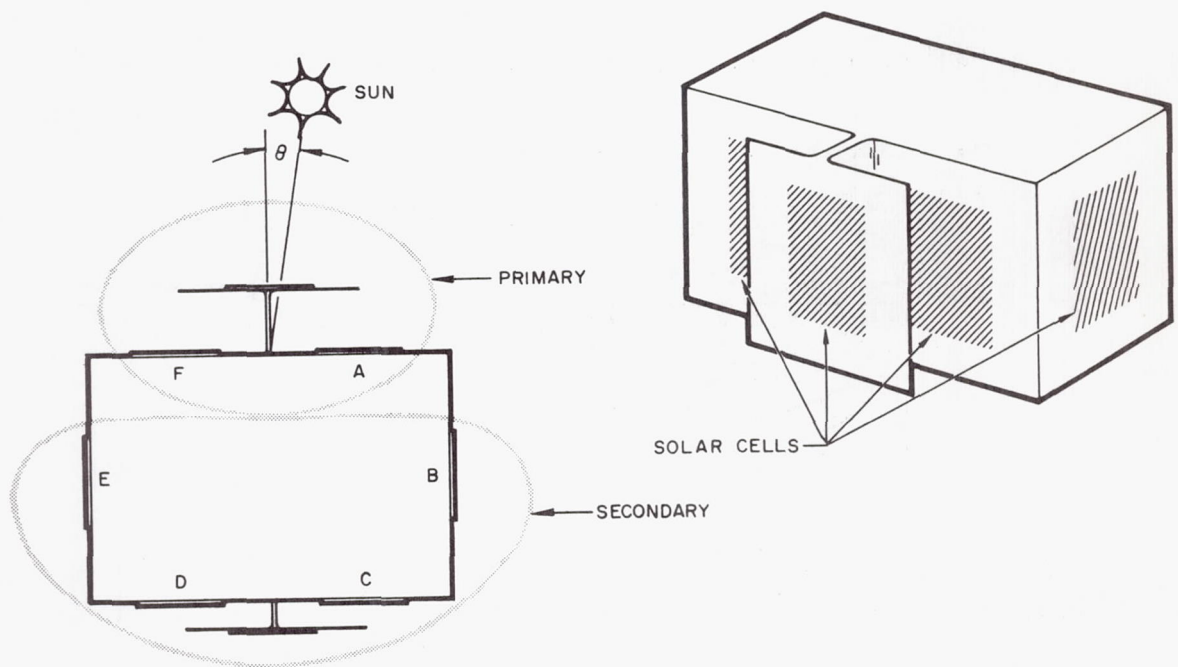


Fig. 36. T Shadow Bar Sun Sensor

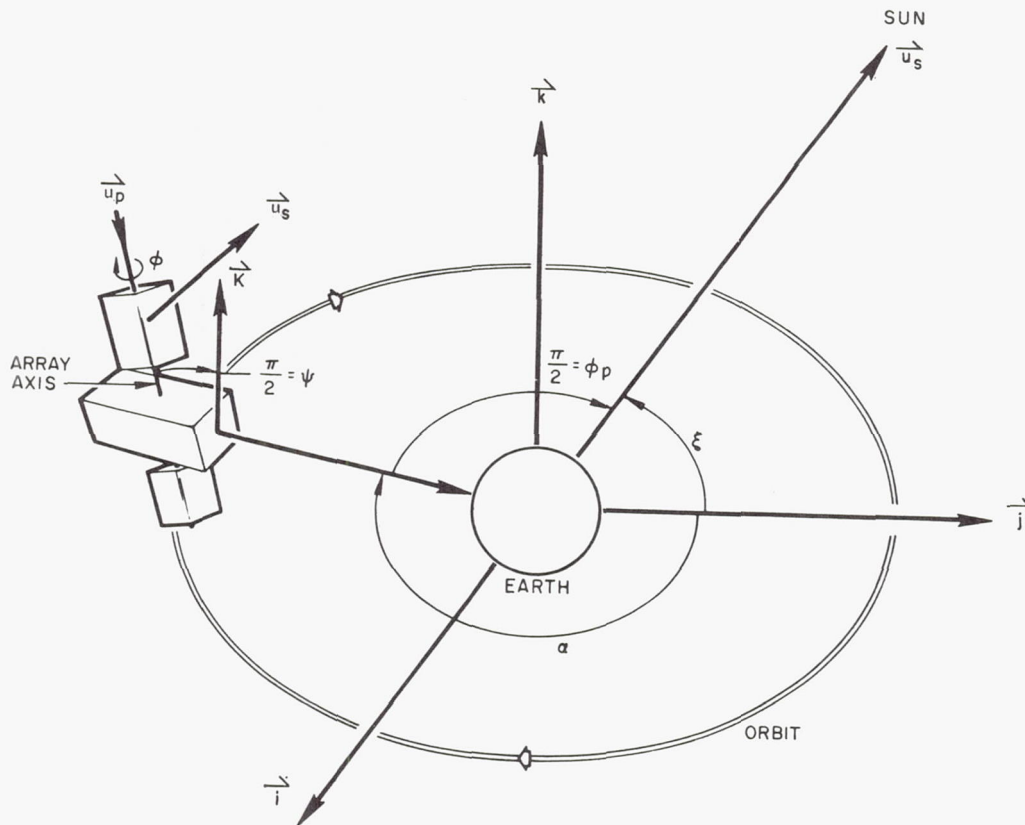


Fig. 37. Coordinate System for Computation of Yaw and Solar Array Laws

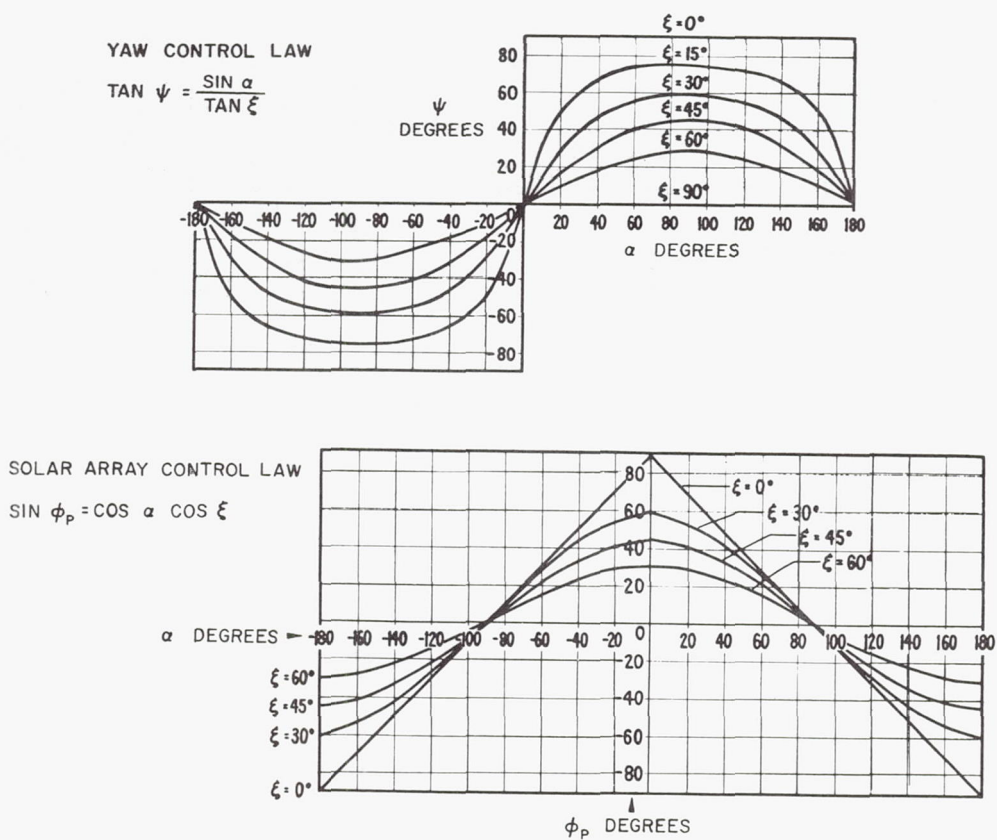


Fig. 38. Yaw and Solar Array Control Laws

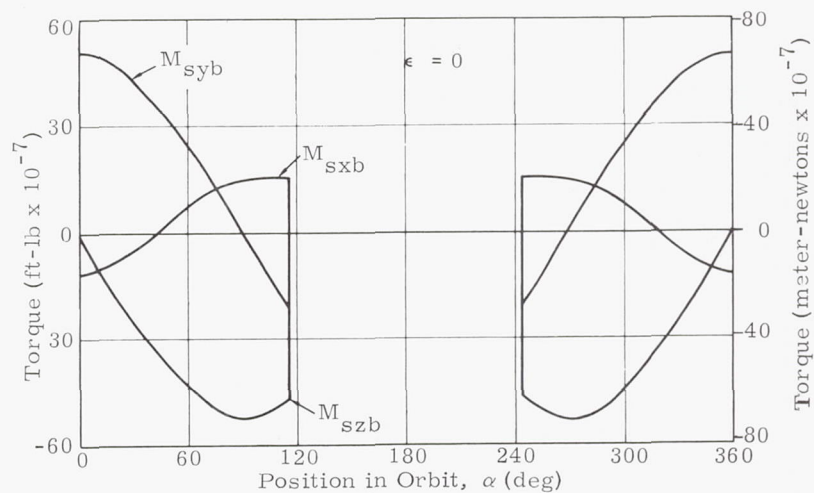


Fig. 39a. Torque in Body Coordinates Due to Solar Radiation Pressure for One Orbit

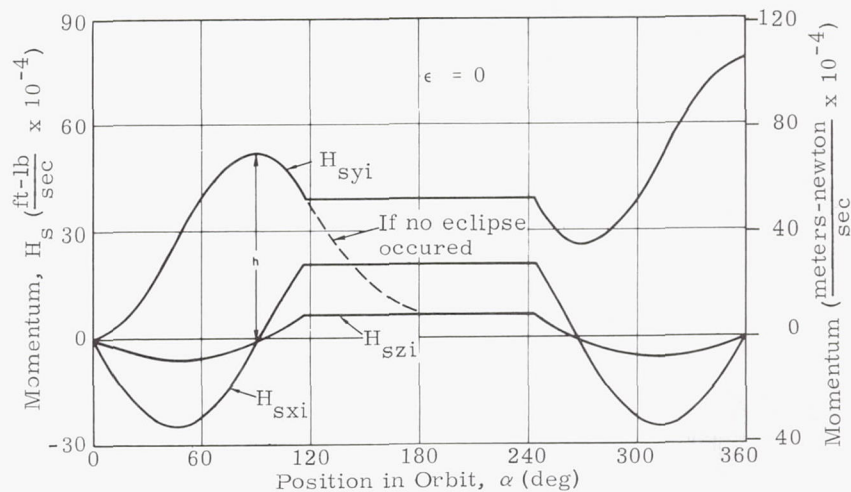


Fig. 39b. Momentum Change in Inertial Coordinates Due to Solar Radiation Pressure for One Orbit

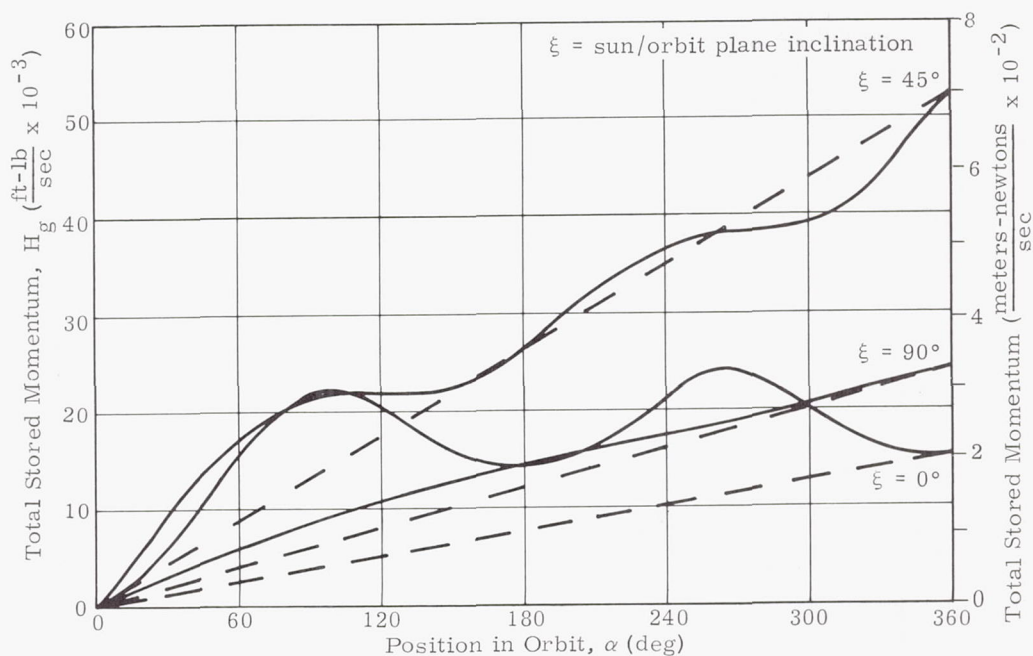


Fig. 40. Total Stored Momentum During One Orbit Due to Gravity Gradient

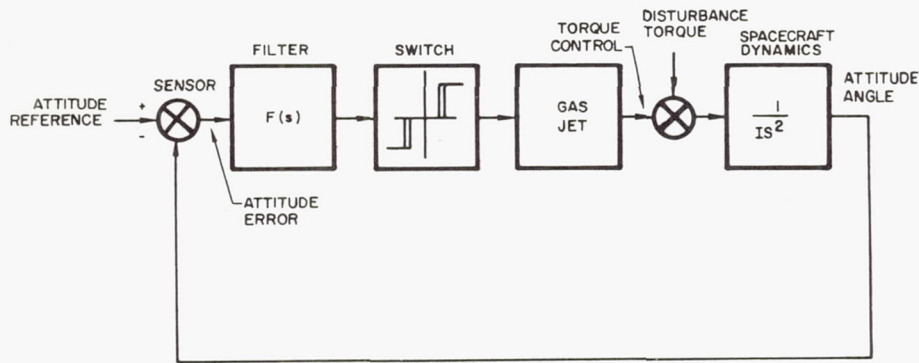


Fig. 41. Block Diagram of Simple On-Off Control System

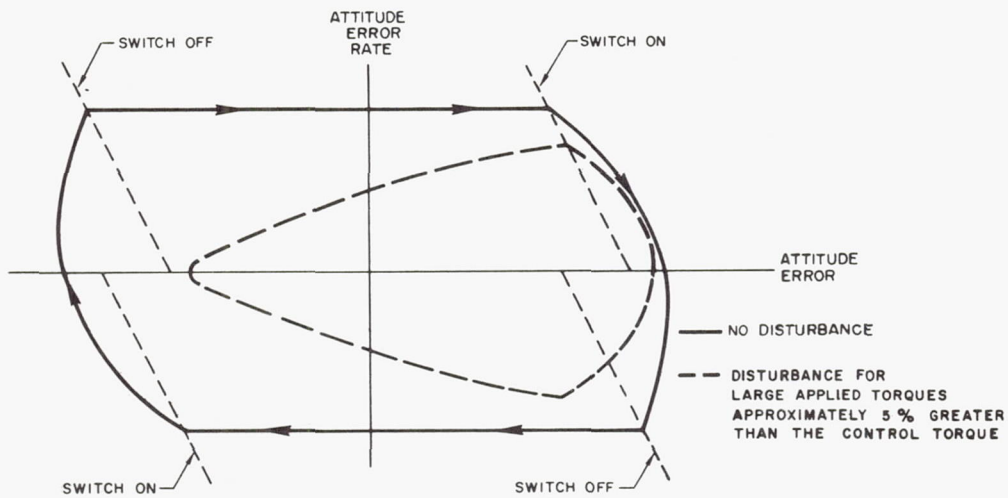


Fig. 42. Phase Plane Portrait of a Contractor Control System

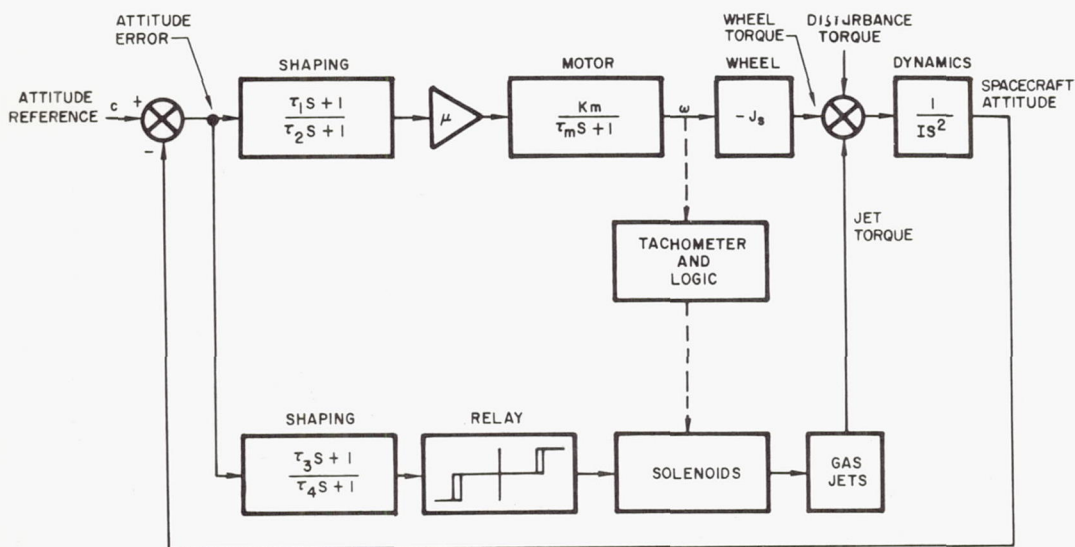


Fig. 43. Block Diagram of Gas Jet Reaction Wheel Dual Mode System

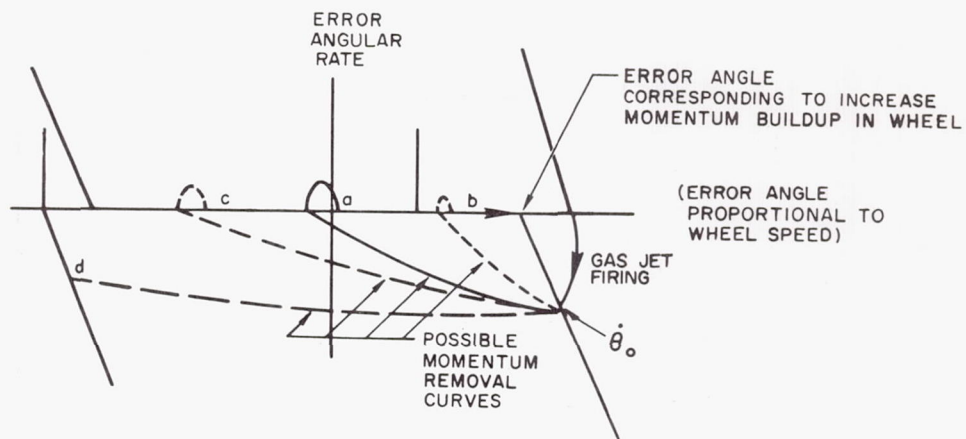


Fig. 44. Typical Phase Portrait Dual Mode System with Constant Disturbance Torque

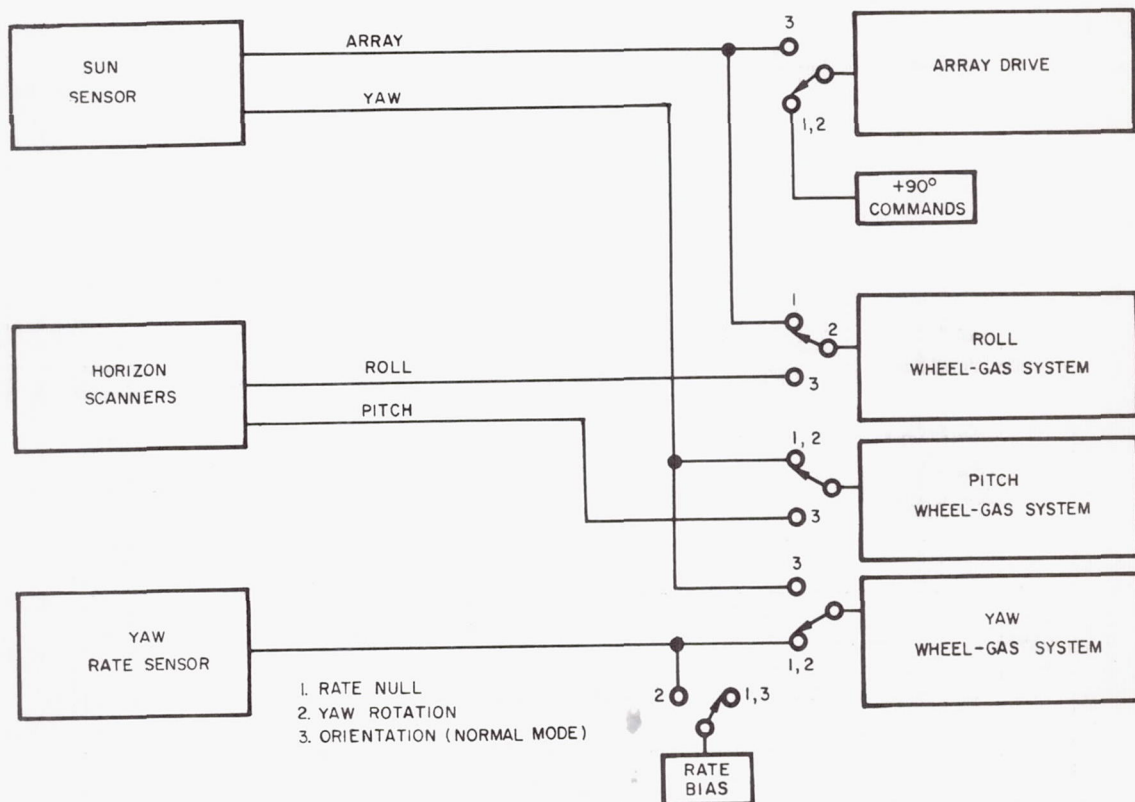


Fig. 45. Example Attitude Control System Block Diagram for Acquisition Mode

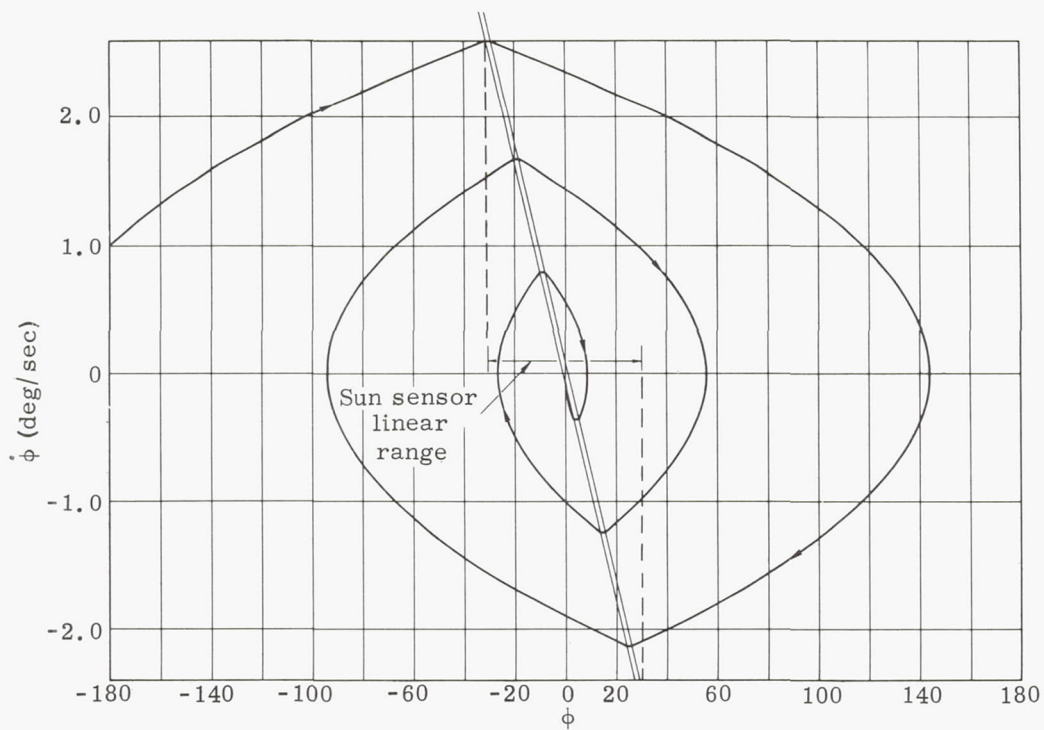


Fig. 46. Phase Portrait of Roll Error and Roll Error Phase of Acquisition

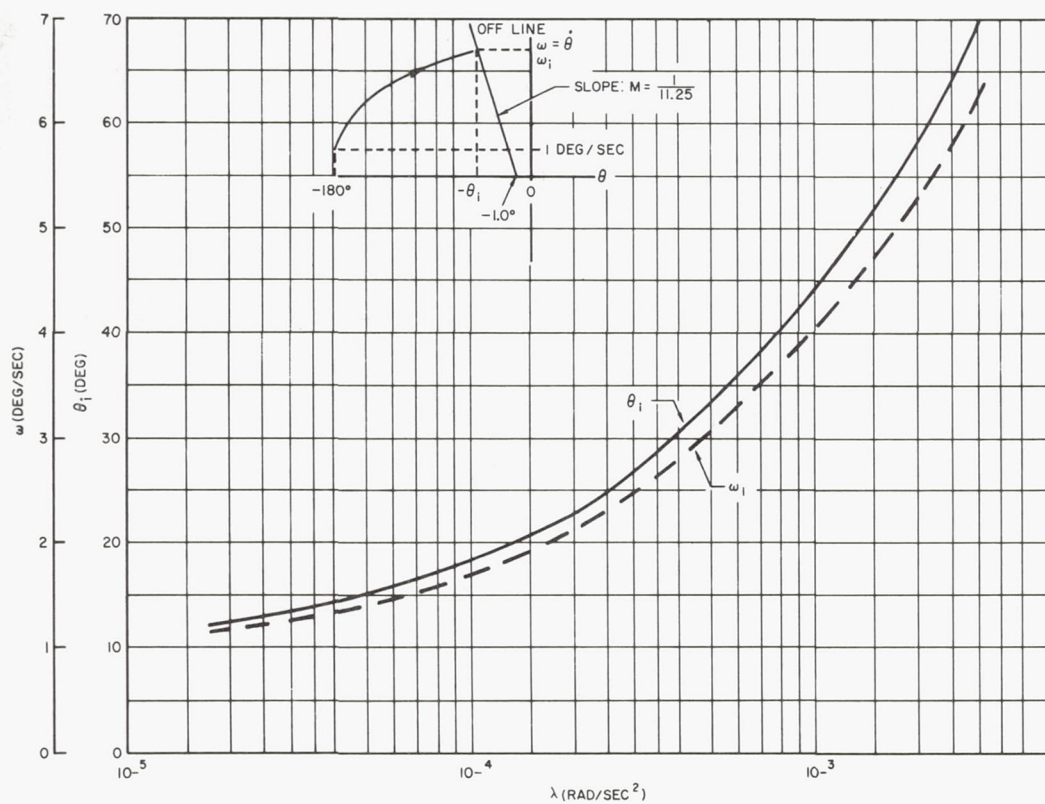


Fig. 47. Angle and Angular Rate at First Switching Line Versus Acceleration for Initial Conditions of 1°/sec and 180° Error

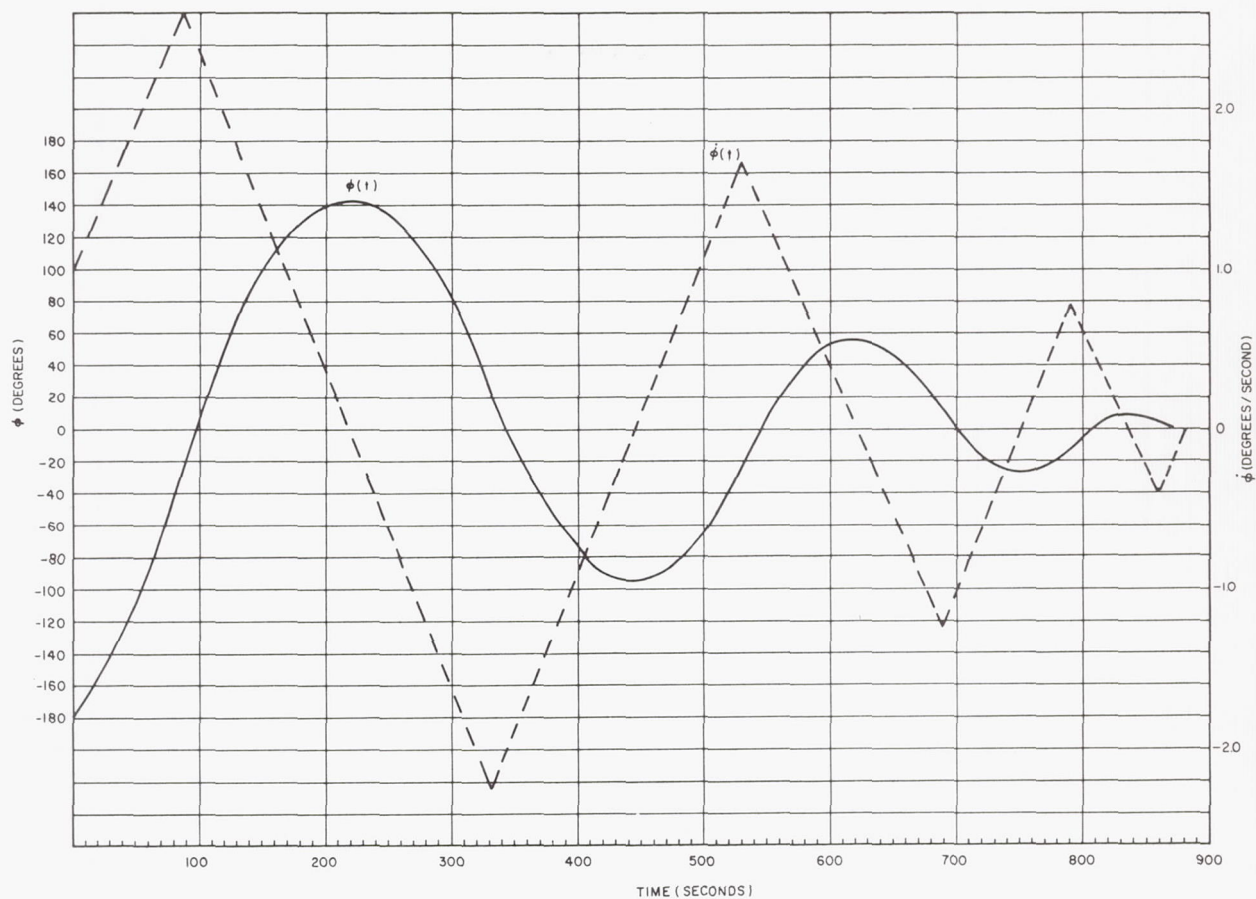


Fig. 48. Angle and Angular Rate Versus Time of Acquisition

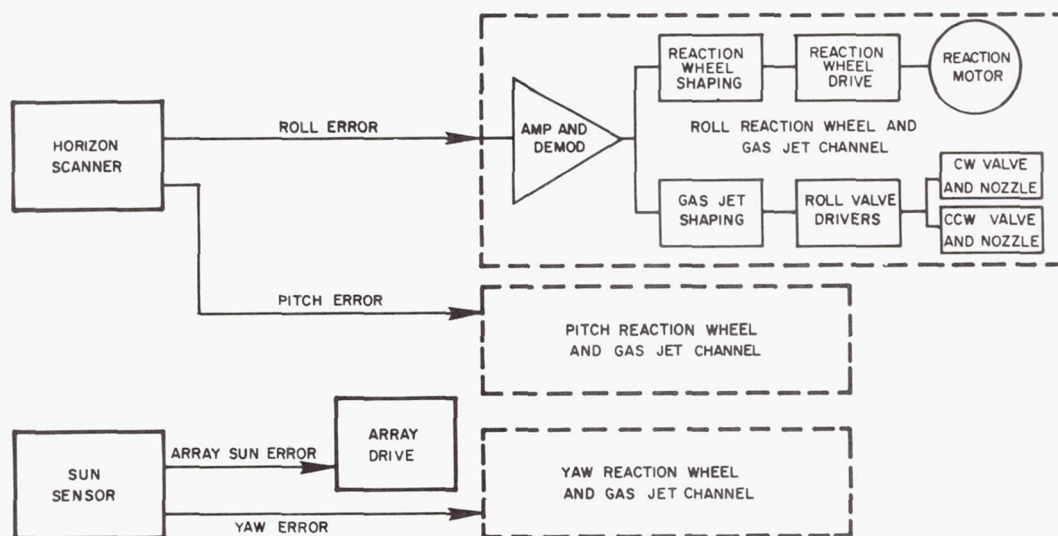


Fig. 49. Basic Attitude Control System Block Diagram for Normal Mode

CHAPTER XIII

MISSION REQUIREMENTS

Prepared by:

J. D. Kraft
Martin Company (Baltimore)
Aerospace Mechanics Department
March 1963

| | Page |
|--|---------|
| Symbols | XIII-1 |
| A. Introduction | XIII-2 |
| B. Mission Considerations. | XIII-2 |
| C. Solar Problems | XIII-6 |
| D. Ground Tracks | XIII-14 |
| E. Satellite Coverage | XIII-17 |
| F. Sensor Limitations on Orbit Selection | XIII-26 |
| G. References | XIII-32 |
| H. Bibliography | XIII-32 |
| Illustrations | XIII-35 |

LIST OF ILLUSTRATIONS

| Figure | | Page |
|--------|--|---------|
| 1 | Sine of the Angle Between the Normal to the Orbit Plane and the Earth-Sun Line, $i = 90^\circ$ | XIII-37 |
| 2 | Cosine of the Angle Between the Normal to the Orbit Plane and the Earth-Sun Line, $i = 90^\circ$ | XIII-38 |
| 3 | Cross Section of Orbit Through Shadow Cone . . . | XIII-39 |
| 4 | Orbit Going Through Shadow When Shadow Is at the Node | XIII-39 |
| 5 | Orbit Going Through Shadow When Shadow Is Not at the Node | XIII-39 |
| 6 | Cross Section of Orbit Through Penumbra Cone | XIII-40 |
| 7 | Orbit Going Through Penumbra When It Is at the Node | XIII-40 |
| 8 | Vector Analysis of Eclipse Time | XIII-41 |
| 9 | Geometry of Eclipse Season. | XIII-41 |
| 10 | Maximum Time in Umbra and Penumbra Versus Semimajor Axis. | XIII-42 |
| 11 | Maximum Time in Umbra and Penumbra Versus Semimajor Axis. | XIII-43 |
| 12 | Maximum Time in Penumbra (No Umbra Eclipse) Versus Semimajor Axis | XIII-44 |
| 13 | Maximum Time in Penumbra (No Umbra Eclipse) Versus Semimajor Axis | XIII-44 |
| 14 | Eclipse Season (Umbra Only) Versus Semimajor Axis | XIII-45 |
| 15 | Eclipse Season (Umbra and Penumbra) Versus Semimajor Axis | XIII-46 |

LIST OF ILLUSTRATIONS (continued)

| Figure | | Page |
|--------|---|---------|
| 16 | Geometry of the Simplified Eclipse Problem | XIII-47 |
| 17 | Time in Sunlight Versus Cosine of Angle Between Earth-Sun Line and Normal to Orbit | XIII-47 |
| 18 | Percent Time in Shadow for Circular Unperturbed Orbits | XIII-48 |
| 19 | Eclipse Durations and Eclipse Seasons for Unper- turbed Circular Orbits | XIII-49 |
| 20 | Eclipse Durations and Eclipse Seasons for Unper- turbed Circular Orbits | XIII-50 |
| 21 | Eclipse Durations and Eclipse Seasons for Unper- turbed Circular Orbits, $i = 90^\circ$, $h = 926$ km | XIII-51 |
| 22 | Eclipse Durations and Eclipse Seasons for an Un- perturbed Circular Orbit, $i = 60^\circ$, $h = 926$ km | XIII-52 |
| 23 | Eclipse Durations and Eclipse Seasons for Unper- turbed Circular Orbits, $i = 32^\circ$, $h = 926$ km | XIII-53 |
| 24 | Inclination with Respect to the Ecliptic (i_ϵ) Versus Longitude of the Node with Respect to the Equator (Ω) for Different Inclinations with Respect to the Equator (i) | XIII-54 |
| 25 | Angular Radius of Shadow Versus Distance from Center of Earth | XIII-55 |
| 26 | Angular Radius of Shadow Versus Distance from Center of Earth | XIII-56 |
| 27 | Flow Chart of a Simple Eclipse Program | XIII-57 |
| 28 | Example of Eclipse Patterns When Launching a Vehicle on Different Dates in 1963 at the Same Time of Day | XIII-58 |
| 29 | Example of Eclipse Patterns When Launching a Vehicle at Different Times on the Same Date | XIII-59 |

LIST OF ILLUSTRATIONS (continued)

| Figure | | Page |
|--------|---|---------|
| 30 | Example of Eclipse Patterns for One Satellite Taking into Account Different Perturbations | XIII-60 |
| 31 | Geometry of the Ground Track Problem | XIII-60 |
| 32 | Ground Tracks of Circular 24-Hr Orbits | XIII-61 |
| 33 | Ground Track of Elliptical 24-Hr Orbits | XIII-61 |
| 34 | Ground Track of an Elliptical 24-Hr Orbit | XIII-61 |
| 35 | Satellite Coverage | XIII-62 |
| 36 | Satellite Coverage | XIII-63 |
| 37 | Longitudinal Ground Track Shift | XIII-64 |
| 38 | Nodal Orbit Period | XIII-65 |
| 39 | Diurnal Longitudinal Shift of the Ground Track . . | XIII-66 |
| 40 | Number and Distribution of Satellites in a Polar Network Providing Complete Global Coverage ($\sigma = 0$ deg) | XIII-67 |
| 41 | Theoretical and Practical Optimum Satellite Utilization in a Polar Network Providing Complete Global Coverage | XIII-67 |
| 42 | Comparison of Polar Satellite Networks Pro- viding Coverage from the Poles to Minimum Latitude, L_{\min} ($\sigma = 0$ deg) | XIII-68 |
| 43 | Comparison of Inclined and Polar Satellite Networks Providing Coverage from the Equator to Maximum Latitude, L_{\max} ($\sigma = 0$ deg) | XIII-68 |
| 44 | Eccentricity Effects on the Spacing of Six Satellites (placed at equal time intervals) | XIII-69 |
| 45 | Ground Track for One Satellite During a Day . . . | XIII-70 |

LIST OF ILLUSTRATIONS (continued)

| Figure | | Page |
|--------|---|---------|
| 46 | Ground Tracks for 16 Satellites During Half a Revolution | XIII-71 |
| 47 | Three-Dimensional Orbit Pattern | XIII-72 |
| 48 | Areas Not Covered by Ground Swaths at Time Zero | XIII-73 |
| 49 | Maximum Longitudinal Increment of Area Not Covered by Ground Swath as a Function of the Orbital Inclination | XIII-74 |
| 50 | The Coordinate System for Satellite Tracking . . . | XIII-75 |
| 51 | Satellite Depression Angle Relative to Local Vertical | XIII-75 |
| 52 | Cosine ψ Versus Nodal Reference Angle | XIII-76 |
| 53 | Cosine ψ Versus Nodal Reference Angle (detailed view) | XIII-77 |
| 54 | Diagram for Finding the Distance at Subsatellite Point and Line-of-Sight Range | XIII-78 |
| 55 | Chart for Determining Elevation and Slant Range of Satellite (0 to 185,000 km) | XIII-79 |
| 56 | Chart for Determining Elevation and Slant Range of Satellite (0 to 8340 km) | XIII-80 |
| 57 | Visibility Time for Circular Orbits (nonrotating earth) | XIII-81 |
| 58 | Effect of Earth Rotation on Visibility Time (circular orbits) | XIII-82 |
| 59 | Maximum Orbit Altitude as a Function of Ground Resolution Desired, Focal Length and System Resolution | XIII-83 |

LIST OF ILLUSTRATIONS (continued)

| Figure | | Page |
|--------|--|---------|
| 60 | Transfer Function (scene-lens combination) | XIII-84 |
| 61 | Transfer Function of Scene Contrast | XIII-84 |
| 62 | Diffraction Limited Lens | XIII-85 |
| 63 | Transfer Function of Diffraction Limited Lens . . . | XIII-85 |
| 64 | Transfer Function of Diffraction Limited Lens . . . | XIII-86 |
| 65 | Transfer Function for Linear Motion | XIII-86 |
| 66 | Typical Photographic Film Transfer Function | XIII-87 |
| 67 | Illustrative Example | XIII-87 |

SYMBOLS

| | |
|---|--|
| a | = orbit semimajor axis |
| b | = orbit semiminor axis |
| d | = ground range |
| e | = orbit eccentricity |
| E | = eccentric anomaly |
| h | = orbit altitude |
| i | = inclination of the orbit plane to the equatorial plane |
| i_e | = inclination of the orbit plane to the ecliptic plane |
| i_\odot | = obliquity of the ecliptic |
| J_2 | = coefficient of the gravitational potential function, 1.0823×10^{-3} |
| ℓ | = Celestial latitude (referenced to ecliptic) |
| L | = geocentric latitude (referenced to equator) |
| M | = mean anomaly |
| n | = mean motion $= \sqrt{\frac{\mu}{a^3}}$ |
| n_1 | = number of orbit planes in a pattern |
| n_2 | = number of satellites in an orbit |
| p | = orbit semilatus rectum |
| r | = radial distance from the center of the earth |
| R | = radius of a sphere of volume equivalent to that of the earth |
| R_e | = equatorial radius of the earth |
| s | = angular radius of shadow |
| t | = time |
| t_v | = visibility time |
| v | = velocity magnitude |
| $\left. \begin{matrix} x \\ y \\ z \end{matrix} \right\}$ | = Cartesian position coordinates |
| α | = central angle between the subsatellite point and the edge of the area visible from the satellite |
| β | = azimuth angle relative to north |
| γ | = flight path angle with respect to local horizontal |

| | |
|--|--|
| γ_n | = angle between the earth-sun line and the normal to the orbit plane |
| $\left. \begin{matrix} \cos \alpha \\ \cos \beta \\ \cos \gamma \end{matrix} \right\}$ | = direction cosines |
| ϵ | = elevation angle with respect to the horizontal plane |
| θ | = true anomaly |
| \ominus | = central angle in the ecliptic plane from vernal equinox to the sun |
| λ | = celestial longitude (referenced to ecliptic) |
| Λ | = geocentric longitude (referenced to equator) |
| μ | = gravitational constant of the earth $(398,601.5 \text{ km}^3/\text{sec}^2)$ |
| ρ | = line-of-sight range |
| σ | = viewing angle with respect to the horizontal plane |
| τ | = Keplerian orbit period |
| τ_{nodal} | = nodal orbit period, the interval between two successive transits through the ascending node |
| τ_{sidereal} | = sidereal orbit period, the interval between two successive crossings of the same hour circle on the celestial sphere |
| τ_e | = period of the earth's rotation |
| ϕ | = central angle in the orbit plane from the ascending node to the satellite |
| ω | = argument of perigee |
| Ω | = right ascension or longitude of the ascending node |
| Ω_e | = rate of rotation of the earth |
| Υ | = vernal equinox |

SUBSCRIPTS

| | |
|------------|---------------|
| o | observer |
| \odot | sun |
| \oplus | earth |
| ϵ | ecliptic |
| 0 | initial value |

A. INTRODUCTION

Once a satellite mission has been conceived to accomplish a given function (e. g., reconnaissance, communications, meteorological determinations, etc.), the question arises as to what orbit or orbits would best be suited to accomplishing the specified mission. Selection of the best orbit depends upon a multitude of factors such as periodicity, area coverage capability, target coverage capability, satellite and sub-satellite point illumination and vehicle tracking considerations. These factors will be investigated in order to provide a basis for orbit selection in a given mission plan. Section B considers the general nature of the various types of missions and indicates how the above factors are involved in orbit design for each mission. Detailed quantitative analyses of the various factors are contained in Sections C, D and E.

B. MISSION CONSIDERATIONS

Although each mission has its individual requirements, most satellites may be categorized for general study as follows:

- (1) Reconnaissance satellites.
- (2) Communications satellites.
- (3) Navigation satellites.
- (4) Meteorological satellites.
- (5) Scientific satellites.

In general, orbit design for each of the missions will require consideration of ground tracks, coverage and sensor limitations. In addition, whenever photographic determinations are made, or solar power supplies are used, various solar problems (e. g., heating, time in sunlight, relative orientation of the vehicle-sun-line, etc.) must be considered. Table 1 lists most of the factors involved in selection of each orbit element. The following subsections qualitatively relate these factors to the above mission types.

1. Reconnaissance Satellites

One function in which satellite systems are well suited is that of scientific or military reconnaissance. Observations made by a satellite system can provide valuable information on the nature of this surface of the earth, and of the number, locations and state of development of installations. In making these observations, a satellite system has the advantage of covering large areas rapidly and periodically with no risk to the observer.

From a general point of view, selection of an optimum reconnaissance satellite orbit, involving specification of six orbit elements, is based upon the following philosophy:

- (1) In most missions, orbits of low eccentricity should be selected to allow uniform sensor performance throughout the orbit. Thus, for the limiting case of $e = 0$, two additional elements ω

and T_p (the argument of perigee and the time of perigee passage) may be selected arbitrarily because they have no real meaning.

- (2) In general, choice of orbit altitude depends on a tradeoff between sensor power and resolution requirements for low altitude on one hand and coverage and orbit lifetime requirements for high altitude on the other. Decay of the orbit altitude due to atmospheric drag is prohibitive for altitudes less than 150 km, and orbits of altitude less than about 225 km will require periodic corrections even for useful lifetimes of a few weeks. The added complexity of orbit correction systems and the added fuel requirement, as determined in Chapter VI, are certainly factors in the selection of an orbit altitude for extended missions. The effect of low altitude in decreasing area coverage is discussed in some detail in Section E. This factor is especially significant for missions requiring continuous photographic coverage for extended periods, where the film bulk can be quite large. The sensor requirement for low altitudes is discussed in Section F.
- (3) For fairly low altitude satellites, the inclination of the orbit to the equatorial plane must be at least as large as the latitude of geographical areas to be observed. Thus, as an example, if there is a requirement for complete coverage with low altitudes, polar orbits are required (Section E).
- (4) The right ascension of the ascending node, as determined by the launch time, could be selected arbitrarily for missions of extended duration or missions aimed at more or less total coverage. However, for short-term missions requiring photographic inspection of a specific geographic area, the node should be selected so that the satellite passes over the area of interest during the local daytime.

2. Communications Satellites

Satellites can be used as component stations of a communication system relaying signals from one point on the earth's surface to another. Their advantage in this application is primarily one of coverage. Range limitations of conventional radio transmission can be overcome and reliable inter-continental radio telephone links established.

Communications satellites may function actively or passively. That is, an active satellite contains receiving and transmitting equipment so that it can receive a signal from earth, amplify it and retransmit the same signal back to earth. A passive satellite, which may take the form of a large, metallic skin balloon, merely reflects incident radiation from the earth so that a portion of this radiation is scattered back in the direction of the earth. Examples of the two types are the ECHO balloon satellites and the TELSTAR active satellites. Passive systems would require ground

TABLE 1
Factors Involved in Orbit Selection

| Altitude | Factor | Eccentricity | Factor | Inclination | Factor | Node | Factor |
|--|---|-----------------------|--|-----------------|---|---------------|---|
| High | (1) Maximum coverage | Low ($e \approx 0$) | (1) Uniform coverage over large areas | Low | (1) Elimination of earth relative motion in the case of the 24-hr orbit | Special value | (1) Selection of daytime over a reconnaissance or coverage area |
| High | (2) Minimum drag perturbations | Low ($e \approx 0$) | (2) Uniform sensor resolution and power requirements | High | (2) Complete global coverage | Special value | (2) Selection of an optimum or uniform coverage pattern |
| High | (3) Minimum oblateness perturbations | | | | | | |
| Low | (4) Sensor resolution and power limitations | Low ($e \approx 0$) | (3) Elimination of earth relative motion in the case of the 24-hr orbit | Specific values | (3) Optimum or uniform coverage | Special value | (3) Maximization of time in sunlight for solar power |
| Low | (5) Minimum solar and lunar perturbations | | | Specific values | (4) Tracking station utilization | | |
| Low | (6) Propellant expenditure in launch | Low ($e \approx 0$) | (4) Ease of position prediction and uniform ground track | Specific values | (5) Reconnaissance or coverage of a particular area | | |
| Specific altitudes (24-hr, 6-hr, etc., see Section D.2.) | (7) Achieving synchronous performance (orbit period a rational fraction of a day) | Low ($e \approx 0$) | (5) Secular perturbations can be largely compensated for in achieving synchronous orbits | Specific values | (6) Regression rate set to $0.986^\circ/\text{day}$ for a given altitude (allows orbit plane to follow the sun) | | |
| See Chapter II | (8) Avoiding Van Allen belts | High | (6) Increased coverage over limited areas for fixed launch propellant expenditure | | | | |

station transmitters of much higher power than would active satellites. On the other hand, the complexity of vehicle-borne equipment leads to limitations on reliability and mission duration for active systems.

Mission requirements for a complete communications system would probably aim for continuous 24-hr coverage between virtually every pair of points on the earth's surface. One orbit design which has been frequently mentioned in connection with this requirement employs the 24-hr satellite orbit. Because this orbit has a period of one day, satellite motion is synchronized with the rotation of the earth. In the case of the 24-hr equatorial circular orbit, the satellite would appear to hang motionless in the sky above an observer on the earth. Elliptic or nonequatorial 24-hr satellites perform diurnal excursions relative to the observer. The 24-hr orbit is described in greater detail in Section D. The advantages of the 24-hr orbit in communications systems lie in the stationary nature of the satellite and the wide coverage of each satellite (the 24-hr circular orbit altitude is 35,777 km). At the 24-hr orbit altitude, each satellite can view very nearly half of the earth's surface. Thus, three satellites could provide very adequate coverage which could only be achieved by hundreds of satellites in low altitude orbits. Also, ground antennas could be fixed, and tracking would be extremely simple. A disadvantage of the 24-hr orbit system is the relatively high power required to transmit to this high altitude.

Whatever altitude is chosen, it should be such that an integral number of periods are contained in a day. Then the ground track, the trace of the subsatellite point on the surface of the rotating earth, will repeat daily. This condition is obviously desirable from the standpoints of ease of prediction of satellite position and utilization of the system. That is, the user would know what satellite service is available at a given time without referring to a complicated ephemeris because a satellite is at the same place at the same time each day. Synchronous orbits, which exhibit a daily repeating ground track, are those of 24, 12, 8, 6, 4, 3 and 2 sidereal hour periods. The altitudes corresponding to these periods are tabulated in Section D.

For communications systems which aim for literally world-wide service, circular orbits offer the advantage of uniformity in coverage. However, if the system is to provide coverage primarily in one hemisphere or primarily during the daytime, high eccentricity orbits could be chosen. These orbits can be achieved more economically than could circular orbits of their apogee altitude (apogee altitude is the criteria here in order to provide a large communication range). The elliptical orbits would, of course, be launched so that apogee conditions occur over the daylight side of the earth or over the hemisphere of interest.

3. Navigation Satellites

Artificial satellites can be used as references for all-weather navigation systems determining position and velocity of a surface vehicle, aircraft or space vehicle. The conventional navigation

methods, e.g., dead-reckoning, star and sun sighting during clear weather and storage of reference information by inertial guidance instruments, provide navigation information of adequate accuracy. However, such information must be periodically corrected to maintain accuracy, and the replacement of star and sun sighting with satellite sighting would permit this updating to be performed at any time, regardless of weather conditions.

a. Satellite navigation methods

Various methods of satellite navigation may be considered, depending on the nature of available equipment, data available from sources other than the satellites and the nature of the position or velocity information to be obtained.

(1) Sphereographical navigation

The position of an observer on the earth's surface can be determined from a pair of observations of the angle between the local vertical and the line of sight to a celestial body. Of course, in order to make these observations, the local vertical must be obtained by means of a pendulum, plumb bob or some other device. Any celestial body, e.g., the sun, a star or a satellite, could be observed as long as its angular position is accurately known. Determinations based on satellite positions will obviously be complicated by the high relative velocity of the observer and the satellite. However, the fundamental technique is the same. The observer, equipped with a vertical reference and an electronic sextant, measures the direction angles of a radio signal continuously emitted from the navigation satellite.

(2) Doppler navigation

The sphereographical technique employs the classical angular measurements of celestial navigation. Satellite systems employing radio techniques are not limited to these methods. One radio technique is based on the Doppler effect. Radio signals received from a moving vehicle appear higher in frequency as the vehicle approaches the observer and lower in frequency as the vehicle recedes from the observer. The difference between the observed frequency and the known transmitter frequency, the "Doppler shift," is a measure of relative motion (or relative position when these shifts are integrated) of the vehicle and observer and, therefore, can serve as input to a navigation system. Knowledge of local vertical is not required. The TRANSIT satellite program employs a purely Doppler system.

(3) Complete geometric determination

Systems for navigation on the surface of the earth can implicitly make use of the knowledge that the observer is a known distance from the center of the earth, the origin of the coordinate system in which the satellite positions are known. A more general problem may be hypothesized as follows: the position and velocity of a vehicle in space is to be determined solely from data consisting of range and range rate relative to the navigation satellites. The observer is assumed to have no knowledge of his orientation, position or velocity

from other sources such as plumb bobs, altimeters, etc. If a complete determination is to be made from a set of observations made at any given time, the observer must simultaneously note the range and range rate of three navigation satellites, the positions and velocities of which are known. Then his position is determined as the intersection of three spheres.

$$(x_o - x_i)^2 + (y_o - y_i)^2 + (z_o - z_i)^2 = \rho_{io}^2 \quad (1)$$

$i = 1, 2, 3$

where

x_o, y_o, z_o = Cartesian position coordinates of observer

x_i, y_i, z_i = known Cartesian position coordinates of the three navigation satellites

ρ_{io} = ranges from the three navigation satellites to the observer.

The observer's velocity is determined from

$$\dot{\rho}_{io} = \frac{(\vec{V}_o - \vec{V}_i) \cdot \vec{\rho}_{io}}{\rho_{io}} \quad (2)$$

where

$$\vec{V}_o - \vec{V}_i = (\dot{x}_o - \dot{x}_i) \vec{i} + (\dot{y}_o - \dot{y}_i) \vec{j} + (\dot{z}_o - \dot{z}_i) \vec{k}$$

$\dot{x}_o, \dot{y}_o, \dot{z}_o$ = Cartesian velocity coordinates of observer

$\dot{x}_i, \dot{y}_i, \dot{z}_i$ = Cartesian velocity components of the three navigation satellites

$\dot{\rho}_{io}$ = the range rate data

and $\vec{\rho}_{io}$ is given from Eq (1).

Differentiation of Eqs (1) and (2) gives the following error formulas.

$$\begin{pmatrix} dx_o \\ dy_o \\ dz_o \end{pmatrix} = \frac{1}{K} \begin{bmatrix} C_{11} & C_{12} & C_{13} \\ C_{21} & C_{22} & C_{23} \\ C_{31} & C_{32} & C_{33} \end{bmatrix} \begin{pmatrix} \Delta_1 \\ \Delta_2 \\ \Delta_3 \end{pmatrix} \quad (3)$$

where

$$\Delta_i = (x_o - x_i) dx_i + (y_o - y_i) dy_i + (z_o - z_i) dz_i + \rho_{io} d\rho_{io} \quad i = 1, 2, 3$$

$$K = |K_{vij}| = \begin{vmatrix} (x_s - x_1) & (y_s - y_1) & (z_s - z_1) \\ (x_s - x_2) & (y_s - y_2) & (z_s - z_2) \\ (x_s - x_3) & (y_s - y_3) & (z_s - z_3) \end{vmatrix}$$

and C_{ij} is the cofactor of the $(ij)^{th}$ element of K^T .

$$\begin{pmatrix} d\dot{x}_o \\ d\dot{y}_o \\ d\dot{z}_o \end{pmatrix} = \frac{1}{K} \begin{bmatrix} C_{11} & C_{12} & C_{13} \\ C_{21} & C_{22} & C_{23} \\ C_{31} & C_{32} & C_{33} \end{bmatrix} \begin{pmatrix} \delta_1 + \frac{\dot{\rho}_{10}}{\rho_{10}} \delta_1' + \delta_1'' \\ \delta_2 + \frac{\dot{\rho}_{20}}{\rho_{20}} \delta_2' + \delta_2'' \\ \delta_3 + \frac{\dot{\rho}_{30}}{\rho_{30}} \delta_3' + \delta_3'' \end{pmatrix} \quad (4)$$

where

$$\delta_i \equiv (\dot{x}_o - \dot{x}_i) (dx_i - dx_o) + (\dot{y}_o - \dot{y}_i) (dy_i - dy_o)$$

$$+ (\dot{z}_o - \dot{z}_i) (dz_i - dz_o)$$

$$\delta_i' \equiv (x_o - x_i) (dx_o - dx_i) + (y_o - y_i) (dy_o - dy_i)$$

$$+ (z_o - z_i) (dz_o - dz_i)$$

$$\delta_i'' \equiv (x_s - x_i) \Delta \dot{x}_i + (y_s - y_i) \Delta \dot{y}_i + (z_s - z_i) \Delta \dot{z}_i$$

$$+ \rho_{is} \Delta \dot{\rho}_{is}$$

and K and C_{ij} are those defined in Eq (3).

b. Selection of navigation satellite orbits

The navigation satellite system is similar in most functional requirement aspects to the communications satellite system, with perhaps more emphasis on precise orbit determination and minimum sensor power requirements in the navigation system case. Here again, the requirements of wide, uniform coverage with the fewest satellites, low transmitter power and synchronous motion are important considerations in specifying optimum orbits. Since navigation requires satellite tracking by each observer as opposed to tracking by a few high-powered transmitters in the communications system, an increased emphasis on lower altitudes is required in navigation system orbit design. Also, since each observer must locate the satellites by means of an accurate ephemeris, the ephemeris should be as simple and easily updated as possible. This requirement makes selection of one of the synchronous orbits attractive. From a general standpoint, the requirements taken as a whole seem to indicate choice of circular 4- or 6-hr orbits for use in navigation system orbit patterns. For specific missions, Sections C, D, E and F offer data upon which a quantitative tradeoff may be based.

4. Meteorological Satellites

Satellite systems offer several advantages in meteorological determinations. The area over which observations can be made is, of course, much larger for a satellite system than for a ground station. By means of this greater coverage, a complete storm structure, as evinced by component cloud formations, may be observed from the satellite. During daylight conditions the satellite determinations can be photographic. The photographs could provide information on the size, structure and location of a storm, and series of photographs would reveal the nature and time history of the storm development and its motion. When the satellite is above the night side of the earth, observations can be made by an infrared scanning system operating at wavelengths which are emitted from the earth and on a spectral band which is reflected or absorbed by clouds.

In addition to storm observations, satellite determinations could include atmospheric moisture content from radar and infrared measurements of water vapor absorption bands, atmospheric density, and radio noise, which indicates the location of thunderstorms, line squalls and fronts where the atmosphere is unstable.

The TIROS satellites, a series of experimental television-equipped meteorological satellites launched in a NASA program, have proved very successful. In addition to known cloud and weather phenomena, processes which apparently had not been previously investigated were observed.

From the standpoint of orbit design the requirements of the meteorological satellite mission primarily involve achieving proper altitude and coverage. The orbit should be high enough to permit adequate area coverage (Section E) of high altitude cloud formations and yet be low enough to provide good resolution with available sensors (Section F). Eccentricity should generally be low to provide uniform coverage and resolution. The TIROS I orbit altitude was approximately 750 km. Required orbit inclination is determined from the latitude range to be covered, as considered in Section E.

C. SOLAR PROBLEMS

For many satellite missions the following considerations involving the relative positions of the sun and the vehicle are important from a mission design standpoint:

- (1) Times of satellite eclipse, i.e., times when a vehicle enters and leaves the shadow of the earth.
- (2) The duration of an eclipse, or the percentage of time spent in shadow.
- (3) The time history of the relative positions of the vehicle, the sun and the earth.

These factors are useful in analysis of the following mission requirements:

- (1) Compensation for radiant heat absorbed through the vehicle skin.

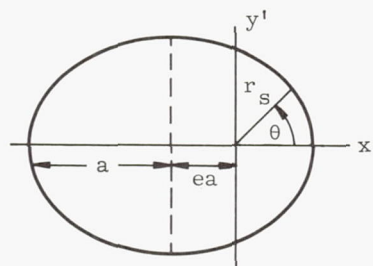
- (2) Provision for adequate power supply by solar cells.
- (3) Provision for tracking the sun.
- (4) Assurance of optimum illumination of the subsatellite point for photographing certain geographical phenomena.

These various problems related to solar effects and their effects on mission performance therefore merit some consideration.

1. Relative Geometry of the Vehicle, Earth and Sun Positions

Since analyses of these solar problems depend on knowledge of the positions of the vehicle, earth and sun relative to each other, it is convenient to first derive equations for the instantaneous relative positions. These equations will provide a basis for the individual analyses.

- a. Position of the satellite in an earth centered inertial (ECI) coordinate system



The equation of an ellipse in polar coordinates is

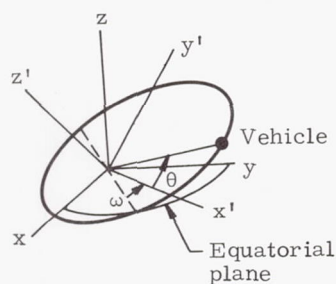
$$r_s = \frac{a(1 - e^2)}{1 + e \cos \theta} \quad (5)$$

or in rectangular coordinates

$$\frac{(x' - ea)^2}{a^2} + \frac{y'^2}{a^2(1 - e^2)} = 1$$

for coordinates in the orbit plane, x' toward perigee. These coordinates may be transformed to ECI by the following rotations as outlined in Chapter XI.

$$\begin{pmatrix} x \\ y \\ z \end{pmatrix} = \begin{bmatrix} \cos \Omega & -\sin \Omega & 0 \\ \sin \Omega & \cos \Omega & 0 \\ 0 & 0 & 1 \end{bmatrix} \begin{bmatrix} 1 & 0 & 0 \\ 0 & \cos i & -\sin i \\ 0 & \sin i & \cos i \end{bmatrix} \begin{pmatrix} x' \\ y' \\ z' \end{pmatrix} \quad (6)$$



The direction cosines of the position of the vehicle in ECI are obtained by substitution of Eq (5) in Eq (6):

$$\frac{x_s}{r_s} = \cos(\theta + \omega) \cos \Omega - \cos i \sin(\theta + \omega) \sin \Omega$$

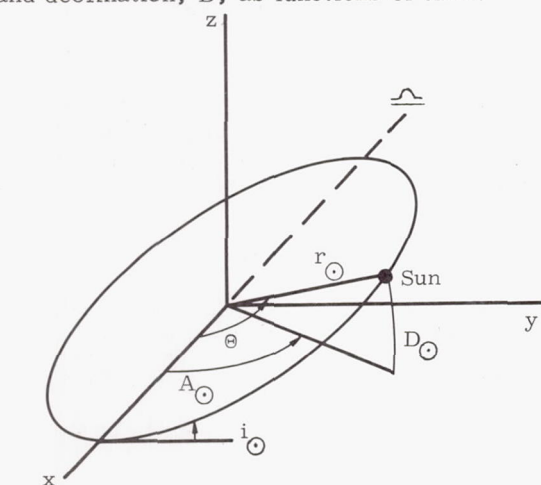
$$\frac{y_s}{r_s} = \cos(\theta + \omega) \sin \Omega + \cos i \sin(\theta + \omega) \cos \Omega$$

$$\frac{z_s}{r_s} = \sin(\theta + \omega) \sin i \quad (7)$$

The rectangular coordinates (x_s , y_s , z_s) are obtained in terms of the parameter θ by substitution of Eq (5) in Eq (7).

b. Position of the sun in an ECI coordinate system

The definition of solar position in the ECI system is simplified by choice of vernal equinox, φ , the direction of the intersection line of the ecliptic and equatorial planes, as one of the system axes. Many astronomical tables provide solar position in terms of right ascension, A , and declination, D , as functions of time.



$$\begin{aligned} x_{\odot} &= r_{\odot} \cos D_{\odot} \cos A_{\odot} \\ y_{\odot} &= r_{\odot} \cos D_{\odot} \sin A_{\odot} \\ z_{\odot} &= r_{\odot} \sin D_{\odot} \end{aligned} \quad (8)$$

However, a more convenient system for study purposes is one employing obliquity, i_{\odot} , and ecliptic angle from equinox, Θ . The obliquity

$$i_{\odot} = 23^{\circ} 27' 08.26'' - 0.4684'' (t - 1900)$$

(where t is the calendar year) is practically constant, and the solar position can then be specified by only two variables, r_{\odot} and Θ . The angle Θ can be found by the inverse solution of Kepler's equation for the eccentric anomaly as a function of time. Then, the Θ can be found as a function of E . However, since the orbit of the earth is nearly circular,

$$e_{\oplus} = 0.0167272,$$

r_{\odot} is nearly constant ($0.983273 \text{ au} \leq r_{\odot} \leq 1.016727 \text{ au}$) and Θ can be approximated as

$$\Theta = 0.98563 d_{\text{ep}}$$

where d_{ep} is the number of days past vernal equinox (\approx March 21).

In either case, the solar position in terms of i_{\odot} and Θ is given as follows:

$$\begin{aligned} x_{\odot} &= r_{\odot} \cos \Theta \\ y_{\odot} &= r_{\odot} \cos i_{\odot} \sin \Theta \\ z_{\odot} &= r_{\odot} \sin i_{\odot} \sin \Theta \end{aligned} \quad (9)$$

c. Position of the sun in a vehicle-centered inertial coordinate system (VCI)

The position of the sun in the VCI system is obtained by subtracting corresponding ECI components of the vehicle and the sun.

$$\begin{aligned} X &= x_{\odot} - x_s \\ Y &= y_{\odot} - y_s \\ Z &= z_{\odot} - z_s \end{aligned} \quad (10)$$

where (x_{\odot} , y_{\odot} , z_{\odot}) and (x_s , y_s , z_s) are given by Eqs (7) and (8) or (9). The distance from the vehicle to the sun is

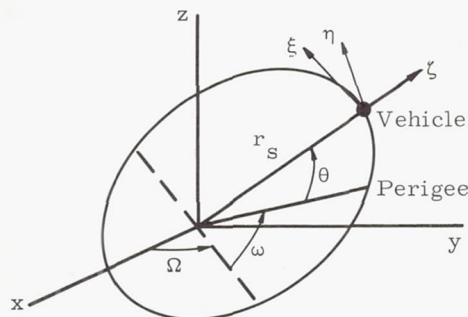
$$r_{s\odot} = \sqrt{(x_{\odot} - x_s)^2 + (y_{\odot} - y_s)^2 + (z_{\odot} - z_s)^2} \quad (11)$$

and so Eq (10) may be expressed in direction cosine form as follows:

$$\begin{aligned} \cos \alpha_X &= \frac{x_{\odot} - x_s}{r_{s\odot}} \\ \cos \beta_Y &= \frac{y_{\odot} - y_s}{r_{s\odot}} \\ \cos \gamma_Z &= \frac{z_{\odot} - z_s}{r_{s\odot}} \end{aligned} \quad (12)$$

- d. Position of the sun in a vehicle-centered local horizontal coordinate system (VCL)

ECI coordinates may be transformed to VCL by successive counterclockwise rotations about z through Ω , about x through i and about z through $(\theta + \omega)$.



$$\begin{bmatrix} \zeta \\ \eta \\ \xi \end{bmatrix} = \begin{bmatrix} \cos(\theta + \omega) & \sin(\theta + \omega) & 0 \\ -\sin(\theta + \omega) & \cos(\theta + \omega) & 0 \\ 0 & 0 & 1 \end{bmatrix}$$

$$\begin{bmatrix} 1 & 0 & 0 \\ 0 & \cos i & \sin i \\ 0 & -\sin i & \cos i \end{bmatrix} \begin{bmatrix} \cos \Omega & \sin \Omega & 0 \\ -\sin \Omega & \cos \Omega & 0 \\ 0 & 0 & 1 \end{bmatrix} \begin{bmatrix} x \\ y \\ z \end{bmatrix}$$

$$\begin{bmatrix} \cos \Omega \cos(\theta + \omega) & \sin \Omega \cos(\theta + \omega) & \sin i \sin(\theta + \omega) \\ -\sin \Omega \cos i \sin(\theta + \omega) & +\cos \Omega \cos i \sin(\theta + \omega) & \sin i \cos(\theta + \omega) \\ -\cos \Omega \sin(\theta + \omega) & -\sin \Omega \sin(\theta + \omega) & \cos i \\ -\sin \Omega \cos i \cos(\theta + \omega) & +\cos \Omega \cos i \cos(\theta + \omega) & \sin i \\ \sin \Omega \sin i & -\cos \Omega \sin i & \cos i \end{bmatrix} \begin{bmatrix} x \\ y \\ z \end{bmatrix} \quad (13)$$

Substitution of Eq (9) in Eq (13), followed by translation of the vehicle radius r_s in the ζ direction, gives the direction cosines of the solar position in VCL coordinates:

$$\cos \alpha_{\zeta} = \frac{\zeta_{\odot}}{r_{s\odot}} = \frac{r_{\odot}}{r_{s\odot}} \left\{ \cos \Theta \left[\cos \Omega \cos(\theta + \omega) - \sin \Omega \cos i \sin(\theta + \omega) \right] + \sin \Theta \cos i_{\odot} \left[\sin \Omega \cos(\theta + \omega) + \cos \Omega \cos i \sin(\theta + \omega) \right] + \sin \Theta \sin i_{\odot} \left[\sin i \sin(\theta + \omega) \right] \right\}$$

$$- \frac{r_s}{r_{s\odot}}$$

$$\cos \beta_{\eta} = \frac{\eta_{\odot}}{r_{s\odot}} = \frac{r_{\odot}}{r_{s\odot}} \left\{ \cos \Theta \left[-\cos \Omega \sin(\theta + \omega) - \sin \Omega \cos i \cos(\theta + \omega) \right] + \sin \Theta \cos i_{\odot} \left[-\sin \Omega \sin(\theta + \omega) + \cos \Omega \cos i \cos(\theta + \omega) \right] + \sin \Theta \sin i_{\odot} \sin i \cos(\theta + \omega) \right\} \quad (14)$$

$$\cos \gamma_{\xi} = \frac{\xi_{\odot}}{r_{s\odot}} = \frac{r_{\odot}}{r_{s\odot}} \left[\cos \Theta \sin \Omega \sin i - \sin \Theta \cos i_{\odot} \cos \Omega \sin i + \sin \Theta \sin i_{\odot} \cos i \right]$$

The last equation of Eq (14) is especially interesting since the true anomaly θ is not involved, i.e., $\cos \gamma_{\xi}$ is a function only of the time of year (Θ) and the orbit orientation (Ω and i). In fact, for low altitude orbits $r_{\odot} \approx r_{s\odot}$ and γ_{ξ} approaches the angle between the earth-sun line and the normal to the orbit plane.

$$\cos \gamma_n = \cos \Theta \sin \Omega \sin i - \sin \Theta \cos i_{\odot} \cos \Omega \sin i + \sin \Theta \sin i_{\odot} \cos i \quad (15)$$

This is a useful parameter in determining time in sunlight (Section E). The $\sin \gamma_n$ and $\cos \gamma_n$ are plotted in Figs. 1 and 2 (Ref. 1) for a particular orbit to show the form.

2. Eclipses of Earth Satellites

There are several important areas to be considered in the study of eclipsing of earth satellites by the earth's shadow. The areas discussed in this section include the following.

- (1) General geometry of eclipses by the shadow.
- (2) Equations leading to the prediction of eclipses by the shadow.

- (3) General geometry of eclipses by the penumbra.
- (4) Equations leading to the prediction of eclipses by the penumbra.
- (5) Eclipse information obtained by analytical means.
- (6) Complications involved in the problem.
- (7) Chart and equations for a computer program.

In the material to be presented, all angular orbital elements are referred to the plane of the ecliptic. Since these angles are referred to the plane of the equator for earth satellites, the reader should see Chapter XI for the appropriate coordinate transformation.

a. General geometry of eclipses by the shadow (Ref. 2)

For simplicity, Figs. 3 through 5 show the orbit of the satellite through the center of the shadow. Figure 5 shows a case where the shadow is not at the node. In all three figures, P_1 is the point where the satellite enters the shadow and P_2 the point where it leaves the shadow. P_3 is some point outside the shadow (that is, in sunlight). Let s be the size (angular radius) of the shadow and θ_s the angular distance from the center of the shadow to any point in the orbit. When $\theta_s > s$ the satellite is in sunlight; when $\theta_s < s$ the satellite is in shadow.

b. Equations involved in prediction of eclipses by the shadow (Ref. 2)

The angular size of the earth's shadow is computed from

$$s = \frac{102}{100} \left[\sin^{-1} \left(\frac{R}{r} \right) - 16' \right] \quad (16)$$

where R is the earth's radius

and

$$r = \frac{a(1-e)^2}{1+e \cos \theta} \quad \begin{cases} a = \text{semimajor axis} \\ e = \text{eccentricity} \\ \theta = \text{true anomaly} \end{cases}$$

and the factor 102/100 is due to the refraction of the atmosphere. Now, using the following sketch

$$\begin{aligned} \cos \theta_s &= \cos \Delta \lambda \cos \Delta \theta \\ &+ \sin \Delta \lambda \sin \Delta \theta \cos i_\epsilon \end{aligned} \quad (17)$$

where

$$\Delta \lambda = \Omega - \lambda \text{ (shadow)}$$

$$\Delta \theta = \theta - \theta (\Omega)$$

and

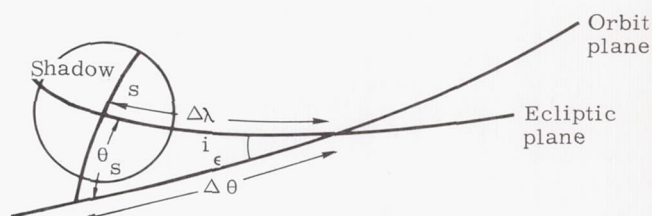
$$\lambda \text{ (shadow)} = \text{longitude of the shadow}$$

$$= \text{longitude of the sun} + 180^\circ$$

$$\theta (\Omega) = \text{true anomaly at the node}$$

$$= -\omega$$

$$i_\epsilon = \text{inclination of orbit plane to ecliptic plane}$$



The solution of the equations for $s = \theta_s$ will give values θ_1 and θ_2 , the true anomaly at the point of entering the shadow (P_1) and at the point of leaving the shadow (P_2) respectively. For each of those conditions

$$\cos E = \frac{\cos \theta + e}{1 + e \cos \theta} \quad (18)$$

$$M = E - e \sin E \quad (19)$$

$$\text{If } 0 \leq \theta \leq 180 \text{ or } \text{If } 180 \leq \theta \leq 360$$

$$\text{then } 0 \leq E \leq 180 \quad \text{then } 180 \leq E \leq 360$$

$$\text{and } 0 \leq M \leq 180 \quad \text{and } 180 \leq M \leq 360$$

$$\text{and } t = \frac{M}{n}, \quad n = \frac{\sqrt{\mu}}{a^{3/2}} \quad (20)$$

where

$$e = \text{eccentricity}$$

$$E = \text{eccentric anomaly}$$

$$M = \text{mean anomaly}$$

$$t = \text{time from perigee passage } (t_p)$$

$$n = \text{mean motion}$$

$$\mu = \text{GM, the product of the universal gravity constant and the mass of the earth}$$

$$= 1.407648 \times 10^{16} \text{ ft}^3/\text{sec}^2 \text{ (adopted value)}$$

$$= 398,601.5 \text{ km}^3/\text{sec}^2$$

then

$$\text{Time in umbra} = t_{2u} - t_{1u} \quad (21)$$

If Eq (21) is negative, add the orbital period to the answer.

To determine eclipse duration on any later revolution, it is necessary to update the past values of the orbital elements which have been changed as a result of various perturbations (see Chapter IV), and the position of the shadow (approximately 0.9856 deg/day). The equations for s and θ_s are again solved for the points where $s = \theta_s$.

c. General geometry of eclipses by the penumbra (Ref. 2)

To find time in penumbra, an approach is followed similar to the study for the time in umbra or shadow. In this case, however, the penumbra is a ring around the umbra as shown in Figs. 6 and 7.

From Fig. 6, it can be seen that, if the satellite orbit is circular (i.e., $r_1 = r_2$),

$$\begin{aligned}\Delta T_1 OP_1 &\approx \Delta T_2 OP_2 \\ \therefore \angle T_1 OP_1 &= \angle T_2 OP_2\end{aligned}$$

But

$$\begin{aligned}\angle T_1 OT_2 &= 180^\circ - \angle O_1 OT_1 - \angle T_2 O O_2 \\ &= 180^\circ - (90^\circ - \alpha) - (90^\circ - \beta) \\ &= \alpha + \beta\end{aligned}$$

and

$$\begin{aligned}\psi &= \angle T_1 OT_2 + \angle T_2 OP_2 - \angle T_1 OP_1 \\ &= \angle T_1 OT_2 = \alpha + \beta.\end{aligned}$$

Thus the angle ψ is very nearly constant regardless of the size of the circular orbit and is approximately equal to 0.54° .

d. Equations involved in prediction of eclipses by the penumbra (Ref. 2)

Whether a satellite enters the penumbra or not (in a particular revolution about the earth) is a similar problem to that of finding out whether it enters the umbra (shadow) or not. We simply increase s by ψ and then compare θ_s with $s + \psi$.

The satellite enters and leaves the penumbra cone at the points $\theta_s = s + \psi$. For these points use Eqs (18), (19) and (20) obtaining t_{1p} and t_{2p} , relative time of entering penumbra and time out of penumbra. If there is not an umbra eclipse in that revolution, then

$$\text{Time in penumbra} = t_{2p} - t_{1p} \quad (22)$$

If there is an umbra eclipse in that revolution, then there will be two times in penumbra (first going from point P_1 to point P_2 and then going from point P_3 to point P_4 as shown in Fig. 7, namely,

$$\text{Time in penumbra (1)} = t_{1u} - t_{1p} \quad (23)$$

$$\text{Time in penumbra (2)} = t_{2p} - t_{2u} \quad (24)$$

If any of Eqs (22), (23) and (24) is negative, add the orbital period to the answer.

e. Alternative solution for eclipse times

An alternative solution for eclipse times may be formulated from consideration of Fig. 9. Let $(\hat{x}, \hat{y}, \hat{z})$ be unit vectors in an ecliptic coordinate system (x_e, y_e, z_e) .

R_\odot = radius of the sun

R_\oplus = radius of the earth

\vec{r} = geocentric radius vector to the satellite (unit vector \hat{r})

r_\oplus = distance between the centers of earth and sun

\hat{s} = unit vector along the direction of the earth-sun line

λ = geocentric celestial longitude of the vehicle (ecliptic)

ℓ = geocentric celestial latitude of the vehicle (ecliptic)

λ_\oplus = heliocentric celestial longitude of the earth (ecliptic)

ϕ = angle between \hat{r} and \hat{s}

Then

$$\hat{r} = \cos \ell \cos \lambda \hat{x} + \cos \ell \sin \lambda \hat{y} + \sin \ell \hat{z}$$

$$\hat{s} = -\cos \lambda_\oplus \hat{x} - \sin \lambda_\oplus \hat{y}$$

and

$$\cos \phi = \hat{r} \cdot \hat{s}$$

The condition for entering or leaving the penumbra is that $\epsilon = 0$ (ϵ defined in Fig. 8). This condition can be determined from

$$\epsilon = \alpha - \beta + \pi - \phi - \sin^{-1} \frac{R_\oplus}{r}$$

where

$$\begin{aligned}\alpha &= \sin^{-1} \frac{R_\odot}{\sqrt{r_\oplus^2 + r^2 - 2 r_\oplus r \cos \phi}} \\ &\approx \frac{R_\odot}{r_\oplus} \left[1 + \frac{1}{6} \left(\frac{R_\odot}{r_\oplus} \right)^2 - \frac{1}{2} \left(\frac{r}{r_\oplus} \right)^2 + \frac{r}{r_\oplus} \cos \phi \right. \\ &\quad \left. + \frac{3}{2} \left(\frac{r}{r_\oplus} \right)^2 \cos^2 \phi \right] \\ &\quad \left[1 \gg \left(\frac{R_\odot}{r_\oplus} \right)^2 ; 1 \gg \left(\frac{r}{r_\oplus} \right)^2 \right]\end{aligned}$$

and

$$\begin{aligned}\beta &= \sin^{-1} \frac{r \sin \phi}{\sqrt{r_{\oplus}^2 + r^2 - 2 r_{\oplus} r \cos \phi}} \\ &\approx \frac{r}{r_{\oplus}} \sin \phi \left[1 - \frac{1}{2} \left(\frac{r}{r_{\oplus}} \right)^2 \right. \\ &\quad \left. + \frac{1}{6} \left(\frac{r}{r_{\oplus}} \right)^2 \sin^2 \phi + \frac{r}{r_{\oplus}} \cos \phi \right. \\ &\quad \left. + \frac{3}{2} \left(\frac{r}{r_{\oplus}} \right)^2 \cos \phi \right] \\ &\quad \left[1 \gg \left(\frac{R_{\odot}}{r_{\oplus}} \right)^2 ; 1 \gg \left(\frac{r}{r_{\oplus}} \right)^2 \right]\end{aligned}$$

The solutions for penumbra entrance and exit thus satisfy

$$\begin{aligned}\epsilon &\approx \frac{R_{\odot}}{r_{\oplus}} \left[1 + \frac{r}{r_{\oplus}} \cos \phi - \frac{r}{R_{\odot}} \sin \phi \right] \\ &\quad + \pi - \phi - \sin^{-1} \frac{R_{\oplus}}{r} = 0 \\ &\quad \left[1 \gg \left(\frac{R_{\odot}}{r_{\oplus}} \right)^2 ; 1 \gg \left(\frac{r}{r_{\oplus}} \right)^2 \right]\end{aligned}$$

The umbra entrance and exit conditions can be written by taking

$$\epsilon = \pi - \phi - (\alpha - \beta) - \sin^{-1} \frac{R_{\oplus}}{r}$$

where

$$\alpha + \beta \approx \frac{R_{\odot}}{r_{\oplus}} \left(1 + \frac{r}{r_{\oplus}} \cos \phi + \frac{r}{R_{\odot}} \sin \phi \right)$$

(as indicated by Fig. 8) and where α is taken in the opposite direction to that for the penumbra solution, i.e., α is the angle between the vehicle-sun line and the lower tangent to the solar surface.

No correction for refraction of the light waves has been made in this material. However, it is noted that the apparent effect at the vehicle will be to make the sun appear larger. Thus, an accurate correction can be made by utilizing the apparent rather than the true radius of the sun.

- f. Eclipse information obtained by analytical means (Refs. 1, 2 and 3)

An exact closed-form analysis of general satellite eclipses is impracticable; however, some useful information can be obtained by this type of analysis. Very little can be done with an eccentric orbit, as may be inferred from the previous sections, but with unperturbed circular orbits several important eclipse properties may be determined.

(1) Eclipse season

If it is desired to find the days on which an eclipse occurs, or so-called eclipse season, one may do so with the aid of Fig. 9

$$\sin \lambda_u = \frac{\sin s}{\sin i_{\epsilon}} \quad (25)$$

where s would be the maximum size of the shadow for an eccentric orbit.

Then

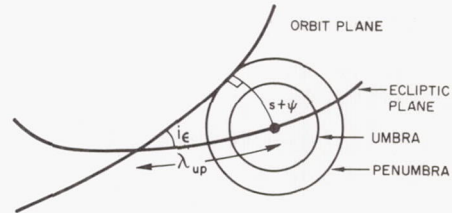
$$\text{eclipse season (umbra only)} \approx 2 \frac{\lambda_u}{0.986} \text{ days} \quad (26)$$

where 0.986 is the mean velocity of the sun in degrees per day.

The exact eclipse season is difficult to compute analytically: (1) due to the regression of the nodes the inclination with respect to the ecliptic varies and it is difficult to predict the inclination when the earth's shadow is near the node; (2) if the orbit is very eccentric the size of the shadow at perigee would be much larger than that at apogee, and again it would be necessary to predict the position of perigee at the time the shadow is approaching the node. For many applications, however, the simple method presented above is adequate.

To determine the eclipse season including the penumbra, the above equations may be used but s must be increased by ψ ($\psi = 0^\circ.54$), as shown in the following sketch.

$$\begin{aligned}\text{eclipse season (umbra and penumbra)} &\approx 2 \frac{\lambda_{up}}{0.98563} \\ &= 2 \frac{\sin^{-1} \left[\frac{\sin(s + \psi)}{\sin i_{\epsilon}} \right]}{0.98563} \quad (27)\end{aligned}$$



Obviously, if the inclination with respect to the ecliptic is smaller than the angular radius of the shadow ($i_{\epsilon} < s$), there will be an eclipse at every revolution.

Also it must be remembered that due to oblateness (and also luni-solar perturbations in certain cases) the nodes regress, and a more realistic expression for Eq (26) would be

$$\text{eclipse season} = 2 \frac{\lambda_u}{0.98563 + \frac{d\Omega}{dt}} \quad (28)$$

where $d\Omega/dt$ = rate of regression of the nodes with respect to the ecliptic. It should be noted that, with proper selection of orbit inclination and altitude, the regression rate can be made

equal to the earth revolution rate, $\frac{d\Omega}{dt} = 0.986^\circ/\text{day}$ (i.e., the orbit would follow the sun). In particular, if the initial orbit were chosen to have this regression rate and, furthermore, to be continuously in sunlight with

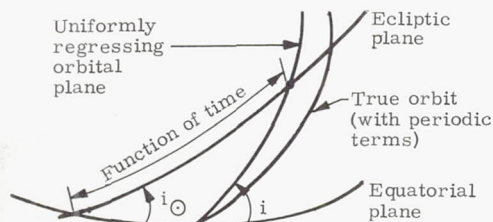
$$i_e > \cos^{-1} \sqrt{1 - \left(\frac{R}{r}\right)^2},$$

the satellite would be in sunlight for its entire lifetime. The orbit condition for $\frac{d\Omega}{dt} = 1^\circ/\text{day}$ is

$$\cos i \approx -0.1 \left(\frac{r}{R}\right)^{7/2}$$

i. e., $90 < i < 180^\circ$.

No straightforward analytical expression exists to give the rate of regression of the nodes with respect to the ecliptic similar to the expression (to first order) which gives the rate of regression of the nodes with respect to the equator. The reason for this fact is shown in the following sketch.



Thus, the equatorial nodal position and the periodic perturbations of the node must both be considered in the definition of nodal position relative to the ecliptic. A graphic study shows, however, that the regression of the nodes with respect to the ecliptic is negligible in most cases. In cases for which it is not, $i_e < s$ and, therefore, is of no consequence in the computation of the eclipse season, since for $i_e < s$ there is an eclipse in every revolution.

(2) Maximum time in umbra (eccentric orbits)

To get an idea of the maximum time in the umbra the following method may be used.

Let the size of the shadow at apogee be s_a and the angular velocity at apogee, w_a

where

$$w_a = \frac{v_a}{r_a} = \sqrt{\frac{\mu}{a^3 (1+e)^3 (1-e)}}$$

$$v_a = \sqrt{\mu \left(\frac{2}{r_a} - \frac{1}{a} \right)}$$

$$r_a = a(1+e)$$

then

$$\text{maximum duration of eclipse} = 2 \left(\frac{s_a}{w_a} \right)$$

where s_a is given by Eq (16).

(3) Curves of maximum eclipse duration and eclipse season (circular orbits)

In the case of unperturbed circular orbits a simplified approach is possible. A set of general curves is included for circular orbits; clearly, the results obtained from these curves cannot be extended to eccentric orbits. A simple method of computing and presenting maximum eclipse durations and eclipse seasons is given in the following material.

Figure 10 shows maximum time in umbra versus semimajor axis, which is obtained from

$$\text{maximum time in umbra} = 2 \frac{s}{n} \quad (29)$$

where n is the mean motion

$$n = \frac{\sqrt{\mu}}{a^{3/2}} \quad (30)$$

Maximum time in umbra and penumbra versus semimajor axis is obtained simply from

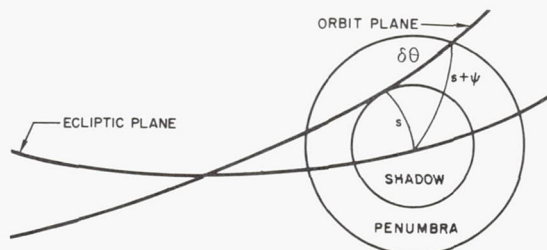
$$\begin{aligned} \text{maximum time in umbra} \\ \text{and penumbra} &= 2 \frac{s + \psi}{n} \end{aligned} \quad (31)$$

Figure 11 shows the same information as Fig. 10, but with expanded scale.

Maximum time in penumbra where there is no umbra eclipse is computed from

$$\cos \delta\theta = \frac{\cos(s + \psi)}{\cos s} \quad (32)$$

which is obtained from the following sketch.



$$\text{Then, maximum time in penumbra} = 2 \frac{\delta\theta}{n}$$

Figure 12 shows maximum time in penumbra versus semimajor axis. Figure 13 shows the same information as Fig. 12, but with expanded scale.

Figure 14 shows eclipse season (umbra only) versus semimajor axis and inclination, which is obtained as illustrated in Fig. 9. Figure 15 shows eclipse season (umbra and penumbra) versus semimajor axis and inclination obtained as illustrated in Fig. 9.

Figure 10 showed that, for fairly low altitude orbits (less than one earth radius), the times in umbra and penumbra differ by a fraction of a minute or less than 1% of the orbit period. In this region the earth shadow can be accurately approximated by a cylinder. With this assumption the eclipse duration solution for unperturbed circular orbits can be further simplified. The simplified problem has been considered in various references, e.g., Refs. 1, 3 and 4.

If the shadow made by the earth is approximated by a cylinder, this cylinder will intersect the orbit plane in an ellipse with semimajor axis of $\frac{R}{\cos \gamma_n}$ and semiminor axis of R , as shown in Fig. 16, where $\cos \gamma_n$ is given in Eq (15) and plotted in Fig. 2. The per cent time in sunlight is then the same as the per cent of the orbit arc not contained in the shadow ellipse, as shown in Fig. 16. The problem then reduces to the simple determination of the angle ϕ from the intersection of the orbit and the projected shadow ellipse:

$$\begin{cases} x^2 + y^2 = r_s^2 \text{ (orbit)} \\ \frac{x^2}{\left(\frac{R}{\cos \gamma_n}\right)^2} + \frac{y^2}{R^2} = 1 \text{ (shadow ellipse)} \end{cases}$$

Substitution of y from the first equation in the second equation gives

$$x^2 \cos^2 \gamma_n + r_s^2 - x^2 = R^2$$

or

$$x = \frac{\sqrt{r_s^2 - R^2}}{\sin \gamma_n}$$

Then

$$\cos \phi = \frac{x}{r_s} = \frac{\sqrt{1 - \left(\frac{R}{r_s}\right)^2}}{\sin \gamma_n}, \quad 0^\circ < \phi < 90^\circ$$

The per cent time in sunlight is

$$\begin{aligned} t_s &= \frac{180 - \phi}{180} \times 100\% \text{ for } \sin \gamma_n > \sqrt{1 - \left(\frac{R}{r_s}\right)^2} \\ &= 100\% \text{ for } \sin \gamma_n \leq \sqrt{1 - \left(\frac{R}{r_s}\right)^2} \end{aligned}$$

Substitution for ϕ in this equation gives

$$\sin \gamma_n = \pm \frac{\sqrt{1 - \left(\frac{R}{r_s}\right)^2}}{\cos (1.8 t_s)} \quad (33)$$

This equation determines the orbit orientation γ_n required for any desired per cent sunlight time t_s . Equation (15) in turn provides the combinations of time of year, orbit ascending node and orbit inclination possible for a given t_s .

As examples, circular orbits of various altitudes and inclinations were considered. The value of $\cos \gamma_n$ for various orbit altitudes as a function of per cent sunlight time is plotted in Fig. 17. Another presentation of the same relationship is given in Fig. 18. These values are obtained from Eq (33). Then horizontal lines across Fig. 1 or Fig. 2 at each t_s level determine the (θ, Ω) loci for the given per cent time in sunlight. These loci have been replotted in different form in Figs. 19 through 23. These figures show

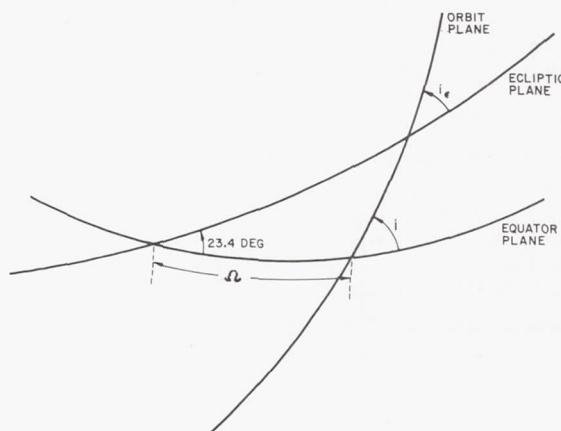
very clearly the required longitude of ascending node, Ω , required to provide a given sunlight time t_s at any given time of the year. For example, for 125-naut mi (232 km) orbits, 100% sunlight may be achieved only in alternate quarters of the year, the quarters near autumnal and vernal equinoxes. During quarters centered about the summer and winter solstices, the maximum time in sunlight is 80%. For 500-naut mi (930 km) orbits, 100% sunlight may be obtained at any time in the year.

Other curves which may prove to be useful are:

- (1) Inclination with respect to the ecliptic (i_e) versus longitude of the node with respect to equator (Ω) for different inclinations with respect to equator (i) (Fig. 24), computed from

$$\cos i_e = \cos 23.4 \cos i + \sin 23.4 \sin i \cos \Omega \quad (34)$$

which is obtained from the following sketch.



- (2) Angular radius of shadow versus distance from center of earth, Fig. 25 [see Fig. 3 and Eq (16)]. Figure 26 shows the same information as Fig. 25, but with expanded scale.

g. Chart and equations for a computer program

The following reasons indicate why a closed-form analytical solution is not easily obtained:

- (1) Time of launch--the longitude of the node at burnout will vary with the time of launch.
- (2) Date of launch--the initial position of the sun will be different for different dates of launch.
- (3) Eccentricity of orbit--the shadow is not a circle, but has an egg-shaped contour.
- (4) Regression of the nodes--the longitude of the node will vary constantly due to oblateness.

- (5) Advance of perigee--the argument of perigee will vary constantly due to oblateness; the size of the shadow at the nodes will vary from maximum if perigee is at the node to minimum if apogee is at the node.
- (6) Drag--the size of the semimajor axis of the orbit will decrease due to atmospheric drag.
- (7) Luni-solar perturbations--all of the orbital elements will vary to some extent due to luni-solar perturbations.

A method for obtaining a more precise solution to the general problem of earth's satellite eclipses is given in this section.

The most efficient method of calculating eclipses is by means of a computer program, a simple example of which is represented in Fig. 27, from Ref. 2.

It must be noted at this point that this program, as well as any of the analytical methods described, will produce only times in umbra and times in penumbra at a given revolution, but not the time of day at which these phenomena happen. This can be roughly determined by knowing the time from perigee passage at which the phenomena occur, the period, and the time of perigee passage for some date. If the time of perigee passage for date D_1 is T_1 and the period is τ , then the approximate time of perigee passage for some other date D_2 , ΔD days from D_1 , is

$$T_2 = T_1 + N\tau \quad (35)$$

where N is the integral number of periods in ΔD . If the motion of perigee due to perturbations is large, the anomalistic period (time from perigee to perigee) should be used in Eq (35).

The results of machine computations are shown in Figs. 28 through 30. The luni-solar perturbations were added by first running another program which computes changes in equatorial elements due to various perturbations (a complicated program in itself), and then using the output as the input to the eclipse program. Also included in the above set of curves is one showing the eclipse pattern when launching the same vehicle at different times of day on the same date and at the same time of day on different dates.

D. GROUND TRACKS (REF. 3)

The equations for the ground track of a satellite orbit may be written, from an application of spherical trigonometry to Fig. 31, as follows:

Geocentric latitude:

$$L = \sin^{-1} (\sin i \sin \phi) \quad (36)$$

Geocentric longitude:

$$\Lambda = \tan^{-1} (\cos i \tan \phi) + \Lambda_{n0} - \Omega_e \Delta t - \frac{3}{2} K n J_2 \Delta t \left(\frac{R_e}{a} \right)^2 \frac{\cos i}{(1 - e^2)^2} \quad (37)$$

where

- i = inclination of the orbit plane to the ecliptic plane, $0 \leq i < 180^\circ$, measured + from east at ascending node
- ϕ = orbit central angle between the satellite and the ascending node
- Λ_{n0} = initial geocentric longitude of the ascending node, $0 \leq \Lambda_{n0} \leq 360^\circ$, measured + toward the east
- Ω_e = rotation rate of the earth, 4.178074×10^{-3} deg/sec
- Λ_{n0} = initial geocentric longitude of the ascending node
- Δt = time measured from the initial condition
- K = 57.2958 deg/rad
- n = mean motion = $\sqrt{\frac{\mu}{a^3}}$
- J_2 = 1.0823×10^{-3}
- R_e = equatorial radius of the earth
- a = orbit semimajor axis
- e = orbit eccentricity.

Equations (36) and (37), presenting satellite position with respect to a rotating oblate earth, neglect second order oblateness perturbations.

These equations may be used to generate the ground track as a series of points (L , Λ) as a function of the parameter ϕ . This determination is simple in the case of circular orbits, but somewhat complicated for elliptical orbits due to the nonlinear behavior of the angular rate.

1. Elliptical Orbit Ground Tracks

The difficulties of ground track predictions for elliptical orbits arise from the fact that the angle in orbit plane (from ascending node to satellite) is a nonlinear function of time. For large eccentricities, Chapter III expresses this angle in the form of a Fourier-Bessel infinite series. For small eccentricities, the angle can be expressed as a simple sine series where the constants are determined by the corresponding eccentricities.

Satellite latitude and longitude are first established with respect to a nonrotating earth, as a function of time. Rotation of the earth, regression of the nodes and precession of the perigee are then used as corrections for longitude and latitude on a rotating earth. Six input parameters are needed (e.g., h_0 , v_0 , γ_0 , L_0 , Λ_0 and β_0).

From these data all the necessary information is obtained by the equations of spherical trigonometry and planetary motion along the Keplerian ellipses.

The geometrical representation of the problem, indicating the most important quantities used in the calculation procedure, is given in Fig. 31. It should be noted that the longitude of the ascending node (Ω), as well as the angle of perigee (ω) and the angle of the satellite (ϕ) from the node are all functions of time.

The properties of the Keplerian ellipse are as follows:

Semimajor axis:

$$a = \frac{r_0}{2 - r_0 v_0^2 / \mu} \quad (38)$$

Eccentricity:

$$e = \sqrt{1 - \frac{r_0^2 v_0^2 \cos^2 \gamma_0}{a \mu}} \quad (39)$$

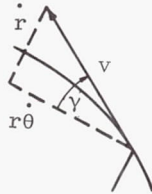
Period:

$$\tau = 2\pi \sqrt{a^3 / \mu} \quad (40)$$

Next the central angle from perigee is derived. First, the local flight path angle is seen from the following geometry to be

$$\tan \gamma = \frac{\dot{r}}{r \dot{\theta}} = \frac{1}{r} \frac{dr}{d\theta}$$

$$r = \frac{p}{1 + e \cos \theta}$$



Therefore,

$$\frac{dr}{d\theta} = \frac{pe \sin \theta}{(1 + e \cos \theta)^2} \quad \text{and} \quad \tan \gamma = \frac{e \sin \theta}{1 + e \cos \theta}$$

This is expressed as

$$\tan \gamma = \frac{e \sqrt{1 - \cos^2 \theta}}{1 + e \cos \theta}$$

and the following is derived.

$$e \cos \theta = \sin^2 \gamma \pm \cos \gamma \sqrt{e^2 - \sin^2 \gamma}$$

From this, the initial central angle from perigee is obtained.

$$\theta_0 = \pm \cos^{-1} \left[\frac{\sin^2 \gamma_0 \pm \cos \gamma_0 \sqrt{e^2 - \sin^2 \gamma_0}}{e} \right] \quad (41)$$

Equation (41) gives four possible answers and the correct one should be selected as follows:

| Flight Path Angle | Radius | θ_0 (from perigee) |
|-------------------|-----------|---|
| $\gamma_0 > 0$ | $r_0 < a$ | $0^\circ < \theta_0 < \theta^*$ |
| $\gamma_0 > 0$ | $r_0 > a$ | $\theta^* < \theta_0 < 180^\circ$ |
| $\gamma_0 < 0$ | $r_0 > a$ | $180^\circ < \theta_0 < 360^\circ - \theta^*$ |
| $\gamma_0 < 0$ | $r_0 < a$ | $360^\circ - \theta^* < \theta_0 < 360^\circ$ |

$$\text{where } \theta^* \equiv 180^\circ - \cos^{-1} e \text{ (see Fig. 31)} \quad (42)$$

Now the inclination of the orbit is obtained by spherical trigonometry.

$$i = \cos^{-1} (\cos L_0 \sin \beta_{0I}), \quad (43)$$

where β_{0I} is obtained as follows.

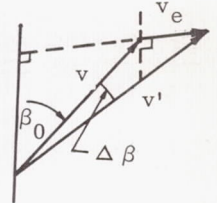
$$\beta_{0I} = \beta_0 + \frac{R_e \Omega_e}{v_0 \cos \gamma_0} \cos L_0 \cos \beta_0$$

The component of velocity parallel to the earth's surface is found by $v' = v_0 \cos \gamma_0$. The component due to the earth's rotation is simply

$$v_e = R \Omega_e \cos L_0.$$

From trigonometry,

$$\begin{aligned} \frac{v_e}{\sin \Delta \beta} &= \frac{v'}{\sin (90^\circ + \beta_0)} \\ &= \frac{v'}{\cos \beta_0}. \end{aligned}$$



Because $\Delta \beta$ is a small angle, $\sin \Delta \beta \approx \Delta \beta$ is a good approximation. Finally, since

$$\Delta \beta = \frac{v_e}{v'} \cos \beta_0 = \frac{R \Omega_e}{v_0 \cos \gamma_0} \cos L_0 \cos \beta_0. \quad (44)$$

Now

$$\beta_{0I} = \beta_0 + \Delta \beta. \quad (45)$$

The initial angle from the ascending node is

$$\phi_0 = \sin^{-1} \left[\frac{\sin L_0}{\sin i} \right] \quad (46)$$

and the initial perigee angle from the node (Eqs (41) and (46)) is

$$\omega_0 = \phi_0 - \theta_0. \quad (47)$$

Denoting the time from the initial point (L_0 , Λ_0 , h_0) by Δt . Then,

$$t = t_0 + \Delta t. \quad (48)$$

where t_0 is the time from perigee found from Kepler's equation

$$t_0 = \frac{\tau}{2\pi} \left\{ \frac{-e \sqrt{1-e^2} \sin \theta_0}{1+e \cos \theta_0} + 2 \tan^{-1} \left[\frac{\sqrt{1-e^2} \tan(\theta_0/2)}{1+e} \right] \right\}. \quad (49)$$

For a nonrotating earth, the following equations are derived from spherical trigonometry.

$$\text{Latitude: } L_1 = \sin^{-1} (\sin i \sin \phi) \quad (50)$$

$$\text{Longitude: } \Lambda_1 = \tan^{-1} (\cos i \tan \phi) + \Lambda_h \quad (51)$$

Next, consider a rotating earth with oblateness effects. Due to the precession of the apsides, the perigee of the orbit is a function of time, and the angle of perigee from the ascending node is given by

$$\begin{aligned} \omega &= \omega_0 + K \dot{\omega} \frac{\Delta t}{\tau} \\ &= \omega_0 + \frac{3}{2} K n J_2 \Delta t \left(\frac{R_e}{a} \right)^2 \frac{(2 - \frac{5}{2} \sin^2 i)}{(1 - e^2)^2} \end{aligned} \quad (52)$$

where

$$n \equiv \frac{2\pi}{\tau} = \sqrt{\frac{\mu}{a^3}} \quad (53)$$

For an easterly launch, the node is given for a rotating oblate earth as

$$\begin{aligned} \Omega &= \Omega_0 - \Omega_e \Delta t - K \dot{\Omega} \frac{\Delta t}{\tau} \\ &= \Omega_0 - \Omega_e \Delta t - K n J_2 \Delta t \left(\frac{R_e}{a} \right)^2 \frac{\cos i}{(1 - e^2)^2} \end{aligned} \quad (54)$$

where $\Omega_0 = \Lambda_{n0} + \text{Greenwich Sidereal Time}$

$$= \Lambda_0 - \cos^{-1} \left(\frac{\cos \phi_0}{\cos L_0} \right) + \text{GST} \quad (55)$$

(Longitudinal shift of the ground track is plotted in Fig. 30.) Now, the angle from node can be found from a Fourier-Bessel series expansion as a function of time.

$$\phi = \omega + nt + 2e \sin nt + \frac{5}{4} e^2 \sin 2nt + \dots \quad (56)$$

Expressing Eq (56) in terms of t_0 and using Eq (52),

$$\begin{aligned} \phi &= \phi_0 + n\Delta t \left[1 + \frac{3}{2} K J_2 \left(\frac{R_e}{a} \right)^2 \frac{(2 - \frac{5}{2} \sin^2 i)}{(1 - e^2)^2} \right] \\ &\quad + 2e (\sin nt - \sin nt_0) + \frac{5}{4} e^2 (\sin 2nt - \sin 2nt_0) + \dots \end{aligned} \quad (57)$$

For a few revolutions, Eq (57) can be approximated by

$$\phi = \phi_0 + n\Delta t + 2e (\sin nt - \sin nt_0). \quad (58)$$

Finally, the desired relations for satellite position with respect to a rotating oblate earth are given by Eqs (36) and (37). Also, the orbit radius can be expressed in series form as

$$r = a \left[1 - e \cos nt - \frac{e^2}{2} (\cos 2nt - 1) - \dots \right]. \quad (59)$$

If extreme accuracies are needed, it should be remembered that $\dot{\Omega}$ and $\dot{\omega}$ in Eqs (52) and (54) can be considered as simple constants only for integral numbers of revolutions. For some fraction of a revolution, the rates of regression of the nodes and precession of the apsides are actually periodic functions, which contain sines or cosines of the geocentric latitude. These functions result in an oscillation about the mean values given by $\dot{\Omega}$ and $\dot{\omega}$ utilized here. The more accurate perturbation models are described in greater detail in Chapter IV.

2. Synchronous Orbits

As noted previously, because synchronous orbits yield ground tracks which repeat daily, they have special advantages for certain missions, e.g., navigation and communication, and, therefore, merit special consideration. The periods and altitudes of the synchronous orbits are given in Table 2. This table is based on the following equation.

$$\tau_{\text{sidereal}} \approx 2\pi a \sqrt{\frac{a}{\mu}} \left[1 - 3J_2 \left(\frac{R_e}{a} \right)^2 \right]$$

Of particular interest, because of limited ground track excursion, is the 24-hr satellite. The circular equatorial 24-hr satellite does not move relative to the rotating earth, and so its ground track is simply a point on the equator. Circular 24-hr orbits of nonzero inclination exhibit limited excursions. The ground tracks for these orbits, shown for $i = 40^\circ$, 50° and 60° in Fig. 32, have the shape of a figure eight. Elliptical inclined 24-hr orbits have ground tracks resembling skewed figure eights. Examples of these are shown in Figs. 33 and 34.

TABLE 2
Synchronous Orbits

| τ_{sidereal} (sid hr) | τ_{sidereal} (sol sec) | Semimajor Axis a (ft $\times 10^8$) | Semimajor Axis a (km) | Circular Orbit Altitude ($R_e = 6378.15$ km) h (km) |
|--------------------------------------|---------------------------------------|---|----------------------------|---|
| 24 | 86,164.09 | 1.383408 | 42,166.28 | 35,788.13 |
| 12 | 43,082.05 | 0.871558 | 26,565.08 | 20,186.93 |
| 8 | 28,721.36 | 0.665182 | 20,274.76 | 13,896.61 |
| 6 | 21,541.02 | 0.549151 | 16,738.13 | 10,359.98 |
| 4 | 14,360.68 | 0.419175 | 12,776.46 | 6,398.31 |
| 3 | 10,770.51 | 0.346109 | 10,549.40 | 4,171.25 |
| 2 | 7,180.34 | 0.264281 | 8,055.28 | 1,677.13 |

E. SATELLITE COVERAGE

Coverage concerns the ability of a satellite-borne observer or sensor to view a point or area on the surface of the earth or, from the opposite standpoint, the ability of a satellite to be viewed from a point or area on the earth. As noted in Section B, most types of satellite missions, including reconnaissance, communications and navigation missions, impose certain coverage requirements. This section considers the degree of coverage available with a given orbit or pattern of orbits. Because of the basic differences in area coverage and point coverage, these topics will be considered separately.

1. Area Coverage

Area coverage, as distinguished from point coverage, will be taken to imply interest in a wide area, e.g., the entire globe, a certain range of latitudes, a continent, etc. Point coverage involves coverage of specific areas of limited extent, such as specified landing sites, tracking stations, small reconnaissance targets, etc.

a. Coverage by a single satellite

The total area on the earth's surface theoretically visible from a satellite at a given instant is given by the following expression:

$$d = R\alpha = R \cos^{-1} \left(\frac{R}{R+h} \right) \quad (60)$$

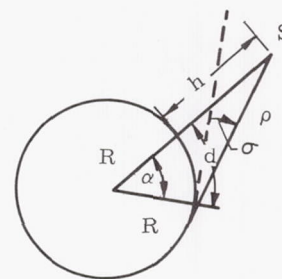
where

R = earth's radius (6371.02 km)

α = central angle between the subsatellite point and the outer edge of area visible from the satellite

h = altitude of the satellite (in km)

If the angle of incidence is restricted to be larger than a given minimum viewing angle σ , then the coverage arc length can be expressed by the following equation (see sketch).



$$d = R\alpha = R \left[\cos^{-1} \left(\frac{R \cos \sigma}{R+h} \right) - \sigma \right] \quad (61)$$

This equation is plotted in Figs. 35 and 36. The coverage angle, α , in degrees can be found from the corresponding arc length by the conversion

$$\alpha = 0.0089929 d \text{ (deg)}$$

where d is in kilometers. This conversion is based on the radius of a sphere of volume equivalent to that of the earth. The percent of earth's surface area visible from the satellite can be found immediately from the coverage angle, α , by comparing the area of the visible segment with the total area of the globe.

Area of segment

$$A_s = 2\pi R^2 (1 - \cos \alpha)$$

Total area

$$A_t = 4\pi R^2$$

Percent area visible

$$A\% = \frac{A_s}{A_t} \times 100\% = \left[\frac{1 - \cos \alpha}{2} \right] \times 100\%$$

If range, in addition to viewing angle, is a sensor limitation, the dashed lines on Fig. 35 (the loci of maximum range) together with the maximum viewing angle loci determine permissible regions of coverage half-angle and altitude.

$$\rho = \frac{R \sin \alpha}{\cos (\alpha + \sigma)} \quad (62)$$

It is frequently necessary to relate the coverage information of Eq (61) and Figs. 35 and 36 to geocentric longitude and latitude on the earth's surface. If at a certain time the subsatellite point is located at geocentric longitude Λ_0 and geocentric latitude L_0 , the circular perimeter of the spherical segment of half-angle α (the area in view of the satellite) may be determined as follows. In the following sketch, let (L, Λ) denote a point of the perimeter to be determined. If

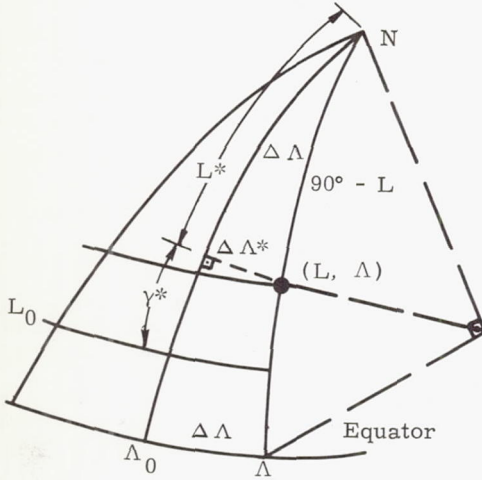
$$\Delta \Lambda \equiv \Lambda - \Lambda_0$$

and $\Delta \Lambda^*$ is measured on a great circle, the law of sines of spherical trigonometry gives

$$\sin \Delta \Lambda^* = \sin \Delta \Lambda \sin (90^\circ - L)$$

or

$$\sin \Delta \Lambda = \frac{\sin \Delta \Lambda^*}{\cos L} \quad (63)$$



From the following sketch, also by the law of sines,

$$\sin \Delta \Lambda^* = \sin \beta \sin \alpha \quad (64)$$

where β is an arbitrary azimuth angle (the parameter of the perimeter solution) and α is the coverage half-angle defined in Eq (60). Equations (63) and (64) give

$$\sin \Delta \Lambda = \frac{\sin \alpha \sin \beta}{\cos L} \quad (65)$$

Also from spherical trigonometry

$$\cos \gamma^* = \frac{\cos \alpha}{\cos \Delta \Lambda^*}$$

Since

$$\gamma^* = 90^\circ - L_0 - L^*,$$

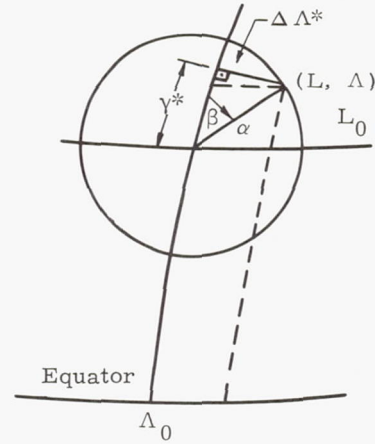
$$90^\circ - L^* = L_0 + \cos^{-1} \left(\frac{\cos \alpha}{\cos \Delta \Lambda^*} \right). \quad (66)$$

But, from the preceding sketch

$$\cos L^* = \frac{\cos (90^\circ - L)}{\cos \Delta \Lambda^*}$$

or

$$\sin (90^\circ - L^*) = \frac{\sin L}{\cos \Delta \Lambda^*} \quad (67)$$



Eqs (66) and (67) give

$$\sin L = \cos \Delta \Lambda^* \sin \left[L_0 + \cos^{-1} \left(\frac{\cos \alpha}{\cos \Delta \Lambda^*} \right) \right]$$

which, after substitution into Eq (64) and simplification, yields

$$\sin L = \sin L_0 \cos \alpha + \cos L_0 \sin \alpha \cos \beta \quad (68)$$

Equations (65) and (68) then comprise a solution for the perimeter of the instantaneous coverage area in terms of the parameter β , the coverage half-angle α , and the geocentric longitude and latitude of the subsatellite point (λ_0, L_0).

Equations (65) and (68) may also be used to define the areas on earth which are not visible from a given ring by making the following substitutions:

$$L_0 = \pm (\pi/2 - i)$$

$$\alpha = \pm (\pi/2 - \alpha).$$

Now, differentiating Eq (65) with respect to β and equating the result to zero yields the maximum longitudinal increment of an area which is uncovered by a particular ground swath. This derivative is

$$\cos \Delta \Lambda \frac{d(\Delta \Lambda)}{d\beta} = \frac{1}{\cos^2 L} \left[\cos \beta \sin \alpha \cos L - \sin \beta \sin \alpha \frac{d}{d\beta} (\cos L) \right] \quad (69)$$

Using Eq (68) and the trigonometric identity

$$\cos^2 L = 1 - \sin^2 L$$

it follows that

$$2 \cos L \frac{d}{d\beta} (\cos L) = 2 \sin L (\cos L_0 \sin \alpha \sin \beta)$$

or

$$\frac{d}{d\beta} (\cos L) = \tan L \cos L_0 \sin \alpha \sin \beta \quad (70)$$

From Eqs (69) and (70),

$$\frac{d(\Delta\Lambda)}{d\beta} = \frac{\cos \beta \sin \alpha \cos L - \sin^2 \beta \sin^2 \alpha \cos L_0 \tan L}{\cos \Delta\Lambda \cos^2 L} \quad (71)$$

If $\frac{d(\Delta\Lambda)}{d\beta} = 0$,

it is implied that

$$\cos \beta \sin \alpha \cos L - \sin^2 \beta \sin^2 \alpha \cos L_0 \tan L = 0 \quad (72)$$

Squaring Eq (68) and substituting into Eq (72) yields

$$\begin{aligned} &(\sin L_0 \cos L_0 \sin \alpha \cos \alpha) \cos^2 \beta - (1 \\ &- \sin^2 L_0 \cos^2 \alpha - \sin^2 \alpha \cos^2 L_0) \cos \beta \\ &+ \sin L_0 \cos L_0 \sin \alpha \cos \alpha = 0 \end{aligned} \quad (73)$$

Equation (73) can be simplified, yielding

$$\cos^2 \beta - 2 \left[\frac{\cot \alpha}{\sin 2 L_0} - \frac{\tan L_0}{\tan 2 \alpha} \right] \cos \beta + 1 = 0 \quad (74)$$

Defining

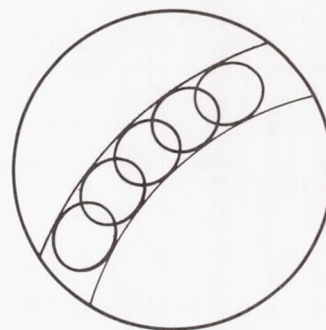
$$K = \frac{\cot \alpha}{\sin 2 L_0} - \frac{\tan L_0}{\tan 2 \alpha} \quad (75)$$

the azimuth for maximum longitude deviation, $\Delta\Lambda_{\max}$ is given by

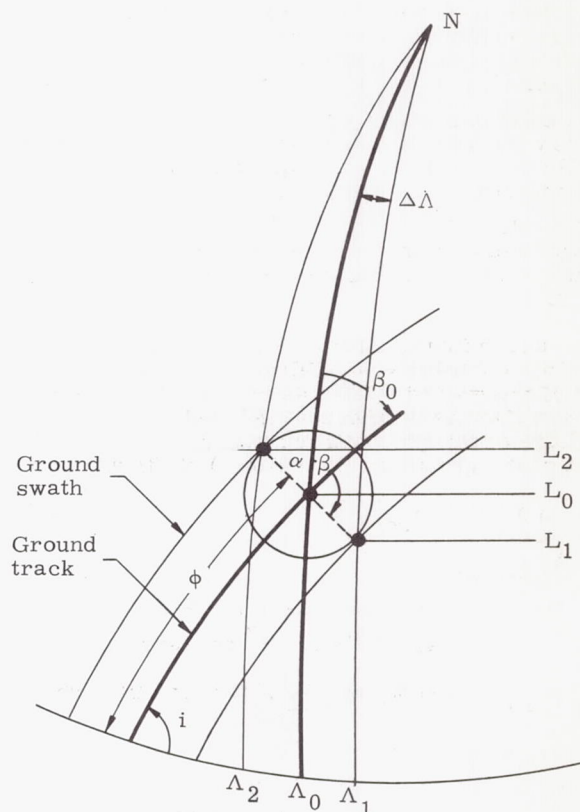
$$\cos \beta_{\Delta\Lambda_{\max}} = K - \sqrt{K^2 - 1} \quad (76)$$

Taking the limit in Eq (75) as $L_0 \rightarrow 0$, $K \rightarrow \infty$ and $\lim_{L_0 \rightarrow 0} (\cos \beta_{\Delta\Lambda_{\max}}) = 0$. Thus, the time that the azimuth angle $\beta_{\Delta\Lambda_{\max}}$ (which locates the maximum value of $\Delta\Lambda$) equals 90° corresponds to the center of the area uncovered by the ground swath on the equator. The angle $\beta_{\Delta\Lambda_{\max}}$ is less than 90° for northern latitudes and greater than 90° for southern latitudes.

The previous analyses concern the instantaneous coverage available from a satellite. Since the satellite is moving relative to the earth's surface, the spherical segment of covered area also moves along the surface, thus generating a track (the "ground swath") of area covered at some time during the lifetime of the satellite.



The edges of the ground swath of a single satellite may be determined from the area coverage perimeter solutions previously obtained and the ground track equations developed in Section D. The problem is illustrated in the following sketch.



Again, let the position of the subsatellite point in geocentric coordinates at a certain time be (L_0, Λ_0) . The locus of points on the perimeter of the area covered when the satellite is located at this position is given by Eqs (65) and (68). Two

of these points will also be points on the ground swath edges to be determined. Namely, the two points are those at the intersections of the circular perimeter and the major circle through (L_0 , Λ_0) and perpendicular to the ground track. Thus, the two intersection points may be determined by solving Eqs (65) and (68) for two particular values of β ,

$$\beta = \beta_0 \pm 90^\circ$$

where β_0 is the orbit azimuth angle relative to the rotating earth defined in the previous ground track analysis, Section D, Eqs (44) and (45). That is, the solution of

$$\sin L = \sin L_0 \cos \alpha \mp \cos L_0 \sin \alpha \sin \beta_0 \quad (77)$$

$$\sin \Delta \Lambda = \pm \frac{\sin \alpha \cos \beta_0}{\cos L} \quad (78)$$

provides two points on the ground swath edges. Then the complete ground swath outline may be generated by solution of Eqs (77) and (78) for sets of values (L_0 , Λ_0 , β_0) generated from the ground track solutions, Eqs (36), (37), (44) and (45). For low altitude orbits, ground swath outlines can usually be calculated to adequate accuracies without correcting the orbit azimuth angle in inertial space, β_{0I} , for rotation of the earth. Of course, rotation must be included in the ground track equations used to generate the set of base points (Λ_0 , L_0).

In determination of the long term coverage available from a given satellite, the longitudinal shift of the ground swath, as computed from Eqs (77) and (78), is of interest. At each latitude, the longitude of the ground track (and hence the longitudes of the ground swath outlines) shifts an amount

$$\Delta \Lambda_\tau = \Omega_e \tau_{\text{nodal}} \quad (79)$$

where

$$\begin{aligned} \Omega_e &= \text{rotation rate of the earth} \\ &= 4.178074 \times 10^{-3} \text{ deg/sec} \end{aligned}$$

$$\tau_{\text{nodal}} = \text{nodal period of the satellite orbit.}$$

For circular orbits,

$$\begin{aligned} \tau_{\text{nodal}} &\approx \tau \left[1 - \frac{3}{2} J_2 \left(\frac{R_e}{r_0} \right)^2 \frac{7 \cos^2 i - 1}{4} \right], \\ 1 &\gg J_3 \end{aligned} \quad (80)$$

where

$$\begin{aligned} \tau &= \text{Keplerian orbit period} = 2\pi r_0 \sqrt{\frac{r_0}{\mu}} \\ r_0 &= \text{circular orbit radius} \end{aligned}$$

Equation (79) is plotted for the case of circular orbits in Fig. 37. The longitudinal shift may be obtained to five place accuracy by multiplying

$\frac{\tau_{\text{nodal}}}{\tau}$ from Fig. 38 by τ from Table 1 of Chapter III and multiplying this result by Ω_e .

The previous analyses, and those of Section D, are concerned with the determination of the ground track and ground swath for a given set of orbit elements and sensor limitations. From the opposite point of view, the equations of these sections can be used to select orbit elements and sensor requirements to achieve total or optimum coverage in a certain area. The typical pattern of area covered by two consecutive ground swaths is shown in the following sketch. During any given day every point in the latitude region of total coverage is in view of the satellite at some time. This region can be determined from the previously derived ground track and ground swath equations by solving for the intersection points of two consecutive swath outlines. However, if mission requirements permit coverage of each point in a latitude band once in several days, the total coverage area may be increased. That is, if the orbit altitude and inclination are selected so that the longitudinal shift

$$\Delta \Lambda = m \Delta \Lambda_\tau (h, i) \quad (81)$$

(where m = number of orbit periods in one day, $\Delta \Lambda_\tau$ is given by Eq (79)) experienced in one day is of such a magnitude that the orbits of the second day are out of phase with those of the first day, then the lune-shaped uncovered areas below the total coverage region will be partially or totally covered by the swaths of the second day. The diurnal longitudinal shift of the ground track is

$$\Delta \Lambda_d = n \Delta \Lambda_\tau - 360^\circ \quad (82)$$

where

$$n = \text{the integral number closest to } \frac{d}{\tau_{\text{nodal}}},$$

or that for which $\Delta \Lambda_d$ is minimum

$$d = \text{one sidereal day, 86,164 mean solar seconds.}$$

Equation 82, plotted in Fig. 39, is then a quantity of interest in determining coverage available over several days. Of course, for missions of long duration, total coverage is available in the latitude range $L = \pm(i + \alpha)$, provided that the ground track does not repeat diurnally. When mission length is limited to a few days or weeks, and total coverage of a specified latitude range is required, optimum coverage is achieved by selection of orbit altitude and inclination such that

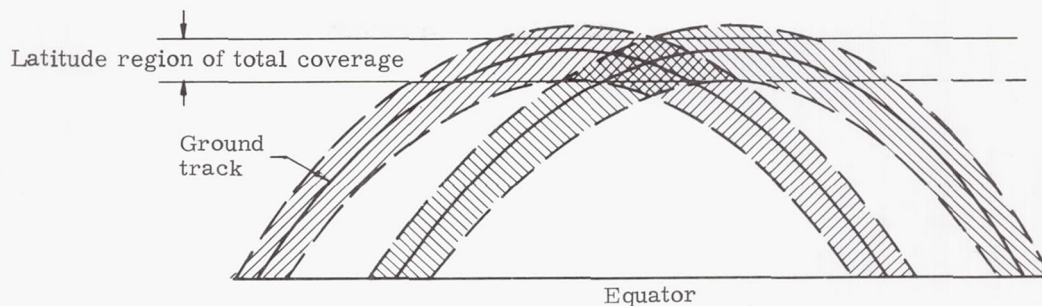
$$\Delta \Lambda_d = \pm \frac{k}{m} \Delta \Lambda_\tau (h, i) \quad (83)$$

where

$$k = \text{an integer}$$

$$m = \text{mission length in days.}$$

An orbit chosen on this basis would obviously provide the most uniform coverage with minimum overlapping of ground swaths.



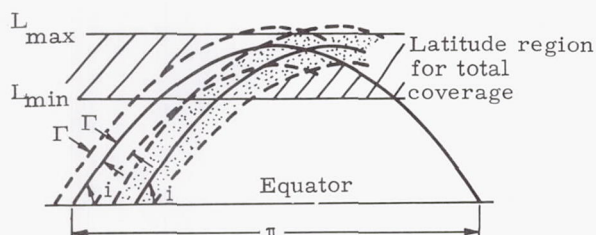
b. Pattern coverage (Ref. 3)

If mission requirements specify continuous total coverage of a large area by at least one satellite or frequent coverage from low altitudes, more than one satellite will be required. Optimization of coverage available from a pattern of several satellite orbits requires a somewhat different approach than that for the single satellite case.

(1) General approach

It is obvious that infinitely many possible arrangements of orbital planes and satellites in orbit could be considered for a satellite pattern covering either some well-defined region or the total surface area of the earth. To simplify the problem and provide for constant angular separations between the orbital planes, consider that the orbit planes are equally inclined to the equator. Second, the uniform coverage requirements can be best met by arranging the nodes of orbital planes at equal distances along the equator, by distributing satellites in equal numbers among all the orbital planes and by placing satellites in circular orbits of common altitude (so that the distances between all the satellites in one ring will be as uniform as possible).

In Ref. 5 the following set of equations is presented for optimization of satellite networks for zonal coverage of a latitude belt in both hemispheres (see the accompanying sketch), considering N the total number of satellites, n_1 the number of orbit planes and n_2 the number of satellites in each orbit plane:



$$h = R \left(\cos \sigma / \cos \left\{ \cos^{-1} \left[\cos \left(\frac{\pi n_1}{N} \right) \cos \Gamma + \sigma \right] - 1 \right\} \right) \quad (84)$$

$$L_{\min} = \tan^{-1} \left\{ \tan i \cos \left[\left(\frac{k+1}{n_1} \right) \pi \right] \right\} - \sin^{-1} \left\{ \frac{\sin \Gamma}{\sqrt{1 - \sin^2 i \sin^2 \left[\left(\frac{k+1}{n_1} \right) \pi \right]}} \right\} \quad (85)$$

where Γ is the ground swath angular half-width, given by

$$\Gamma = \sin^{-1} \left[\sin L_{\max} \cos i - \cos \frac{\pi}{n_1} \cos L_{\max} \sin i \right] \quad (86)$$

Note: $0 < \Gamma < 90^\circ$ is required, also

$$\Gamma \leq \cos^{-1} \sqrt{1 - \sin^2 i \sin^2 \frac{\pi}{n_1}} \quad (87)$$

k = the least integer such that

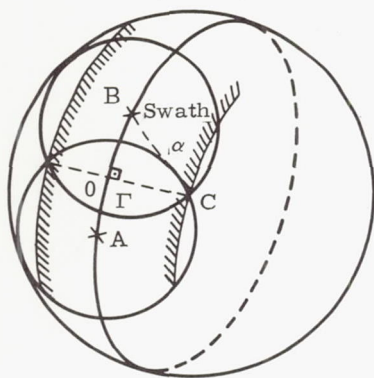
$$k \geq \frac{n_1}{2} - 2 - \frac{n_1}{\pi} \tan^{-1} \left[\frac{\cos i}{\sin \Gamma} \sqrt{\frac{\cos^2 \Gamma}{1 - \sin^2 i \sin^2 \frac{\pi}{n_1}} - 1} \right] \quad (88)$$

σ = minimum incidence angle for the sensor.

The relationship between the ground swath angular half-width, Γ , and the ground coverage angle, α , is given by

$$\cos \alpha = \cos \Gamma \cos \frac{\pi}{n_2}, \quad (89)$$

as shown in the accompanying sketch, in which consecutive satellites in the same orbit are located at A and B.



In Ref. 5 the above equations are solved for various polar and inclined orbit planes, as shown in Figs. 40 through 43.

Figure 40 gives the total number of satellites, N , required for polar orbits consisting of from 2 to 6 orbit planes. As a numerical example, a reconnaissance system of 36 satellites providing complete global coverage is considered. The results are shown in the following table:

| Orbit Planes n_1 | Satellites/ Plane n_2 | Required Altitude h (km) |
|--------------------------|-------------------------------|----------------------------------|
| 2 | 18 | 2780 |
| 3 | 12 | 1245 |
| 4 | 9 | 968 |
| 6 | 6 | 1245 |
| 9 | 4 | 2780 |

Considering sensor limitations, the 4-orbit plane system is obviously optimum for the case considered.

Figure 41 gives the comparison between the theoretical optimum curve and the practical optimum curve for polar orbits with minimum incidence angle $\sigma = 0^\circ$. The effects of increasing minimum incidence angles are also shown.

Figure 42 gives the comparison of polar satellite networks providing coverage from the poles to a fixed minimum latitude L_{\min} , considering $\sigma = 0^\circ$ and $L_{\min} = 60^\circ, 30^\circ$ and 0° (note that $L_{\min} = 0^\circ$ gives the complete global coverage given by the step-function on Fig. 41).

Finally, Fig. 43 shows the comparison of inclined satellite patterns to the polar pattern for complete coverage. It can be seen that polar orbits are preferable, at least under 3500-km altitudes.

As a more particular example, following slightly different lines of approach, the optimization of a specific orbit pattern is analyzed more fully in the next subsection.

(2) Specific example: 6-hour orbit pattern

Although the equations and data presented in the preceding subsection provide a general basis for orbit pattern selection, a specific mission may present special problems. As an interesting example, consider the selection of a navigation satellite orbit pattern which must fulfill the requirement that at least three satellites be visible from any point on the earth's surface (and, therefore, from any point in space near the earth) at any given time. Definition of the required pattern entails specification of each of the following parameters:

- (1) Orbital period (i. e., altitude).
- (2) Number of satellites in each ring.
- (3) Orbital nodal positions (number of rings).
- (4) Orbital inclination.
- (5) Orbital eccentricity.

The synchronized pattern obtained from these considerations must also be subjected to a pattern proof, including the effects of small changes in inclination. The earth's oblateness effects are included in the determination of the exact orbital altitude.

The altitude of the navigation satellites depends on a large number of factors as noted in Section A. Some of the most important are:

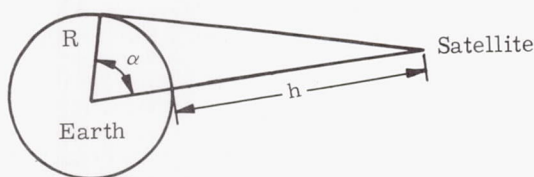
- (1) Resolution limitations.
- (2) Perturbations.
- (3) Repeatable daily ground track.
- (4) Number of satellites employed.
- (5) Van Allen radiation belts.

For the best resolution at sea level, the satellite orbits should be as low as possible. On the other hand, oblateness perturbations are largest for low altitude orbits; for higher orbits the perturbations caused by the sun and the moon increase in relative importance. A repeatable daily ground track will simplify the preparation of the required ephemeris which makes navigation possible; therefore, it is desirable to have an integral number of revolutions per day. The number of satellites in a given ring will further define the necessary altitude and period for the desired ground coverage. To keep the molecular breakdown of the solar cells and similar electronic apparatus to a minimum, the Van Allen radiation belts should be avoided as much as possible.

From all the above considerations, the 6-hr orbit was considered as the most promising for the present application.

The 6-hr orbit retraces its ground track on a daily basis and that ground track results from four orbital revolutions. For an ideal spherical earth, the period of this orbit would be exactly one-fourth of a sidereal day. Since the earth is actually oblate, the orbit plane regresses slowly; and in order to repeat the desired ground track (i. e., to achieve a sidereal period of 21,541.02 mean solar seconds), the semimajor axis required is 16738.13 km. (A complete set of synchronous orbit semimajor axes is included in Section D.2.) The circular orbit altitude corresponding to this value of semimajor axis is about 10,360 km.

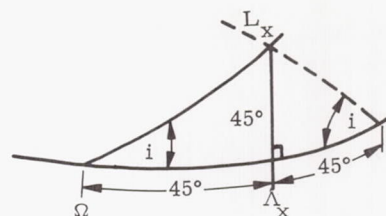
At this altitude, the ground coverage is 135.26°, as can be seen in the following sketch:



$$2\alpha = 2 \cos^{-1} \left(\frac{R}{R+h} \right) = 135.26^\circ$$

Thus, three or more satellites will be required to provide continuous coverage of a band on the earth (the width of this band being a function of the number of satellites). Because the overlap of the covered areas is small with only three satellites per ring, four satellites will be placed in each ring at 90° intervals. In general, only one satellite is seen on the earth's surface from a given satellite ring. Furthermore, there are two areas around the axis perpendicular to the orbital plane of a given satellite ring where no satellites from this ring are visible. To ensure that in these regions at least three satellites are visible, three more satellite rings are required, placed so as to make at least one satellite visible from each additional ring at all times. Since uniform ground coverage is desirable, the nodes for the four satellite rings must be displaced from each other by 90° on the equator. This brings the total number of satellites employed in the navigation pattern to 16.

To equalize oblateness perturbations for the four orbital planes, the inclinations must be equal. From this condition, it can be seen that the most symmetrical distribution of orbital planes in inertial space results if each set of two planes intersects at a latitude of 45° (that is, halfway between the poles and the equator). The orbital inclination which satisfies these conditions was found from spherical trigonometry as:



$$i = \tan^{-1} \left[\frac{\tan L_x}{\sin (\Lambda_x - \Omega)} \right] = 54.736^\circ$$

Orbital eccentricity produces periodic relative motion of the satellites in each ring (Fig. 44) which, in turn, produces irregular ground coverage. While this in itself does not eliminate eccentric orbits from consideration, it does make the resulting analysis and pattern utilization more difficult, because the solution for position as a function of time becomes transcendental. For these reasons, the orbits considered are circular (i. e., zero eccentricity).

To avoid crowding a considerable number of satellites over the same region of the globe, one satellite was placed at the node for Planes I and II (which are consecutive), while the positions in Planes III and IV were displaced by 45°. The initial latitudes, longitudes and central angles of all 16 satellites are given in Table 3.

TABLE 3
Initial Positions of 16 Satellites

| Orbit Plane and Satellite Numbers | Latitude (L_0) (deg) | Longitude (Λ_0) (deg) | Initial Central Angle (θ_0) (deg) |
|---|--------------------------------|---------------------------------------|---|
| I-1 | 0 | 180 W | 0 |
| I-2 | 54.7 N | 90 W | 90 |
| I-3 | 0 | 0 | 180 |
| I-4 | 54.7 S | 90 E | 270 |
| II-1 | 0 | 90 W | 0 |
| II-2 | 54.7 N | 0 | 90 |
| II-3 | 0 | 90 E | 180 |
| II-4 | 54.7 S | 180 E | 270 |
| III-1 | 35.3 N | 30 E | 45 |
| III-2 | 35.3 N | 150 E | 135 |
| III-3 | 35.3 S | 150 W | 225 |
| III-4 | 35.3 S | 30 W | 315 |
| IV-1 | 35.3 N | 120 E | 45 |
| IV-2 | 35.3 N | 120 W | 135 |
| IV-3 | 35.3 S | 60 W | 225 |
| IV-4 | 35.3 S | 60 E | 315 |

The ground track of a satellite, as noted in Section C, is given by the equations:

$$L = \sin^{-1} \left[\sin i \sin (\theta_0 + \theta) \right] \quad (90)$$

$$\Lambda = \tan^{-1} \left[\cos i \tan (\theta_0 + \theta) \right] + \Omega_0 - \Omega_e t \quad (91)$$

where flight time is given for a circular orbit by the equation

$$t = \left(\frac{\tau}{2\pi} \right) \theta. \quad (92)$$

A complete ground track during one day was computed for the first satellite in the first orbit plane by Eqs (90) and (91). The result was plotted in Fig. 45. It should be noted that the same pattern of four revolutions is identically repeated during each day. This is due to the fact that the sidereal period is exactly one-fourth of a sidereal day.

Initial positions and ground tracks for one-half of a revolution are given in Fig. 46. It is obvious from this figure that the distribution of satellites is not completely uniform over the earth's surface at all times. However, there are no serious crowding problems and thus, this pattern is satisfactory.

The placement of the four orbit planes in three-dimensional space is indicated in Fig. 47. The first of the two drawings shows the intersections of the orbital planes in inertial space (the earth should be visualized as rotating within this fixed framework). The second drawing shows the initial positions of the 16 satellites as given in Table 3 and Fig. 46 (except the ones hidden by the earth).

The proof of satellite pattern. It must now be shown that the pattern specified actually satisfies the requirement that at least three of the vehicles are always visible at any point on earth's surface. Secondly, small changes in the orbit inclination must be investigated in order to justify the optimum inclination selected ($i = 54.736^\circ$).

In order to rigorously prove the satellite pattern, the concept of ground swath was used. Swath in the case of this problem is defined as the region on a nonrotating earth where at least one of the four satellites in the ring is always visible.

From Eq (89), it can be seen that the width of the ground swath (to either side of the ground track) is given by:

$$\Gamma = \cos^{-1} \left(\frac{\cos \alpha}{\cos \frac{180^\circ}{n_2}} \right) = 57.421^\circ$$

$$\frac{180^\circ}{n_2} = \frac{180^\circ}{4} = 45^\circ$$

Outlines of ground swaths were obtained as indicated in Section E.1.a. Areas not included by

the swath generated by the satellites in four orbit planes are shown in Fig. 48. No satellite from the ring indicated by the Roman numeral is visible inside either cross-hatched area of the same number. Because no cross-hatched areas intersect, the figure proves that at least three satellites are visible at all times at every point on the earth's surface. On a rotating earth the eight cross-hatched areas must be visualized as moving with a 24-hour period but maintaining the given topological pattern. The horizontal and vertical distances between any two adjacent cross-hatched areas are essentially equal (5.4° on a great circle).

The effects of small changes in orbit inclination on the pattern of circular areas shown in Fig. 48 may be investigated by means of the equations of Section E.1.a, with swath width denoted by Γ instead of α .

The results of the foregoing analysis are presented in Fig. 49 which shows that the requirements placed upon the pattern can only be met in the range of orbital inclinations between 49.6° and 57.4° . The selection of the optimum inclination with this range must be based on visibility criteria because there are definite limits which must be imposed on the minimum elevation angle between the satellites of the pattern and the horizon to make navigation practical. This optimum inclination angle is 54.736° because only this inclination ensures that all of the visible satellites will be at least 5° above the horizon. This analysis also proves that the minimum altitude for a pattern of 16 satellites, which will ensure a minimum elevation angle above the horizon of 5° for at least three of the satellites at all times, is that of the 6-hr orbit.

2. Point Coverage

In many satellite missions, area coverage as discussed in the previous section is not a firm requirement; rather, it is desired to maximize the time spent over a specific set of points on the earth. These locations may be tracking stations, ground data links, landing sites, or points under surveillance. Various problems connected with point coverage are considered in this section.

a. Determination of the zenith angle of a satellite

A problem of interest to satellite tracking and communication is that of determining the conditions under which the satellite is visible, or above the horizon, when viewed from a point on the earth.

To solve this problem assume that a satellite S is in an orbit inclined at angle i to the earth's equator, and assume a point of observation P on the earth at a latitude L . Consider a coordinate system, its origin at the point of observation, with the Z-axis vertical, the X-axis due east (i.e., in the direction of motion of the point of observation) and the Y-axis due north. Let the distance from the center of earth to the point of observation be R_e and the distance from the center of the earth to the satellite be r .

The satellite's position is determined by a central angle ϕ_s measured in the orbital plane from the ascending node, and the position of the point of

observation is determined by an angle ϕ_e measured from the longitude of the ascending node (Fig. 50). In terms of the usual variables, the angles ϕ_s and ϕ_e are given as

$$\begin{aligned}\phi_s &= \omega + \theta & \text{where } \Lambda_p &= \text{longitude of observation point} \\ \phi_e &= \Lambda_p - \Lambda_n & \Lambda_n &= \text{longitude of nodal point}\end{aligned}$$

The coordinates of the satellite in the X, Y, Z system are as follows:

$$\begin{aligned}x &= r (\cos i \sin \phi_s \cos \phi_e - \cos \phi_s \sin \phi_e) \\ y &= r \left[\cos L \sin i \sin \phi_s - \sin L (\cos \phi_s \cos \phi_e + \cos i \sin \phi_s \sin \phi_e) \right] \\ z &= r \left[\sin L \sin i \sin \phi_s + \cos L (\cos \phi_s \cos \phi_e + \cos i \sin \phi_s \sin \phi_e) \right] - R\end{aligned}$$

The distance between the point of observation and the satellite is

$$\rho = \sqrt{r^2 + R^2 - 2rR \cos \psi}$$

where

$$\begin{aligned}\cos \psi &= \sin L_p \sin i \sin \phi_s + \cos L_p (\cos \phi_e \cos \phi_s \\ &\quad + \cos i \sin \phi_e \sin \phi_s)\end{aligned}$$

and ψ is the angle between the radius vectors from the earth's center to the point of observation and to the satellite (see Fig. 50).

The direction cosine, l_z , (i.e., the cosine of the angle δ between the Z-axis and the radius vector from P to S) is

$$\begin{aligned}l_z &= \frac{z}{\rho} = \frac{r \cos \psi - R}{\sqrt{r^2 + R^2 - 2rR \cos \psi}} \\ &= \frac{\frac{r}{R} \cos \psi - 1}{\sqrt{1 + \left(\frac{r}{R}\right)^2 - 2\frac{r}{R} \cos \psi}}\end{aligned}$$

The satellite is above the horizon as viewed from the point of observation if $l_z > 0$ and, since l_z is the cosine of the satellite's zenith angle, any value of the satellite elevation angle can be specified and the corresponding l_z determined. Any l_z above this value corresponds to a satellite passage at an elevation angle equal to, or higher than, the specified value.

For the point of observation $\phi_e = (\Omega_e + \dot{\Omega})t + \phi_1$,

where

$\dot{\Omega}$ = the rate of regression of the nodes of the satellite (rad/sec)

$$\phi_1 = \Lambda_{p0} - \Lambda_{n0}$$

For the satellite $\phi_s = \phi_s(t) + \phi_0$, where $\phi_s(t)$ is the equation relating the central angle to time in the general elliptical case, and ϕ_0 is the initial angle of the satellite with respect to the ascending node. For a circular orbit $\phi_s(t) = \omega_s t$, where ω_s is the angular velocity of the satellite. The use of these equations is illustrated by the following example.

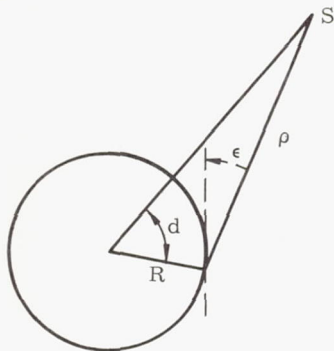
Assume an orbital inclination angle of 30° and a point of observation at a latitude of 30° . Assume further that the satellite is in a circular orbit at an altitude such that it makes 15 revolutions relative to the ascending node in the time it takes the earth to make one revolution relative to this node. The regression period is then about 50 days and the period of the satellite about 1.59 hr, rather than the 1.6-hr period if the regression were neglected. For this example this small difference is neglected and a satellite altitude of 357 stat mi and $r/R_e = 1.0902$ is assumed. To find when the satellite is above the horizon for a point originally along the meridian through the node at the time the satellite was at the node (i.e., $\phi_1 = \phi_0 = 0$, $\phi_e = \Omega_e t$ and $\phi_s = 15 \Omega_e t$), the procedure is first to plot

$$l_z = \cos \delta = \frac{1.0902 \cos \psi - 1}{\sqrt{1 + (1.0902)^2 - 2(1.0902 \cos \psi)}}$$

as a function of $\cos \psi$ (Fig. 51). Note that $l_z > 0$ for $0.9173 \cos \psi < 1$. Next plot $\cos \psi$ as a function of $\phi_e = \Omega_e t$ (Figs. 52 and 53). The values of ϕ_e for which $0.9173 < \cos \psi$ (indicated on the figure by a solid line) then represent the values of $t = \phi_e / \Omega_e$, for which the satellite is above the horizon. If it is required that the satellite be 30° above the horizon, then $0.5 < l_z$ and $0.9916 \leq \cos \psi$. This line is indicated on the figure by a dotted line. The angle δ , defined by $\cos \delta = l_z$, is actually the zenith distance of the satellite and the angle ϕ_e can be considered the "hour angle" of P with respect to satellite node.

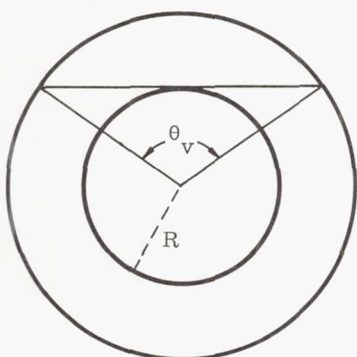
Finally, Fig. 54 presents in English units a solution for the line-of-sight range to the satellite and the distance of the subsatellite point from the observation point on the earth's surface. This information is presented in different form in Figs. 55 and 56, also in English units. It should be noted that Figs. 35 and 36 present the same information in metric units when the coverage

half-angle, α , is interpreted as ground range, d , and the minimum viewing angle, σ , is interpreted as elevation, ϵ .



b. Visibility time durations

Visibility times for satellites in elliptical orbits must be computed from Kepler's equation, tabulated in Chapter 3. However, in the case of circular orbits, the equations for visibility time are sufficiently simple to warrant presenting parametric results. Visibility time from a point on a nonrotating earth is then



$$t_v = \frac{\cos^{-1} \frac{R}{r}}{180^\circ} \left(2\pi r \sqrt{\frac{r}{\mu}} \right) \quad (93)$$

where r = circular orbit radius. The visibility time of a satellite moving in a circular orbit exactly in the direction of the earth's rotation is

$$t_{v+} = t_v \frac{\tau_e}{\tau_e - \tau} \quad (94)$$

where

τ_e = period of earth rotation, 86,164 sec

τ = orbit period = $2\pi r \sqrt{\frac{r}{\mu}}$

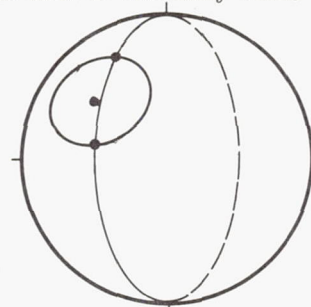
For satellites moving directly opposite to the direction of the earth's rotation, the visibility time is

$$t_v - t_v \frac{\tau_e}{\tau_e + \tau} \quad (95)$$

Equations (93), (94) and (95) are plotted in Figs. 57 and 58.

c. Visibility and call-down time computation

The computation of call-down time (the time interval during which a vehicle may initiate a landing sequence terminating at a specified landing site) or visibility time proceeds by solution for the intersections of the ground track, as given by the equations of Section D, and the perimeter of a test region. In the case of visibility time, the test region is simply the spherical segment determined by the maximum ground range of the tracking station. The perimeter of the test region is then given by Eqs (65) and (68) where (L_0, Λ_0) is interpreted as the location of the tracking station and α is the maximum ground range. In the case of call-down time the shape of the test region is a function of the maneuverability of the landing vehicle. This particular subject is treated in some length in Chapter VIII.



F. SENSOR LIMITATIONS ON ORBIT SELECTION

The selection of orbit elements to best fulfill given mission requirements must obviously be subject to any sensor limitations. Although sensors may take a wide variety of forms, consideration will be limited to the two largest classes, optical and radio systems. The primary limitations of these systems are power and resolution requirements.

1. Radio Systems

An important limitation of radio systems and the primary limitation for communication applications is the restriction on range imposed by transmission power limits. The range equation may be written in several forms:

$$\begin{aligned} \frac{P_r}{P_t} &= \frac{G_t A_r}{4\pi \rho^3} \\ &= \frac{G_r A_t}{4\pi \rho^2} \\ &= \frac{G_t G_r \lambda^2}{(4\pi \rho)^2} \\ &= \frac{A_t A_r}{(\lambda \rho)^2} \end{aligned} \quad (96)$$

for simple one-way transmission.

Where

P_r = received signal power

P_t = transmitted power

A_r = effective area of the receiving antenna

A_t = effective area of the transmitting antenna

G_r = receiving antenna gain

G_t = transmitting antenna gain

λ = wavelength

ρ = range from the transmitter to the receiver.

In skin tracking, the transmitted radio beam is reflected by the object tracked, and a portion of the reflected energy is then received at the transmitter station. For skin tracking, then,

$$\frac{P_r}{P_t} = \frac{A_o A_r G_t}{(4\pi \rho^2)^2} = \frac{G_t G_r \lambda^2 A_o}{4\pi (4\pi \rho^2)^2} \quad (97)$$

where

A_o = scattering cross-section area.

Typical gains and effective areas for use in the above equations are contained in Table 4 from Ref. 6.

TABLE 4

| Antenna | Gain | Effective Area |
|----------------------|---|-------------------------------|
| Isotropic | 1 | $\frac{\lambda^2}{4\pi}$ |
| Infinitesimal dipole | 1.5 | $\frac{1.5 \lambda^2}{4\pi}$ |
| Half-wave dipole | 1.64 | $\frac{1.65 \lambda^2}{4\pi}$ |
| Optimum horn | $\frac{10.0 A}{\lambda^2}$ | 0.81 A |
| Parabola or lens | $\frac{(6.3 \text{ to } 7.5) A}{\lambda^2}$ | (0.5 to 0.6) A |
| Broadside array | $\frac{4\pi A}{\lambda^2}$ (maximum) | A (maximum) |

The minimum detectable signal is not determined by the ability to amplify the signal, but by the noise which obscures the signal. That is, if no interference were present, any signal transmitted over any distance could be detected by providing sufficient amplification in the receiver. Noise limiting the usable range may enter the radio system at the transmitter, at the receiver or in the space link. The noise power produced in a bandwidth Δf is given by

$$P_n = kT \Delta f \quad (98)$$

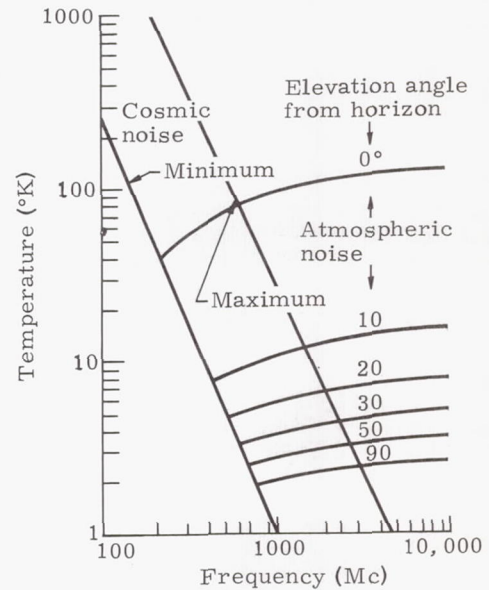
where

k = Boltzmann's constant = 1.38×10^{-23} , w-sec/°K

T = absolute temperature of the circuitry, °K

Δf = bandwidth, cps

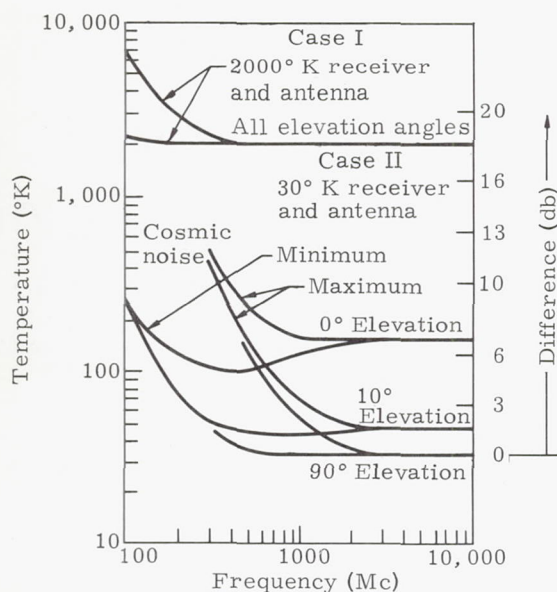
The temperature T is the weighted sum of the various component source temperatures, the weights being high (unity) for noise sources internal to or surrounding the receiver or low if the noise enters through a fraction of the receiver surroundings. Typical equivalent temperatures of internal receiver noise are 2000° K for conventional receivers, 100° K for parametric amplifier receivers and 10° K for masers. Equivalent temperatures of external noise are dependent on frequency and, in the case of atmospheric noise, on elevation angle. External noise is shown in the following sketches from Ref. 6. The blackbody radiation of the earth also comprises a noise source which increases for low elevation angles. Thus, low altitude satellites, which spend relatively long times near the horizon of an observer on earth, entail greater noise problems. Other sources of noise are the sun, the moon and the planets.



The ratio of received power, P_r , to interference power in the bandwidth Δf determines the range at which communication is feasible. A ratio of unity is defined as threshold reception. The threshold reception range for space-to-earth communication is

$$\rho' = \sqrt{\frac{P_t A_t G_r}{4\pi k T \Delta f}} \quad (99)$$

Usable ranges may be about one-third of this value.



In addition to range limitations, missions employing radar systems may encounter resolution problems. The angular resolution of a radar is determined by the narrowness of the antenna beam. The apparent angular extent of an object detected is increased by the width of the antenna beam, and objects separated by less than the beamwidth are interpreted as a single object. Consequently, for a given system bandwidth, the minimum resolution distance increases with increased altitude. Range resolution depends mainly on the pulse duration of the transmitted signal.

Just as noise determines the minimum detectable signal for range limitations, the obscuring of echoes by ground clutter and sea return is closely related to resolution capability. For example, in detection of a ship by means of an overhead airborne radar, difficulty is experienced in distinguishing the ship from the sea because the ranges differ by less than the pulse duration. The problem of relating radar resolution in the presence of clutter to orbit altitude is too complex to consider here except by generally noting the importance of low altitudes in achieving high resolution and minimizing power consumption.

2. Satellite Photography Systems

Resolution attainable in satellite photography is related to orbit altitude, and so the photographic system limitations are factors in choice of orbit elements. Investigation of this relationship, in order to be meaningful, must consider the entire photographic system performance in some detail.

Among the factors which determine the degree of detail that can be detected or identified by a visual or photographic system are the object distance and the focal length of the viewing lens. The ratio of object distance, d , to focal length, f , is referred to as the scale number, S .

$$S = \frac{d}{f} \quad (100)$$

Then one cm on a photograph corresponds to S cms on the ground. Thus larger scale numbers mean greater difficulty in discerning fine detail.

A second parameter useful in defining optical system capability is resolution, the ability to distinguish parts of an image. In photography, resolution is the ability of a film-lens system to distinguish a standard pattern of black and white lines. Thus a film-lens system may be described as providing resolution of r_f lines per millimeter. Ground resolution is the distance on the ground equivalent to one barely resolvable line. Thus, if a film-lens system provides a system resolution of r_f lines per mm, and the scale number is S , the ground resolution, r_g , is

$$r_g = \frac{S}{r_f} \quad (102)$$

In terms of commonly used units,

$$r_g \text{ (meters)} = \frac{S}{1000 r_f \text{ (lines per millimeter)}} \cdot$$

Although ground resolution is a ratio, the effects of graininess influence a selection of lower values of S and r_f to attain a given r_g . From Eqs (101) and (102), the maximum orbit altitude can be determined as a function of system resolution, focal length and ground resolution.

$$h = 1000 f r_f r_g \quad (103)$$

where

h = orbit altitude in meters

f = focal length in meters

r_g = ground resolution in meters

r_f = system resolution in lines per mm.

Equation (103) is plotted in Fig. 59. However, in order to use this data or Eq (103) it is necessary to describe the quantity r_f (or system resolution). This resolution is a function of many separate factors and will be discussed in the following paragraphs.

The overall performance of a photographic system depends on the contribution of each element of the system. The elements of a photographic system are:

- (1) The scene, with its contrasts.
- (2) The atmosphere, which modifies the light from the scene before it enters the optical system.
- (3) The optical system, which images the scene on the film.
- (4) The camera system, through which uncompensated motion and vibration enter the system.

- (5) The film, which records the final image.

Each of the elements which follows the scene alters the contrast in a different manner. It is desirable to have a method of analysis which permits the examination of each of these elements in the same terms so that the individual elements can be compared on a common basis, and which presents the result in the same terms.

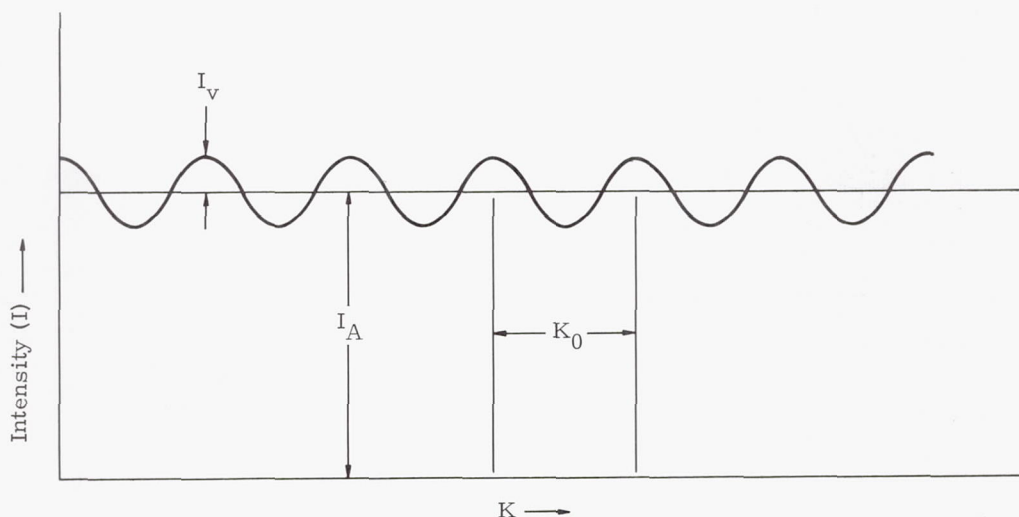
Such a method is the sine wave response analysis which describes the effects of each element in terms of its modulation transfer function, $T(K)$. The method is analogous to the transfer function analysis of servomechanisms in which the modulation transfer function describes the response of the element as a function of the spatial frequency. The overall system performance is then the product of the modulation transfer functions of the individual elements.

a. Modulation transfer function

Consider a scene in which the intensity varies according to the following relation

$$I = I_A + I_V \sin \left(\frac{2\pi K}{K_0} \right).$$

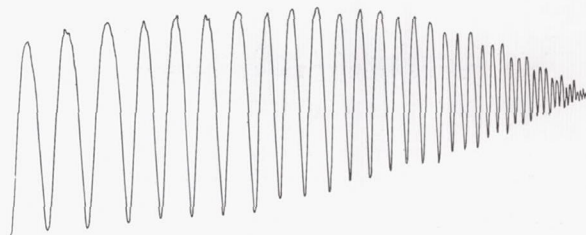
This is a series of lines spaced K_0 units apart (see following sketch). The maximum intensity is $I_A + I_V$ and the minimum intensity is $I_A - I_V$, with the intensity varying sinusoidally between these limits. Since all of the lines are the same distance apart, they represent a constant spatial frequency, K_0 . The modulation transfer function can be defined as the ratio of I_V to I_A . Therefore for this scene the modulation transfer function $T(K_0)$ is given by I_V/I_A .



Now consider the image which is produced when light from a scene (see following sketch) which has a modulation transfer function of unity but



increasing spatial frequency is passed through a diffraction limited lens. At some spatial frequency the diffraction patterns of the individual lines begin to overlap and the contrast in the image is reduced. As the lines become closer together the contrast becomes further reduced until at some frequency the lens gives essentially no response to the modulation in the scene. The modulation of the scene-lens combination might appear as shown in the following sketch. The corresponding transfer function is given in Fig. 60. Since the scene has a modulation transfer function of unity, Fig. 60 is the transfer function of the lens alone.



By determining the modulation transfer function of each element of the system, the modulation transfer function of the final image as recorded on film can be determined, thereby determining the

performance of the system. The modulation transfer function of each of the elements of the system is discussed in the following paragraphs.

b. The scene

The scene to be photographed is usually a complex mixture of contrasts and spacings, and its transfer function, although theoretically obtainable, is too complex to be of practical value. Fortunately, we are rarely interested in the performance of the system against a particular scene; we are usually interested in the ability of the system to resolve detail. This can be done by evaluating the system performance against an artificial scene which lends itself to analysis, such as the scene represented in the foregoing sketch.

Such artificial "target" scenes are characterized by a constant contrast, and therefore a constant transfer function, for all spatial frequencies. The transfer function varies with the contrast in the following manner:

$$T_C = \frac{C - 1}{C + 1} \quad (104)$$

where C is the brightness ratio of the peaks to the valleys of the sine wave.

Equation (104) is plotted in Fig. 61. The scene contrast is seen to act as a "gain" factor which multiplies the system sine wave response, and, therefore, to compare systems on a common basis, it is necessary to use a common value of scene contrast. For satellite photography a brightness ratio of 8.1 is usually assumed.

c. The atmosphere

In addition to the obvious effect of clouds, the atmosphere affects the system in two ways. The first of these, scattering, causes some light from the sun to be scattered directly into the system and some image forming light from the scene is scattered out of the system. From a satellite, looking through the entire thickness of the atmosphere, the scattering causes the target contrast to be reduced by a factor of four, so that the effective contrast seen by the system is 2:1, giving a transfer function of 0.33 from Eq (104).

The second effect is due to turbulence, and it affects only very high acuity systems. The turbulence causes a random angular displacement of the rays making up the image, and its value for satellite photography has not yet been adequately determined. It is felt that it will limit the ultimate system performance to the order of one foot.

d. The lens

The transfer function of the lens depends on its diffraction pattern and aberrations, and for a particular lens this can be measured after the lens is manufactured. For system design, which must be performed before the lens is manufactured, it can be assumed that the lens has no aberrations and is diffraction limited. For a well designed lens, this will be very nearly true on axis, but at the edges of the field the performance will be considerably reduced.

The modulation transfer function for a diffraction limited circular aperture, when viewing a line image, is given by Ref. 7

$$T(K) = \frac{2}{\pi} \left[\cos^{-1} (AK) - AK \sqrt{1 - (AK)^2} \right] \quad (105)$$

where

$$A = N\lambda$$

$$\lambda = \text{wavelength of light}$$

$$N = \text{focal ratio (f-number) of the lens}$$

$$K = \text{spatial frequency}$$

The transfer function of an f/4 lens for light of 6000 Å was given in Fig. 60. Equation (102) is plotted in Fig. 62 and the transfer function for f/1 to f/12 lenses is given in Figs. 63 and 64.

e. Image motion

The camera introduces two types of image motion into the system, vibration and linear motion. Although it is generally impossible to determine the expected vibration environment at the time of system design, the transfer function for vibration is useful in that it can be used to determine an allowable vibration level which will not seriously degrade the system. By finding that transfer function which degrades the system performance by the allowable amount, the vibration level which produces the transfer function is determined.

The transfer function for vibration is given by

$$T(K) = J_0(\pi AK) \quad (\text{Ref. 7}) \quad (106)$$

where

$$J_0 = \text{zero order Bessel function}$$

$$A = \text{amplitude of the vibration}$$

$$K = \text{spatial frequency}$$

Linear motion between the film and the image during the exposure time can arise from several sources. These include:

- (1) Uncompensated vehicle rotation rates.
- (2) V/H measurement errors.
- (3) Camera pointing errors.
- (4) Film drive speed errors.

The magnitude of the motion from these sources can usually be predicted at the system design stage and the effects of the motion can be calculated.

The transfer function for linear motion is given by Ref. 7.

$$T(K) = \frac{\sin \pi AK}{\pi AK} \quad (107)$$

where

A = distance of the motion (in the focal plane)

K = spatial frequency

Equation (107) is plotted in Fig. 65.

f. The film

The modulation transfer function of the photographic film is determined experimentally and can be obtained from the film manufacturer. An example of the transfer function that might be obtained from satellite photography films is shown in Fig. 66.

g. Interpretation

The overall system transfer function represents the response of the system to lines of width which vary from very broad, to lines which are finer than the system can resolve, and therefore is a good description of the system performance. However, it is often desirable to describe the system performance in terms of a single number, the resolution. It has been found that the minimum detectable resolution occurs at a response of 0.04, and the spatial frequency at which 4% response occurs is becoming accepted as the system resolution.

h. Illustrative example

To illustrate the use of modulation transfer functions in analyzing systems, the following example is presented. Assume the following system characteristics:

Aperture--18 in. or 0.492 m

Focal ratio--f/4

Orbital altitude--125 naut mi or 232 km

Image motion--equivalent to 2.5×10^{-6} rad

Target contrast 8:1, reduced to 2:1 by the atmosphere.

These values lead to the following transfer functions:

The lens, being f/4, is described in Fig. 60.

The image motion is determined as follows:

$$A = 2.5 \times 10^{-6} \text{ rad} \times 72 \text{ in. (focal length)} \\ \times 25.4 \text{ millimeters/in.} = 4.57 \times 10^{-3} \text{ mm.}$$

This yields the transfer function shown in Fig. 67 for image motion. The film will be represented by the transfer function of Fig. 66. Table 5 gives the values of the transfer function for the example, and they are plotted in Fig. 67.

The 4% response point is seen to occur at 140 lines per millimeter. The corresponding resolution in the scene is determined by multiplying the distance in the image (1/140 mm), by the scale number, as in Eq (103)* or utilizing Fig. 59.

TABLE 5
Transfer Functions for Illustrative Example

| Spatial Frequency (lines/mm) | The Scene + Atmosphere | Lens | Image Motion | Film | Overall System |
|------------------------------|------------------------|------|--------------|------|----------------|
| 10 | 0.33 | 0.96 | 0.99 | 0.96 | 0.30 |
| 20 | | 0.93 | 0.98 | 0.90 | 0.27 |
| 30 | | 0.90 | 0.96 | 0.85 | 0.24 |
| 40 | | 0.87 | 0.94 | 0.80 | 0.22 |
| 50 | | 0.84 | 0.91 | 0.74 | 0.19 |
| 60 | | 0.81 | 0.88 | 0.70 | 0.16 |
| 70 | | 0.78 | 0.84 | 0.66 | 0.14 |
| 80 | | 0.75 | 0.79 | 0.63 | 0.12 |
| 90 | | 0.72 | 0.74 | 0.60 | 0.11 |
| 100 | | 0.69 | 0.68 | 0.58 | 0.09 |
| 110 | | 0.66 | 0.63 | 0.55 | 0.08 |
| 120 | | 0.63 | 0.57 | 0.53 | 0.06 |
| 130 | | 0.60 | 0.51 | 0.51 | 0.05 |
| 140 | | 0.57 | 0.45 | 0.50 | 0.04 |
| 150 | | 0.54 | 0.39 | 0.48 | 0.03 |
| 160 | | 0.51 | 0.33 | 0.47 | 0.026 |
| 170 | | 0.48 | 0.27 | 0.45 | 0.019 |
| 180 | | 0.45 | 0.21 | 0.44 | 0.013 |
| 190 | | 0.43 | 0.16 | 0.43 | 0.010 |
| 200 | | 0.40 | 0.10 | 0.41 | 0.005 |

$$r_f = \frac{1}{140} \text{ mm} \times \frac{125 \text{ miles}}{72 \text{ in.}} \times \frac{1 \text{ in.}}{25.4 \text{ mm}} \\ \times 6076 \frac{\text{ft}}{\text{mi}} = 2.97 \text{ ft} \\ = 0.974 \text{ m}$$

i. Tabulation of transfer function values

Reference 7 also presents the following table of values for the transfer functions.

TABLE 6
Values of T(K)

| AK | $J_0(\pi AK)$ | $\sin \pi AK / \pi AK$ | $\frac{2}{\pi} \left[\cos^{-1}(AK) - AK \sqrt{1 - (AK)^2} \right]$ |
|------|---------------|------------------------|---|
| 0.05 | 0.994 | 0.996 | 0.963 |
| 0.10 | 0.975 | 0.983 | 0.873 |
| 0.15 | 0.945 | 0.963 | 0.810 |
| 0.20 | 0.904 | 0.935 | 0.747 |
| 0.25 | 0.854 | 0.900 | 0.685 |
| 0.30 | 0.790 | 0.858 | 0.623 |
| 0.40 | 0.646 | 0.756 | 0.506 |
| 0.45 | 0.560 | 0.699 | 0.442 |

(continued)

TABLE 6 (continued)

| AK | $J_0 (\pi AK)$ | $\sin \pi AK / \pi AK$ | $\frac{2}{\pi} [\cos^{-1} (AK) - AK \sqrt{1 - (AK)^2}]$ |
|------|----------------|------------------------|---|
| 0.50 | 0.473 | 0.636 | 0.389 |
| 0.60 | 0.293 | 0.525 | 0.285 |
| 0.70 | 0.110 | 0.368 | 0.188 |
| 0.75 | 0.025 | 0.300 | 0.138 |
| 0.80 | | 0.234 | 0.104 |
| 0.90 | | 0.109 | 0.038 |
| 0.95 | | 0.052 | 0.015 |
| 1.00 | | 0 | 0 |

G. REFERENCES

1. Kraft, D., "Position of the Sun with Respect to an Earth Satellite," Martin Company, ER 12507, April 1962.
2. Wolverton, R. (editor), "Flight Performance Handbook for Orbital Operations," STL, September 1961.
3. Jensen, J., Townsend, G., Kork, J. and Kraft, D., "Design Guide to Orbital Flight," McGraw-Hill, 1962.
4. Patterson, G., "Graphical Method for Prediction of Time in Sunlight for a Circular Orbit," ARS Journal, Vol. 31, No. 3, p 441.
5. Lüders, R. D., "Satellite Networks for Continuous Zonal Coverage," ARS Journal, Vol. 31, No. 2, February 1961, p 179.
6. Rechtin, E., "Deep Space Communications," Astronautics, Vol. 6, No. 4, April 1961, p 37.
7. Scott, R. M., "Contrast Rendition as a Design Tool," Photographic Science and Engineering, Vol. 3, No. 5, September to October 1959.

H. BIBLIOGRAPHY

Vargo, L. G., Pasquall, J., and Gersten, R. H., "Observation Satellite Orbits," ARS Journal, Vol. 32, pp 105 to 106, 1962.

Kaula, W. M., "Analysis of Gravitational and Geometric Aspects of Geodetic Utilization of Satellites," National Aeronautics and Space Administration, (NASA Technical Note D-572), March 1961.

Levin, E., "The Reflected Radiation Received by an Earth Satellite," Aerospace Corporation, El Segundo, California (Report No. TDR-594 (1560-01) TN-3), 8 May 1961, 21 p incl illus.

Greenwood, S. W., "Reconnaissance Orbits Normal to the Ecliptic Plane," Royal Aeron Soc, J, Vol. 65, No. 606, June 1961, pp 437 to 438.

Cunningham, F. G., "Calculation of the Eclipse Factor for Elliptical Satellite Orbits," National Aeronautics and Space Administration (NASA) Technical Note D-1347, June 1962.

Katz, A. H., "Observation Satellites," Astronautics:

- Part I, Vol. 5, No. 5, May 1960.
 Part II, Vol. 5, No. 6, June 1960, p 26.
 Part III, Vol. 5, No. 7, July 1960, p 28.
 Part IV, Vol. 5, No. 8, August 1960, p 30.
 Part V, Vol. 5, No. 9, September 1960, p 32.
 Part VI, Vol. 5, No. 10, October 1960, p 36.

Rechtin, E., "Deep Space Communications," Astronautics:

- Part I, Vol. 6, No. 4, April 1961, p 37.
 Part II, Vol. 6, No. 5, May 1961, p 26.

Mueller, G. E., Hebenstreit, W. B., and Spangler, E. R., "Communication Satellites--How High?," Astronautics, Vol. 6, No. 7, July 1961, p 42.

Tepper, M., "Tiros Program Results," Astronautics, Vol. 6, No. 5, May 1961, p 28.

Kershner, R. B., "Transit Program Results," Astronautics, Vol. 6, No. 5, May 1961, p 30.

Jaffe, L., "Project Echo Results," Astronautics, Vol. 6, No. 5, May 1961, p 32.

Pierce, J. R., "Practical Problems of Satellite Communication," Astronautics, Vol. 6, No. 5, May 1961, p 34.

Ziemer, R. R., "Orbiting Astronomical Observatories," Astronautics, Vol. 6, No. 5, May 1961, p 36.

Freitag, R. F., "Project Transit: A Navigation Satellite," Navigation, Summer-Autumn 1960, Vol. 7, Nos. 2 and 3.

Holahan, J., "Transit: Navy Claims World's First Operational Satellite," Space Aeronautics, June 1960, Vol. 33, No. 6, p 154.

Kershner, R. B., "The Transit Program," Astronautics, June 1960, Vol. 5, No. 6, p 30.

Graves, C. D., "Radio Propagation Measurements Using the Explorer Six Satellite," Journal of Geophysical Research, September 1960, Vol. 65, No. 9, p 2585.

Heller, G., "Thermal Control of the Explorer Satellites," ARS Journal, April 1960, Vol. 30, No. 4.

Keigler, J. E., and Krawitz, L., "Weather Radar Observation from an Earth Satellite," Journal of Geophysical Research, September 1960, Vol. 65, No. 9, p 2793.

"First Navigation Satellite," Missiles and Rockets, 18 April 1960, Vol. 6, No. 16, p 15.

"Navy Tests Transit Navigational Potential," Aviation Week, 18 April 1960, Vol. 72, No. 16, pp 29 to 30.

"Refraction Error No Problem in Transit," Missiles and Rockets, 14 November 1960, Vol. 7, No. 20, p 19.

Mueller, G. E., "Telebit--An Integrated Space Navigation and Communication System," Astronautics, May 1960, Vol. 5, No. 5, p 26.

"Explorer Eight Mapping Ionosphere," Aviation Week, 7 November 1960, Vol. 73, No. 19, p 31.

"Explorer Eight Probes Ionosphere," Missiles and Rockets, 14 November 1960, Vol. 7, No. 20, p 42.

"Explorer Eight Relays Ionospheric Data," Aviation Week, 21 November 1960, Vol. 73, No. 21, p 71.

Basler, R. P., Dewitt, R. N., and Reid, G. C., "Radiation Information from 1958 Delta 2," Journal of Geophysical Research, April 1960, Vol. 65, No. 4, p 1135.

Davies, M. E.,
"Are the Lunik III Photos Fake?," Astronautics, June 1960, Vol. 5, No. 6, p 46.
"How Good Is the Lunik III Photography?," Astronautics, May 1960, Vol. 5, No. 5, p 28.

Krasovskii, V. I., "Results of Scientific Investigations Made by Soviet Sputniks and Cosmic Rockets," ARS Journal, January 1960, Vol. 30, No. 1, p 27.

Clarke, E., "Tiros Exceeds Weather Bureau Hopes," Aviation Week, 2 May 1960, Vol. 72, No. 18, p 30.

Goldberg, E. A., and Landon, V. D., "Key Equipment for Tiros I," Astronautics, June 1960, Vol. 5, No. 6, p 36.

Holmes, J., "Tiros II Maps Hurt by Poor TV Photos," Missiles and Rockets, 5 December 1960, Vol. 7, No. 23, p 15.

Keigler, J. E. and Krawitz, L., "Weather Radar Observations from an Earth Satellite," Journal of Geophysical Research, September 1960, Vol. 65, No. 9, p 2793.

Keigler, J. E., and Oakley, C. B., "The Tiros System on the Ground," Astronautics, June 1960, Vol. 5, No. 6, p 44.

Lewis, C., "NASA Tiros I Demonstrates Potential Satellite Reconnaissance Utility," Aviation Week, 11 April 1960, Vol. 72, No. 15, p 28.

Means, P., "Tiros Presages Long-Range Forecasts," Missiles and Rockets, 11 April 1960, Vol. 6, No. 14, p 21.

Osgood, C. C., "Structural Design of Tiros I," Astronautics, June 1960, Vol. 5, No. 6, p 42.

Perkel, H., "Tiros I Spin Stabilization," Astronautics, June 1960, Vol. 5, No. 6, p 38.

Ritter, M., "Thermal Design for Tiros," Astronautics, June 1960, Vol. 5, No. 6, p 40.

Sternberg, S., and Stroud, W. G., "Tiros I--Meteorological Satellite," Astronautics, June 1960, Vol. 5, No. 6, p 32.

Wexler, H., and Fritz, S., "Tiros Reveals Cloud Formation," Science, 10 June 1960, Vol. 131, No. 3415, p 1708.

"Aerospace Engineering Intelligence--Tiros Satellite is Powered by 9200 Solar Cells," Space Astronautics, May 1960, Vol. 33, No. 5, p 31.

"The Satellite Echo One," Nature, 27 August 1960, Vol. 187, No. 4739, p 741.

"The Echo Communications Satellite," IGY Bulletin, September 1960, No. 39, p 14.

"Tiros II Transmits Cloud, Infrared Data," Aviation Week, 28 November 1960, Vol. 73, No. 22, p 32.

"NASA Tiros I Demonstrates Potential Satellite Reconnaissance Utility," Space Technology, July 1960, Vol. 3, No. 3, p 24.

"Sputnik III Results," Missiles and Rockets, 11 January 1960, Vol. 6, No. 2, p 38.

"Sputnik IV," Spaceflight, October 1960, Vol. 11, No. 8, p 230.

"The Other Side of the Moon," Spaceflight, January 1960, Vol. 11, No. 5, p 130.

"Triumph of Sputnik V," Spaceflight, October 1960, Vol. 11, No. 8, p 225.

Heppner, J. P., Stolarik, J. D., Shapiro, I. R., and Cain, J. C., "Project Vanguard Magnetic-Field Instrumentation and Measurements," NASA TN D-486, September 1960. (Also, Nice, France, First International and Space Symposium, January 1960.)

Mansir, D., "Magnetic Measurements in Space," Electronics, 5 August 1960, Vol. 33, No. 32, p 47.

O'Keefe, J. A., Eckels, A., and Squires, R. K., "Vanguard Measurements Give Pear-Shaped Component of Earth's Figure," Science, 27 February 1959, Vol. 129, No. 3348, pp 565 to 566.

Siry, J. W., "The Vanguard IGY Earth Satellite Program," Moscow, 5th General Assembly of CSAGI, 30 July to 10 August.

ILLUSTRATIONS

Preceding Page Blank

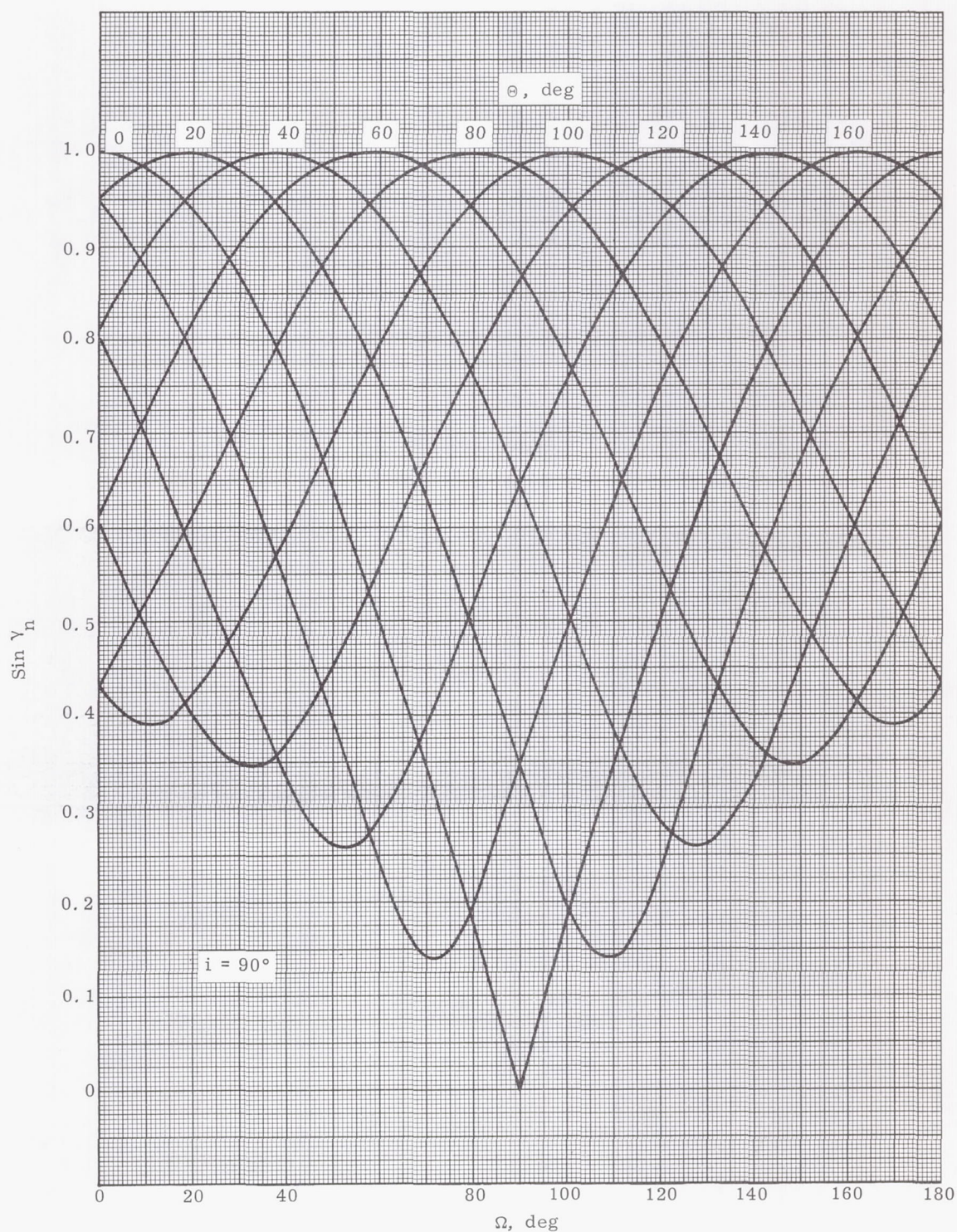


Fig. 1. Sine of the Angle Between the Normal to the Orbit Plane and the Earth-Sun Line, $i = 90^\circ$

Preceding Page Blank

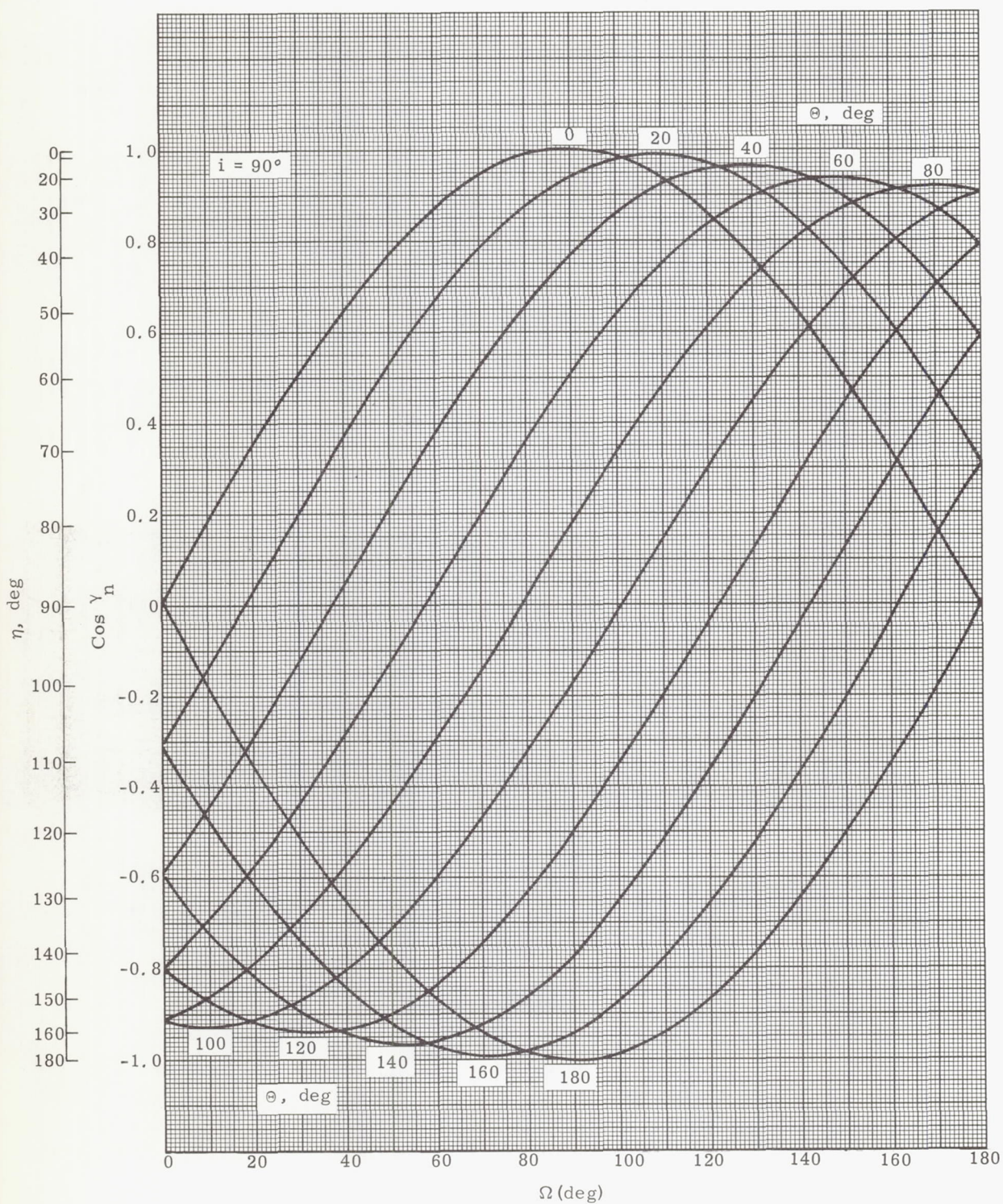


Fig. 2. Cosine of the Angle Between the Normal to the Orbit Plane and the Earth-Sun Line, $i = 90^\circ$

Fig. 3. Cross Section of Orbit Through Shadow Cone

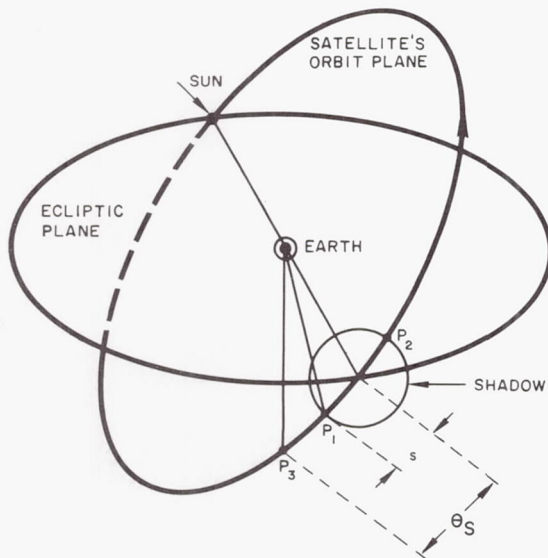
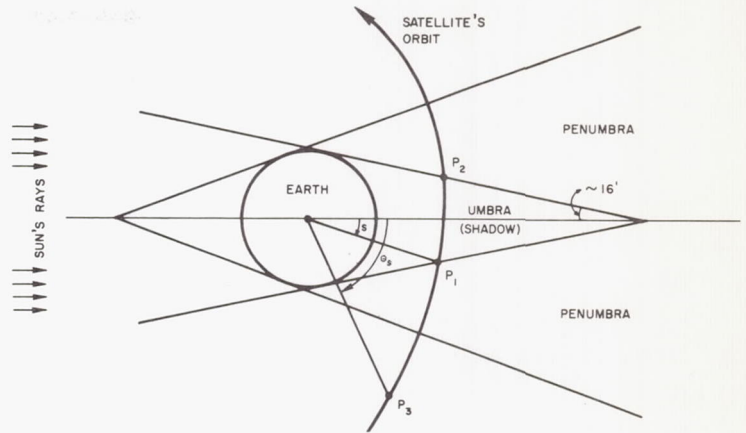
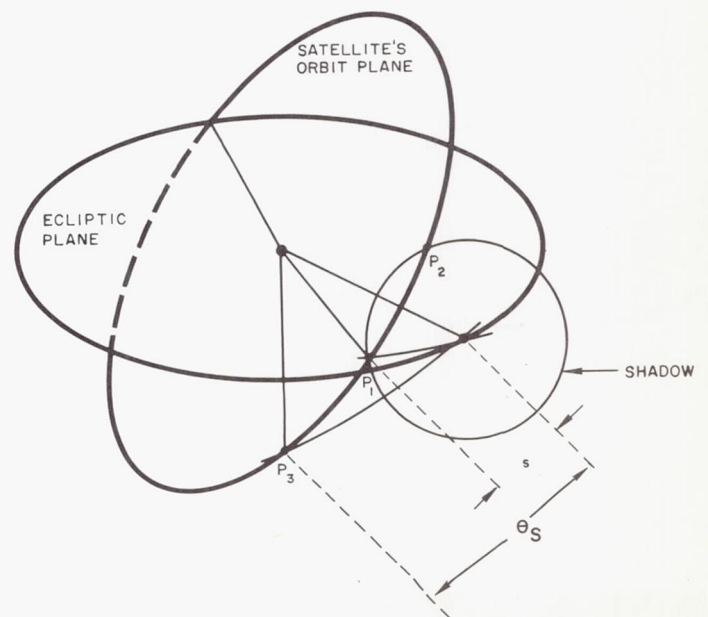


Fig. 4. Orbit Going Through Shadow When Shadow Is at the Node

Fig. 5. Orbit Going Through Shadow When Shadow Is Not at the Node



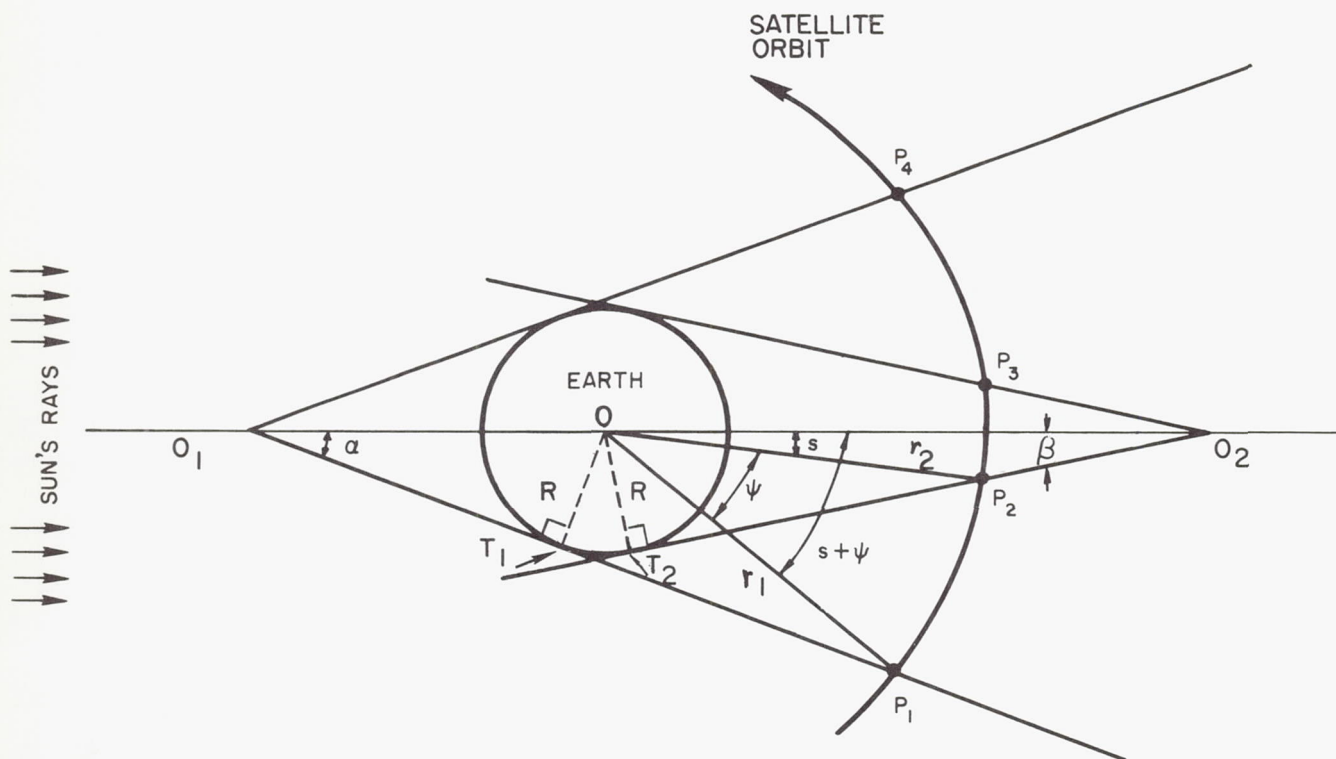


Fig. 6. Cross Section of Orbit Through Penumbra Cone

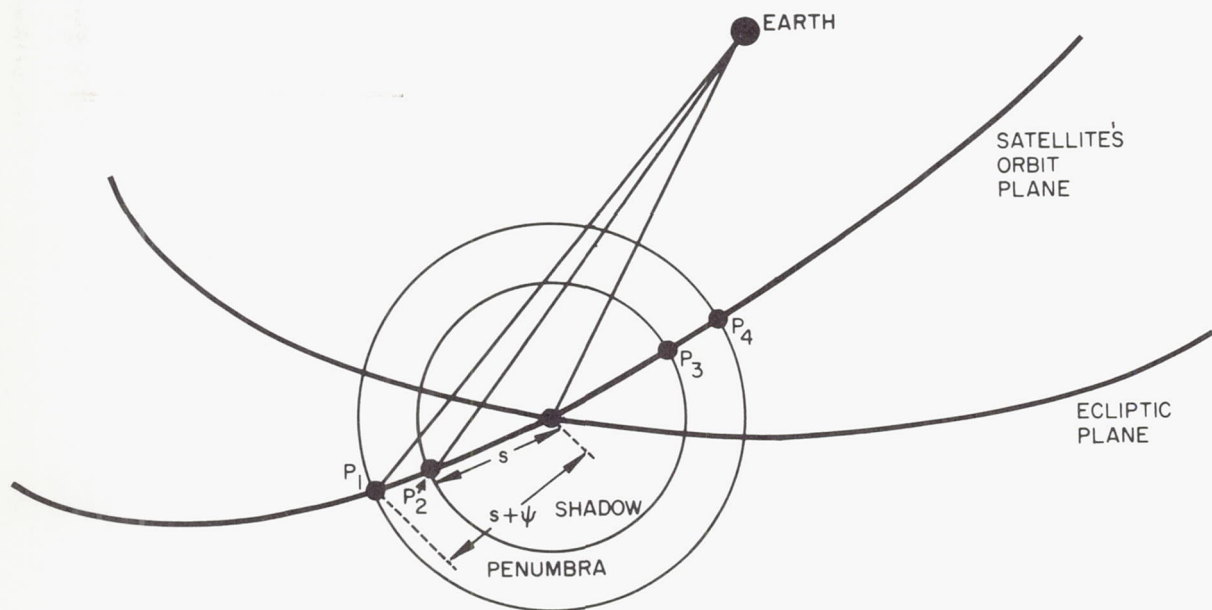


Fig. 7. Orbit Going Through Penumbra When It Is at the Node

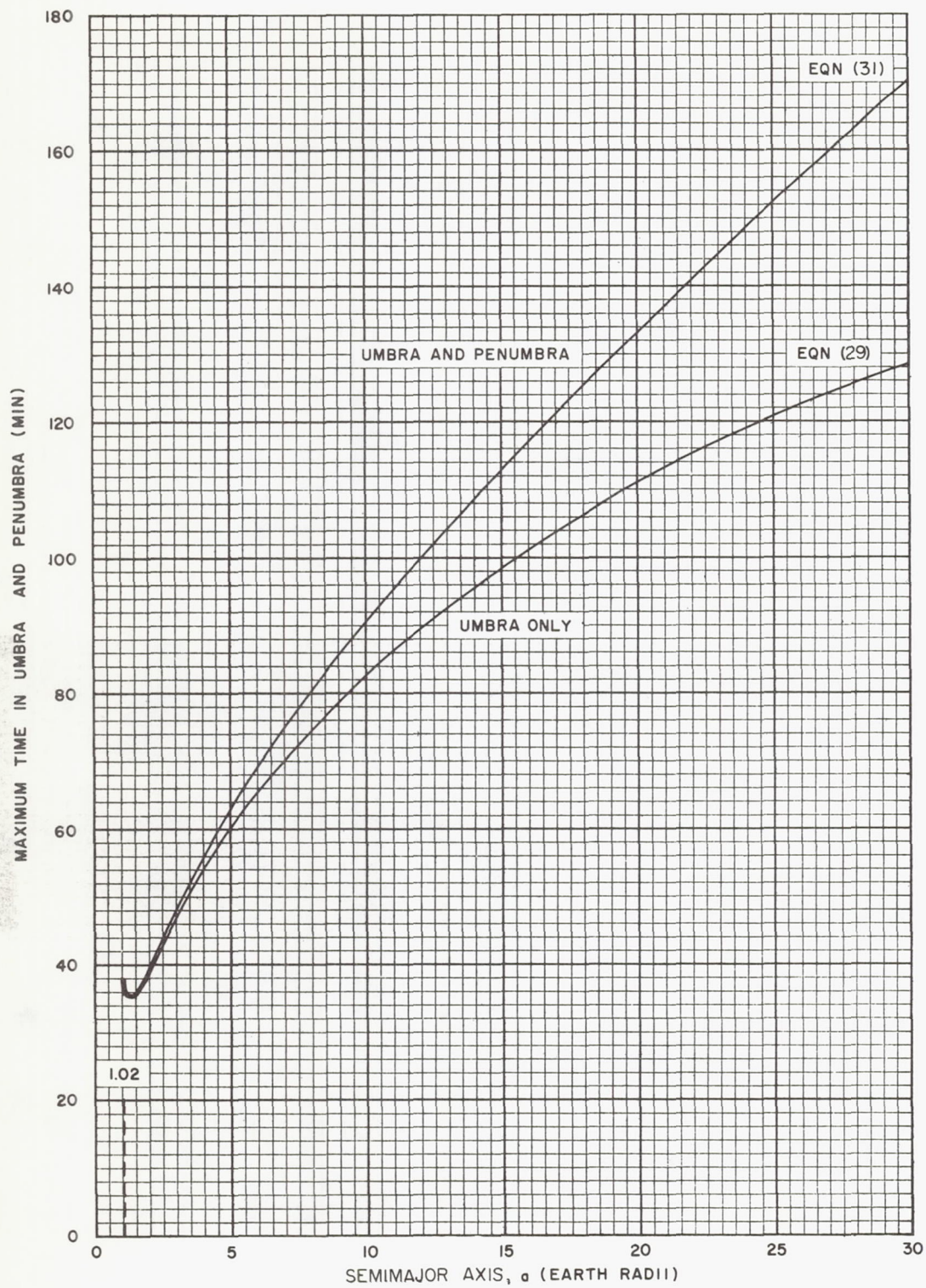


Fig. 10. Maximum Time in Umbra and Penumbra Versus Semimajor Axis

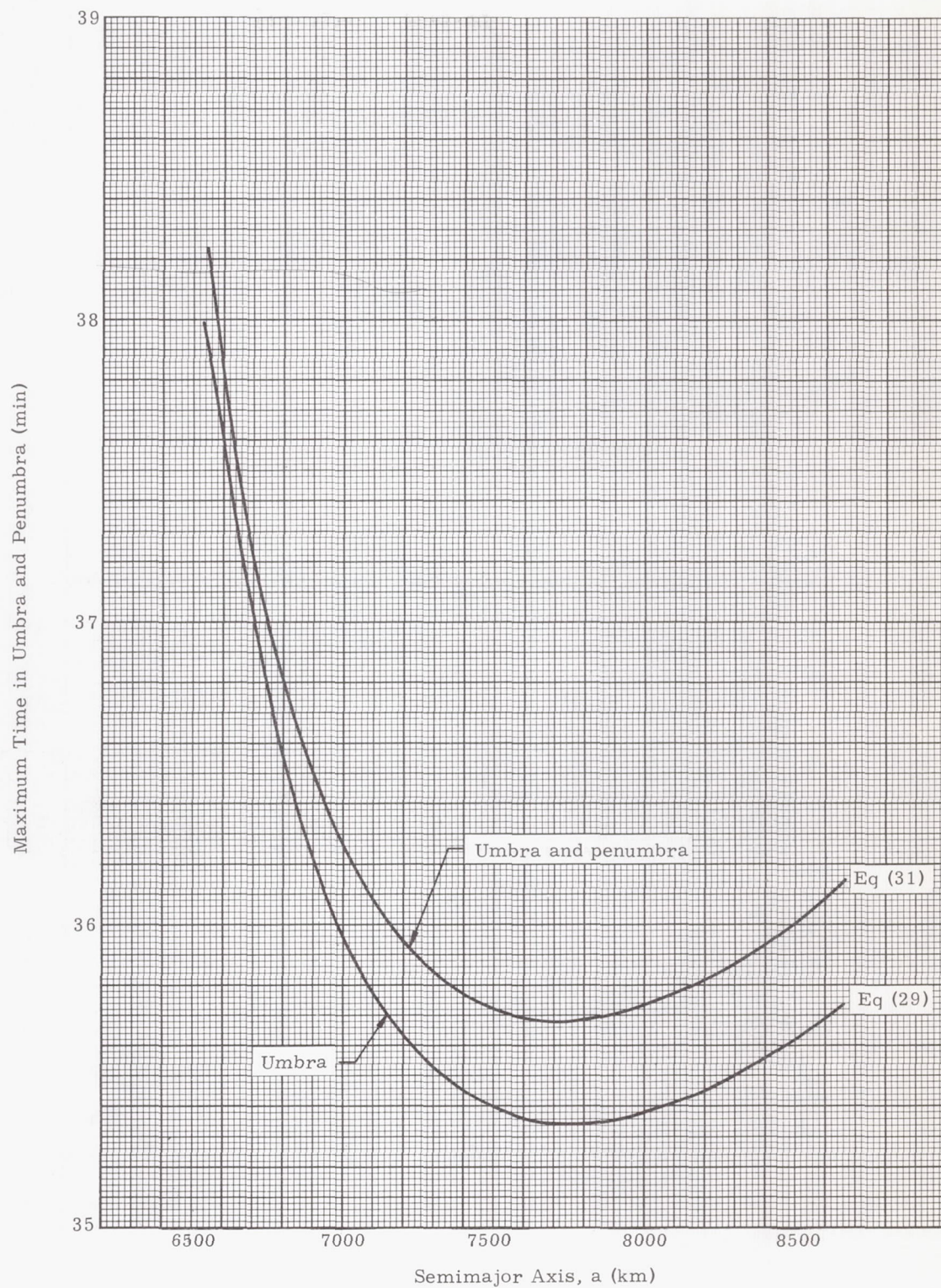


Fig. 11. Maximum Time in Umbra and Penumbra Versus Semimajor Axis

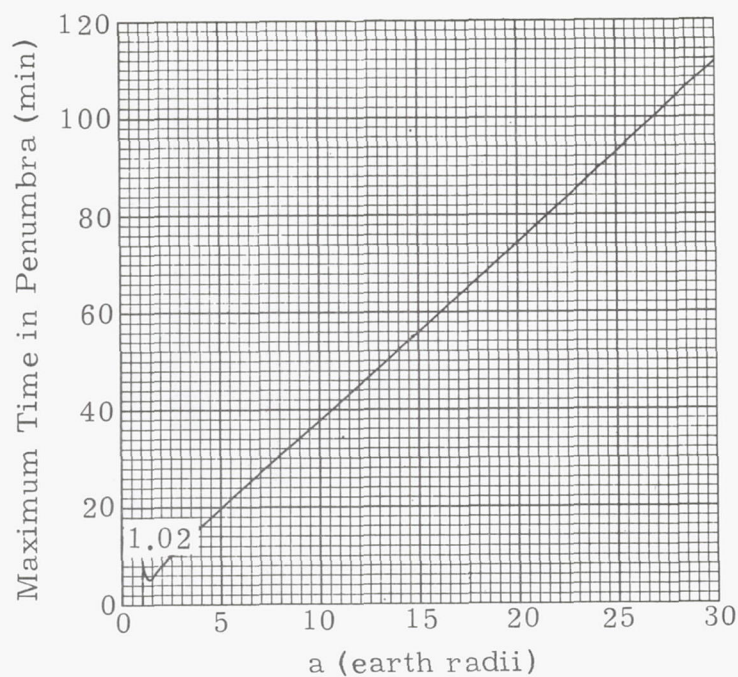


Fig. 12. Maximum Time in Penumbra (No Umbra Eclipse) Versus Semimajor Axis

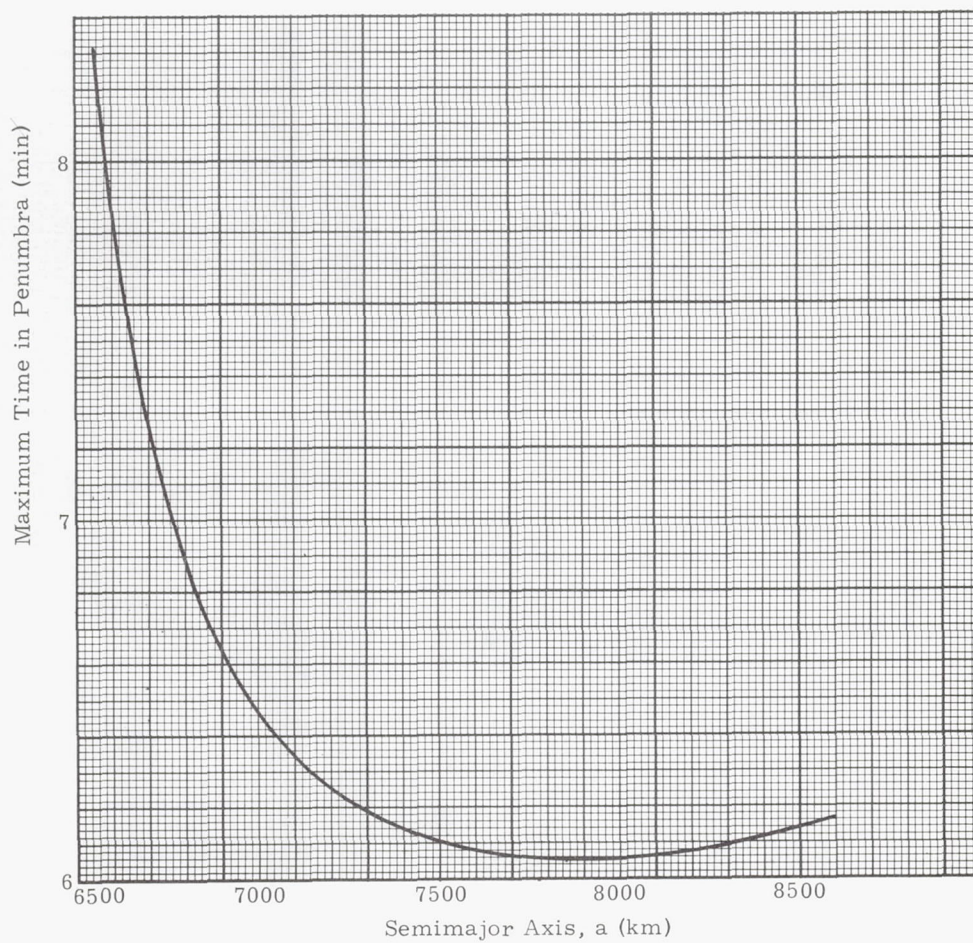


Fig. 13. Maximum Time in Penumbra (No Umbra Eclipse) Versus Semimajor Axis

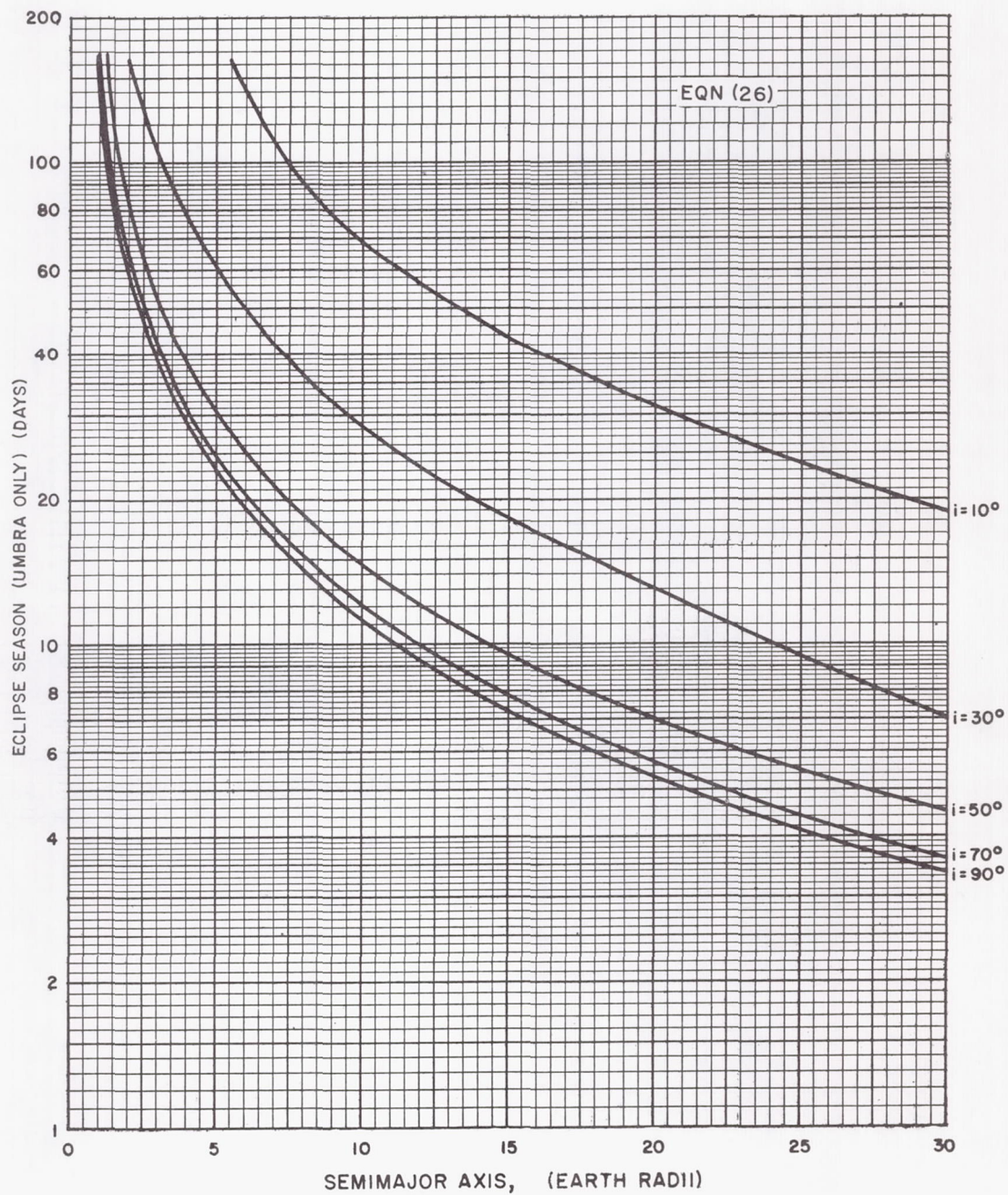


Fig. 14. Eclipse Season (Umbra Only) Versus Semimajor Axis

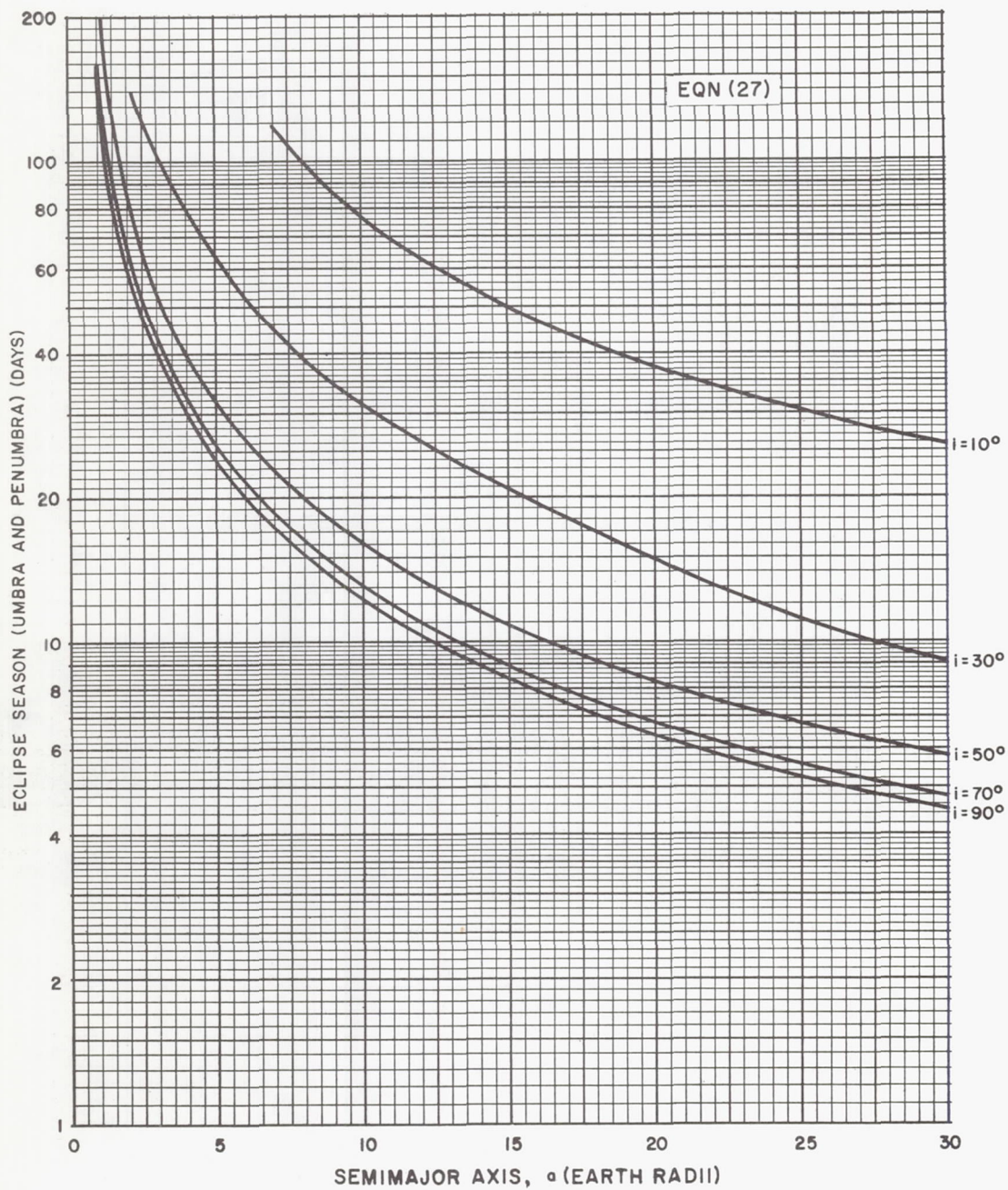


Fig. 15. Eclipse Season (Umbra and Penumbra) Versus Semimajor Axis

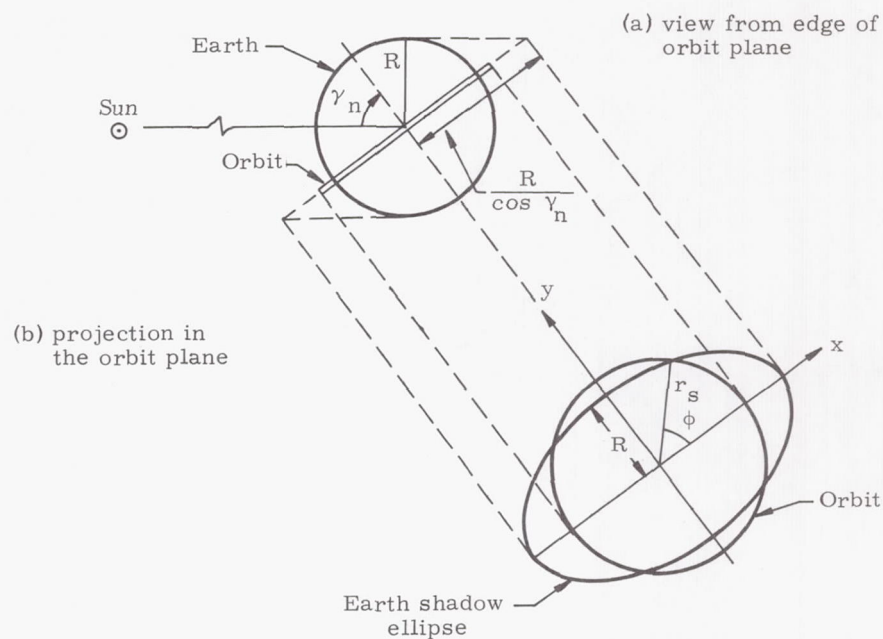


Fig. 16. Geometry of the Simplified Eclipse Problem

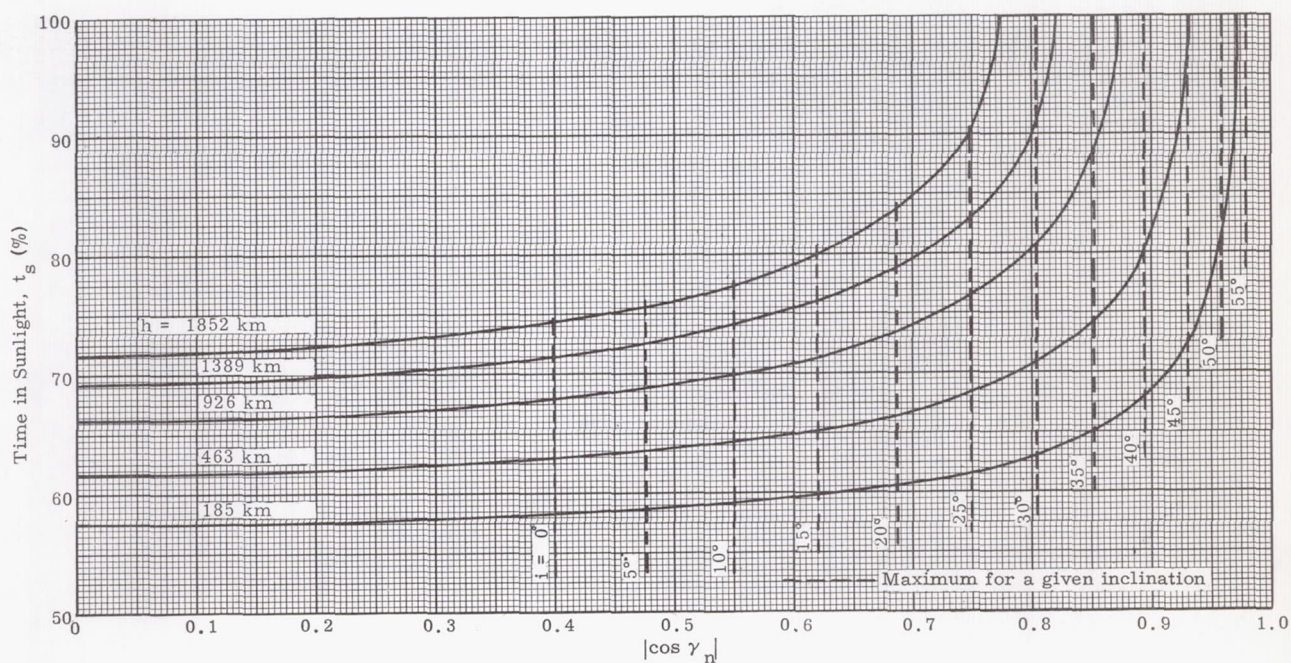


Fig. 17. Time in Sunlight Versus Cosine of Angle Between Earth-Sun Line and Normal to Orbit

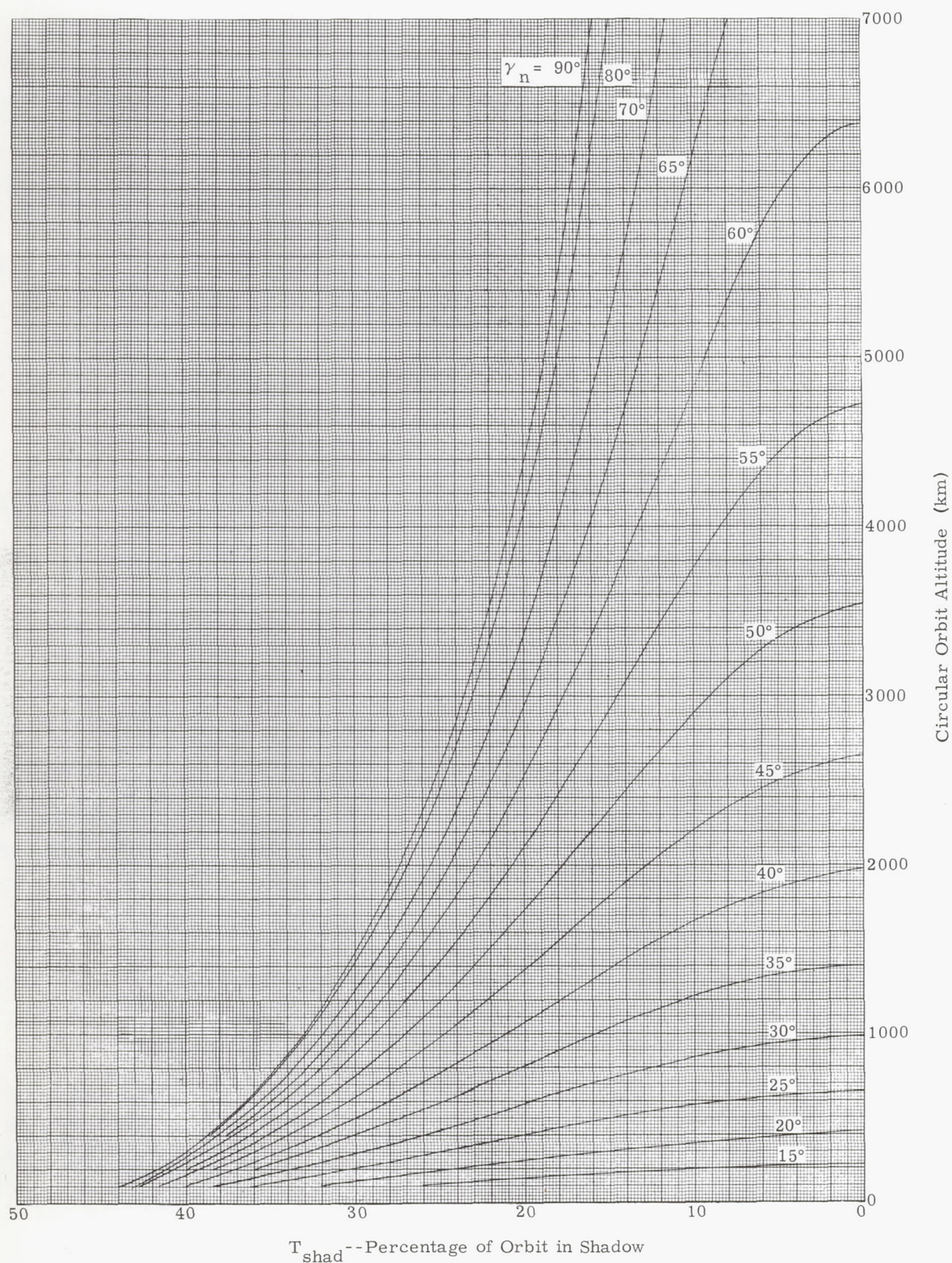


Fig. 18. Percent Time in Shadow for Circular Unperturbed Orbits

$h = 231.5 \text{ km}$
polar orbit

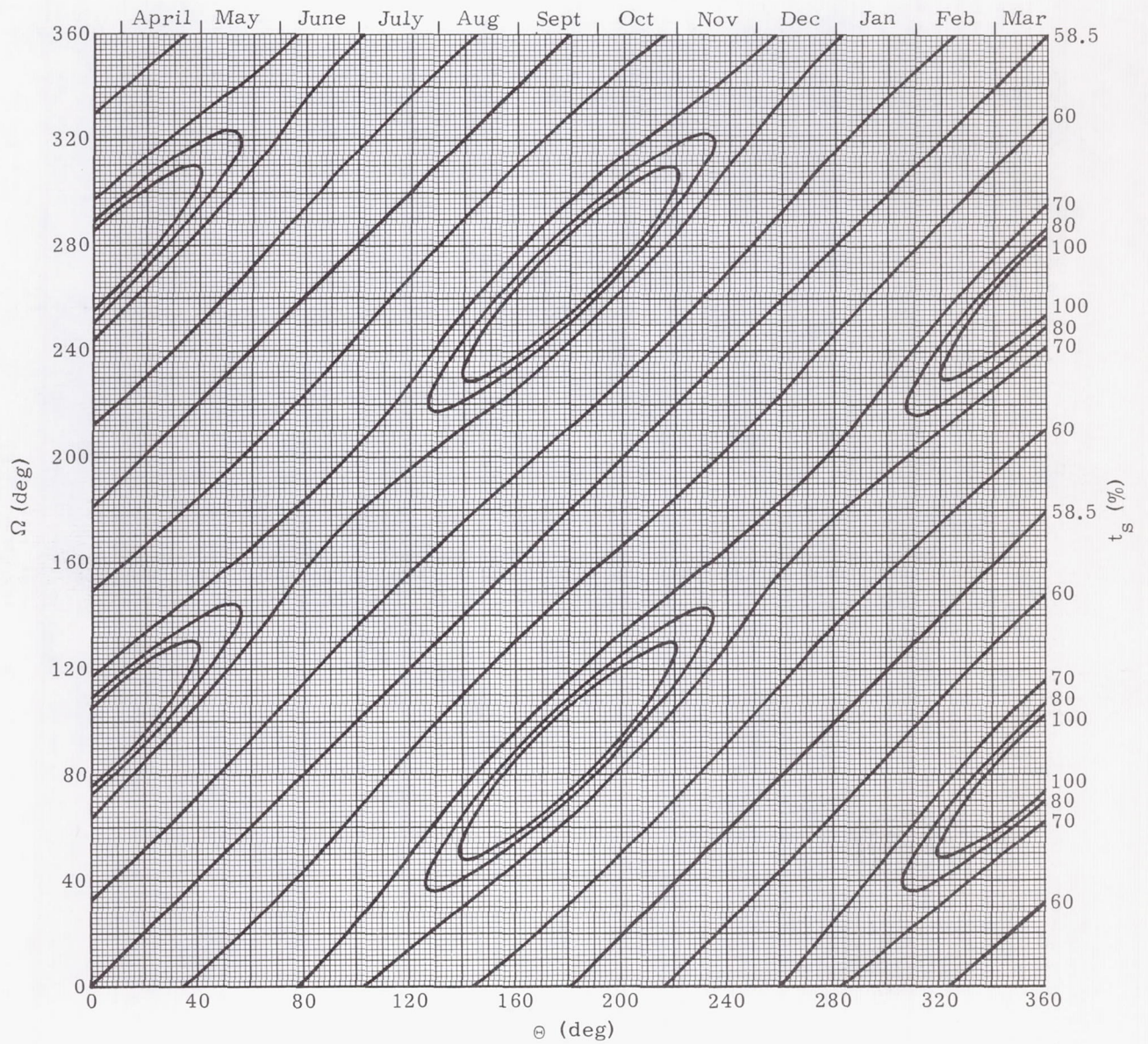


Fig. 19. Eclipse Durations and Eclipse Seasons for Unperturbed Circular Orbits

$h = 463 \text{ km}$
polar orbit

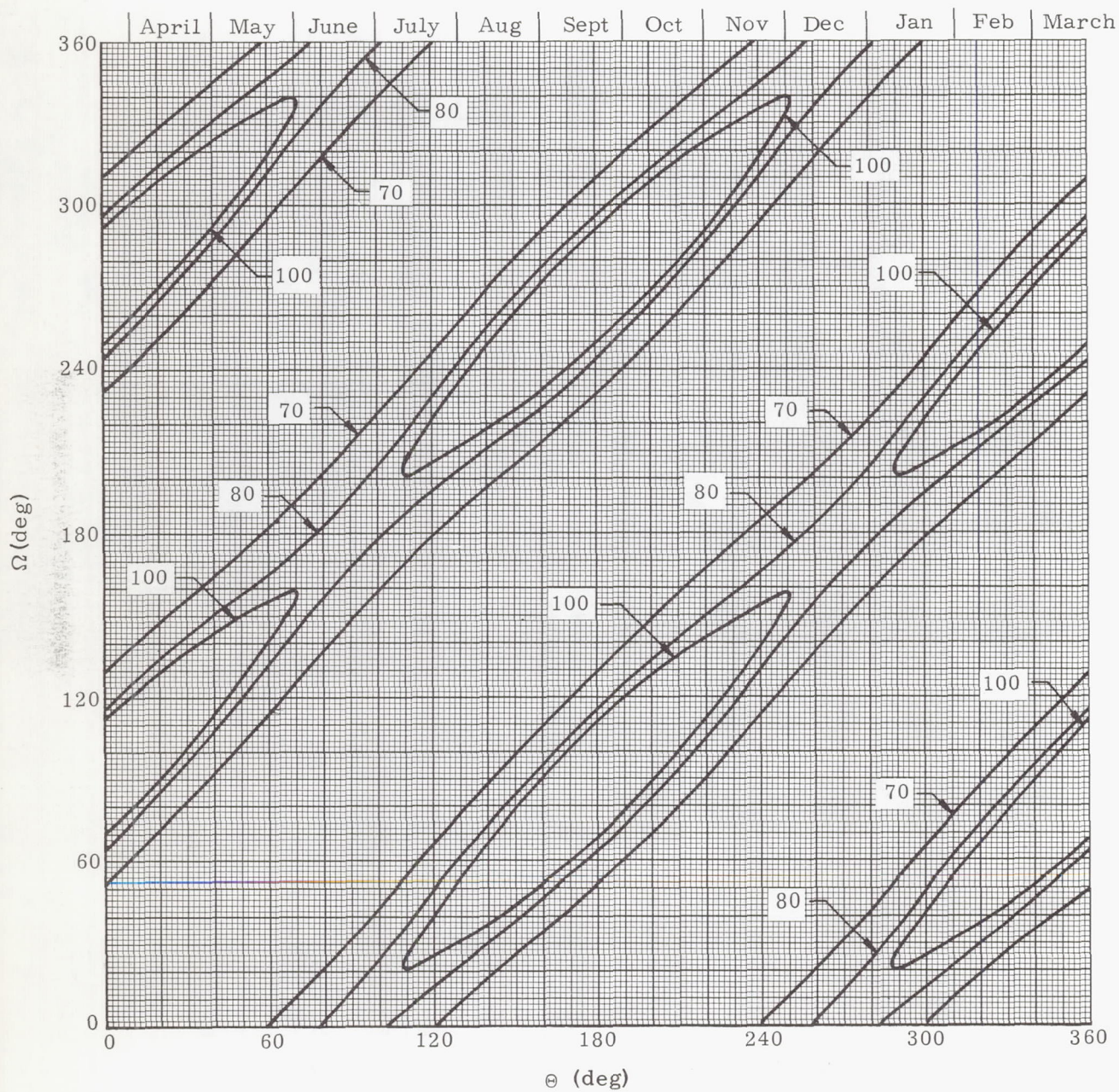


Fig. 20. Eclipse Durations and Eclipse Seasons for Unperturbed Circular Orbits

$h = 926 \text{ km}$
polar orbit

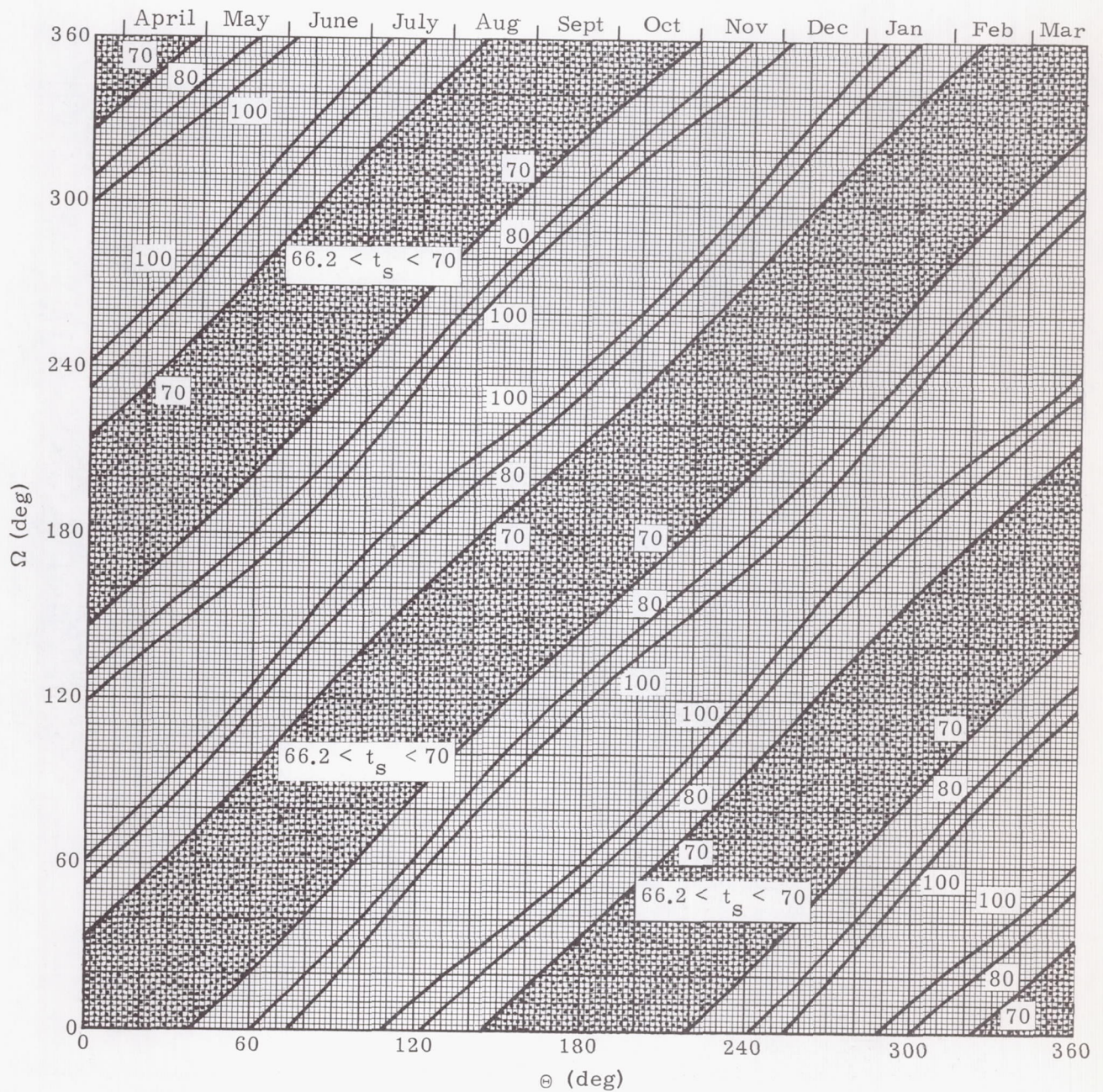


Fig. 21. Eclipse Durations and Eclipse Seasons for Unperturbed Circular Orbits, $i = 90^\circ$, $h = 926 \text{ km}$

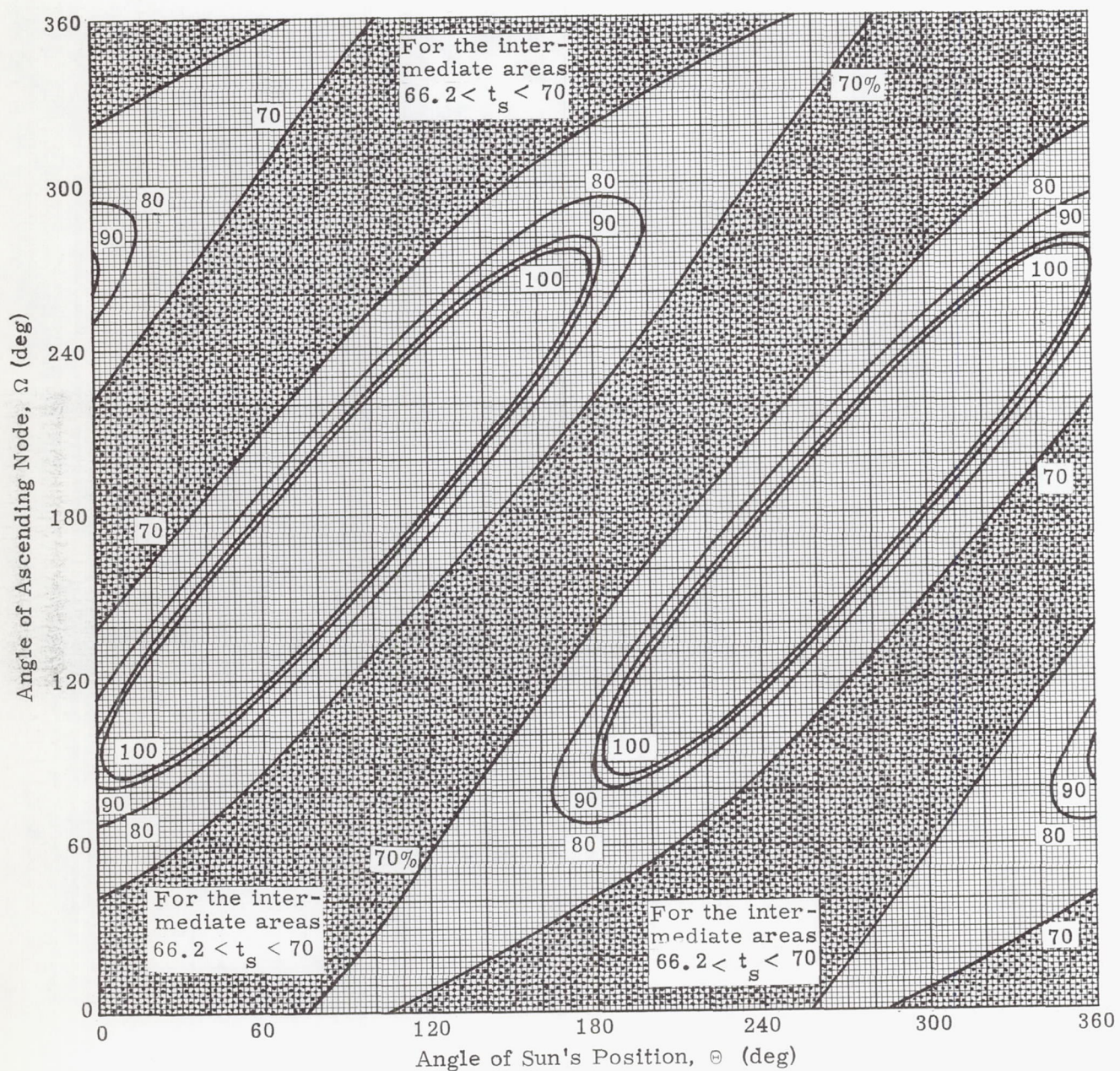


Fig. 22. Eclipse Durations and Eclipse Seasons for an Unperturbed Circular Orbit, $i = 60^\circ$, $h = 926$ km

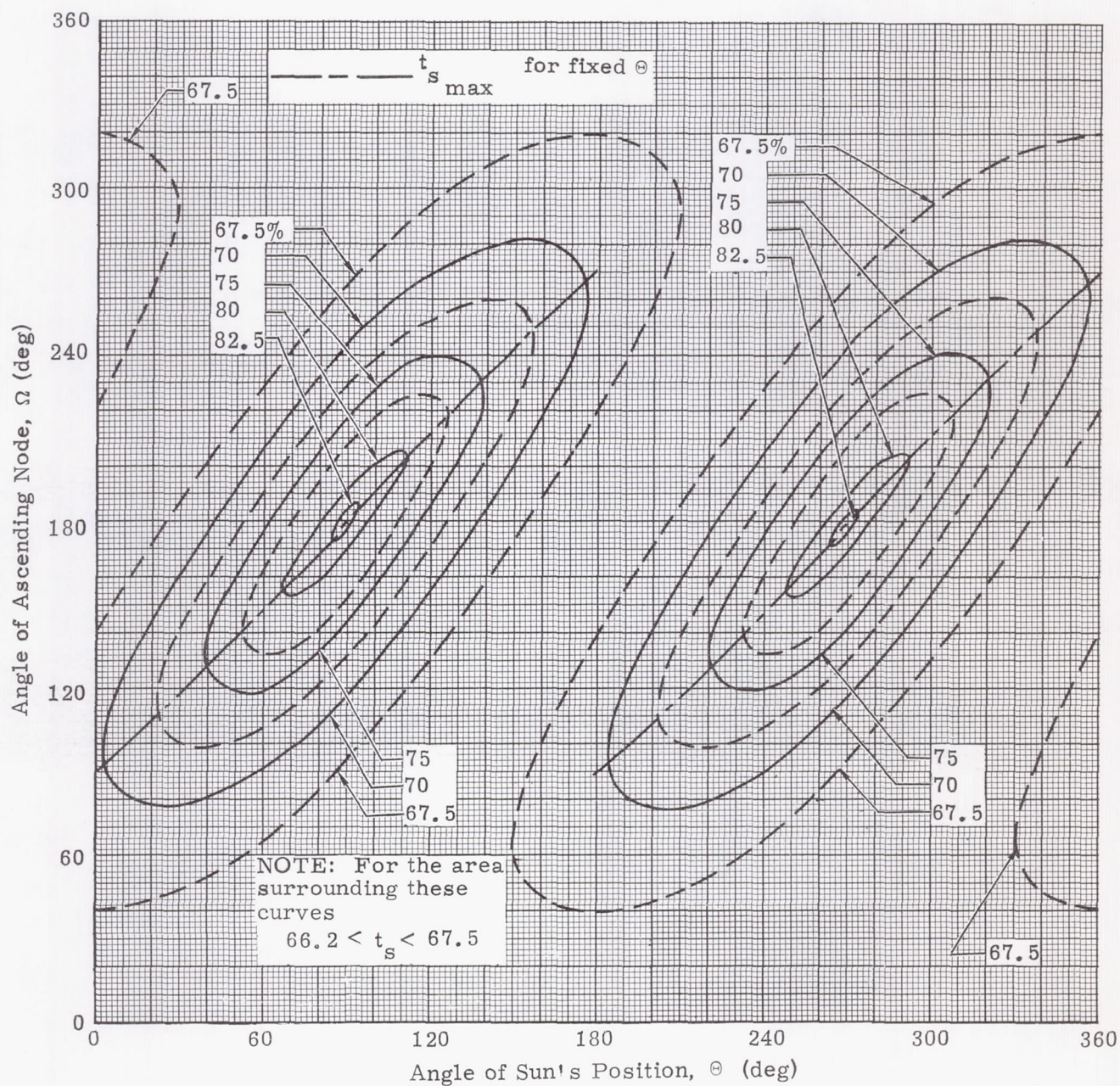


Fig. 23. Eclipse Durations and Eclipse Seasons for Unperturbed Circular Orbits, $i = 32^\circ$, $h = 926$ km

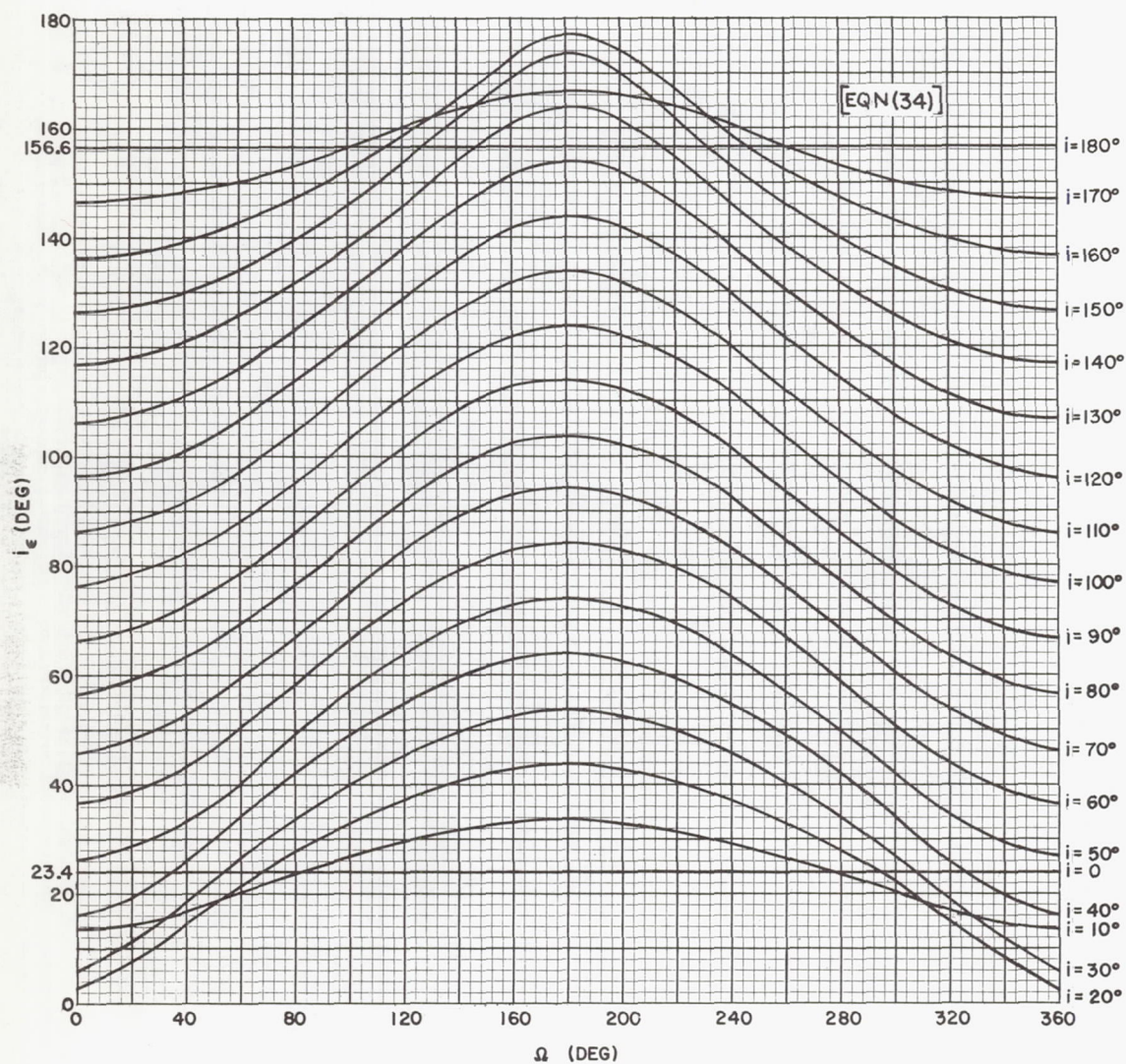


Fig. 24. Inclination with Respect to the Ecliptic (i_e) Versus Longitude of the Node with Respect to the Equator (Ω) for Different Inclinations with Respect to the Equator (i)

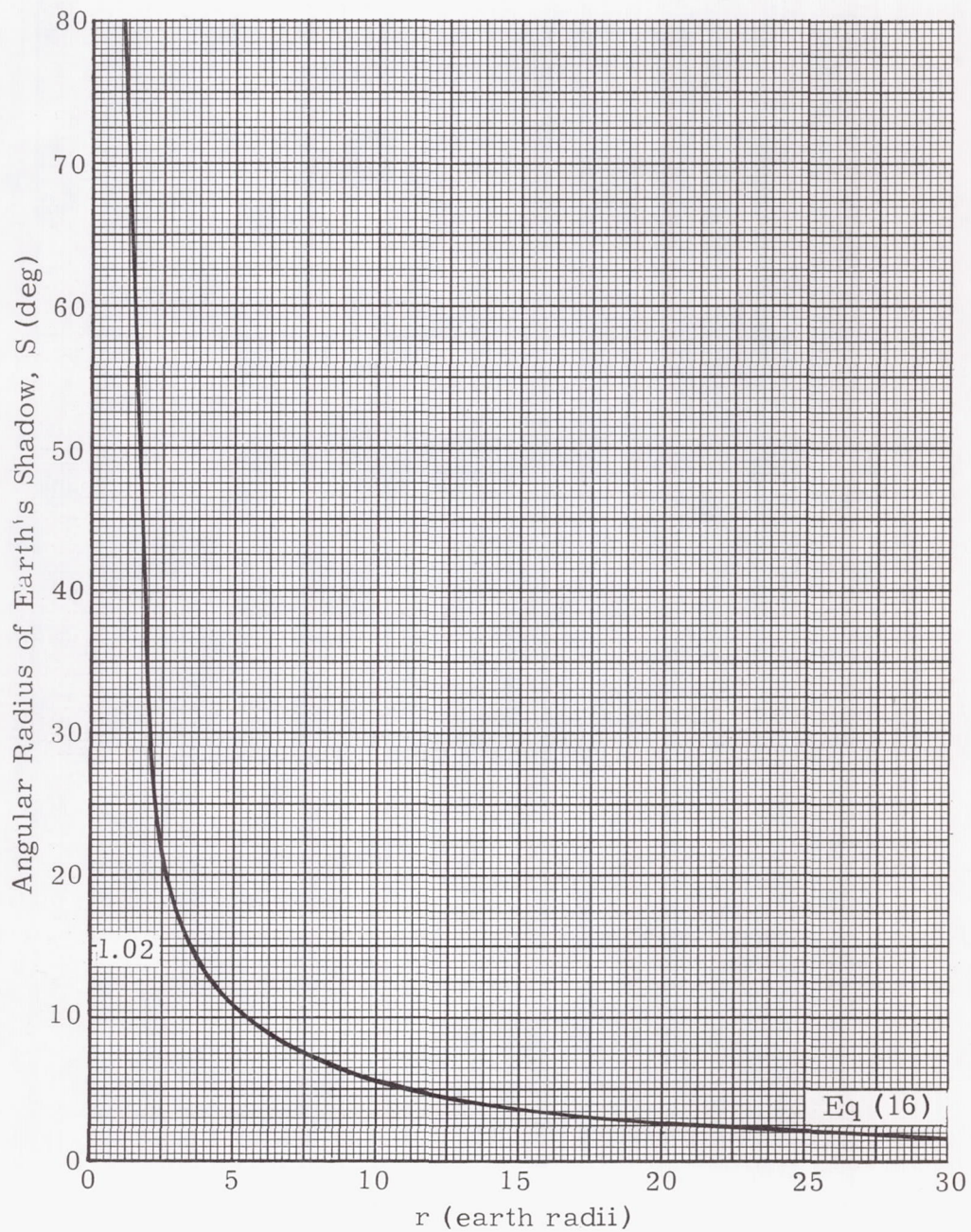


Fig. 25. Angular Radius of Shadow Versus Distance from Center of Earth

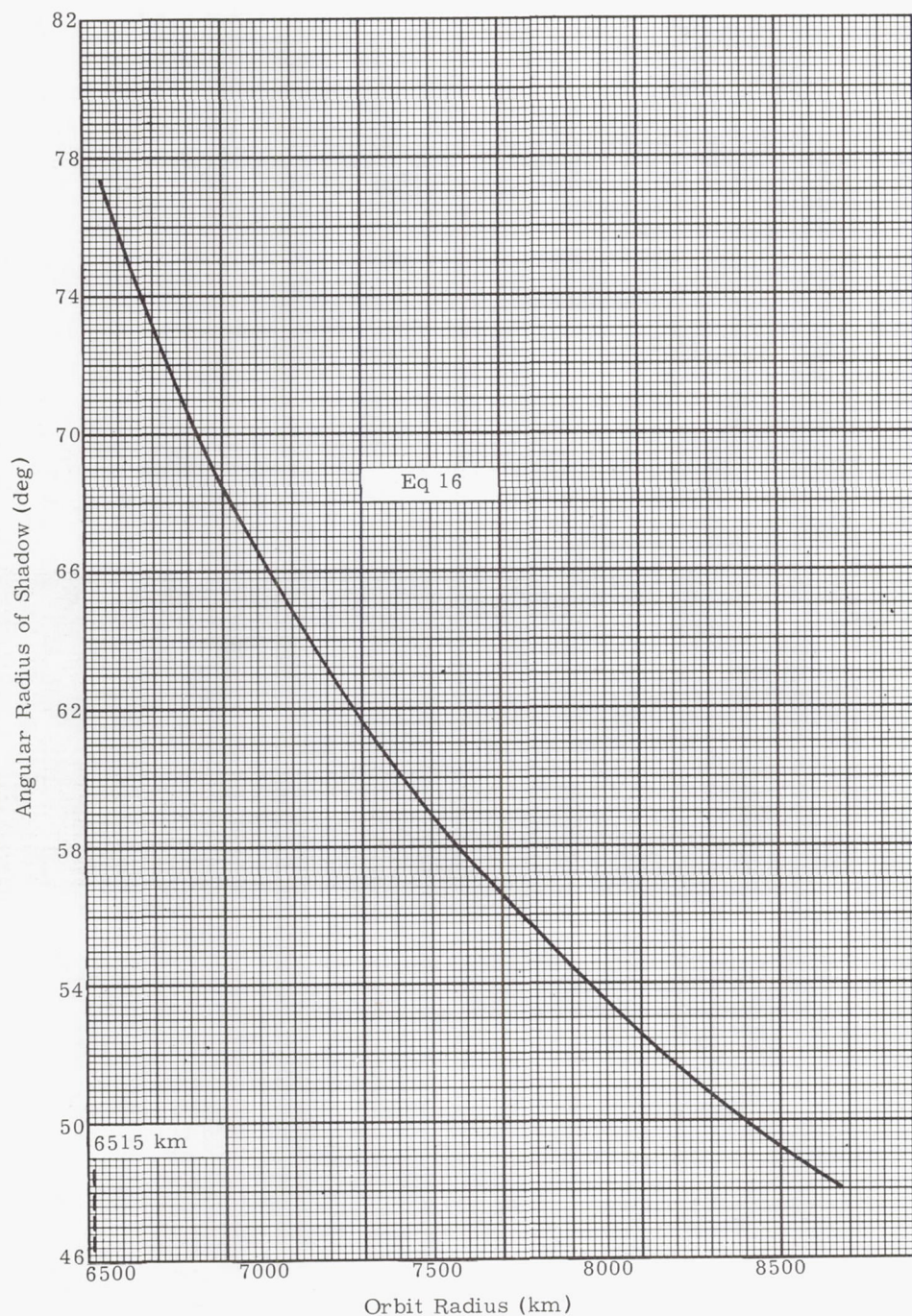


Fig. 26. Angular Radius of Shadow Versus Distance from Center of Earth

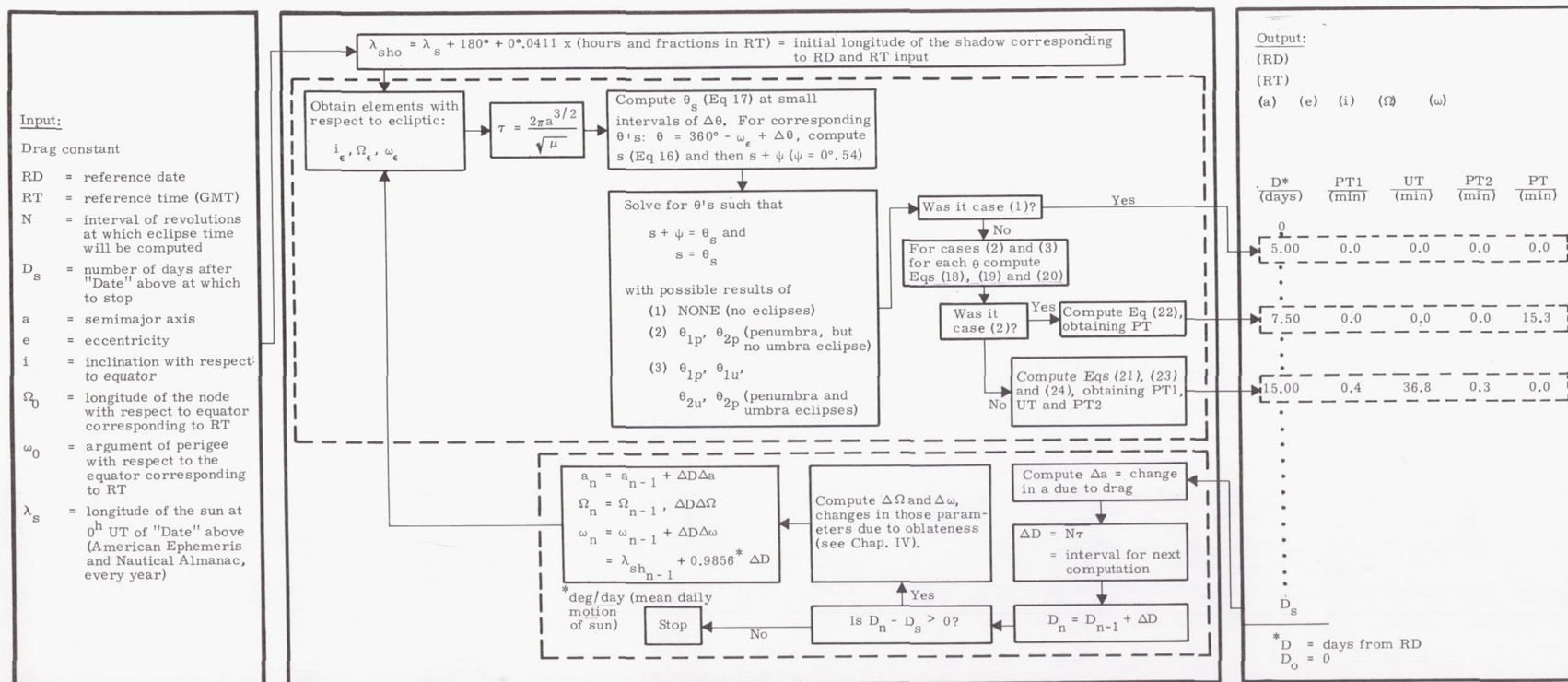


Fig. 27. Flow Chart of a Simple Eclipse Program

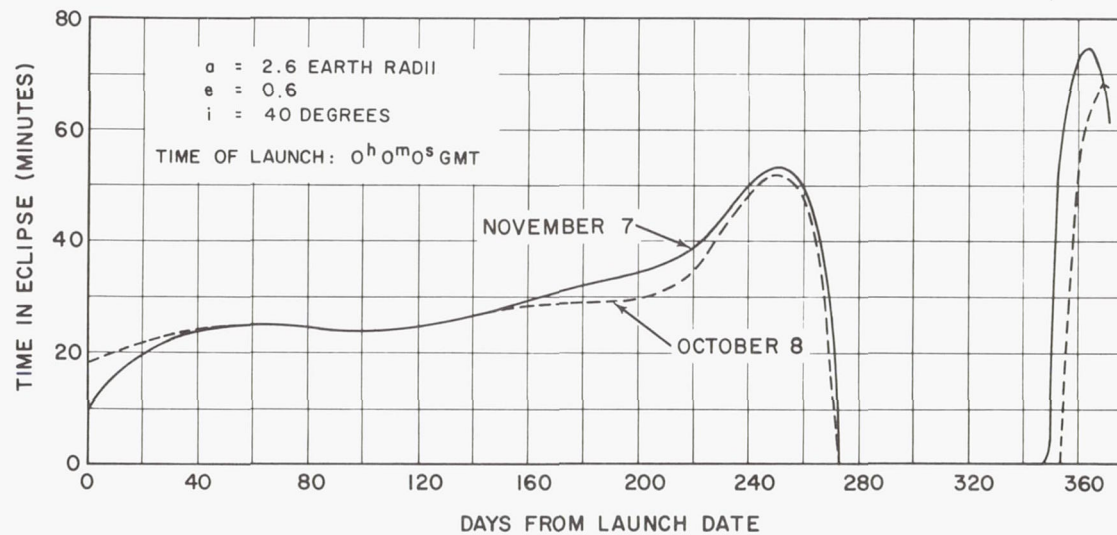
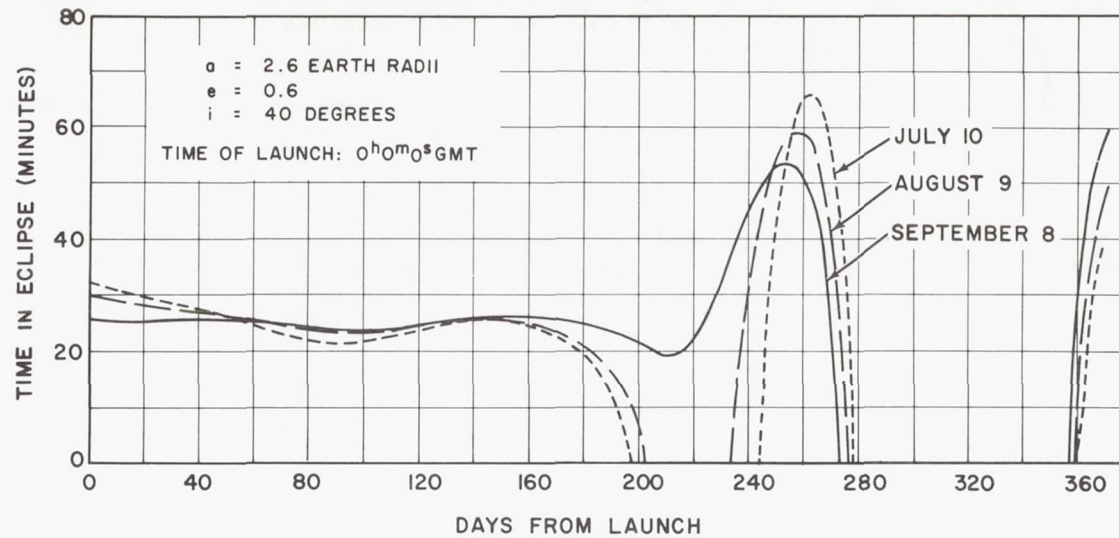


Fig. 28. Example of Eclipse Patterns When Launching a Vehicle on Different Dates in 1963 at the Same Time of Day

- Townsend, G. and Leach, R., "Guidance and Control Requirements," Design Guide to Orbital Flight, McGraw-Hill Book Company, New York, Chapter 12, 1962.
- Townsend, G., Kork, J. and Kraft, D.
 "Guidance Requirements for a 24-hr Satellite," the Martin Company, Baltimore, Maryland, Engineering Report No. ER 10718-6, October 1959.
 "Orbital Guidance Systems Study," The Martin Company, Baltimore, Maryland, Engineering Report No. ER 11439-3, November 1960.
- Tripp, C. N. and Boardman, W. P., "Attitude Control Rocket Requirements for Space Vehicles," Marquardt Corporation, presented at the National IAS-ARS Joint Meeting, Los Angeles, Calif., June 13 to 16, 1961.
- Vertregt, M., "Orientation in Space," Journal of the British Interplanetary Society, Vol. 15, No. 6, pp 324 to 338, November and December 1956.
- Wheelon, A. D., "Midcourse and Terminal Guidance," University of California, Engineering Extension, Berkeley, California, April 1958, Eng X461-AEC, Space Technology Lecture 12B. (Also, Space Technology, John Wiley & Sons, New York, 1959 (Siefert, H., ed.))
- White, J. A.
 "A Study of the Guidance of Space Vehicles Returning to a Braking Ellipse About the Earth," NASA TN D-191, January 1960.
 "A Study of the Effect of Errors in Measurement of Velocity and Flight-Path Angle on the Guidance of a Space Vehicle Approaching the Earth," NASA TN D-957, October 1961.
- Wing, W. G., "State of the Art: Inertial Guidance," Space/Aeronautics, Vol. 31, p 24, January 1959.
- West, C. T. and Goodstein, R., "On the Simplification of the Attitude Equations of a Satellite," American Astronautical Society, Preprint No. 60-13, 1960.
- Widrow, B., "Rate of Adaptation in Control Systems," ARS Journal, Vol. 32, No. 9, p 1378, September 1962.
- Windeknecht, T. G., "A Simple System of Sun Orientation for a Spinning Satellite," Institute of Aerospace Sciences, Preprint No. 61-204-1898, June 1961.
- Williams, O. S. and Wiseman, J. R., "Low-Thrust Bipropellant Pulse-Rockets for Satellite Attitude Control," American Rocket Society, Preprint No. 1503-60, 1960.
- Williams, O. S., "Performance and Reliability of Rocket Attitude Control Systems," Thiokol Astronaut, Vol. 2, No. 1, pp 3 to 6, 1960.
- Wilson, R. H., Jr., "Magnetic Field Effects on Artificial Satellites," Sky and Telescope, Vol. 20, No. 2, pp 77 to 79, August 1960.
- Wisneski, M. L., "Error Matrix for a Flight on a Circular Orbit," ARS Journal, Vol. 32, No. 9, p 1416, September 1962.
- Wolaver, L. E., "Derivation and Burnout Errors," "A Study of the Satellite Equations of Motion," WADC Aeronautical Research Laboratory, WCLJY Internal Memo 58-0, Part I, March 1958.
- Zajac, E. E., "Damping of a Gravitationally Oriented Two-Body Satellite," ARS Journal, Vol. 32, No. 12, p 1871, December 1962.
- "Analytical Investigation to Determine the Dynamic Requirements of Missile Flight Control Systems," Systems Technology, Inc., Report No. TN-3, 6 January 1959.
- "Detection and Analysis of Missile Guidance Systems," ITT Laboratories, Fort Wayne, Indiana, August 1958 to February 1961.
- 1st Quarterly Report, August 1958.
 2nd Quarterly Report 72001, March 1959.
 3rd Quarterly Report 72027, October 1959.
 4th Quarterly Report 72037, November 1959.
 5th Quarterly Report 72042, November 1959.
 6th Quarterly Report 72050, December 1959.
 7th Quarterly Report 72082, May 1960.
 8th Quarterly Report 72095, July 1960.
 9th Quarterly Report 72143, January 1961.
 10th Quarterly Report 72155, February 1961.
- "Developmental Star Tracker Final Report," Santa Barbara Research Department, Santa Barbara, California, Report No. 1030-F, July 1956.
- "Doppler Velocity for Space Navigation," General Precision Laboratory, New York, Interim Engineering Reports Nos. A18-3 and A18-4.
- "First Quarterly Engineering Report on the Study of Electromagnetic Phenomena for Space Navigation," The Franklin Institute, Philadelphia, Pennsylvania, Report No. Q-A2183-1, 1 July to 30 September 1958.
- "First Quarterly Technical Note on Study of Automatic Position Fixing," General Precision Laboratory, New York, Report No. A20-1, 1 December 1958.
- "Guidance and Control; Trajectories; Radio Propagation," Transactions of Second Technical Symposium on Ballistic Missiles, Ramo-Woolbridge, AFBMD, ARDC, Vol. II, 12 to 14 June 1957.
- "Proceedings of the National Specialists Meetings on Guidance of Aerospace Vehicles," Institute of the Aeronautical Sciences, New York, 1960.
- Antes, L. L.
 "Command and Data Link for an Astronomical Satellite."
 Spradlin, L. W.
 "The Long-Time Satellite Rendezvous Trajectory."
 Lowry, J. H., Jr. and Buehrle, C. D.
 "Guidance and Control of Point Return Vehicles,"

- Haywood, W. J., Jr.
"Application of Optical Techniques to Interplanetary Navigation."
Ormsby, R. D.
"A Free Reaction Sphere Satellite Attitude Control System."
Useller, J. W. and Algranti, J. S.
"Pilot Control of Space Vehicle Tumbling."
Alonso, R. L. and Laning, J. H., Jr.
"Design Principles for a Control Computer for Space Guidance."
Grube, R. H.
"Terminal Guidance for Lunar and Planetary Probes."
- "Study of Satellite Guidance Sensors," Radiation, Inc., Final Technical Report No. IR-1761-VI, Orlando, Florida, 2 Vols., January 1961.
- "Technique Development of Orbital Guidance Equipment for Satellite Vehicles," Radiation, Inc., Orlando, Florida, April 1959 to July 1960.
Quarterly Technical Note 1188-59-01, April 1959.
Quarterly Technical Note 1188-59-02, July 1959.
Quarterly Technical Note 1188-59-03, October 1959.
Quarterly Technical Note 1188-59-04, January 1960.
Quarterly Technical Note 1188-60-01, April 1960.
Quarterly Technical Note 1188-60-02, July 1960.
- Techniques of Indication and Control for Inertial Guidance of Ballistic Missiles," Massachusetts Institute of Technology, Cambridge, Massachusetts, Instrumentation Laboratory, February 1959.
- "Radio and Inertial Guidance," Transactions of the First Technical Symposium on Ballistic Missiles, Ramo-Wooldridge, Report No. GM 01.1-266, Vols. 1 and 2, 21 and 22 June 1956.
- "Radio and Inertial Guidance," Transactions of the Second Technical Symposium on Ballistic Missiles. Ramo-Wooldridge, Report No. GM TR 202, Vols. 1 and 2, 12 to 14 June 1957.
- "Radio and Inertial Guidance," Transactions of the Third Technical Symposium on Ballistic Missiles, Ramo-Wooldridge, Vols. 1 and 2, 14 to 15 July 1958.
- "USAF Symposium on Guidance of Ballistic Missiles and Space Vehicles," WADC TR 58-270, March 1958.
- Adams, J. J. and Chilton, R. E.
"A Weight Comparison of Several Attitude Control Systems for Satellites," NASA Memorandum 12-30-586, February 1959
- Arck, M. H. and Merlen, M. M.
"Horizon Sensors for Vertical Stabilization of Satellites and Space Vehicles," IAS Symposium, Boston, May 1960.
- Barnes, J. L., "Precision Position and Attitude Control for Synchronous Satellites," Stockholm, XIth International Astronautical Congress, Astrodynamics Colloquium, 1960.
- Chatkoff, M. and Lynch, G., "Attitude Control of a Space Vehicle by a Gyroscopic Reference Unit," Aero/Space Engineering, Vol. 19, May 1960.
- Davis, W. R., "Determination of a Unique Attitude for an Earth Satellite," American Astronautical Society, 4th Annual Meeting, New York, January 1958.
- DeLisle, J. E., et al., "Attitude Control of Spacecraft," Astronautics, Vol. 6, No. 11, November 1961.
- Freed, L. E., "Attitude Control System for a Spinning Body," Institute of Aerospace Sciences, Preprint No. 61-207-1901, June 1961.
- Gates, C. R., "Attitude Control of Space Vehicles," California Institute of Technology, Pasadena, California, Jet Propulsion Laboratory, JPL Report No. EP 795, February 5, 1960. (Presented at the National Automatic Control Conference, Dallas, Texas, November 4 to 6, 1959.)
- Gillespie, W., Jr., "Some Notes on Attitude Control on Earth Satellite Vehicles," NASA TN D-40, December 1959.
- Grasshoff, L., "Method for Controlling the Attitude of a Spin-Stabilized Satellite," ARS Journal, Vol. 31, No. 5, 1961.
- Haeussermann, W. E., "Recent Advances in Attitude Control of Space Vehicles," ARS Journal Vol. 32, No. 2, p 188, February 1962.
- Kalman, R. E. and Bertrom, J. E., "Control System Analyses and Design via the Second Method of Liapunov," RIAS, Inc., Baltimore, Maryland, Monograph 59-13. (Also, ASME Paper No. 59-NAC-2, 1959.)
- Levin, S. M. and Manusevich, L. G., "A Vector Method for Calculating One Class of Control Systems," Automation and Remote Control, Vol. 21, No. 10, pp 962 to 970, October 1960.
- Lillestrand, R. L., "Use of a Stellar Aberrator in Space Systems," XIth International Astronautical Congress, Astrodynamics Colloquium, Stockholm, 1960.
- Litovchenko, I. A., "On a Problem of Optimum Control," Automation and Remote Control, Vol. 21, No. 8, pp 791 to 798, August 1960.
- Mueller, H., "An Attitude Control System for Extremely Small Control Forces," XIth International Astronautical Congress, Astrodynamics Colloquium, Stockholm, 1960.
- Ormsby, R., "Capabilities and Limitations of Reaction Spheres for Attitude Control," ARS Journal, Vol. 31, No. 6, 1961.

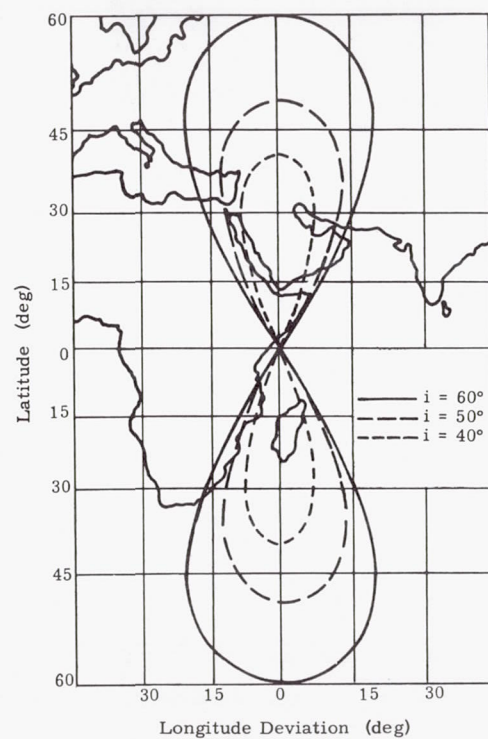


Fig. 32. Ground Tracks of Circular 24-hr Orbits

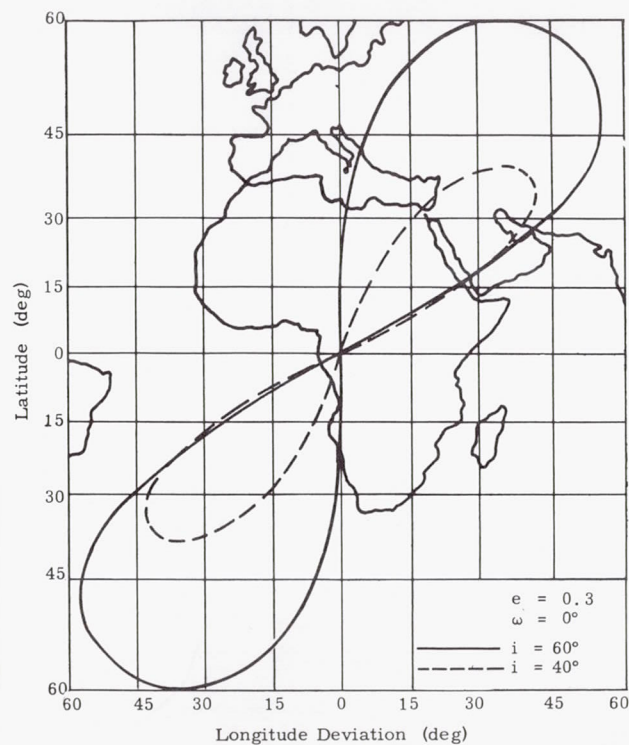


Fig. 33. Ground Tracks of Elliptical 24-hr Orbits

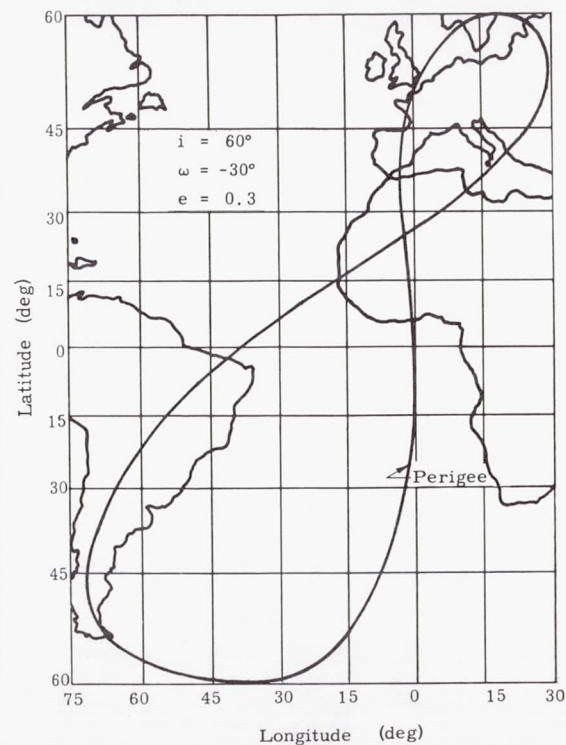


Fig. 34. Ground Track of an Elliptical 24-hr Orbit

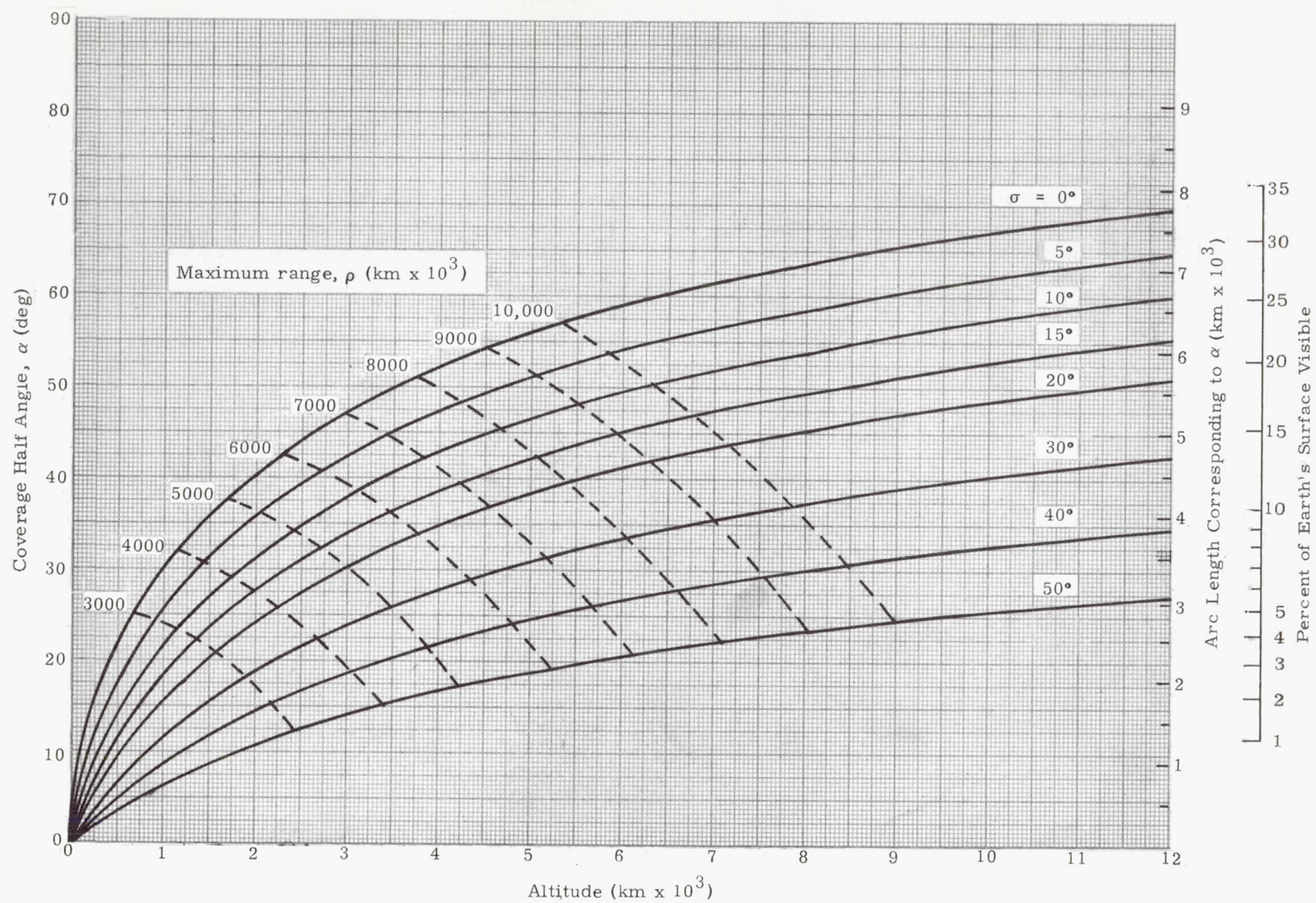


Fig. 35. Satellite Coverage

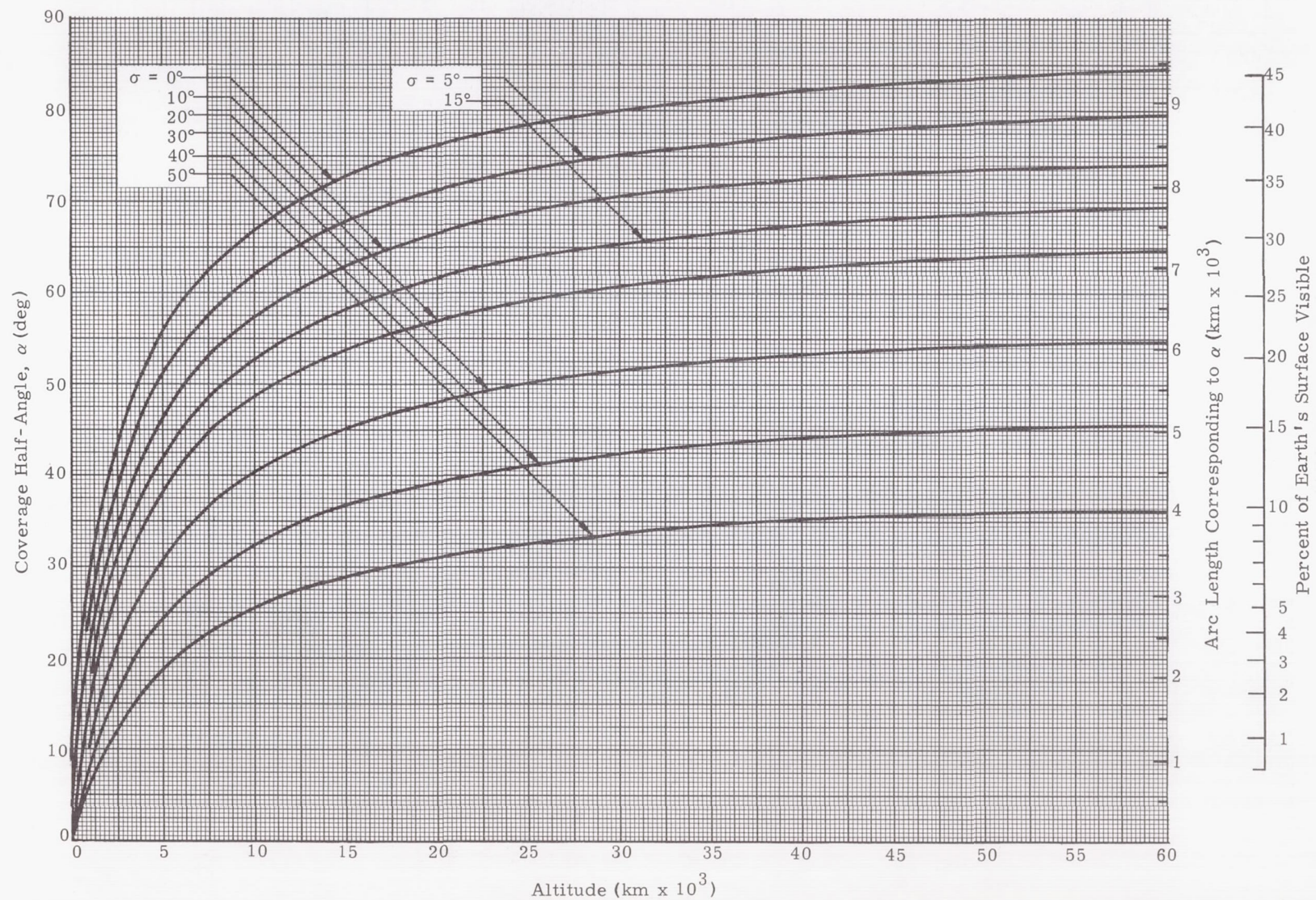


Fig. 36. Satellite Coverage

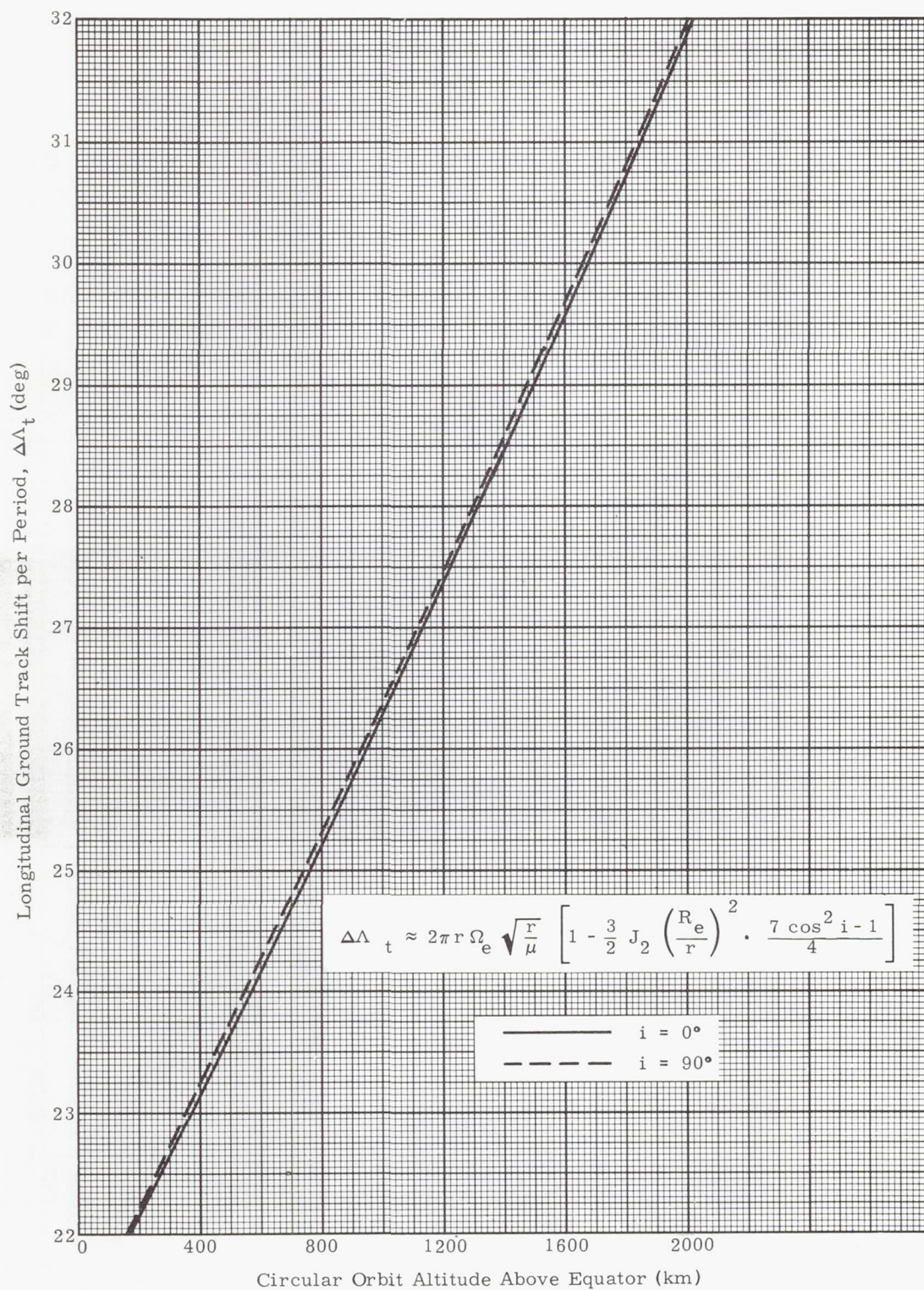


Fig. 37. Longitudinal Ground Track Shift

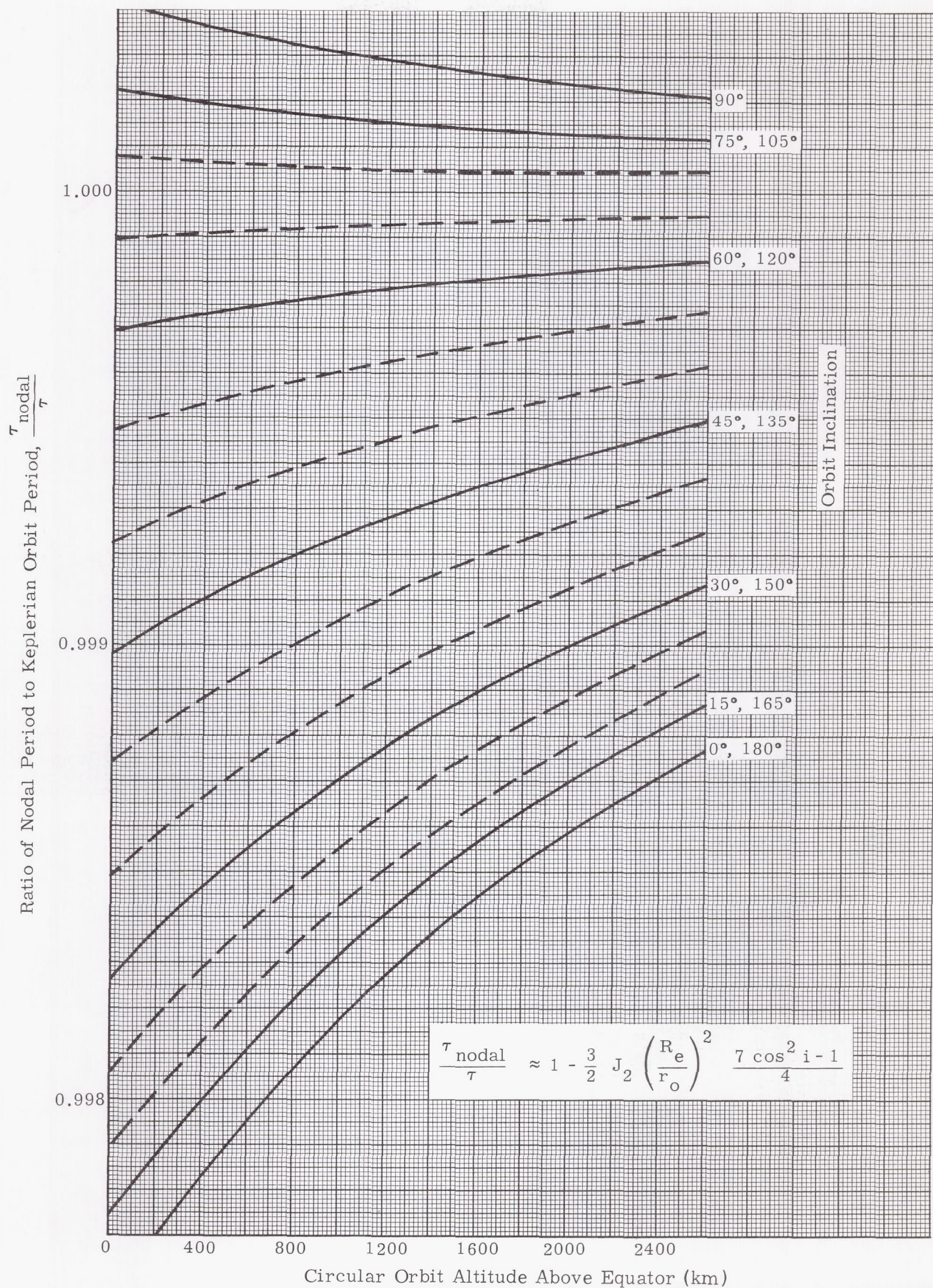


Fig. 38. Nodal Orbit Period

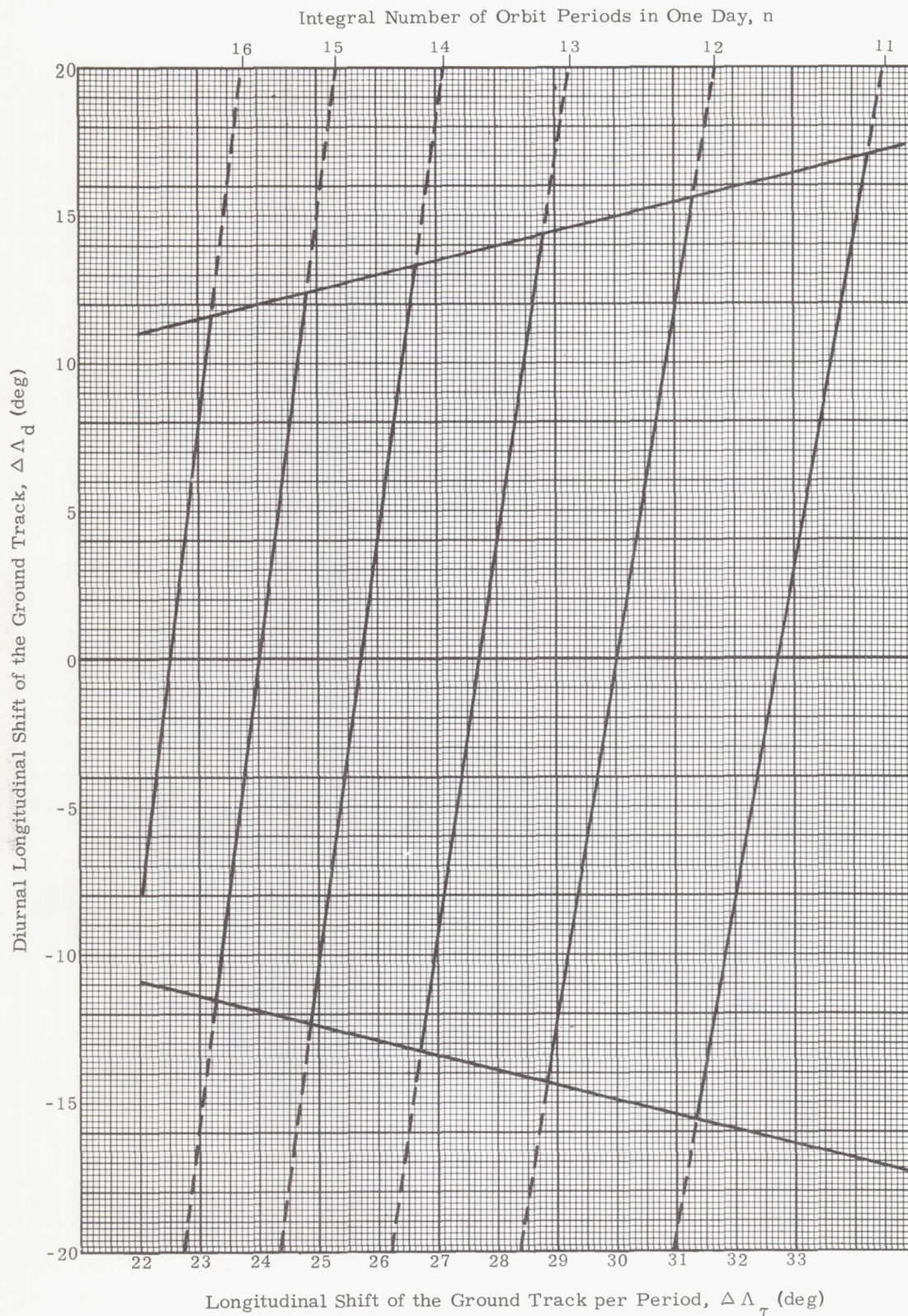


Fig. 39. Diurnal Longitudinal Shift of the Ground Track

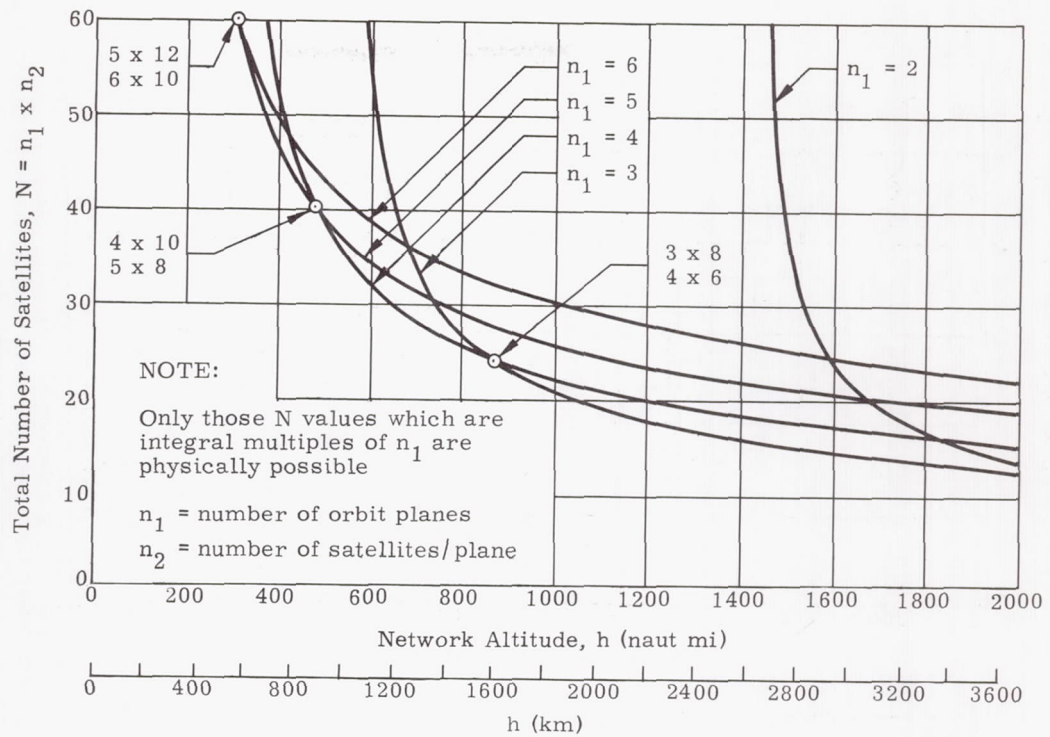


Fig. 40. Number and Distribution of Satellites in a Polar Network Providing Complete Global Coverage ($\sigma = 0$ deg)

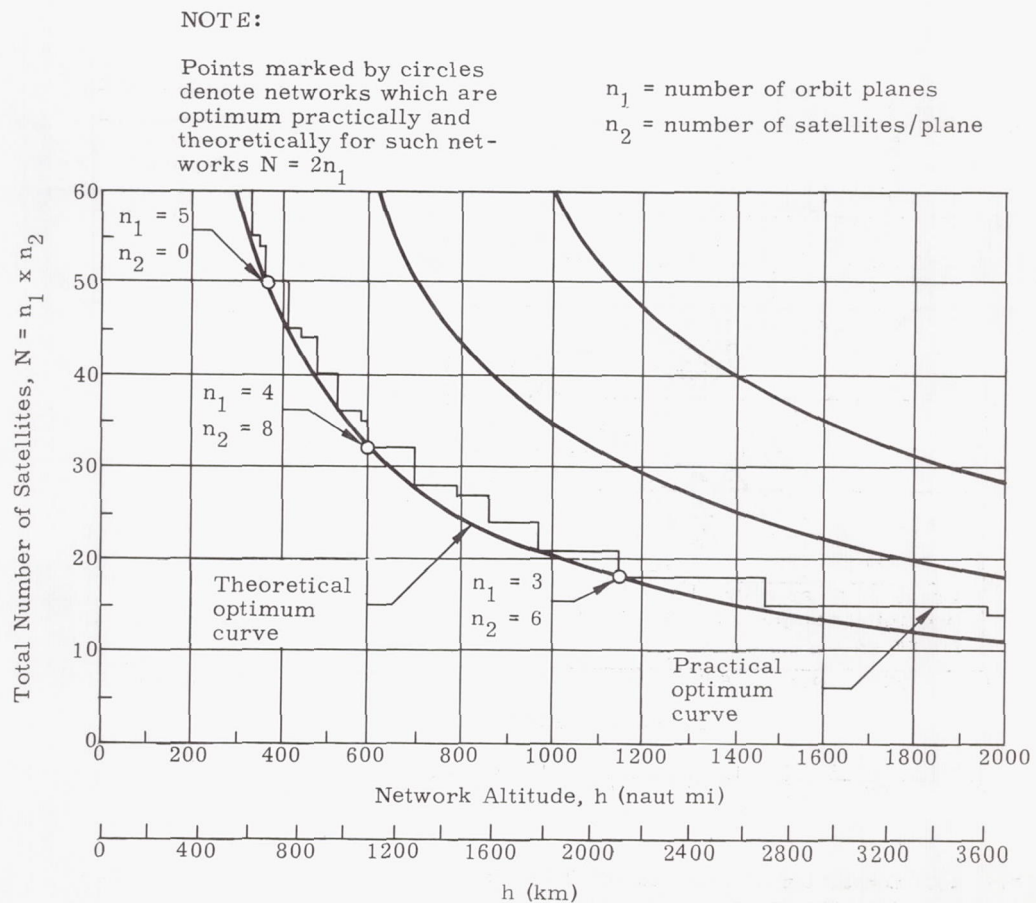


Fig. 41. Theoretical and Practical Optimum Satellite Utilization in a Polar Network Providing Complete Global Coverage

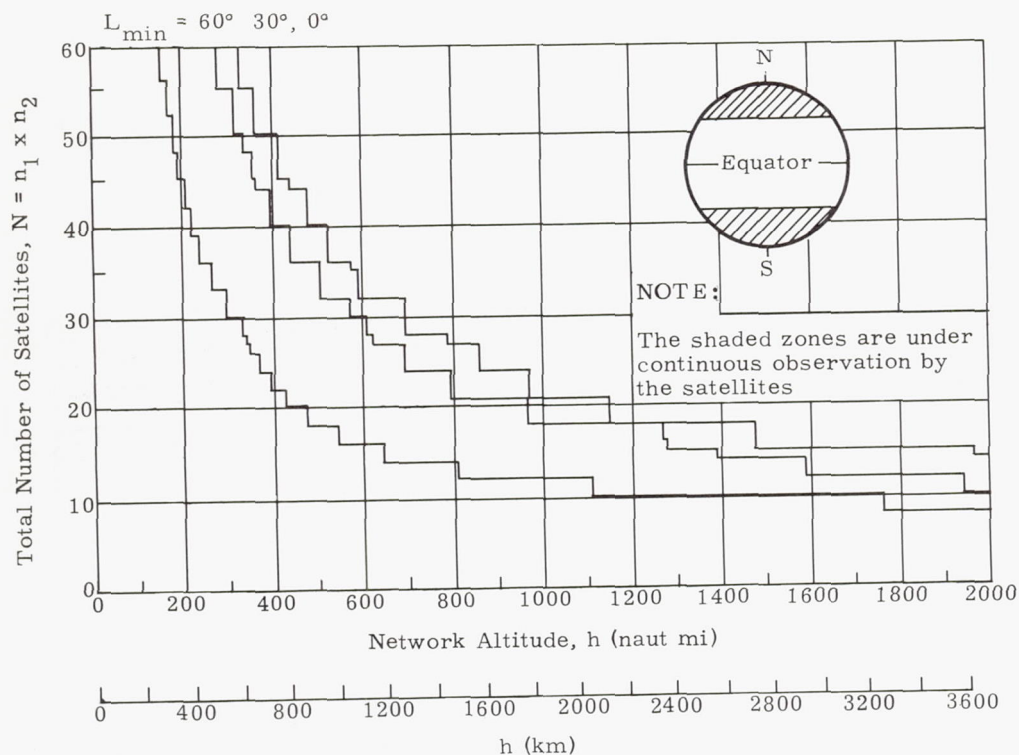


Fig. 42. Comparison of Polar Satellite Networks Providing Coverage from the Poles to Minimum Latitude, L_{\min} ($\sigma = 0$ deg)

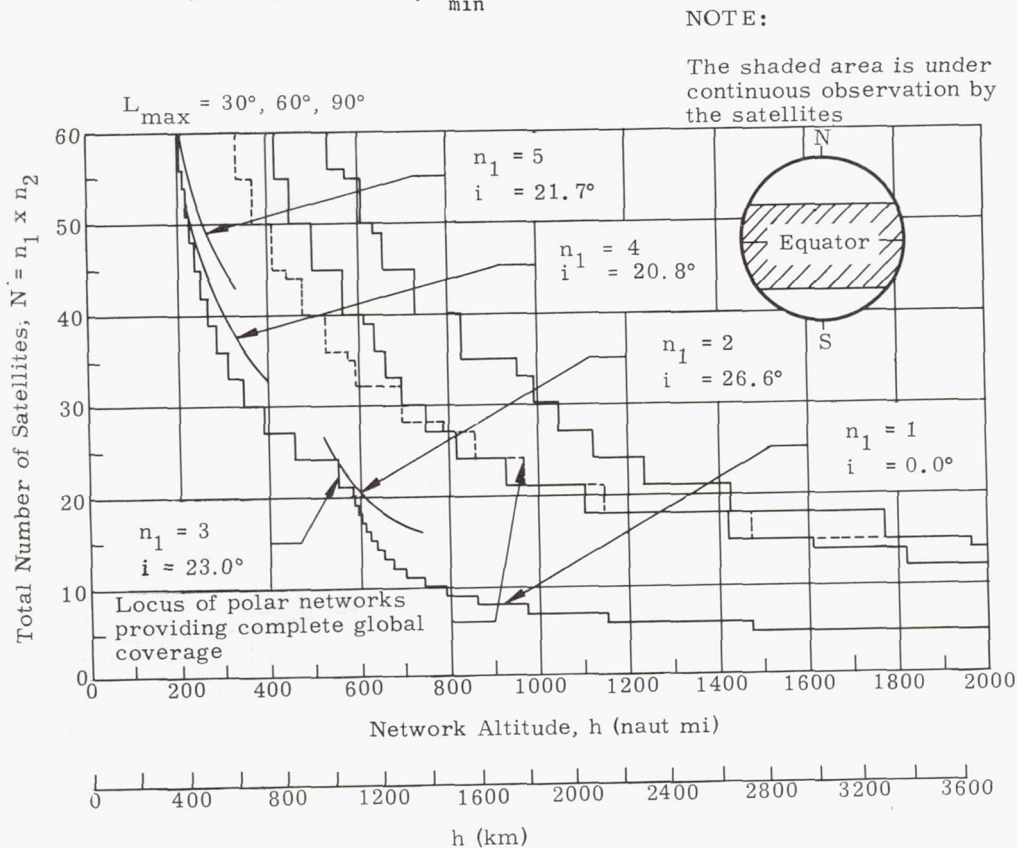


Fig. 43. Comparison of Inclined and Polar Satellite Networks Providing Coverage from the Equator to Maximum Latitude, L_{\max} ($\sigma = 0$ deg)

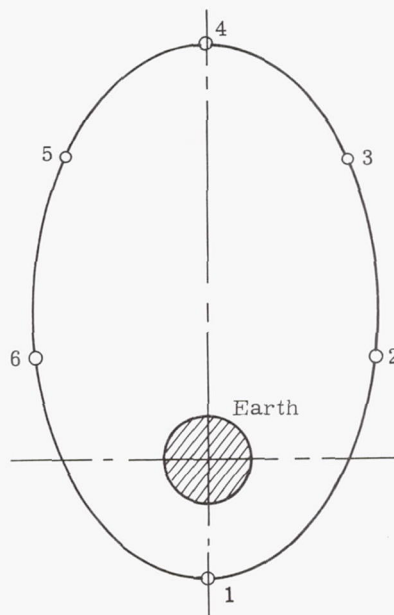
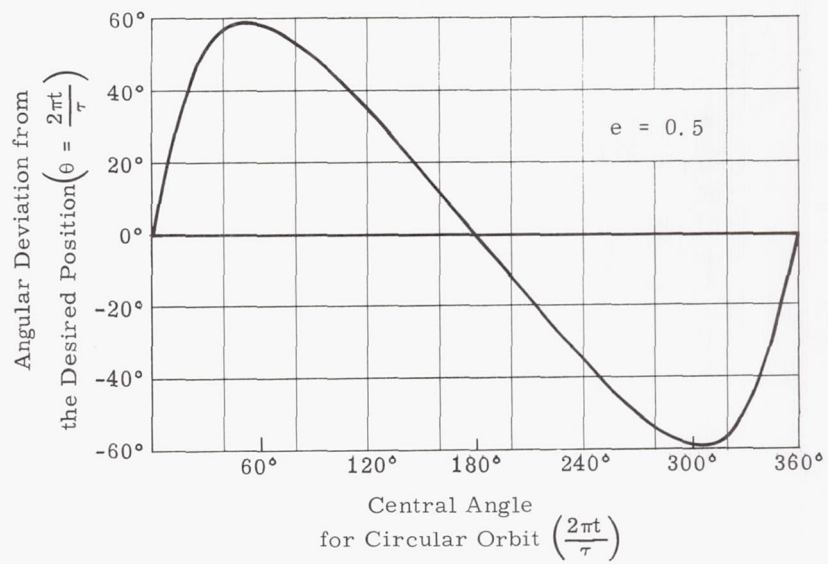


Fig. 44. Eccentricity Effects on the Spacing of Six Satellites (placed at equal time intervals)

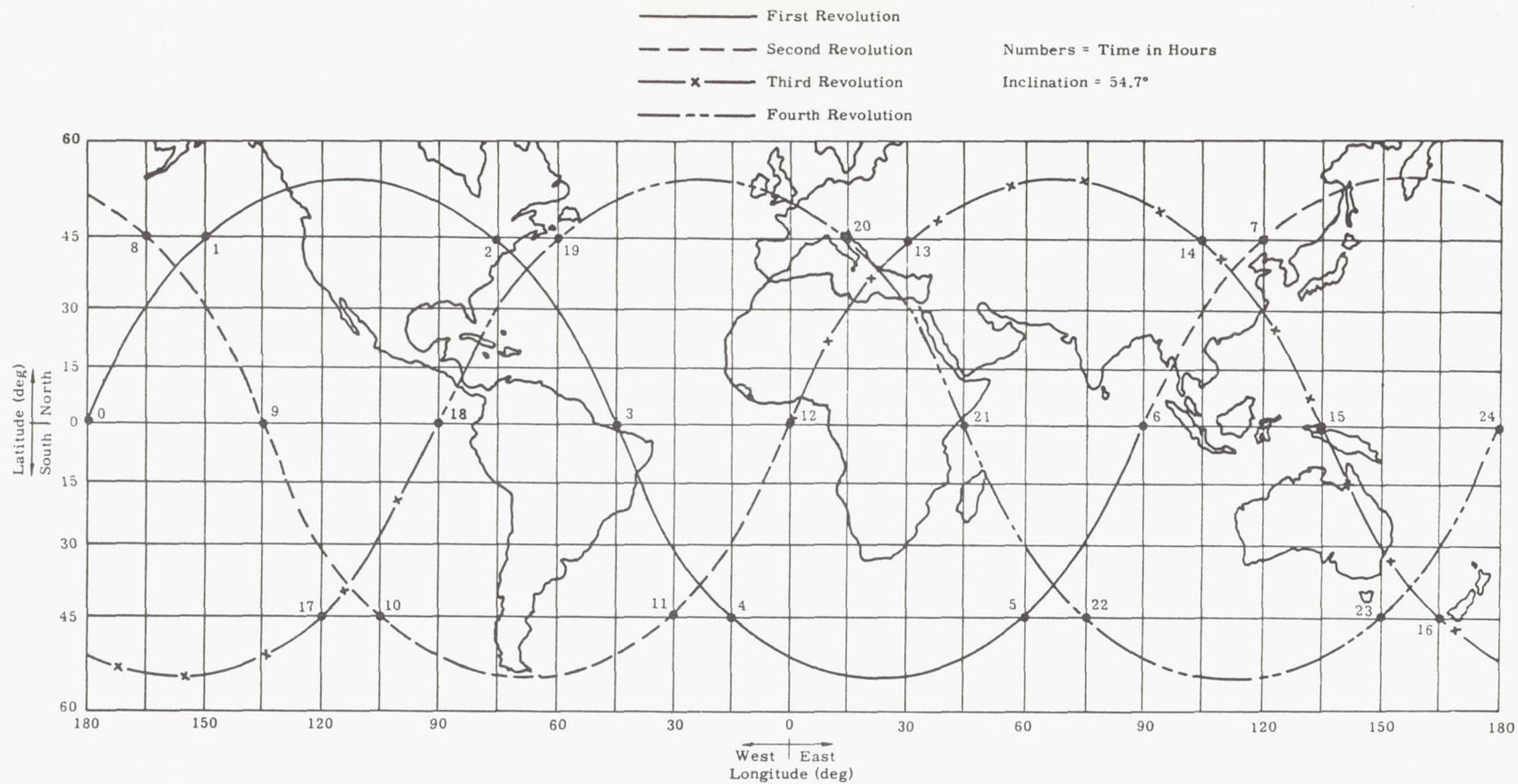


Fig. 45. Ground Track for One Satellite During a Day

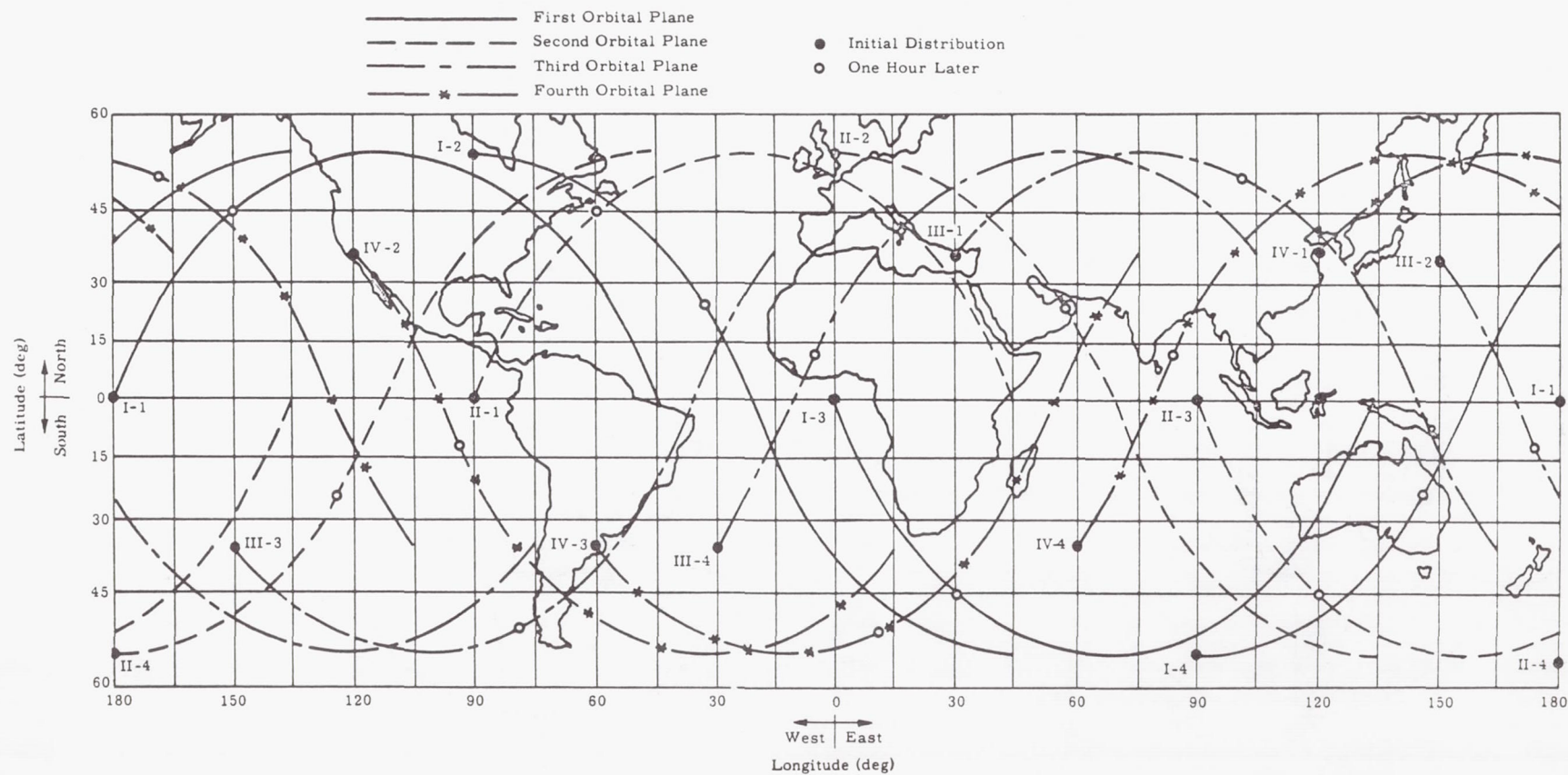


Fig. 46. Ground Tracks for 16 Satellites During Half a Revolution

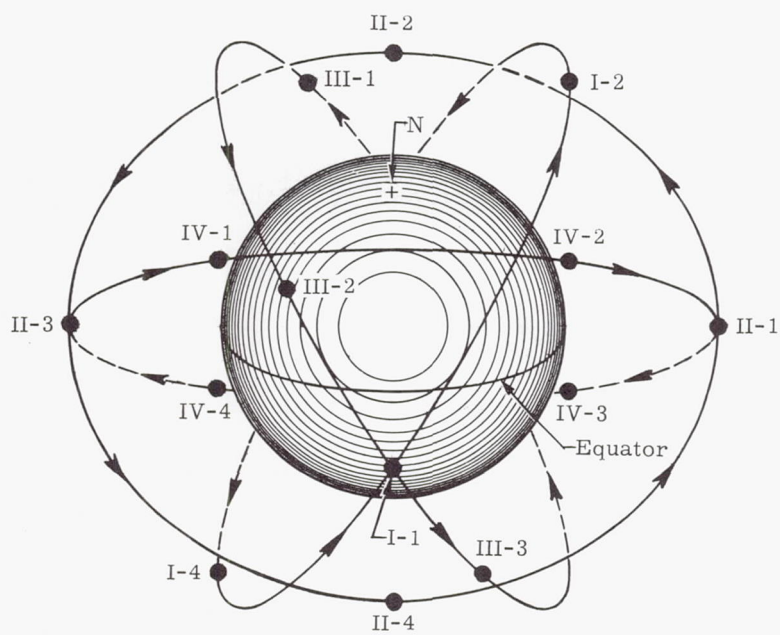
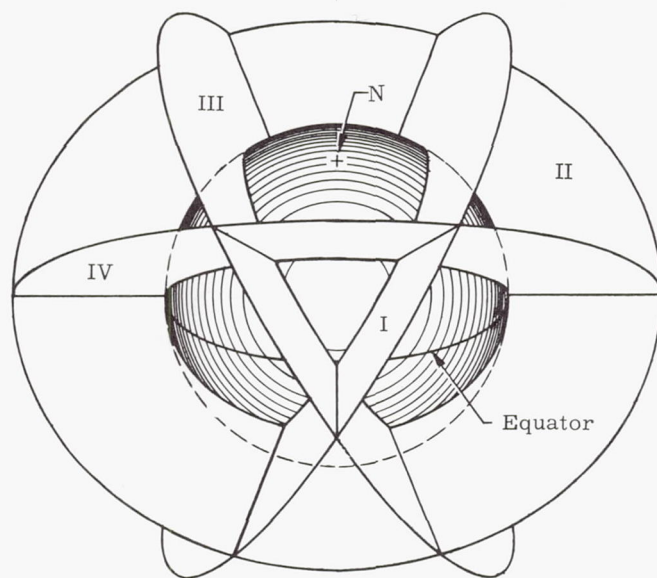


Fig. 47. Three-Dimensional Orbit Pattern

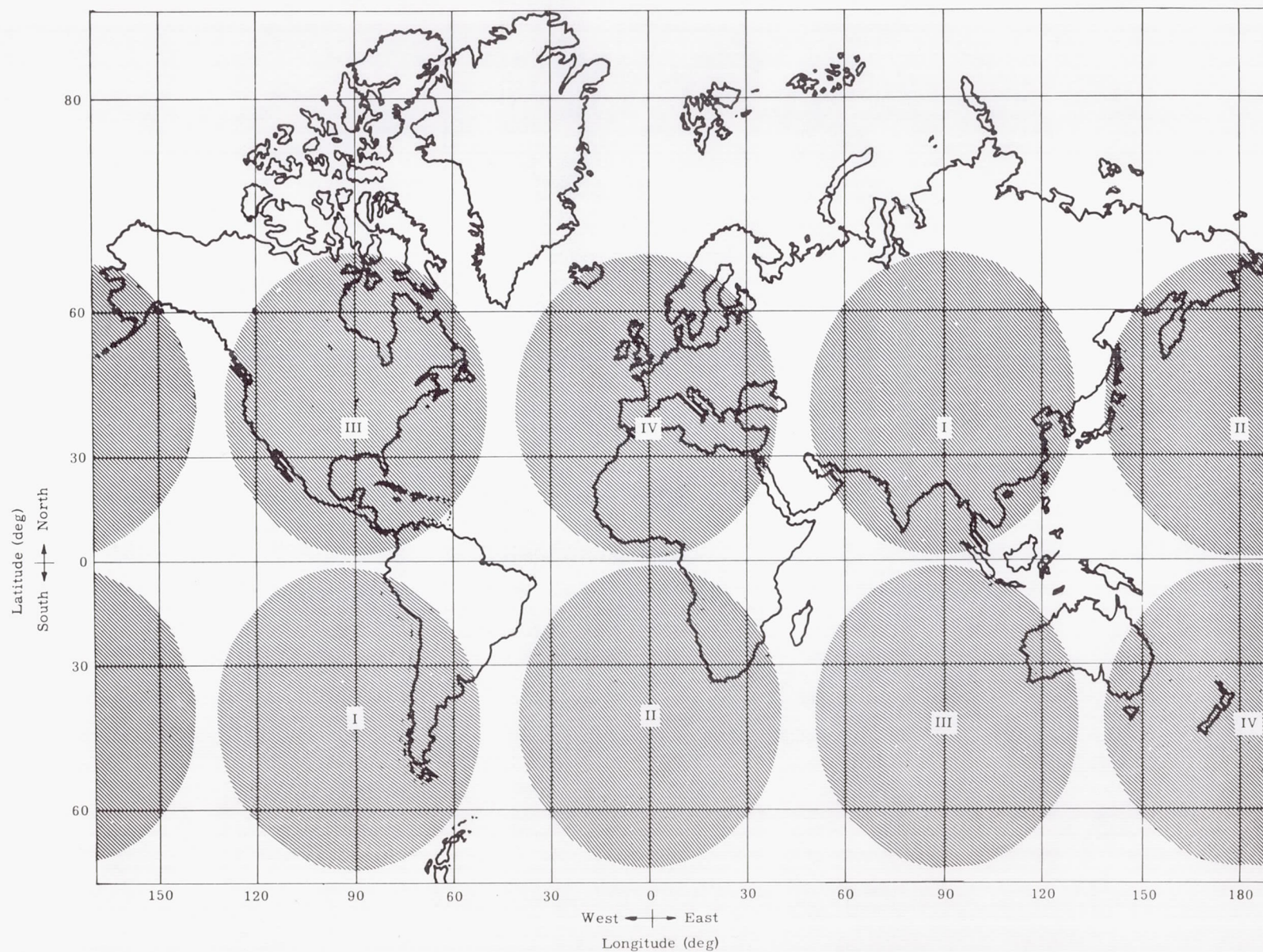


Fig. 48. Areas Not Covered by Ground Swaths at Time Zero

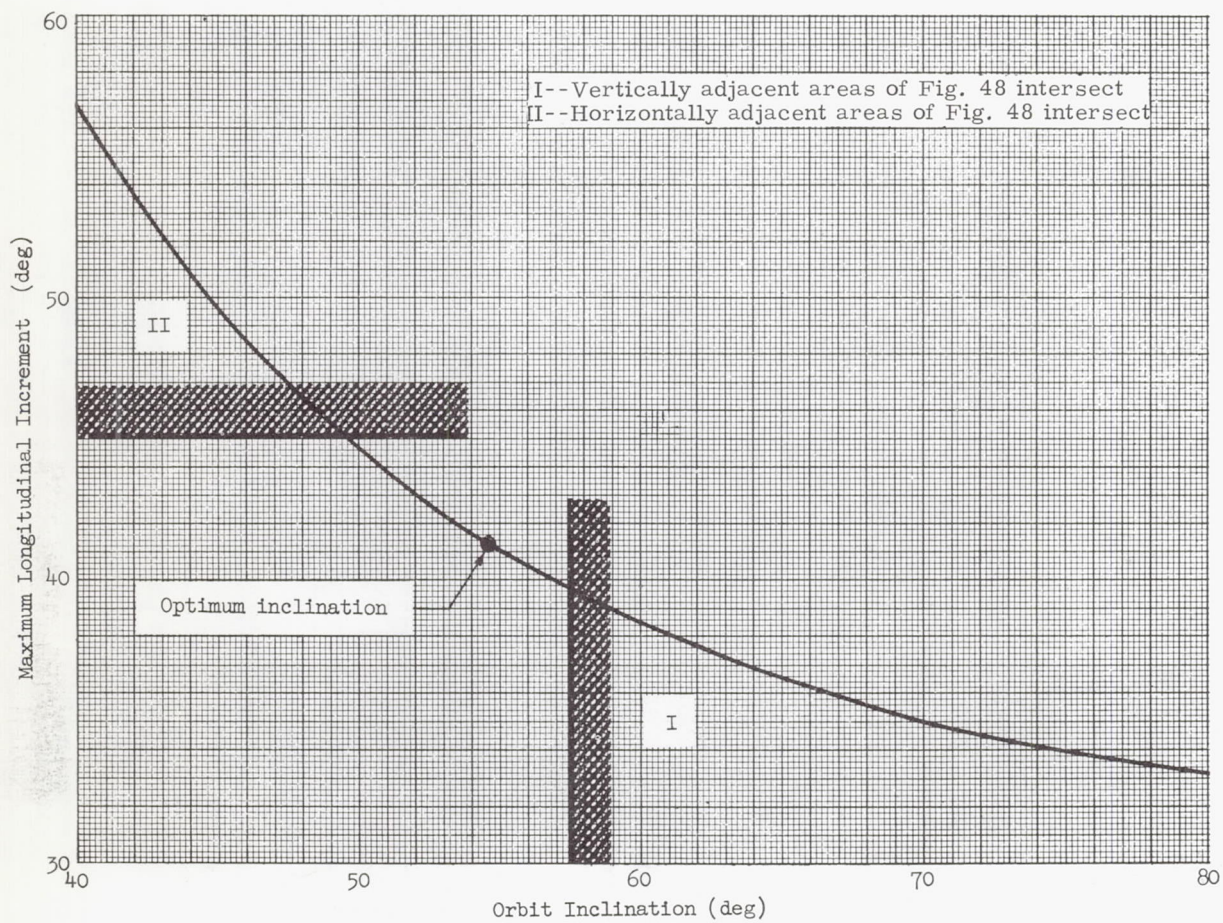


Fig. 49. Maximum Longitudinal Increment of Area Not Covered by Ground Swath as a Function of the Orbital Inclination

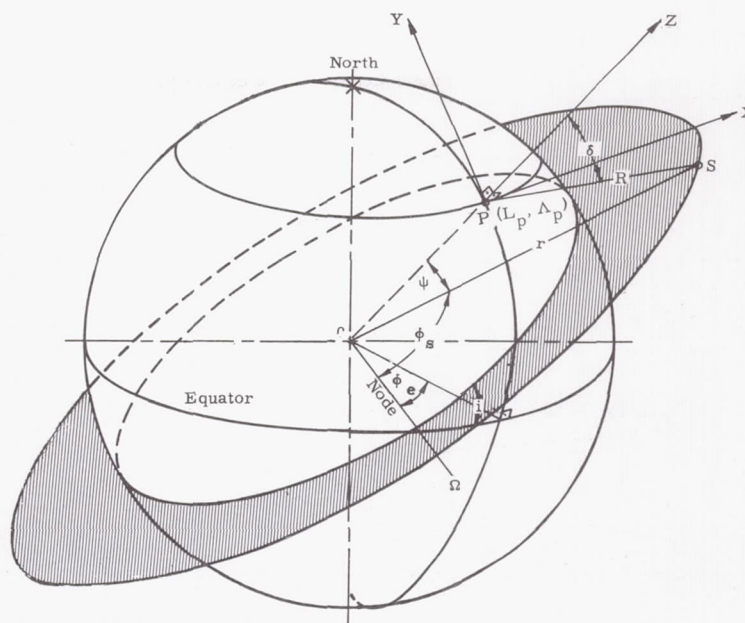


Fig. 50. The Coordinate System for Satellite Tracking

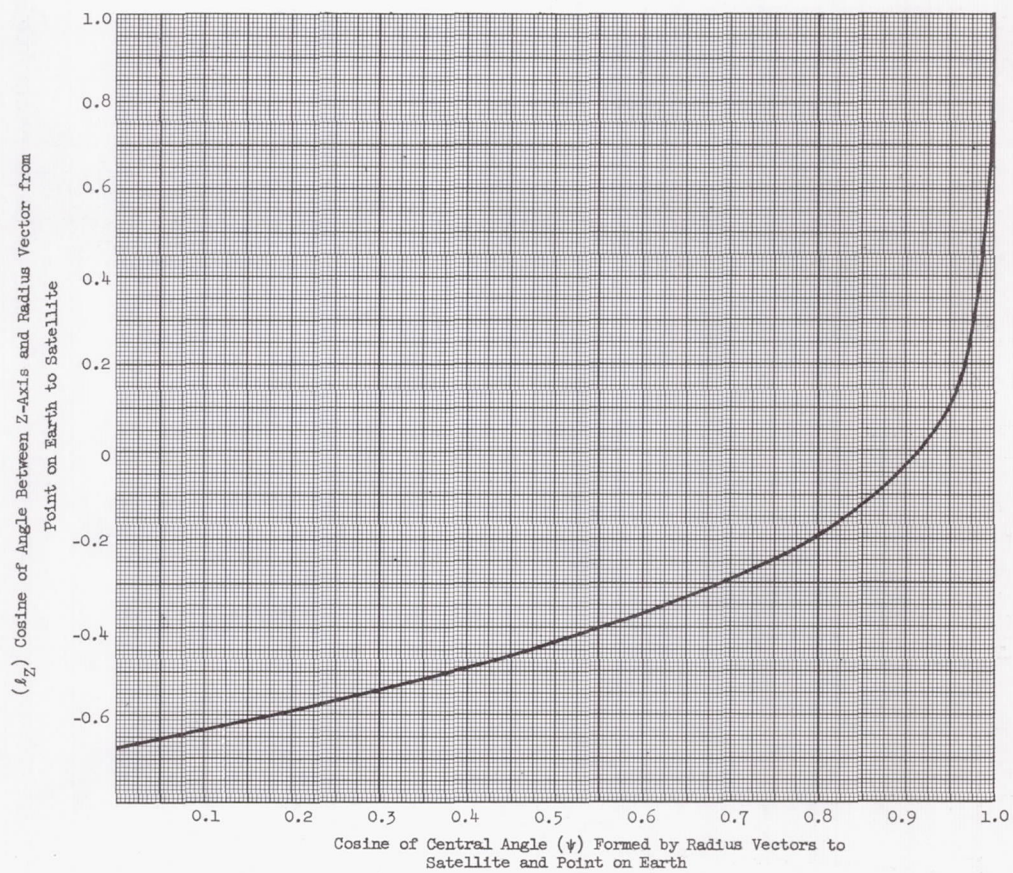
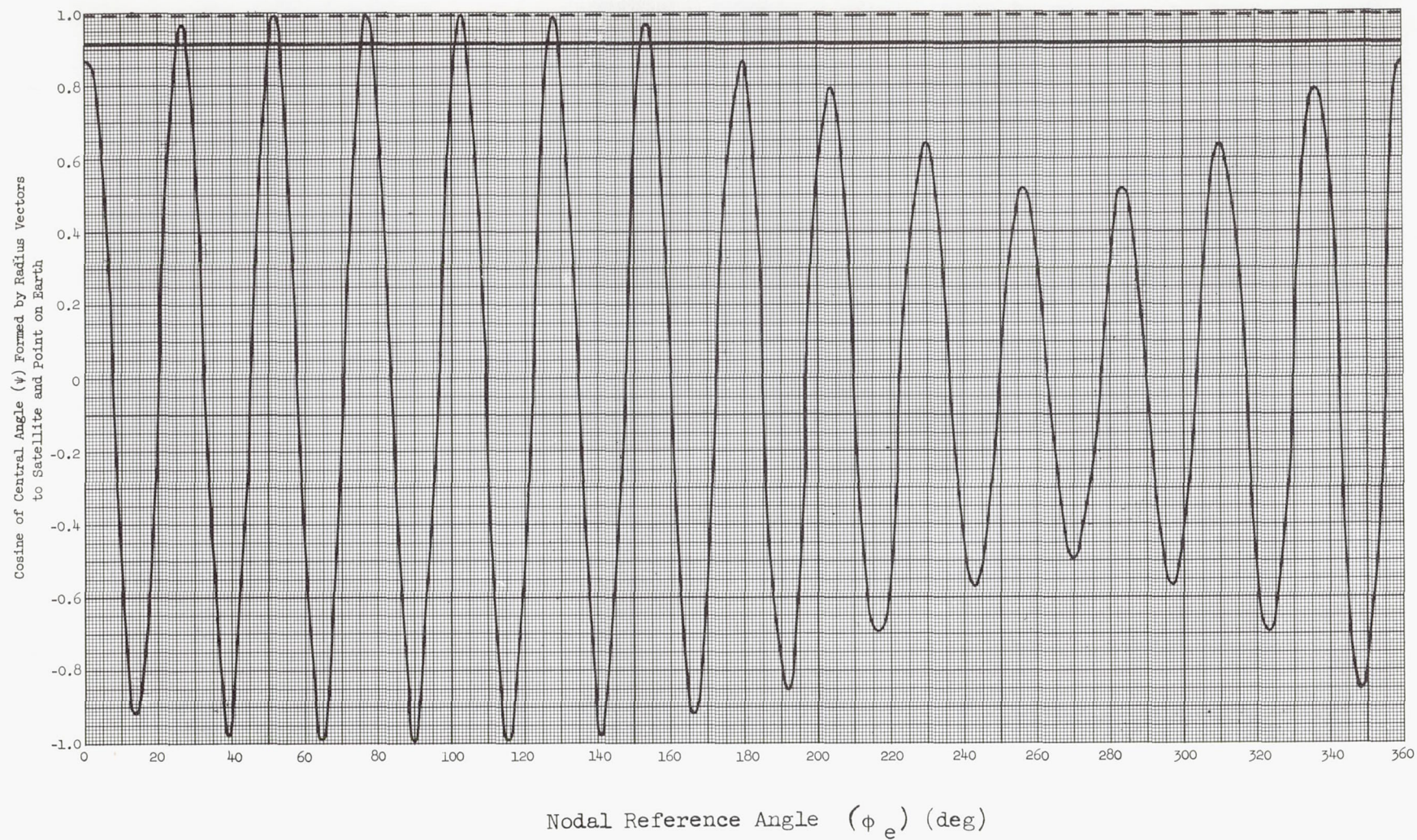


Fig. 51. Satellite Depression Angle Relative to Local Vertical

Fig. 52. Cosine ψ Versus Nodal Reference Angle

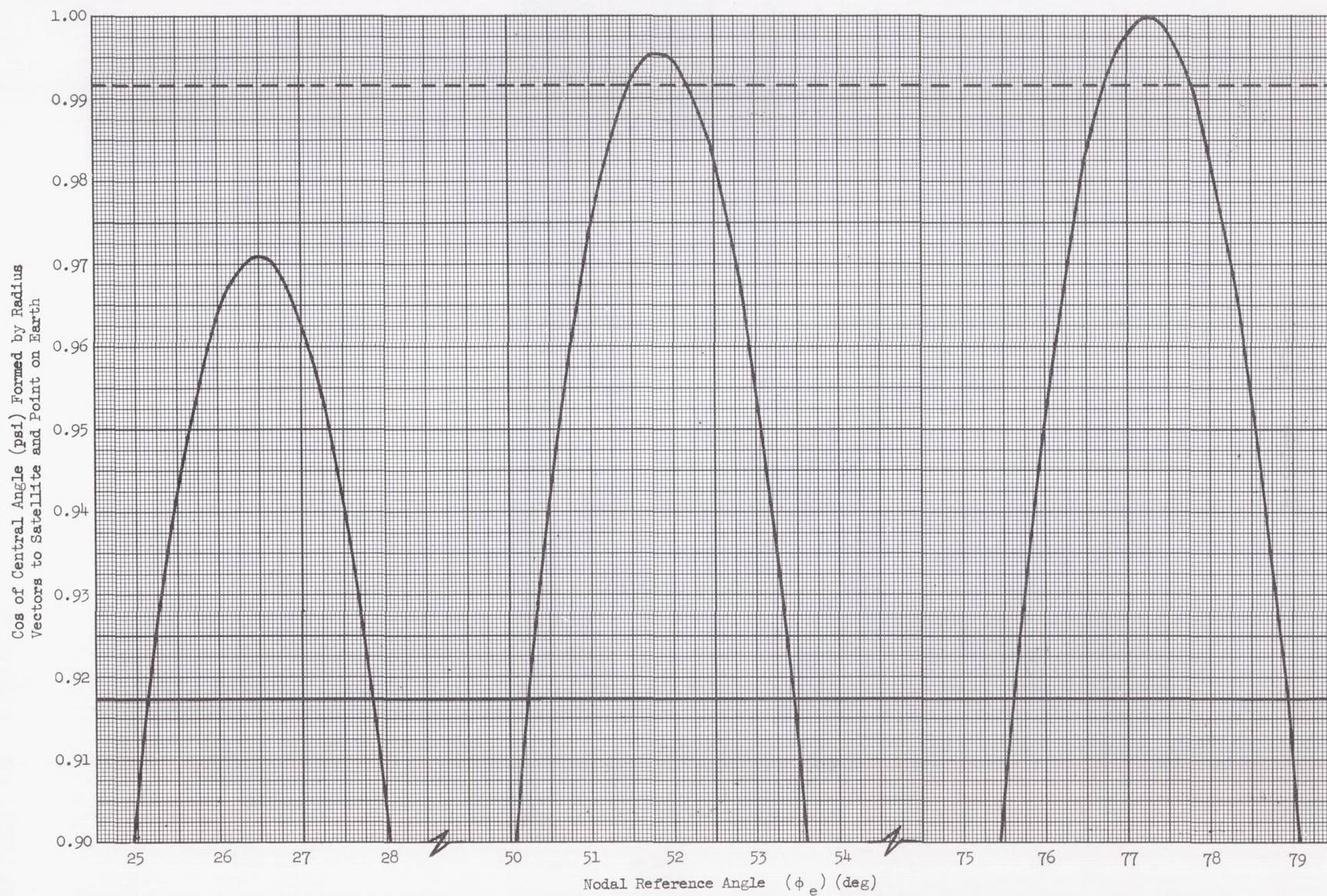


Fig. 53. Cosine ψ Versus Nodal Reference Angle (detailed view)

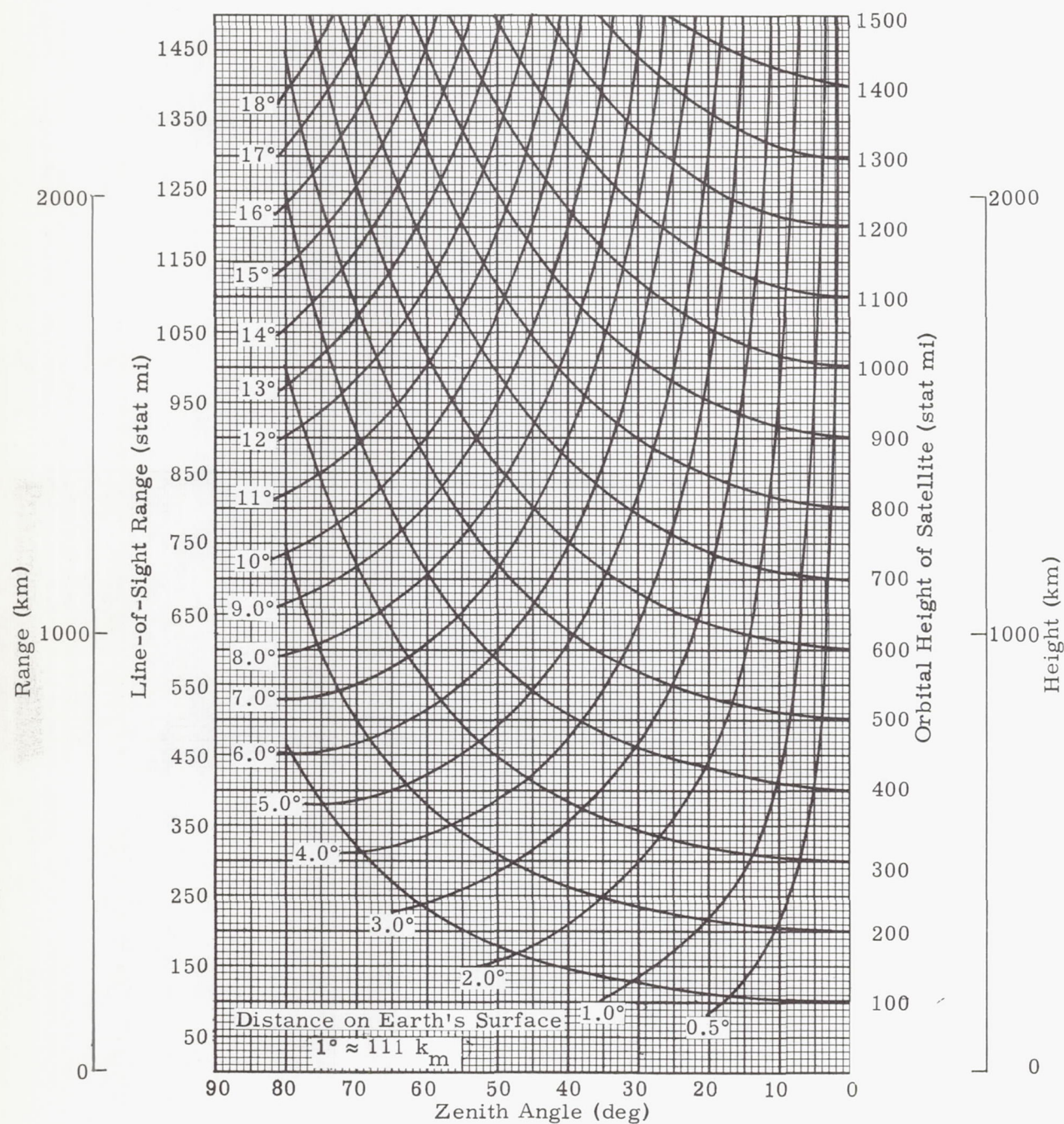


Fig. 54. Diagram for Finding the Distance at Subsattelite Point and Line-of-Sight Range

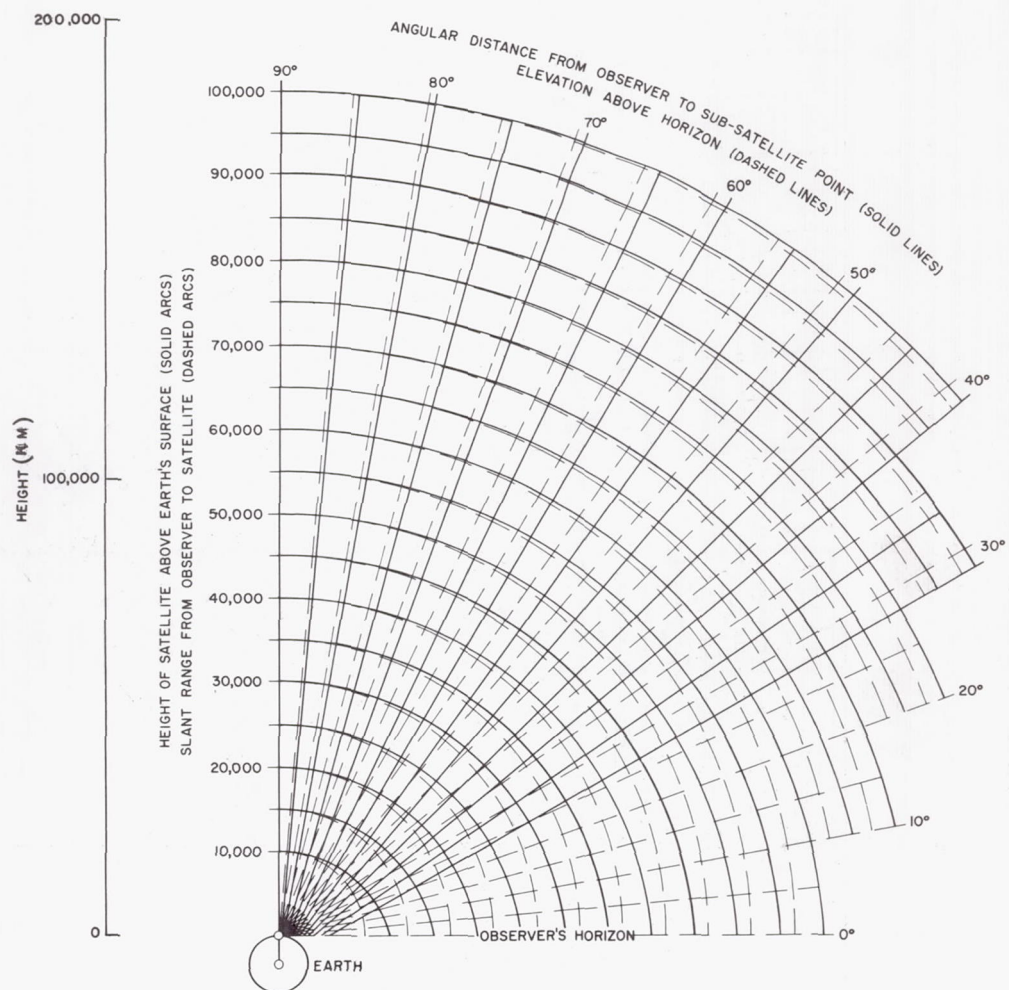


Fig. 55. Chart for Determining Elevation and Slant Range of Satellite (0 to 100,000 naut mi, 185,000 km)

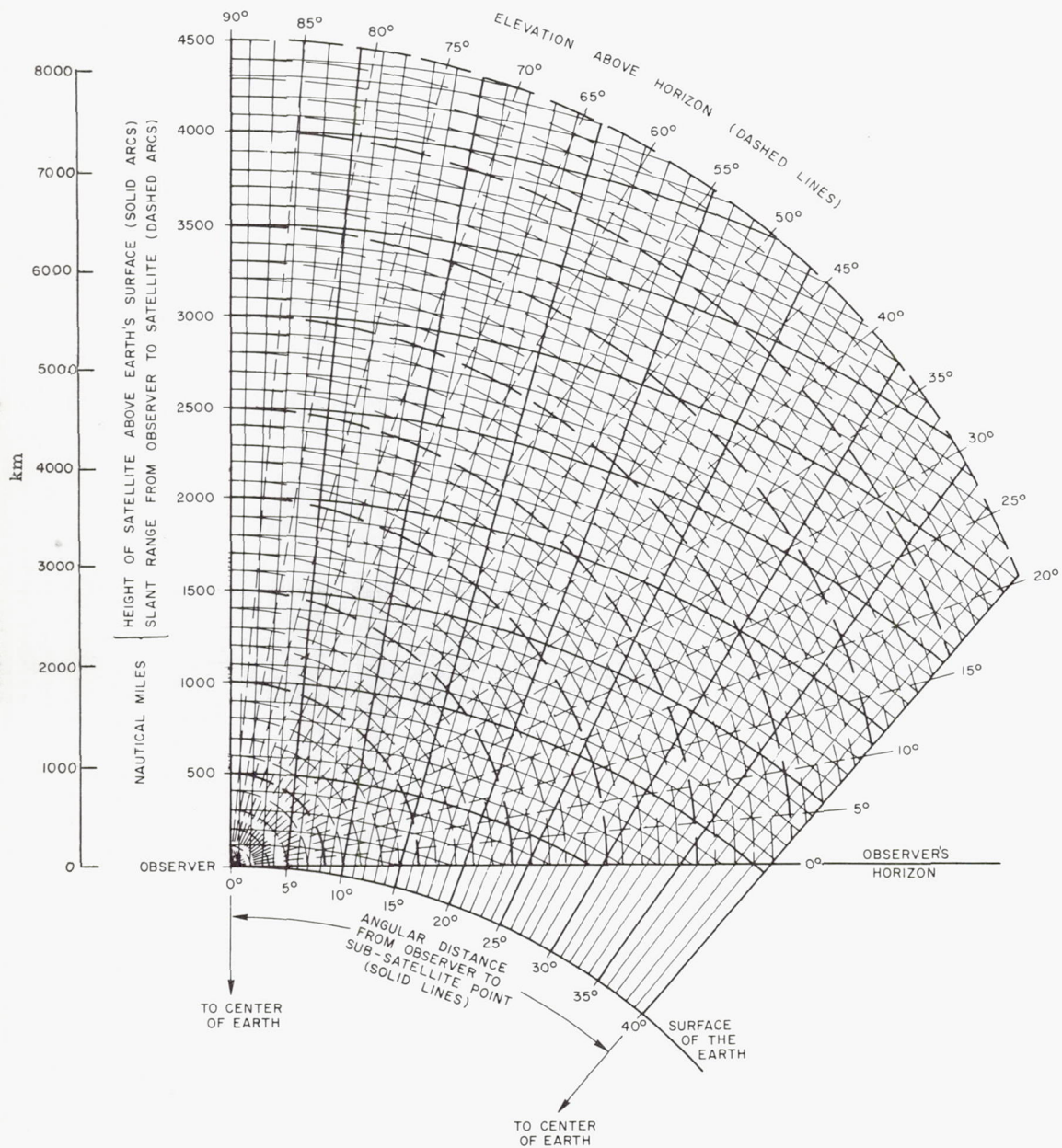


Fig. 56. Chart for Determining Elevation and Slant Range of Satellite (0 to 4500 naut mi, 8150 km)

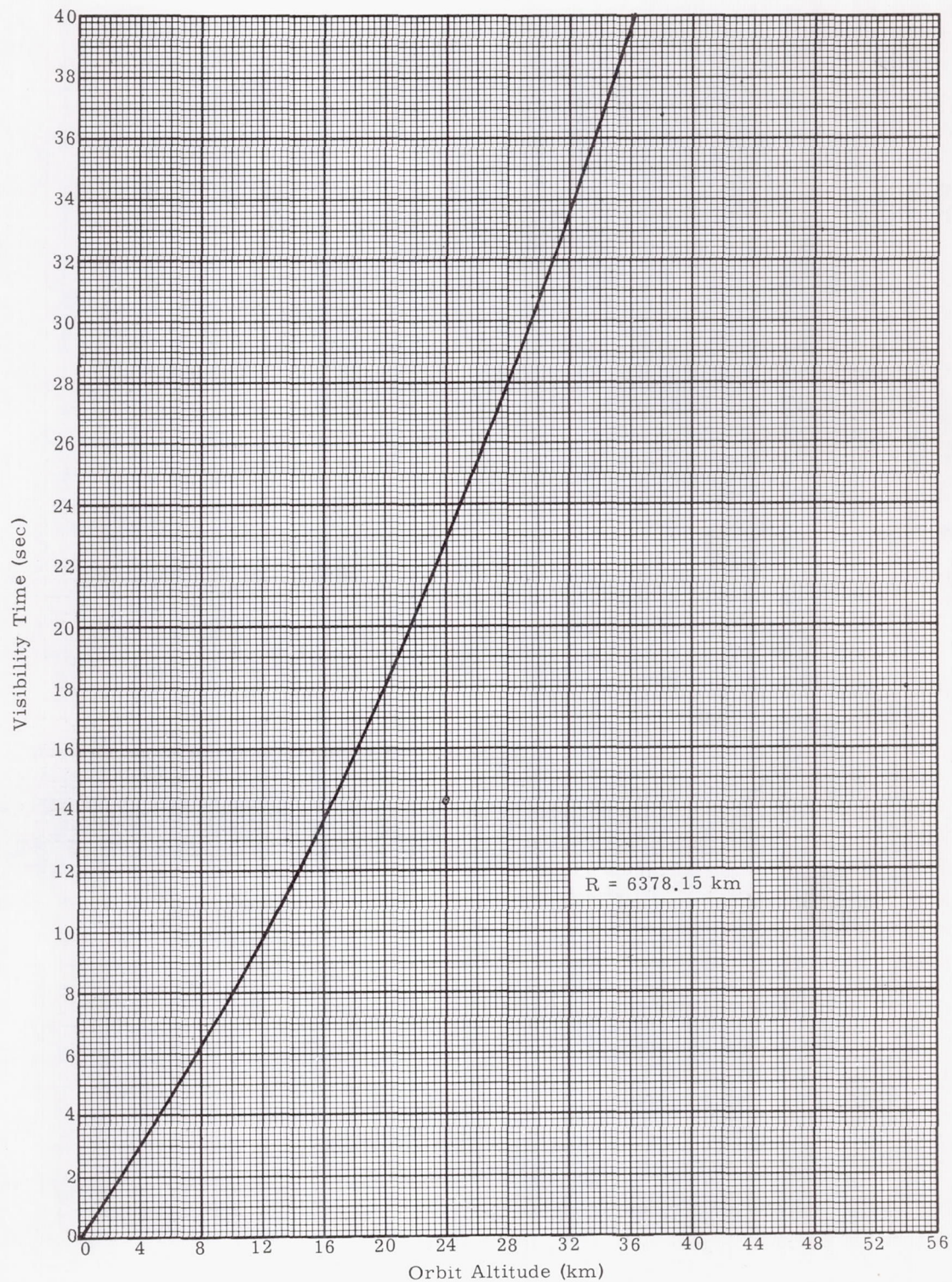


Fig. 57. Visibility Time for Circular Orbits (nonrotating earth)

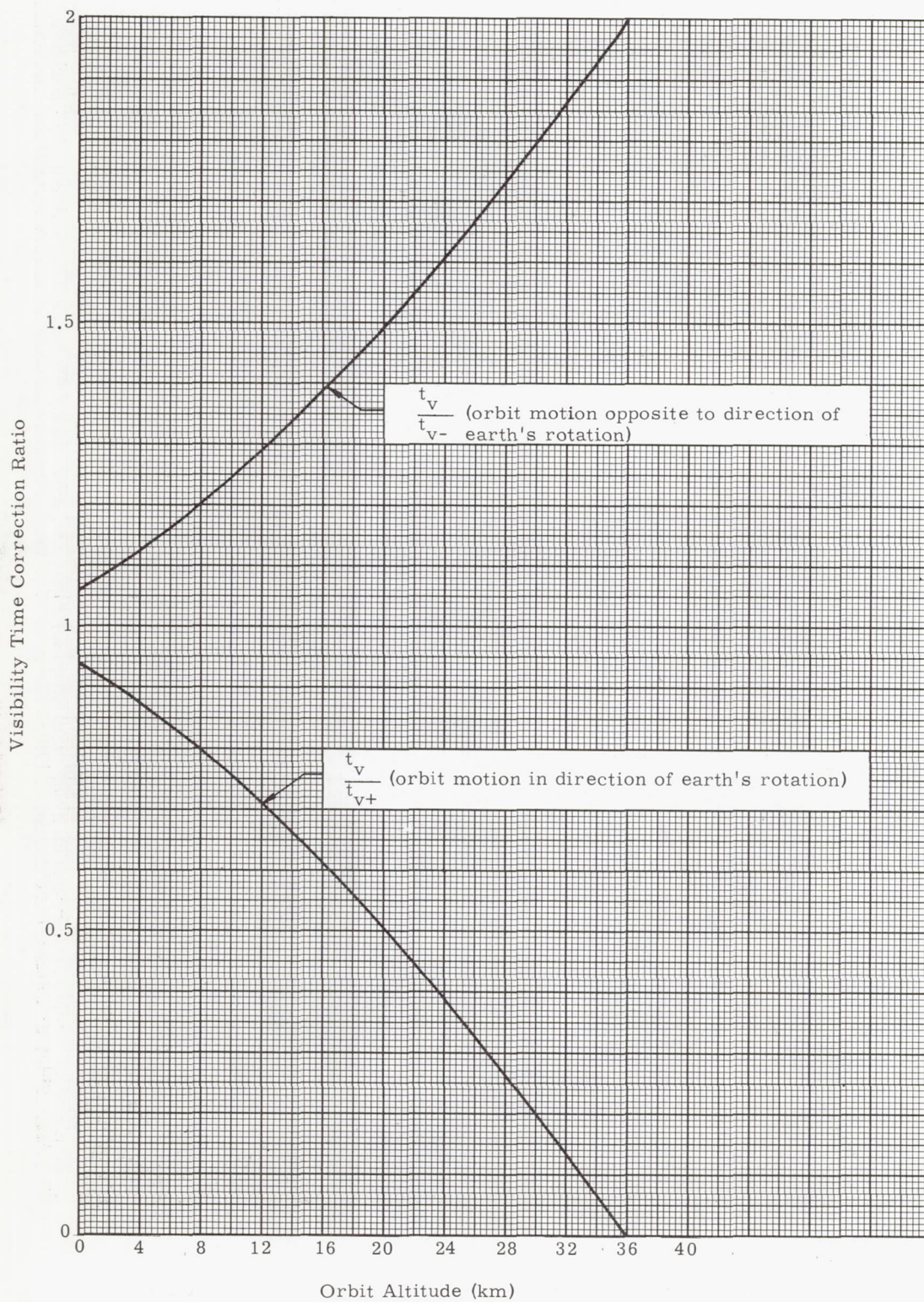


Fig. 58. Effect of Earth Rotation of Visibility Time (circular orbits)

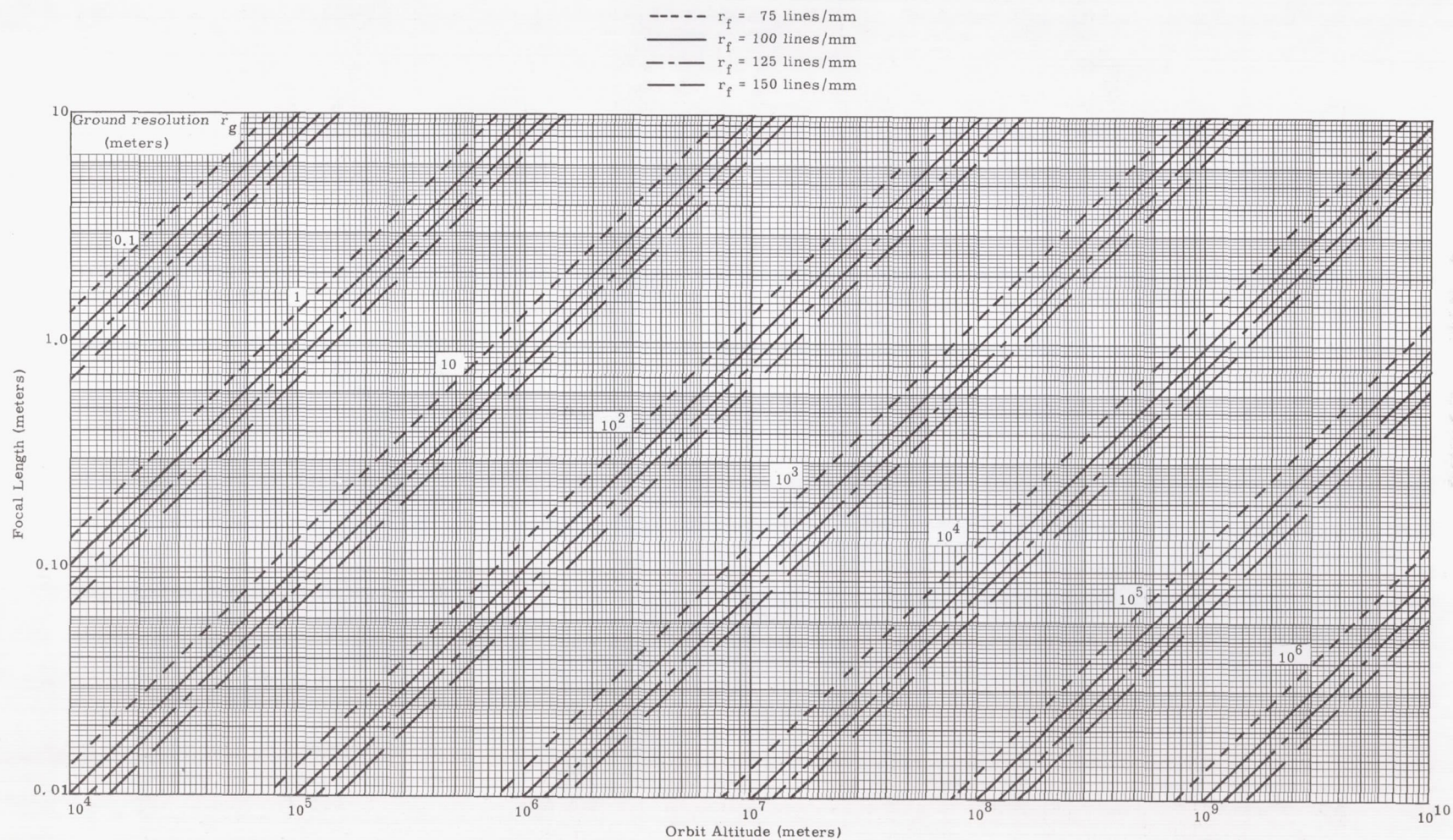


Fig. 59. Maximum Orbit Altitude as a Function of Ground Resolution Desired, Focal Length and System Resolution

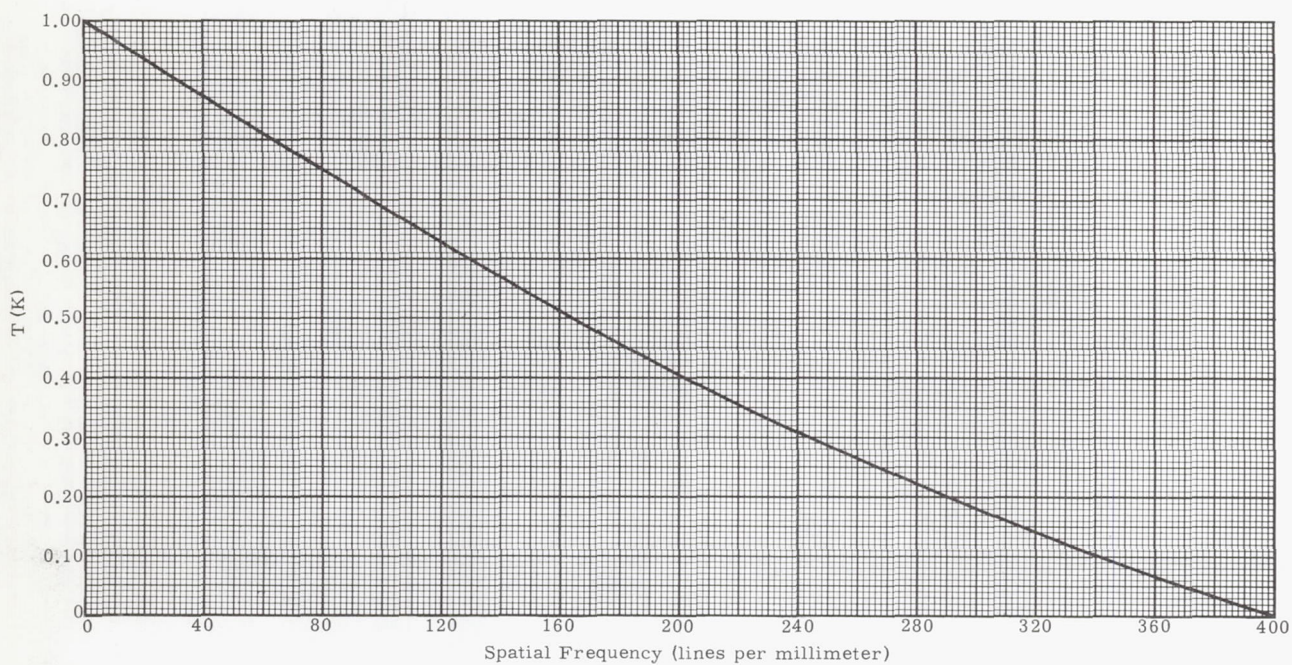


Fig. 60. Transfer Function (scene-lens combination)

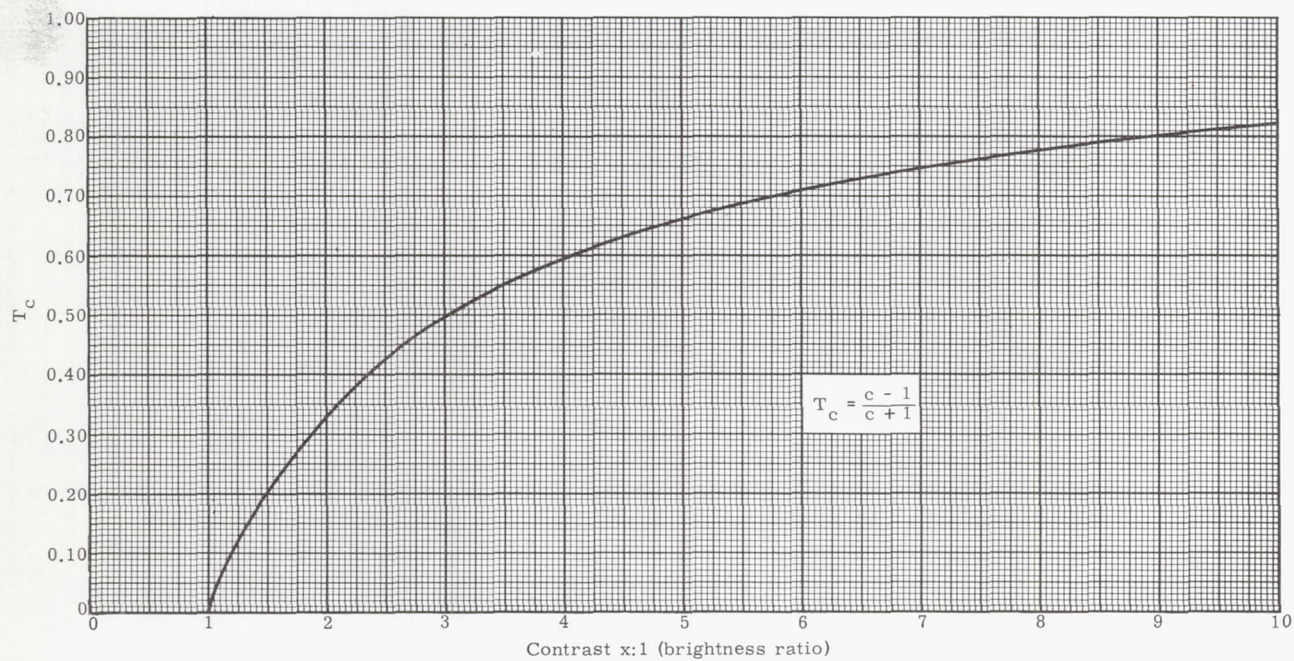


Fig. 61. Transfer Function of Scene Contrast

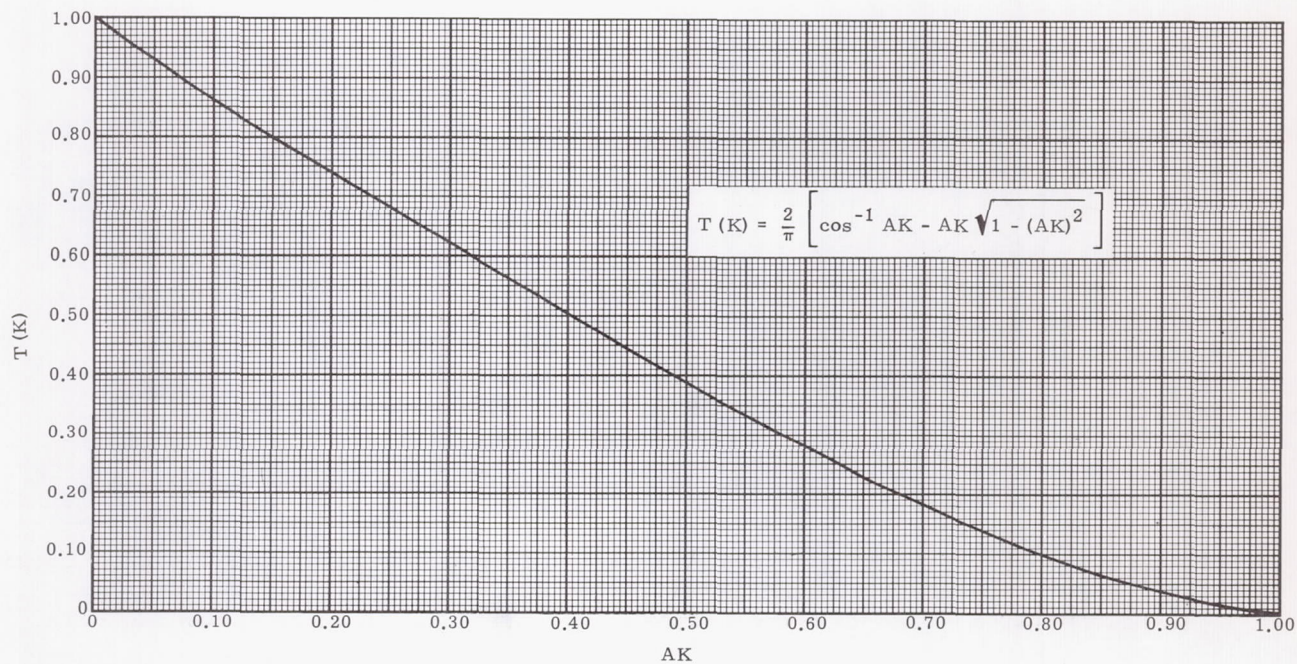


Fig. 62. Diffraction Limited Lens

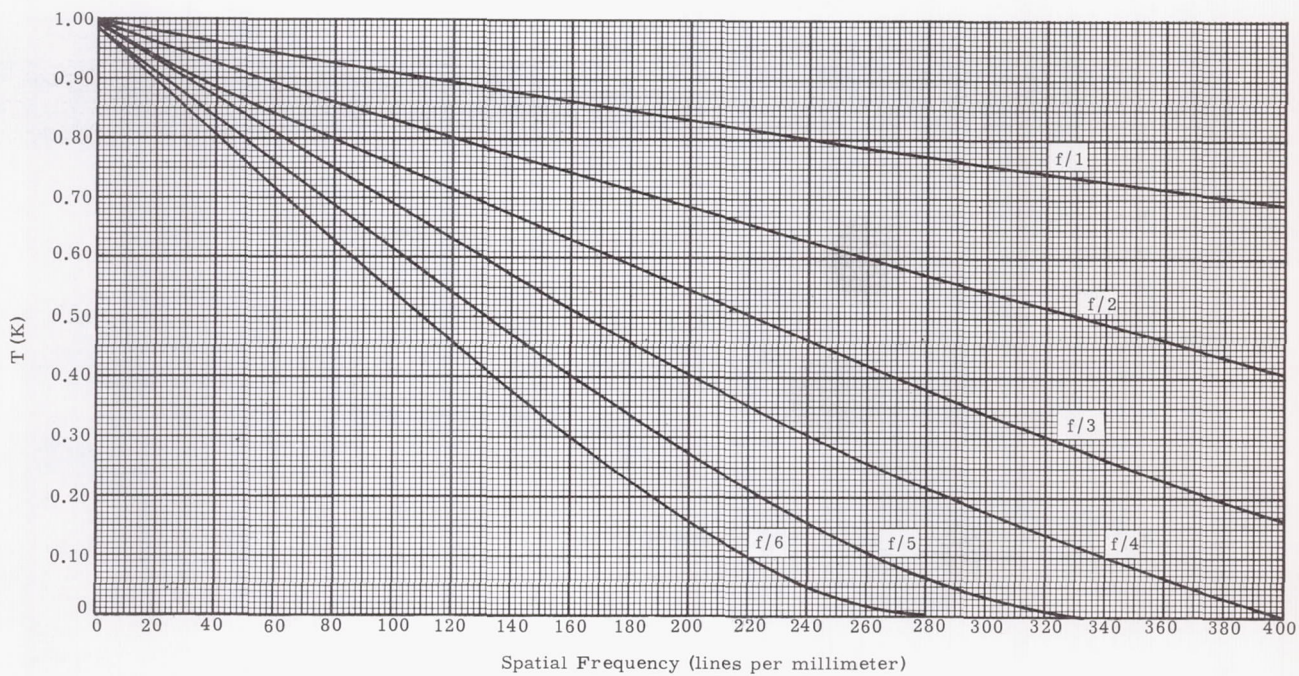


Fig. 63. Transfer Function of Diffraction Limited Lens

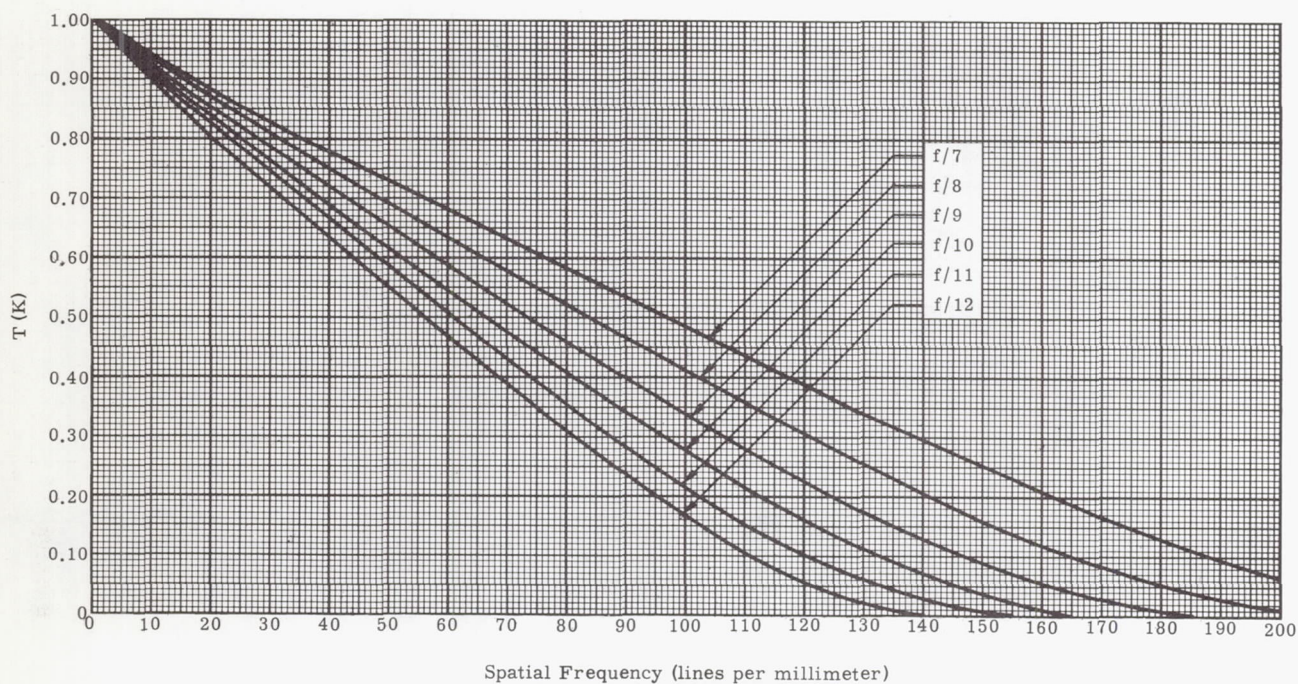


Fig. 64. Transfer Function of Diffraction Limited Lens

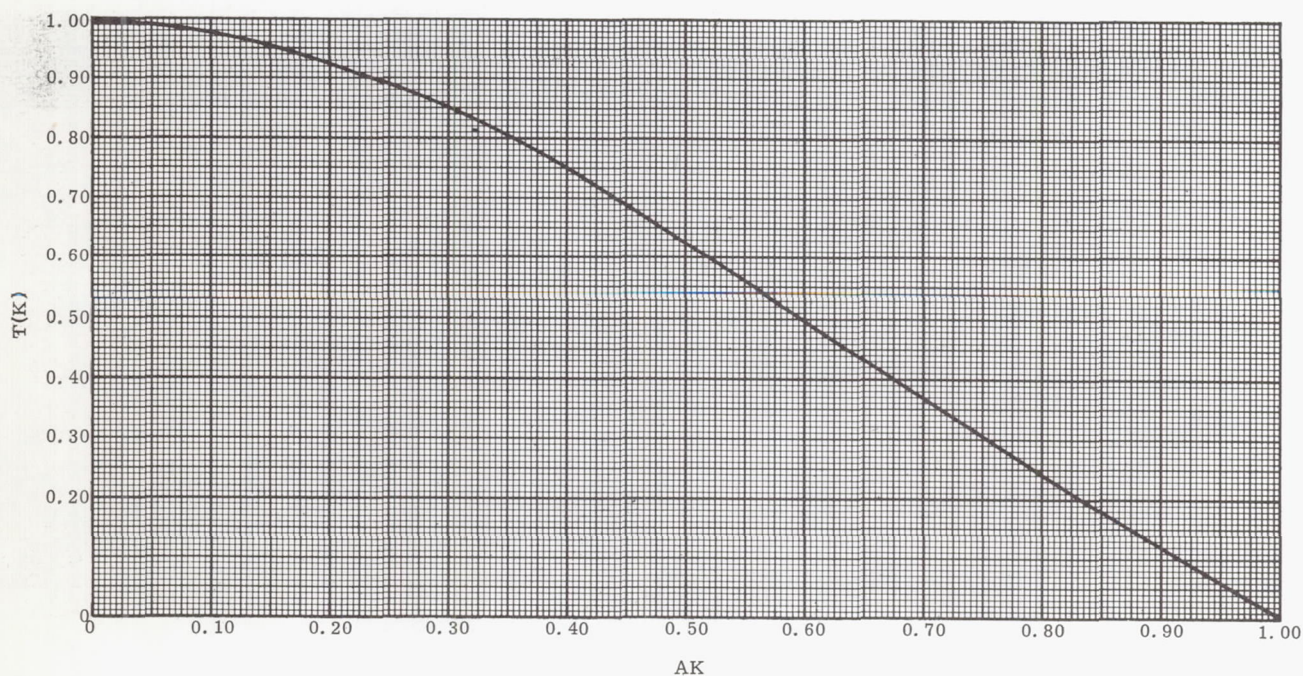


Fig. 65. Transfer Function for Linear Motion

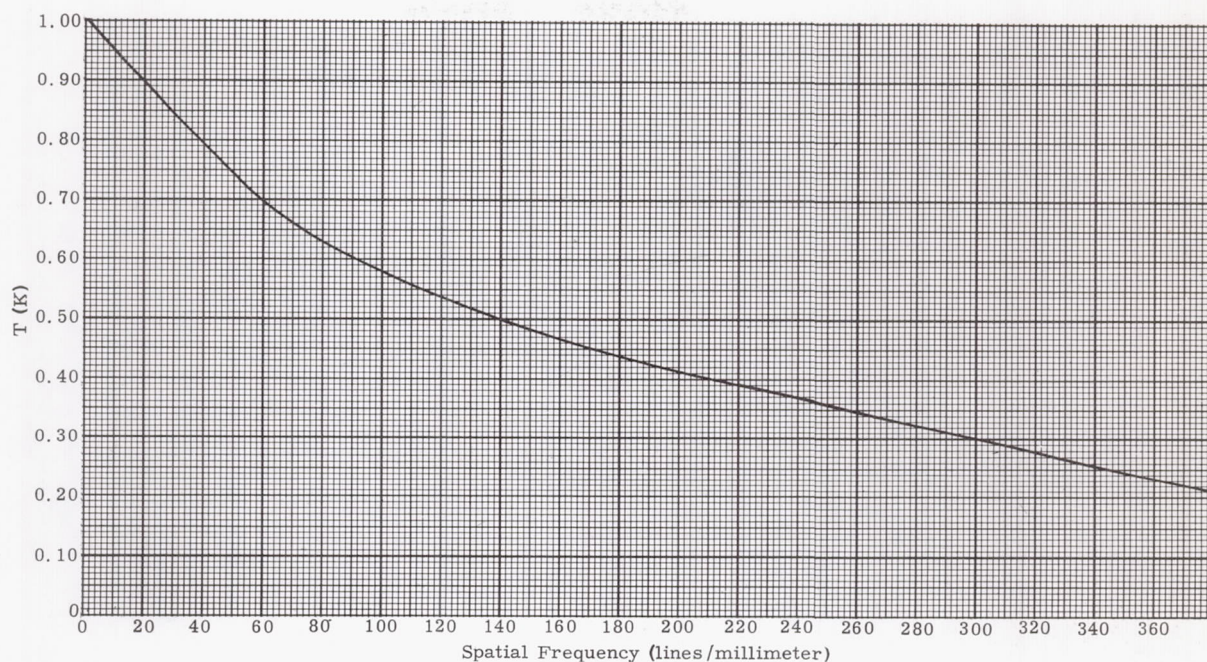


Fig. 66. Typical Photographic Film Transfer Function

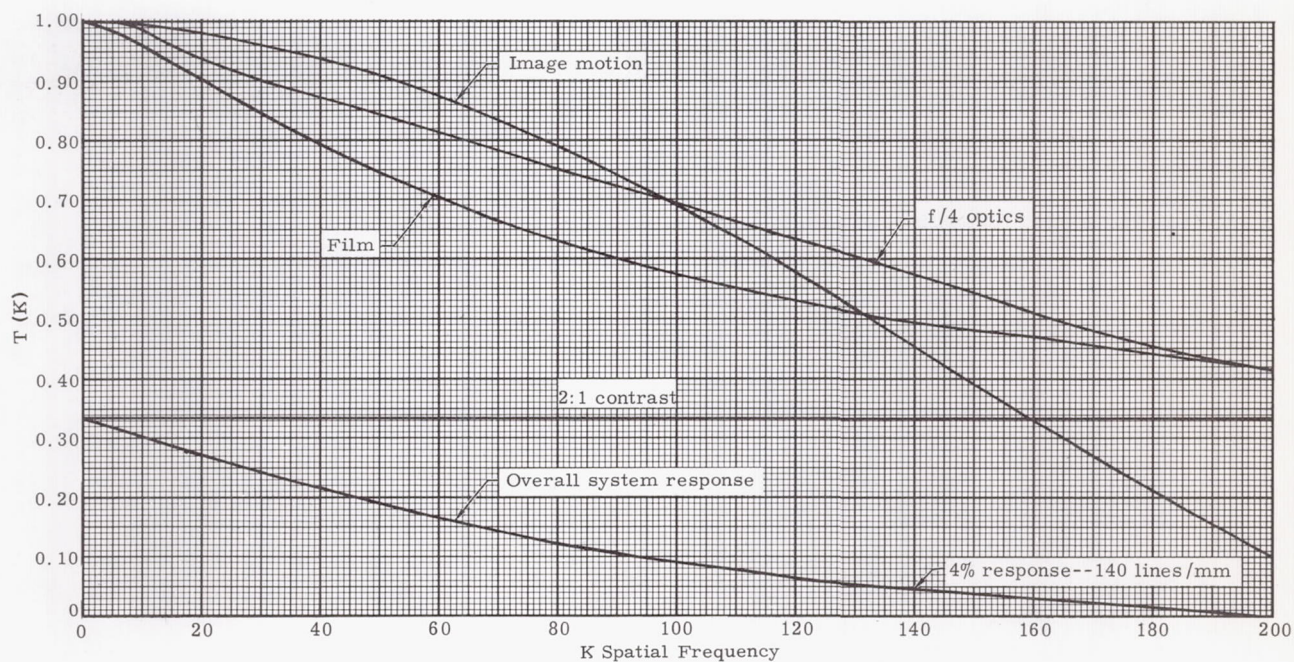


Fig. 67. Illustrative Example

APPENDIX A

APPENDIX A

GLOSSARY (REF. 1)

A

Aberration: apparent displacement of a body from its actual position due to the observer's motion, the object's motion and the finite speed of light.

Aberration, planetary: aberration including effects of the object's motion as well as the observer's motion during the time light travels from the object to the observer.

Aberration, stellar: aberration including only the effect of the earth's motion around the sun, mean value 29.9 km/sec.

Ablation: the gradual removal or erosion of an exposed surface of an object resulting from its high speed passage through a resistive medium.

Abort: the termination of a space mission after an emergency forces return to earth.

Albedo: fraction of total incident light reflected by a body.

Albedo, average geometric: ratio between the average brightness of the object to the brightness of a white screen of the same size normal to the incident light (lunar albedo 0.105).

Albedo, spherical: ratio of the light scattered in all directions by the object to the total incident light (lunar albedo = 0.073).

Almucantar: a parallel to the horizon.

Altitude (also elevation): a topocentric coordinate in the horizon system; the angular distance of an object above the horizon, measured on a vertical circle. Also synonymous with the height of an object above some surface.

Analytical integration: the specification of an explicit closed algebraic or series relation to represent the integral of a given function.

Angular momentum: the quantity $m\vec{r} \times \dot{\vec{r}}$ ($= r^2 \dot{\theta}$ in polar coordinates) constant for conic motion.

Anomaly: or angle; see true anomaly, mean anomaly, and eccentric anomaly.

Aphelion: the point on a heliocentric ellipse farthest from the sun.

Apocynthion (also aposelene or apolune): the point on a selenocentric elliptic orbit farthest from the moon's center.

Apofocus: the apsis on an elliptic orbit farthest from the principal focus or center of force.

Apogee: the point on a geocentric elliptical orbit farthest from the earth's center.

Apsis (plural, apsides): the point on a conic where the radius vector is a maximum or minimum.

The line of apsides is the major axis extended indefinitely.

Argument of latitude: the angle in the orbit from the ascending node to the object in the direction of motion; the sum of the argument of perifocus and the true anomaly.

Argument of perifocus: the angular distance measured in the orbit plane in the direction of motion from the lines of nodes to line of apsides.

Aries: an astronomical constellation; a portion of the celestial sphere which contained the vernal equinox.

Aries, first line of: the direction of the vernal equinox (the name is a carryover from a time that the vernal equinox was in the constellation Aries).

Aspect: angular position of a body relative to its line of advance in orbit.

Astrodynamics: the engineering or practical application of celestial mechanics and other allied fields such as high altitude aerodynamics; geophysics; attitude dynamics; and electromagnetic, optimization, observation, navigation, and propulsion theory, to the contemporary problems of space vehicles. Astrodynamics is sometimes also meant to include the study of natural objects such as comets, meteorites and planets.

Astronomical unit (AU): the mean distance or semimajor axis of the orbit of a fictitious unperturbed planet having the mass (0.000,002,819 solar masses) and sidereal period (365.256,383,5 mean solar days) that Gauss adopted for the earth in his original determination of the gravitational constant K_s ($= 0.017,202,089,95$).

Approximately equal to 92,914,000 statute miles or 149,530,000 km.

Azimuth: a topocentric coordinate measured in the plane of the horizon from the north (or south) point on the horizon clockwise to the object.

B

Ballistic trajectory (also coast trajectory or free-flight trajectory): motion of the space vehicle without rocket burning or thrust forces.

Barker's equation: an equation that relates position to time for an object traveling in a parabolic orbit.

Barycenter: center of mass of a system of masses.

Base altitudes: reference altitudes or levels of the atmosphere between which the atmospheric temperature gradient is assumed to be a constant.

Boltzmann's constant: the ratio of the mean total energy of a molecule to its absolute temperature. Its value is 1.380×10^{-23} joule/ $^{\circ}$ K.

Braking: the deceleration of a space vehicle by rocket thrust or by atmospheric drag.

Braking ellipses: a series of ellipses whose semi-major axes decrease due to the atmosphere of a planet when a vehicle attempts a landing on that planet.

Burnout: end of rocket burning for a particular rocket engine in a given stage of the rocket.

C

Call-down frequency: the frequency with which a vehicle can be recalled from orbit and landed at a specific site.

Cartesian coordinate system: a set of (usually three) mutually orthogonal straight coordinate axes which form a right-handed coordinate system.

Celestial equator: the great circle in which the plane of the terrestrial equator intersects the celestial sphere. The north celestial pole is the point of intersection of the earth's spin vector with the celestial sphere.

Celestial sphere: a hypothetical sphere of infinite dimensions, centered at the observer (or center of the earth or sun, etc.), on the inner surface of which the celestial bodies are projected and appear to move. This sphere is fixed in space, and thus, because of the earth's rotation, appears to rotate from east to west.

Centrifugal force: a fictitious position-dependent force that apparently arises when the motion of an object is observed with respect to a rotating coordinate system. The relationship yielding this "force" is $-m\vec{\omega} \times (\vec{\omega} \times \vec{r})$, where m is the mass of the object and $\vec{\omega}$ is the angular velocity vector of the rotating coordinate system.

Characteristic velocity: the sum of all absolute velocity changes required of a vehicle for a particular space flight (a measure of the total energy requirement for a flight).

Circle, galactic: fundamental plane of the galactic reference system (north pole at $12^{\text{h}} 44^{\text{m}}$ right ascension and $+27^{\circ}$ declination), inclined 62° to the celestial equator.

Circle, hour: secondary circles of the equatorial coordinate system, i.e., planes normal to the celestial equator.

Circle, secondary: great circles (or planes through the origin) which pass through the poles of a given coordinate system.

Circle, vertical: intersections of the celestial sphere by vertical planes in a horizontal coordinate system.

Circumlunar trajectory: a trajectory from the vicinity of the earth which passes behind the moon and returns ballistically to the vicinity of the earth.

Cislunar space: the region of space around the earth and moon, usually taken as being synonymous with the sphere of influence of the earth-moon system.

Collision parameter: the offset distance between the extension of a velocity vector of an object at a great distance from a center of attraction or repulsion and this center.

Colure, equinoctial: the plane, secondary to the equator, which passes through both the celestial poles and the equinoxes.

Colure, solstitial: the plane, secondary to the equator, which passes through both the celestial poles and the solstices.

Conjunction: a point in the orbit of a planet (or moon) where its celestial longitude equals that of the sun. If the alignment is sun-planet-earth, the planet is said to be in "inferior conjunction." This configuration is possible only with inferior planets; if it is planet-sun-earth, the planet is in "superior conjunction." Similarly, when the moon (or a superior planet) is between the earth and the sun, i.e., "new," it is said to be at conjunction.

Coordinate systems: one of a number of sets of celestial coordinate systems used in astronautics (Chapter XI).

- (1) Ecliptic System uses the plane of the earth's orbit (ecliptic) as the reference. The axis of the poles of the ecliptic is at right angles to this plane. This system is most useful for intrasolar system work since all the planets move in or near the plane of the ecliptic.
- (2) Equatorial System uses the celestial equator as the reference plane. The celestial equator and celestial poles coincide with extensions of the earth's equator and poles on the celestial sphere. This system is the one most commonly used in astronomy.
- (3) Horizon System uses the observed horizon as the reference plane and is the common system of celestial navigation.

Coriolis force: a fictitious velocity dependent force that apparently arises when the motion of an object is reckoned with respect to a rotating coordinate system. The relationship yielding this "force" is $-2m\vec{\omega} \times \vec{r}_r$, where m is the mass of the object, $\vec{\omega}$ is the angular velocity vector of the rotating coordinate system, and \vec{r}_r is the velocity of the object reckoned with respect to the rotating system.

Cosmic dust: fine dust particles (micrometeorites) that are concentrated in the solar system in the plane of the ecliptic (e.g., giving rise to the phenomenon of "zodiacal light") and also dispersed in a more rarefied manner in interstellar space, being more concentrated in the galactic spiral arms; also a component of comets.

Cosmic rays (direct): high-energy charged particles (e.g., with energies in excess of 100 Mev) such as protons, alpha particles and heavy nuclei which have apparently been ejected by stars and accelerated by vast magnetic fields in interstellar space.

Cosmoparticle: discrete material entities of sub-meteoritic mass, either in or from space. They may be "free" or individual molecules or atoms, or molecular or atomic constituents of any kind, e.g., ions, atomic nuclei, protons, neutrons, electrons, positrons, etc.

Cross product: or vector product (denoted by $\vec{A} \times \vec{B}$) of two typical vector quantities \vec{A} and \vec{B} can be defined either as a vector mutually perpendicular to both \vec{A} and \vec{B} with magnitude $AB \sin(A, B)$ or equivalently as

$$(A_y B_z - A_z B_y) \mathbf{I} + (A_z B_x - A_x B_z) \mathbf{J} \\ + (A_x B_y - A_y B_x) \mathbf{K}$$

where the subscripts denote the components of the vectors on the three orthogonal axes denoted by the unit vectors \mathbf{I} , \mathbf{J} , \mathbf{K} .

Culmination: The time at which a heavenly body reaches the meridian of an observer. Upper culmination occurs near zenith, lower culmination near nadir.

D

Day, sidereal: the period of one rotation of the earth relative to inertial space (the stars), $23^h 56^m 04^s.090$ mean solar time.

Day, solar: the time between two successive upper (or lower) culminations of the sun, $24^h 03^m 56^s.556$ sidereal time.

Declination: the arc of an hour circle (great circles passing through the poles) intercepted between the celestial equator and the object; angular distance north or south of the celestial equator.

Definitive orbit: an orbit that is defined in a highly precise manner with due regard taken for accurate constants and observational data, and precision computational techniques including perturbations.

Differential correction: a method for finding from the observed minus computed (O - C) residuals small corrections which, when applied to the elements or constants, will reduce the deviations from the observed motion to a minimum.

Dip: the angular distance between the true horizontal and the observed horizon for an observer above ground level.

Direct motion: the term applied to eastward or counterclockwise motion of a planet or other object as seen from the North Pole (i.e., in the direction of increasing right ascension). Thus, it is motion on an orbit in which $i \leq 90$ degrees.

Diurnal: daily.

Diurnal motion: the apparent revolution of the heavenly bodies around the earth.

Dot product: or scalar product (denoted by $\vec{A} \cdot \vec{B}$) of two typical vector quantities \vec{A} and \vec{B} can be defined as $AB \cos(A, B)$ or equivalently as $A_x B_x + A_y B_y + A_z B_z$ where the subscripts denote the components of the vectors on three orthogonal axes.

Drag: the force occasioned by the passage of an object through a resistive medium acting in a direction opposite to that of the object's motion relative to the medium.

Drag coefficient: the total drag force acting on an object divided by one-half the local atmospheric density, the projected frontal area of the object, and the square of the magnitude of the velocity of the object relative to the resistive medium.

Drift, anomalistic: the variation or drift of a frequency source (e.g., a crystal oscillator) such that the frequency changes due to a variety of causes (e.g., temperature variation, component aging, etc.), none of which can be predicted in advance or completely controlled.

E

Eccentric anomaly: an angle at the center of an ellipse between the line of apsides and the radius of the auxiliary circle (which has radius equal to semimajor axis of ellipse and center at center of ellipse) through a point that has the same x-coordinate as a given point on the ellipse.

Eccentricity: the ratio of the radius vector through a point on a conic to the distance from the point to the directrix.

Eclipse: a name applied to cases where a non-luminous body passes into the shadow of another; eclipse of the sun means the interposition of the moon's disc between the observer and the sun.

Ecliptic: the great circle formed by the intersection of the orbital plane of the earth (the ecliptic plane) and the celestial sphere.

Ecliptic coordinate system: axes with the ecliptic as the fundamental plane and with spherical coordinates: celestial longitude and latitude.

Elements of orbit: any six independent constants defining the orbit, e.g., (1) orientation elements: Ω longitude of ascending node; i inclination of orbit plane; ω argument of perifocus; (2) dimensional elements: e eccentricity; a semimajor axis; (3) time element: T time of perifocus passage.

Elevation, angle of: the angle between the inertial velocity vector \vec{r} and the local horizontal, i.e., the plane normal to \vec{r} passing through the vehicle.

Eliminant: a determinant that is formed when $n - 1$ linear unknowns are eliminated from a set of n equations. The elimination of x and y , for example, from

$$a_1x + b_1y = c_1$$

$$a_2x + b_2y = c_2$$

$$a_3x + b_3y = c_3$$

yields the eliminant:

$$\begin{vmatrix} a_1 & b_1 & c_1 \\ a_2 & b_2 & c_2 \\ a_3 & b_3 & c_3 \end{vmatrix} = 0$$

Elongation, angle of: the angle between the direction to an object and to the center of the coordinate system reckoned at the observer.

Energy integral: one of the integrals of two-body motion expressing conservation of energy.

Entry angle: the angle between the velocity vector of a space vehicle relative to a resistive medium and the local horizontal.

Ephemeris (plural, ephemerides): a table of calculated coordinates of an object with equidistant dates as arguments.

Ephemeris time (ET): uniform or Newtonian time, defined by mean frequency of rotation of the earth around the sun for the year 1900.

Epoch: arbitrary instant of time for which the elements of an orbit are valid (e.g., initial, injection, or correction time).

Equator, celestial: the great circle in which the plane of the terrestrial equator intersects the celestial sphere.

Equator, terrestrial: the circle in which the plane through the earth's center normal to its axis of rotation (the equatorial plane) intersects the earth's surface.

Equatorial bulge: the excess of the earth's equatorial diameter over the polar diameter (i.e., about 27 miles, 43 km); oblateness.

Equatorial satellite: a satellite whose orbit plane coincides with the earth's equatorial plane.

Equatorial system: rectangular axes referred to the equator as the fundamental plane and having spherical coordinates, right ascension and declination.

Equilateral triangle solutions: a particular solution of the three-body problem in which an object situated at one vertex of an equilateral triangle formed with the sun and a planet has a stable orbit. It was predicted by Lagrange (1772) and amply confirmed in the case of Jupiter. See Trojan asteroids.

Equinox, nutation of: arises from nutation of equator.

Equinox of date: position of equinox at epoch being used in discussion.

Equinox, precession of: arises from precession of equator.

Equinox, true: equals equinox or vernal equinox, q.v., "true" being used to emphasize distinction from mean equinox.

Equinoxes: intersections of the equator and ecliptic, the vernal equinox being the point where the sun crosses the equator going from south to north (descending node of earth's orbit).

Euler's equation: a relation in a parabolic orbit involving two radii vectors, their chord, and the time interval between them; discovered by Euler (1744).

Evection: a large perturbative term in the moon's longitude discovered by Hipparchus, amounting to $1^\circ 15'$ at maximum.

F

Feasibility orbit: an orbit that can be rapidly and inexpensively computed on the basis of simplifying assumptions (e.g., two-body motion, circular orbit, three-body motion approximated by 2 two-body orbits, etc.) and yields an indication of the general feasibility of a system based upon the orbit without having to carry out a definitive orbit computation.

Free-molecule flow (or free-molecular flow): flow regime in aerodynamics in which molecules emitted from an object, as it passes through a resistive medium, do not affect the flow of oncoming molecules by scattering interactions, i.e., the mean free path of the

emitted molecules is much longer than a characteristic linear dimension of an object.

G

Galactic system: a system based on the center-line of the milky way.

Gaussian gravitational constant, K_g : factor of proportionality in Kepler's third law; the numerical value depending on the units employed. See astronomical unit.

Geocentric: referred to the center of the earth as origin.

Geocentric parallax: see parallax.

Geocentric subvehicle point: the point where the radius vector from the geocenter to a space vehicle intersects the spheroid.

Geodetic subvehicle point: the point where a line through a space vehicle normal to the spheroid intersects the spheroid.

Geoid: the mean sea-level figure of the earth.

Geoidal surface: the mean sea-level surface of the earth; surface of gravitational equipotential.

Geometric meter: the standard meter.

Geopotential meter: a unit of length employed in reckoning geopotential altitude.

Gravitational potential: at a point, the work required to remove unit mass from that point to infinity.

Greenwich meridian: the zero meridian from which geographical longitude is measured (passes through the Greenwich Observatory, England).

Ground trace: a succession of subvehicle points on earth or on any other celestial body.

Ground swath: a region around the ground trace, the boundaries of which are specified by the lateral distance from the ground trace.

Guidance and control system: a system that actively counteracts or overcomes the effects of deviations (from nominal conditions) in order to accomplish the given mission with the desired degree of exactness. Navigational inputs allow the guidance and control system to sense these deviations.

Guidance law: the equations which are mechanized in the guidance and control system.

Guidance law, explicit: the guidance computer in the vehicle predicts and the vehicle is steered along a trajectory which brings it to the desired end conditions.

Guidance law, implicit: the vehicle follows a nominal trajectory while the guidance system is active.

H

Harmonics of the earth's gravitational field: a series representing the gravitational potential of the earth whose terms form a harmonic progression, i.e., include powers of the reciprocal of distance.

Heliocentric: referred to the center of the sun as origin.

Hohmann orbit: an elliptic heliocentric trajectory for interplanetary flight, having tangency to the earth at one apsis and to another planetary orbit (e.g., that of Venus or Mars) at the opposite apsis. More generally stands for any such doubly tangent transfer ellipse.

Horizon, apparent: the horizon formed by the horizontal plane through the position of the observer.

Horizon, rational: the horizon formed by the plane through the center of the earth parallel to the observer's horizon.

Horizon coordinate system: a system of topocentric coordinates either spherical (azimuth and altitude) or rectangular, having as reference plane the celestial horizon, which is perpendicular to the direction of gravity at the observer.

Horizon scanner: an optical device that senses the radiation discontinuity between a planet or lunar surface and the stellar background of space. It can be utilized to establish a "vertical" reference based upon a "visual" horizon (which differs from both the astronomical and geodetic horizon).

Horizontal plane: that plane perpendicular to the direction of gravity at any place.

Hour angle (LHA): angle between the observer's meridian and the hour circle passing through the object, a coordinate in the rotating equator system, positive toward west, 0 to 24 hr.

Hour circle: any one of the great circles that pass through the celestial poles and, therefore, are at right angles to the equator.

I

Inclination i : angle between orbit plane and reference plane (e.g., the equator is the reference plane for geocentric orbits and the ecliptic for heliocentric orbits).

Inertial axes: axes that are not in accelerated or rotational motion.

Injection: the addition of an "instantaneous" incremental velocity vector to the satellite velocity vector at a prescribed time and place to establish a new orbit.

Injection conditions: position and velocity of rocket at the instant when the thrusting of rocket motor ends and the ballistic portion of the trajectory begins.

Intermediate orbit: an orbit tangent to the actual (or disturbed) orbit, having the same coordinates but not velocity at point of tangency.

Inversion: in this context is meant to be synonymous with the numerical solution of a set of linear algebraic equations.

Ionosphere: the ionized portion of the atmosphere above about 60 km.

Isostatic equilibrium: a situation in which the pressure under the earth's surface is the same regardless of whether it is measured under a mountain, valley or ocean, i.e., lower density strata underlie mountains while higher density strata underlie oceans.

J

Jacobi's integral: an integral of the equations of motion in a rotating coordinate system which relates the square of the velocity and the coordinates of an infinitesimal body referred to the rotating coordinate system. The constant of integration associated with Jacobi's integral is known as Jacobi's constant.

Julian date: the number of mean solar days that have elapsed since midnight, January 1, 4713 BC; e.g., the Julian date of January 1, 1960 is 2,436,934, and of February 1, 1965 is 2,438,792, etc.

K

Kepler's planetary laws: (1) every planet moves in an ellipse about the sun with the sun at one focus; (2) every planet moves in such a way that its radius vector sweeps over equal areas in equal intervals of time; (3) the squares of the periods of revolution of two planets are to each other as the cubes of their mean distances from the sun.

K_e^{-1} min: the characteristic time for geocentric orbits, i.e., the time required by hypothetical satellites to move 1 radian in a circular orbit of radius a_e (equatorial earth's radius); equal to 13,447,052 min.

K_s^{-1} day: the characteristic time for heliocentric orbits, i.e., the time required for a planet at 1 astronomical unit to move 1 radian (or 1 a.u.) along its orbit; equal to 58.132,440,87 days.

L

Lagrangian solutions: particular solutions of the three-body problem in which an infinitesimal object moves under the attraction of two finite bodies (e.g., the sun and Jupiter) which revolve in circles around their center of mass and in which the distances from the infinitesimal object to the finite bodies remain constant. See also equilateral triangle solutions and synodic satellites, i.e., the so-called straight line solutions.

Lambert's equation: an equation of the 8th degree expressing the curvature of the apparent path of a body moving around the sun, as seen from the earth: discovered by Lambert (1771).

Latitude, astronomical: the angle between the direction of gravity through a point and the equatorial plane.

Latitude, celestial: the angular distance of an object north (+) or south (-) of the ecliptic plane; a coordinate in the ecliptic system.

Latitude, geocentric: the angle between the equatorial plane and a straight line from the observer to the center of the earth. It differs from astronomical and geodetic latitudes because of the oblateness of the earth, 0° to 90° north or south.

Latitude, geodetic (or geographic latitude): the angle between the plane of the equator and a normal to a reference spheroid. Geodetic and astronomical latitudes differ only because of local deviations in the direction of gravity, 0° to 90° north or south.

Least squares inversion: a solution of a set of overdetermined linear equations such that the sum of the squares of the residuals is a minimum.

Legendre polynomials: the coefficients $P_n(c)$ in the expansion $(1 - 2ch + h^2)^{-1/2} = \sum_{n=0}^{\infty} P_n(c) h^n$ where $P_0(c) = 1$, $P_1(c) = 1/2(3c^2 - 1)$, $P_3(c) = 1/2(5c^3 - 3c)$, or, in general, $(n+1)P_{n+1}(c) - (2n+1)cP_n(c) + nP_{n-1}(c) = 0$.

Libration: (1) apparent or optical and physical tilting and side-to-side movements of the moon that render 18 percent of its surface alternately visible and invisible, (2) long-period orbital motions of the Trojan asteroids around the equilateral triangle points of the three-body Lagrangian solutions, (3) periodic perturbative oscillations in orbital elements.

Lift: the force arising from the passage of a vehicle through a resistive medium when the vehicle presents an asymmetrical form or orientation; which force acts in a direction normal to the object's motion relative to the medium.

Limb: the edge of the visible disk of the sun, moon, planet, etc.

Line of apsides: a line connecting the near to the far apsis, i.e., defines the major or transverse axis.

Line of nodes: the intersection of a reference plane and the orbit plane.

Line-of-sight: the apparent or observed direction of an object.

Longitude, celestial: the angular distance measured along the ecliptic from the vernal equinox eastward to the great circle passing through the object and normal to the ecliptic.

Longitude, ephemeris: analogous to ordinary geographic longitude, but referred to the ephemeris meridian, rather than to the Meridian of Greenwich.

Longitude, geocentric: the angular distance from the foot of the Greenwich meridian, measured along the equator, east or west, to the foot of the meridian through the place.

Longitude of ascending node: the angular distance from the vernal equinox measured eastward in the fundamental plane (ecliptic or equator) to the point of intersection with the orbit plane at the point that the object crosses from south to north.

Longitude of perifocus: sum of the angle in the fundamental plane between the vernal equinox and the line of nodes and the angle in the orbit plane between the line of nodes and the line of apsides, measured in the direction of motion.

Lunar equation: a factor required for reducing observations to the barycenter of the earth/moon system.

Lunar theory: the analytical theory of the motion of the moon. The lunar theories of Delavny, Hansen, and Hill-Brown are used most frequently today.

Lunar unit (LU): the mean distance from the center of the earth to the center of a fictitious unperturbed moon having the mass and sidereal period of the moon. One lunar unit is approximately equal to 384,747 km or 239,122 statute miles.

Lunicentric: referred to the moon's center as origin; selenocentric.

M

Mach number: the ratio of the speed of a vehicle to the local speed of sound.

Macrometeorites: meteorites that are sufficiently massive to become fallen meteorites (and whose origin appears to be related to that of minor planets).

Magnetic storms: extensive disturbances in the earth's magnetic field.

Magnitude, stellar: a measure of the brightness of a star. A difference of five magnitudes represents a factor of 100 in brightness.

Mean anomaly: the angle through which an object would move at the uniform average angular speed n , measured from perifocus; $M = t \sqrt{\frac{\mu}{a^3}}$.

Mean center of moon (MCP): the point on the lunar surface intersected by the lunar radius that is directed toward the earth's center when the moon is at the mean ascending node and when the node coincides with the mean perigee or the mean apogee. The MCP is a specified distance from the crater Mösting A in the Sinus Medii.

Mean distance: the semimajor axis (it can be considered as an historical term).

Mean equinox of date: a fictitious equinox whose position is that of the vernal equinox at a particular date with the effect of nutation removed.

Mean free path: the path of a molecule when molecules are assumed to be smooth, rigid spheres with no external field of force acting on them; each molecule travels freely on a straight line between impacts with other molecules. The distance traversed between two successive impacts is called the free path and the average value of this distance the mean free path.

Mean solar day: the elapsed time between successive passage of the mean fictitious sun across the observer's meridian, 86,400 mean solar sec, the mean fictitious sun being a fictitious sun that moves along the celestial equator with the mean speed with which the true sun apparently moves along the ecliptic throughout the year.

Meridian: (1) Terrestrial meridians: great circles passing through North and South Poles, e.g., the observer's local meridian passes through his local zenith and the North and South Poles. (2) Celestial meridian: a great circle on the celestial sphere in the plane of the observer's terrestrial meridian.

Meridian, ephemeris: the geographical meridian which lies east of Greenwich by the amount 1.002738 times the difference (ET-UT).

Meridian passage: also called "transit" or "culmination" of a celestial object is marked by its crossing an observer's meridian.

Mesometeorites: intermediate meteorites having characteristic dimension of the order of a fraction of an inch that are stopped by the atmosphere, consumed, and are seen as common "meteors." The origin of these bodies appears to be related to that of comets

Meteor swarms: a large collection of mesometeorites (probably the remains of an "old" comet) that enters the earth's atmosphere and is seen as a swarm of meteors. The term is often applied to the actual collection of mesometeorites on heliocentric orbits in space.

Micrometeorites: very small meteorites (having a characteristic dimension of a few microns) that are stopped by the atmosphere without being consumed in flight or without producing luminous phenomena visible at the earth's surface.

Minor planets (or asteroids): small planets revolving about the sun, estimated to number more than 30,000, with diameters of more than 1 mile. The largest, Ceres, has a diameter of 488 miles.

Molecular scale temperature: the actual temperature of the atmosphere at any given height multiplied by the ratio of the mean molecular weight of the atmosphere at sea level to the mean molecular weight of the atmosphere at the given height.

Month, nodal: the time for one revolution of the moon with respect to either node.

Month, sidereal: the time between two successive arrivals of the moon at a given apparent place on the celestial sphere as indicated by the stars.

Month, synodic: the time for one revolution of the moon with respect to the apparent place of the sun, e.g., the time between conjunctions.

Moon's celestial equator: a great circle on the celestial sphere in the plane of the moon's equator, i.e., in a plane perpendicular to the moon's axis of rotation.

Moon's orbital plane (MOP): the instantaneous orbital plane of the moon around the earth, defined by the moon's geocentric radius and velocity vectors.

N

Nadir: the downward plumb-bob direction, or the point where the downward extension of the direction of a plumb-bob intersects the celestial sphere.

Navigation: the process of determining the position and velocity of a submarine, ship, airplane, or space vehicle by making observations from the vehicle of objects in the environment of the vehicle.

n-body problem: concerned with the gravitational interactions of masses m_1, m_2, \dots, m_n , $i, j = 1, 2, \dots, n$ which are assumed homogeneous in spherical layers, under the Newtonian law. If $n = 2$, one has a two-body problem, while $n = 3$ is known as the three-body problem.

Newton's laws: Law of gravitation: Every particle of matter in the universe attracts every other particle with a force varying directly as the product of their masses and inversely as the square of the distance between them. Laws of motion: (1) Every particle continues in its state of rest, or of uniform motion in a straight line, unless it is compelled to change that state by a force impressed upon it. (2) The rate of change of momentum is proportional to the force impressed, and takes place in the direction of the straight line in which the force acts. (3) To every action there is an equal and opposite reaction; or the mutual actions of two bodies are always equal and oppositely directed.

Nodal passage, time of: the time T_Ω when an object passes through the node from the southern hemisphere to the northern hemisphere.

Node: the points of intersection of the great circle on the celestial sphere cut by the orbit plane and a reference plane (e.g., the ecliptic or equator reference plane).

Node, ascending: the node in the reference plane through which the body passes from South to North.

Node, descending: the node in the reference plane through which the body passes from North to South.

Node, longitude of ascending: see longitude of ascending node.

Nominal orbit: the true or ideal orbit in which space vehicle is expected to travel.

Normal places: curve formed, when several observations are available very close together in time, by smoothing observed coordinates.

Numerical differentiation: a process that allows for the numerical evaluation of the derivative of quantity, given tabular values of the quantity.

Numerical integration: a process that allows for the numerical evaluation of a definite integral.

Nutation: short period terms in the precession arising from the obliquity, the eccentricity, and the inclination of the moon's orbit and the regression of its nodes (approximately a 19-year period).

O

Obliquity of the ecliptic: the inclination of the ecliptic to the celestial equator; the angle of approximately $23^\circ 27'$ between the earth's orbital plane and its equator.

Occultation: the interruption of the light from one celestial body by the intervention of another.

Opposition: the position of an object when its celestial longitude is 180° from sun, i.e., opposite to sun. (Configuration possible only with moon and superior planets.)

Orientation angles: the classical orientation elements, i.e., the inclination, longitude of the ascending node, and longitude of perifocus.

Osculating orbit: an orbit tangent to the actual or disturbed trajectory, having the same coordinates and velocity at that instant.

P

Parallactic angle: the angle between the hour circle of and the vertical circle through a body.

Parallactic inequality: a secondary effect on the solar perturbations in the moon's longitude due to the ellipticity of the earth's orbit.

Parallax: (1) Geocentric parallax: the angle at the object subtended by the earth's equatorial radius; applied to objects in the solar system. (2) Heliocentric parallax: the angle at a star, etc., subtended by the radius of the earth's orbit; applied to objects outside the solar system.

Pericyynthion: the point on a selenocentric orbit nearest the moon's center.

Perifocus: the point on an orbit nearest the central force.

Perigee: the point on a geocentric orbit nearest the earth's center.

Perihelion: the point on a heliocentric orbit nearest the sun.

Period: the time required for one complete circuit of the orbit.

Period, anomalistic: interval of time from one perifocus passage to the next.

Period, nodal (also draconic): interval of time from one nodal crossing to the next.

Period, sidereal: the time required for the projection of a planet or other body to make a complete circuit of the celestial sphere. This is the true period.

Period, synodic: the time between successive oppositions of a superior planet or successive inferior conjunctions of an inferior planet.

Perturbations: deviations from exact reference motion caused by the gravitational attractions of other bodies or other forces.

General perturbations: A method of calculating the perturbative effects by expanding and integrating in series.

Special perturbations: methods of deriving the disturbed orbit by numerically integrating the rectangular coordinates or the elements.

Piecewise continuous: a function that can be divided into a finite number of pieces such that the function is continuous on the interior of each piece and such that the function approaches a finite limit at the point of connection of one piece with another. In the context of the temperature profile discussion the term is used in a more restricted sense to imply a function that is divided into a finite number or series of connected linear pieces (straight line segments).

Planetocentric: referred to the center of a planet as dynamical center or origin of coordinates.

Planets: bodies in the solar system which move in essentially elliptical paths around the sun (see Kepler's laws).

| | |
|-------------------|---------------------------------|
| Inferior planets: | Inner, or terrestrial, planets: |
| Mercury | Mercury |
| Venus | Venus |
| Superior planets: | Earth |
| | Mars |
| Mars | |
| Asteroids | Asteroids, or minor planets. |
| Jupiter | |
| Saturn | |
| Uranus | Outer, or major, planets: |
| Neptune | Jupiter |
| Pluto | Saturn |
| | Uranus |
| | Neptune |
| | Pluto |

Plasma: a collection of positive and negative ions that has no overall or gross charge.

Polar satellite: a satellite that passes over the north and south poles of the earth, i.e., that has an inclination of 90° with respect to the earth's equator.

Polar distance, ecliptic: complement of the celestial latitude.

Polar distance, north: complement of the declination.

Poles, celestial: the points in which the axis of rotation intersects the celestial sphere.

Poles, ecliptic: the points in which the normal to the ecliptic through the origin intersects the celestial sphere.

Poles, galactic: the points in which the fundamental galactic axis intersects the celestial sphere. The north galactic pole is at $12^{\text{h}} 44^{\text{m}}$ right ascension and $+27^{\circ}$ declination.

Position, apparent: coordinates of a celestial body as seen by an observer at the center of the earth referred to a coordinate system defined by the instantaneous equator, ecliptic, and equinox. The tabulated positions of the sun, moon, and planets in the American Ephemeris and Nautical Almanac are usually apparent positions.

Position, mean: coordinates of a celestial body referred to a coordinate system defined by the mean equator, ecliptic and equinox of date. This means that the periodic effects of nutation have been neglected.

Position, true: coordinates of a celestial body if corrections for planetary aberration are applied to the apparent position. A sequence of true positions as a function of time is known as a geometric ephemeris.

Potential function: see gravitational potential.

Poynting-Robertson effect: the gradual decrease in the orbital semimajor axis and eccentricity of a micrometeorite caused by the re-emission of radiant energy from the micrometeorite. The theory was first announced by Poynting and later improved and brought into conformity with the theory of relativity by Robertson.

Precession of the equinoxes: the slow, 26,000-year period westward motion of the equinoxes (and equator) along the ecliptic, arising from solar and lunar perturbations on the earth's equatorial bulge, which cause the earth's axis to precess.

Predicting a satellite's position: the six elements are the same in number as the three coordinates of position and the three components of velocity required to specify the launching conditions completely.

Primary: the body having the strongest gravitational field (most ponderous mass) in a system of bodies revolving about their common center of gravity. (Sun is the solar system's primary, earth is earth-moon system primary, etc.)

Prime meridian: the meridian defining 0° and 180° E or 180° W longitude. On earth the Greenwich meridian is the prime meridian.

R

Radiation pressure: the pressure acting on a surface exposed to incident electromagnetic radiation caused by the momentum transferred to the surface by the absorption and reflection of the radiation.

Ratios of the triangles: in the orbit determination methods of Gauss, Olbers, et al., the ratios of the triangles formed by the radii and the chords are assumed in a first approximation to be ratios of the sectors, which are the ratios of the corresponding time intervals by Kepler's second law.

Rectilinear orbit: a trajectory for which perifocus distance is zero and eccentricity is one.

Red shift, gravitational: an effect predicted by the General Theory of Relativity in which the frequency of light emitted by atoms in stellar atmospheres is decreased by a factor proportional to the (mass/radius) quotient of the star: confirmed observationally by the spectra of white dwarfs.

Re-entry: portion of a trajectory in the atmosphere of a planet; in the case of the earth it is usually taken as the portion below 400,000 ft or 122 km.

Re-entry corridor: all possible re-entry trajectories which do not produce excessive aerodynamic heating or deceleration.

Reduction to orbit: quantity added to celestial heliocentric longitude to give true longitude, q. v.

Reference ellipsoid (or spheroid): oblate spheroid closely approximating the geoid.

Reference orbit: an orbit, usually but not exclusively the best two-body orbit available, on the basis of which the perturbations are computed.

Refractive index (of a medium): the ratio of the speed of light in a vacuum to that in the medium, hence it is a measure of how greatly electromagnetic radiation rays are bent during their transit through a medium such as the earth's atmosphere.

Regression of the moon's nodes: the movement of the nodes of the moon's orbit westward along the ecliptic, due to solar perturbations, with period ≈ 19 years.

Relativity effects: effects on a space vehicle trajectory and on time measurement arising by use of Einstein's special theory of relativity or of Einstein's general theory of relativity instead of the customary Newtonian mechanics for determining the trajectory. The fundamentals of these theories of relativity are discussed in Chapter IV of the Lunar Flight Handbook. Relativity effects are small in the weak gravitational field of the solar system if the space vehicle velocity is small compared to the speed of light. There are many such effects, the most prominent of which are: the time dilation predicted from the Lorentz transformation of special relativity; the time dilation, secular advance of perigee, and red-shift of spectral lines predicted by general relativity.

Rendezvous: the approach and contact of two vehicles in space.

Representation: the computation of the position of a space vehicle given the orbital elements and the time.

Residuals (O - C): differences between the observed and computed coordinates in the sense observed minus computed.

Residuals (O - 1): differences between the pre-computed ideal observational data and the actual observed data on, for example, an interplanetary voyage.

Restricted n-body problem: the motion of n masses under their mutual gravitational attraction, but with one of the n masses having negligible mass and hence not influencing the motion of the other (n - 1) masses. This term is usually applied to n = 3 (see also n-body problem).

Retrograde motion: westward or clockwise motion as seen from the North Pole, i.e., motion in an orbit in which $i > 90$ degrees (opposite earth's rotation).

Retrorocket: a rocket attached to a space vehicle whose thrust is directed in a general direction against the inertial velocity of the space vehicle.

Reynolds number: the ratio of inertial forces to viscous forces--it is proportional to the Mach number, vehicle diameter, and the density, or, in equivalent terms, proportional to the diameter of the space vehicle in mean free paths and the vehicle speed measured in terms of the average thermal speeds of gas molecules that constitute the oncoming flow.

Right ascension: angular position of an object (e.g., star) measured eastward along the celestial equator from the vernal equinox to the great circle passing through the north celestial pole and the star (hour circle). Right ascension is often expressed in hours, minutes, and seconds ($1^h = 15^\circ$).

S

Scale height: the distance in which an isothermal atmosphere decreases in density from 1 to $1/e$.

Secular terms: expressions for perturbations that are proportional to the time.

Selenocentric: referred to the center of the moon; lunocentric.

Selenocentric equatorial coordinates: a right-handed coordinate system centered at the moon with its three axes defined by the vernal equinox, north celestial pole (of the earth), and a direction perpendicular to these two, i.e., an equatorial coordinate system translated to the moon.

Selenographic coordinates: coordinates that are rigidly attached to the moon (as geographic coordinates are attached to the earth) defined by the moon's equator and prime meridian. See mean center of moon.

Semimajor axis: the distance from the center of an ellipse to an apsis; one-half the longest diameter; one of the orbital elements.

Seminor axis: one-half the shortest diameter of an ellipse.

Semiparameter: semilatus rectum; the perpendicular distance from the conic to the semimajor axis through either focus (not to be confused with the generic term "parameters").

Setting circles: a graduated scale that can be read visually and indicates the direction (e.g., altitude and azimuth or right ascension and declination) in which a telescope is pointed. Ordinarily they are employed to set or point a conventional astronomical telescope in the proper direction to make a given observation.

Sidereal period of a planet: see period, sidereal.

Sidereal time: the hour angle of the vernal equinox. (See Chapter II for conversion of sidereal time to mean solar time).

Sidereal year: time required by the earth to complete one revolution of its orbit; equal to 365.25636 mean solar days.

Slip flow: a flow regime in aerodynamics in which there is some departure from continuum flow and the layer of compressible fluid immediately adjacent to the surface of an object is no longer at rest but has a finite tangential "slipping" velocity.

Solar flares: short-lived areas of brilliance (covering areas of 10 million square miles or so) on the sun's chromosphere that are associated with other solar activity. Often accompanied by bursts of emitted charged corpuscles and electromagnetic radiation. They reach several times normal brightness within one or two minutes and then subside slowly over 15 to 30 minutes.

Solar parallax: the ratio of the earth's equatorial radius to its mean distance from the sun.

Solar time, mean: hour angle of fictitious mean sun increased by 12 hours. (The fictitious mean sun is a fictitious sun moving on the celestial equator with a mean motion of the real sun.) See pages 474 to 476, American Ephemeris and Nautical Almanac for conversion of mean solar time to sidereal time.

Solar wind: those low energy particles, i.e., corpuscular radiation (electrons and protons) emanating from the sun. Typical flux rates are 10^8 to 10^{10} particles per cm^2 per second, and typical energies are 1000 to 100,000 electron volts for the protons and a few electron volts for the electrons.

Solstices: the two times a year when the sun's declination is greatest north or south (about June 22 and December 22).

Space range system: a system or network of observation stations, together with their associated communication links and computational facilities, that are utilized to observe and track space vehicles, e.g., the Pacific Missile Range, the National Space Surveillance System, etc.

Specular reflection: characterized by the relation that the angle of incidence equals the angle of reflection, in contrast to diffuse reflection.

Sphere, celestial: an imaginary reference sphere; generally considered to be of infinite radius, and having its visible representation in the sky.

Spheroid: an oblate ellipsoid which closely approximates the mean sea-level figure of the earth or geoid.

Stability of a point or orbit: a point or orbit is stable if the space vehicle will remain near the point or orbit if given a small displacement and velocity. The point or orbit is unstable if the space vehicle will depart from it rapidly.

Standard atmosphere: a table of atmospheric density as a function of altitude which is accepted as a standard and used as a model to portray a typical average atmospheric density variation.

Standard deviation: the square root of the arithmetic mean of the squares of the deviations from the mean; also called root mean square error and sigma deviation.

Stationary points: points in the apparent path of a planet, etc., against the star background where the object appears to stand still because relative to the observer it is moving only in the line of sight. Such a point occurs when a planet changes its apparent motion from direct to retrograde and vice-versa.

Station error: small, usually negligible, differences between the astronomical and geodetic latitudes, due to certain anomalies (such as a mountain) in the local gravitational field.

Stratosphere: a region in which the temperature remains constant from about 18 km up to a height of 30 to 35 km.

Surface-circular satellite: a hypothetical satellite on a circular orbit about the earth having a semimajor axis equal to the earth's equatorial radius. Hence, such a satellite would "skim the surface of the earth" as it revolved on its orbit.

Synodic satellite: a hypothetical satellite, situated 0.84 of the distance to the moon on a line joining the centers of the earth and moon and having the same period of revolution as the moon, according to the Lagrangian "straight line solution" of the three-body problem.

T

Terminator: the boundary between the illuminated and dark sides of a planet or satellite. Usually one distinguishes between a morning and an evening terminator.

Three-body problem: the problem of integrating the equations of motion of three bodies (e.g., sun-moon-earth) moving under their mutual gravitational attractions: directly soluble only in particular cases. See Lagrangian solutions.

Thrust: the force exerted on a vehicle, by the discharge of a gas or propellant, in accordance with the conservation of linear momentum.

Time, ephemeris: time reckoning based upon "constant" frequency rather than frequency of earth's rotation. The current difference between ephemeris and universal time is about 35 seconds.

Time dilation: the apparent slowing-down of moving clocks. This effect arises from the special and general theory of relativity.

Time of perifocal passage: the time when a space vehicle traveling upon an orbit passes by the nearer apsis or perifocal point.

Topocentric: referred to the position of the observer on the surface of the earth, as origin.

Topocentric parallax: the difference between the geocentric and topocentric positions of a satellite.

Topocentric equatorial coordinates: a right-handed coordinate system centered at the observer with its three axes defined by the vernal equinox, north celestial pole, and a direction perpendicular to these two, i.e., an equatorial coordinate system translated to the topos.

Tracking: the process of determining the position and velocity of a celestial body by making observations from earth by optical or electromagnetic means.

Trajectory sensitivities: the partial derivatives of dependent trajectory variables with respect to independent trajectory variables.

Transitional flow: a flow regime in aerodynamics between the free-molecule flow and slip-flow regimes in which the molecules emitted from the surface of an object affect the flow of oncoming molecules, i.e., in which the mean free path of the emitted molecules becomes comparable to a characteristic linear dimension of an object.

Transearth trajectory: trajectory from the vicinity of the moon to the vicinity of the earth.

Translunar trajectory: trajectory from the vicinity of the earth to the vicinity of the moon.

Transverse axis: the distance between the apsides --identical to the semimajor axis for elliptical orbits.

Triaxial ellipsoid: a solid aspherical figure which when cut or sectioned in three (orthogonal, normal or mutually perpendicular) directions exhibits three elliptical cross sections of differing semimajor axes and eccentricities.

Tropopause: the height (varying from about 9 km over the poles to 18 km over the equator) where the gradual decrease in temperature with elevation above sea level ceases.

True anomaly: the angle about the focus between the perifocus and the radius vector in the direction of the motion.

True equinox of date: the actual position of the equinox including both precession and nutation.

Twenty-four-hour satellite: a satellite whose orbital period is approximately 24 hr. If such a satellite is on circular equatorial orbit, then it will theoretically remain fixed or "stationary" relative to the rotating earth.

Two-body orbit: the motion of a body of negligible mass around a center of attraction.

U

Umbra: the dark central portion of the shadow of a large body such as the earth or moon (used in connection with eclipses). The outer, less dark shadow is known as the penumbra.

Unit vector: a vector whose magnitude or length is unity--utilized to define directions in space.

Universal time (UT): mean solar time referred to the meridian of Greenwich, slightly non-uniform owing to the irregular rotation of the earth.

V

Van Allen radiation belt: two toroidal-shaped zones or belts of charged particles roughly situated in the plane of earth's equator. The inner belt commences at about one-fifth on an earth's radius above the equator and extends out to a little less than one earth's radius. The outer belt is located at about two-and one-half earth radii from the earth at the equator and is about one-earth radius thick. Actually the outer belt has a cross section that is shaped somewhat like a banana and extends north and south of the equatorial plane two earth radii. The northern and southern extremes of the belt's cross section (at about 45 degrees latitude) approach the earth one-half of an earth radius closer than at the equator.

Variant orbits: computed orbits in which one of the initial conditions (or parameters) is varied slightly from those of the nominal trajectory--such orbits are utilized to compute numerical partial derivatives or to determine the effects of errors in launch conditions.

Variation of latitude: small periodic changes in the position of the earth's poles due to a "wobbling" of the axis of rotation about the geometrical axis (the shortest diameter) of the earth.

Vector component: the projection of a vector on a given axis in space, e.g., if it is the X-axis then the component of the vector A on this axis is denoted by A_x .

Vector equation: an equation, whose terms include vectors, that can be resolved into

component equations; e.g., $\ddot{\vec{r}} = \frac{-\mu \vec{r}}{r^3}$

actually represents the three component equations:

$$\ddot{x} = -\mu x/r^3$$

$$\ddot{y} = -\mu y/r^3$$

$$\ddot{z} = -\mu z/r^3$$

where $\ddot{\vec{r}}$ has been replaced by its three components \ddot{x} , \ddot{y} , and \ddot{z} and \vec{r} by its three components x , y , and z .

Velocity, circular: the magnitude of the velocity required of a body at a given point in a gravitational field which will result in the body following a circular orbital path about the center of the field.

Velocity, escape (also parabolic velocity): the minimum magnitude of the velocity required of a body at a given point in a gravitational field which will permit the body to escape from the field.

Velocity, orbital: with respect to the planets, usually the mean magnitude of the velocity in orbit--computed as the total distance traveled in one circuit divided by the period.

Vernal equinox: that point of intersection of the ecliptic and celestial equator where the sun crosses the equator from south to north in its apparent annual motion along the ecliptic.

Vis viva integral: see energy integral.

Voice trajectory program (Volume of Influence Calculated Envelopes): a patched conic lunar mission trajectory program. It uses the analytical solutions of the two-body trajectories to construct a complete trajectory from the vicinity of the earth to the moon and back.

Y

Year: the orbital period of the earth. When unqualified, it refers to the equatorial or to the calendar year, depending on its use.

Year, anomalistic: the time interval between successive passes through perihelion = $365.259,641,34 + 0.000,003,04 T$ days (T denotes centuries since 1900).

Year, Besselian: a time reckoning in terms of actual rather than calendar years.

Year, calendar: a variable year containing either 365 or 366 days.

Year, equatorial (also tropical or ordinary year, not calendar year): interval between transits of the sun through the moon equator $365.242,198,79 - 0.000,006,14 T$ days.

Year, Julian: the year of the Julian calendar = 365.25 days.

Year, sidereal: the period of the earth relative to the stars = $365.256,360,42 + 0.000,000,11 T$ days.

Z

Zedir technique: the use of two cameras on a satellite whose optical axes are parallel, one of which photographs the sky (zenith) while the other simultaneously photographs the ground (nadir). Upon development and measurement, the photographs can be utilized to find the attitude of the camera's optical axis at the time of photograph.

Zenith: the point where the upward extension of the plumb-bob direction intersects the celestial sphere.

REFERENCE

1. "Flight Performance Handbook for Orbital Operations," Appendix A, Space Technology Laboratories, Inc. (Redondo Beach, California), September 1961.

APPENDIX B

ACKNOWLEDGEMENT

The Martin Company expresses its grateful appreciation to Dr. Helmut G. L. Krause of NASA for his permission to reproduce his study, "On a Consistent System of Astrodynamic Constants." It was formerly published by the George C. Marshall Space Flight Center, Propulsion and Vehicle Engineering Division, Huntsville, Alabama.

1. THE ASTRONOMICAL UNIT AND THE SOLAR PARALLAX

The astronomical unit (A.U.), or the Earth's mean distance from the Sun, is connected with the solar parallax (π_0) by the following relation (with $R_e = 6378.170 \pm 0.020$ km the equatorial radius of the Earth):

$$1 \text{ A.U.} = \frac{R_e}{\sin \pi_0} = \frac{R_e}{\pi_0'' \sin 1''} = \frac{206264.806247}{\pi_0''} R_e = \frac{1315592000 \pm 4000}{\pi_0''} \quad (1)$$

Modern determinations of the solar parallax usually are included between the two values $\pi_0 = 8.790 \pm 0.001$ (H. Spencer Jones, 1941) and $\pi_0 = 8.79835 \pm 0.00039$ (E. Rabe, 1949). The mean value of both determinations, $\pi_0 = 8.794 \pm 0.002$, has been accepted by C. W. Allen (Ref. 1, p. 131) in his book on "Astrophysical Quantities" (1955). Exactly in the middle of these two values are also the recently obtained data of radar echoes from Venus, which have a considerably higher accuracy than previous determinations. Furthermore, agreement of the different radio observatories is also very good, as shown in the following table:

| Radio Observatory | Author (Year) | Ref. | Radar Frequency (MC/sec) | Astronomical Unit (km) | Solar Parallax ($R_e = 6378.170$ km) |
|----------------------------------|--------------------------------------|------|-----------------------------|---------------------------|--|
| Millstone (Lincoln Lab., M.I.T.) | Pettengill, Price et. al. (1961) | 2 | 440 | 149597850 ± 400 | 8.79419_1 |
| Goldstone (J.P.L.) | Victor, Stevens and Muhlemann (1961) | 3 | 2388 | 149598845 ± 250 | 8.79413_2 |
| Jodrell Bank (U. of Manchester) | Thomson et. al. (1961) | | 408 | 149601000 ± 5000 | 8.79400_5 |
| Moorestown (R.C.A.) | Maron et. al. (1961) | | --- | 149596000 | 8.79429_9 |
| U. S. S. R. | Kotelnikov (1961) | | 700 | 149599500 ± 800 | 8.79409_4 |
| | | | | | 8.79414_4 |

According to Newcomb and de Sitter the semimajor axis of the Earth's orbit around the Sun is given by $a_\oplus = 1.000000236 \pm 0.000000004$ A.U. (or approximately 35 km more than 1 A.U.). For practical purposes both distances will be assumed equal to

$$a_\oplus = 149598700 \pm 400 = 149598700 (1 \pm 2.7 \times 10^{-6}) \text{ km} \quad (2)$$

The corresponding solar parallax will be

$$\pi_0 = \frac{R_e}{a_\oplus \sin 1''} = 206264.806247 \frac{6378.170 \pm 0.020}{149598700 \pm 400} = 8.79414 \pm 0.00005 \quad (3)$$

Taking as best value for the light velocity the value determined by Froome (Ref. 4) in 1958:

$$c = 299792.5 \pm 0.1 = 299792.5 (1 \pm 3.3 \times 10^{-7}) \text{ km/sec} \quad (4)$$

the light-time for unit distance (1 A.U.) is therefore

$$\tau = \frac{a_{\oplus}}{c} = 499.007_5 \pm 0.018 = 499.007_5 (1 \pm 3.6 \times 10^{-5}) \text{ sec} \quad (5)$$

2. DEFINITION OF TIME UNITS, MEAN ORBITAL MOTIONS, AND ROTATIONAL ANGULAR VELOCITIES OF EARTH AND MOON

There are three different times which are in use, namely, the Greenwich mean solar time or universal time (U.T.), the Greenwich mean sidereal time (G.M.S.T.) and the ephemeris time (E.T.) or Newtonian time. Due to the variable rotation of the Earth, the mean solar time and the mean sidereal time do not have a constant rate. The observations are therefore functions of a variable time, while the gravitational theories for the Sun and the planets use a uniform time. The ephemeris time, having a constant rate is defined by the orbital motion of the Earth as given by Newcomb's Tables of the Sun. It is therefore necessary to apply corrections to our practical determinations of time. In addition to the fluctuations and the tidal slowing down of the Earth's rotation, the Moon also shows a real diminution in the angular mean motion which is not given by Brown's lunar theory.

The correction to Newcomb's tabulated tropical mean longitude of the Sun (Ref. 5)

$$L_{\odot} = 279^{\circ} 41' 48''.04 + 129 602 768''.13 T_E + 1''.089 T_E^2 \quad (6)$$

is, according to H. Spencer Jones (Ref. 6),

$$\Delta L_{\odot} = + 1''.00 + 2''.97 T + 1''.23 T^2 + 0.0748 B \quad (7)$$

when the observation times are in U.T. The time T is in Julian centuries of 36525^d counted from 1900 Jan. 0, 12^h U.T. (Greenwich mean noon) and B is the irregular fluctuation in the Moon's mean longitude in arc seconds (time of observation again expressed in U.T.). The Sun's tropical mean longitude, L_{\odot} , increases at the rate of 1'' in $86400 / (0.9856473354 \times 3600) = 24.34948$ sec, so that the correction to universal time, required to obtain ephemeris time is, according to H. Clemence (Ref. 7),

$$\Delta t \equiv t_E - t_U = 24.34948 \Delta L_{\odot} = + 24''.5349 + 72''.318 T + 29''.5950 T^2 + 1.82134 B \quad (8)$$

H. Spencer Jones gives for the irregular fluctuation (Ref. 6)

$$B = (L_{\text{obs.}} - L_{\text{tabular}}) + 10''.71 \sin(140^{\circ} 0 T + 240^{\circ} 7) - 4''.65 - 12''.96 T - 5''.22 T^2 \quad (9)$$

The periodic term is Brown's empirical term in his lunar theory. Therefore the correction to the Moon's mean longitude, as given by Brown's Tables of the Motion of the Moon (Ref. 8), is

$$\Delta L_{\text{L}} \equiv L_{\text{obs.}} - L_{\text{tabular}} = + 4''.65 + 12''.96 T + 5''.22 T^2 + B - 10''.71 \sin(140^{\circ} 0 T + 240^{\circ} 7) \quad (10)$$

in order to obtain the actual mean longitude determined by observations in U.T. In the time

interval $\Delta t = t_E - t_U$ the Moon's mean longitude increases by ($n = 13.176\,396\,5268 \times 3600/86400 = 0.549\,016\,522''/\text{sec}$)

$$\Delta L_t = 0.549 \Delta t = 13.368 \Delta L_0 = +13.''37 + 39.''70 T + 16.''44 T^2 + B \quad (11)$$

Therefore the correction to Brown's Tables is

$$\Delta L_t - \Delta L_t = -8.''72 - 26.''74 T - 11.''22 T^2 - 10.''71 \sin(140^\circ 0' T + 240^\circ 7') \quad (12)$$

when the observations are in ephemeris time. Brown's theory is now reduced to a gravitational theory with the same measure of time as defined by Newcomb's Tables of the Sun. Clemence's corrected value for the Moon's mean longitude (Ref. 7)

$$L_t = 270^\circ 26' 2.''99 + 1\,732\,564\,379.''31 T_E - 4.''08 T_E^2 + 0.''0068 T_E^3 \quad (13)$$

is used in the American Ephemeris and Nautical Almanac.

By means of equation (6) the tropical year, from mean equinox to mean equinox, thus has the length

$$\begin{aligned} P_{\text{trop}} &= \frac{2\pi}{L_0} = \frac{1\,296\,000'' \times 36\,525^{dE}}{129\,602\,768.''13 + 2.''178 T} = 365.^{dE}242\,198\,78 - 0.^{dE}000\,006\,138 T \\ &= 365.^{dE}05^{hE}48^{mE}45.^{sE}9747 - 0.^{sE}5303 T = 31\,556\,925.^{sE}9747 - 0.^{sE}5303 T \quad (14) \end{aligned}$$

In 1957 the ephemeris second has been adopted as the fundamental invariable unit of time, and it is the fraction $1/31\,556\,925.9747$ of the tropical year for 1900 Jan. 0, 12^h E.T. (Ref. 9)

The basis for all civil time-keeping is the universal time which is non-uniform. In practical life, however, the difference between mean solar time and ephemeris time can be neglected because there is $1^d \approx (1 \pm 10^{-8})^{dE}$. To define universal time Newcomb introduced a fictitious mean Sun which moves with the same constant sidereal rate, in the equator, as the mean sidereal motion is for the true Sun, affected by aberration ($20.''50$) in the ecliptic. According to Newcomb, the right ascension of the fictitious mean Sun is (neglecting nutation in right ascension)

$$\begin{aligned} R_E &= 279^\circ 41' 27.''54 + 129\,602\,768.''13 T_E + 1.''394 T_E^2 \\ &= 18^h 38^m 45.^s836 + 8640184.^s542 T_E + 0.^s0929 T_E^2 \quad (15) \end{aligned}$$

Defining a point on the equator whose right ascension, measured from the mean equinox of date, is

$$R_U = 18^h 38^m 45.^s836 + 8640184.^s542 T_U + 0.^s0929 T_U^2, \quad (16)$$

and where R_E differs from R_U by $0.002738 \Delta t$ (see equation 8), the Greenwich hour angle

$\tau_{Gr(R_U)}$ of the point whose right ascension is R_U [equal to universal time (U.T.) $\pm 12^h$], increased by the right ascension R_U , is the Greenwich hour angle, $\tau_{Gr}(\gamma)$, of the mean vernal equinox of date which is Greenwich mean sidereal time, Θ_{Gr} . That is,

$$\text{U.T.} \pm 12^h + R_U = \tau_{Gr(R_U)} + R_U = \tau_{Gr}(\gamma) \equiv \Theta_{Gr} \quad (17)$$

Adding the East longitude to both sides gives the local mean time on the left side of the equation and the local mean sidereal time on the right side, because

$$\Theta = \Theta_{Gr} + \lambda_{\text{east.}}$$

The time rate of the right ascension, given by differentiation of equation (16), is

$$\begin{aligned} \dot{R}_U &= 8640184.542 + 0.1858 T_U [\text{sec/Jul. century}] \\ &= 129602768.13 + 2.788 T_U ["/\text{Jul. century}] \\ &= 3548.3304074 + 0.00007633 T_U ["/\text{d}] \\ &= 0.9856473354 + 2.1203 \times 10^{-8} T_U [^\circ/\text{d}], \end{aligned} \quad (18)$$

Adding to this the time rate of the hour angle, $\dot{\tau} = 360^\circ/\text{d} = 1296000 "/\text{d}$, the time rate of the mean sidereal time is then

$$\begin{aligned} \dot{\Theta}_m &= 1299548.3304074 + 0.00007633 T ["/\text{d}] \\ &= 360.9856473354 + 2.1203 \times 10^{-8} T [^\circ/\text{d}] \\ &= 15.04106863897 + 8.835 \times 10^{-10} T ["/\text{s} \text{ or } ^\circ/\text{h}] \\ &= 1.002737909265 + 0.5890 \times 10^{-10} T [\text{d}_*/\text{d} \text{ or } \text{s}_*/\text{s}] \\ &= 7.29211585458 \times 10^{-5} + 4.283 \times 10^{-15} T [\text{rad/s}] \end{aligned} \quad (19)$$

This motion is the result of the spin of the Earth and the motion of the vernal equinox (precession). Because the latter motion takes place in the ecliptic the equatorial component or the general precession in right ascension, m , must be used here. The mean angular velocity of the Earth's rotation is, therefore,

$$\Omega_m = \dot{\Theta}_m - m \quad (20)$$

It is very probable that Newcomb's value for the general precession in longitude, p , must be increased by $\Delta p = + 0.780$ per tropical century (see Part 9), thus

$$\begin{aligned} p &= 5026.441 + 2.2229 T + 0.00026 T^2 ["/\text{trop. century}] \\ &= 0.1376194 + 0.000060861 T + 0.712 \times 10^{-8} T^2 ["/\text{d}] \\ &= 0.00003822761 + 0.00000016906 T + 1.98 \times 10^{-12} T^2 [^\circ/\text{d}] \end{aligned} \quad (21)$$

Neglecting the correction in planetary precession ($\Delta\lambda = 0$) the correction for the general precession in right ascension would be $\Delta m = \Delta p \cdot \cos \epsilon = 0''.80 \times 0.917 = + 0''.73$. Thus,

$$\begin{aligned} m &= 4609.236 + 2.7945 T + 0.00012 T^2 ["/\text{trop. century}] \\ &= 0.1261967 + 0.000076511 T + 0.33 \times 10^{-8} T^2 ["/\text{d}] \\ &= 0.00003505464 + 0.000000021253 T + 0.92 \times 10^{-12} T^2 [^\circ/\text{d}] \end{aligned} \quad (22)$$

The angular velocity of the Earth's rotation is, therefore,

$$\begin{aligned} \Omega_m &= 1299548.2042107 - 0.00000018 T ["/\text{d}] \\ &= 360.9856122808 - 0.0050 \times 10^{-8} T [^\circ/\text{d}] \\ &= 15.04106717837 - 0.021 \times 10^{-10} T ["/\text{s or } ^\circ/\text{h}] \\ &= 1.002737811891 - 0.0014 \times 10^{-10} T [\text{rot}/\text{d}] \\ &= 7.29211514646 \times 10^{-5} - 0.010 \times 10^{-15} T [\text{rad}/\text{s}] \end{aligned} \quad (23)$$

Using equations (19) and (23) the following periods are obtained:

1. Mean solar day (culmination period of the mean Sun)

$$\begin{aligned} 1^d &= 1^d \cdot 002737909265 + 0^d \cdot 589 \times 10^{-10} T \\ &= 86636^s \cdot 55536050 + 0^s \cdot 0508896 \times 10^{-4} T \\ &= 24^h \cdot 03^m \cdot 56^s \cdot 55536050 + 0^s \cdot 0508896 \times 10^{-4} T \\ &= 1^{\text{rot}} \cdot 002737811891 - 0^{\text{rot}} \cdot 0014 \times 10^{-10} T \\ &= (1 + 10^{-8})^{dE} \end{aligned} \quad (24)$$

2. Mean sidereal day or mean equinoctial day (culmination period of the vernal equinox)

$$\begin{aligned} 1^{d*} &= 1^d - 0^d \cdot 002730433586 - 0^d \cdot 587 \times 10^{-10} T \\ &= 0^d \cdot 997269566414 - 0^d \cdot 587 \times 10^{-10} T \\ &= 86164^s \cdot 09053817 - 0^s \cdot 0507168 \times 10^{-4} T \\ &= 23^h \cdot 56^m \cdot 04^s \cdot 09053817 - 0^s \cdot 0507168 \times 10^{-4} T \\ &= \frac{\Omega}{\Theta} = 1 - \frac{m}{\Theta} = (1 - 0.00000097108)^{\text{rot}} - 0^{\text{rot}} \cdot 589 \times 10^{-10} T \\ &= 0^{\text{rot}} \cdot 999999902892 - 0^{\text{rot}} \cdot 589 \times 10^{-10} T \end{aligned} \quad (25)$$

3. Period of the Earth's rotation (culmination period of an equatorial star without proper motion)

$$\begin{aligned}
 1^{\text{rot}} &= \frac{\dot{\Theta}}{\Omega} = 1 + \frac{m}{\Omega} = 1^{\text{d}} \cdot 000\,000\,097\,108 + 0^{\text{d}} \cdot 589 \times 10^{-10} T \\
 &= 86400^{\text{s}} \cdot 008\,390\,13 + 0^{\text{s}} \cdot 050\,889\,6 \times 10^{-4} T \\
 &= 1^{\text{d}} - 0^{\text{d}} \cdot 002\,730\,336\,743 + 0^{\text{d}} \cdot 001\,4 \times 10^{-10} T \\
 &= 1^{\text{d}} - 235^{\text{s}} \cdot 901\,094\,60 + 0^{\text{s}} \cdot 000\,120\,96 \times 10^{-4} T \\
 &= 0^{\text{d}} \cdot 997\,269\,663\,257 + 0^{\text{d}} \cdot 001\,4 \times 10^{-10} T \\
 &= 86\,164^{\text{s}} \cdot 098\,905\,40 + 0^{\text{s}} \cdot 001\,209\,6 \times 10^{-5} T
 \end{aligned} \tag{26}$$

Because

$$\begin{aligned}
 1^{\text{d}} - 1^{\text{d}*} &= 236^{\text{s}} \cdot 555\,360\,50 + 0^{\text{s}} \cdot 050\,889\,6 \times 10^{-4} T \\
 &= 235^{\text{s}} \cdot 909\,461\,83 + 0^{\text{s}} \cdot 050\,716\,8 \times 10^{-4} T
 \end{aligned}$$

or

$$1^{\text{h}} - 1^{\text{h}*} = 9^{\text{s}} \cdot 856\,473 = 9^{\text{s}} \cdot 829\,561$$

the change of mean sidereal time against mean solar time is $9^{\text{s}} \cdot 856\,47$ in a mean solar hour and $9^{\text{s}} \cdot 829\,56$ in a mean sidereal hour.

In order to apply Kepler's third law, the sidereal mean angular motions of the Earth about the Sun and the Moon about the Earth will be needed. Differentiation of equation (6) gives the tropical mean motion of the Earth:

$$\begin{aligned}
 n_{\oplus}(\text{trop.}) &= \dot{L}_{\odot} = 129\,602\,768.13 + 2.178 T \text{ [''/Jul. century]} \\
 &= 3548.330\,407\,4 + 0.000\,059\,63 T \text{ [''/d]} \\
 &= 0.985\,647\,335\,4 + 1.6564 \times 10^{-8} T \text{ [°/d]}
 \end{aligned} \tag{27}$$

Subtracting from this the general precession in longitude (equation 21) yields the sidereal mean motion of the Earth:

$$\begin{aligned}
 n_{\oplus}(\text{sid.}) &= \dot{L}_{\odot} - p = 3548.192\,788\,0 - 0.000\,001\,23 T \text{ [''/d]} \\
 &= 0.985\,609\,1078 - 0.0342 \times 10^{-8} T \text{ [°/d]} \\
 &= 0.041\,067\,046\,16 - 0.1424 \times 10^{-10} T \text{ [''/s]} \\
 &= 1.990\,986\,582\,0 \times 10^{-7} - 0.690\,374\,68 \times 10^{-16} T \text{ [rad/s]}
 \end{aligned} \tag{28}$$

Differentiating equation (13) provides the tropical mean motion of the Moon:

$$\begin{aligned}
n_{\bullet} (\text{trop}) &= \dot{L}_{\bullet} = 1732564379.31 - 8.16 T + 0.0204 T^2 [''/\text{Jul. century}] \\
&= 47435.0274965 - 2.234 \times 10^{-4} T + 0.559 \times 10^{-6} T^2 [''/\text{d}] \\
&= 13.1763965268 - 6.206 \times 10^{-8} T + 1.55 \times 10^{-10} T^2 [^{\circ}/\text{d}] \\
&= 0.549016521950 - 2.586 \times 10^{-9} T + 6.46 \times 10^{-12} T^2 [''/\text{s}] \quad (29)
\end{aligned}$$

and subtraction of the general precession in longitude, p , gives the sidereal mean motion of the Moon:

$$\begin{aligned}
n_{\bullet} (\text{sid.}) &= \dot{L}_{\bullet} - p = 47434.8898771 - 2.843 \times 10^{-4} T + 0.552 \times 10^{-6} T^2 [''/\text{d}] \\
&= 13.1763582992 - 7.897 \times 10^{-8} T + 1.53 \times 10^{-10} T^2 [^{\circ}/\text{d}] \\
&= 0.549014929133 - 3.290 \times 10^{-8} T + 6.38 \times 10^{-12} T^2 [''/\text{s}] \\
&= 2.66169948773 \times 10^{-6} - 1.595 \times 10^{-13} T + 3.09 \times 10^{-17} T^2 [\text{rad/s}] \quad (30)
\end{aligned}$$

Because the distance of the Earth to the Sun is now known more accurately than before, it is possible to give the mean orbital velocity of the Earth about the Sun with high accuracy, namely

$$v_{\oplus} = a_{\oplus} n_{\oplus} = 29784.90 \pm 0.08 [\text{m/s}] \quad (31)$$

There are two constants connected with this velocity. Taking $e = 0.01675$ for the orbital eccentricity of the Earth the value for the constant of aberration will be

$$K = \frac{v_{\oplus}/c}{\sqrt{1-e^2} \sin 1''} = \frac{\tau n_{\oplus}}{\sqrt{1-e^2} \sin 1''} = 20.''4956 \pm 0.''0007, \quad (32)$$

and using the formula of de Sitter (Ref. 10) the geodetic precession, due to the special theory of relativity, is

$$p_g = \frac{3}{2} (v_{\oplus}/c)^2 n_{\oplus} = \frac{3}{2} (K \sin 1'' \sqrt{1-e^2})^2 n_{\oplus} = 1.''9188 \pm 0.''0002 \quad (33)$$

3. THE LUNAR DISTANCE AND THE LUNAR PARALLAX

The mean observed distance, \bar{r}_{\bullet} , of the Moon from the Earth is connected with the mean perturbed lunar parallax, π_{\bullet} , and the constant π'_{\bullet} of the sine of the perturbed lunar parallax by the following relation:

$$\frac{\bar{r}_{\bullet}}{R_e} = \frac{1}{\sin \pi_{\bullet}} = \frac{1}{\pi'_{\bullet} \sin 1''} \quad (34)$$

Dividing both sides of the series development

$$\pi_{\bullet} = \sin \pi_{\bullet} + \frac{1}{6} \sin^3 \pi_{\bullet} + \dots$$

by $\sin 1''$ yields (because $\pi'_i = \sin \pi_i / \sin 1''$)

$$\begin{aligned}\pi''_i &= \pi'_i + \frac{1}{6} (\pi'_i)^3 (\sin 1'')^2 + \dots = \pi'_i \left[1 + \frac{1}{6} \left(\frac{R_e}{\bar{r}_i} \right)^2 + \dots \right] \\ &= \pi'_i \times 1.000045885 = \pi'_i + 0.''157\end{aligned}\quad (35)$$

Newer determinations are

| | | |
|----------------------|----------------------|--------------------------------|
| $\pi'_i = 3422.''54$ | $\pi_i = 3422.70$ | (E.W. Brown, Ref. 8) |
| 3422.526 ± 0.009 | 3422.683 ± 0.009 | (W. deSitter, Ref. 10) |
| 3422.419 ± 0.024 | 3422.576 ± 0.024 | (H. Jeffreys, Ref. 11, p. 193) |
| 3422.493 | 3422.650 | (Herrick, Baker, Ref. 12) |

Recent determinations of the mean lunar distance, \bar{r}_i , by means of radar echoes to the Moon are in very close agreement (see Reference 13). This value is given by

$$\bar{r}_i = 384402.0 + 1.0 = 384402.0 (1 \pm 2.6 \times 10^{-6}) \text{ km} \quad (36)$$

thus

$$\frac{\bar{r}_i}{R_e} = \frac{384402.0 (1 \pm 2.6 \times 10^{-6})}{6378.170 (1 \pm 3.2 \times 10^{-6})} = 60.26838 (1 \pm 5.8 \times 10^{-6}) = 60.26838 \pm 0.00035 \quad (37)$$

and

$$\pi'_i = \frac{\sin \pi_i}{\sin 1''} = \frac{206264.''806247}{(\bar{r}_i/R_e)} = 3422.''438 \pm 0.''020 \quad (38)$$

$$\pi_i = 3422.''595 + 0.''020 \quad (39)$$

To obtain the semi-major axis, a_i , it is necessary to add to the mean lunar distance the constant part of the solar perturbations according to Brown's lunar theory. There is now

$$a_i = 1.000907681 \bar{r}_i = 384750.9 \pm 1.0 \text{ km} \quad (40)$$

and the mean orbital velocity of the Moon about the Earth is

$$v_i = a_i n_i = 1024.091 \pm 0.003 \text{ m/s} \quad (41)$$

4. MASS RATIOS OF THE SUN AND THE EARTH-MOON SYSTEM

Taking the already given values for a_\oplus , n_\oplus (sid.), and a_i , n_i (sid.) then Kepler's third law gives

$$n_\oplus^2 a_\oplus^3 = G (M_\odot + M_\oplus + M_i) = G M_\oplus (\nu + 1)(1 + \kappa) \quad (42)$$

$$n_i^2 a_i^3 = G (M_\oplus + M_i) = G M_\oplus (1 + \kappa) \quad (43)$$

with

$$\nu = \frac{M_{\odot}}{M_{\oplus} + M_{\ddagger}} \gg 1 \quad ; \quad \kappa = \frac{M_{\ddagger}}{M_{\oplus}} \ll 1 \quad (44)$$

Dividing the two equations yields

$$\begin{aligned} \nu &\equiv \frac{M_{\odot}}{M_{\oplus} + M_{\ddagger}} = \left(\frac{n_{\oplus}}{n_{\ddagger}}\right)^2 \left(\frac{a_{\oplus}}{a_{\ddagger}}\right)^3 - 1 = \left(\frac{v_{\oplus}}{v_{\ddagger}}\right)^2 \left(\frac{a_{\oplus}}{a_{\ddagger}}\right) - 1 \\ &= 328898.6 (1 \pm 1.6 \times 10^{-5}) = 328898.6 \pm 5.2 \end{aligned} \quad (45)$$

This value is approximately in the middle between the value 329390 obtained by S. Newcomb (Ref. 14), adopted by Am. Ephemeris, and the value 328446 ± 43 determined by E. Rabe (Ref. 15).

The second equation gives

$$\mu_{\oplus} (1 + \kappa) = n_{\ddagger}^2 a_{\ddagger}^3 = v_{\ddagger}^2 a_{\ddagger} = 403512.3 \pm 3.2 \text{ km}^3/\text{s}^2 \quad (46)$$

which connects the gravitational parameter $\mu_{\oplus} = G M_{\oplus}$ for the Earth with κ , the ratio of the Moon's mass to the Earth's mass.

5. THE CONSTANT OF LUNAR INEQUALITY AND THE PARALLACTIC INEQUALITY IN MOON'S ECLIPTIC LONGITUDE

The Parallactic Inequality in the Moon's ecliptic longitude is given by E. W. Brown's lunar theory as follows

$$P_* = (49853.''2 \pm 1.''2) \frac{1 - \kappa}{1 + \kappa} \frac{\pi_{\odot}}{\pi_{\ddagger}} = (49853.''2 \pm 1.''2) \frac{1/\kappa - 1}{1/\kappa + 1} \frac{\overline{r}_e}{a_{\oplus}} \quad (47)$$

or with the newest data for the lunar distance and the astronomical unit

$$P_* = (128.''1005 \pm 0.''0037) \frac{1/\kappa - 1}{1/\kappa + 1} \quad (48)$$

Newer determinations are:

$$\begin{aligned} P_* &= 124.''86 \pm 0.''15 && (\text{J. Bauschinger, Ref. 16}) \\ &= 125.154 && (\text{E. W. Brown, Ref. 8}) \\ &= 124.93 && (\text{H. Battermann, Ref. 17}) \\ &= 124.969 \pm 0.042 && (\text{D. Brouwer and O. B. Watts, Ref. 18}) \end{aligned}$$

On the other hand, the constant of Lunar Inequality is defined by W. deSitter (Ref. 10) as

$$L = \frac{\kappa}{1 + \kappa} \frac{\pi_{\odot}}{\sin \pi_{\ddagger}} = \frac{206264.''806247}{1/\kappa + 1} \frac{\pi_{\odot}}{\pi_{\ddagger}} = \frac{530.''0089 \pm 0.''0028}{1/\kappa + 1} \quad (49)$$

Newcomb used the lunar inequality in the Sun's longitude which is, according to deSitter, $L_s = 1.00450 L$. The ratio of P_* and L , depending only on κ , is

$$P_*/L = \frac{49853.''2 \pm 1.''2}{206264.''806247} (1/\kappa - 1) = (0.241695 \pm 0.000006) (1/\kappa - 1) \quad (50)$$

The mass ratio is therefore

$$1/\kappa = (4.13744_4 \pm 0.00010) \frac{P_*}{L} + 1 = \frac{530.''0089 \pm 0.''0028}{L} - 1 = \frac{128.''1005 + P_*}{128.''1005 - P_*} \quad (51)$$

Observed values for the constant of Lunar Inequality are:

| | | | |
|---------------------------|-----------------------------|----------------------|---------------------|
| $L = 6.''456 \pm 0.''012$ | (Newcomb, Ref. 14) | From observations of | Sun |
| 6.414 ± 0.009 | (D. Gill, Ref. 19) | " | Victoria |
| 6.4305 ± 0.0031 | (A.R. Hinks, Ref. 20) | " | Eros (opp. of 1901) |
| 6.4390 ± 0.0015 | (H. Spencer Jones, Ref. 21) | " | Eros (opp. of 1931) |
| 6.450 ± 0.010 | (Morgan and Scott, Ref. 22) | " | Sun |
| 6.4378 ± 0.0015 | (H. Jeffreys, Ref. 23) | " | Eros (opp. of 1931) |
| 6.4356 ± 0.0028 | (E. Rabe, Ref. 15) | " | Eros (opp. of 1931) |
| 6.4428 ± 0.0014 | | " | |
| 6.4430 ± 0.0017 | (E. Delano, Ref. 24) | " | Eros (opp. of 1931) |

The latest reevaluation of all Eros observations during the opposition of 1930/31 by E. Delano (Ref. 24) gave

$$\begin{aligned} L &= 6.''4428 \pm 0.''0014 && \text{(from right ascensions of Eros)} \\ L &= 6.4430 \pm 0.0017 && \text{(from declinations of Eros)} \end{aligned}$$

Delano used the old value $\pi_0 = 8.''790$ for the solar parallax and obtained therefore $1/\kappa = 81.222 \pm 0.027$ and 81.219 ± 0.030 , respectively. With the newest values for π_0 and π'_1 there is now

$$1/\kappa = 81.263_7 \quad \text{and} \quad 1/\kappa = 81.261_2$$

respectively.

6. ANOTHER METHOD FOR THE DETERMINATION OF THE RATIO OF THE MASSES OF EARTH AND MOON

The mass of the Earth is given by

$$M_{\oplus} = \frac{4}{3} \pi R_{\oplus}^3 (1-f) \rho_{\oplus} \quad (52)$$

where f is the flattening (oblateness) and ρ_{\oplus} is the mean density of the Earth. On the other hand the mass of the triaxial figure of the Moon is given by

$$M_{\bullet} = \frac{4}{3} \pi a b c \rho_{\bullet} = \frac{4}{3} \pi a^3 \left(\frac{b}{a}\right) \left(\frac{c}{a}\right) \rho_{\bullet} \quad (53)$$

Because the longest axis is always directed to the Earth (neglecting the small librations) and can never be seen, the lunar radius of the visible disk is

$$R_{\bullet} = \frac{b+c}{2} \quad ; \quad \frac{R_{\bullet}}{a} = \frac{1}{2} \left(\frac{b}{a} + \frac{c}{a} \right) = \sigma \quad (54)$$

That yields for the mass of the moon

$$M_{\bullet} = \frac{4}{3} \pi R_{\bullet}^3 \frac{(b/a)(c/a)}{\sigma^3} \rho_{\bullet} \quad (55)$$

The mass ratio is therefore

$$1/\kappa \equiv M_{\oplus}/M_{\bullet} = \left(\frac{R_{\oplus}}{R_{\bullet}} \right)^3 \frac{(1-f) \sigma^3}{(b/a)(c/a)} \left(\frac{\rho_{\oplus}}{\rho_{\bullet}} \right) \frac{(1-f) \sigma^3}{(b/a)(c/a)} \frac{\rho_{\oplus}/\rho_{\bullet}}{k^3} \quad (56)$$

where

$$k = \frac{R_{\bullet}}{R_e} = \frac{\sin s_{\bullet}}{\sin \pi_{\bullet}} = \frac{s'_{\bullet}}{\pi'_{\bullet}} = \frac{s_{\bullet} - 0.''003}{\pi_{\bullet} - 0.''157} \quad (57)$$

is given by the lunar parallax, π_{\bullet} , and the apparent semi-diameter of the Moon, s_{\bullet} .

A reevaluation of Sir Harold Jeffrey's best data on the Moon's figure by the author gave (see section 12)

$$\frac{b}{a} = 0.9998116 \quad ; \quad \frac{c}{a} = 0.9993720 \quad ; \quad \sigma = 0.9995918$$

From the secular perturbations of artificial Earth satellites there follows as best value for the Earth oblateness

$$1/f = 298.30 \quad ; \quad 1-f = 0.99664767$$

so that

$$1/\kappa = 0.9962409 \frac{\rho_{\oplus}/\rho_{\bullet}}{k^3} \quad (58)$$

Taking for the mean densities the well-known and frequently used values

$$\rho_{\oplus} = 5.517 \pm 0.004 \text{ g/cm}^3 \text{ (Heyl)} \quad ; \quad \rho_{\bullet} = 3.342 \pm 0.005 \text{ g/cm}^3 \text{ (Jeffreys)}$$

the density ratio, independent from the assumed value of the gravitational constant, G , becomes $\rho_{\oplus}/\rho_{\bullet} = 1.6508$. Therefore

$$1/\kappa = 1.6446/k^3 \quad (59)$$

With $\pi'_4 = 3422.''438$ and various values for s_4 the following table is obtained

| s_4 | k | $1/\kappa$ |
|--|-----------|------------|
| 932.''58 (Newcomb, Ref. 25) | 0.2724891 | 81.286 |
| 932.63 (American Ephemer., Ref. 26) | 0.2725037 | 81.272 |
| 932.80 + 0.07 (Hirose & Manabe, Ref. 27) | 0.2725534 | 81.228 |

The American Ephemeris is using $k = 0.2724953$, based on Brown's lunar parallax. The values for $1/\kappa$ obtained in the previous paragraph are between the two latter values in this table. The arithmetic mean of these two latter values will be taken as the presently best value, namely

$$1/\kappa \equiv \frac{M_{\oplus}}{M_4} = 81.250 (1 \pm 3 \times 10^{-4}) = 81.250 \pm 0.024 \quad (60)$$

and therefore

$$k \equiv \frac{R_4}{R_e} = 0.2725289 \pm 0.0000273 \quad (61)$$

The last equation of paragraph 4 now gives

$$\mu_{\oplus} \equiv GM_{\oplus} = \frac{403512.3}{1.0123077} = 398606.4 \pm 4.9 \text{ km}^3/\text{sec}^2 \quad (62)$$

for the Earth, while, for the Moon,

$$\mu_4 \equiv GM_4 = \kappa \mu_{\oplus} = 4905.92 \pm 1.52 \text{ km}^3/\text{sec}^2 \quad (63)$$

7. GEODYNAMIC (TERRESTRIAL) RELATIONS

The surface of the Earth (geoid) can be approximated as the surface of an spheroid assumed as an equipotential surface. The equation for the Earth's radius, as function of the latitude, is then given by

$$R = R_e \left[1 - f \sin^2 \varphi + \left(\frac{5}{8} f^2 - \kappa \right) \sin^2 2\varphi \right] = R_e \left[1 - f \sin^2 \phi - \left(\frac{3}{8} f^2 + \kappa \right) \sin^2 2\phi \right] \quad (64)$$

where φ is the geodetic (geographic) latitude and ϕ the geocentric latitude. They are related by

$$\tan \phi = (1 - f)^2 \tan \varphi = (1 - e^2) \tan \varphi \quad (65)$$

where $e = \sqrt{f(2 - f)}$ is the eccentricity of the meridian ellipse of the Earth. The equation of the Earth-ellipsoid is obtained by setting $\kappa = 0$. The maximum depression, $-\kappa R_e$, of the spheroid from the ellipsoid is reached at the latitude 45° . It will never be more than 5.17 m. For the spheroid as equipotential surface there is

$$\begin{aligned} U &= \frac{GM}{R} \left[1 - \frac{2}{3} J \left(\frac{R}{R_e} \right)^2 P_2(\sin \phi) + \frac{4}{15} K \left(\frac{R}{R_e} \right)^4 P_4(\sin \phi) + \dots \right] + \frac{1}{2} \Omega^2 R^2 \cos^2 \phi \\ &= \frac{GM}{R} \left[1 - \sum_{n=2}^{\infty} J_n \left(\frac{R}{R_e} \right)^n P_n(\sin \phi) \right] + \frac{1}{2} \Omega^2 R^2 \cos^2 \phi = \text{const.} \end{aligned} \quad (66)$$

and the acceleration of gravity at this surface is

$$g = |\text{grad } U| = g_e [1 + \beta \sin^2 \varphi + \gamma \sin^2 2\varphi] = g_e [1 + \beta \sin^2 \phi + (\gamma + \beta f) \sin^2 2\phi] \quad (67)$$

where Ω is the angular velocity of the Earth's rotation, β and γ are constant gravity coefficients and J_n or J and K are constant oblateness coefficients. These coefficients depend only on f , κ , and a parameter containing Ω^2 (centrifugal force parameter). This latter parameter is a little different in the various second-order theories which have been developed. Taking

$$\Omega = 7.292115146 \times 10^{-5} \text{ rad/sec}$$

$$1/f = 298.30 \quad ; \quad 1 - f = 0.996647670$$

$$G = 6.670 \times 10^{-8} \text{ cm}^3/(\text{g-sec}^2) \quad ; \quad \rho_m = 5.517 \text{ g/cm}^3 \quad ; \quad G \rho_m = 3.679839 \times 10^{-7} \quad (68)$$

then the following parameters could be used

$$\tilde{\omega} = \frac{\Omega^2 R_e^3}{GM} = \frac{\Omega^2}{4/3 \pi G \rho_m (1-f)} = 0.003461369 \text{ [Herrick, (Ref.12)]} \quad (69)$$

$$\tilde{\omega}' = \frac{\Omega^2 R_v^3}{GM} = \frac{\Omega^2}{4/3 \pi G \rho_m} = \tilde{\omega} (1-f) = 0.003449766 \text{ [Jeffreys, Ref.11]} \quad (70)$$

$$\tilde{\omega}_1 = \frac{\Omega^2 R_1^3}{GM} = \tilde{\omega} \left(1 - f + 2f^2 - \frac{8}{3} \kappa\right) = \tilde{\omega}' \left(1 + 2f^2 - \frac{8}{3} \kappa\right) = 0.003449843 \text{ [deSitter, Ref.10]} \quad (71)$$

$$m = \frac{\Omega^2 R_e}{g_e} = \frac{\tilde{\omega}}{1 - A - \frac{3}{2} \tilde{\omega} + f + f^2 - \frac{3}{7} f \tilde{\omega} + \frac{16}{7} \kappa} = \frac{\tilde{\omega}}{1 - A - \tilde{\omega} + J + 1/2 K} \\ = 0.003467730 \text{ [Darwin, Ref.28; Helmert, Ref.29]} \quad (72)$$

where $R_v = R_e (1-f)^{1/3}$ is the radius for a sphere of same volume as the Earth and $R_1 = R_e (1 - 1/3 f + 5/9 f^2 - 8/9 \kappa)$ is the mean radius for which $P_2(\sin \varphi) = 0$ or $\varphi = \sin^{-1} \sqrt{1/3} = 35^\circ 15' 51''.8$. $A = 0.88 \times 10^{-6}$ is the mass of the Earth's atmosphere (expressed in mass of the Earth) which does not contribute to the surface gravity of the Earth. Different assumptions have been made for κ . Bullard (Ref.30) found $10^6 \kappa = 0.68$. This value was accepted later by Herrick, Baker, and Hilton (Ref.12). On the other hand, deSitter found values of only $10^6 \kappa = 0.47$ to 0.52 and used the round mean value $10^6 \kappa = 0.50$. The theoretical limits are according to deSitter (Ref. 31)

$$0 \leq \kappa \leq \frac{5}{16} f \tilde{\omega} - \frac{1}{4} f^2 = (3.62 - 2.81) \times 10^{-6} = 0.81 \times 10^{-6} \quad (73)$$

The different formula systems now yield

$$\begin{aligned}
J &= f - \frac{1}{2} \varpi - \frac{1}{2} f^2 + \frac{9}{14} f \varpi + \frac{4}{7} \kappa \\
&= f - \frac{1}{2} \varpi' - \frac{1}{2} f^2 + \frac{1}{7} f \varpi' + \frac{4}{7} \kappa \\
&= f - \frac{1}{2} \varpi_1 - \frac{1}{2} f^2 + \frac{1}{7} f \varpi_1 + \frac{4}{7} \kappa \\
&= f - \frac{1}{2} m - \frac{1}{2} f^2 + \frac{1}{7} f m + \frac{3}{4} m^2 + \frac{4}{7} \kappa
\end{aligned} \tag{74}$$

$$\begin{aligned}
K = \frac{6}{7} D &= 3 f^2 - \frac{15}{7} f \varpi + \frac{24}{7} \kappa \\
&= 3 f^2 - \frac{15}{7} f \varpi' + \frac{24}{7} \kappa \\
&= 3 f^2 - \frac{15}{7} f \varpi_1 + \frac{24}{7} \kappa \\
&= 3 f^2 - \frac{15}{7} f m + \frac{24}{7} \kappa
\end{aligned} \tag{75}$$

$$\begin{aligned}
\beta &= \frac{5}{2} \varpi - f - \frac{26}{7} f \varpi + \frac{15}{4} \varpi^2 + \frac{8}{7} \kappa \\
&= \frac{5}{2} \varpi' - f - \frac{17}{14} f \varpi' + \frac{15}{4} \varpi'^2 + \frac{8}{7} \kappa \\
&= \frac{5}{2} \varpi_1 - f - \frac{17}{14} f \varpi_1 + \frac{15}{4} \varpi_1^2 + \frac{8}{7} \kappa \\
&= \frac{5}{2} m - f - \frac{17}{14} f m + \frac{8}{7} \kappa
\end{aligned} \tag{76}$$

$$\begin{aligned}
\gamma &= \frac{1}{8} f^2 - \frac{5}{8} f \varpi - 3 \kappa \\
&= \frac{1}{8} f^2 - \frac{5}{8} f \varpi' - 3 \kappa \\
&= \frac{1}{8} f^2 - \frac{5}{8} f \varpi_1 - 3 \kappa \\
&= \frac{1}{8} f^2 - \frac{5}{8} f m - 3 \kappa
\end{aligned} \tag{77}$$

$$\begin{aligned}
\chi &\equiv g_e / (GM/R_e^2) = 1 - A - \omega + J + \frac{1}{2} K \\
&= 1 - A - \frac{3}{2} \omega + f + f^2 - \frac{3}{7} f \omega + \frac{16}{7} \kappa \\
&= 1 - A - \frac{3}{2} \omega' + f + f^2 - \frac{27}{14} f \omega' + \frac{16}{7} \kappa \\
&= 1 - A - \frac{3}{2} \omega_1 + f + f^2 - \frac{27}{14} f \omega_1 + \frac{16}{7} \kappa \\
&= 1 - A - \frac{3}{2} m + f + f^2 - \frac{27}{14} f m + \frac{9}{4} m^2 + \frac{16}{7} \kappa
\end{aligned} \tag{78}$$

Using these equations and the above-given constants for the Earth then the following table is obtained with $J_2 \equiv (C - A)/(M R_e^2) = \frac{2}{3} J$ and $J_4 = -\frac{4}{15} K = -\frac{8}{35} D$:

| Coefficient | $\kappa = 0$ | $\kappa = 0.50 \times 10^{-6}$ | $\kappa = 0.68 \times 10^{-6}$ |
|-------------------------------|-------------------|--------------------------------|--------------------------------|
| $10^6 J$ $10^6 K$ | 1623.48 8.85 | 1623.77 10.56 | 1623.87 11.18 |
| $10^6 J_2$ $10^6 J_4$ | 1082.32 - 2.36 | 1082.51 - 2.82 | 1082.58 - 2.98 |
| $10^6 \beta$ $10^6 \gamma$ | 5302.92 - 5.85 | 5303.49 - 7.35 | 5303.70 - 7.89 |
| χ | 0.9981 6566 | 0.9981 6680 | 0.9981 6721 |

The numerical values for $|J_4|$ are a little higher than the values derived from the observed secular perturbations of artificial satellites. Thus the data for $\kappa = 0$ will be used here.

The gravitational parameter of the Earth is now given by

$$\mu_{\oplus} \equiv GM_{\oplus} = \frac{4}{3} \pi G \rho_{\oplus} R_e^3 (1 - f) = \frac{g_e R_e^2}{\chi} = 398606.4 \pm 4.9 \text{ km}^3/\text{sec}^2 \tag{79}$$

which corresponds to $1/\kappa = 81.250$. Taking, furthermore, $\frac{4}{3} \pi = 4.188790204$; $1 - f = 0.996647670$; $\chi = 0.99816566$ that yields

$$g_e R_e^2 = \chi \mu_{\oplus} = 397875.2 \pm 4.9 \text{ km}^2/\text{sec}^2 = 3.978752 \times 10^{14} \text{ m}^3/\text{sec}^2 \tag{80}$$

and

$$\frac{g_e}{R_e} = \frac{4}{3} \pi (1 - f) \chi G \rho_{\oplus} = 4.167090090 G \rho_{\oplus} \tag{81}$$

or with $G = 6.670 \times 10^{-8} \text{ cm}^3/\text{g} \cdot \text{sec}^2$

$$\rho_{\oplus} = \frac{(g_e/R_e) \times 10^7}{2.77945} \quad [\text{g/cm}^3] \quad (82)$$

8. EXPERIMENTAL VALUES OF THE GRAVITATIONAL ACCELERATION OF THE EARTH

The observed gravitational acceleration at the surface of the rotating Earth can be represented by the formula

$$g = g_e [1 + \beta \sin^2 \varphi + \gamma \sin^2 2\varphi + \delta \cos^2 \varphi \cos 2(\lambda - \lambda_0)] \quad (83)$$

where λ is the geographic longitude measured eastwards of Greenwich meridian. The first term corresponds to a sphere. The next two terms give the contribution due to the oblateness of the Earth spheroid, while the longitude term is due to the non-ellipticity of the equator when the Earth is assumed as a triaxial figure. The longitude, λ_0 , gives the direction of the longest semi-axis of the equator. δ is connected with the difference $B - A$ of the equatorial moments of inertia or with the flattening, f_e , of the equator by the relation

$$\delta = \frac{9}{4} \frac{B - A}{M_{\oplus} R_e^2} = \frac{9}{4} \Lambda f_e (2 - f_e) \approx \frac{3}{8} f_e \quad (84)$$

because the inhomogeneity factor of the Earth is given by

$$\Lambda = \frac{C}{M_{\oplus} (a^2 + b^2)} \approx \frac{C}{2M_{\oplus} R_e^2} \approx \frac{1}{6} \quad (85)$$

The most important determinations from gravity measurements since 1915 have been compiled in a table on the following page.

All these gravity measurements are still based on the standard gravity value of Potsdam ($\varphi = 52^\circ 22' 86''$; $\lambda = +13^\circ 4' 06''$; $b = 87 \text{ m}$)

$$g = 981.2740 \text{ gal}$$

obtained by F. Kuhnen and Ph. Furtwangler (Ref. 43). It is necessary to revise the Potsdam system. For the correction of the Potsdam value, the following data are given (Refs. 44 and 45):

| | | | |
|--|----------------|----------|--|
| P. R. Heyl and G. S. Cook (Wash. D.C.) | : - 20 | milligal | } according to absolute gravity measurements |
| Bullard (Teddington, G. Brit.) | : - 15 | " | |
| J. S. Clarke (Teddington, Gt. Brit.) | : - 13 | " | |
| Ivanoff (Leningrad, U.S.S.R.) | : - 4 | " | |
| P. R. Heyl | : - 15 | " | } according to recalculations |
| Bullard and Browne | : - 16 | " | |
| Morelli (1954) | : - 16 | " | |
| H. Jeffreys | : - 13.4 | " | |
| Wollard | : - 14 to - 18 | " | |
| A. Berroth | : - 12.5 | " | |
| Morelli (1959) | : - 12.9 | " | |

| Author | Year | Ref. | g_e (gal) | $10^6 \beta$ | $10^6 \gamma$ | $10^6 \delta$ | λ_0 | ΔR_e (m) | $1:f_1$ | $1:f_2$ | $1:f_m$ | $1:f_e$ |
|--------------------|------|------|----------------------|---------------------|---------------|---------------|--------------------|---------------------|-----------------|-----------------|-------------------|---------|
| F. R. Helmert | 1915 | 32 | 978.052 ± 3 | 5285 ± 5 | - 7 | 18 ± 3 | $- 17^\circ \pm 4$ | 230 ± 51 | | | 296.7 ± 0.4 | 28 000 |
| A. Berroth | 1916 | 33 | 978.046 | 5296 | | 11.6 ± 4 | - 10 | 150 ± 58 | 296.7 | 298.8 | 297.8 ± 0.7 | 42 000 |
| W. Heiskanen | 1924 | 34 | 978.048 ± 3 | 5293 ± 6 | | --- | --- | --- | --- | --- | 297.4 ± 0.5 | --- |
| " | 1924 | 34 | 978.052 ± 3 | 5285 ± 6 | | 27 ± 3 | $+ 18 \pm 5$ | 345 ± 38 | 294.3 ± 0.6 | 299.0 ± 0.6 | 296.7 ± 0.5 | 18 700 |
| " | 1928 | 35 | 978.049 ± 1 | 5289 | | --- | --- | --- | --- | --- | 297.06 | --- |
| " | 1928 | 35 | 978.049 ± 1 | 5293 | | 19 ± 3 | 0 ± 5 | 242 | 295.7 | 299.0 | 297.3 | 26 703 |
| " | 1938 | 36 | 978.0451 | 5302.7 | | --- | --- | --- | --- | --- | 298.25 ± 0.3 | --- |
| " | 1938 | 36 | 978.0524 | 5297.0 | -5.9 | 27.6 | - 25 | 352 ± 30 | $295.3 + 0.4$ | $300.2 + 0.4$ | 297.8 ± 0.4 | 18 314 |
| N. F. Shuravlev | 1940 | 37 | 978.0484 | 5303 | | --- | --- | --- | --- | --- | 298.3 | --- |
| E. Niskanen | 1945 | 38 | 978.0468 | 5297.8 | | 23.0 | - 3.9 | 293 | 295.7 ± 0.2 | 299.8 ± 0.2 | 297.8 ± 0.2 | 21 550 |
| H. Jeffreys | 1948 | 39 | 978.0513 | 5285.9 | | --- | --- | --- | --- | --- | 296.85 ± 0.66 | --- |
| H. Schütte | 1950 | 40 | 978.0520 ± 33 | 5282.7 ± 6.0 | | --- | --- | --- | --- | --- | 296.3 | --- |
| U. A. Uotila | 1957 | 41 | 978.0516 | 5291.0 | | 10.6 | - 6 | --- | --- | --- | 297.2 | 47 600 |
| Heiskanen & Uotila | 1957 | 42 | 978.0496 | 5293.4 | | --- | --- | --- | --- | --- | 297.4 | --- |
| Mean Value | | | 978.049 ₅ | 5292.4 | | | | | | | 297.3 | |

Taking for g_e the latest determination of Heiskanen and Uotila (Ref. 42) which is nearly in agreement with the average value of all determinations, and using the correction due to H. Jeffreys (Ref. 39) the following value is obtained

$$g_e = 978.0496 - 0.0134 = 978.0362 \text{ gal} = 9.780362 \text{ m/sec}^2 \quad (86)$$

9. THE DYNAMIC OBLATENESS AND THE CONSTANTS OF PRECESSION AND NUTATION

The dynamic flattening $H = (C - A)/C$ is connected with Newcomb's constant of precession, P , by the relation

$$\frac{P}{H} = 530977.''04 + \frac{94419319''}{1/\kappa + 1} = 1678932.''29 \text{ for } 1/\kappa = 81.250 \quad (87)$$

while the constant of nutation, N , is given by

$$\frac{N}{H} = \frac{252871''}{1/\kappa + 1} \cos \epsilon = \frac{231982''}{1/\kappa + 1} = 2820.''45 \text{ for } 1/\kappa = 81.250 \quad (88)$$

where $\cos \epsilon = 0.9173917$ (for 1900.0) has been used for the cosine of the obliquity, ϵ , of the ecliptic. The constants in the equations are obtained from Brown's theory of the motion of the Moon and are well known. Both equations yield

$$\frac{P}{N} = 2.288872 (1/\kappa + 1) + 407.01140 = 595.271 \text{ for } 1/\kappa = 81.250$$

while observed modern values of P and N lead to

$$\frac{P}{N} = \frac{5493.''62}{9.''208} = 596.614 \text{ and thus } 1/\kappa = \frac{P/N}{2.288872} - 178.8218 = 81.84$$

This value for $1/\kappa$ is by far too large. H. Jeffreys (Ref. 39) has shown that in the equation for the constant of nutation, N , another constant H' for the dynamic flattening must be used due to the deviation of the Earth's interior from the isostatic equilibrium ($H' < H$). Therefore H' can be determined only from P and $1/\kappa$. With $p_0 = p_g + p$, the lunisolar precession, $p_g = \frac{3}{2} \frac{v_g^2}{c^2} n_g$, the geodetic precession (a relativistic term due to W. deSitter), p , the general precession in longitude, and λ , the planetary precession in right ascension, Newcomb's precessional constant is

$$P = \frac{p_0}{\cos \epsilon} = \frac{p + p_g}{\cos \epsilon} + \lambda \quad (89)$$

Values for 1900.0 derived from observations are (for a tropical century)

| | | | |
|----------------------|------------------|----------------------|--|
| $P = 5490.''66$ | $p = 5025.''641$ | $\lambda = 12.''473$ | $p_g = 0$ (Newcomb & Andoyer, Ref. 46) |
| 5493.156 ± 0.175 | 5026.000 | 12.493 | 1.915 (deSitter & Brouwer, Ref. 10) |
| 5493.847 | $5026.''650$ | 12.469 | 1.921 (Clemence, Ref. 7) |

According to newer investigations, Newcomb's value of the general precession in longitude

must be corrected by $\Delta p = + 0.''75$ (H. R. Morgan, Ref. 47), $\Delta p = + 0.''71$ (J. H. Oort, Ref. 48), $\Delta p = + 0.''86$ (Dirk Brouwer, Ref. 48), $\Delta p = + 0.''84$ (Poulkovo Obs., Ref. 48). The average value for the correction may be $\Delta p = + 0.''80$. All these investigators take $\Delta\lambda = 0$. In another paper, J. H. Oort (1943, Ref. 49) takes $\Delta\lambda = + 0.''02$, a correction also used by deSitter. The correction for P is therefore

$$\Delta P = \frac{\Delta p + \Delta p_g}{\cos \epsilon} + \Delta\lambda = \frac{0.''80 + 1.92}{0.9173917} + 0.00 = 2.''96 \quad (90)$$

The value

$$P = 5490.''66 + 2.''96 = 5493.''62 \quad (91)$$

will be accepted here. The dynamic flattening is now

$$H \equiv \frac{C - A}{C} = \frac{5493.''62}{1678932.''29} = 0.003272091 = \frac{1}{305.615 \pm 0.05} \quad (92)$$

and thus

$$q \equiv \frac{3}{2} \frac{C}{M_{\oplus} R_e^2} = \frac{J}{H} = 0.49616_0 \pm 0.00017 \quad (93)$$

and

$$\frac{C}{m_{\oplus} R_e^2} = \frac{J_2}{H} = 0.33077_3 \pm 0.00011 \quad (94)$$

The quantity q may be calculated in another way. Clairant's theory for the Earth in hydrostatic equilibrium has been developed to the second order by Radau (Ref. 50), Callandreau (Ref. 51), and Darwin (Ref. 28). deSitter (Ref. 31) gives

$$q \equiv \frac{3}{2} \frac{C}{M R_e^2} = 1 - \frac{1}{3} \varpi_1 - \frac{2}{5} \left(1 - \frac{2}{3} f\right) \frac{\sqrt{1 + \eta_1}}{1 + \lambda_1} \quad (95)$$

where

$$\eta_1 = \frac{\frac{5}{2} \varpi_1 + \frac{10}{21} \varpi_1^2 + \frac{4}{7} f^2 - \frac{6}{7} f \varpi_1}{f - \frac{5}{42} f^2 + \frac{4}{7} \kappa} - 2 \quad (96)$$

and $1 + \lambda_1$ is an average value of Radau's function, $f(\eta)$, depending on the internal density distribution of the Earth. The most reliable value, $1 + \lambda_1 = 1.00016$, was derived by Bullard (Ref. 30). With the above data for f and ϖ_1 the above-mentioned equations give, for $\kappa = 0$,

$$\eta_1 = 0.57440 \quad ; \quad q = 0.49815$$

$$\frac{C}{M R_e^2} = \frac{2}{3} \quad q = 0.33210$$

These data are not compatible with the previously derived data (eqs. 93 and 94), showing that the hypothesis of hydrostatic equilibrium is not fulfilled for the Earth.

10. DENSITY DISTRIBUTION WITHIN THE MOON

It is very difficult to derive a consistent system of lunar constants. Most reports on this subject are based on the work of Sir Harold Jeffreys. However, not even this source is free of inconsistencies. The reason is that many lunar constants are coupled with each other by relations. Therefore a systematic investigation of these relations will be necessary.

It is assumed that the density ρ within the Moon is constant over concentric ellipsoidal shells

$$\frac{\xi^2}{a^2} + \frac{\eta^2}{b^2} + \frac{\zeta^2}{c^2} = \mu^2 \quad (97)$$

where μ varies from 0 at the center to 1 at the surface, and where

$$\begin{aligned} \xi/a &= \mu \cos \phi \cos \theta \\ \eta/b &= \mu \cos \phi \sin \theta \\ \zeta/c &= \mu \sin \phi \end{aligned} \quad (98)$$

are the relative coordinates of the mass element

$$dm = \rho(\mu) d\xi d\eta d\zeta = \rho(\mu) a b c \mu^2 \cos \phi d\mu d\phi d\theta \quad (99)$$

The angle ϕ is the lunicentric latitude and θ the longitude. a is the longest semi-axis of the surface ellipsoid pointing toward the Earth, b the smallest semi-axis in the lunar equator, and c the rotational or polar semi-axis.

Using equations (98) and (99) after observing that

$$\int_0^{2\pi} \sin^2 \theta d\theta = \int_0^{2\pi} \cos^2 \theta d\theta = \pi; \quad \int_{-\pi/2}^{\pi/2} \cos^3 \phi d\phi = \frac{4}{3}; \quad \int_{-\pi/2}^{\pi/2} \sin^2 \phi \cos \phi d\phi = \frac{2}{3}$$

the moments of inertia around the a , b , c axes, respectively, become

$$\begin{aligned} A &= \int_0^M (\eta^2 + \zeta^2) dm = \lambda M (b^2 + c^2) \\ B &= \int_0^M (\zeta^2 + \xi^2) dm = \lambda M (c^2 + a^2) \\ C &= \int_0^M (\xi^2 + \eta^2) dm = \lambda M (a^2 + b^2) \end{aligned} \quad (100)$$

where the integrations are taken from 0 to 2π with respect to θ , from $-\pi/2$ to $\pi/2$ with respect to ϕ and from 0 to 1 with respect to μ . In the last equation $M = 4/3 \pi a b c \rho_m$ is the total mass (ρ_m is the mean density) and the inhomogeneity factor, λ , is given by

$$\lambda = \frac{\int_0^1 \rho \mu^4 d\mu}{\rho_m} = \frac{\int_0^1 \rho \mu^4 d\mu}{3 \int_0^1 \rho \mu^2 d\mu} \quad (101)$$

Because $a > b > c$, there is $A < B < C$. A constant density model gives $\lambda = 1/5 = 0.2$. For Jeffreys compressional model with constant bulk modulus (Ref. 52) Roche's density law [with $\rho_m = 3.342 \text{ g/cm}^3$ (mean density), $\rho_0 = 3.290 \text{ g/cm}^3$ (surface density) and $\rho_c = 3.420 \text{ g/cm}^3$ (central density)] becomes

$$\rho = \rho_c - (\rho_c - \rho_0) \mu^2 = 3.420 - 0.130 \mu^2 [\text{g/cm}^3] \quad (102)$$

The inhomogeneity factor is, therefore,

$$\begin{aligned} \lambda &= \frac{1}{5} \frac{\rho_c - \frac{5}{7}(\rho_c - \rho_0)}{\rho_m} = \frac{1}{5} \frac{\rho_c - \frac{5}{7}(\rho_c - \rho_0)}{\rho_c - \frac{3}{5}(\rho_c - \rho_0)} = \frac{0.9955}{5} = \\ &= 0.1991 \pm 0.0001 \end{aligned} \quad (103)$$

11. CONSTANTS OF THE PHYSICAL LIBRATION OF THE MOON

The values of $f \equiv \frac{C-B}{C-A}$ and the inclination of the Moon's equator to the ecliptic can be determined from observations of the physical libration of the Moon. Due to the difficulty of observations near the irregular limb of varied illumination the values for f scatter widely, as can be seen from the following table (Refs. 11 and 13):

| Author | Year | $f \equiv \frac{C-B}{C-A}$ |
|-----------------|------|----------------------------|
| F. Hayn | 1907 | 0.75 ± 0.04 |
| F. Hayn | | 0.85 ± 0.07 |
| J. Stratton | 1909 | 0.50 ± 0.03 |
| I. V. Belkovich | 1936 | 0.84 ± 0.08 |
| I. V. Belkovich | 1949 | 0.67 ± 0.03 |
| K. Koziel | 1949 | 0.71 ± 0.051 |
| K. Koziel | 1949 | 0.60 ± 0.055 |
| A.A. Nefedjev | 1950 | 0.65 ± 0.045 |
| A.A. Yakovkin | 1950 | 0.85 ± 0.03 |
| T. Weimer | 1954 | 0.60 |
| Mean Value | | 0.70_2 |

Sir Harold Jeffreys used $f = 0.84$ in his book *The Earth* (Ref. 11). Later he recommended $f = 0.67$ (Ref. 53) and used $f = 0.639 \pm 0.014$ in his latest paper (Ref. 54).

The secular motions of the perigee and node of the lunar orbit are also influenced by the Moon's oblateness coefficients (L and K). From Jeffreys equation for the perigee motion follows (Ref. 11):

$$380 L - 1192 K = 6.420 - 3896 J_{\oplus} \geq 0$$

and thus

$$f = 1 - \frac{K}{L} \geq 1 - \frac{380}{1192} = \frac{812}{1192} = 0.6812$$

The mean value of the table is consistent with this lower limit for f and therefore

$$f = 0.70 \pm 0.02 \quad (104)$$

will be adopted in this paper.

A new investigation of the libration of the Moon's axis by H. Jeffreys (Ref. 54) leads to

$$\beta \equiv \frac{C-A}{C} = 0.0006279 \pm 0.0000010 \quad (105)$$

taking into account a solar effect not evaluated by Hayn.

The three quantities λ , f , and β are sufficient to calculate all other quantities, provided the mass and the mean radius of the Moon are known.

12. RELATIONS AND NUMERICAL VALUES FOR THE DIMENSIONLESS MOMENT OF INERTIA PARAMETERS

The same symbols for moment of inertia parameters will be used as they have been introduced mainly by H. Jeffreys (Ref. 11). The numerical values are based on the above-given parameters λ , f , and β ; namely

$$\begin{aligned} \lambda &= \frac{A}{M(b^2 + c^2)} = \frac{B}{M(c^2 + a^2)} = \frac{C}{M(a^2 + b^2)} \\ &= \frac{C-B}{M(b^2 - c^2)} = \frac{C-A}{M(a^2 - c^2)} = \frac{C-B}{M(b^2 - c^2)} = 0.1991 \pm 0.0001 \end{aligned} \quad (106)$$

$$f = \frac{a}{\beta} = \frac{C-B}{C-A} = \frac{2J-K}{2J+K} = \frac{J - 1/2 K}{L} = \frac{b^2 - c^2}{a^2 - c^2} = 0.70 \pm 0.02 \quad (107)$$

$$\beta = \frac{C-A}{C} = \frac{J + 1/2 K}{g} = \frac{L}{g} = \frac{a^2 - c^2}{a^2 + b^2} = 0.0006279 \pm 0.0000010 \quad (108)$$

The other parameters can be derived from these as follows:

$$\begin{aligned} 1-f &= \frac{\gamma}{\beta} = \frac{B-A}{C-A} = \frac{K}{J + 1/2 K} = \frac{K}{L} = \frac{a^2 - b^2}{a^2 - c^2} = \frac{3\lambda - g}{L} = \frac{3\lambda/g - 1}{\beta} = \\ &= 0.30 \pm 0.02 \end{aligned} \quad (109)$$

$$\alpha = \frac{C - B}{C} = f\beta = \frac{J - 1/2 K}{g} = \frac{L - K}{g} = \frac{b^2 - c^2}{a^2 + b^2} = 0.0004395 \pm 0.0000133 \quad (110)$$

$$\gamma = \frac{B - A}{C} = \beta - \alpha = \frac{K}{g} = (1 - f)\beta = \frac{a^2 - b^2}{a^2 + b^2} = 0.0001884 \pm 0.0000129 \quad (111)$$

$$g = \frac{3}{2} \frac{C}{Ma^2} = \frac{3\lambda}{1 + \gamma} = \frac{3}{2} \lambda \frac{a^2 + b^2}{a^2} = 0.5972 \pm 0.0003 \quad (112)$$

$$L = \frac{3}{2} \frac{C - A}{Ma^2} = J + \frac{1}{2} K = g\beta = \frac{3}{2} \lambda \frac{a^2 - c^2}{a^2} = 0.0003750 \pm 0.0000008 \quad (113)$$

$$\begin{aligned} J &= \frac{3}{2} \frac{C - \frac{A+B}{2}}{Ma^2} = L - \frac{1}{2} K = \frac{1+f}{2} L = \frac{1}{2} \frac{1+f}{1-f} K = \frac{3}{2} \lambda \frac{\frac{a^2 + b^2}{2} - c^2}{a^2} \\ &= g \left(\beta - \frac{1}{2} \gamma \right) = g \frac{\alpha + \beta}{2} = g \left(\alpha + \frac{1}{2} \gamma \right) = 0.00031875 \pm 0.0000044 \end{aligned} \quad (114)$$

$$K = \frac{3}{2} \frac{B - A}{Ma^2} = (1 - f)L = g\gamma = \frac{3}{2} \lambda \frac{a^2 - b^2}{a^2} = 0.0001125 \pm 0.0000077 \quad (115)$$

The dimensionless moments of inertia and their differences are obtained from the above-mentioned data as:

$$\frac{C - A}{Ma^2} = \frac{2}{3} L = \frac{2J + K}{3} = \lambda \frac{a^2 - c^2}{a^2} = 0.0002500 \pm 0.0000005 \quad (116)$$

$$\frac{C - B}{Ma^2} = \frac{2}{3} fL = \frac{2J - K}{3} = \lambda \frac{b^2 - c^2}{a^2} = 0.0001750 \pm 0.0000054 \quad (117)$$

$$\frac{B - A}{Ma^2} = \frac{2}{3} (1 - f)L = \frac{2}{3} K = \lambda \frac{a^2 - b^2}{a^2} = 0.0000750 \pm 0.0000051 \quad (118)$$

$$\frac{A}{Ma^2} = \frac{2}{3} g (1 - \beta) = \frac{2}{3} (g - L) = \lambda \frac{b^2 + c^2}{a^2} = 0.3978_{77} \pm 0.0002 \quad (119)$$

$$\frac{B}{Ma^2} = \frac{2}{3} g (1 - \alpha) = \frac{2}{3} (g - fL) = \lambda \frac{c^2 + a^2}{a^2} = 0.3979_{52} \pm 0.0002 \quad (120)$$

$$\frac{C}{Ma^2} = \frac{2}{3} g = \frac{2\lambda}{1+\gamma} = \lambda \frac{a^2 + b^2}{a^2} = 0.3981_{27} \pm 0.0002 \quad (121)$$

The ratios of the semi-axes now become

$$\frac{b}{a} = \sqrt{\frac{1-\gamma}{1+\gamma}} = \sqrt{1 - \frac{2\gamma}{1+\gamma}} = 0.9998116 \pm 0.0000129 \quad (122)$$

$$\frac{c}{a} = \sqrt{1 - \frac{2\beta}{1+\gamma}} = \sqrt{1 - \frac{2\gamma}{(1-f)(1+\gamma)}} = 0.9993720 \pm 0.0000010 \quad (123)$$

These data seem, at present, to be the most reasonable. H. Jeffreys' value

$$g \equiv \frac{3}{2} \frac{C}{Ma^2} = 0.5956 \pm 0.0010$$

is slightly low, and affords a higher density concentration towards the center as has been assumed by Jeffreys.

13. THE FINAL DETERMINATION OF THE DIMENSIONS, MASSES AND MOMENTS OF INERTIA FOR THE EARTH AND THE MOON

Using the obtained value of the gravitational acceleration, g_e , at the equator (eq. 86) in the relations (eq. 80) and (eq. 82) at the end of Section 7 there follows at once $R_e = \sqrt{\chi \mu_\oplus / g_e} = 6378169.835 \text{ m}$ and $\rho_\oplus = 5.516964 \text{ g/cm}^3$. The final values, adopted for the Earth, will be taken as

$$R_e = 6378170 (1 \pm 3.2 \times 10^{-6}) \text{ m} = 6378170 \pm 20 \text{ m} \quad (124)$$

and

$$\rho_\oplus = 5.5170 (1 \pm 7.3 \times 10^{-4}) \text{ g/cm}^3 = 5.5170 \pm 0.0040 \text{ g/cm}^3 \quad (125)$$

The volume of the Earth is

$$\begin{aligned} V_\oplus &= \frac{4}{3} \pi R_e^3 (1-f) = 1.083225 \times 10^{27} (1 \pm 1.02 \times 10^{-5}) \text{ cm}^3 \\ &= (1.083225 \pm 0.000011) \times 10^{27} \text{ cm}^3 \end{aligned} \quad (126)$$

while the mass is given by

$$M_\oplus = \frac{\mu_\oplus}{G} = V_\oplus \rho_\oplus = 5.9761 \times 10^{27} (1 \pm 7.2 \times 10^{-4}) \text{ g} = (5.9761 \pm 0.0043) \times 10^{27} \text{ g} \quad (127)$$

and the polar radius now becomes

$$R_p = R_e (1-f) = 6356788 (1 \pm 3.7 \times 10^{-6}) \text{ m} = 6356788 \pm 24 \text{ m} \quad (128)$$

The unit for the moments of inertia is

$$M_{\oplus} R_e^2 = 2.4311_4 \times 10^{45} (1 \pm 7.3 \times 10^{-4}) g \text{ cm}^2 = (2.4311_4 \pm 0.0018) \times 10^{45} g \text{ cm}^2 \quad (129)$$

and therefore

$$C - A = J_2 \times M_{\oplus} R_e^2 = 2.6313 \times 10^{42} (1 \pm 9.1 \times 10^{-4}) g \text{ cm}^2 = (2.6313 \pm 0.0024) \times 10^{42} g \text{ cm}^2 \quad (130)$$

$$C = \frac{2}{3} q \times M_{\oplus} R_e^2 = 8.0415 \times 10^{44} (1 \pm 1.07 \times 10^{-3}) g \text{ cm}^2 = (8.0415 \pm 0.0086) \times 10^{44} g \text{ cm}^2 \quad (131)$$

It is now possible to give corresponding data for the Moon. The mass is given by

$$M_{\bullet} = \kappa M_{\oplus} = 7.3552 \times 10^{25} (1 \pm 1.02 \times 10^{-3}) g = (7.3552 \pm 0.0075) \times 10^{25} g \quad (132)$$

while the mean visible radius is

$$R_{\bullet} = k R_e = 1738236 (1 \pm 1.0 \times 10^{-4}) = 1738236 \pm 174 \text{ m} \quad (133)$$

and therefore the semi-axes of the three-axial Moon are

$$a = \frac{R_{\bullet}}{\sigma} = 1738946 \pm 186 \text{ m} \quad (134)$$

$$b = a \left(\frac{b}{a} \right) = 1738618 \pm 209 \text{ m} \quad (135)$$

$$c = a \left(\frac{c}{a} \right) = 1737854 \pm 188 \text{ m} \quad (136)$$

The unit for the Moon's moments of inertia is

$$M_{\bullet} a^2 = 2.2241_6 \times 10^{42} (1 \pm 1.23 \times 10^{-3}) g \text{ cm}^2 = (2.2241_6 \pm 0.0027) \times 10^{42} g \text{ cm}^2 \quad (137)$$

and thus the moments of inertia are

$$A = 0.8849_{42} \times 10^{42} (1 \pm 1.73 \times 10^{-3}) g \text{ cm}^2 = (0.8849_{42} \pm 0.0015_3) \times 10^{42} g \text{ cm}^2 \quad (138)$$

$$B = 0.8851_{09} \times 10^{42} (1 \pm 1.73 \times 10^{-3}) g \text{ cm}^2 = (0.8851_{09} \pm 0.0015_3) \times 10^{42} g \text{ cm}^2 \quad (139)$$

$$C = 0.8854_{98} \times 10^{42} (1 \pm 1.73 \times 10^{-3}) g \text{ cm}^2 = (0.8854_{98} \pm 0.0015_3) \times 10^{42} g \text{ cm}^2 \quad (140)$$

$$C - \frac{A+B}{2} = (0.000473 \pm 0.000007) \times 10^{42} g \text{ cm}^2 \quad (141)$$

$$B - A = (0.000167 \pm 0.000012) \times 10^{42} g \text{ cm}^2 \quad (142)$$

The oblateness coefficients of the potential function of the Moon are

$$J_2 = \frac{C - (A+B)/2}{M_{\bullet} a^2} = \frac{2}{3} J = 0.0002125 \pm 0.0000029 \quad (143)$$

$$J_2^{(2)} = \frac{B-A}{4 M_e a^2} = \frac{1}{6} K = 0.000\,0188 \pm 0.000\,0013 \quad (144)$$

The derived value for the equatorial radius of the Earth (eq. 124) is in good agreement with the following values:

| Author | Year | Ref. | R_e |
|-------------------|------|------|------------------------|
| W. M. Kaula | 1961 | 55 | $6\,378\,163 \pm 21$ m |
| V. C. Clarke, Jr. | 1962 | 56 | $6\,378\,165 \pm 25$ |
| I. Fischer | 1962 | 57 | $6\,378\,166$ |
| Present Report | 1962 | | $6\,378\,170 \pm 20$ |

I. Fisher's value for $1/\kappa = M_\oplus / M_e = 81.268$ is also in good agreement with the value in this report. The presented system of constants is not only a consistent one, but the most serious discrepancy has been removed in determining the gravitational parameter μ_\oplus from terrestrial data and, on the other hand, from the lunar mean motion in combination with radar measurements of the Moon's distance.

Finally, the present data for the Moon's moments of inertia are compared with the values of other authors in the following table:

| Author | Ref. | A $10^{35} \text{ kg}\cdot\text{m}^2$ | B $10^{35} \text{ kg}\cdot\text{m}^2$ | C $10^{35} \text{ kg}\cdot\text{m}^2$ | $C - (A+B)/2$ $10^{35} \text{ kg}\cdot\text{m}^2$ | $B - A$ $10^{35} \text{ kg}\cdot\text{m}^2$ |
|--------------------------|------|--|--|--|--|--|
| B. E. Kalensher | 58 | 0.87976 | 0.87985 | 0.88032 | 0.00051 | 0.00009 |
| Makemson, Baker, Westrom | 13 | 0.88837 | 0.88856 | 0.88893 | 0.00047 | 0.00019 |
| V. C. Clarke, Jr. | 56 | 0.88746 | 0.88764 | 0.88801 | 0.00046 | 0.00018 |
| Present Report | --- | 0.88494 | 0.88511 | 0.88550 | 0.00047 | 0.00017 |

The values of V. C. Clarke, Jr. are used for the Ranger Program.

14. THE EARTH ELLIPSOID

The equation of the rotational ellipsoid or spheroid is

$$\frac{x^2 + y^2}{R_e^2} + \frac{z^2}{R_p^2} = 1 \quad (145)$$

where

$$x = R \cos \phi \cos \lambda = R_e \cos \psi \cos \lambda = \rho_n \cos \varphi \cos \lambda \quad (146)$$

$$y = R \cos \phi \sin \lambda = R_e \cos \psi \sin \lambda = \rho_n \cos \varphi \sin \lambda \quad (147)$$

$$z = R \sin \phi = R_p \sin \psi = \rho_n (1-e^2) \sin \varphi \quad (148)$$

and R_e is the equatorial Earth radius, R_p the polar Earth radius, R the local Earth radius, ρ_n the normal radius of curvature, λ the geographic longitude (positive eastward of Greenwich), ϕ the geocentric latitude, ψ the reduced latitude, φ the geodetic or geographic (\approx astronomical) latitude, and e the first eccentricity of the meridian ellipse. Introducing the second eccentricity, ϵ , and the flattening (oblateness, ellipticity), f , the following relations hold

$$f = \frac{R_e - R_p}{R_e} = 1 - \sqrt{1 - e^2} = 1 - \frac{1}{\sqrt{1 + \epsilon^2}} \approx \frac{1}{2} e^2 + \frac{1}{8} e^4 + \dots + \frac{1 \cdot 1 \cdot 3 \cdot 5 \dots (2\kappa - 3)}{2 \cdot 4 \cdot 6 \cdot 8 \dots (2\kappa)} e^{2\kappa} + \dots \quad (149)$$

$$e^2 = \frac{R_e^2 - R_p^2}{R_e^2} = \frac{\epsilon^2}{1 + \epsilon^2} = f(2 - f) = 2f - f^2 \quad (150)$$

$$\epsilon^2 = \frac{R_e^2 - R_p^2}{R_e^2} = \frac{e^2}{1 - e^2} = \frac{f(2 - f)}{(1 - f)^2} = 2f + 3f^2 + \dots + (\kappa + 1)f^\kappa + \dots \quad (151)$$

thus

$$\frac{R_p}{R_e} = 1 - f = \sqrt{1 - e^2} = \frac{1}{\sqrt{1 + \epsilon^2}} \quad (152)$$

The different latitude angles are related by

$$\tan \phi = \sqrt{1 - e^2} \tan \psi = (1 - e^2) \tan \varphi \quad (153)$$

$$\tan \phi = (1 - f) \tan \psi = (1 - f)^2 \tan \varphi \quad (154)$$

By differentiation the relation

$$\frac{R^2}{R_p} d\phi = R_e d\psi = \rho d\varphi \quad (155)$$

follows.

Thus the line element is

$$ds^2 = dx^2 + dy^2 + dz^2 = dr^2 + r^2 d\phi^2 + r^2 \cos^2 \phi d\lambda^2 = R_e^2 (1 - e^2 \cos^2 \psi) d\psi^2 + R_e^2 \cos^2 \psi d\lambda^2 \quad (156)$$

The parameter ρ is the mean radius of curvature, and is correlated with the normal radius of curvature

$$\begin{aligned} \rho_n &= \frac{R_e}{(1 - e^2 \sin^2 \varphi)^{1/2}} = \frac{R_e^2 / R_p}{(1 + \epsilon^2 \cos^2 \varphi)^{1/2}} = R \frac{\cos \phi}{\cos \varphi} = \\ &= R_e \left[1 + \frac{1}{2} e^2 \sin^2 \varphi + \frac{3}{8} e^4 \sin^4 \varphi + \frac{5}{16} e^6 \sin^6 \varphi + \dots \right] \end{aligned} \quad (157)$$

and to the meridional radius of curvature

$$\begin{aligned}\rho_m &= \frac{R_e (1 - e^2)}{(1 - e^2 \sin^2 \varphi)^{3/2}} = \frac{R_p^2 / R_e}{(1 - e^2 \sin^2 \varphi)^{3/2}} = \frac{R_e^2 / R_p}{(1 + e^2 \cos^2 \varphi)^{3/2}} \\ &= R_e (1 - e^2) \left[1 + \frac{3}{2} e^2 \sin^2 \varphi + \frac{15}{8} e^4 \sin^4 \varphi + \frac{35}{16} e^6 \sin^6 \varphi + \dots \right]\end{aligned}\quad (158)$$

by the relation

$$\rho = \sqrt{\rho_m \rho_n} = \frac{R_p}{1 - e^2 \sin^2 \varphi} = \frac{R_e^2 / R_p}{1 + e^2 \cos^2 \varphi} = R_p [1 + e^2 \sin^2 \varphi + e^4 \sin^4 \varphi + e^6 \sin^6 \varphi + \dots] \quad (159)$$

The radius of a parallel of latitude is $\rho_n \cos \varphi = R_e \cos \psi = R \cos \phi$. Because f or e^2 are small quantities the latitudes ϕ , ψ , and φ will not differ very much from each other. Therefore it is very useful to have rapidly converging series developments available for the differences $\phi - \varphi$ and $\psi - \varphi$. With

$$m = \frac{R_e^2 - R_p^2}{R_e^2 + R_p^2} = \frac{1 - (1 - e^2)}{1 + (1 - e^2)} = \frac{e^2}{2 - e^2} = f + \frac{1}{2} f^2 - \frac{1}{4} f^4 + \dots \quad (160)$$

there is

$$\phi = \varphi - m \sin 2 \varphi + \frac{m^2}{2} \sin 4 \varphi - \frac{m^3}{3} \sin 6 \varphi \pm \dots \quad (161)$$

$$\varphi = \phi + m \sin 2 \phi + \frac{m^2}{2} \sin 4 \phi + \frac{m^3}{3} \sin 6 \phi + \dots \quad (162)$$

and with

$$n = \frac{R_e - R_p}{R_e + R_p} = \frac{1 - (1 - f)}{1 + (1 - f)} = \frac{f}{2 - f} = \frac{1}{2} f + \frac{1}{4} f^2 + \dots \quad (163)$$

there is

$$\psi = \varphi - n \sin 2 \varphi + \frac{n^2}{2} \sin 4 \varphi - \frac{n^3}{3} \sin 6 \varphi \pm \dots \quad (164)$$

$$\varphi = \psi + n \sin 2 \psi + \frac{n^2}{2} \sin 4 \psi + \frac{n^3}{3} \sin 6 \psi + \dots \quad (165)$$

An accurate formula for the difference $\varphi - \phi$ is given by

$$\tan(\varphi - \phi) = \frac{e^2 \tan \varphi}{1 + (1 - e^2) \tan^2 \varphi} = \frac{e^2 \sin \varphi \cos \varphi}{1 - e^2 \sin^2 \varphi} \quad (166)$$

The local Earth radius (radius vector) can be accurately calculated from the relations

$$\begin{aligned}R &= \sqrt{x^2 + y^2 + z^2} = \frac{R_p}{\sqrt{1 - e^2 \cos^2 \phi}} = R_e \sqrt{1 - e^2 \sin^2 \psi} = R_e \sqrt{\frac{1 - e^2 (2 - e^2) \sin \varphi}{1 - e^2 \sin^2 \varphi}} \\ &= R_e \sqrt{\frac{1 - 4m(1+m)^{-2} \sin^2 \varphi}{1 - 4n(1+n)^{-2} \sin^2 \varphi}} = \frac{1+n}{1+m} R_e \sqrt{\frac{1 + m^2 + 2m \cos 2\varphi}{1 + n^2 + 2n \cos 2\varphi}}\end{aligned}\quad (167)$$

By taking the logarithm of the last relation there follows

$$\ln \frac{R}{R_e} = \ln \frac{1+n}{1+m} + \frac{1}{2} \ln (1+m^2+2m \cos 2\varphi) - \frac{1}{2} \ln (1+n^2+2n \cos 2\varphi)$$

or, using a known series development,

$$\log \frac{R}{R_e} = \log \frac{1+n}{1+m} + M \left[(m-n) \cos 2\varphi - \frac{m^2-n^2}{2} \cos 4\varphi + \frac{m^3-n^3}{3} \cos 6\varphi \mp \dots \right] \quad (168)$$

where M is the module ($M = 0.4342944819$). This series is due to Encke.

Conventional power series for R/R_e can be obtained as follows:

$$\frac{R}{R_e} = (1 + \epsilon^2 \sin^2 \phi)^{-1/2} = 1 - \frac{1}{2} \epsilon^2 \sin^2 \phi + \frac{3}{8} \epsilon^4 \sin^4 \phi - \frac{5}{16} \epsilon^6 \sin^6 \phi \pm \dots \quad (169)$$

The above-mentioned power series for the local Earth radius can also be written

$$\frac{R}{R_e} = 1 - \left(\frac{1}{2} \epsilon^2 - \frac{3}{8} \epsilon^4 + \frac{5}{16} \epsilon^6 \right) \sin^2 \phi - \left(\frac{3}{32} \epsilon^4 - \frac{5}{64} \epsilon^6 \right) \sin^2 2\phi + \frac{5}{64} \epsilon^6 \sin^2 \phi \sin^2 2\phi + \dots \quad (170)$$

or

$$\frac{R}{R_e} = 1 - f \sin^2 \phi - \left(\frac{3}{8} f^2 + \frac{1}{2} f^3 \right) \sin^2 2\phi + \frac{5}{8} f^3 \sin^2 \phi \sin^2 2\phi + \dots \quad (171)$$

using eq. (151).

In order to obtain power series for the local Earth radius as a function of the geodetic latitude, φ , it is useful to set

$$k = \frac{4m}{(1+m)^2} = e^2 (2 - e^2) ; k' = \frac{4n}{(1+n)^2} = f (2 - f) = e'^2 ; k/k' = 2 - e^2 \quad (172)$$

the non-dimensional local Earth radius is now

$$\frac{R}{R_e} = 1 - \frac{1}{2} (k - k') \sin^2 \varphi - \frac{1}{8} (k^2 + 2kk' - 3k'^2) \sin^4 \varphi - \frac{1}{16} (k^3 + k^2 k' + 3kk'^2 - 5k'^3) \sin^6 \varphi - \dots \quad (173)$$

or

$$\begin{aligned} \frac{R}{R_e} = 1 - \frac{1}{2} e^2 [(2 - e^2) - 1] \sin^2 \varphi - \frac{1}{8} e^4 [(2 - e^2)^2 + 2(2 - e^2) - 3] \sin^4 \varphi \\ - \frac{1}{16} e^6 [(2 - e^2)^3 + (2 - e^2)^2 + 3(2 - e^2) - 5] \sin^6 \varphi - \dots \end{aligned} \quad (174)$$

Because

$$e^2 = 2f - f^2 ; \quad 2 - e^2 = 2 - 2f + f^2$$

there is, also,

$$\begin{aligned} \frac{R}{R_e} &= 1 - \left(f - \frac{5}{2}f^2 + 2f^3\right)\sin^2 \varphi - \left(\frac{5}{2}f^2 - \frac{17}{2}f^3\right)\sin^4 \varphi - \frac{13}{2}f^3\sin^6 \varphi - \dots \\ &= 1 - f\sin^2 \varphi + \left(\frac{5}{8}f^2 - \frac{1}{2}f^3\right)\sin^2 2\varphi + \frac{13}{8}f^3\sin^2 \varphi \sin^2 2\varphi + \dots \\ &= 1 - \frac{1}{2}f + \frac{5}{16}f^2 + \frac{5}{32}f^3 + \left(\frac{1}{2}f - \frac{13}{64}f^3\right)\cos 2\varphi - \left(\frac{5}{16}f^2 + \frac{5}{32}f^3\right)\cos 4\varphi + \frac{13}{64}f^3\cos 6\varphi + \dots \end{aligned} \quad (175)$$

It is also important to know the arc corresponding to 1° in longitude, namely

$$\begin{aligned} \nu &= \frac{\pi}{180} \rho_n \cos \varphi = \frac{\pi}{180} \frac{R_e \cos \varphi}{(1 - e^2 \sin^2 \varphi)^{1/2}} \\ &= \frac{\pi}{180} R_e \cos \varphi \left(1 + \frac{1}{2}e^2 \sin^2 \varphi + \frac{3}{8}e^4 \sin^4 \varphi + \dots\right) \\ &= \frac{\pi}{180} R_e \left(1 + \frac{1}{8}e^2 + \frac{3}{64}e^4\right) \cos \varphi - \left(\frac{e^2}{8} + \frac{9}{128}e^4\right) \cos 3\varphi + \frac{3}{128}e^4 \cos 5\varphi \mp \dots \end{aligned} \quad (176)$$

and the arc corresponding to 1° in latitude, namely

$$\begin{aligned} \mu &= \frac{\pi}{180} \rho_m = \frac{\pi}{180} \frac{R_e (1 - e^2)}{(1 - e^2 \sin^2 \varphi)^{3/2}} = \frac{\pi}{180} R_e (1 - e^2) \left[1 + \frac{3}{2}e^2 \sin^2 \varphi + \frac{15}{8}e^4 \sin^4 \varphi + \dots\right] \\ &= \frac{\pi}{180} \frac{R_e^2}{R_e} \left[1 + \frac{3}{4}e^2 + \frac{45}{64}e^4 - \left(\frac{3}{4}e^2 + \frac{15}{16}e^4\right)\cos 2\varphi + \frac{15}{64}e^4 \cos 4\varphi \mp \dots\right] \end{aligned} \quad (177)$$

The length of a meridian quadrant is given by

$$\begin{aligned} Q_m &= \frac{\pi}{2} \overline{\rho_m} = \int_0^{\pi/2} \frac{R_e(1 - e^2)}{(1 - e^2 \sin^2 \varphi)^{3/2}} d\varphi = R_e (1 - e^2) \int_0^1 \frac{dz}{(1 - e^2 z^2) \sqrt{(1 - z^2)(1 - e^2 z^2)}} \\ &= R_e (1 - e^2) \prod\left(\frac{\pi}{2}, -e^2, e\right) = R_e (1 - e^2) \int_0^{\pi/2} \left[1 + \frac{3}{2}e^2 \sin^2 \varphi + \frac{15}{8}e^4 \sin^4 \varphi + \frac{35}{16}e^6 \sin^6 \varphi + \dots\right] d\varphi \\ &= \frac{\pi}{2} R_e (1 - e^2) \left[1 + \frac{3}{4}e^2 + \frac{45}{64}e^4 + \frac{175}{256}e^6 + \dots\right] \\ &= \frac{\pi}{2} R_e \left(1 - \frac{1}{4}e^2 - \frac{3}{64}e^4 - \frac{5}{256}e^6 - \dots\right) \\ &= \frac{\pi}{2} R_e \left(1 - \frac{1}{2}f + \frac{1}{16}f^2 + \frac{1}{32}f^3 + \dots\right) \end{aligned} \quad (178)$$

The volume of the Earth spheroid is simply given by

$$V = \frac{4}{3} \pi R_e^2 R_p = \frac{4}{3} \pi R_e^3 (1 - f) \quad (179)$$

while the surface area follows from

$$\begin{aligned} S &= 4\pi R_e R_p \int_0^1 \sqrt{1 + \epsilon^2 z^2} dz = 2\pi R_e R_p \left[\sqrt{1 + \epsilon^2} + \frac{1}{\epsilon} \sinh^{-1} \epsilon \right] \\ &= 2\pi R_e^2 \left[1 + \frac{\sinh^{-1} \epsilon}{\epsilon \sqrt{1 + \epsilon^2}} \right] = 2\pi R_e^2 \left[1 + \frac{\ln(\epsilon + \sqrt{1 + \epsilon^2})}{\epsilon \sqrt{1 + \epsilon^2}} \right] \\ &= 2\pi R_e^2 \left[1 + \left(1 - \frac{1}{6} \epsilon^2 + \frac{3}{40} \epsilon^4 - \frac{5}{112} \epsilon^6 \pm \dots \right) \left(1 - \frac{1}{2} \epsilon^2 + \frac{3}{8} \epsilon^4 - \frac{5}{16} \epsilon^6 \pm \dots \right) \right] \\ &= 4\pi R_e^2 \left(1 - \frac{1}{3} \epsilon^2 + \frac{4}{15} \epsilon^4 - \frac{8}{35} \epsilon^6 - \dots \right) = 4\pi R_e^2 \left(1 - \frac{2}{3} f + \frac{1}{15} f^2 + \frac{4}{105} f^3 + \dots \right) \quad (180) \end{aligned}$$

These formulas will now be used to derive the Earth's dimensions and other Earth parameters. Taking $R_e = 6378170 \pm 20$ m and $1/f = 298.30 \pm 0.05$ yields

$$e^2 = 0.006693422, \quad e = 0.081813334$$

$$\epsilon^2 = 0.006738525, \quad \epsilon = 0.082088522$$

$$m = 0.003357949 = 692.''627$$

$$n = 0.001678979 = 346.''314$$

The mean radius is

$$\bar{R} = \frac{2R_e + R_p}{3} = 6371043 \pm 21 \text{ m} \quad (181)$$

The radius for the geodetic latitude $\varphi = \sin^{-1} \sqrt{1/3} = 35^\circ 15' 51.''8$ ($\phi = 35^\circ 4' 59.''5$) is

$$R_1 = R_e \sqrt{1 - \frac{e^2(1 - e^2)}{3 - e^2}} = R_e \left[1 - \frac{1}{3} f + \frac{5}{9} f^2 + \frac{1}{3} f^3 + \dots \right] = 6371083 \pm 21 \text{ m} \quad (182)$$

The radius for the geocentric latitude $\phi = \sin^{-1} \sqrt{1/3} = 35^\circ 15' 51.''8$ ($\varphi = 35^\circ 26' 45.''5$) is

$$R_2 = R_e \sqrt{1 - \frac{e^2}{3 - 2e^2}} = R_e \left[1 - \frac{1}{3} f - \frac{1}{3} f^2 - \frac{7}{27} f^3 - \dots \right] = 6371019 \pm 21 \text{ m} \quad (183)$$

The radius for a sphere of equal area is

$$R_s = (S/4\pi)^{1/2} = R_e \left(1 - \frac{1}{3} f^2 - \frac{1}{45} f^3 + \frac{11}{945} f^4 + \dots \right) = 6371041 \pm 21 \text{ m} \quad (184)$$

while the radius for a sphere of equal volume is

$$R_v = (3V/4\pi)^{1/3} = R_e (1 - f)^{1/3} = R_e \left(1 - \frac{1}{3} f - \frac{1}{9} f^2 - \frac{5}{81} f^3 - \dots \right) = 6371035 \pm 21 \text{ m} \quad (185)$$

The surface area is

$$S = 4\pi R_e^2 \left(1 - \frac{2}{3}f + \frac{1}{15}f^2 + \frac{4}{105}f^3 + \dots\right) = (5.100711 \pm 0.000034) \times 10^{14} \text{ m}^2 \quad (186)$$

while the volume is given by

$$V = \frac{4}{3}\pi R_e^3 (1 - f) = (1.083225 \pm 0.000011) \times 10^{21} \text{ m}^3 \quad (187)$$

The radius of curvature at the pole is

$$\rho_p = R_e^2 / R_p = R_e / (1 - f) = 6399624 \pm 24 \text{ m} \quad (188)$$

while the meridional radius of curvature at the equator is given by

$$\rho_{me} = R_p^2 / R_e = R_e (1 - f)^2 = R_e (1 - e^2) = 6335478 \pm 27 \text{ m} \quad (189)$$

The length of an equatorial quadrant is

$$Q_e = \frac{\pi}{2} R_e = 10018806 \pm 31 \text{ m} \quad (190)$$

while the length of a meridional quadrant is

$$Q_m = \frac{\pi}{2} R_e \left(1 - \frac{1}{2}f + \frac{1}{16}f^2 + \frac{1}{32}f^3 + \dots\right) = 10002020 \pm 34 \text{ m} \quad (191)$$

Therefore the arc corresponding to 1° in longitude is at the equator

$$\nu_e = Q_e / 90 = \frac{\pi}{180} R_e = 111320.07 \pm 0.35 \text{ m} \quad (192)$$

while the arc corresponding to 1° in latitude is at the equator

$$\mu_e = \frac{\pi}{180} \rho_{me} = \frac{\pi}{180} R_e (1 - f)^2 = 110574.95 \pm 0.47 \text{ m} \quad (193)$$

at the pole

$$\mu_p = \frac{\pi}{180} \rho_p = \frac{\pi}{180} R_e / (1 - f) = 111694.51 \pm 0.41 \text{ m} \quad (194)$$

and in the average

$$\bar{\mu} = Q_m / 90 = \frac{\pi}{180} R_e \left(1 - \frac{1}{2}f + \frac{1}{16}f^2 + \frac{1}{32}f^3 + \dots\right) = 111133.56 \pm 0.38 \text{ m} \quad (195)$$

Finally, a few series developments are given for the Earth radius, for the various definitions of latitude, and for the radii of curvature:

$$\phi = \varphi - 692.''627 \sin 2 \varphi + 1.''163 \sin 4 \varphi \mp \dots$$

$$\varphi = \phi + 692.''627 \sin 2 \phi + 1.''163 \sin 4 \phi + \dots \quad (196)$$

and

$$\psi = \varphi - 346.''314 \sin 2 \varphi + 0.''291 \sin 4 \varphi \mp \dots$$

$$\varphi = \psi + 346.''314 \sin 2 \psi + 0.''291 \sin 4 \psi + \dots \quad (197)$$

furthermore

$$\log \frac{R}{R_e} = 9.99927266 + 0.00072917 \cos 2 \varphi - 0.00000184 \cos 4 \varphi + \dots \quad (198)$$

and

$$\begin{aligned} \frac{R}{R_e} &= 1 - 0.003369263 \sin^2 \phi + 0.000017028 \sin^4 \phi - 0.000000096 \sin^6 \phi \pm \dots \\ &= 1 - 0.003352330 \sin^2 \phi - 0.000004233 \sin^2 2 \phi + 0.000000024 \sin^2 \phi \sin^2 2 \phi + \dots \\ &= 0.998321724 + 0.001676162 \cos 2 \phi + 0.000002111 \cos 4 \phi + 0.000000003 \cos 6 \phi + \dots \end{aligned} \quad (199)$$

or

$$\begin{aligned} R &= 6378170.0 - 21489.7 \sin^2 \phi + 108.6 \sin^4 \phi - 0.6 \sin^6 \phi \pm \dots \\ &= 6378170.0 - 21381.7 \sin^2 \phi - 27.0 \sin^2 2 \phi + 0.2 \sin^2 \phi \sin^2 2 \phi + \dots \\ &= 6367465.7 + 10690.8 \cos 2 \varphi + 13.5 \cos 4 \varphi + 0.0_2 \cos 6 \varphi + \dots \end{aligned} \quad (200)$$

and

$$\begin{aligned} \frac{R}{R_e} &= 1 - 0.003324310 \sin^2 \varphi - 0.000027777 \sin^4 \varphi - 0.000000241 \sin^6 \varphi - \dots \\ &= 1 - 0.003352330 \sin^2 \varphi - 0.000007004 \sin^2 2 \phi + 0.000000060 \sin^2 \phi \sin^2 2 \phi + \dots \\ &= 0.998320349 + 0.001676156 \cos 2 \varphi + 0.000003487 \cos 4 \varphi + 0.000000008 \cos 6 \varphi + \dots \end{aligned} \quad (201)$$

or

$$\begin{aligned} R &= 6378170.0 - 21203.0 \sin^2 \varphi - 177.2 \sin^4 \varphi - 1.5 \sin^6 \varphi - \dots \\ &= 6378170.0 - 21381.7 \sin^2 \varphi - 44.7 \sin^2 2 \varphi + 0.4 \sin^2 \varphi \sin^2 2 \varphi + \dots \\ &= 6367456.9 + 10690.8 \cos 2 \varphi + 22.2 \cos 4 \varphi + 0.0_5 \cos 6 \varphi + \dots \end{aligned} \quad (202)$$

and

$$\begin{aligned}\frac{\mu}{\mu_e} &= \frac{\rho_m}{\rho_{m_e}} = 1 + 0.010040132 \sin^2 \varphi + 0.000084004 \sin^4 \varphi \\ &= 1.005051568 - 0.005062068 \cos 2 \varphi + 0.000010500 \cos 4 \varphi \mp \dots\end{aligned}\quad (203)$$

or

$$\begin{aligned}\mu &= 110574.95 + 1110.19 \sin^2 \varphi + 9.29 \sin^4 \varphi + \dots \\ &= 111133.53 - 559.74 \cos 2 \varphi + 1.16 \cos 4 \varphi \mp \dots\end{aligned}\quad (204)$$

$$\frac{\nu}{\nu_e} = \frac{\rho_n}{R_e} \cos \varphi = 1.000838785 \cos \varphi - 0.000839841 \cos 3 \varphi + 0.000001059 \cos 5 \varphi + \dots\quad (205)$$

or

$$\nu = 111413.44 \cos \varphi - 93.49 \cos 3 \varphi + 0.12 \cos 5 \varphi\quad (206)$$

and

$$\begin{aligned}\frac{\rho_n}{R_e} &= 1 + 0.003346711 \sin^2 \varphi + 0.000016801 \sin^4 \varphi + 0.000000094 \sin^6 \varphi + \dots \\ &= 1 + 0.003363605 \sin^2 \varphi - 0.000004224 \sin^2 2 \varphi - 0.000000023 \sin^2 \varphi \sin^2 2 \varphi \\ &= 1.001679685 - 0.001681800 \cos 2 \varphi + 0.000002118 \cos 4 \varphi - 0.000000003 \cos 6 \varphi\end{aligned}\quad (207)$$

or

$$\begin{aligned}\rho_n &= 6378170.0 + 21345.9 \sin^2 \varphi + 107.2 \sin^4 \varphi + 0.6 \sin^6 \varphi + \dots \\ &= 6378170.0 + 21453.6 \sin^2 \varphi - 26.9 \sin^2 2 \varphi - 0.15 \sin^2 \varphi \sin^2 2 \varphi + \dots \\ &= 6388883.3 - 10726.8 \cos 2 \varphi + 13.5 \cos 4 \varphi - \dots\end{aligned}\quad (208)$$

REFERENCES

1. C. W. Allen: *Astrophysical Quantities*. 263pp., The Athlone Press, University of London, 1955.
2. G. W. Pettengill, H. W. Briscoe, J. V. Evans, E. Gehrels, G. M. Hyde, L. G. Kraft, R. Price, and W. B. Smith: *A Radar Investigation of Venus*. The Astronomical Journal, vol. 67, no. 4, pp. 181-190, May 1962.
3. D. O. Muhleman, D. B. Holdridge, and N. Block: *The Astronomical Unit Determined by Radar Reflections from Venus*. The Astronomical Journal, vol. 67, no. 4, pp. 191-203, May 1962.
4. K. D. Froome: *Precision Determination of the Velocity of Electromagnetic Waves*. Nature, vol. 181, no. 4604, p. 258, 25 Jan. 1958.
5. Simon Newcomb: *Tables of the Motion of the Earth on Its Axis and Around the Sun*. Astronomical Papers prepared for the use of the American Ephemeris and Nautical Almanac, vol. vi, part 1, 1895.
6. H. Spencer Jones: *The Rotation of the Earth, and the Secular Accelerations of the Sun, Moon and Planets*. Monthly Notices, Royal Astron. Soc., vol. 99, no. 7, pp. 541-558, 1939.
7. G. M. Clemence: *On the System of Astronomical Constants*. The Astronomical Journal, vol. 53, no. 6, pp. 169-179, May 1948.
8. E. W. Brown: *Tables of the Motion of the Moon*. Yale University Press, New Haven, 1919.
9. *Procès Verbaux des Séances du Comité International des Poids et Mesures*, deuxième Série, tome 25, p. 77, 1957.
10. W. deSitter and Dirk Brouwer: *On the System of Astronomical Constants*. Bulletin of the Astronomical Institutes of the Netherlands, vol. VIII, no. 307, pp. 213-231, 8 July 1938.
11. Harold Jeffreys: *The Earth. Its Origins, History and Physical Constitution*. Cambridge University Press, Fourth Edition, 1959.
12. S. Herrick, R.M.L. Baker, Jr. and C. G. Hilton: *Gravitational and Related Constants for Accurate Space Navigation*. American Rocket Society Paper 497-57, October 1957.
13. M. W. Makemson, R.M.L. Baker, Jr. and G. B. Westrom: *Analysis and Standardization of Astrodynamical Constants*. Univ. of California, Los Angeles. Astrodynamical Report no. 12, February 1961. Journal of the Astronautical Sciences, vol. VIII, no. 1, Spring 1961; AAS Preprint 61-27, January 1961.
14. Simon Newcomb: *The Elements of the Four Inner Planets and the Fundamental Constants of Astronomy*. Washington, D.C., 1895 (Supplement to The American Ephemeris and Nautical Almanac for 1897).

REFERENCES (Continued)

15. Eugene Rabe: *Derivation of Fundamental Astronomical Constants from Observations of Eros During 1926-1945*. The Astronomical Journal, vol. 55, no. 1184, pp. 112-126, 1950. *Additional Note on the Solar Parallax from Eros*. The Astronomical Journal, vol. 59, pp. 409-411, 1954.
16. Julius Bauschinger: Enzykl. d. Math. Wiss. 6 II, no. 17, 1919. (The value is given in Ref. 45, p. 51).
17. H. Battermann: Veröffentl. d. Sternw. Königsberg/Pr. (The value is given in Ref. 45, p. 51)
18. Dirk Brouwer and O. B. Watts: Unpublished. (The value is given in Ref. 45, p. 52).
19. David Gill: *Determination of the Solar Parallax and the Mass of the Moon from Heliometer Observations of Iris, Victoria and Sappho Made in the Years 1888 and 1890*. Ann. Cape Observatory, vol. 6, 1896, and vol. 7, 1897.
20. A. R. Hinks: *Solar Parallax*. Monthly notices, Royal Astronomical Soc., vol. 70, no. 9, p. 588, 1909.
21. H. Spencer Jones: *The Solar Parallax and the Mass of the Moon from Observations of Eros at the Opposition of 1931*. Mem. Royal Astr. Soc., vol. 66, pt. 2, 56pp., London, 1941.
22. H. R. Morgan and F. P. Scott: *Observations of the Sun 1900-1937 Compared with Newcomb's Tables*. The Astronomical Journal, vol. 47, p. 193, 1939.
23. Harold Jeffreys: *On the Lunar Equation*. Monthly Notices of the Royal Astronomical Soc. (London), vol. 102, no. 4, pp. 194-204, 1942.
24. Erwin Delano: *The Lunar Equation from Observations of Eros 1930-31*. The Astronomical Journal, vol. 55, pp. 129-132, 1950.
25. Simon Newcomb: *Researches on the Motion of the Moon, Part II*. Astr. Paper. Amer. Eph., vol. IX, p. 39, 1912.
26. The American Ephemeris and Nautical Almanac for the Year 1962, U.S. Government Printing Office, Washington, D.C., 1960. Explanatory Supplement to the Astronomical Ephemeris and the American Ephemeris and Nautical Almanac, London, 1961.
27. H. Hirose and R. Manabe: *Motion and Figure of the Moon*. Transactions I.A.U., vol. 9, p. 265, 1955.
28. George H. Darwin: *The Theory of the Figure of the Earth, Carried to the Second Order of Small Quantities*. Monthly Notices Roy. Astron. Soc., vol. 60, pp. 82-124, 1899.
29. F. R. Helmert: *Die mathematischen und physikalischen Theorien der Höheren Geodäsie*. I. *Die mathematischen Theorien*. Leipzig, 1880. II. *Die physikalischen Theorien*. Leipzig, 1884.

REFERENCES (Continued)

30. E. C. Bullard: *The Figure of the Earth*. Monthly Notices Roy. Astron. Soc., Geophys. Suppl., vol. 5, no. 6, 1948.
31. W. deSitter: *On the Flattening and the Constitution of the Earth*. Bulletin of the Astronomical Institutes of the Netherlands, vol. II, no. 55, pp. 97-108, 14 May 1924.
32. F. R. Helmert: *Neue Formeln für den Verlauf der Schwerkraft im Meeresniveau beim Festland*. Sitz-Ber. d. Kgl. Preuss. Akad. d. Wiss., vol. 41, pp. 676-68, Berlin 1915.
33. A. Berroth: *Die Erdgestalt und die Hauptträgheitsmomente A und B im Äquator aus Messungen der Schwerkraft*. Gerl. Beitr. Geophys., vol. 14, pp. 215-257, Leipzig, 1915-1918.
34. W. A. Heiskanen: *Untersuchungen über Schwerkraft und Isostasie*. Publ. Finn. Geod. Inst., no. 4, Helsinki, 1924.
35. W. A. Heiskanen: *Ist die Erde ein dreiaxsiges Ellipsoid?* Gerlands Beitr. Geophys., vol. 19, pp. 356-377, Leipzig, 1928, Astr. Nachr., vol. 234, no. 5562, Kiel, 1928.
36. W. A. Heiskanen: *Investigations on the Gravity Formula*. Ann. Acad. Scient. Fennicae, series A, vol. 51, no. 8, Helsinki, 1938.
37. N. F. Shuravlev: *Die Bestimmung der Abplattung des Erdellipsoides aus gravimetrischen Messungen* (in Russian with English Abstract) Publ. Astro. Inst. Sternberg, vol. 14, pt. 2, Moscow, 1940.
38. Erkki Niskanen: *Gravity Formulas Derived by the Aid of the Level Land Stations*. Publ. Isos. Inst. IAG (Helsinki), no. 16, 1945; Ann. Acad. Scient. Fennicae, series A, no. III, 10, pp. 1-16, Helsinki, 1945.
39. Harold Jeffreys: *The Figures of the Earth and Moon* (Third Paper). Monthly Notices of the Roy. Astr. Soc., Geophys. Suppl. vol. 5, no. 7, pp. 219-247, July 1948.
40. H. Schütte: *Die Bestimmung der Abplattung der Erde aus der Schwereverteilung nach dem Schwereverzeichnis von N. F. Shuravlev*. Gerl. Beitr. Geophys., vol. 62, pp. 9-26, Leipzig, 1950.
41. U. A. Uotila: *Determination of the Shape of the Geoid*. Symposium: Size and Shape of the Earth, held at the Ohio State University, Columbus, Ohio, Nov. 13-15, 1956. Publ. no. 7, Inst. of Geodesy, Photogrammetry and Cartography, 1957.
42. W. A. Heiskanen; *Achievements of the World-wide Gravity Program of the Mapping and Charting Research Laboratory of the Ohio State University*. Report to the Toronto General Assembly of the IUGG in 1957.
43. F. Kühnen und Ph. Furtwängler: *Bestimmung der absoluten Grösse der Schwerkraft zu Potsdam mit Reversionspendeln*. Veröff. d. Preuss. Geod. Inst. N.F. 27, 1906.
44. W. A. Heiskanen and F. A. Vening Meinesz: *The Earth and Its Gravity Field*. x + 470 pp., McGraw-Hill Book Co., New York, 1958 (p. 75).

REFERENCES (Continued)

45. Landolt-Börnstein: *Zahlenwerte und Funktionen aus Physik, Chemie, Astronomie, Geophysik und Technik*. Vol. III, pp. 43-52 (A. Kopff: Astrometrische Konstanten) and pp. 256-270 (K. Jung: Schwerkraft und Erdfigur), Springer-Verlag, Berlin, 1952.
46. H. Andoyer: *Les formules de la précession après S. Newcomb*. Bulletin Astronomique (Paris), vol. 28, p. 67-76, 1911.
47. H. R. Morgan: *Systematic Corrections to the Albany General Catalogue*. The Astron. Jour., vol. 54, no. 1, pp. 1-9, Sept. 1948; Corrections to the Fundamental Catalogs. The Astron. Jour., vol. 54, no. 6, pp. 145-150, June 1949
48. Landolt-Börnstein: *Zahlenwerte und Funktionen*. (Ref. 45, p. 52)
49. J. H. Oort: *The Constants of Precession of Galactic Rotation*. Bulletin of the Astron. Institutes of the Netherlands, vol. 9, p. 424 - 427, 1943.
50. R. R. Radau: *Sur la loi des densités à l'intérieur de la Terre*. Comptes Rendus Acad. Sci. (Paris), vol. 100, pp. 972-974, 1885; Bulletin Astronomique 2, p. 157, 1885.
51. O. Callandreau: *Sur le développement en série du potential*. J. Polytech., 1889; Ann. de l'Observ. de Paris 19 E, 1889.
52. Harold Jeffreys: *On the Figures of the Earth and Moon*. Monthly Notices of the Roy. Astr. Soc., vol. 97, no. 1, pp. 3-15, Nov. 1936 or Geophys. Suppl., vol. 4, no. 1, pp. 1-13, Jan. 1937.
53. Harold Jeffreys: *The Moon's Libration in Longitude*. Monthly Notices of the Roy. Astr. Soc., vol. 117, no. 5, pp. 475-477, 1957.
54. Harold Jeffreys: *On the Figure of the Moon*. Monthly Notices Roy. Astr. Soc., vol. 122, pp. 421-432, 1961.
55. W. M. Kaula: *A Geoid and World Geodetic System Based on a Combination of Gravimetric, Astrogeodetic, and Satellite Data*. Jour. Geophys. Res., vol. 66, no. 6, pp. 1799-1811, June 1961.
56. Victor C. Clarke Jr.: *Constants and Related Data Used in Trajectory Calculations at the Jet Propulsion Laboratory*. Jet Propulsion Laboratory, Technical Report No. 32-273, 14 pp., 1 May 1962.
57. Irene Fischer: *Parallax of the Moon in Terms of a World Geodetic System*. The Astronomical Jour., vol. 67, no. 6, pp. 373-378, Aug. 1962.
58. B. E. Kalensher: *Selenographic Coordinates*. Jet Propulsion Laboratory, Technical Report No. 32-41, 31 pp., 24 February 1961.

SUMMARY

An internally consistent system of astrodynamic constants is derived based upon theoretical coupling relationships and the most recent available experimental data. A previously existing discrepancy in the value of the gravitational parameter of the earth (as derived by different methods) has been eliminated. Likewise, several inconsistencies in the previously available system of lunar constants have been removed.

A new method of determining the ratio of the masses of the Earth and Moon has been derived and the results are in agreement with other determinations.

An error study of each constant is presented; both relative and absolute probable errors are listed.

The results of this study can be summarized in the following list of astrodynamic constants:

1. GENERAL CONSTANTS

1. Newton's gravitation constant:

$$G = 6.670 (1 \pm 0.0007) \times 10^{-8} = (6.670 \pm 0.005) \times 10^{-8} \text{ cm}^3 \text{ g}^{-1} \text{ s}^{-2} (\text{dyn cm}^2 \text{ g}^{-2})$$

2. Velocity of light:

$$c = 299\,792.5 (1 \pm 3.3 \times 10^{-7}) = 299\,792.5 \pm 0.1 \text{ km/s}$$

3. Solar parallax (Sun's equatorial horizontal parallax):

$$\pi_{\odot} = 8.''794\,14 (1 \pm 5.8 \times 10^{-6}) = 8.''794\,14 \pm 0.''000\,05$$

4. Astronomical unit (mean Earth-Sun distance = $R_{\odot} / \pi_{\odot} \sin 1''$):

$$\text{a. u.} = 149\,598\,700 (1 \pm 2.7 \times 10^{-6}) = 149\,598\,700 \pm 400 \text{ km}$$

5. Light year (distance which light travels in a year = $P_{\oplus} c$):

$$1. \text{ y.} = 31\,556\,925.9747 c = (9.460\,530 \pm 0.000\,003) \times 10^{12} \text{ km} = 63\,239.39 \pm 0.15 \text{ a. u.}$$

6. Parsec (distance in which 1 a. u. appears as $1'' = 1 \text{ a. u.} / \sin 1''$):

$$p c = 206\,264.806\,247 \text{ a. u.} = (3.085\,695 \pm 0.000\,008) \times 10^{13} \text{ km} = 3.261\,651 \pm 0.000\,008 \text{ l. y.}$$

7. Light time for 1 a. u. :

$$\tau = \text{a.u.}/c = 499.008 (1 \pm 3.6 \times 10^{-5}) = 499.008 \pm 0.018 \text{ s}$$

8. Constant of aberration:

$$K = 20.''4956 (1 \pm 3.5 \times 10^{-5}) = 20.''4956 \pm 0.''0007$$

9. Obliquity of ecliptic

$$\epsilon = 23^{\circ}27'8.''26 - 46.''844 T - 0.''0060 T^2 + 0.''00183 T^3$$

$$\cos \epsilon = 0.917\,3917 ; \sin \epsilon = 0.397\,985\,5 (1900.0)$$

10. Newcomb's constant of precession (per tropical century):

$$P = \frac{p_0}{\cos \epsilon} = 5493.''62 - 0.''003\,64 T = (N + 2.''96) *$$

11. Luni-solar precession in longitude:

$$p_0 = p_{\odot} + p_{\text{M}} = 5039.''804 + 0.''4930 T - 0.''000\,04 T^2 = (N + 2.''72)$$

* N refers to Newcomb's precessional data

12. Geodetic precession in longitude:

$$p_g = \frac{3}{2} (v_{\oplus}/c)^2 n_{\oplus} = 1.''9188 \pm 0.''0002 = (N + 1.''92)$$

13. Observed luni-solar precession in longitude:

$$p_1 = p_0 - p_g = 5037.''885 + 0.''4930 T - 0.''00004 T^2 = (N + 0.''80)$$

14. Planetary precession in right ascension:

$$\lambda = -m + n \cot \epsilon = 12.''473 - 1.''8870 T - 0.''00014 T^2 = (N + 0.''00)$$

15. General precession in longitude:

$$p = p_1 - \lambda \cos \epsilon = m \cos \epsilon + n \sin \epsilon = 5026.''441 + 2.''2229 T + 0.''00026 T^2 = (N + 0.''80)$$

16. General precession in right ascension:

$$\begin{aligned} m = p_1 \cos \epsilon - \lambda &= 4609.''236 + 2.''7945 T + 0.''00012 T^2 = (N + 0.''73) \\ &= 307.^s 2824 + 0.^s 18630 + 0.^s 000008 T^2 = (N + 0.^s 0487) \end{aligned}$$

17. General precession in declination:

$$\begin{aligned} n = p_1 \sin \epsilon &= 2005.''005 - 0.''8533 T - 0.''00037 T^2 = (N + 0.''32) \\ &= 133.^s 6670 - 0.^s 05689 T - 0.^s 000025 T^2 = (N + 0.^s 0213) \end{aligned}$$

18. Mean sidereal time rate (for 1950.0):

$$\begin{aligned} \dot{\Theta}_m &= 7.29211585479 \times 10^{-5} \text{ rad/s} = 1.002737909294 \text{ d}_*/\text{d} (s_*/s) \\ &= 15.04106863941 \text{ ''/s } (^{\circ}/\text{h}) = 360.9856473460 \text{ }^{\circ}/\text{d} \end{aligned}$$

2. EARTH CONSTANTS

19. Semi-major axis of the Earth's orbit:

$$a_{\oplus} = 149\,598\,700 (1 \pm 2.7 \times 10^{-6}) = 149\,598\,700 \pm 400 \text{ km}$$

20. Sidereal mean orbital motion (for 1950.0):

$$\begin{aligned} n_{\oplus} &= 0.9856091080 \text{ }^{\circ}/\text{d} = 0.04106704615 \text{ ''/s } (^{\circ}/\text{h}) \\ &= 1.9909865817 \times 10^{-7} \text{ rad/s} \end{aligned}$$

21. Mean orbital velocity:

$$v_{\oplus} = a_{\oplus} n_{\oplus} = 29\,784.90 (1 \pm 2.7 \times 10^{-6}) = 29\,784.90 \pm 0.08 \text{ m/s}$$

22. Mass ratio of the Sun to the Earth-Moon system:

$$\nu = \frac{M_{\odot}}{M_{\oplus} + M_{\text{A}}} = 328\,898.6 (1 \pm 1.6 \times 10^{-5}) = 328\,898.6 \pm 5.2$$

23. Mass ratio of the Sun to the Earth:

$$\nu (1 + \kappa) = \frac{M_{\odot}}{M_{\oplus}} = 332\,947.6 (1 \pm 2.0 \times 10^{-5}) = 332\,947.6 \pm 6.7$$

24. Gravitational parameter of the Earth:

$$\mu_{\oplus} = G M_{\oplus} = 398\,606.4 (1 \pm 1.23 \times 10^{-5}) = 398\,606.4 \pm 4.9 \text{ km}^3/\text{s}^2$$

25. Mass:

$$M_{\oplus} = 5.9761 \times 10^{27} (1 \pm 7.2 \times 10^{-4}) = (5.9761 \pm 0.0043) \times 10^{27} \text{ g}$$

26. Equatorial radius:

$$R_{\text{e}} = 6\,378\,170 (1 \pm 3.14 \times 10^{-6}) = 6\,378\,170 \pm 20 \text{ m}$$

27. Polar radius:

$$R_{\text{p}} = 6\,356\,788 (1 \pm 3.70 \times 10^{-6}) = 6\,356\,788 \pm 24 \text{ m}$$

28. Flattening (oblateness, ellipticity):

$$f = \frac{R_{\text{e}} - R_{\text{p}}}{R_{\text{e}}} = 0.003\,352\,33 (1 \pm 1.7 \times 10^{-4}) = 0.003\,352\,33 \pm 0.000\,000\,56 = 1: (298.30 \pm 0.05)$$

$$1 - f = (1 - e^2)^{1/2} = (1 + \epsilon^2)^{-1/2} R_{\text{p}}/R_{\text{e}} = 0.996\,647\,67 (1 \pm 5.6 \times 10^{-7})$$

29. First eccentricity of the meridian ellipse:

$$e = 0.081\,813\,33 + 0.000\,006\,80$$

$$e^2 = f(2 - f) = 0.006\,693\,42 + 0.000\,001\,11$$

30. Second eccentricity of the meridian ellipse:

$$\epsilon = 0.082\,088\,52 \pm 0.000\,006\,87$$

$$\epsilon^2 = \frac{e^2}{1 - e^2} = 0.006\,738\,53 \pm 0.000\,001\,13$$

31. Mean radius:

$$\bar{R} = (2 R_{\text{e}} + R_{\text{p}}) / 3 = 6\,371\,043 (1 \pm 3.3 \times 10^{-6}) = 6\,371\,043 \pm 21 \text{ m}$$

32. Radius for geodetic latitude $\varphi = \sin^{-1} \sqrt{1/3} = 35^\circ 15' 51.''8$

$$R_1 = 6\,371\,083 (1 \pm 3.3 \times 10^{-6}) = 6\,371\,083 \pm 21 \text{ m}$$

33. Radius for geocentric latitude $\phi = \sin^{-1} \sqrt{1/3} = 35^\circ 15' 51.''8$

$$R_2 = 6\,371\,019 (1 \pm 3.3 \times 10^{-6}) = 6\,371\,019 \pm 21 \text{ m}$$

34. Radius for sphere of same surface area:

$$R_s = 6\,371\,041 (1 \pm 3.3 \times 10^{-6}) = 6\,371\,041 \pm 21 \text{ m}$$

35. Radius for sphere of same volume:

$$R_v = 6\,371\,035 (1 \pm 3.3 \times 10^{-6}) = 6\,371\,035 \pm 21 \text{ m}$$

36. Surface area:

$$S_\oplus = 5.100\,711 \times 10^{14} (1 \pm 6.6 \times 10^{-6}) = (5.100\,711 \pm 0.000\,034) \times 10^{14} \text{ m}^2$$

37. Volume:

$$V_\oplus = 1.083\,225 \times 10^{21} (1 \pm 1.0 \times 10^{-5}) = (1.083\,225 \pm 0.000\,011) \times 10^{21} \text{ m}^3$$

38. Mean density:

$$\bar{\rho}_\oplus = 5.5170 (1 \pm 7.3 \times 10^{-4}) = 5.5170 \pm 0.0040 \text{ g/cm}^3$$

39. Angular velocity of the Earth's rotation:

$$\begin{aligned} \Omega_m &= 7.292\,115\,146\,46 \times 10^{-5} \text{ rad/s} = 1.002\,737\,811\,891 \text{ rot/d} \\ &= 15.041\,067\,178\,37 \text{ ''/s } (^\circ/\text{h}) = 360.985\,612\,280\,8 \text{ }^\circ/\text{d} \end{aligned}$$

40. Rotational velocity at the equator:

$$\Omega_m R_e = 465.1035 (1 \pm 3.2 \times 10^{-6}) = 465.1035 \pm 0.0015 \text{ m/s}$$

41. Centrifugal acceleration at the equator:

$$\Omega_m^2 R_e = 0.033\,915\,88 (1 \pm 3.2 \times 10^{-6}) = 0.033\,915\,88 \pm 0.000\,000\,11 \text{ m/s}^2$$

42. Centrifugal acceleration factor:

$$\tilde{\omega}_\oplus = \frac{\Omega_m^2 R_e^3}{G M_\oplus} = 3461.369 \times 10^{-6} (1 \pm 2.2 \times 10^{-5}) = (3461.369 \pm 0.076) \times 10^{-6}$$

43. Oblateness coefficients of the Earth's potential:

$$J = 1623.48 \times 10^{-6} (1 \pm 1.8 \times 10^{-4}) = (1623.48 \pm 0.29) \times 10^{-6}$$

$$K = \frac{6}{7} D = 8.85 \times 10^{-6}$$

$$J_2 = \frac{2}{3} J = 1082.32 \times 10^{-6} (1 \pm 1.8 \times 10^{-4}) = (1082.32 \pm 0.19) \times 10^{-6}$$

$$J_4 = -\frac{4}{15} K = -\frac{8}{35} D = -2.36 \times 10^{-6}$$

44. Coefficients of the Earth's gravity formula:

$$\beta = 5302.92 \times 10^{-6}; \quad \gamma = -5.85 \times 10^{-6}$$

45. Mass of the Earth's atmosphere:

$$M_{\text{atm}} = \frac{p_0}{g} \cdot S_{\oplus} = (10332.275 \text{ kg/m}^2) \cdot S_{\oplus} \\ = 5.270195 \times 10^{18} (1 \pm 6.6 \times 10^{-6}) = (5.270195 \pm 0.000035) \times 10^{18} \text{ kg}$$

46. Relative mass of the Earth's atmosphere:

$$A = M_{\text{atm}} / M_{\oplus} = 0.88188 \times 10^{-6} (1 \pm 7.3 \times 10^{-4}) = (0.88188 \pm 0.00064) \times 10^{-6}$$

47. Gravity acceleration correction factor:

$$\chi = g_e / (GM_{\oplus} / R_e^2) = 0.99816566 (1 \pm 4.0 \times 10^{-7}) = 0.99816566 \pm 0.00000040 \\ 1 - \chi = A + \tilde{\omega} - J - \frac{1}{2} K = 1834.34 \times 10^{-6} (1 \pm 2.2 \times 10^{-4}) = (1834.34 \pm 0.40) \times 10^{-6}$$

48. Gravity acceleration at the Earth's equator:

$$g_e = 9.780362 (1 \pm 3.3 \times 10^{-6}) = 9.780362 \pm 0.000032 \text{ m/s}^2$$

49. Dynamic oblateness:

$$H = \frac{C - A}{C} = 3272.09 \times 10^{-6} (1 \pm 1.6 \times 10^{-4}) = (3272.09 \pm 0.54) \times 10^{-6} = 1/305.615 \pm 0.05$$

50. Moment of inertia parameter:

$$q = \frac{3}{2} \frac{C}{M_{\oplus} R_e^2} = \frac{J}{H} = 0.49616 (1 \pm 3.4 \times 10^{-4}) = 0.49616 \pm 0.00017$$

51. Dimensionless moments of inertia:

$$\frac{A}{M_{\oplus} R_e^2} = J_2 \left(\frac{1}{H} - 1 \right) = 0.32969 \pm 0.00011$$

$$\frac{C}{M_{\oplus} R_e^2} = J_2 / H = 0.33077 \pm 0.00011$$

52. Unit for the Earth's moments of inertia:

$$M_{\oplus} R_e^2 = 2.4311_4 \times 10^{38} (1 \pm 7.3 \times 10^{-4}) = (2.4311_4 \pm 0.0018) \times 10^{38} \text{ kg m}^2$$

53. Earth's moments of inertia:

$$A = 0.80152 \times 10^{38} (1 \pm 1.07 \times 10^{-3}) = (0.80152 \pm 0.00086) \times 10^{38} \text{ kg m}^2$$

$$C = 0.80415 \times 10^{38} (1 \pm 1.07 \times 10^{-3}) = (0.80415 \pm 0.00086) \times 10^{38} \text{ kg m}^2$$

$$C - A = 2.6313 \times 10^{35} (1 \pm 9.1 \times 10^{-4}) = (2.6313 \pm 0.0024) \times 10^{35} \text{ kg m}^2$$

54. Angular momentum:

$$C \Omega = 5.8640 \times 10^{33} (1 \pm 1.07 \times 10^{-3}) = (5.8640 \pm 0.0063) \times 10^{33} \text{ kg m}^2/\text{s}$$

55. Rotational energy:

$$\frac{1}{2} C \Omega^2 = 2.1380 \times 10^{29} (1 \pm 1.07 \times 10^{-3}) = 2.1380 \pm 0.0023 \times 10^{29} \text{ kg m}^2/\text{s}^2 (\text{joule})$$

56. Circular velocity at the Earth's equator:

$$v_{\text{cir}} = \sqrt{\mu_{\oplus}/R_e} = 7905.404 (1 \pm 7.7 \times 10^{-6}) = 7905.404 \pm 0.061 \text{ m/s}$$

3. LUNAR CONSTANTS

57. Mean observed distance from the Earth:

$$\bar{r}_{\text{e}} = 384402.0 (1 \pm 2.6 \times 10^{-6}) = 384402.0 \pm 1.0 \text{ km}$$

58. Relative mean lunar distance:

$$\bar{r}_{\text{e}}/R_e = 1/\sin \pi_{\text{e}} = 60.26838 (1 \pm 5.8 \times 10^{-6}) = 60.26838 \pm 0.00035$$

59. Constant part of the sine of the perturbed lunar parallax:

$$\pi'_{\text{e}} = \frac{\sin \pi_{\text{e}}}{\sin 1''} = 3422.''438 (1 \pm 5.8 \times 10^{-6}) = 3422.''438 \pm 0.''020$$

60. Mean perturbed equatorial horizontal parallax:

$$\pi_{\text{e}} = 3422.''595 (1 \pm 5.8 \times 10^{-6}) = 3422.''595 \pm 0.''020$$

61. Semi-major axis of the Moon's orbit:

$$a_{\text{e}} = 1.000907681 \bar{r}_{\text{e}} = 384750.9 (1 \pm 2.6 \times 10^{-6}) = 384750.9 \pm 1.0 \text{ km}$$

62. Sidereal mean orbital motion (for 1950.0):

$$\begin{aligned} n_{\text{e}} &= 13.1763582598 \text{ }^{\circ}/\text{d} = 0.549014912685 \text{ ''/s } (^{\circ}/\text{h}) \\ &= 2.66169940799 \times 10^{-6} \text{ rad/s} \end{aligned}$$

63. Mean orbital velocity:

$$v_{\text{e}} = a_{\text{e}} n_{\text{e}} = 1024.091 (1 \pm 2.9 \times 10^{-6}) = 1024.091 \pm 0.003 \text{ m/s}$$

64. Lunar inequality in the Moon's ecliptic longitude:

$$L = 6.''4439 (1 \pm 3.0 \times 10^{-4}) = 6.''4439 \pm 0.''0019$$

65. Parallax inequality in the Moon's ecliptic longitude:

$$P_{\star} = 124.''986 (1 \pm 3.3 \times 10^{-5}) = 124.''986 \pm 0.''004$$

66. Mass ratio of the Earth to the Moon:

$$1/\kappa = M_{\oplus}/M_{\text{e}} = 81.250 (1 \pm 3.0 \times 10^{-4}) = 81.250 \pm 0.024$$

67. Mass ratio of the Earth-Moon system to the Earth:

$$1 + \kappa = (M_{\oplus} + M_{\text{e}})/M_{\oplus} = 1.0123077 (1 \pm 3.7 \times 10^{-6}) = 1.0123077 \pm 0.0000037$$

68. Gravitational parameter of the Moon:

$$\mu_{\text{e}} = GM_{\text{e}} = 4905.92 (1 \pm 3.1 \times 10^{-4}) = 4905.92 \pm 1.52 \text{ km}^3/\text{s}^2$$

69. Mass:

$$M_{\text{e}} = 7.3552 \times 10^{25} (1 \pm 1.02 \times 10^{-3}) = (7.3552 \pm 0.0075) \times 10^{25} \text{ g}$$

70. Moon's semi-diameter at mean distance:

$$s_{\text{e}} = 932.''72 (1 \pm 1.0 \times 10^{-4}) = 932.''72 \pm 0.''09$$

71. Relative radius of the visible disk of the Moon:

$$k = R_{\text{e}}/R_{\oplus} = 0.2725289 (1 \pm 1.0 \times 10^{-4}) = 0.2725289 \pm 0.0000273$$

72. Radius of the visible disk of the Moon:

$$R_{\text{e}} = \frac{b+c}{2} = 1738236 (1 \pm 1.0 \times 10^{-4}) = 1738236 \pm 174 \text{ m}$$

73. Longest semi-axis directed to the Earth:

$$a = R_{\text{e}}/0.9995918 = 1738946 (1 \pm 1.07 \times 10^{-4}) = 1738946 \pm 186 \text{ m}$$

74. Medium semi-axis in orbital direction:

$$b = 0.9998116 a = 1738618 (1 \pm 1.20 \times 10^{-4}) = 1738618 \pm 209 \text{ m}$$

75. Shortest semi-axis (rotational or polar radius):

$$c = 0.9993720 a = 1737854 (1 \pm 1.08 \times 10^{-4}) = 1737854 \pm 188 \text{ m}$$

76. Volume:

$$V_{\bullet} = \frac{4}{3} \pi a b c = 2.20086 \times 10^{25} (1 \pm 3.35 \times 10^{-4}) = (2.20086 \pm 0.00074) \times 10^{25} \text{ cm}^3$$

77. Mean density:

$$\bar{\rho}_{\bullet} = 3.3420 (1 \pm 1.5 \times 10^{-3}) = 3.3420 \pm 0.0050 \text{ g/cm}^3$$

78. Surface density:

$$\rho_0 = 3.290 \text{ g/cm}^3$$

79. Central density:

$$\rho_c = 3.420 \text{ g/cm}^3$$

80. Inhomogeneity factor of the Moon:

$$\lambda = 0.1991 (1 \pm 5.0 \times 10^{-4}) = 0.1991 \pm 0.0001$$

81. Dimensionless moment of inertia parameters:

$$f = \frac{C - B}{C - A} = 0.70 (1 \pm 2.86 \times 10^{-2}) = 0.70 \pm 0.02$$

$$\alpha = \frac{C - B}{C} = 0.0004395 (1 \pm 3.03 \times 10^{-2}) = 0.0004395 \pm 0.0000133$$

$$\beta = \frac{C - A}{C} = 0.0006279 (1 \pm 1.6 \times 10^{-4}) = 0.0006279 \pm 0.0000001$$

$$\gamma = \frac{B - A}{C} = 0.0001884 (1 \pm 6.85 \times 10^{-2}) = 0.0001884 \pm 0.0000129$$

$$g = \frac{3}{2} \frac{C}{M_{\bullet} a^2} = 0.5972 (1 \pm 5.0 \times 10^{-4}) = 0.5972 \pm 0.0003$$

$$J = \frac{3}{2} \frac{C - 1/2 (A + B)}{M_{\bullet} a^2} = 0.0003187 (1 \pm 1.38 \times 10^{-2}) = 0.0003187 \pm 0.0000044$$

$$K = \frac{3}{2} \frac{B - A}{M_{\bullet} a^2} = 0.0001125 (1 \pm 6.84 \times 10^{-2}) = 0.0001125 \pm 0.0000077$$

$$L = \frac{3}{2} \frac{C - A}{M_{\bullet} a^2} = 0.0003750 (1 \pm 2.1 \times 10^{-3}) = 0.0003750 \pm 0.0000008$$

82. Dimensionless moment of inertia differences:

$$\frac{C - A}{M_{\bullet} a^2} = 0.0002500 (1 \pm 2.1 \times 10^{-3}) = 0.0002500 \pm 0.0000005$$

$$\frac{C - B}{M_{\bullet} a^2} = 0.0001750 (1 \pm 3.09 \times 10^{-2}) = 0.0001750 \pm 0.0000054$$

82. Dimensionless moment of inertia differences (Continued):

$$\frac{B-A}{M_{\bullet} a^2} = 0.000\,0750 (1 \pm 6.84 \times 10^{-2}) = 0.000\,0750 \pm 0.000\,0051$$

83. Dimensionless moments of inertia:

$$\frac{A}{M_{\bullet} a^2} = 0.397\,87_7 (1 \pm 5.0 \times 10^{-4}) = 0.397\,87_7 \pm 0.00020$$

$$\frac{B}{M_{\bullet} a^2} = 0.397\,95_2 (1 \pm 5.0 \times 10^{-4}) = 0.397\,95_2 \pm 0.000\,20$$

$$\frac{C}{M_{\bullet} a^2} = 0.398\,12_7 (1 \pm 5.0 \times 10^{-4}) = 0.398\,12_7 \pm 0.000\,20$$

84. Axial ratios of the Moon:

$$\frac{b}{a} = \sqrt{1 - \frac{2\gamma}{1+\gamma}} = 0.9998\,116 (1 \pm 1.3 \times 10^{-5}) = 0.9998\,116 \pm 0.0000\,129$$

$$\frac{c}{a} = \sqrt{1 - \frac{2\beta}{1+\gamma}} = 0.9993\,720 (1 \pm 1.0 \times 10^{-6}) = 0.9993\,720 \pm 0.0000\,010$$

$$\sigma = R_{\bullet}/a = \frac{1}{2} \left(\frac{b}{a} + \frac{c}{a} \right) = 0.9995\,918 (1 \pm 7.0 \times 10^{-6}) = 0.9995\,918 \pm 0.0000\,070$$

85. Oblateness coefficients of the potential function of the Moon:

$$J_2 = \frac{C - 1/2 (A+B)}{M_{\bullet} a^2} = \frac{2}{3} J = 0.000\,2125 \pm 0.000\,0029$$

$$J_2^{(2)} = \frac{B-A}{4 M_{\bullet} a^2} = \frac{1}{6} K = 0.000\,0188 \pm 0.000\,0013$$

86. Unit for the Moon's moments of inertia:

$$M_{\bullet} a^2 = 2.224\,1_6 \times 10^{35} (1 \pm 1.2 \times 10^{-3}) = (2.224\,1_6 \pm 0.0027) \times 10^{35} \text{ kg m}^2$$

87. Moment of inertia differences:

$$C - \frac{1}{2} (A+B) = 0.000\,473 \times 10^{35} (1 \pm 1.50 \times 10^{-2}) = (0.000\,473 \pm 0.000\,007) \times 10^{35} \text{ kg m}^2$$

$$B-A = 0.000\,167 \times 10^{35} (1 \pm 6.96 \times 10^{-2}) = (0.000\,167 \pm 0.000\,012) \times 10^{35} \text{ kg m}^2$$

88. Moon's moments of inertia:

$$A = 0.884\,94 \times 10^{35} (1 \pm 1.73 \times 10^{-3}) = (0.884\,94 \pm 0.001\,53) \times 10^{35} \text{ kg m}^2$$

$$B = 0.885\,11 \times 10^{35} (1 \pm 1.73 \times 10^{-3}) = (0.885\,11 \pm 0.001\,53) \times 10^{35} \text{ kg m}^2$$

$$C = 0.885\,50 \times 10^{35} (1 \pm 1.73 \times 10^{-3}) = (0.885\,50 \pm 0.001\,53) \times 10^{35} \text{ kg m}^2$$

INDEX

(A)

| | Page |
|--|--------------|
| Acceleration, gravitational, | II-9-14 |
| Accuracy, tracking, | XI-12-20 |
| Adams-Bashforth method, | IV-9-10 |
| Aerodynamic heating, | IX-14-17 |
| Air drag, perturbation of satellite orbits by, | V-1-55, IV-3 |
| Angular momentum smoothing, | VII-44-46 |
| Angular orbital elements, | III-4-37 |
| Anomaly, eccentric, equations for, | III-21 |
| series expansions, | III-26 |
| mean, equations for, | III-25 |
| figures, | III-76-87 |
| series in, | III-26-34 |
| true, equations for, | III-23 |
| series for, | III-27 |
| Apogee radius, equations for, | III-19 |
| Apogee velocity, equations for, | III-20 |
| Area coverage, | XIII-17-26 |
| Areas, law of, | III-2 |
| Argument of perigee, equations for, | III-24 |
| Ascending node, equations for, | III-24 |
| Astronomical unit, | II-2-15 |
| Astronautical constants, | II-4 |
| Atmospheric density, U.S. Standard 1962, | II-21-31 |
| variability, | II-31-38 |
| Attitude control, modes of, | XII-31-55 |
| Attitude sensing, methods of, | XII-44-48 |
| Axis, semimajor, equations for, | III-17 |
| semiminor, equations for, | III-17 |
| Azimuth, equations for, | III-37 |

| | Page |
|----------------------------------|-------|
| (B) | |
| Ballistic coefficient, | V-4-6 |
| effective, | V-20 |
| tumbling, | V-6-8 |
| Bessel functions, | V-16 |
| asymptotic series, | V-17 |
| integrals, | V-16 |
| modified, | V-17 |
| reduction formulas, | V-17 |
| Bibliographies (see references) | |

| | |
|---|------------|
| (C) | |
| Central force field, | III-2 |
| Change in orbital velocity due to | |
| impulsive burning of an injection rocket, | VI-2, 6 |
| in satellite in-orbit position, | VI-6-8, 11 |
| Closure (rendezvous), (see final closure) | |
| Coefficient of drag, | V-3-6 |
| effective, | V-20 |
| Coefficients of potential, function, | II-9-14 |
| Compatible orbits rendezvous, | VII-9-12 |
| Computation of orbits, | IX-25-30 |
| Conic motion, | III-1-7 |
| Constants, astronomical, | II-2 |
| conversion, | II-50-56 |
| geocentric, | II-9-14 |
| heliocentric, | II-4-5 |
| planetocentric, | II-5-8 |
| selenocentric, | II-14-15 |
| Control requirements, | XII-47-55 |
| Conversion factors, table of, | II-50-56 |

| | Page |
|--|------------|
| Coordinate systems, geometrical properties of, | IX-2 |
| Coordinate systems, important, summary, | IX-3 |
| Coordinates and transformations, | IX-2-6 |
| Cosmic radiation, | II-41-45 |
| Cryogenic fluids, properties of, | X-10 |
| Cryogenic tanks, design of, | X-11 |
| Coverage, area, | XIII-17-24 |
| effects of sensor limitations, | XIII-26-31 |
| Cowell's method, | IV-4 |

(D)

| | |
|--|------------|
| Decay histories, | IX-2-18 |
| circular orbits, | V-9-10 |
| effects on coverage, | VIII-25-26 |
| elliptic orbits, | V-13-21 |
| Decay rates, circular orbits, | V-18 |
| elliptic orbits, | V-19 |
| expansions for small parameter, | V-11 |
| Deceleration, re-entry, | IX-12-14 |
| Declination, equations, | III-37 |
| Definitions, | Appendix A |
| Density, atmospheric (see atmospheric density) | |
| Departure, orbital (see Orbital Departure) | |
| Direct launch (rendezvous), | VII-12-13 |
| Docking, orbital (see Rendezvous) | |
| Drag, atmospheric, | V-3-8 |
| in circular orbits, | V-9-10 |
| coefficient, | V-4-8 |
| effect on the orbit (perturbations), | V-8-55 |
| for tumbling bodies, | V-6-8 |
| Differential corrections, maneuvers, | VI-33-39 |
| orbit improvement, | XI-37-43 |

| | Page |
|---|-----------------|
| (E) | |
| Eccentricity, equations for, | III-18 |
| series expansions in, | III-26-34 |
| Eckert-Brouwer differential corrections, | XI-37-42 |
| Eclipses of earth satellites, | XIII-6-14 |
| Ecliptic coordinates, | XI-2-6 |
| Elements, elliptic, equations for, | III-16-34 |
| hyperbolic, equations for, | III-34-38 |
| Elliptic orbits, computation of, | XI-22-47 |
| correction of, | VI-2-52 |
| discussion of, | III-2-13 |
| Encke's method, | IV-4-5 |
| Energy, equation, | III-5 |
| kinetic, | II-5 |
| loss due to drag, | V-9 |
| minimization of, | VI-43-50 |
| potential, | II-5 |
| total, | II-5 |
| Error analysis, of elliptic orbits, | XII-2-28 |
| of orbital departure, | VIII-5-6, 22-23 |
| of maneuvers, | VI-39-42 |
| Errors in numerical integration, | IV-7-14 |
| Extraction of information (see Orbit Computation) | XI-12-22 |

| | |
|---|------------|
| (F) | |
| Final closure (rendezvous), | VII-15-54 |
| analytic solutions, | VII-50-54 |
| techniques, | VII-26-54 |
| energy and time requirements, | VII-40-44 |
| terminal smoothing, | VII-44-50 |
| Finite burning times--effects on departure, | VIII-19-22 |
| effects on maneuvers, | VI-50-53 |

| | Page |
|---|---------------|
| Flight path angle, equations for, | III-22 |
| Flight time, equations for, | III-6 |
| figures, | III-45, 76-87 |
| lifetimes, | V-2-30 |
| re-entry, | IX-2-12 |
| rendezvous, | VII-40-44 |
| return from orbit, | VIII-19-22 |
| Flow regimes, | V-2-3 |
| Force, central, | III-2 |
| Formulations for elliptic orbits, | III-16-34 |
| Fourier-Bessel expansions, | III-30-34 |
| Frequency-departure, | VIII-24-30 |

(G)

| | |
|---|------------|
| Gauss-Jackson method, | IV-11 |
| General maneuver, | VI-23-26 |
| General perturbations, | IV-14-50 |
| Geocentric constants, | II-9-14 |
| coefficients of the potential function, | II-12 |
| flattening and equatorial radius, | II-12-14 |
| gravitational constant, | II-11 |
| Geodetic latitude, | XI-4 |
| Geometry, of ellipse, | III-46 |
| of hyperbola, | III-47 |
| of orbit in 3-D, | III-46 |
| of parabola, | III-47 |
| Geophysical data, | II-15-50 |
| Glossary, | Appendix A |
| Ground resolution, | XIII-26-32 |
| Ground swath, | XIII-17-26 |
| Guidance and control requirements, | XII-2-28 |

(H)

| | |
|---|-----------|
| Heat balance, | X-4 |
| Heat input, | X-5 |
| Heat transfer, | X-11 |
| Heliocentric constants, | II-4-5 |
| planetary geometry, | II-5-8 |
| planetary masses, | II-5 |
| planetary orbits, | II-8-9 |
| solar gravitation constant, | II-4 |
| solar parallax, | II-4 |
| Hyperbolic orbits, element relations, | III-35-36 |
| time variant relations, | III-36-37 |

(I)

| | |
|--|-----------|
| Illumination of satellites, | XIII-6-14 |
| Improvement of orbit, | XI-37-43 |
| Impulsive maneuvers, | VI-2-38 |
| Inclination, equations for, | III-24 |
| Integration, numerical, errors in, | IV-12-14 |
| Intermediate orbits, rendezvous, | VII-5-9 |

(J)

| | |
|--|---------|
| J_i (coefficients of the gravitational potential), | II-9-14 |
|--|---------|

(K)

| | |
|--|----------|
| Keplerian orbits, | III-1-14 |
| Kepler's equation, | III-6 |
| solution by Newton's method, | III-6 |
| Krylov-Bogoliuboff averaging method, | V-15 |

(L)

| | |
|---|----------|
| Lagrange's planetary equations, | IV-20-21 |
| Lambert's theorem, | III-7-9 |

| | Page |
|--|---------------|
| Lifetimes, | V-1-29 |
| drag coefficients, | V-4-6 |
| drag force, | V-3-4 |
| drag on tumbling bodies, | V-6-8 |
| effect of density variability, | V-25-30 |
| flow regimes, | V-2-3 |
| three dimensional perturbation, | V-21-25 |
| change in elements, | V-22-25 |
| perturbing force, | V-21-22 |
| two-dimensional perturbation, | V-8-21 |
| elliptic orbits, | V-10-12 |
| near circular orbits, | V-9-10, 18-19 |
| variation of elements, | V-12-18 |
| Low altitude orbits, departure from, | VIII-17-23 |
| Low level thrust maneuvers, | VI-56-64 |
| Lunar perturbations, | IV-36-40 |

(M)

| | |
|--|----------|
| Maneuverability, | IX-18-21 |
| envelopes, | IX-21 |
| lifting bodies, | IX-21 |
| re-entry, | IX-18-21 |
| Maneuvers, | VI-1-64 |
| differential corrections, | VI-33-39 |
| distribution of the resulting orbit, | VI-39-43 |
| effects of finite burning time, | VI-50-53 |
| general, | VI-23-26 |
| impulsive corrections, | VI-2-3 |
| in orbit propulsion system, | VI-53-56 |
| independent adjustment of elements, | VI-3-15 |
| microthrust study, | VI-56-64 |
| optimization, | VI-43-50 |

| | Page |
|--|------------|
| propulsion for canceling drag and | |
| oblateness, | VI-26-33 |
| small maneuvers in nearly circular orbits, | VI-15-23 |
| Mean anomaly (see Anomaly, mean) | |
| Meteoroid, data, | II-46-50 |
| hazard and shielding, | II-50 |
| penetration, | II-49 |
| Method of least squares, | XI-30-36 |
| Microthrust, normal to the plane, | VI-60 |
| circumferential, | VI-58 |
| general, | VI-60-64 |
| radial, | VI-57-58 |
| tangential, | VI-58 |
| Minimum energy transfers, | VI-43-50 |
| Mission requirements, | XIII-1-32 |
| area coverage, | XIII-17-21 |
| communication satellites, | XIII-2-4 |
| eclipses, | XIII-8-14 |
| ground tracks, | XIII-14-17 |
| meteorological satellites, | XIII-6 |
| mission considerations, | XIII-2-6 |
| navigation satellites, | XIII-4-6 |
| pattern coverage, | XIII-21-24 |
| point coverage, | XIII-24-26 |
| reconnaissance satellites, | XIII-2 |
| relative geometry vehicle, earth, sun, | XIII-6-8 |
| satellite coverage, | XIII-17-26 |
| sensor limitations, | XIII-26-32 |
| solar problems, | XIII-6-14 |
| synchronous orbits, | XIII-16-17 |
| Model atmospheres, | II-15-38 |

| | Page |
|--|------------|
| Molecular speed ratio, | V-4 |
| Motion, equations of, | III-2 |
| (N) | |
| Node, ascending, equations for, | III-24 |
| Nomography, | III-14-15 |
| Nongravitational forces, | IV-3-4 |
| Numerical integration, | IV-7-14 |
| (O) | |
| Orbit computation, | XI-1-47 |
| accuracy determination, | XI-43-47 |
| acquisition of data, | XI-14-22 |
| coordinate systems and transformations, | XI-2-14 |
| data correction, | XI-2-11 |
| Gibbs' modification, | XI-26-27 |
| maximum likelihood, | XI-36 |
| method of Laplace, | XI-22-25 |
| method of least squares, | XI-30-37 |
| method of Gauss, | XI-25-26 |
| method of moments, | XI-36-37 |
| minimum variance, | XI-36 |
| observational error, | XI-28-37 |
| orbit improvement, | XI-37-43 |
| preliminary orbits, | XI-22-28 |
| station properties, | XI-14-16 |
| tracking techniques, | XI-12-14 |
| Orbital departure, | VIII-3-30 |
| analysis of departure frequencies, | VIII-24-30 |
| generalized return problem, | VIII-3-17 |
| planar analysis of deorbit from low altitude circular orbits, | VIII-17-23 |
| three-dimensional impulse analyses, | VIII-23-24 |

| | Page |
|---|------------|
| Orbit mechanics, | III-1-39 |
| graphical data, | III-39-87 |
| Lagrangian equations, | III-3 |
| Lambert's theorem, | III-7-9 |
| motions in central force field, | III-2-3 |
| motion in 3-D, | III-4 |
| N-body problem, | III-9-12 |
| nomograms, | III-14-15 |
| orbital elements, | III-3 |
| properties of elliptic motion, | III-4-7 |
| series expansion for elliptic orbits, | III-12-14 |
| tables of equations for elliptic motion, | III-15-38 |
| Oblate earth, | II-9-14 |
| Oblateness, comparison of theories, | IV-31-36 |
| perturbations, | IV-21-31 |
| long period, | IV-24 |
| secular, | IV-23-24 |
| short period, | IV-24-25 |
| Observational theory and trajectory prediction, | XI-28-37 |
| Optimization, of area coverage, | XIII-17-26 |
| of maneuvers, | VI-43-50 |
| of satellite patterns, | XIII-21-26 |
| Orbit determination, | XI-22-28 |
| Orbit improvement, | XI-37-42 |
| Orbital parameters, equations for, | III-17-38 |
| Orbital perturbations, equations for, | IV-23-40 |
| Orientation, satellite, | XIII-6-14 |
| Osculating orbital elements, | IV-15-21 |

(P)

| | |
|----------------------------|-------|
| Parallax, lunar, | II-14 |
| solar, | II-4 |

| | Page |
|--|--------------|
| Parameters, variation of, | IV-15-21 |
| Parking orbits, utilization of, | VII-5-9 |
| Penetration, meteorite, | VIII-3-17 |
| Perigee advance, due to drag, | V-13 |
| due to oblateness, | IV-23-24 |
| Perigee radius, equations for, | III-19 |
| Perigee velocity, equations for, | III-20 |
| Period, anomalistic, | IV-22 |
| changes due to drag, | VIII-25-27 |
| changes due to oblateness, | IV-21-22 |
| nodal, | IV-22 |
| sidereal, | IV-22 |
| Perkins' method for decay rates, | V-18-19 |
| Perturbation theories, analytic comparison of, | IV-31-36 |
| Cowell's method, | IV-4-5 |
| drag perturbations, | IV-40-45 |
| Encke's method, | IV-5-6 |
| first order secular, | IV-21-23 |
| general, | IV-15-40 |
| higher order, | IV-23-31 |
| numerical integration, | IV-7-14 |
| oblateness, | IV-21-31 |
| precession of apsides, | IV-24 |
| regression of nodes, | IV-24 |
| solar-lunar, | IV-36-40 |
| special, | IV-2-7 |
| stability, | IV-47-50 |
| variation of parameters, | IV-6-7-15-21 |
| Physical data, | II-2-56 |
| astronomical constants, | II-2-15 |

| | Page |
|---|------------|
| astrophysical data, | II-15-50 |
| conversion data, | II-50-56 |
| Planets, geometry of, | II-5-9 |
| masses of, | II-5 |
| elements of orbits, | II-8 |
| Potential function, | II-9 |
| Precession of apsides, | IV-24 |
| Primary cosmic radiation, | II-43-45 |
| Propellant storage in orbit, | X-10-15 |
| Propulsion requirements to cancel effects | |
| of oblateness, | VI-26-33 |
| Propulsion system, | VI-53-56 |
| chamber sizing, | VI-55 |
| nozzle sizing, | VI-54 |
| propellant flow rates, | VI-56 |
| requirements, | VI-53 |
| thrust level, | VI-54 |
| (R) | |
| Radar data, | XI-12-22 |
| Radial acceleration, equations for, | III-22 |
| Radial velocity, equations for, | II-21, 22 |
| Radiation, damage thresholds, | II-45 |
| penetrating electromagnetic, | II-45 |
| primary cosmic, | II-41-45 |
| solar flare radiations, | II-39, 40 |
| Van Allen belts, | II-40, 41 |
| Radius, earth's equatorial, | II-12-14 |
| equivalent, | II-19 |
| polar, | II-12-14 |
| orbital, equations for, | III-21 |
| series, | III-27, 28 |

| | Page |
|--|------------|
| Range, descent from orbit to re-entry, | VIII-17-23 |
| ballistic vehicles re-entry to impact, | IX-17, 18 |
| equilibrium glide re-entry to impact, | IX-19 |
| lateral re-entry to impact, | IX-18-21 |
| lifting vehicles re-entry to impact, | IX-17-21 |
| Re-entry, aerodynamic heating, | IX-14-17 |
| deceleration and loads, | IX-12-14 |
| range and maneuverability, | IX-17-21 |
| theory, | IX-2-22 |
| trajectories, | IX-2-12 |
| References and bibliography, guidance and control, . | XII-56-63 |
| lifetime, | V-30-35 |
| maneuvers, | VI-64-75 |
| mission requirements, | XIII-32-35 |
| orbit computation, | XI-47-49 |
| orbit mechanics, | III-39-41 |
| orbital departure, | VIII-30 |
| perturbations, | IV-50-59 |
| physical data, | II-56-63 |
| re-entry, | IX-21-29 |
| rendezvous, | VII-54-57 |
| waiting orbit criteria, | X-15-21 |
| Regression of the nodes, | IV-24 |
| Rendezvous, | VII-1-53 |
| compatible orbits, | VII-9-12 |
| direct launch, | VII-12-13 |
| energy and time requirements, | VII-40-44 |
| final closure techniques, | VII-26-40 |
| gross maneuvers, | VII-3-13 |
| homing phase errors, | VII-53-59 |
| intermediate orbits, | VII-2-9 |
| long time closures, | VII-50-53 |

| | Page |
|---|------------|
| relative motion, | VII-13-26 |
| terminal guidance smoothing, | VII-44-50 |
| terminal maneuver, | VII-13-54 |
| Return from orbit (see Re-entry and Orbit Departure) | |
| Runge-Kutta method, | IV-7-8 |
| (S) | |
| Satellite, energy, | III-5 |
| ground tracks, | XIII-14-17 |
| illumination, | XIII-6-14 |
| orbital data, | III-15-39 |
| orientation with respect to the sun, | XIII-6-14 |
| recovery, | VIII, IX |
| Selenocentric constants, | II-14-15 |
| Simulatus rectum (see Semiparameter) | |
| Semimajor axis, equations for, | III-17 |
| Semiparameter, equations for, | III-18 |
| Sensitivities, trajectories, | XII-2-28 |
| Series expansions of orbital parameters, | III-26-34 |
| Smoothing techniques, general, | XI-28-42 |
| rendezvous, | VII-44-50 |
| Solar, gravitational constant, | II-5 |
| parallax, | II-4 |
| perturbations, | IV-36-40 |
| radiation, | II-39-40 |
| Special perturbations, | IV-2-14 |
| Spherical trigonometric relations, | III-37, 38 |
| Statistical error analysis (maneuvers), | IV-39-43 |
| Storability, cryogenic, | X-10-15 |
| Swath, | XIII-17-26 |

(T)

| | |
|---|-----------|
| Temperatures, histories for re-entry, | IX-14-17 |
| parameters, | IX-14-17 |
| radiation equilibrium, | IX-16 |
| skin, | IX-14-17 |
| stagnation point, | IX-14-17 |
| Terminal guidance for rendezvous, | VII-13-54 |
| Theory of errors in orbital prediction, | XII-2-2 |
| Three dimensional elliptic relations, | III-4 |
| Time dependent variables for elliptic orbits, | III-21-23 |
| Time standards and conversions, | II-50-56 |
| Tracking facilities, | XI-12-22 |
| Trajectories, re-entry, | IX-2-12 |
| Transfer maneuvers, | VI-2-33 |
| Transformation of coordinates, | XI-2-12 |
| True anomaly, equations for, | III-23 |
| series expansions, | III-27 |

(U)

| | |
|--|-----------|
| Umbra, time in, | XIII-6-14 |
| Upper atmosphere, models of, | II-15-38 |
| Universal gravitation, low of, | II-2 |

(V)

| | |
|------------------------------------|------------|
| Van Allen radiation, | II-40, 41 |
| Variation of parameters, | IV-15-21 |
| Vis Viva integral, | III-5 |
| Visibility times, | XIII-17-26 |

(W)

| | |
|---|---------|
| Waiting orbit criteria, | X-2-15 |
| cryogenic propellant storage, | X-10-15 |

| | Page |
|---|------------|
| payload and geometrical restrictions | X-2-4 |
| vehicle temperature control, | X-4-10 |
| Weights and volume conversions, | II-50-56 |
| (Z) | |
| Z function for re-entry, | IX-2-12 |
| Zenith angle of a satellite, | XIII-24-25 |